Utilisation of Cashew Nut Shell Liquid as a Starting Material for the Synthesis of Difunctional Monomers Useful in the Preparation of High Performance Polymers

A thesis submitted to the

Savitribai Phule Pune University
for the degree of

DOCTOR OF PHILOSOPHY

in

CHEMISTRY

by

Deepshikha Chatterjee

Research Guide
Dr. Prakash P. Wadgaonkar

Polymers and Advanced Materials Laboratory,
Polymer Science and Engineering Division,
CSIR-National Chemical Laboratory,
PUNE 411 008

OCTOBER 2018

To my dear Father, Late Robindra Nath Chatterjee, my Grandfather, Late Dr. (Brig) M. N. Chatterjee, my Grandmother Late Sondhya Chatterjee and my dearest Mom, Sumita Chatterjee.

सीएसआईआर - राष्ट्रीय रासायनिक प्रयोगशाला
(वैज्ञानिक तथा औद्योगिक अनुसंधान परिषद)
डॉ. होमी भाभा मार्ग, पुणे - 411 008, भारत
CSIR - NATIONAL CHEMICAL LABORATORY
(Council of Scientific & Industrial Research)
Dr. Homi Bhabha Road, Pune - 411 008, India

Certificate of the Guide

This to certify that the work incorporated in the Ph.D thesis entitled **"Utilisation of cashew nut shell liquid as a starting material for the synthesis of difunctional monomers useful in the preparation of high performance polymers"** submitted by **Deepshikha Chatterjee** to **Savitribai Phule Pune University** in fulfilment of the requirements for the award of the Degree of **Doctor of Philosophy in Chemistry,** embodies original research work done under my supervision. I further certify that this work has not been submitted to any other University or Institution in part or full for the award of any degree or diploma. Any text, illustration, table etc., used in the thesis from other sources, have been duly cited and acknowledged.

Deepshikha Chatterjee
(Student)
October, 2018

Prakash P. Wadgaonkar
(Research Guide)

Communication Channels
NCL Level DID : 2590
NCL Board No. : +91-20-25902000
EPABX : +91-20-25893300
: +91-20-25893400
FAX
Director's Office : +91-20-25902601
COA's Office : +91-20-25902660
SPO's Office : +91-20-25902664
WEBSITE
www.ncl-india.org

DECLARATION BY THE CANDIDATE

I hereby declare that the research work embodied in this thesis entitled, **"Utilisation of cashew nut shell liquid as a starting material for the synthesis of difunctional monomers useful in the preparation of high performance polymers"** submitted to the Savitribai Phule Pune University for the award of the **Degree of the Doctor of Philosophy (Ph.D.)** is the outcome of experimental investigations carried out by me at the Polymer Science and Engineering Division of CSIR-National Chemical Laboratory, Pune, India, under the supervision of **Dr. Prakash P. Wadgaonkar**, Chief Scientist, CSIR-National Chemical Laboratory, Pune. I affirm that the work incorporated is original, and has not been submitted to any other Academy, University or Institute for the award of any Degree or Diploma.

Deepshikha Chatterjee
(Research Student)
October, 2018
Polymer Science and Engineering Division
CSIR-National Chemical Laboratory
Pune-411008

Acknowledgement

I express sincere heartfelt gratitude towards the Almighty for giving me the courage and strength to endure when faced with hardships. I take this moment to fondly remember and thank my late grandfather for instilling in me discipline, hardwork and an undying love for science....my PhD thesis would not exist without his moulding influence. Also, I remember and thank my late father and grandmother for their care, understanding and wisdom; who would be happiest to see me complete my PhD journey, from up above. Thanks are due to my mother, for supporting me, every step of the way.

I take intense pleasure in thanking my supervisor, Dr. Prakash P. Wadgaonkar, for giving me the opportunity to do research and providing invaluable guidance, support, encouragement and intellectual stimulation throughout my PhD tenure. His astute observations and comments helped me to establish the overall direction of my research. He taught me how to understand a scientific problem and logically arrive at a solution through scientific enquiry. His invaluable guidance has helped in making me a better person and professional. When it comes down to my PhD thesis: I owe it all to him!

I am extremely grateful to the Council of Scientific and Industrial Research (CSIR) for providing me research fellowship and financial support. I extend my gratitude to Prof Ashwinikumar Nangia (Director, CSIR-NCL), Dr. Vijayamohanan Pillai (Former Director, CSIR-NCL), Dr. Sourav Pal (Former Director, CSIR-NCL) and Dr. S. Sivaram (Former Director, CSIR-NCL) for allowing me to pursue research in CSIR-NCL. I greatly appreciate Dr. U. K. Kharul (Chair, PSE Division), Dr.Ashish Lele (Former Chair, PSE Division), Dr. A. J. Varma (Former Chair, PSE Division) and Dr. M. G. Kulkarni (Former Chair, PSE Division) for giving me the opportunity to work in Polymer Science and Engineering Division and providing the instrumental facilities and infrastructure to perform my research work.

I owe my sincere thanks to Dr. C. V. Avadhani, Mr. S. K. Menon, Mr. Anandrao Patil, Dr. Ashootosh Ambade and Dr. Nilakshi V. Sadavarte for their kind support and help throughout my PhD tenure.

I would also like to thank my research progress monitoring committee members: Dr. U. P. Mulik (C-MET, Pune), Dr.Vaishali Shinde (Savitribai Phule Pune University), Dr. U. K. Kharul (CSIR-NCL, Pune) and Dr. Ashootosh Ambade (CSIR-NCL, Pune) for their insightful comments.

My special thanks are due to Uday Jadhav, for helping me accomplish memory device characterisation. My heartfelt gratitude extends to Dr. Tukaram Dongale (Assistant Professor, School of

Nanoscience and Technology, Shivaji University, Kolhapur) and Dr. P. S. Patil (Professor, Founder and Coordinator, School of Nanoscience and Technology, Shivaji University, Kolhapur) for making memory device evaluation possible. I am especially indebted to Dr. Dongale for his insightful help and guidance in data interpretation. Special thanks are due to Dr. K. Krishnamoorthy (CSIR-NCL, Pune) and Dr. Chayanika Das for their help in carrying out electrochemical and spectroelectrochemical characterisations.

I would like to express my sincere thanks to Dr. Suresh Bhat, Mrs. Deepa Dhoble, Dr. Neelima Bulakh, Mrs. Sangeeta Hambir, Mrs. Poorvi Purohit, Dr. B. Santhakumari and Mr. R. Gholap for allowing me to use instruments and providing analytical facilities. Many special thanks to Dr. P. R. Rajamohanan, Dr. T. G. Ajithkumar and the entire NMR facility for helping me in NMR characterisations. I also thank the members of Glass Blowing, Workshop, Stores, Purchase, Accounts and Bills section and other office staff for their timely help. I deeply appreciate Student Academic Office (SAO) Chairman Dr. M. S. Shashidhar, Dr. C. G. Suresh and other staff members including Mrs. P. Kolhe and Shri S. Iyer for their continual cooperation and support.

I am deeply indebted to my past colleages in our group: Dr. Rahul Shingte, Dr. Anjana Sarkar, Dr. Pandurang Honkhambe, Palaskar, Nagendra Bhairamdgi, Dr. Snehalata Bapat, Dr. Arvind More, Dr. Arun Kulkarni, Dr. Prakash Sane, Dr. Savita Kumari, Dr. Mahesh Biyani, Dr. Sharad Pasale, Kishor Kumbhar, Dr. Nagendra Kalva, Dr. Naganath Patil, Dr. Aarti ,Dr. Bhausaheb Tawade, Dr. Indravadan Parmar, Dr. Sachin Patil, Dr. Sachin Kuhire, Jagdish Salunke, Vikas Kumar, Dr. Kavita Garg, Dr. Shyambo Chatterjee, Dr. Murugesan, Vishal, Dr. Shraddha Chhatre, Dr. Sayali Shaligram, Sachin Basutkar, Nitin Valsange, as well as present members: Samadhan, Dr. Bharat Shrimant, Deepak, Rupali, Nitin Basutkar, Geethika, Ashwini, Uday, Durgaprasad, Amol, Shakeb, Dr. Ikhlas Gadwal, Yogesh Neware, Ketan and Dr. Prakash Babu. All of them made my life in the lab easier and more enjoyable.

Finally, I thank all the other people in CSIR-NCL, who cannot be named due to space constraints for their valuable helping hands.

Deepshikha Chatterjee
October, 2018

Table of Contents

Description			Page no
➢ Abstract			i
➢ List of Abbreviations			vii
➢ List of Tables			ix
➢ List of Schemes			xi
➢ List of Figures			xiii
Chapter 1	**Introduction and Literature Survey**		
1.1	Introduction		1
	1.1.1	Background	1
	1.1.2	Cashew Nut Shell Liquid (CNSL)	3
	1.1.3	Components of CNSL	4
	1.1.4	Reactivity of cardanol	6
1.2.	Difunctional monomers based on CNSL and step-growth polymers therefrom		6
	1.2.1	CNSL-based aromatic difunctional condensation monomers	6
	1.2.2	Step-growth polymers from CNSL-based aromatic difunctional monomers	12
		1.2.2.1 Aromatic polyimides	13
		1.2.2.2 Aromatic polyamides	19
		1.2.2.3 Aromatic polyazomethines	23
		1.2.2.4 Poly(arylene ether)s	25
1.3	General trends in properties of high performance polymers from CNSL-based aromatic difunctional monomers		27
1.4	The potential for CNSL-based step-growth polymers for optoelectronic applications: literature and prospects		28
1.5	Summary		35
References			36
Chapter 2	**Scope and Objectives**		47
References			49

Chapter 3 Synthesis and Characterisation of Monomers Starting from CNSL

3.1 Introduction 53

3.2 Experimental 55

3.2.1 Materials 55

3.2.2 Measurements 55

3.3 Preparations 56

3.3.1 Synthesis of 4, 4’-diamino-4"pentadecyltriphenylamine (DPTA) 56

3.3.1.1 Synthesis of 1-nitro-4-pentadecyl benzene 56

3.3.1.2 Synthesis of 4-pentadecylaniline 56

3.3.1.3 Synthesis of 4, 4’-dinitro-4"pentadecyltriphenylamine 57

3.3.1.4 Synthesis of 4, 4’-diamino-4"pentadecyltriphenylamine (DPTA) 58

3.3.2 Synthesis of 4-methoxy-6-pentadecylisophthalaldehyde (MPIAL) 58

3.3.2.1 Synthesis of 1-methoxy-3-pentadecylbenzene 58

3.3.2.2 Synthesis of 1,5-dibromo-2-methoxy-4-pentadecylbenzene 59

3.3.2.3 Synthesis of 4-methoxy-6-pentadecylisophthalonitrile 60

3.3.2.4 Synthesis of 4-methoxy-6-pentadecylisophthalaldehyde (MPIAL) 61

3.3.3 Synthesis of diacid with pendent pentadecyl chain 62

3.3.3.1 Synthesis of 4-methoxy-6-pentadecylisophthalic acid (MPIA) 62

3.3.4 Synthesis of 4-(4-hydroxyphenoxy)-3-pentadecylphenol (HPPDP) 62

3.3.4.1 Synthesis of 1-bromo-4-methoxy-2-pentadecylbenzene 62

	3.3.4.2	Synthesis of 4-methoxy-1-(4-methoxyphenoxy)-2-pentadecylbenzene	63
	3.3.4.3	Synthesis of 4-(4-hydroxyphenoxy)-3-pentadecylphenol (HPPDP)	64
3.3.5	Synthesis of 3-pentadecyl 4,4' biphenol (PDBP)		64
	3.3.5.1	Synthesis of 4, 4'-dimethoxy-2-pentadecyl-1,1'-biphenyl	64
	3.3.5.2	Synthesis of 3-pentadecyl 4, 4' biphenol (PDBP)	65
3.3.6	Synthesis of 4,4'-(3-pentadecylcyclohexane-1,1-diyl)diphenol (BPC15)		66
	3.3.6.1	Synthesis of 3-pentadecyl cyclohexanol	66
	3.3.6.2	Synthesis of 3-pentadecyl cyclohexanone	66
	3.3.6.3	Synthesis of 4,4'-(3-pentadecylcyclohexane-1,1-diyl)diphenol (BPC15)	67
3.3.7	Synthesis of bisphenol based on 3-pentadecyl cyclohexanone		67
	3.3.7.1	Synthesis of 2,6-bis(4-hydroxybenzylidene)-3-pentadecylcyclohexanone (BPC)	67
3.3.8	Synthesis of 4,4'-((2-pentadecyl-[1,1'-biphenyl]-4,4'-diyl)bis(oxy))dianiline (PBD)		68
	3.3.8.1	Synthesis of 4,4'-bis(4-nitrophenoxy)-2-pentadecyl-1,1'-biphenyl	68
	3.3.8.2	Synthesis of 4,4'-((2-pentadecyl-[1,1'-biphenyl]-4,4'-diyl)bis(oxy))dianiline (PBD)	69
3.3.9	Synthesis of bispropargyl ether with biphenylene linkage		69
	3.3.9.1	Synthesis of 2-pentadecyl-4,4'-bis(prop-2-yn-1-yloxy)-1,1'-biphenyl (PPB)	69
3.3.10	Synthesis of bispropargyl ether with multiple ether linkages		70
	3.3.10.1	Synthesis of 2-pentadecyl-4-(prop-2-yn-1-yloxy)-1-(4-(prop-2-yn-1-yloxy)phenoxy)benzene (PPPB)	70

3.3.11	Synthesis of phthalonitrile with multiple ether linkages		71
	3.3.11.1	Synthesis of 4-(4-(4-(3,4-dicyanophenoxy)-2-pentadecylphenoxy)phenoxy)phthalonitrile (DCPP)	71
3.3.12	Synthesis of phthalonitrile with biphenylene linkage		72
	3.3.12.1	Synthesis of 4,4'-((2-pentadecyl-[1,1'-biphenyl]-4,4'-diyl)bis(oxy))diphthalonitrile (PBP)	72
3.3.13	Synthesis of phthalonitrile with cyclohexylidene moiety		73
	3.3.13.1	Synthesis of 4,4'-(((3-pentadecylcyclohexane-1,1-diyl)bis(4,1-phenylene))bis(oxy))diphthalonitrile (CPP)	73
3.4	Results and Discussion		74
3.4.1	Synthesis of 4, 4’-diamino-4"pentadecyltriphenylamine (DPTA)		74
3.4.2	Synthesis of 4-methoxy-6-pentadecylisophthalaldehyde (MPIAL)		78
3.4.3	Synthesis of 4-methoxy-6-pentadecylisophthalic acid (MPIA)		81
3.4.4	Synthesis of 4-(4-hydroxyphenoxy)-3-pentadecylphenol (HPPDP)		84
3.4.5	Synthesis of 3-pentadecyl biphenol (PDBP)		88
3.4.6	Synthesis of 4,4'-(3-pentadecylcyclohexane-1,1-diyl)diphenol (BPC15)		91
3.4.7	Synthesis of 2,6-bis(4-hydroxybenzylidene)-3-pentadecylcyclohexanone (BPC)		95
3.4.8	Synthesis of 4,4'-((2-pentadecyl-[1,1'-biphenyl]-4,4'-diyl)bis(oxy))dianiline (PBD)		100
3.4.9	Synthesis of 2-pentadecyl-4,4'-bis(prop-2-yn-1-yloxy)-1,1'-biphenyl (PPB)		104
3.4.10	Synthesis of 2-pentadecyl-4-(prop-2-yn-1-yloxy)-1-(4-(prop-2-yn-1-yloxy)phenoxy)benzene (PPPB)		108

	3.4.11	Synthesis of 4-(4-(4-(3,4-dicyanophenoxy)-2-pentadecylphenoxy)phenoxy)phthalonitrile (DCPP)	112
	3.4.12	Synthesis of 4,4'-((2-pentadecyl-[1,1'-biphenyl]-4,4'-diyl)bis(oxy))diphthalonitrile (PBP)	116
	3.4.13	Synthesis of 4,4'-(((3-pentadecylcyclohexane-1,1-diyl)bis(4,1-phenylene))bis(oxy))diphthalonitrile (CPP)	120
3.5	Conclusions		126
References			127
Supporting Information			131
Chapter 4	**Partially Bio-Based Triarylamine-Containing High Performance Polymers**		
Chapter 4a	**Partially Bio-Based Triarylamine-Containing Polyimides: Synthesis, Characterisation and Evaluation for Memory Devices**		
4a.1	Introduction		133
4a.2	Experimental		134
	4a.2.1	Materials	134
	4a.2.2	Measurements	135
	4a.2.3	Polyimide synthesis: typical procedure	135
	4a.2.4	Optical, electrochemical and spectroelectrochemical measurements	136
	4a.2.5	Memory device characterisation	136
4a.3	Results and Discussion		137
	4a.3.1	Polyimide synthesis	137
	4a.3.2	Solubility and X-ray diffraction studies	142
	4a.3.3	Thermal properties	143
	4a.3.4	Optical and electrochemical properties	147
	4a.3.5	Spectroelectrochemical properties	149
	4a.3.6	Memory device characterisation	151
4a.4	Conclusions		161
References			162

Supporting Information 166

Chapter 4b Partially Bio-Based Triarylamine-Containing Polyamides: Synthesis, Characterisation and Evaluation for Memory Devices

4b.1 Introduction 169

4b.2 Experimental 169

4b.2.1 Materials 169

4b.2.2 Measurements 170

4b.2.3 Polyamide synthesis: typical procedure 170

4b.2.4 Optical and electrochemical characterisation 171

4b.2.5 Memory device characterisation 171

4b.3 Results and Discussion 172

4b.3.1 Polyamide synthesis 172

4b.3.2 Solubility and X-ray diffraction studies 178

4b.3.3 Thermal Properties 179

4b.3.4 Optical and electrochemical properties 183

4b.3.5 Memory device characterisation 185

4b.4 Conclusions 193

References 194

Supporting Information 198

Chapter 4c Partially Bio-Based Triarylamine-Containing Polyazomethines: Synthesis, Characterisation and Evaluation for Memory Devices

4c.1 Introduction 201

4c.2 Experimental 202

4c.2.1 Materials 202

4c.2.2 Measurements 202

4c.2.3 Polyazomethine synthesis: typical procedure 203

4c.2.4 Optical measurements 203

4c.2.5 Memory device characterisation 203

4c.3 Results and Discussion 204

4c.3.1 Polyazomethine synthesis 204

4c.3.2 Solubility and X-ray diffraction studies 209
4c.3.3 Thermal Properties 210
4c.3.4 Optical properties 213
4c.3.5 Memory device characterisation 215
4c.4 Conclusions 223
References 224
Chapter 5 Partially Bio-Based Poly(arylene ether)s Containing pendent Pentadecyl Chains
Chapter 5a Synthesis and Characterisation of Partially Bio-Based Poly(ether ether ether ketone)s Containing Pendent Pentadecyl Chains
5a.1 Introduction 229
5a.2 Experimental 230
5a.2.1 Materials 230
5a.2.2 Measurements 230
5a.2.3 Synthesis of (co)poly(ether ether ether ketone)s: typical procedure 231
5a.3 Results and Discussion 231
5a.3.1 Synthesis of (co)poly(ether ether ether ketone)s 231
5a.3.2 Solubility and X-ray diffraction studies 238
5a.3.3 Thermal properties 241
5a.4 Conclusions 244
References 245
Chapter 5b Synthesis and Characterisation of Partially Bio-Based Poly(ether sulfone)s Containing Pendent Pentadecyl Chains
5b.1 Introduction 249
5b.2 Experimental 250
5b.2.1 Materials 250
5b.2.2 Measurements 250
5b.2.3 Synthesis of (co)poly(ether sulfones)s: typical procedure 251
5b.3 Results and Discussion 251

5b.3.1 Synthesis of (co)poly(ether sulfone)s 251
5b.3.2 Solubility and X-ray diffraction studies 258
5b.3.3 Thermal properties 260
5b.4 Conclusions 264
References 265
Chapter 6 Synthesis and Characterisation of Partially Bio-Based Polycarbonates Containing Pendent Pentadecyl Chains
6.1 Introduction 269
6.2 Experimental 270
6.2.1 Materials 270
6.2.2 Measurements 270
6.2.3 Synthesis of (co)polycarbonates: typical procedure 271
6.3 Results and Discussion 272
6.3.1 Synthesis of (co)polycarbonates 272
6.3.2 Solubility and X-ray diffraction studies 280
6.3.3 Thermal properties 281
6.4 Conclusions 285
References 285
Chapter 7 Synthesis and Characterisation of Partially Bio-Based Polyimides Containing Pendent Pentadecyl Chains
7.1 Introduction 289
7.2 Experimental 290
7.2.1 Materials 290
7.2.2 Measurements 290
7.2.3 Polyimide synthesis: typical procedure 291
7.3 Results and Discussion 292
7.3.1 Synthesis of polyimides 292
7.3.2 Solubility and X-ray diffraction studies 296
7.3.3 Thermal properties 298
7.4 Conclusions 301

References 302

Chapter 8 Summary and Conclusions

8.1 Summary 305

8.2 Future Perspectives 312

Synopsis 315

List of Publications 325

Abstract

The present day age of polymers, ushered in by the development of the first synthetic polymer by Leo Hendrik Bakeland in 1907, has seen unprecedented and explosive growth in the past century. For the 335 million metric tonnes of man-made plastics produced worldwide per annum, the core source for their chemical synthesis has always been petrochemical resources. The exploration of alternative sources for the synthesis of polymers is an attractive and challenging prospect faced by chemical industry and academia, necessary for the achievement of sustainability. Biomass constitutes an attractive source of renewable bio-derived chemicals, including lignins, natural phenols, tannins, etc.

Cashew nut shell liquid (CNSL) is a natural phenol obtained as a by-product of the cashew processing industry and its constituents are: anacardic acid, cardanol, cardol, and 2-methyl cardol. These bio-derived chemicals provide a naturally occurring 15-carbon hydrocarbon chain and hydroxyl moiety in the same molecule opening up several opportunities for chemical modifications. This allows chemists to design new monomers starting from these bio-derived chemicals by employing basic chemical transformations. Additionally, pentadecyl chains, when incorporated into synthesised high performance polymers which are notorious for their intractability and solvent resistance, can enhance solubility and processability.

The present research work is centred on the utilisation of cashew nut shell liquid as a starting material for the synthesis of difunctional monomers and the preparation of high performance polymers therefrom. For this purpose, a number of monomers were synthesised from CNSL, which are potentially useful for the synthesis of polymers. Furthermore, several high performance polymers containing triarylamine units were investigated for optoelectronic applications, such as OLEDs, electrochromic devices, memory devices, etc.

Chapter 1 presents a brief account of cashew nut shell liquid (CNSL) as an important bio-based chemical abundantly available in the form of a by-product of the cashew processing industry. An overview has been provided pertaining to difunctional monomers obtained from CNSL and the preparation of step-growth polymers therefrom.

The properties of polymers are discussed in brief. The potential of the utilisation of CNSL in smart materials, especially in the field of optoelectronics, has been considered.

Chapter 2 enumerates the scope and objectives of the present work.

Chapter 3 describes the synthesis of monomers as depicted in **Tables 1 and 2**:

Table 1 Difunctional condensation monomers starting from CNSL

Sr. No.	Monomer Structure	Monomer
1.	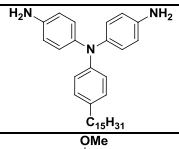	4, 4’-Diamino-4"pentadecyltriphenylamine
2.	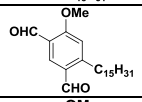	4-Methoxy-6-pentadecylisophthalaldehyde
3.	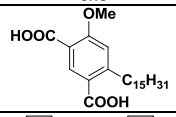	4-Methoxy-6-pentadecylisophthalic acid
4.	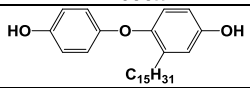	4-(4-Hydroxyphenoxy)-3-pentadecylphenol
5.	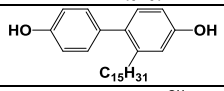	2-Pentadecyl-[1,1'-biphenyl]-4,4'-diol
6.	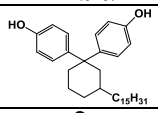	4,4'-(3-Pentadecylcyclohexane-1,1-diyl)diphenol
7.	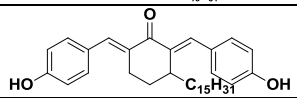	2,6-Bis(4-hydroxybenzylidene)-3-pentadecylcyclohexanone
8.	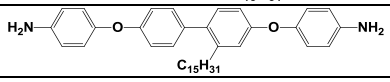	4,4'-((2-Pentadecyl-[1,1'-biphenyl]-4,4'-diyl)bis(oxy))dianiline

Table 2 Monomers for thermosetting resins starting from CNSL

Sr. No.	Monomer Structure	Monomer
1.	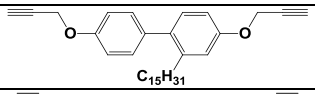	2-Pentadecyl-4,4'-bis(prop-2-yn-1-yloxy)-1,1'-biphenyl
2.	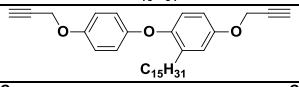	2-Pentadecyl-4-(prop-2-yn-1-yloxy)-1-(4-(prop-2-yn-1-yloxy)phenoxy)benzene
3.	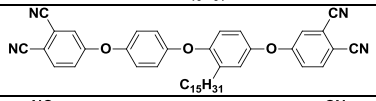	4-(4-(4-(3,4-Dicyanophenoxy)-2-pentadecylphenoxy)phenoxy)phthalonitrile
4.	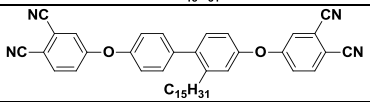	4,4'-((2-Pentadecyl-[1,1'-biphenyl]-4,4'-diyl)bis(oxy))diphthalonitrile
5.	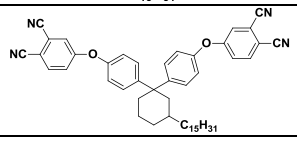	4,4'-(((3-Pentadecylcyclohexane-1,1-diyl)bis(4,1-phenylene))bis(oxy))diphthalonitrile

The synthesised monomers and the intermediates involved were characterised by FT-IR, ^{1}H-NMR spectroscopy, ^{13}C-NMR spectroscopy and HRMS.

Chapter 4 has been divided into three sections

Chapter 4a provides a study on the synthesis of triarylamine-containing polyimides bearing pendent pentadecyl chains by polycondensation of 4, 4'-diamino-4"pentadecyltriphenylamine with commercially available aromatic dianhydrides *viz*. 3,3',4,4'-biphenyltetracarboxylic dianhydride (BPDA), 4,4'-oxydiphthalic anhydride (ODPA) and 4,4'-(hexafluoroisopropylidene) diphthalic anhydride (6-FDA). The synthesised polyimides exhibited inherent viscosities and number average molecular weights in the range 0.54 – 0.60 dL g^{-1} and 26800 – 43500 g mol^{-1}, respectively, indicating the formation of polyimides with reasonably high molecular weights. Polyimides were readily soluble in common organic solvents including chloroform. T_{10} values were observed in the range 418–447 °C, suggesting good thermal stability. T_g values were observed in the range 165– 225 °C. Polyimides displayed optical and electrochemical band-gap values in the range 1.95 – 1.98 eV and 1.42– 1.49 eV respectively, showing good potential for semiconductor applications. Polyimides also exhibited electrochromic properties. Fabricated memory devices based on the three

polyimides displayed non-volatile rewritable memory characteristics with good uniformity of memory characteristics.

Chapter 4b describes the synthesis of three new triarylamine-containing polyamides with pendent pentadecyl chains by the polycondensation of 4, 4'-diamino-4"pentadecyltriphenylamine with commercially available aromatic diacids viz. 4,4′-(hexafluoroisopropylidene)bis(benzoic acid) (HBBA), isophthalic acid (IPA) and 4,4′-oxybis(benzoic acid) (OBBA) by Yamazaki polymerisation at 120 °C. Polyamides were designated as PA-HBBA, PA-IPA and PA-OBBA. Polyamides obtained were of reasonably high molecular weights. T_{10} values were in the range 420 – 448 °C, suggesting that the polyamides possessed good thermal stability. Optical band-gap values were observed in the range 1.58 – 1.6 eV. Memory devices were fabricated from PA-HBBA and PA-IPA. Both memory devices were non-volatile in nature. Memory device based on PA-HBBA displayed WORM type behaviour, while memory device based on PA-IPA was rewritable in nature.

Chapter 4c discusses the synthesis of three aromatic polyazomethines synthesised by solution polycondensation of 4, 4'-diamino-4"pentadecyltriphenylamine with aromatic dialdehydes such as terephthaldehyde, isophthaldehyde and a mixture of terephthaldehyde and isophthaldehyde in 1-methyl-2-pyrrolidinone and hexamethyl phosphoramide at room temperature. Polyazomethines synthesised were of reasonably high molecular weights and soluble in chloroform, tetrahydrofuran, *m*-cresol, pyridine and nitro benzene at room temperature. Observed T_{10} values were in the range 431 – 463 °C while T_g values were in the range 53 – 78 °C. Optical band-gap values were in the range 1.26 – 1.3 eV, indicating that the polyazomethines were well qualified for semiconductor applications. Memory devices based on the three polyazomethines exhibited non-volatile rewritable memory characteristics. Multilevel memory in addition to excellent uniformity of memory states was observed.

Chapter 5 is subdivided into two sections

Chapter 5a deals with the synthesis of a series of (co)poly(ether ether ether ketone)s containing pendent pentadecyl chains by polycondensation of 4-(4-hydroxyphenoxy)-3-pentadecylphenol or a mixture of 4-(4-hydroxyphenoxy)-3-pentadecylphenol and bisphenol A with 4,4'-difluorobenzophenone *via* nucleophilic

aromatic substitution polycondensation in DMAc at 180 °C. Inherent viscosities and number average molecular weights were in the range 0.61 – 0.73 dL g^{-1} and 26900 – 93400 g mol^{-1}, respectively, suggestive of the formation of polymers of reasonably high molecular weights. The polymers were readily soluble in common organic solvents and formed flexible, free-standing, transparent films from chloroform solutions. All the synthesised (co)poly(ether ether ether ketone)s were found to be amorphous in nature. Observed T_{10} values were in the range 431 – 463 °C indicating good thermal stability. T_g and T_{10} values progressively decreased with increase in % incorporation of 4-(4-hydroxyphenoxy)-3-pentadecylphenol.

Chapter 5b describes the synthesis of a series of (co)poly(ether sulfone)s from the nucleophilic substitution polycondensation of 4-(4-hydroxyphenoxy)-3-pentadecylphenol or a mixture of 4-(4-hydroxyphenoxy)-3-pentadecylphenol and bisphenol A with bis(4-fluorophenyl)sulfone in *N*,*N*-dimethylacetamide at 180 °C. Inherent viscosities obtained were in the range 0.56 – 0.69 dL g^{-1} while number average molecular weights were observed to be in the range 46000 – 87000 g mol^{-1}, which indicated the formation of (co)poly(ether sufone)s of reasonably high molecular weights. (Co)poly(ether sulfone)s were readily soluble in common organic solvents and were amorphous in nature. Good thermal stability was observed as indicated by T_{10} values in the range 414 – 444 °C. T_g values were in the range 47 – 149 °C. Both T_g and T_{10} values showed a progressive decrease with increase in % incorporation of 4-(4-hydroxyphenoxy)-3-pentadecylphenol.

Chapter 6 deals with the synthesis of a series of (co)polycarbonates containing cyclohexylidene and pendent pentadecyl chains by polycondensation of 1,1-bis(4-hydroxyphenyl)-3-pentadecylcyclohexane or a mixture of 1,1-bis(4-hydroxyphenyl)-3-pentadecylcyclohexane and bisphenol A with triphosgene *via* low temperature solution polymerisation. Polycarbonates synthesised were found to be of reasonably high molecular weights, as suggested by the inherent viscosity measurements (0.71 – 0.86 dL g^{-1}) and GPC (40200 – 69800 g mol^{-1}) analysis. (Co)polycarbonates formed flexible, transparent and free-standing films from chloroform solutions. The T_{10} values were observed in the range 438 – 450 °C indicating good thermal stability. The T_g values were

observed in the range 47 – 79 °C. The T_{10} values and the T_g values decreased with increase in content of 1,1-bis(4-hydroxyphenyl)-3-pentadecylcyclohexane.

Chapter 7 provides the study of the synthesis of a series of aromatic polyimides containing ether linkages in the backbone and pendent pentadecyl chains by polycondensation of 4,4'-((2-pentadecyl-[1,1'-biphenyl]-4,4'-diyl)bis(oxy))dianiline with commercially available aromatic dianhydrides, namely, 3,3',4,4'-biphenyltetracarboxylic dianhydride (BPDA), 4,4'-oxydiphthalic anhydride (ODPA), 4,4'-(hexafluoroisopropylidene) diphthalic anhydride (6-FDA) and 4,4′-(4,4′-isopropylidenediphenoxy)bis(phthalic anhydride) (IDBP). Polyimides obtained were of reasonably high molecular weights as suggested by inherent viscosity values which were in the range 0.5 – 1.53 dL g^{-1} and number average molecular weights were in the range 19600 – 46500 g mol^{-1}. Polyimides were soluble in common organic solvents including chloroform and formed flexible, free-standing and transparent films from chloroform solutions. Polyimides were found to be amorphous in nature as deduced from XRD analysis. Observed T_{10} values were in the range 460 °C – 476 °C suggesting good thermal stability. T_g values of polyimides were in the range 100 – 134 °C.

Chapter 8 summarises the results and describes salient conclusions along with future prospects of the investigations reported in this thesis.

List of Abbreviations

CNSL	Cashew nut shell liquid
T_g	Glass transition temperature
T_{10}	10% Decomposition temperature
T_m	Melting transition
DPTA	4, 4’-Diamino-4"pentadecyltriphenylamine
MPIAL	4-Methoxy-6-pentadecylisophthalaldehyde
MPIA	4-Methoxy-6-pentadecylisophthalic acid
HPPDP	4-(4-Hydroxyphenoxy)-3-pentadecylphenol
PDBP	3-Pentadecyl 4,4' biphenol
BPC15	4,4'-(3-Pentadecylcyclohexane-1,1-diyl)diphenol
BPC	2,6-Bis(4-hydroxybenzylidene)-3-pentadecylcyclohexanone
PBD	4,4'-((2-Pentadecyl-[1,1'-biphenyl]-4,4'-diyl)bis(oxy))dianiline
PPPB	2-Pentadecyl-4-(prop-2-yn-1-yloxy)-1-(4-(prop-2-yn-1-yloxy)phenoxy)benzene
DCPP	4-(4-(4-(3,4-Dicyanophenoxy)-2-pentadecylphenoxy)phenoxy)phthalonitrile
PBP	4,4'-((2-Pentadecyl-[1,1'-biphenyl]-4,4'-diyl)bis(oxy))diphthalonitrile
CPP	4,4'-(((3-Pentadecylcyclohexane-1,1-diyl)bis(4,1-phenylene))bis(oxy))diphthalonitrile
BPA	2,2-Bis(4-hydroxyphenyl)propane or bisphenol-A
PES	Poly(ether sulfone)
PEEK	Poly(ether ether ketone)
BPDA	3,3’,4,4’-Biphenyl tetracarboxylic dianhydride
ODPA	4,4’-Oxydiphthalic anhydride
6-FDA	4,4’-(Hexafluoro isopropylidene)diphthalic anhydride
HBBA	4,4′-(Hexafluoroisopropylidene)bis(benzoic acid)
IPA	Isophthalic acid
OBBA	4,4′-Oxybis(benzoic acid)
IDBP	4,4′-(4,4′-Isopropylidenediphenoxy)bis(phthalic anhydride)
NMP	1-Methyl-2-pyrrolidinone
HMPA	Hexamethylphosphoramide
DMAc	*N*,*N*-Dimethylacetamide
DMF	*N*,*N*-Dimethylformamide
THF	Tetrahydrofuran

DCM	Dichloromethane
DMSO	Dimethyl sulfoxide
RRAM	Resistive random access memory
CMOS	Complementary metal oxide semiconductor
DRAM	Dynamic random access memory
SRAM	Static random access memory
SDRAM	Synchronous dynamic random access memory
WORM	Write once read many times
HRS	High resistance State
LRS	Low resistance state
CTC	Charge transfer complex
ITO	Indium tin oxide
FTO	Fluorine doped tin oxide
TBAP	Tetrabutylammonium perchlorate
CV	Cyclic voltammetry
HOMO	Highest occupied molecular orbital
LUMO	Lowest unoccupied molecular orbital
GPC	Gel permeation chromatography
M_n	Number average molecular weight
M_w	Weight average molecular weight
η_{inh}	Inherent viscosity
WAXD	Wide angle X-ray diffraction
TGA	Thermogravimetric analysis
DTG	Differential thermogravimetric analysis
DSC	Differential scanning calorimetry
COSY	Correlation spectroscopy
HSQC	Heteronuclear single-quantum correlation spectroscopy

List of Tables

Table No	Description	Page No
1.1	Components of natural and technical CNSL (in wt %)	**5**
1.2	CNSL-based difunctional condensation monomers	**7**
1.3	Condensation monomers prepared from cardanol through metathesis	**10**
1.4	Aromatic polyimides containing pendent pentadecyl chains derived from difunctional monomers based on cardanol	**14**
1.5	Aromatic polyamides containing pendent pentadecyl chains derived from difunctional monomers based on cardanol	**20**
1.6	Aromatic polyazomethines containing pendent pentadecyl chains derived from difunctional monomers based on cardanol	**24**
1.7	Aromatic poly(arylene ether)s containing pendent pentadecyl chains derived from difunctional monomers based on cardanol	**25**
1.8	Influence of the pentadecyl chain on polymer properties	**27**
1.9	Triarylamine-containing high performance polymers investigated for memory devices	**29**
3.1	Difunctional condensation monomers starting from CNSL	**54**
3.2	Monomers for thermosetting resins starting from CNSL	**54**
4a.1	Results of synthesis of triarylamine-containing polyimides	**138**
4a.2	Solubility of triarylamine-containing polyimides	**142**
4a.3	Thermal properties of triarylamine-containing polyimides	**144**
4a.4	Optical and electrochemical properties of triaryamine-containing polyimides	**148**
4a.5	Performance comparison of triarylamine-containing polyimide memory devices	**156**
4b.1	Results of synthesis of triarylamine-containing polyamides	**174**
4b.2	Solubility of triarylamine-containing polyamides	**178**
4b.3	Thermal properties of triarylamine-containing polyamides	**180**
4b.4	Optical and electrochemical properties of triarylamine-containing polyamides	**183**
4b.5:	Performance comparison of triarylamine-containing polyamide memory devices	**190**

4c.1	Results of synthesis of triarylamine-containing polyazomethines	**205**
4c.2	Solubility of triarylamine-containing polyazomethines	**209**
4c.3	Thermal properties of triarylamine-containing polyazomethines	**211**
4c.4	Optical properties of triarylamine-containing polyazomethines	**214**
4c.5	Performance comparison of triarylamine-containing polyazomethine memory devices	**220**
5a.1	Results of synthesis of (co)poly(ether ether ether ketone)s	**233**
5a.2	Composition of copoly(ether ether ether ketone)s determined from ^{1}H-NMR spectra	**238**
5a.3	Solubility of (co)poly(ether ether ether ketone)s	**239**
5a.4	Thermal properties of (co)poly(ether ether ether ketone)s	**241**
5b.1	Results of synthesis of (co)poly(ether sulfone)s	**253**
5b.2	Composition of copoly(ether sulfone)s determined from ^{1}H-NMR spectra	**258**
5b.3	Solubility of (co)poly(ether sulfone)s	**259**
5b.4	Thermal properties of (co)poly(ether sulfone)s	**261**
6.1	Results of synthesis of (co)polycarbonates	**274**
6.2	Composition of copolycarbonates determined from ^{1}H-NMR spectra	**280**
6.3	Thermal properties of (co)polycarbonates	**281**
7.1	Results of synthesis of polyimides	**293**
7.2	Solubility of polyimides	**297**
7.3	Thermal properties of polyimides	**299**
8.1	Difunctional condensation monomers starting from CNSL	**306**
8.2	Monomers for thermosetting resins starting from CNSL	**306**

List of Schemes

Scheme No	Description	Page No
1.1	Synthesis of polyimides based on CNSL-derived aromatic difunctional monomers	**14**
1.2	Synthesis of polyamides based on CNSL-derived aromatic difunctional monomers	**20**
1.3	Synthesis of aromatic polyazomethines based on CNSL-derived aromatic diamine monomers	**24**
1.4	Synthesis of poly(arylene ether)s based on CNSL-derived aromatic biphenol monomers	**25**
1.5	Synthesis of poly(*m*-phenylenevinylene)s based on cardanol-derived diphosphonate monomers	**34**
3.1	Synthesis of 4, 4'-diamino-4"pentadecyltriphenylamine (DPTA)	**74**
3.2	Synthesis of 4-methoxy-6-pentadecylisophthalaldehyde (MPIAL)	**78**
3.3	Synthesis of 4-methoxy-6-pentadecylisophthalic acid (MPIA)	**82**
3.4	Synthesis of 4-(4-hydroxyphenoxy)-3-pentadecylphenol (HPPDP)	**85**
3.5	Synthesis of 3-pentadecyl biphenol (PDBP)	**88**
3.6	Synthesis of 4,4'-(3-pentadecylcyclohexane-1,1-diyl)diphenol (BPC15)	**91**
3.7	Synthesis of 2,6-bis(4-hydroxybenzylidene)-3-pentadecylcyclohexanone (BPC)	**96**
3.8	Synthesis of 4,4'-((2-pentadecyl-[1,1'-biphenyl]-4,4'-diyl)bis(oxy))dianiline (PBD)	**100**
3.9	Synthesis of 2-pentadecyl-4,4'-bis(prop-2-yn-1-yloxy)-1,1'-biphenyl (PPB)	**104**
3.10	Synthesis of 2-pentadecyl-4-(prop-2-yn-1-yloxy)-1-(4-(prop-2-yn-1-yloxy)phenoxy)benzene (PPPB)	**108**
3.11	Synthesis of 4-(4-(4-(3,4-dicyanophenoxy)-2-pentadecylphenoxy)phenoxy)phthalonitrile (DCPP)	**112**
3.12	Synthesis of 4,4'-((2-pentadecyl-[1,1'-biphenyl]-4,4'-diyl)bis(oxy))diphthalonitrile (PBP)	**116**
3.13	Synthesis of 4,4'-(((3-pentadecylcyclohexane-1,1-diyl)bis(4,1-	**120**

	phenylene))bis(oxy))diphthalonitrile (CPP)	
4a.1	Synthesis of triarylamine-containing polyimides	**138**
4b.1	Synthesis of triarylamine-containing polyamides	**173**
4c.1	Synthesis of triarylamine-containing polyazomethines	**205**
5a.1	Synthesis of (co)poly(ether ether ether ketone)s	**232**
5b.1	Synthesis of (co)poly(ether sulfone)s	**252**
6.1	Synthesis of (co)polycarbonates	**273**
7.1	Synthesis of polyimides	**292**

List of Figures

Figure No	Description	Page No
1.1	Sources of bio-chemicals	**2**
1.2	The cashew fruit	**4**
1.3	Components of CNSL	**5**
1.4	Reactive sites in cardanol	**6**
1.5	Possible sequences arising due to constitutional isomerism	**17**
2.1	The theme of the thesis	**48**
3.1	FT-IR spectrum of 4, 4'-diamino-4"pentadecyltriphenylamine (DPTA)	**75**
3.2	^{1}H-NMR spectrum ($CDCl_3$) of 4, 4'-diamino-4"pentadecyltriphenylamine (DPTA)	**76**
3.3	^{13}C-NMR spectrum ($CDCl_3$) of 4, 4'-diamino-4"pentadecyltriphenylamine (DPTA)	**77**
3.4	FT-IR spectrum of 4-methoxy-6-pentadecylisophthalaldehyde (MPIAL)	**79**
3.5	^{1}H-NMR spectrum ($CDCl_3$) of 4-methoxy-6-pentadecylisophthalaldehyde (MPIAL)	**80**
3.6	^{13}C-NMR spectrum (Acetone-d_6) of 4-methoxy-6-pentadecylisophthalaldehyde (MPIAL)	**81**
3.7	FT-IR spectrum of 4-methoxy-6-pentadecylisophthalic acid (MPIA)	**82**
3.8	^{1}H-NMR spectrum (DMSO-d_6) of 4-methoxy-6-pentadecylisophthalic acid (MPIA)	**83**
3.9	^{13}C-NMR spectrum (DMSO-d_6) of 4-methoxy-6-pentadecylisophthalic acid (MPIA)	**84**
3.10	FT-IR spectrum 4-(4-hydroxyphenoxy)-3-pentadecylphenol (HPPDP)	**86**
3.11	^{1}H-NMR spectrum ($CDCl_3$) of 4-(4-hydroxyphenoxy)-3-pentadecylphenol (HPPDP)	**86**
3.12	^{13}C-NMR spectrum ($CDCl_3$) of 4-(4-hydroxyphenoxy)-3-pentadecylphenol (HPPDP)	**87**
3.13	FT-IR spectrum of 3-pentadecyl biphenol (PDBP)	**89**
3.14	^{1}H-NMR spectrum ($CDCl_3$) of 3-pentadecyl biphenol (PDBP)	**89**
3.15	^{13}C-NMR spectrum ($CDCl_3$) of 3-pentadecyl biphenol (PDBP)	**90**
3.16	FT-IR spectrum of 4,4'-(3-pentadecylcyclohexane-1,1-diyl)diphenol	**92**

(BPC15)

3.17 ^{1}H-NMR spectrum ($CDCl_3$) of 4,4'-(3-pentadecylcyclohexane-1,1-diyl)diphenol (BPC15) **93**

3.18 HSQC spectrum ($CDCl_3$) of 4,4'-(3-pentadecylcyclohexane-1,1-diyl)diphenol (BPC15) **94**

3.19 ^{13}C-NMR spectrum ($CDCl_3$) of 4,4'-(3-pentadecylcyclohexane-1,1-diyl)diphenol (BPC15) **95**

3.20 FT-IR spectrum of 2,6-bis(4-hydroxybenzylidene)-3-pentadecylcyclohexanone (BPC) **97**

3.21 ^{1}H-NMR spectrum ($CDCl_3$) of 2,6-bis(4-hydroxybenzylidene)-3-pentadecylcyclohexanone (BPC) **98**

3.22 ^{13}C-NMR spectrum ($CDCl_3$) 2,6-bis(4-hydroxybenzylidene)-3-pentadecylcyclohexanone (BPC) **99**

3.23 FT-IR spectrum of 4,4'-((2-pentadecyl-[1,1'-biphenyl]-4,4'-diyl)bis(oxy))dianiline (PBD) **101**

3.24 ^{1}H-NMR spectrum ($CDCl_3$) of 4,4'-((2-pentadecyl-[1,1'-biphenyl]-4,4'-diyl)bis(oxy))dianiline (PBD) **102**

3.25 ^{13}C-NMR spectrum ($CDCl_3$) 4,4'-((2-pentadecyl-[1,1'-biphenyl]-4,4'-diyl)bis(oxy))dianiline (PBD) **103**

3.26 FT-IR spectrum of 2-pentadecyl-4,4'-bis(prop-2-yn-1-yloxy)-1,1'-biphenyl (PPB) **105**

3.27 ^{1}H-NMR spectrum ($CDCl_3$) of 2-pentadecyl-4,4'-bis(prop-2-yn-1-yloxy)-1,1'-biphenyl (PPB) **106**

3.28 ^{13}C-NMR spectrum ($CDCl_3$) of 2-pentadecyl-4,4'-bis(prop-2-yn-1-yloxy)-1,1'-biphenyl (PPB) **107**

3.29 FT-IR spectrum of 2-pentadecyl-4-(prop-2-yn-1-yloxy)-1-(4-(prop-2-yn-1-yloxy)phenoxy)benzene (PPPB) **109**

3.30 ^{1}H-NMR spectrum ($CDCl_3$) of 2-pentadecyl-4-(prop-2-yn-1-yloxy)-1-(4-(prop-2-yn-1-yloxy)phenoxy)benzene (PPPB) **110**

3.31 ^{13}C-NMR spectrum ($CDCl_3$) of 2-pentadecyl-4-(prop-2-yn-1-yloxy)-1-(4-(prop-2-yn-1-yloxy)phenoxy)benzene (PPPB) **111**

3.32 FT-IR spectrum of 4-(4-(4-(3,4-dicyanophenoxy)-2-pentadecylphenoxy)phenoxy)phthalonitrile (DCPP) **113**

3.33 ^{1}H-NMR spectrum ($CDCl_3$) of 4-(4-(4-(3,4-dicyanophenoxy)-2- **114**

	pentadecylphenoxy)phenoxy)phthalonitrile (DCPP)	
3.34	^{13}C-NMR spectrum ($CDCl_3$) of 4-(4-(4-(3,4-dicyanophenoxy)-2-pentadecylphenoxy)phenoxy)phthalonitrile (DCPP)	**115**
3.35	FT-IR spectrum of 4,4'-((2-pentadecyl-[1,1'-biphenyl]-4,4'-diyl)bis(oxy))diphthalonitrile (PBP)	**117**
3.36	^{1}H-NMR spectrum ($CDCl_3$) of 4,4'-((2-pentadecyl-[1,1'-biphenyl]-4,4'-diyl)bis(oxy))diphthalonitrile (PBP)	**118**
3.37	^{13}C-NMR spectrum ($CDCl_3$) of 4,4'-((2-pentadecyl-[1,1'-biphenyl]-4,4'-diyl)bis(oxy))diphthalonitrile (PBP)	**119**
3.38	FT-IR spectrum of 4,4'-(((3-pentadecylcyclohexane-1,1-diyl)bis(4,1-phenylene))bis(oxy))diphthalonitrile (CPP)	**121**
3.39	^{1}H-NMR spectrum ($CDCl_3$) of 4,4'-(((3-pentadecylcyclohexane-1,1-diyl)bis(4,1-phenylene))bis(oxy))diphthalonitrile (CPP)	**122**
3.40	COSEY spectrum ($CDCl_3$) of 4,4'-(((3-pentadecylcyclohexane-1,1-diyl)bis(4,1-phenylene))bis(oxy))diphthalonitrile (CPP)	**123**
3.41	HSQC spectrum ($CDCl_3$) of 4,4'-(((3-pentadecylcyclohexane-1,1-diyl)bis(4,1-phenylene))bis(oxy))diphthalonitrile (CPP)	**124**
3.42	^{13}C-NMR spectrum ($CDCl_3$) of 4,4'-(((3-pentadecylcyclohexane-1,1-diyl)bis(4,1-phenylene))bis(oxy))diphthalonitrile (CPP)	**125**
SI 3.1	HRMS of 4, 4’-diamino-4"pentadecyltriphenylamine (DPTA)	**131**
SI 3.2	HRMS of 4-methoxy-6-pentadecylisophthalaldehyde (MPIAL)	**131**
SI 3.3	HRMS of 4-methoxy-6-pentadecylisophthalic acid (MPIA)	**132**
SI 3.4	HRMS of 4,4'-((2-pentadecyl-[1,1'-biphenyl]-4,4'-diyl)bis(oxy))dianiline (PBD)	**132**
4a.1	Schematic structure of triarylamine-containing polyimide based memory devices	**137**
4a.2	PI-6FDA film cast from chloroform	**139**
4a.3	FT-IR spectrum of PI-6FDA film	**139**
4a.4	^{1}H-NMR spectrum ($CDCl_3$) of PI-6FDA.	**140**
4a.5	^{13}C-NMR spectrum ($CDCl_3$) of PI-6FDA	**141**
4a.6	X-Ray diffractograms of triarylamine-containing polyimides	**143**
4a.7	TG curves of triarylamine-containing polyimides	**145**
4a.8	DTG curve of PI-ODPA	**146**
4a.9	DSC curves of triarylamine-containing polyimides	**146**

4a.10	Oxidative cyclic voltammograms of triarylamine-containing polyimides.	**148**
4a.11	Electrochromic behaviour of **(a)** PI-6FDA thin film, **(b)** PI-ODPA thin film and **(c)** PI-BPDA thin film	**150**
4a.12.	Bipolar resistive switching characteristics of **(a-b)** PI-ODPA, **(c-d)** PI-BPDA, and **(e-f)** PI-6FDA memory devices in linear and semilog scale, respectively. The direction of resistive switching is indicated by arrows	**152**
4a.13	Endurance and retention memory performance of **(a-b)** PI-ODPA, **(c-d)** PI-BPDA, and **(e-f)** PI-6FDA memory devices	**155**
4a.14	Resistive switching cumulative probability of **(a-b)** PI-ODPA, **(c-d)** PI-BPDA, and **(e-f)** PI-6FDA memory devices	**156**
4a.15	Conduction mechanisms of **(a-b)** PI-ODPA, **(c-d)** PI-BPDA, and **(e-f)** PI-6FDA memory devices in positive and negative bias	**159**
4a.16	Schottky conduction mechanism fitting to the high slope part data of the **(a-b)** PI-ODPA, **(c-d)** PI-BPDA, and **(e-f)** PI-6FDA memory devices	**160**
SI 4a.1	^{1}H-NMR spectrum ($CDCl_3$) of PI-ODPA	**166**
SI 4a.2	^{13}C-NMR spectrum ($CDCl_3$) of PI-ODPA	**166**
SI 4a.3	^{1}H-NMR spectrum ($CDCl_3$) of PI-BPDA	**167**
SI 4a.4	^{13}C-NMR spectrum ($CDCl_3$) of PI-BPDA	**167**
SI 4a.5	UV-Vis absorption spectra of triarylamine-containing polyimides	**168**
SI 4a.6	Reductive cyclic voltammograms of triarylamine-containing polyimides	**168**
4b.1	Schematic structure of the triarylamine-containing polyamide based memory devices	**172**
4b.2	PA-HBBA film cast from DMAc	**174**
4b.3	FT-IR spectrum of PA-HBBA film	**175**
4b.4	^{1}H-NMR spectrum (DMSO-d_6 + $CDCl_3$) of PA-HBBA.	**176**
4b.5	^{13}C-NMR spectrum (DMSO-d_6 + $CDCl_3$) of PA-HBBA	**177**
4b.6	X-Ray diffractograms of triarylamine-containing polyamides	**179**
4b.7	TG curves of triarylamine-containing polyamides	**181**
4b.8	DTG curve of PA-IPA	**182**
4b.9	DSC curves of triarylamine-containing polyamides	**182**
4b.10	UV-Vis spectra of triarylamine-containing polyamides.	**184**
4b.11	Oxidative cyclic voltammograms of triarylamine-containing polyamides	**184**
4b.12	Bipolar resistive switching characteristics of **(a-b)** PA-HBBA and **(c-d)** PA-IPA memory devices in linear and semilog scale, respectively	**186**

4b.13	Endurance and retention memory performance of **(a-b)** PA-HBBA and **(c-d)** PA-IPA memory devices	**189**
4b.14	LRS and HRS cumulative probability of **(a)** PA-HBBA and **(b)** PA-IPA memory devices	**190**
4b.15	Conduction mechanisms of **(a-b)** PA-HBBA and **(c-d)** PA-IPA memory devices in positive and negative bias, respectively	**192**
4b.16	Schottky conduction mechanism fitting to the high slope part data of **(a)** PA-HBBA (positive bias) memory device and **(b)** PA-IPA memory device in positive bias and **(c)** negative bias	**193**
SI 4b.1	^{1}H-NMR spectrum ($CDCl_3$ + DMSO-d_6) of PA-IPA	**198**
SI 4b.2	^{13}C-NMR spectrum ($CDCl_3$ + DMSO-d_6) of PA-IPA	**199**
4c.1	Schematic structure of the triarylamine-containing polyazomethine based memory devices	**204**
4c.2	PAZ-TPA film cast from chloroform	**206**
4c.3	FT-IR spectrum of PAZ-TPA film	**206**
4c.4	^{1}H-NMR spectrum ($CDCl_3$) of PAZ-TPA.	**207**
4c.5	^{13}C-NMR spectrum ($CDCl_3$) of PAZ-TPA.	**208**
4c.6	X-Ray diffractograms of triarylamine-containing polyazomethines	**210**
4c.7	TG curves of triarylamine-containing polyazomethines	**211**
4c.8	DTG curve of PAZ-TPA	**212**
4c.9	DSC curves of triarylamine-containing polyazomethines	**213**
4c.10	UV-Vis spectra of triarylamine-containing polyazomethines	**214**
4c.11	Current-voltage (I-V) characteristics of **(a-b)** PAZ-TPA, **(c-d)** PAZ-IPA, and **(e-f)** PAZ-TPA+IPA memory devices in linear and semilog scale respectively. The arrows indicate the direction of resistive switching.	**216**
4c.12	**(a)** Endurance and **(b)** retention memory performance of PAZ-TPA, PAZ-IPA, and PAZ-TPA+IPA memory devices. Three resistance states *viz*. LRS, IRS, and HRS are observed in the developed devices	**219**
4c.13	Cumulative probability of resistive switching states of **(a-b)** PAZ-TPA, **(c-d)** PAZ-IPA, and **(e-f)** PAZ-TPA+IPA memory devices.	**220**
4c.14	Conduction mechanisms and high slope part data fitting of **(a-b)** PAZ-TPA, **(c-d)** PAZ-IPA, and **(e-f)** PAZ-TPA+IPA memory devices.	**223**
5a.1	PEK-25 film cast from chloroform	**234**
5a.2	FT-IR spectrum of PEK-100 film	**234**

5a.3	^{1}H-NMR spectrum ($CDCl_3$) of PEK-100	**235**
5a.4	^{13}C-NMR spectrum ($CDCl_3$) of PEK-100	**236**
5a.5	^{1}H-NMR spectra ($CDCl_3$) of copolycarbonates derived from HPPDP, BPA and 4,4'-difluorobenzophenone	**237**
5a.6	X-Ray diffractograms of (co)poly(ether ether ether ketone)s	**240**
5a.7	TG curves of (co)poly(ether ether ether ketone)s	**242**
5a.8	DTG curve of PEK-100	**242**
5a.9	DSC curves of (co)poly(ether ether ether ketone)s	**243**
5a.10	T_g as a function of composition of HPPDP in copoly(ether ether ether ketone)s derived from polycondensation of a mixture of HPPDP and BPA with 4,4'-difluorobenzophenone	**244**
5b.1	PES-100 film cast from chloroform	**253**
5b.2	FT-IR spectrum of PES-100 film	**254**
5b.3	^{1}H-NMR spectrum ($CDCl_3$) of PES-100	**255**
5b.4	^{13}C-NMR spectrum ($CDCl_3$) of PES-100	**256**
5b.5	^{1}H-NMR ($CDCl_3$) spectra of (co)poly(ether sulfone)s derived from HPPDP, BPA and bis(4-fluorophenyl)sulfone	**257**
5b.6	X-Ray diffractograms of (co)poly(ether sulfone)s	**260**
5b.7	TG curves of (co)poly(ether sulfone)s	**261**
5b.8	DTG curve of PES-100	**262**
5b.9	DSC curves of (co)poly(ether sulfone)s	**263**
5b.10	T_g as a function of composition of HPPDP in copoly(ether sulfone)s derived from polycondensation of a mixture of HPPDP and BPA with bis(4-fluorophenyl)sulfone	**264**
6.1	PC-100 film cast from chloroform	**274**
6.2	FT-IR spectrum of PC-100 film	**275**
6.3	^{1}H-NMR spectrum ($CDCl_3$) of PC-100	**276**
6.4	HSQC spectrum ($CDCl_3$) of PC-100	**277**
6.5	^{13}C-NMR spectrum ($CDCl_3$) of PC-100	**278**
6.6	^{1}H-NMR ($CDCl_3$) spectra of (co)polycarbonates derived from BPC15, BPA and triphosgene	**279**
6.7	X-Ray diffractograms of (co)polycarbonates	**281**
6.8	TG curves of (co)polycarbonates	**282**
6.9	DTG curve of PC-100	**283**

6.10	DSC curves of (co)polycarbonates	**283**
6.11	T_g as a function of composition of BPC15 in copolycarbonates derived from polycondensation of a mixture of BPC15 and BPA with triphosgene	**284**
7.1	PEI-IDBP film cast from chloroform	**293**
7.2	FT-IR spectrum of PEI-6FDA film	**294**
7.3	^{1}H-NMR spectrum ($CDCl_3$) of PEI-6FDA	**295**
7.4	^{13}C-NMR spectrum ($CDCl_3$) of PEI-6FDA	**296**
7.5	X-Ray diffractograms of polyimides	**298**
7.6	TG curves of polyimides	**299**
7.7	DTG curve of PEI-BPDA	**300**
7.8	DSC curves of polyimides	**301**

CHAPTER 1

*Introduction and Literature Survey**

*Partly adapted from D. Chatterjee et al. (2017) Step-Growth Polymers from Cashew Nut Shell Liquid (CNSL)-Based Aromatic Difunctional Monomers. In: Anilkumar P. (eds) Cashew Nut Shell Liquid. A Goldfield for Functional Materials, Springer, (10.1007/978-3-319-47455-7_9)

1.1 Introduction

1.1.1 Background

Unquestionably, today we live in the "Plastics Age". An estimated average worldwide production of plastics is around 355 million metric tonnes per year, with a yearly average growth of 10 %.[1,2] Plastics are mostly derived from fossil resources. Almost all organic chemicals can be derived from seven basic building blocks, namely, syngas, ethylene, propylene, butanes, butylenes, butadiene and BTX (mixture of benzene, toluene and xylene) which are mostly obtained from fossil resources *viz*., natural gas, petroleum and coal.[3,4]

Over the past several years, spectacular progress has been made in petrochemical industry, so much so, that one might even question the need to investigate the area of renewable resources. However, complete dependence on fossil resources has its own limitations. Fossil resources are generated through chemical and biological processes occurring over millions of years, while the rate of consumption of these resources is several times the rate of their formation.[5–8] Fossil resources being non-renewable in nature, it is logically advisable to investigate the use and consumption of renewable resources for production of chemicals. One of the promising renewable resources is biomass. Biomass refers to any organic matter having recent biological origin, including plant materials, agricultural crops and animal residues.[9] Biomass remains an attractive resource for obtaining chemicals, especially platform chemicals.[10] Platform chemicals are defined as chemicals from which many value added chemicals may be derived, which in turn can be used to manufacture end use commodities like plastics, resins, etc.[11] A biomass-based economy will require a well developed bio-refinery system.[12,13] The products (bio-chemicals) obtained from biomass can be intermediates, final products or other materials.[14–17] International Energy Agency (IEA) Bioenergy (task 42) has defined bio-refinery[12] as the sustainable processing of biomass into a spectrum of marketable products and energy. This simply implies the concept of separating the components of biomass obtained from a source and their valorisation. There is presently a huge potential for bio-derived chemicals to share markets with fossil based counterparts.

Major renewable resources include wood, plant residues, algae, animal residues and bacterial biomass (**Figure 1.1**).[9,18]

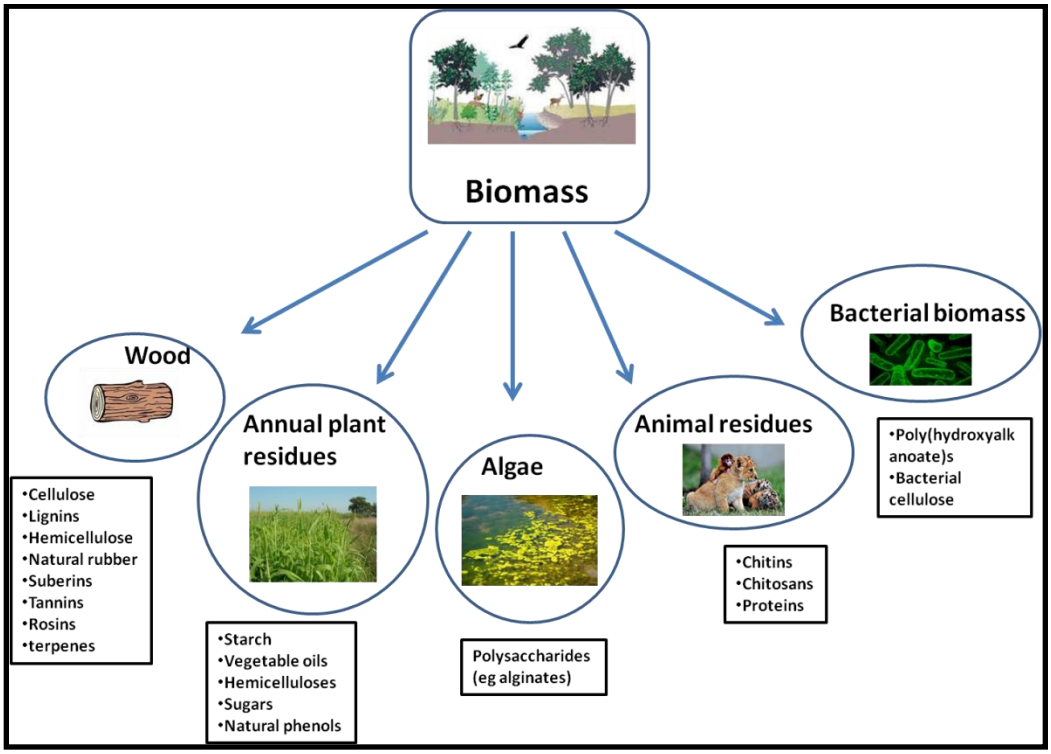

Figure 1.1 Sources of bio-chemicals

Edible bio-chemicals include starch, vegetable oils and sugars. Natural phenols, hemicelluloses and other bio-chemicals derived from wood, animal residues, algae and bacterial biomass are non-edible. Such non-edible bio-resources are preferred as starting materials for chemicals as they do not put undue pressure on the food industry. Bio-chemicals are attractive sources of both aliphatic and aromatic monomers. Rich sources of aromatic monomers include lignins, tannins and natural phenols such as Cashew Nut Shell Liquid (CNSL). Lignin is an important bio-polymer present in plant cell walls, which is industrially obtained as a co-product of paper manufacture. Lignin is an important source for obtaining vanillin, which has huge potential as a source for bio-based monomers.[19] Naturally occurring vegetable tannins are mainly phenolic in nature and are classified into two broad classes, namely, condensed/ polyflavonoid tannins and hydrolysable tannins. 2,5-Furan dicarboxylic acid (FDCA), 5-hydroxymethyl furfural and a variety of FDCA-based materials, which can be readily and economically prepared from a vast variety of agricultural and forestry wastes[20] are important precursors for the synthesis of aromatic monomers.

Several biomass-based programmes and projects have been funded by Governments and Industries around the world. 'CatchBIO' is a Dutch research programme in the field of catalytic biomass conversion with 21 partners which include research institutes and companies such as BASF.[21] 'BIO-TIC' is a project funded by the European Union.[22] 'ARENA' (Australian Renewable Energy Agency) is an independent agency of the Australian Federal Government to manage renewable energy programmes in the country.[23] Delft Advanced Biorenewables (DAB) is a private company in The Netherlands dealing with bio-renewables.[24] These are just a few representative programmes involved in bio-renewables.

A number of researchers have reviewed monomers and polymers synthesised from various biomass resources,[16,25–31] including various furan and vegetable oil-based monomers and polymers.[32,33] Tschan *et al*[34] have discussed biodegradable polymers from biomass while Zhang *et al*[35] have summarised recent advances in utilisation of biomass as separators, binders and electrode materials. Datta *et al*[36] have discussed bio-based epoxy resins. Wilbon *et al*[37] have reviewed the details of polymerisation and copolymerisation of terpenes, terpenoids and rosin-derived monomers. Llevot *et al*[38] and Upton *et al*[39] have reviewed various lignin-derived aromatic compounds and polymers while Galbis *et al*[40] have reviewed various monomers and polymers derived from carbohydrates. Arbenz *et al*[41] have discussed chemical modification and synthesis of polymeric materials from tannins.

CNSL, as an interesting bio-derived chemical, with enormous potential in the field of polymer chemistry has been discussed in the subsequent sections.

1.1.2 Cashew Nut Shell Liquid (CNSL)

CNSL belongs to the class of naturally occurring phenols, a non-edible by-product of cashew (*Anacardium occidentale* L) industry and is a promising renewable resource. It is abundantly available (4,898,360 tonnes worldwide and 671,000 tonnes in India in 2016) at low cost (around 0.27 $/Kg in 2017). Cashew tree originated in Brazil, but is presently cultivated in many countries. The top five cashew producers (as of 2016) are Vietnam, Nigeria, India, Cote d'Ivoire and Phillipines.[42] The actual fruit of the cashew tree is a 'drupe' out of which grows the oval or pear-shaped cashew apple, which is an accessory (or false) fruit. It is edible and is used for making jams, jellies and

alcoholic drinks. The distal end of the cashew apple is attached to the cashew nut, the edible portion of which is encased in a double-layered shell. The shell has a honeycomb structure and contains CNSL- a greenish yellow viscous liquid (**Fig 1.2**). The cashew nut and cashew apple are the cash crops yielded by the cashew tree, while CNSL is an agricultural by-product.[43–46]

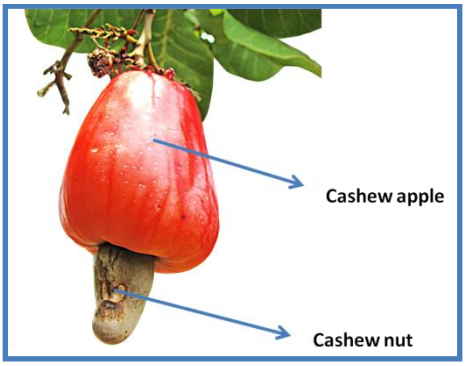

Figure 1.2 The cashew fruit

Traditionally, CNSL is obtained as a by-product during the process of removing the cashew kernel (edible part) from the nut, by the hot oil process or roasting process.[47] More recent and improved methods of extraction include solvent extraction technique[46,48] and supercritical extraction using CO_2 and isopropyl alcohol and vacuum pyrolysis.[49,50] CNSL is purified by chemical treatment with sulphuric acid and other acid treatments before further use. Subsequently, it may be distilled under reduced pressure or hydrogenated.[51]

A number of review articles have dealt with the extraction, isolation and applications of CNSL.[20,52–59] Blazdell[56] has discussed the usefulness of cashew nut, dealing with its history, cultivation, extraction and various products. Mele *et al*[57] have reviewed CNSL-based fine chemicals as well as cardanol hybrids. Balachandran *et al*[58] have discussed the generation of soft nanomaterials from cardanol. Voirin *et al*[59] have reviewed purification, separation methods, reactivity and applications of CNSL.

1.1.3 Components of CNSL

Naturally occurring CNSL consists of four major components *viz*., anacardic acid, cardanol, cardol and 2-methyl cardol (**Fig 1.3**). Commercial grade CNSL mainly consists of cardanol, 2-methyl cardol and cardol as anacardic acid gets almost completely converted to cardanol due to decarboxylation occurring during the extraction and refining

processes.[60] Composition of natural and technical CNSL is depicted in **Table 1.1**. Each component of CNSL is a mixture of four constituents differing in the side chain unsaturation, namely saturated (~5-8 %), monoene (~48-49 %), diene (16-17 %) and triene (29-30 %).[61]

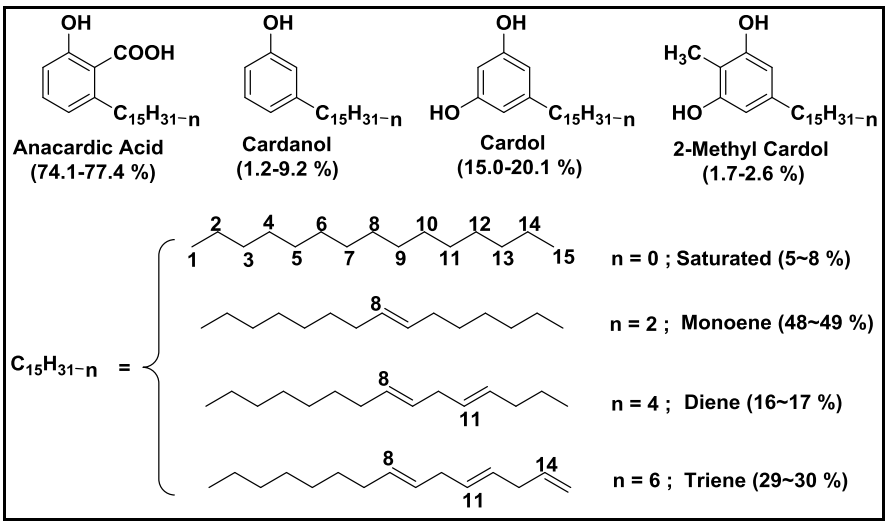

Figure 1.3 Components of CNSL[59] (Reproduced by permission of The Royal Society of Chemistry)

Table 1.1 Components of natural and technical CNSL (in wt %)[59] (Reproduced by permission of The Royal Society of Chemistry)

Component/ other material	**Natural CNSL**	**Technical CNSL**
Cardanol (%)	1.20	62.86
Cardol (%)	11.31	11.25
2-Methyl cardol (%)	2.04	2.08
Anacardic acid (%)	64.93	N. D.*
Polymer (and minor materials)	20.3	23.8

*N.D Not detected.

M/s Cardolite Corporation, USA is the world leader in developing and manufacturing products based on CNSL.[62]

1.1.4 Reactivity of cardanol

Cardanol possesses a C-15 hydrocarbon chain *meta* to the phenolic –OH, an unique orientation which would be difficult to achieve synthetically. Moreover, cardanol provides a number of sites for functionalisation and modification which include the phenolic –OH, the aromatic ring and the unsaturation(s) in the side chain (**Fig 1.4**).

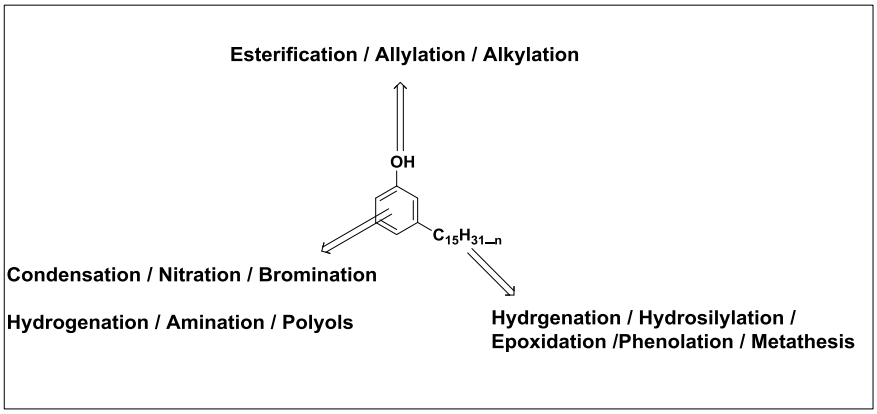

Figure 1.4 Reactive sites in cardanol[59] (Reproduced by permission of The Royal Society of Chemistry)

The aromatic ring can undergo various electrophilic substitution reactions such as nitration, bromination, alkylation, acylation, etc. The unsaturated C-15 side chain provides sites for epoxidation, hydrogenation, phenolation, metathesis, etc while the phenolic –OH group can undergo modification through esterification, alkylation, etc. Such possibilities for modifications can be utilised to synthesise designed monomers and polymers, as has been discussed in the subsequent sections.

Pertinent research efforts expended towards the synthesis of aromatic difunctional monomers based on CNSL and their utilisation for the preparation of step-growth polymers have been briefly reviewed in the following sections.

1.2. Difunctional monomers based on CNSL and step-growth polymers therefrom

1.2.1 CNSL-based aromatic difunctional condensation monomers

Aromatic diamines, diacids, diphenols, diisocyanates, dialdehydes, etc are the main classes of condensation monomers useful for the preparation of high performance polymers. A large number of difunctional monomers possessing special structural features have been synthesised till date. Researchers still continue to synthesise new difunctional monomers which simply serve as "drop-in substitutes" for commercial

monomers already in practice for the purpose of imparting special properties to the existing polymers.

Cardanol, due to its interesting reactive sites (phenolic –OH, aromatic ring and unsaturation in the pentadecenyl chain), has been utilised as a starting material for the synthesis of difunctional condensation monomers.[59] Furthermore, cardanol is derived from biomass, which makes it an even more attractive starting material for synthesis of aromatic difunctional monomers useful in polycondensation chemistry. Cardanol possesses a long hydrocarbon chain (C-15), which is expected to impart interesting properties to the synthesised polymers. Difunctional condensation monomers possessing long pendent hydrocarbon chains are difficult to synthesise traditionally from petrochemical resources. Various difunctional condensation monomers such as diamines, diacids, diphenols, dialdehydes, diacylhydrazides, diisocyanates, etc were derived from cardanol, as listed in **Table 1.2** and **Table 1.3**. The listed monomers have been synthesised either from cardanol or 3-pentadecyl phenol, which in turn is obtained from cardanol through side chain hydrogenation.

Table 1.2 CNSL-based difunctional condensation monomers[a]

Sr. No	Monomers	Polymers	Ref.
	Diphenols/Diols		
1.	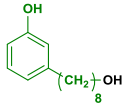	Polycarbonates	63
2.	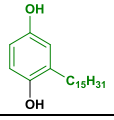	Polyesters	64
3.	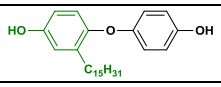	(Co)polyesters	65
4.	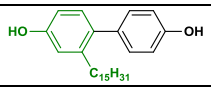	Poly(arylene ether)s	66
5.	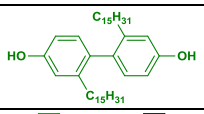	-[b]	67
6.	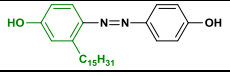	Polyurethanes	68,69
7.	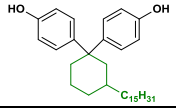	(Co)polyesters and Poly(arylene ether)s	70–72

8.	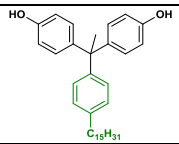	(Co)polyesters and Poly(arylene ether)s	72–75
9.	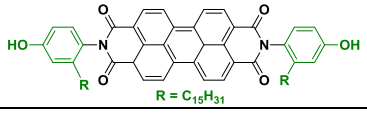	-[b]	76
10.	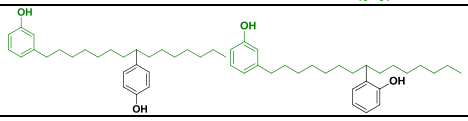	-[c]	77
	Diamines		
11.	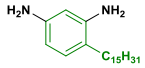	Polyimides, Polyamides and Poly(azomethine)s	78,79
12.	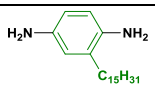	Polyimides	80
13.	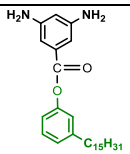	Polyimides and Polyamides	81,82
14.	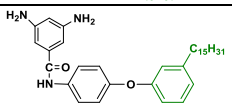	Polyimides and Polyamides	81,82
15.	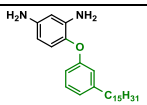	Polyimides and Polyamides	81,82
16.	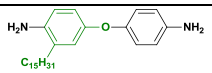	Poly(azomethine)s	83
17.	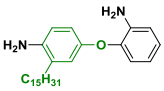	-[b]	75
18.	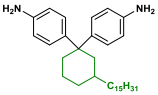	(Co)polyimides	70,84
19.	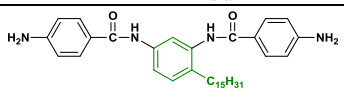	Poly(amideimide)s	85
20.	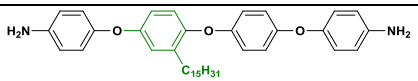	Polyimides	86
21.	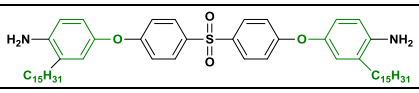	Polyamides and Polyimides	87
22.	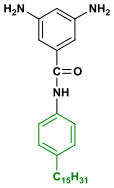	-[b]	64

23.	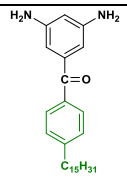	-[b]	64
	Diacids		
24.	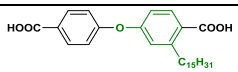	Polyamides	88
25.	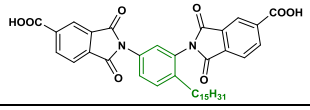	Poly(esterimide)s	89
26.	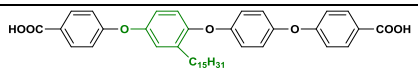	-[b]	67
27.	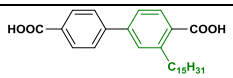	-[b]	67
	Diacylhydrazides		
28.	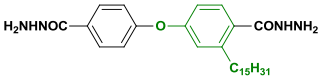	Poly(amideimide)s, Polyhydrazides and Poly(1,3,4-oxadiazole)s	90–92
29.	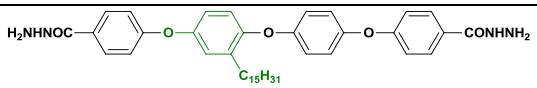	Polyhydrazides and Poly(1,3,4-oxadiazole)s	67
30.	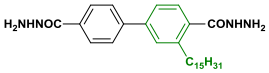	-[b]	67
	Diisocyanates		
31.	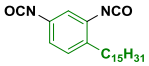	-[b]	64
32.	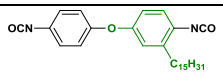	-[b]	75
	Miscellaneous monomers		
33.	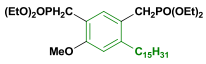	Poly(*m*-phenylenevinylene)s	93
34.	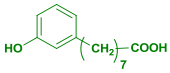	Polyesters	94–96
35.	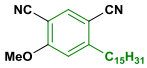	-[b]	64
36.	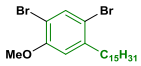	-[b]	64
37.	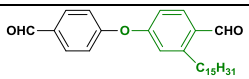	-[b]	67
38.	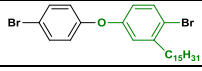	-[b]	75

[a]green colour indicates structural components derived from cardanol, [b]polymers not reported, [c]not used for synthesis of thermoplastic polymers.

Majority of the monomers listed in **Table 1.2** are of AA type while entry no. 34, is of AB type. Cardanol possesses an –OH group and a hydrocarbon chain *meta* to each

other, thus providing a useful means of designing *meta* substituted monomers. Besides this in-built *meta* relationship, *meta* substituted monomers (**Table 1.2**, entries 11, 13, 14, 15, 22, 23, 31, 33, 35 and 36) have also been designed through typical electrophilic substitution reactions guided by the electron rich –OH group. The cardanol molecule has been suitably modified to synthesise asymmetrical monomers (**Table 1.2**, entries 1, 2, 3, 4, etc). Subsequently, monomers containing flexible ether linkages (**Table 1.2**, entries 3, 16, 17, 20, 21, 24, 26, 28, 29, 32, 37 and 38) were synthesised. Monomers possessing aromatic ring(s) derived solely from cardanol contribute more towards their 'greenness' (**Table 1.2**, entries 1, 2, 5, 10-12, 31, 33-36). Cardbisphenol, i.e. 1,8-bis(hydroxyphenyl)pentadecane (**Table 1.2**, entry 10) was prepared from cardanol and phenol. This has been shown to consist of two isomers and is used in the preparation of resins useful in surface coating industries.[77] Cardanol was converted to 3-(8-hydroxy-octyl) phenol (**Table 1.2**, entry 1) through ozonolysis followed by reduction using sodium borohydride.

The difunctional monomers listed in **Table 1.2**, except for the monomers represented by entries 1 and 34, have been synthesised through functional group transformations and coupling reactions, wherein the C-15 hydrocarbon chain remains unaltered with respect to carbon number. Another interesting strategy exists, wherein the unsaturation in the C-15 hydrocarbon chain of cardanol is exploited; through olefin metathesis reactions.

Olefin metathesis involves redistribution of fragments of alkenes by scission and recombination by carbon–carbon double bonds. CNSL is comprised of components which have fifteen carbon unsaturated chains. Hence application of olefin metathesis on cardanol can give rise to interesting monomers which may be difficult to access by conventional routes. Monomers prepared by metathesis reaction involving cardanol are listed in **Table 1.3**.[97–104]

Table 1.3 Condensation monomers prepared from cardanol through metathesis[a]

Sr. No	Metathesis products based on cardanol	Ref.
1.	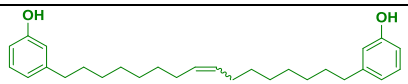	97–99

2.	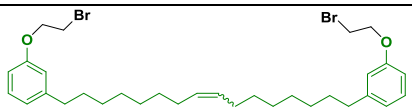	97–99
3.	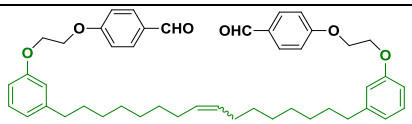	97–99
4.	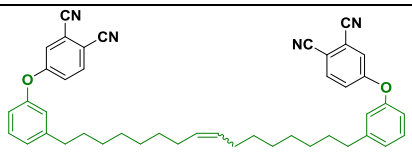	97–99
5.	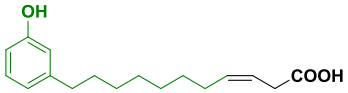	100–103
6.	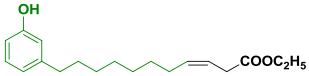	100–103
7.	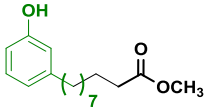	104
8.	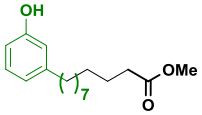	104
9.	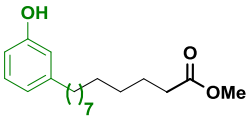	104
10.	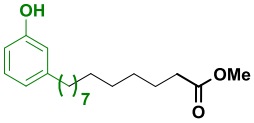	104
11.	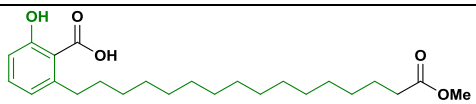	104
12.	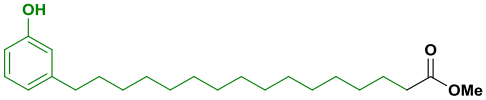	104

[a]green colour indicates structural components derived from cardanol.

Table 1.3, entries 1-4, represent difunctional monomers obtained through self-metathesis reactions of cardanol while monomers represented by entries 5-12 (**Table 1.3**), are synthesised by cross metathesis reaction involving cardanol. In 2016, Mgaya *et*

al[104] synthesised a series of difunctional monomers of various chain lengths from cardanol by metathesis chemistry (**Table 1.3**, entries 7 to 12).

Metathesis thus provides a tool by which the carbon atom number of the hydrocarbon chain can be tuned (**Table 1.3**, entries 1-12). It also presents a means to functionalise the hydrocarbon chain (**Table 1.3**, entries 5-12) and provides mixed aliphatic-aromatic difunctional monomers (**Table 1.3**, entries 5-12).

Several monomers listed in **Table 1.2** and **Table 1.3** have been utilised to synthesise step-growth polymers, while some monomers have not yet been polymerised. The properties of the synthesised polymers are discussed in the subsequent sections.

1.2.2 Step-growth polymers from CNSL-based aromatic difunctional monomers

Aromatic polyimides, polyamides, etc are important classes of high performance polymers which possess excellent thermo-oxidative stability, mechanical strength, electrical properties, and high radiation and solvent resistance.[105,106] These find applications in fields such as aerospace, automobiles, electronics and other industries as films, coatings, adhesives, membranes for separation of gases or liquids, etc.[107–111]

High performance polymers generally possess high glass transition temperatures, which are sometimes above their decomposition temperatures, and exhibit poor solubility in common organic solvents, which results into processing difficulties. Several approaches have been used to modify/ improve processability of high performance polymers, which include: (1) the insertion of flexible spacers between the rigid units; (2) the insertion of bent or 'crankshaft' units or "kinks" along the aromatic backbone and (3) the introduction of bulky side groups or flexible side chains to the aromatic backbone.[112,113]These structural modifications disrupt molecular symmetry, inhibit close packing of the chains and increase the free volume, consequently leading to improved solubility and processability.

Some of the difunctional monomers derived from CNSL as listed in **Table 1.2** have been utilised for the synthesis of a variety of step-growth polymers such as aromatic polyimides, polyamides, poly(azomethine)s, poly(amideimide)s, poly(esterimide)s, polyesters, polyhydrazides, poly(1,3,4-oxadiazole)s, polyurethanes, etc. The special structural features of aromatic difunctional monomers such as a long C-15 alkyl chain, *meta*-substitution and asymmetrical nature have been exploited to synthesise processable

high performance polymers. Cardanol-based monomers possessing pendent C-15 alkyl chain reduce co-planarity of the aromatic rings and disrupt the inter-chain packing of the macromolecular chains, which in turn leads to processable polymers. *Meta* substituted monomers introduce "kinks" in the macromolecular chain resulting into processable polymers. The asymmetrical monomers cause disruption of symmetry in the polymer chain leading to decrease in the inter-chain interactions between the polymer chains and also give rise to constitutional isomerism. Monomers containing flexible ether linkages provide polymers with lower internal energy of rotation and disrupt the linear progression in the polymer backbone.

Properties of certain high performance polymers derived from the listed cardanol-derived difunctional monomers with a particular emphasis on processability characteristics are discussed in the following sections.

1.2.2.1 Aromatic polyimides

Aromatic polyimides are generally synthesised by the polycondensation of aromatic diamines and tetracarboxylic dianhydrides, mainly involving a two-step method *via* poly(amic acid) formation or by one-step high temperature solution polymerisation[114] besides other synthetic routes.[115–123] **Table 1.4** represents the repeating units of aromatic polyimides derived from CNSL-based aromatic difunctional monomers and data concerning their solubility and thermal properties.

Aromatic polyimides containing pendent pentadecyl chains (**Table 1.4**) were mostly synthesised through one-step high temperature solution polycondensation, except for polyimides represented by entries 10 and 11 in **Table 1.4**, which were synthesised by two-step method involving thermal imidisation (**Scheme 1.1**).

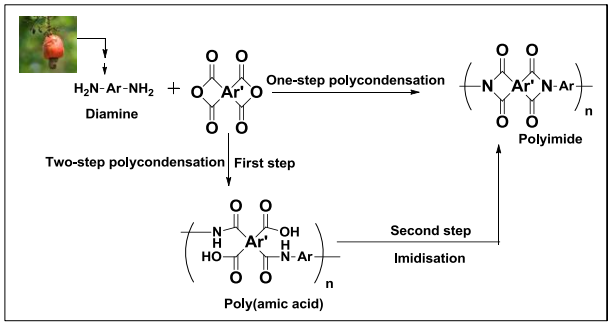

Scheme 1.1 Synthesis of polyimides based on CNSL-derived aromatic difunctional monomers

Table 1.4 Aromatic polyimides containing pendent pentadecyl chains derived from difunctional monomers based on cardanol[a]

Sr. No	Polyimide	η_{inh}[b] (dL/g)	Solubility[c]		T_g(^{0}C)[d]	T_{10} (^{0}C)[e]	Ref.
			$CHCl_3$	THF			
1.	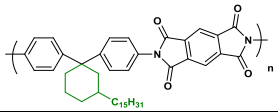	0.33	++	++	191	493	70
2.	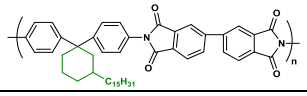	0.40	++	++	209	513	70
3.	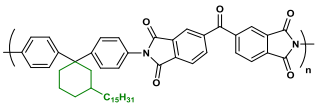	0.40	++	++	178	512	70
4.	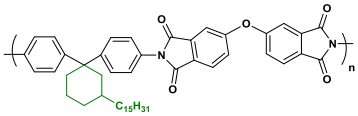	0.33	++	++	161	503	70
5.	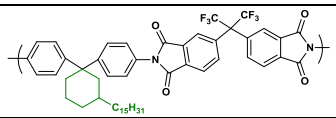	0.30	++	++	165	509	70
6.	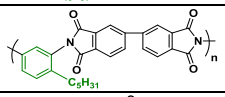	0.67	++	++	206 (330)	475	78
7.	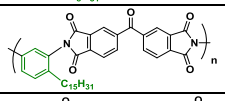	0.49	++	--	176 (320)	470	78
8.	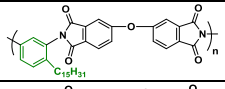	0.56	++	++	159 (305)	480	78
9.	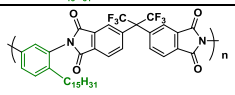	0.33	++	++	158 (297)	480	78
10.	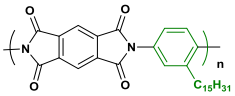	0.56*	N.R.	N.R.	N.R.	430	80

11.	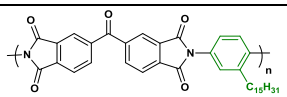	0.49*	N.R.	N.R.	N.R.	430	80
12.	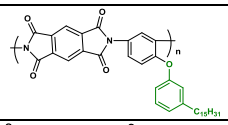	N.R.	+-	+-	212	451	82
13.	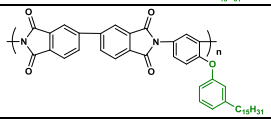	N.R.	+-	+-	226	460	82
14.	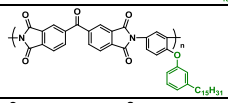	N.R.	++	++	171	468	82
15.	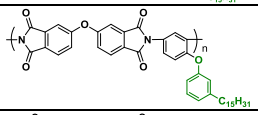	0.45	++	++	146	457	82
16.	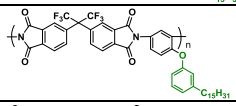	0.62	++	++	156	456	82
17.	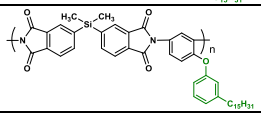	0.42	++	++	123	450	82
18.	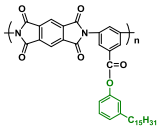	N.R.	--	--	228	514	82
19.	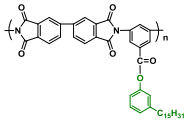	N.R.	--	+-	241	449	82
20.	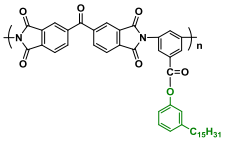	0.25*	--	++	237[#]	487	82
21.	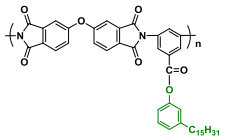	0.55*	+-	++	216	443	82
22.	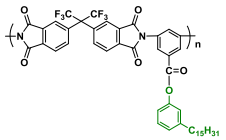	0.45*	++	++	174	488	82

23.	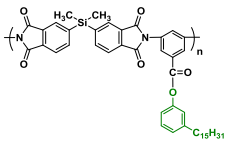	0.35*	++	++	185	436	82
24.	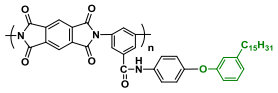	N.R.	--	--	219	445	82
25.	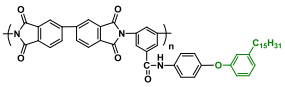	N.R.	--	--	224	443	82
26.	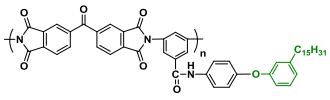	0.23*	--	--	237#	446	82
27.	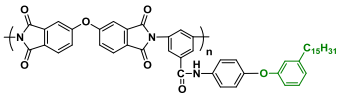	0.55*	++	+-	216#	449	82
28.	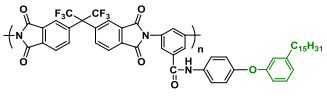	0.32	++	++	186	444	82
29.	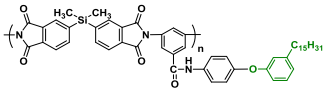	0.30	++	++	193	447	82
30.	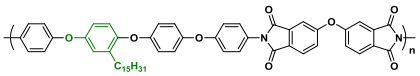	0.70	++	++	113	460	86
31.	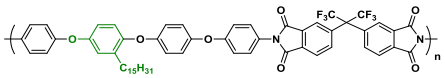	0.67	++	++	122	470	86
32.	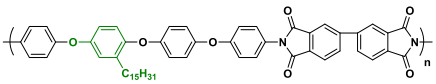	0.66	++	++	131	460	86

*$\eta_{inh}$was measured with 0.5% (w/v) solution of polyimides in *N,N*-dimethylacetamide at 30 ± 0.1°C, #sample was heated to the softening point and then quenched in liquid nitrogen before determining T_g, [a]green colour indicates structural components derived from cardanol, [b]$\eta_{inh}$was measured with 0.5% (w/v) solution of polyimides in chloroform at 30 ± 0.1°C, [c]solubility measured at 3 % (w/v) concentration --, Insoluble; +- partially soluble or swollen; ++, soluble at room temperature, [d]T_g values obtained from DSC curves from the second heating scans of polyimide samples, values in the bracket are T_g values of reference polyimides, [e]temperature at which 10 % weight loss was observed from TGA under nitrogen atmosphere, N.R. not reported.

Mathew[82] synthesised a series of copolyimides by polycondensation of a mixture of pentadecyl chain containing aromatic diamine corresponding to entry 15 (**Table 1.2**) and 4,4'-oxydianiline (ODA) at 5, 20, 50 mol %, with a number of commercially

available aromatic dianhydrides. Another series of copolyimides was synthesised by polycondensation of the same diamine (**Table 1.2**, entry 15) with 50 mol % of bis(3,4-dicarboxyphenyl) dimethylsilane dianhydride (SiDA) and other commercially available aromatic dianhydrides. The reported inherent viscosities (η_{inh}) of polyimides (0.23-0.70 dL/g) indicated the formation of medium to reasonably high molecular weight polymers which formed transparent and flexible films from their solutions.

^{1}H-NMR studies of polyimides (**Table 1.4**, entries 30-32) indicated the presence of constitutional isomerism based on appearance of four signals corresponding to aromatic protons *ortho* to imide nitrogen, instead of the expected doublet.[86]Constitutional isomerism arises when an asymmetrical monomer reacts with a symmetrical monomer. The presence of pentadecyl chain on the phenyl ring imparts asymmetry to the polymer backbone leading to constitutional isomerism (**Figure 1.5**). Theoretically, four probable structural orientations occur, *viz.*, (a) Head-to-Head, (b) Tail-to-Tail, (c) Head-to-Tail and (d) Tail-to-Head, out of which Head-to-Tail and Tail-to-Head would be indistinguishable by ^{1}H-NMR spectroscopy.[64]

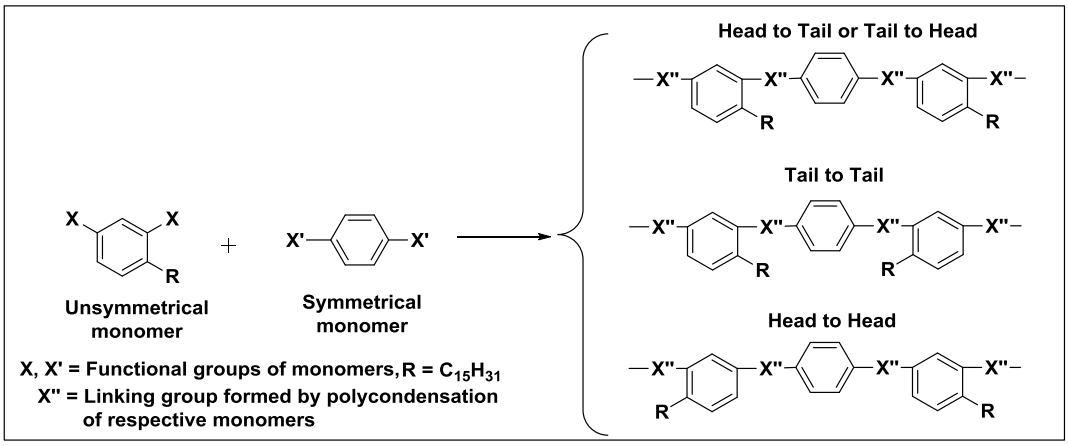

Figure 1.5 Possible sequences arising due to constitutional isomerism

The results of solubility tests demonstrated that solubility of polyimides was considerably enhanced compared with reference polymers, i.e. polymers without C_{15} alkyl chain. The C_{15} alkyl chain disrupts inter-chain packing, thus allowing solvent molecules to penetrate inside the polymer chains, consequently improving polymer solubility. Additionally, the pentadecyl chain provides a handle for interaction with solvent molecules. For example, the polymers represented in **Table 1.4** (entries 1, 2, 6, 32

etc) were soluble in chloroform and tetrahydrofuran at room temperature in spite of possessing rigid aromatic rings in the backbone, while the reference polyimides were insoluble in the respective solvents.

Thermogravimetric (TG) analysis data indicated that polyimides possessed good thermal stability (T_{10} values above 430 °C). Differential thermogravimetric analysis (DTG) of the synthesised polyimides (Table 4, entries 6-9) revealed a two stage weight loss: the first stage weight loss was due to decomposition of pendent alkyl groups while the second stage weight loss was due to decomposition of polyimide backbone. Polyimides containing pendent pentadecyl chains showed a significant drop in glass transition temperatures (T_g) values (113 – 241 °C) when compared with reference polyimides (**Table 1.4**, entries 6-9). The lowering in T_g values was attributed to disruption of inter-chain packing and increased segmental mobility imparted by the pentadecyl chain.

Alkyl groups are known to improve the solubility, liquid crystal alignment properties, dielectric and gas permeability properties of polymers. Polyimides have applications as organic alignment films due to good chemical resistance, abrasion resistance and thermal stability. Long alkyl chains and fluorinated alkyl side chains generate high pretilt angles of liquid crystals due to hydrophobic interaction with the polar liquid crystal molecules.[82] Polyimide corresponding to entry 15 (**Table 1.4**) provided pretilt angle in the range of 0.46° – 6.6° when used in combination with various commercial liquid crystals. It showed potential as alignment layers for super twisted nematic liquid crystal devices where a tilt angle of 5° – 14° is required.[82]

Dielectric properties of polymers are dependent on their hydrophobicity and therefore polymers containing pendent alkyl groups are expected to have low dielectric constant, which makes them useful as interlayer dielectrics. Dielectric constant (ε) was calculated from capacitance measurements over a range of frequencies for the polyimides represented by entries 15-17 of **Table 1.4** and copolyimides composed of 20 mol % and 50 mol % diamine derived from cardanol (**Table 1.2**, entry 15) over a range of frequencies. Polyimides (**Table 1.4**, entries 15, 16 and copolyimide composed of 20 mol % diamine derived from cardanol) showed dielectric constant values in the range 0.4 – 1.7 which were lower than that of polyimide (Kapton) "H" film (ε = 3.5), a preferred

dielectric material in microelectronics applications. Polyimides derived from CNSL-based monomers offer a good choice for microelectronic devices as interlayer dielectrics owing to their low dielectric constant values ($\varepsilon < 3.5$) coupled with good processability.[82]

The presence of pendent alkyl groups along the polymer backbone is important in gas separation applications since they cause an increase in the free volume of the resulting polymer and thereby increase the permeability. Gas permeability studies were performed on polyimides containing pendent pentadecyl chains corresponding to entries 15-16, 21-23 and 27-29 of **Table 1.4**. Polyimides corresponding to entries numbered 16 and 22, in **Table 1.4**, displayed high oxygen permeability coefficients and high O_2/N_2 selectivity, showing promise as gas separation membrane materials.[82]

Transmission electron micrographs (TEM) of grids coated with copolyimides based on diamine possessing pendent pentadecyl chain corresponding to entry 15 (**Table 1.2**) with ODA and SiDA were obtained. All the films showed hole-like structures. Copolyimides based on 20 mol % of the diamine (**Table 1.2**, entry 15) with SiDA, 3,3',4,4'-oxydiphthalicdianhydride (ODPA) and 4,4'-(hexafluoroisopropylidene)diphthalic anhydride (6-FDA) showed resemblance with commercial grids. A holey grid with uniform holes was obtained by using a copolyimide solution of 0.1% and a lacey grid was obtained when the concentration was 0.07 %.[82]

1.2.2.2 Aromatic polyamides

Wholly aromatic polyamides are high-performance organic materials possessing excellent thermal and mechanical resistance arising from their stiff rod-like macromolecular chains that interact with each other *via* strong and highly directional hydrogen bonds.[105,124–126] Aromatic polyamides can be prepared mainly by low temperature interfacial polycondensation of a diamine and a diacid chloride or high temperature solution polycondensation of an activated dicarboxylic acid and a diamine, besides other methods. Aromatic polyamides containing pendent pentadecyl chains are collected in **Table 1.5**.

Aromatic polyamides presented in **Table 1.5**, containing pendent pentadecyl chains, were synthesised by phosphorylation polycondensation of diamines with diacids (**Table 1.5**, entries 1-4, 10-14) or by low temperature interfacial polycondensation of diamines with diacyl chlorides (**Table 1.5**, entries 5-9, 15-23) (**Scheme 1.2**).

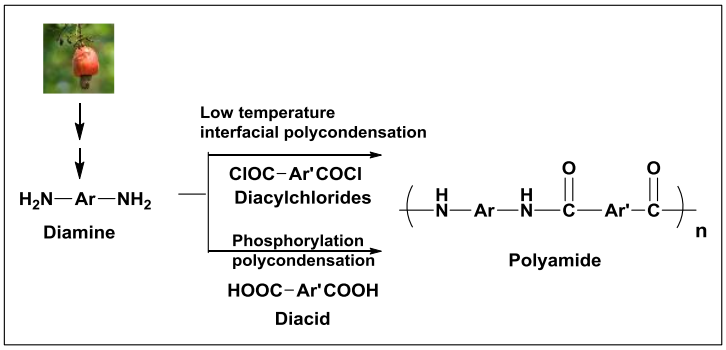

Scheme 1.2 Synthesis of polyamides based on CNSL-derived aromatic difunctional monomers

Table 1.5 Aromatic polyamides containing pendent pentadecyl chains derived from difunctional monomers based on cardanol[a]

Sr. No	Polyamide	η_{inh}(dL/g)[b]	Solubility[c]		T_g(^{0}C)[d]	T_{10} (^{0}C)[e]	Ref
			DMAc	THF			
1	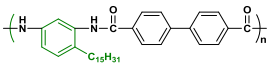	0.56	+	--	215	450 (531)	79
2	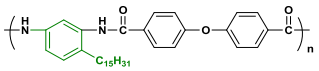	0.52	++	--	169 (232)	435 (510)	79
3	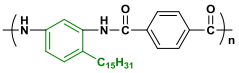	0.43	++	--	206 (295)	460 (524)	79
4	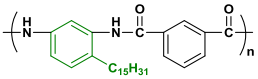	0.35	++	+-	189 (276)	430	79
5	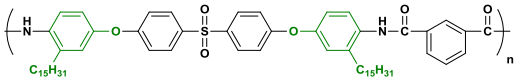	0.17*	++	++	N.R.	479[##]	87

6	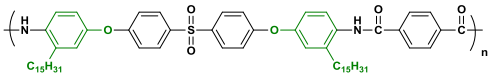	0.15	+	+-	N.R.	490[##]	87
7	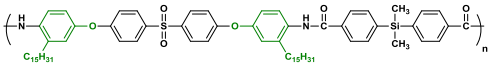	0.23*	++	++	N.R.	493[##]	87
8	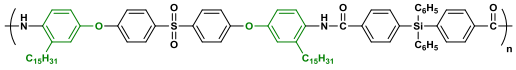	0.17*	++	++	N.R.	498[##]	87
9	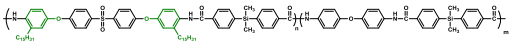 (50:50 mol%)	0.56	++	+	N.R.	482[##]	87
10	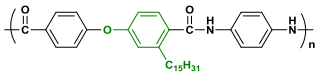	0.45	+-	N.R.	189	430	88
11	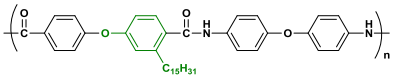	0.66	++	N.R.	160 (231)	425 (515)	88
12	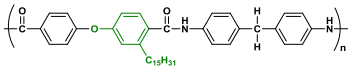	0.62	++	N.R.	139 (255)	440 (483)	88
13	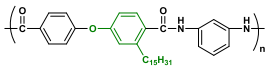	0.58	++	++	148 (250)	439 (467)	88
14	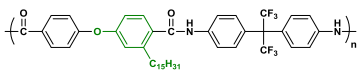	0.66	++	++	154	453	88

15	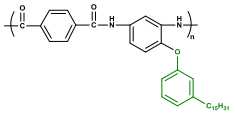	N.R.	+-	+-	164	422	82
16	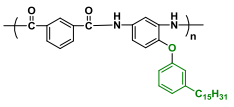	N.R.	+-	N.R.	150	422	82
17	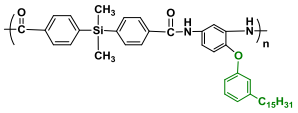	0.45	++	++	111	439	82
18	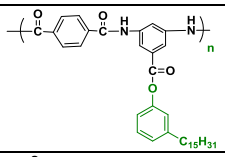	0.6**	++	N.R.	232	340	82
19	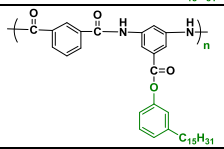	0.55**	++	++	221	365	82
20	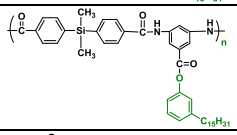	0.5**	++	++	186	354	82
21	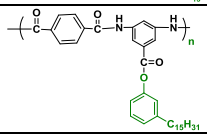	N.R.	--	--	279	417	82
22	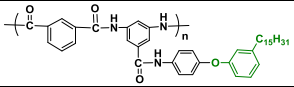	0.56**	++	++	262	401	82
23	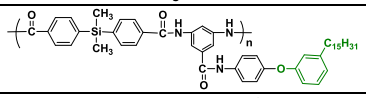	0.65**	++	++	225	437	82

*η_{inh} was measured with 0.5% (w/v) solution of polyamides in $CHCl_3$ at 30 ± 0.1°C, **η_{inh} was measured with 0.5% (w/v) solution of polyamides in NMP at 30 ± 0.1°C, ##T_{max} maximum degradation temperature obtained from DTG curve, [a]green colour indicates structural components derived from cardanol, [b]η_{inh} was measured with 0.5% (w/v) solution of polyamides in *N*,*N*-dimethylacetamide at 30 ± 0.1°C, [c]solubility measured at 3 % (w/v) concentration --, Insoluble; +- partially soluble or swollen; + soluble on heating; ++, soluble at room temperature, [d]T_g values obtained from DSC curves from the second heating scans of polyamide samples, values in the bracket are T_g values of reference polyamides, [e]temperature at which 10 % weight loss was observed from TGA under nitrogen atmosphere, values in the bracket are T_{10} values of reference polyimides, N.R. not reported.

The reported inherent viscosities (0.15 – 0.66 dL/g) implied that the synthesised polyamides were of medium to high molecular weights. Polyamides represented in **Table 1.5** formed self-standing, transparent and flexible films. ^{1}H-NMR studies of the polyamides containing pendent pentadecyl chains (**Table 1.5**, entries 1-4, 10-14)

exhibited appearance of four different peaks corresponding to the amide protons, indicating the existence of constitutional isomerism resulting from the use of an asymmetrical monomer.[79,88] Polyamides corresponding to entries 5, 7, 8, 13, 14, 17, 19, 20, 22, 23 of **Table 1.5** showed room temperature solubility in *N*,*N*-dimethylacetamide (DMAc) and tetrahydrofuran (THF), due to chain disruptive effect of the pentadecyl chain. Jadhav *et al*[87] synthesised a series of copolyamides by polycondensation of a mixture of pentadecyl chain containing diamine and ODA (**Table 1.5**, entry 9) at 25, 50, 75 mol % with commercial diacids that demonstrated improvement in solubility with increasing incorporation of pentadecyl chain containing monomer.

The reported T_{10} values (above 340 °C) suggested that the synthesised polyamides possessed good thermal stability. The pentadecyl chain containing polyamides exhibited lower T_g values (111 – 279 °C) compared to reference polyamides (for example, **Table 1.5**, entries 2-4, 11-13) due to increased segmental mobility imparted by the long alkyl chain. The silicon containing polyamides (entries 17, 20, 23) showed good permeability towards gases such as nitrogen, oxygen, hydrogen and carbon dioxide.[82]

1.2.2.3 Aromatic polyazomethines

Aromatic polyazomethines find applications in opto-electronics[127–133]and are high-performance fibre and film-forming polymers with remarkable thermal stability, high strength, high modulus,[134] and an ability to form chelates.[135–137] However, their high melting temperatures and poor solubilities in common organic solvents make both their characterisation and processing difficult. Therefore, it is desirable to improve the processability of polyazomethines. **Table 1.6** represents aromatic polyazomethines containing pendent pentadecyl chains synthesised from monomers derived from cardanol.

Polyazomethines reported in **Table 1.6** were synthesised by solution polycondensation of diamines containing pentadecyl chains with commercially available aromatic dialdehydes (**Scheme 1.3**).

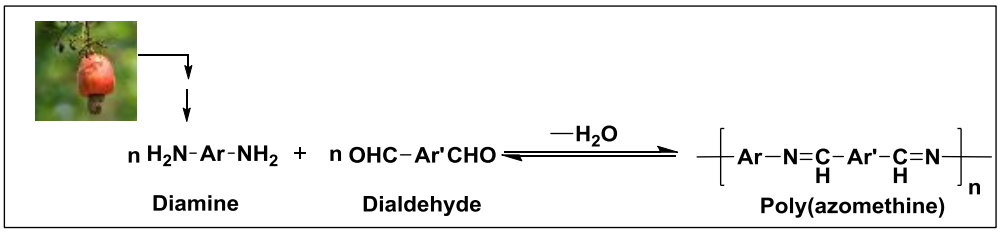

Scheme 1.3 Synthesis of aromatic polyazomethines based on CNSL-derived aromatic diamine monomers

Table 1.6 Aromatic polyazomethines containing pendent pentadecyl chains derived from difunctional monomers based on cardanol[a]

Sr. No	Polyazomethine	η_{inh}(dL/g)[b]	Solubility[c]		T_g (°C)[d]	T_{10} (°C)[e]	Ref.
			$CHCl_3$	THF			
1.	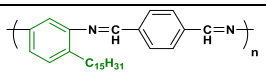	0.38	++	+-	55	440	79
2.	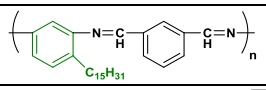	0.36	++	++	16	440	79
3.	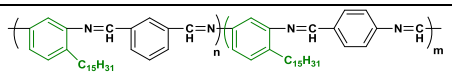 (50:50 mol%)	0.33	++	++	45	425	79
4.	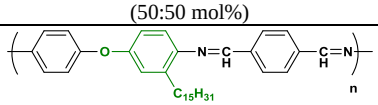	0.70	++	+-	48	435	83
5.	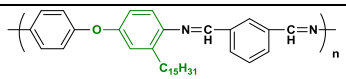	0.56	++	++	21	438	83
6.	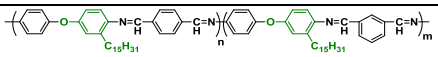 (50:50 mol%)	0.52	++	++	27	441	83

[a]green colour indicates structural components derived from cardanol, [b]η_{inh} was measured with 0.5% (w/v) solution of polyazomethines in $CHCl_3$ at 30 ± 0.1°C, [c]solubility measured at 3 % (w/v) concentration, +- partially soluble or swollen; ++, soluble at room temperature, [d]T_g values obtained from DSC curves from the second heating scans of polyazomethine samples, [e]temperature at which 10 % weight loss was observed from TGA under nitrogen atmosphere.

The reported inherent viscosity values (0.33 – 0.70 dL/g) showed that the polyazomethines were of medium to reasonably high molecular weights. Transparent, flexible and stretchable films of polyazomethines could be cast from chloroform solution. Polyazomethines corresponding to entries 4-5 of **Table 1.6** exhibited constitutional isomerism due to the unsymmetrical diamine as indicated by ^{1}H-NMR studies.[83] The synthesised polyazomethines exhibited good solubility in chloroform and THF at room temperature.

The T_{10} values (above 425 °C), as exhibited in **Table 1.6**, indicated that synthesised polyazomethines possessed good thermal stability. The low T_g (16 – 55 °C)

values are due to increase in segmental mobility and the chain –disruptive effect of the long alkyl chain.

1.2.2.4 Poly(arylene ether)s

Poly(arylene ether)s such as poly(ether ketone)s, poly(ether sulfone)s, etc, constitute an important class of high performance thermoplastics because of their attractive properties such as high thermo-oxidative and chemical stability and excellent mechanical strength. Poly(arylene ether)s are therefore extensively used in aviation, spacecrafts, automobile, food processing sectors, medical devices, gas separation membranes, ultrafilration, fuel cells, electronic/electrical industries, etc. Poly(arylene ether)s can be synthesised by a number of methods such as i) electrophilic substitution[138–142] ii) nucleophilic aromatic substitution,[143–155] and other methods.[156]

Table 1.7 summarises the solubility and thermal properties of poly(arylene ether)s containing pendent pentadecyl chains. Poly(arylene ether)s presented in **Table 1.7** were synthesised through nucleophilic aromatic substitution polycondensation of aromatic biphenols and activated aromatic difluorides (**Scheme 1.4**).

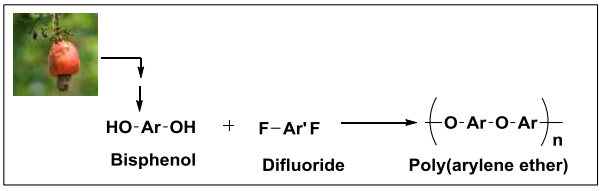

Scheme 1.4 Synthesis of poly(arylene ether)s based on CNSL-derived aromatic biphenol monomers

Table 1.7 Aromatic poly(arylene ether)s containing pendent pentadecyl chains derived from difunctional monomers based on cardanol[a]

Sr. No	Poly(arylene ether)	η_{inh} (dL/g)[b]	Solubility[c]		T_g (°C)[d]	T_{10} (°C)[e]	Ref.
			$CHCl_3$	THF			
1.	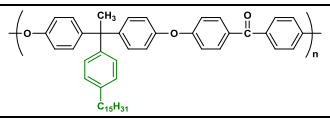	1.07	++	++	68	440	72
2.	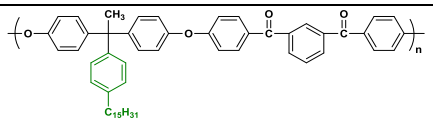	0.70	++	++	75	429	72
3.	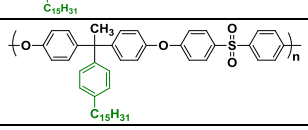	0.64	++	++	93	416	72

4.	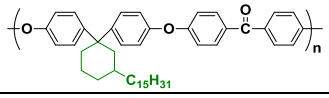	1.27	++	++	69	459	72
5.	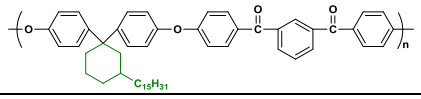	1.0	++	++	78	416	72
6.	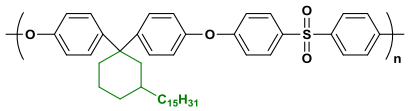	1.12	++	++	95	443	72
7.	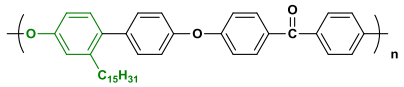	0.81	++	++	35	455	66
8.	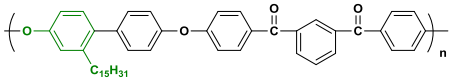	0.50	++	++	51	455	66
9.	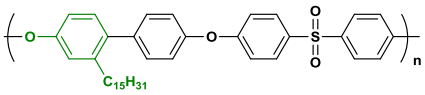	0.67	++	++	60	410	66

[a]green colour indicates structural components derived from cardanol, [b]η_{inh} was measured with 0.5% (w/v) solution of poly(arylene ether)s in $CHCl_3$ at 30 ± 0.1°C, [c]solubility measured at 3 % (w/v) concentration; ++, soluble at room temperature, [d]T_g values obtained from DSC curves from the second heating scans of poly(arylene ether) samples; [e]temperature at which 10 % weight loss was observed from TGA under nitrogen atmosphere.

The reported inherent viscosity values of poly(arylene ether)s (0.50 – 1.27 dL/g) suggested the formation of reasonably high molecular weight polymers. Poly(arylene ether)s exhibited good solubility in chloroform and THF and formed transparent, tough and self-standing films from their solutions. The existence of constitutional isomerism in poly(arylene ether)s (**Table 1.7** entries 7-9) was evidenced from detailed NMR spectroscopic studies.[66] The synthesised poly(arylene ether)s possessed bulky pendent aryl groups (**Table 1.7** entries 1-3) or cardo moieties such as cyclohexylidene groups (**Table 1.7** entries 4-6) along with pendent pentadecyl chains. Consequently, they exhibited excellent solubility in common solvents such as chloroform and tetrahydrofuran due to packing disruptive effects of the pendent groups. The pendent pentadecyl chain along the polymer backbone acts as a handle for interaction with solvent molecules. T_{10} values (above 410 °C) indicated that these polymers possessed good thermal stability. Poly(arylene ether)s exhibited low glass transition temperatures (35 – 95 °C) due to increased polymer chain mobility imparted by the pendent pentadecyl chains. The data on the properties of polymers suggests that bisphenols containing pentadecyl chains are useful comonomers to tune the thermal and other properties of commercial poly(arylene ether)s.

1.3 General trends in properties of high performance polymers from CNSL-based aromatic difunctional monomers

As has been discussed in the previous sections, the C-15 alkyl chain present in the aromatic difunctional monomers derived from cardanol influences the properties of polymers synthesised therefrom in several ways. Overall, the polymer processability/ solubility was improved by the incorporation of pendent pentadecyl chains. The presence of C-15 alkyl chain disrupts inter-chain packing of the polymers, enhances chain mobility and facilitates interaction of solvent molecules with the polymer chains. All these effects are manifested into interesting changes in polymer properties as summarised in **Table 1.8.**

Table 1.8 Influence of the pentadecyl chain on polymer properties

Property	Remark
Crystallinity	Decrease in crystallinity leading to amorphous polymers, contributes to enhancement in solubility characteristics.
Solubility in (common) organic solvents	Improvement in solubility characteristics, solution processability
Temperature at 10 wt % decomposition in TGA (T_{10})	Decrease in T_{10} (TGA) and T_{max} (DTG)
Glass transition temperature (T_g)	Depression in T_g when compared to reference polymers; a large gap between T_g and T_{10}, wider processing window, possibilities of compression moulding.

A large gap between T_g and T_{10} values was observed with the studied high performance polymers. This offers polymers a wide processing window. Thus improved solubility coupled with reasonably good thermal stability of these polymers makes them attractive candidates for high performance polymer applications.

1.4 The potential for CNSL-based step-growth polymers for optoelectronic applications: literature and prospects

By virtue of their lower cost, solution processability, deformation and deterioration resistance and rich versatility of structure, polymeric materials have captivated the attention of researchers world-wide for exploration in the field of optoelectronics, especially light emitting devices,[157–160] solar cells,[161–167]electrochromic devices,[168–172] memory devices,[173–175] etc. Such polymers generally include conjugated polymers and certain non-conjugated donor-acceptor polymers. Conjugated polymers generally include polymer classes such as poly(phenylenevinylene)s, poly(*m*-phenylenevinylene)s, etc. Additionally, step-growth polymers with triarylamine[176–178] or carbazole[179,180] units in the backbone or pendent show good potential for applications in optoelectronics. The triaryamine moiety refers to a tertiary amine with two aryl groups. The triarylamine moiety possesses several interesting features, which include a low ionisation potential, contributing to efficient hole injection. The nitrogen atom has a strong tendency to undergo oxidation, leading to the formation of radical cation species. Therefore, the triarylamine group can effectively transport charges (holes) *via* the formation of radical cations. As a result, triarylamine moieties can act as good donors with strong charge transfer effect.[181,182] Triarylamine-containing polymers have been investigated for electrochromic applications, OLED devices, memory devices, etc. Selected examples of triarylamine-containing high performance polymers investigated for memory devices, which is presently a hot area of research, are summarised in **Table 1.9**.

Table 1.9 Triarylamine-containing high performance polymers investigated for memory devices

S. R. No.	Polymer	Comment	Reference
1.	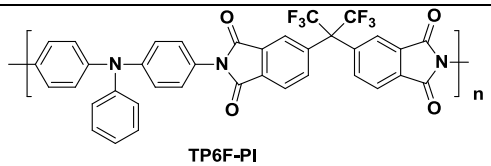 TP6F-PI	TP6F-PI displayed volatile, DRAM (Dynamic Random Access Memory) behaviour.	183
2.	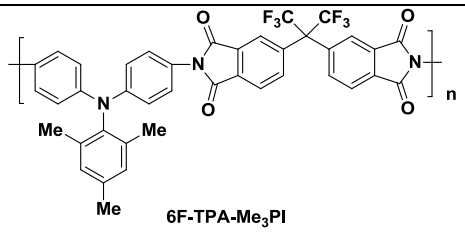 6F-TPA-Me_3PI 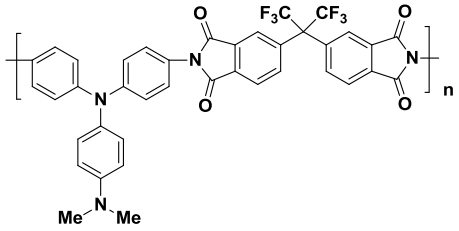 6F-TPA-NMe_3PI	6F-TPA-Me_3PI was observed to display unipolar WORM behaviour while 6F-TPA-NMe_3PI displayed unipolar rewritable memory behaviour	184
3.	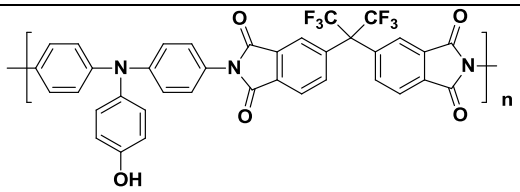 6F-HTPA-PI	Films of 6F-HTPA-PI established excellent unipolar WORM memory behaviour	185

4.	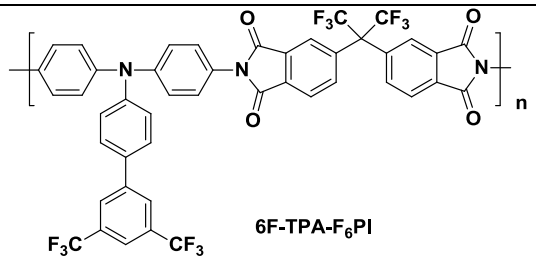 6F-TPA-F_6PI 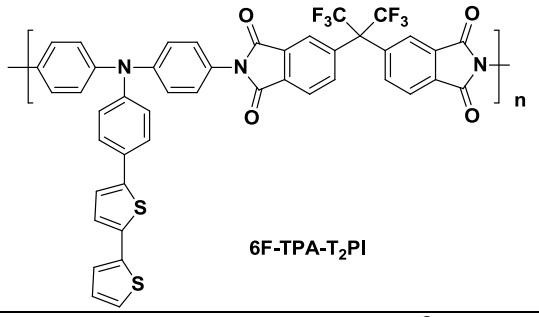 6F-TPA-T_2PI	Memory devices fabricated from 6F-TPA-F_6PI exhibited sDRAM memory. 6F-TPA-T_2PI film exhibited unipolar WORM memory behaviour.	186
5.	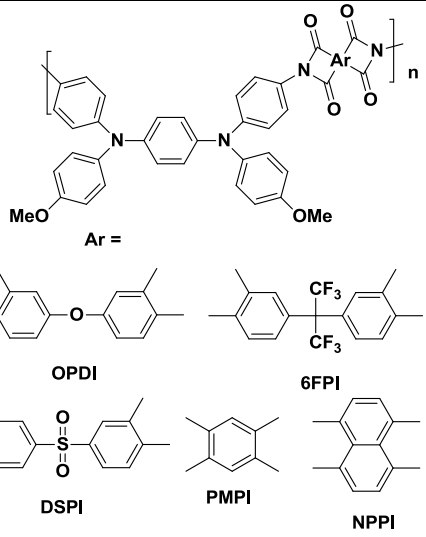	It was observed that $(OMe)_2$TPPA-ODPI did not display any memory behaviour while $(OMe)_2$TPPA-6FPI exhibited DRAM and $(OMe)_2$TPPA-PMPI displayed SRAM. $(OMe)_2$TPPA-DSPI and $(OMe)_2$TPPA-NPPI exhibited WORM memory behaviour.	187
6.	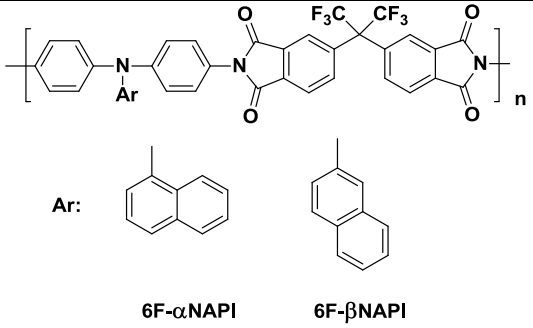 6F-αNAPI 6F-βNAPI	It was observed that 6F-αNAPI displayed WORM type memory while 6F-βNAPI exhibited programmable flash type memory behaviour.	188

7.	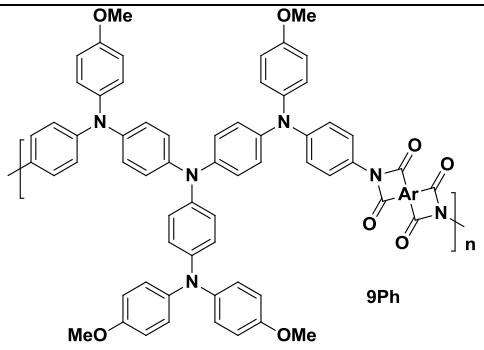 9Ph Ar = 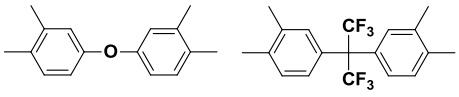 OPDI 6FPI 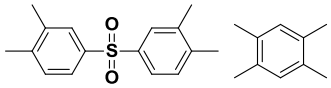 DSPI PMPI	9Ph-ODPI displayed DRAM characteristics while 9Ph-6FPI displayed SRAM characteristics. 9Ph-DSPI and 9Ph-PMPI both displayed WORM behaviour.	189
8.	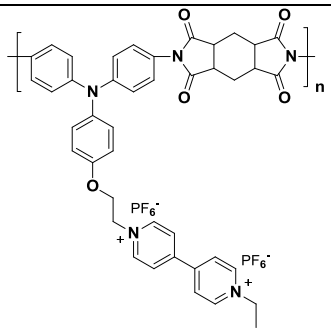 Vio-CH	Vio-CH was observed to display non-volatile WORM memory characteristics	190

9.	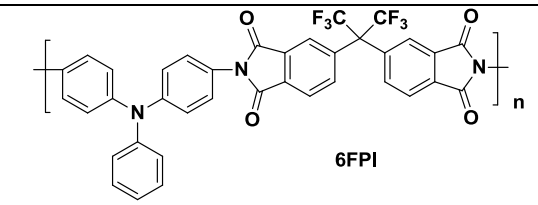 6FPI 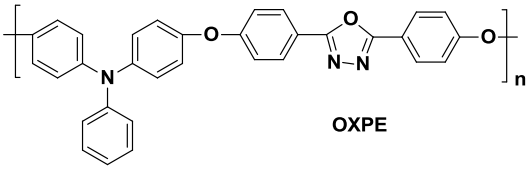 OXPE 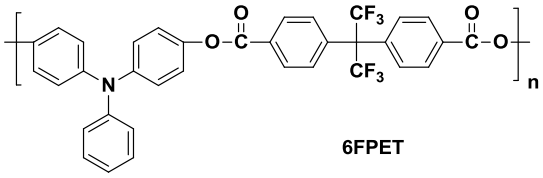 6FPET 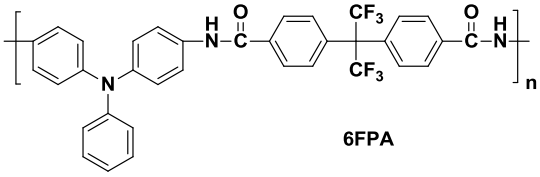 6FPA 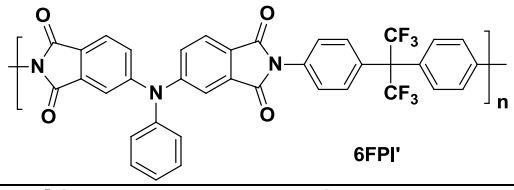 6FPI'	6FPI' did not display any memory characteristics. 6FPI exhibited DRAM characteristics while OXPE, 6FPET and 6FPA displayed SRAM characteristics.	191
10.	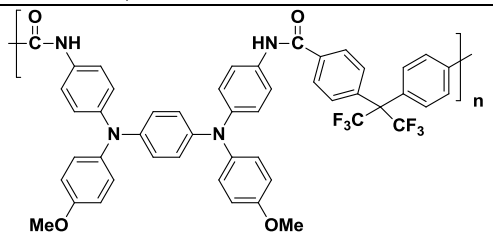 (OMe)$_2$TPPA-6FPA	Device fabricated from (OMe)$_2$TPPA-6FPA displayed SRAM characteristics.	192

11.	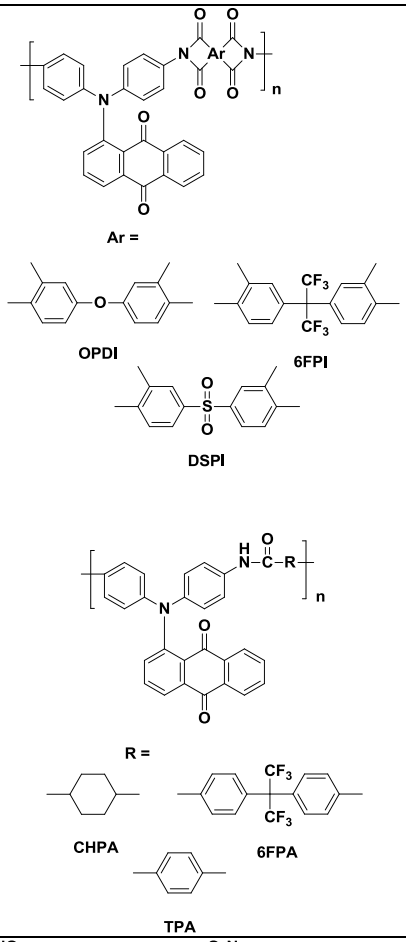	The synthesised polyimides and polyamides displayed non-volatile WORM memory behaviour.	193
12.	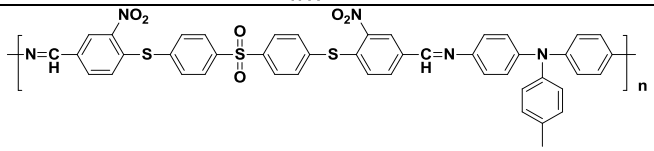	The synthesised polyazomethines after doping with PTSA displayed rewritable memory behaviour with multilevel storage capacity and excellent uniformity of the resistance states. The undoped polyazomethines exhibited rewritable memory characteristics but did not display multilevel memory.	194

13.	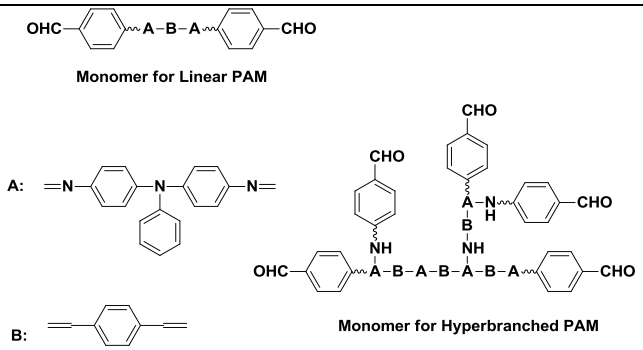	The synthesised PAMs displayed non-volatile rewritable memory behaviour. The hyperbranched PAM thin film demonstrated more uniform distribution of the HRS and LRS.	195

Polymers investigated for optoelectronic applications are generally derived from petrochemical sources. It is of great interest to develop polymer-based smart materials from renewable resources. A few reports are known regarding the exploration of polymers based on CNSL for optoelectronic applications. Cyriac *et al*[93] reported synthesis of bisylide monomer based on 3-pentadecyl phenol. The bisylide monomer was polymerised with bisaldehyde under Wittig-Horner reaction conditions to prepare poly [(4-methoxy-6-pentadecyl-1,3-phenylenevinylene)-alt-(1,3-phenylenevinylene)] (m-PPV) and its *para*-counterpart *viz*., poly [(4-methoxy-6-pentadecyl-1, 3-phenylenevinylene)-alt-(1, 4-phenylenevinylene)] (p-PPV) (**Scheme 1.5**).

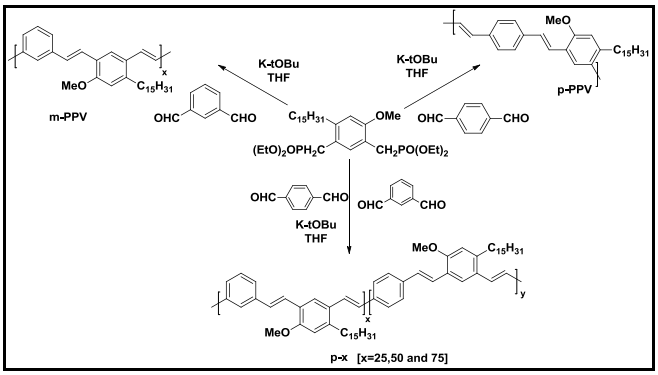

Scheme 1.5 Synthesis of poly(*m*-phenylenevinylene)s based on cardanol-derived diphosphonate monomers

The cardanol based *m*-PPV and *p*-PPV polymers were used to trace energy transfer process and molecular aggregation phenomena in the π-conjugated system. The detailed photophysical studies by absorption and emission spectroscopes indicated efficient

Forster energy transfer from the *m*-conjugated segments to the *p*-counterpart in solution as well as in the solid state.

Seo *et al*[92] have reported CNSL-based poly(1,3,4-oxadiazole)s used in a leak-free electrochemical switching device, which showed reversible fluorescent switching. There remains a lot of scope for designing step-growth polymers from CNSL for use in optoelectronic applications. It would be an intriguing strategy to design triarylamine containing difunctional monomers from CNSL for the purpose of synthesis of high performance polymers. This strategy has been further pursued in this work, as discussed in **Chapter 4**.

1.5 Summary

1. Cardanol, a major constituent of CNSL, is a by-product of cashew industry and a non-edible oil. Cardanol possesses a number of reactive sites for functionalisation and chemical modification, which makes it an attractive bio-based starting material for synthesis of various types of monomers and polymers.

2. This chapter has summarised the library of difunctional monomers synthesised from cardanol/CNSL. Olefin metathesis reactions have opened up interesting opportunities to synthesise new cardanol-derived monomers and polymers possessing side chains of variable lengths and functionalised alkyl chains. These difunctional monomers are a welcome addition to the existing portfolio of difunctional condensation monomers and represent useful (co)monomers for the synthesis of step-growth polymers with attractive processability characteristics.

3. Polymers derived from cardanol bear pendent C-15 chains which have been amply exploited by researchers to modify polymer properties and thereby improve solubility and processability of various polymer classes *viz.* polyimides, polyamides, etc. The literature account presented in the chapter provides a comprehensive summary of several difunctional monomers synthesised from cardanol/ CNSL and the preparation, solubility and thermal properties of various step-growth polymers. The incorporation of pendent flexible pentadecyl chains resulted into significant improvement in solubility characteristics of polymers and induced the depression of T_g. High performance polymers derived from CNSL-based aromatic difunctional monomers exhibited reasonably good thermal stability. However, T_{10} values were lower than the corresponding reference

polymers without containing pentadecyl chains. Furthermore, a large gap between T_g and T_{10} values of polymers based on CNSL-derived monomers offers a broad processing window. The data on solubility and thermal properties of (co)polymers revealed that even at low concentration of cardanol-derived monomers, there is a significant enhancement in solubility and reduction in T_g.

4. With growing demand for renewables, it is only a matter of time for CNSL-based difunctional condensation monomers to find widespread commercial applications.

5. There is a huge potential for designing and developing CNSL-based high performance polymers for optoelectronic applications.

6. A lot of scope exists for the further exploration of high performance polymers containing pentadecyl chains.

References

1 S. Muñoz-Guerra, C. Lavilla, C. Japu and A. Martínez de Ilarduya, *Green Chem.*, 2014, **16**, 1716–1739.

2 M. Meier, *Green Chem.*, 2014, **16**, 1672.

3 Y. Xu, M. A. Hanna and L. Isom, *Open Agric. J.*, 2008, **2**, 54–61.

4 Big Chemical Encyclopedia, http://chempedia.info/info/151307/, (accessed September 19, 2018).

5 R. A. Berner, *Nature*, 2003, **426**, 323–326.

6 J. D. Brooks and J. W. Smith, *Geochim. Cosmochim. Acta*, 1969, **33**, 1183–1194.

7 B. P. Tissot and D. H. Welte, *Petroleum Formation and Occurrence*, Springer Berlin Heidelberg, Berlin, Heidelberg, Heidelberg, 1984.

8 F. D. Mango, *Org. Geochem.*, 1997, **26**, 417–440.

9 M. Crocker and C. Crofcheck, *Energeia*, 2006, **17**, 1–6.

10 C. Okkerse and H. van Bekkum, *Green Chem.*, 1999, **1**, 107–114.

11 U.S. Biobased Products: Market Potential and Projections Through 2025., https://www.usda.gov/oce/reports/energy/BiobasedReport2008.pdf, (accessed September 19, 2018).

12 E. de Jong and G. Jungmeier, in *Industrial Biorefineries & White Biotechnology*, Elsevier, 2015, pp. 3–33.

13 F. Cherubini, *Energy Convers. Manag.*, 2010, **51**, 1412–1421.

14 M. FitzPatrick, P. Champagne, M. F. Cunningham and R. A. Whitney, *Bioresour. Technol.*, 2010, **101**, 8915–8922.

15 S. N. Naik, V. V. Goud, P. K. Rout and A. K. Dalai, *Renew. Sustain. Energy Rev.*, 2010, **14**, 578–597.

16 M. Stöcker, *Angew. Chemie Int. Ed.*, 2008, **47**, 9200–9211.

17 C. Williams and M. Hillmyer, *Polym. Rev.*, 2008, **48**, 1–10.

18 M. N. Belgacem and A. Gandini, *Monomers, Polymers and Composites from Renewable Resources*, Elsevier, 2008.

19 M. Fache, E. Darroman, V. Besse, R. Auvergne, S. Caillol and B. Boutevin, *Green Chem.*, 2014, **16**, 1987–1998.

20 B. Lochab, S. Shukla and I. K. Varma, *RSC Adv.*, 2014, **4**, 21712–21752.

21 CatchBio, http://www.catchbio.com/, (accessed September 19, 2018).

22 BIO-TIC, http://industrialbiotech-europe.eu/, (accessed September 19, 2018).

23 ARENA, https://arena.gov.au/, (accessed September 19, 2018).

24 Delft Advanced Biorenewables, http://delftab.com/, (accessed September 19, 2018).

25 A. Gandini and T. M. Lacerda, *Prog. Polym. Sci.*, 2015, **48**, 1–39.

26 C. Vilela, A. F. Sousa, A. C. Fonseca, A. C. Serra, J. F. J. Coelho, C. S. R. Freire and A. J. D. Silvestre, *Polym. Chem.*, 2014, **5**, 3119–3141.

27 M. A. Hillmyer, *Science*, 2017, **358**, 868–870.

28 S. A. Miller, *ACS Macro Lett.*, 2013, **2**, 550–554.

29 D. K. Schneiderman and M. A. Hillmyer, *Macromolecules*, 2017, **50**, 3733–3749.

30 B. Gyarmati and B. Pukánszky, *Eur. Polym. J.*, 2017, **93**, 612–617.

31 R. Mülhaupt, *Macromol. Chem. Phys.*, 2013, **214**, 159–174.

32 A. Gandini, T. M. Lacerda, A. J. F. Carvalho and E. Trovatti, *Chem. Rev.*, 2016, **116**, 1637–1669.

33 A. F. Sousa, C. Vilela, A. C. Fonseca, M. Matos, C. S. R. Freire, G.-J. M. Gruter, J. F. J. Coelho and A. J. D. Silvestre, *Polym. Chem.*, 2015, **6**, 5961–5983.

34 M. J. L. Tschan, E. Brulé, P. Haquette and C. M. Thomas, *Polym. Chem.*, 2012, **3**, 836–851.

35 L. Zhang, Z. Liu, G. Cui and L. Chen, *Prog. Polym. Sci.*, 2015, **43**, 136–164.

36 J. Datta and M. Włoch, *Polym. Bull.*, 2014, **71**, 3035–3049.

37 P. A. Wilbon, F. Chu and C. Tang, *Macromol. Rapid Commun.*, 2013, **34**, 8–37.

38 A. Llevot, E. Grau, S. Carlotti, S. Grelier and H. Cramail, *Macromol. Rapid Commun.*, 2016, **37**, 9–28.

39 B. M. Upton and A. M. Kasko, *Chem. Rev.*, 2016, **116**, 2275–2306.

40 J. A. Galbis, M. D. G. García-Martín, M. V. de Paz and E. Galbis, *Chem. Rev.*, 2016, **116**, 1600–1636.

41 A. Arbenz and L. Avérous, *Green Chem.*, 2015, **17**, 2626–2646.

42 Food and Agriculture Organisation of the United Nations Statistics Division (FAOSTAT), http://www.fao.org/faostat/en/#home, (accessed September 19, 2018).

43 J. H. P. Tyman, *Synthetic and Natural Phenols*, Elsevier, Amsterdam, 1st edn., 1996.

44 O. A. Attanasi, *Chim. Oggi*, 1983, **8**, 11–14.

45 M. T. Harvey and S. Caplan, *Ind. Eng. Chem.*, 1940, **32**, 1306–1310.

46 R. Paramashivappa, P. P. Kumar, P. J. Vithayathil and A. S. Rao, *J. Agric. Food Chem.*, 2001, **49**, 2548–2551.

47 S. Manjula, C. K. S. Pillai and V. G. Kumar, *Thermochim. Acta*, 1990, **159**, 255–266.

48 J. H. P. Tyman, R. A. Johnson, M. Muir and R. Rokhgar, *J. Am. Oil Chem. Soc.*, 1989, **66**, 553–557.

49 R. K. Jain and S. Kumar, *J. Food Eng.*, 1997, **32**, 339–345.

50 R. N. Patel, S. Bandyopadhyay and A. Ganesh, *Energy*, 2011, **36**, 1535–1542.

51 T. Gandhi, M. R. Patel and B. Z. Dholakiya, *J. Nat. Prod. Plant Resour.*, 2012, **2**, 135–142.

52 D. Chatterjee, N. V. Sadavarte, R. D. Shingte, A. S. More, B. V. Tawade, A. D. Kulkarni, A. B. Ichake, C. V. Avadhani and P. P. Wadgaonkar, in *Cashew Nut Shell Liquid, A Goldfield for Functional Materials*, ed. P. Anilkumar, Springer International Publishing, Cham, 2017, pp. 163–214.

53 M. C. Lubi and E. T. Thachil, *Des. Monomers Polym.*, 2000, **3**, 123–153.

54 P. H. Gedam and P. S. Sampathkumaran, *Prog. Org. Coatings*, 1986, **14**, 115–157.

55 S. Caillol, *Curr. Opin. Green Sustain. Chem.*, 2018, **14**, 26–32.

56 P. Blazdell, *Interdiscip. Sci. Rev.*, 2000, **25**, 220–226.

57 G. Mele and G. Vasapollo, *Mini. Rev. Org. Chem.*, 2008, **5**, 243–253.

58 V. S. Balachandran, S. R. Jadhav, P. K. Vemula and G. John, *Chem. Soc. Rev.*, 2013, **42**, 427–438.

59 C. Voirin, S. Caillol, N. V. Sadavarte, B. V. Tawade, B. Boutevin and P. P. Wadgaonkar, *Polym. Chem.*, 2014, **5**, 3142–3162.

60 J. H. P. Tyman, D. Wilczynski and M. A. Kashani, *J. Am. Oil Chem. Soc.*, 1978, **55**, 663–668.

61 M. T. S. Trevisan, B. Pfundstein, R. Haubner, G. Würtele, B. Spiegelhalder, H. Bartsch and R. W. Owen, *Food Chem. Toxicol.*, 2006, **44**, 188–197.

62 Cardolite, https://www.cardolite.com/, (accessed September 19, 2018).

63 A. J. Varma and S. Sivaram, US6451957B1, 2002.

64 N. V. Sadavarte, Ph. D. Thesis, University of Pune, 2012.

65 B. V. Tawade, J. K. Salunke, P. S. Sane and P. P. Wadgaonkar, *J. Polym. Res.*, 2014, **21**, 617.

66 B. V. Tawade, S. V. Shaligram, N. G. Valsange, U. K. Kharul and P. P. Wadgaonkar, *Polym. Int.*, 2016, **65**, 567–576.

67 B. V. Tawade, Ph. D. Thesis, Savitribai Phule Pune University, 2014.

68 H. P. Bhunia, R. N. Jana, A. Basak, S. Lenka and G. B. Nando, *J. Polym. Sci. Part A Polym. Chem.*, 1998, **36**, 391–400.

69 H. P. Bhunia, A. Basak, T. K. Chaki and G. B. Nando, *Eur. Polym. J.*, 2000, **36**, 1157–1165.

70 R. D. Shingte, Ph. D. Thesis, University of Pune, 2006.

71 C. V. Avadhani, P. P. Wadgaonkar and S. Sivaram, US6255439B1, 2001.

72 A. S. More, S. K. Pasale, P. N. Honkhambe and P. P. Wadgaonkar, *J. Appl. Polym. Sci.*, 2011, **121**, 3689–3695.

73 A. S. More, P. V. Naik, K. P. Kumbhar and P. P. Wadgaonkar, *Polym. Int.*, 2010, **59**, 1408–1414.

74 A. S. More and P. P. Wadgaonkar, US7446234B2, 2008.

75 A. S. More, Ph. D. Thesis, University of Pune, 2009.

76 G. A. Bhavsar and S. K. Asha, *Chem. - A Eur. J.*, 2011, **17**, 12646–12658.

77 M. Ramasri, G. S. Srinivasa Rao, P. S. Sampatkumaran and M. M. Shirsalkar, *Indian J. Chem.*, 1987, **26B**, 683–684.

78 N. V. Sadavarte, M. R. Halhalli, C. V. Avadhani and P. P. Wadgaonkar, *Eur. Polym. J.*, 2009, **45**, 582–589.

79 N. V. Sadavarte, C. V. Avadhani and P. P. Wadgaonkar, *High Perform. Polym.*, 2011, **23**, 494–505.

80 N. D. Ghatge and N. N. Maldar, *Polymer*, 1984, **25**, 1353–1356.

81 J. S. Mathew, S. P. Vernekar, R. Mercier and R. Kerboua, US6500913B2, 2002.

82 J. S. Mathew, Ph. D. Thesis, University of Pune, 2001.

83 A. S. More, P. S. Sane, A. S. Patil and P. P. Wadgaonkar, *Polym. Degrad. Stab.*, 2010, **95**, 1727–1735.

84 R. D. Shingte and P. P. Wadgaonkar, US6790993B1, 2004.

85 N. V. Sadavarte, C. V. Avadhani, P. V. Naik and P. P. Wadgaonkar, *Eur. Polym. J.*, 2010, **46**, 1307–1315.

86 B. V. Tawade, A. D. Kulkarni and P. P. Wadgaonkar, *Polym. Int.*, 2015, **64**, 1770–1778.

87 A. S. Jadhav, S. P. Vernekar and N. N. Maldar, *Polym. Int.*, 1993, **32**, 5–11.

88 A. S. More, S. K. Pasale and P. P. Wadgaonkar, *Eur. Polym. J.*, 2010, **46**, 557–567.

89 N. V. Sadavarte, S. S. Patil, C. V. Avadhani and P. P. Wadgaonkar, *High Perform. Polym.*, 2013, **25**, 735–743.

90 A. S. More, A. S. Patil and P. P. Wadgaonkar, *Polym. Degrad. Stab.*, 2010, **95**, 837–844.

91 A. S. More, S. K. Menon and P. P. Wadgaonkar, *J. Appl. Polym. Sci.*, 2012, **124**, 1281–1289.

92 S. Seo, Y. Kim, J. You, B. D. Sarwade, P. P. Wadgaonkar, S. K. Menon, A. S. More and E. Kim, *Macromol. Rapid Commun.*, 2011, **32**, 637–643.

93 A. Cyriac, S. R. Amrutha and M. Jayakannan, *J. Polym. Sci. Part A Polym. Chem.*, 2008, **46**, 3241–3256.

94 C. K. S. Pillai, D. C. Sherrington and A. Sneddon, *Polymer*, 1992, **33**, 3968–3970.

95 S. Abraham, V. Prasad, C. Pillai and M. Ravindranathan, *Polym. Int.*, 2002, **51**, 475–480.

96 D. G. Lee and V. S. Chang, *J. Org. Chem.*, 1978, **43**, 1532–1536.

97 R. H. Grubbs, *Tetrahedron*, 2004, **60**, 7117–7140.

98 D. Astruc, *New J. Chem.*, 2005, **29**, 42–56.

99 R. H. Grubbs, *Adv. Synth. Catal.*, 2007, **349**, 34–40.

100 F. Martina, Ph. D. Thesis, University of Salento, 2008.

101 G. Vasapollo, G. Mele and R. Del Sole, *Molecules*, 2011, **16**, 6871–6882.

102 E. Bloise, L. Carbone, G. Colafemmina, L. D'Accolti, S. E. Mazzetto, G. Vasapollo and G. Mele, *Molecules*, 2012, **17**, 12252–12261.

103 O. A. Attanasi, G. Ciccarella, P. Filippone, G. Mele, J. Spadavecchia and G. Vasapollo, *J. Porphyr. Phthalocyanines*, 2003, **07**, 52–57.

104 J. E. Mgaya, S. A. Bartlett, E. B. Mubofu, Q. A. Mgani, A. M. Z. Slawin, P. J. Pogorzelec and D. J. Cole-Hamilton, *ChemCatChem*, 2016, **8**, 751–757.

105 P. E. Cassidy, *Thermally stable polymers*, Marcel Dekker, New York, 1980.

106 P. M. Hergenrother, *High Perform. Polym.*, 2003, **15**, 3–45.

107 O. J. Dautel, G. Wantz, D. Flot, J.-P. Lere-Porte, J. J. E. Moreau, J.-P. Parneix, F. Serein-Spirau and L. Vignau, *J. Mater. Chem.*, 2005, **15**, 4446–4452.

108 M.-S. Jung, T.-W. Lee, J. Hyeon-Lee, B. Hee Sohn and I.-S. Jung, *Polymer*, 2006, **47**, 2670–2676.

109 A. Kausar, S. Zulfiqar, Z. Ahmad and M. Ilyas Sarwar, *Polym. Degrad. Stab.*, 2010, **95**, 2611–2618.

110 M. Rubal, C. W. Wilkins, P. E. Cassidy, C. Lansford and Y. Yamada, *Polym. Adv. Technol.*, 2008, **19**, 1033–1039.

111 B. Zhang, W. Li, J. Yang, Y. Fu, Z. Xie, S. Zhang and L. Wang, *J. Phys. Chem. C*, 2009, **113**, 7898–7903.

112 C. W. Ulmer II, D. A. Smith, B. G. Sumpter and D. I. Noid, *Comput. Theor. Polym. Sci.*, 1998, **8**, 311–321.

113 A. P. Dove and M. A. R. Meier, *Macromol. Chem. Phys.*, 2014, **215**, 2135–2137.

114 K. L. Mittal, *Polyimides and Other High Temperature Polymers: Synthesis, Characterization and Applications.*, CRC Press, Taylor and Francis group, Boca

Raton, 2001.

115 W. Volksen, in *High Performance Polymers*, Springer-Verlag, Berlin/Heidelberg, 1994, pp. 111–164.

116 D. Wilson, D. Stenzenberger, Horst and P. M. Hergenrother, *Polyimides*, Springer Netherlands, Dordrecht, 1990.

117 M. Sato, in *Handbook of Thermoplastics*, ed. O. Olabisi, 1997, p. 665.

118 H. Yeganeh, B. Tamami and I. Ghazi, *Eur. Polym. J.*, 2004, **40**, 2059–2064.

119 Y. Imai and K. Kojima, *J. Polym. Sci. Part A-1 Polym. Chem.*, 1972, **10**, 2091–2096.

120 S. Di Bella, G. Consiglio, N. Leonardi, S. Failla, P. Finocchiaro and I. Fragalà, *Eur. J. Inorg. Chem.*, 2004, **2004**, 2701–2705.

121 R. Gheneim, C. Perez-Berumen and A. Gandini, *Macromolecules*, 2002, **35**, 7246–7253.

122 J. H. Chi, G. J. Shin, Y. S. Kim and J. C. Jung, *J. Appl. Polym. Sci.*, 2007, **106**, 3823–3832.

123 D. M. Muñoz, J. G. de la Campa, J. de Abajo and A. E. Lozano, *Macromolecules*, 2007, **40**, 8225–8232.

124 H. H. Yang, *Aromatic High-Strength Fibers*, Wiley Interscience, New York, 1989.

125 J. K. Fink, *High Performance Polymers*, William Andrew Inc., Burlington, 2008.

126 L. Volbracht, in *Comprehensive Polymer Science Vol 5*, eds. G. Allen, B. Bevington, G. V Eastmond, A. Ledwith, S. Russo and P. Sigwald, Pergamon Press, Oxford, 1989, p. 373.

127 M. Grigoras and C. O. Catanescu, *J. Macromol. Sci. Part C Polym. Rev.*, 2004, **44**, 131–173.

128 M. Grigoras and L. Stafie, *Des. Monomers Polym.*, 2009, **12**, 177–196.

129 M. Bagheri and A. Entezami, *Eur. Polym. J.*, 2002, **38**, 317–326.

130 P. K. Dutta, P. Jain, P. Sen, R. Trivedi, P. K. Sen and J. Dutta, *Eur. Polym. J.*, 2003, **39**, 1007–1011.

131 S. C. Suh and S. C. Shim, *Synth. Met.*, 2000, **114**, 91–95.

132 D. Sek, A. Iwan, B. Jarzabek, B. Kaczmarczyk, J. Kasperczyk, Z. Mazurak, M. Domanski, K. Karon and M. Lapkowski, *Macromolecules*, 2008, **41**, 6653–6663.

133 A. Iwan and D. Sek, *Prog. Polym. Sci.*, 2008, **33**, 289–345.

134 P. W. Morgan, S. L. Kwolek and T. C. Pletcher, *Macromolecules*, 1987, **20**, 729–739.

135 W. E. Rudzinski, S. R. Guthrie and P. E. Cassidy, *J. Polym. Sci. Part A Polym. Chem.*, 1988, **26**, 1677–1680.

136 S. Banerjee, P. K. Gutch and C. Saxena, *J. Polym. Sci. Part A Polym. Chem.*, 1995, **33**, 1719–1725.

137 K. H. Park, T. Tani, M. Kakimoto and Y. Imai, *Macromol. Chem. Phys.*, 1998, **199**, 1029–1033.

138 V. Jansons and K. Dahl, *Makromol. Chemie. Macromol. Symp.*, 1991, **51**, 87–101.

139 Y. Iwakura, K. Uno and T. Takiguchi, *J. Polym. Sci. Part A-1 Polym. Chem.*, 1968, **6**, 3345–3355.

140 M. Ueda and M. Sato, *Macromolecules*, 1987, **20**, 2675–2678.

141 B. M. Marks, US3441538, 1969.

142 B. E. Jennings, M. E. B. Jones and J. B. Rose, *J. Polym. Sci. Part C Polym. Symp.*, 1967, **16**, 715–724.

143 H. R. Kricheldorf and G. Bier, *Polymer*, 1984, **25**, 1151–1156.

144 P. M. Hergenrother, B. J. Jensen and S. J. Havens, *Polymer*, 1988, **29**, 358–369.

145 H. R. Kricheldorf and G. Bier, *J. Polym. Sci. Polym. Chem. Ed.*, 1983, **21**, 2283–2289.

146 R. N. Johnson, A. G. Farnham, R. A. Clendinning, W. F. Hale and C. N. Merriam, *J. Polym. Sci. Part A-1 Polym. Chem.*, 1967, **5**, 2375–2398.

147 F. Liu, J. Ding, M. Li, M. Day, G. Robertson and M. Zhou, *Macromol. Rapid Commun.*, 2002, **23**, 844–848.

148 V. Percec, R. S. Clough, M. Grigoras, P. L. Rinaldi and V. E. Litman, *Macromolecules*, 1993, **26**, 3650–3662.

149 K. Maeyama and S. Ito, *Polym. Bull.*,2018 , DOI:10.1007/s00289-018-2347-5.

150 V. Percec, M. Grigoras, R. S. Clough and J. Fanjul, *J. Polym. Sci. Part A Polym. Chem.*, 1995, **33**, 331–344.

151 S. K. Park and S. Y. Kim, *Macromolecules*, 1998, **31**, 3385–3387.

152 V. Percec, R. S. Clough, P. L. Rinaldi and V. E. Litman, *Macromolecules*, 1991,

24, 5889–5892.

153 J. W. Labadie, J. L. Hedrick and M. Ueda, in *Step-Growth Polymers for High-Performance Materials*, eds. J. L. Hedrick and J. W. Labadie, American Chemical Society, Washington, DC, 1996, pp. 210–225.

154 P. T. McGrail, *Polym. Int.*, 1996, **41**, 103–121.

155 J. Ding, X. Du, M. Day, J. Jiang, C. L. Callender and J. Stupak, *Macromolecules*, 2007, **40**, 3145–3153.

156 A. Ben-Haida, H. M. Colquhoun, P. Hodge and D. J. Williams, *Macromolecules*, 2006, **39**, 6467–6472.

157 R. H. Friend, R. W. Gymer, A. B. Holmes, J. H. Burroughes, R. N. Marks, C. Taliani, D. D. C. Bradley, D. A. Dos Santos, J. L. Brédas, M. Lögdlund and W. R. Salaneck, *Nature*, 1999, **397**, 121–128.

158 K. Lee, J. Y. Kim, S. H. Park, S. H. Kim, S. Cho and A. J. Heeger, *Adv. Mater.*, 2007, **19**, 2445–2449.

159 Y. Shao, G. C. Bazan and A. J. Heeger, *Adv. Mater.*, 2008, **20**, 1191–1193.

160 Y. Shao, X. Gong, A. J. Heeger, M. Liu and A. K. Y. Jen, *Adv. Mater.*, 2009, **21**, 1972–1975.

161 G. Yu, J. Gao, J. C. Hummelen, F. Wudl and A. J. Heeger, *Science*, 1995, **270**, 1789–1791.

162 C. J. Brabec, N. S. Sariciftci and J. C. Hummelen, *Adv. Funct. Mater.*, 2001, **11**, 15–26.

163 G. Li, V. Shrotriya, J. Huang, Y. Yao, T. Moriarty, K. Emery and Y. Yang, *Nat. Mater.*, 2005, **4**, 864–868.

164 M.-H. Chen, J. Hou, Z. Hong, G. Yang, S. Sista, L.-M. Chen and Y. Yang, *Adv. Mater.*, 2009, **21**, 4238–4242.

165 J. Hou, T. L. Chen, S. Zhang, L. Huo, S. Sista and Y. Yang, *Macromolecules*, 2009, **42**, 9217–9219.

166 L. Huo, J. Hou, S. Zhang, H.-Y. Chen and Y. Yang, *Angew. Chemie Int. Ed.*, 2010, **49**, 1500–1503.

167 S. Sista, Z. Hong, M.-H. Park, Z. Xu and Y. Yang, *Adv. Mater.*, 2010, **22**, E77–E80.

168 B. Yao, J. Zhang and X. Wan, in *Electrochromic Materials and Devices*, Wiley-VCH Verlag GmbH & Co. KGaA, Weinheim, Germany, 2015, vol. 44, pp. 211–240.

169 A. Iwan and D. Sek, *Prog. Polym. Sci.*, 2011, **36**, 1277–1325.

170 T. Abidin, Q. Zhang, K.-L. Wang and D.-J. Liaw, *Polymer*, 2014, **55**, 5293–5304.

171 H.-J. Yen and G.-S. Liou, *Polym. Chem.*, 2018, **9**, 3001–3018.

172 H.-J. Yen and G.-S. Liou, *Polym. Chem.*, 2012, **3**, 255–264.

173 H.-J. Yen and G.-S. Liou, *Polym. J.*, 2016, **48**, 117–138.

174 W.-P. Lin, S.-J. Liu, T. Gong, Q. Zhao and W. Huang, *Adv. Mater.*, 2014, **26**, 570–606.

175 T. Kurosawa, T. Higashihara and M. Ueda, *Polym. Chem.*, 2013, **4**, 16–30.

176 S.-H. Hsiao, G.-S. Liou, Y.-C. Kung, H.-Y. Pan and C.-H. Kuo, *Eur. Polym. J.*, 2009, **45**, 2234–2248.

177 H.-M. Wang and S.-H. Hsiao, *J. Polym. Sci. Part A Polym. Chem.*, 2014, **52**, 1172–1184.

178 S.-H. Hsiao, Y.-H. Hsiao and Y.-R. Kung, *J. Electroanal. Chem.*, 2016, **764**, 31–37.

179 J. Li and A. C. Grimsdale, *Chem. Soc. Rev.*, 2010, **39**, 2399–2410.

180 S.-H. Hsiao, S.-C. Peng, Y.-R. Kung, C.-M. Leu and T.-M. Lee, *Eur. Polym. J.*, 2015, **73**, 50–64.

181 J. Wang, K. Liu, L. Ma and X. Zhan, *Chem. Rev.*, 2016, **116**, 14675–14725.

182 Z. Ning and H. Tian, *Chem. Commun.*, 2009, **0**, 5483–5495.

183 Q.-D. Ling, F.-C. Chang, Y. Song, C.-X. Zhu, D.-J. Liaw, D. S.-H. Chan, E.-T. Kang and K.-G. Neoh, *J. Am. Chem. Soc.*, 2006, **128**, 8732–8733.

184 T. J. Lee, Y.-G. Ko, H.-J. Yen, K. Kim, D. M. Kim, W. Kwon, S. G. Hahm, G.-S. Liou and M. Ree, *Polym. Chem.*, 2012, **3**, 1276–1283.

185 D. M. Kim, S. Park, T. J. Lee, S. G. Hahm, K. Kim, J. C. Kim, W. Kwon and M. Ree, *Langmuir*, 2009, **25**, 11713–11719.

186 D. M. Kim, Y.-G. Ko, J. K. Choi, K. Kim, W. Kwon, J. Jung, T.-H. Yoon and M. Ree, *Polymer*, 2012, **53**, 1703–1710.

187 C.-J. Chen, H.-J. Yen, W.-C. Chen and G.-S. Liou, *J. Mater. Chem.*, 2012, **22**,

14085–14093.

188 L. Shi, H. Ye, W. Liu, G. Tian, S. Qi and D. Wu, *J. Mater. Chem. C*, 2013, **1**, 7387–7399.

189 C.-J. Chen, H.-J. Yen, Y.-C. Hu and G.-S. Liou, *J. Mater. Chem. C*, 2013, **1**, 7623–7634.

190 H.-J. Yen, C.-L. Tsai, S.-H. Chen and G.-S. Liou, *Macromol. Rapid Commun.*, 2017, **38**, 1600715.

191 C.-J. Chen, Y.-C. Hu and G.-S. Liou, *Polym. Chem.*, 2013, **4**, 4162–4171.

192 C.-J. CHen, H.-J. Yen, W.-C. Chen and G.-S. Liou, *J. Polym. Sci. Part A Polym. Chem.*, 2011, **49**, 3709–3718.

193 H.-J. Yen, J.-H. Chang, J.-H. Wu and G.-S. Liou, *Polym. Chem.*, 2015, **6**, 7758–7763.

194 B. Hu, X. Zhu, X. Chen, L. Pan, S. Peng, Y. Wu, J. Shang, G. Liu, Q. Yan and R.-W. Li, *J. Am. Chem. Soc.*, 2012, **134**, 17408–17411.

195 W. Zhang, C. Wang, G. Liu, J. Wang, Y. Chen and R.-W. Li, *Chem. Commun.*, 2014, **50**, 11496–11499.

CHAPTER 2

Scope and Objectives

Polymers comprise such an important part of our life, that all the comforts of modern life would be inconceivable in their absence. Synthetic polymers are strongly and positively linked to sustainability (e.g., reduced fuel costs due to lower transportation weight, food packaging which prevents spoilage, etc). Modern synthetic polymers, in reality, form a conduit for us to experience modern technology. However, a major issue regarding synthetic polymers is the fact that they are derived from petrochemical sources.[1] Today, ~ 8 % of the oil produced annually is utilised for the production of synthetic polymers.[2,3] It has been projected that this number would rise to almost 20 % by 2050. This statistic is worrisome due to the impending problems of energy security and the rising environmental costs of polymer manufacture and disposal.[4] The problem stems from the simple fact that the time scale during which petroleum forms is much slower than the service life of the manufactured polymers.[5–8] Regardless of the present abundance and competitive cost of oil available today, it would be erroneous to be lulled into a false state of security. In the face of rising costs of fossil resources and upcoming government policies incentivising a low carbon footprint, it is advisable to explore the renewable carbon sources embodied in abundant biomass, before a crisis point is breached. Amongst various approaches currently being pursued in academia and industries, is the concept of biorefinery, which refers to the sustainable processing of biomass into a spectrum of marketable products.[9] Exploration of abundantly available biomass and its valorisation into useful platform chemicals is an attractive concept.[10–13] The utilisation of non-edible biomass is prudent to avoid stressing the food industry.[14,15] Non-edible bio-derived chemicals include lignins, tannins, natural phenols, etc, which are being actively investigated for the synthesis of monomers and polymers.[2,14,16–22]

Majority of the reported bio-based polymers are generally aliphatic or semi-aromatic in nature.[23] High performance polymers, such as aromatic polyamides, polyimides, polyazomethines etc are endowed with excellent thermo-oxidative stability, mechanical strength, good electrical properties and solvent resistance.[24] It is therefore of interest to develop bio-based aromatic monomers which would be suitable for the synthesis of high performance polymers. Cashew nut shell liquid (CNSL) comprises an important source of aromatic chemicals which totally fits the bill as a source for bio-derived chemicals suitable for the synthesis of high performance polymers. CNSL is a

natural phenol (as enumerated in **Chapter 1**) and by-product of the cashew processing industry.[25,26] CNSL provides a 15-carbon alkyl chain as a natural gift, along with a phenolic functionality positioned (1,3) to the alkyl chain, which is difficult to attain from petrochemical sources. Thus, the synthesis of difunctional monomers from CNSL and the preparation of polymers has proven to be a profitable pursuit.[12,27–35] The present work builds on this concept. The following graphic (**Fig 2.1**) captures the theme of the present thesis.

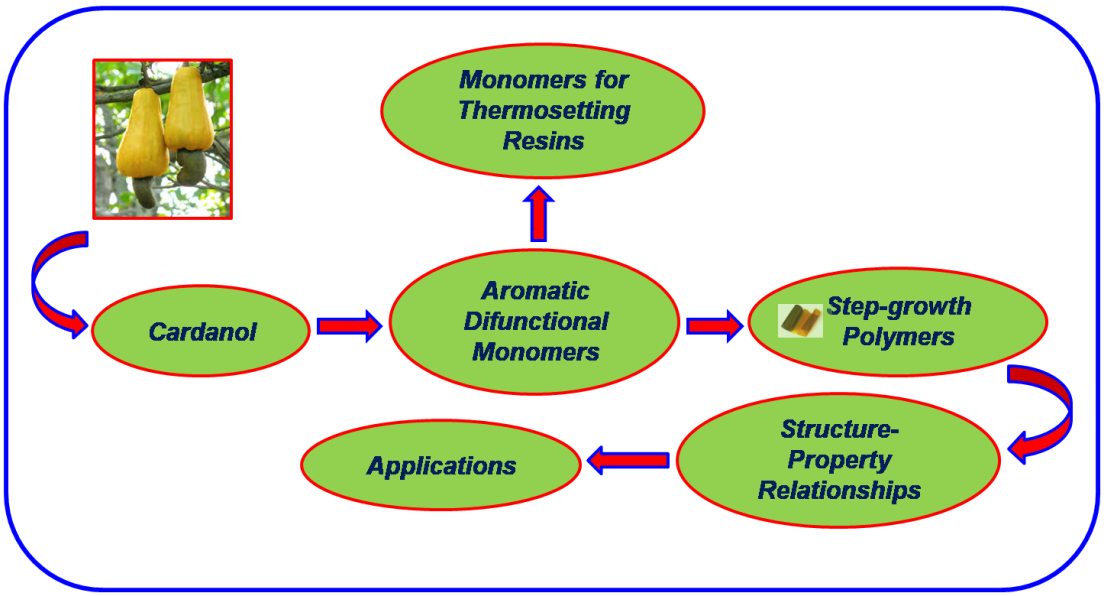

Figure 2.1 The theme of the thesis

The overall objectives of this thesis are firstly, to synthesise partially bio-based difunctional monomers starting from 3-pentadecyl phenol (which is derived from CNSL). Secondly, our objective is to synthesise a novel aromatic diamine from 3-pentadecyl phenol with an in-built triarylamine moiety. The triarylamine moiety is expected to impart interesting hole transporting and donor-acceptor properties to the synthesised polymers.[36–39] Another objective is to incorporate the flexible 15-carbon hydrocarbon chain pendent to the polymer backbone. The flexibilising nature and packing disruptive effect of the pentadecyl chain is expected to improve solubility and processability of synthesised high performance polymers, besides imparting other interesting properties.[24,40]

The specific objectives of the present thesis are:

1. The design and synthesis of aromatic difunctional monomers, *viz.* aromatic diamines, diacid, dialdehyde and bisphenol starting from CNSL.

2. The design and synthesis of triarylamine-containing diamine starting from 3-pentadecyl phenol.

3. The design and synthesis of bispropargyl ethers and bisphthalonitriles starting from 3-pentadecyl phenol.

4. Synthesis of partially bio-based triarylamine-containing polymers such as polyimides, polyamides and polyazomethines.

5. Exploration of triarylamine-containing polyimides, polyamides and polyazomethines for memory device applications.

6. Synthesis of aromatic polyimides, poly(arylene ether)s and polycarbonates containing pendent pentadecyl chains and study of the effect of incorporation of pentadecyl chains on polymer properties.

References

1 Y. Xu, M. A. Hanna and L. Isom, *Open Agric. J.*, 2008, **2**, 54–61.

2 D. K. Schneiderman and M. A. Hillmyer, *Macromolecules*, 2017, **50**, 3733–3749.

3 J. Hopewell, R. Dvorak and E. Kosior, *Philos. Trans. R. Soc. B Biol. Sci.*, 2009, **364**, 2115–2126.

4 S. C. Finney and L. E. Edwards, *GSA Today*, 2016, **26**, 4–10.

5 R. A. Berner, *Nature*, 2003, **426**, 323–326.

6 J. D. Brooks and J. W. Smith, *Geochim. Cosmochim. Acta*, 1969, **33**, 1183–1194.

7 F. D. Mango, *Org. Geochem.*, 1997, **26**, 417–440.

8 B. P. Tissot and D. H. Welte, *Petroleum Formation and Occurrence*, Springer Berlin Heidelberg, Berlin, Heidelberg, Heidelberg, 1984.

9 E. de Jong and G. Jungmeier, in *Industrial Biorefineries & White Biotechnology*, Elsevier, 2015, pp. 3–33.

10 M. FitzPatrick, P. Champagne, M. F. Cunningham and R. A. Whitney, *Bioresour. Technol.*, 2010, **101**, 8915–8922.

11 S. N. Naik, V. V. Goud, P. K. Rout and A. K. Dalai, *Renew. Sustain. Energy Rev.*, 2010, **14**, 578–597.

12 M. Stöcker, *Angew. Chemie Int. Ed.*, 2008, **47**, 9200–9211.

13 C. Williams and M. Hillmyer, *Polym. Rev.*, 2008, **48**, 1–10.

14 R. Mülhaupt, *Macromol. Chem. Phys.*, 2013, **214**, 159–174.

15 R. Mülhaupt, *Angew. Chemie Int. Ed.*, 2004, **43**, 1054–1063.

16 A. Gandini and T. M. Lacerda, *Prog. Polym. Sci.*, 2015, **48**, 1–39.

17 C. Vilela, A. F. Sousa, A. C. Fonseca, A. C. Serra, J. F. J. Coelho, C. S. R. Freire and A. J. D. Silvestre, *Polym. Chem.*, 2014, **5**, 3119–3141.

18 A. Gandini, T. M. Lacerda, A. J. F. Carvalho and E. Trovatti, *Chem. Rev.*, 2016, **116**, 1637–1669.

19 A. F. Sousa, C. Vilela, A. C. Fonseca, M. Matos, C. S. R. Freire, G.-J. M. Gruter, J. F. J. Coelho and A. J. D. Silvestre, *Polym. Chem.*, 2015, **6**, 5961–5983.

20 M. A. Hillmyer, *Science*, 2017, **358**, 868–870.

21 S. A. Miller, *ACS Macro Lett.*, 2013, **2**, 550–554.

22 B. Gyarmati and B. Pukánszky, *Eur. Polym. J.*, 2017, **93**, 612–617.

23 H. T. H. Nguyen, P. Qi, M. Rostagno, A. Feteha and S. A. Miller, *J. Mater. Chem. A*, 2018, **6**, 9298–9331.

24 P. M. Hergenrother, *High Perform. Polym.*, 2003, **15**, 3–45.

25 M. T. Harvey and S. Caplan, *Ind. Eng. Chem.*, 1940, **32**, 1306–1310.

26 R. Paramashivappa, P. P. Kumar, P. J. Vithayathil and A. S. Rao, *J. Agric. Food Chem.*, 2001, **49**, 2548–2551.

27 C. Voirin, S. Caillol, N. V. Sadavarte, B. V. Tawade, B. Boutevin and P. P. Wadgaonkar, *Polym. Chem.*, 2014, **5**, 3142–3162.

28 D. Chatterjee, N. V. Sadavarte, R. D. Shingte, A. S. More, B. V. Tawade, A. D. Kulkarni, A. B. Ichake, C. V. Avadhani and P. P. Wadgaonkar, in *Cashew Nut Shell Liquid, A Goldfield for Functional Materials*, ed. P. Anilkumar, Springer International Publishing, Cham, 2017, pp. 163–214.

29 B. Lochab, S. Shukla and I. K. Varma, *RSC Adv.*, 2014, **4**, 21712–21752.

30 M. C. Lubi and E. T. Thachil, *Des. Monomers Polym.*, 2000, **3**, 123–153.

31 P. H. Gedam and P. S. Sampathkumaran, *Prog. Org. Coatings*, 1986, **14**, 115–157.

32 P. Blazdell, *Interdiscip. Sci. Rev.*, 2000, **25**, 220–226.

33 G. Mele and G. Vasapollo, *Mini. Rev. Org. Chem.*, 2008, **5**, 243–253.

34 V. S. Balachandran, S. R. Jadhav, P. K. Vemula and G. John, *Chem. Soc. Rev.*,

2013, **42**, 427–438.

35 S. Caillol, *Curr. Opin. Green Sustain. Chem.*, 2018, **14**, 26–32.

36 H.-J. Yen and G.-S. Liou, *Polym. Chem.*, 2018, **9**, 3001–3018.

37 S. Gong, M. Liu, S. Xia and Y. Wang, *J. Polym. Res.*, 2014, **21**, 542.

38 Q.-D. Ling, F.-C. Chang, Y. Song, C.-X. Zhu, D.-J. Liaw, D. S.-H. Chan, E.-T. Kang and K.-G. Neoh, *J. Am. Chem. Soc.*, 2006, **128**, 8732–8733.

39 D. M. Kim, S. Park, T. J. Lee, S. G. Hahm, K. Kim, J. C. Kim, W. Kwon and M. Ree, *Langmuir*, 2009, **25**, 11713–11719.

40 A. P. Dove and M. A. R. Meier, *Macromol. Chem. Phys.*, 2014, **215**, 2135–2137.

CHAPTER 3

Synthesis and Characterisation of Monomers Starting from CNSL

3.1 Introduction

Step-growth polymers contribute significantly to the present "Age of Polymers".[1–3] Step-growth polymers such as polyimides, polyamides, polyesters, etc possess attractive and useful properties which include good mechanical properties, superior toughness, stiffness and high temperature resistance, when contrasted with polymers derived from addition polymerisation. Step-growth polymers find applications in automobiles, packaging, textiles, etc as fibres, resins and so on.[4] Applications of step-growth polymers depend on polymer properties, which, in turn, can be tuned most commonly by varying the monomer structure.[5] Several examples exist in literature dealing with modification of polymer properties, *viz*., T_g, T_m, solubility, etc, for the purpose of improving polymer processability[2,6] through the logical design and synthesis of difunctional monomers. In the past few decades, step-growth polymers are increasingly being investigated for applications in emerging fields such as optoelectronics, especially for organic light emitting devices,[7–9] solar cells,[10–16] electrochromic devices[17–21] and memory devices.[22–25] Incorporation of the triarylamine moiety either in the polymer backbone or as a pendent through synthesis of triarylamine-based difunctional monomers, constitutes a significant strategy for the development of step-growth polymers for emerging applications.

The sizeable chemical industry, of which polymers form a significant part, consumes majorly fossil feedstocks, in the form of oil and gas. However, continued indefinite dependence on non-renewable fossil feedstocks is not prudent due to impending fossil fuel depletion, non-renewability and environmental issues.[26–28] Hence, considerable research efforts have been expended towards the exploration of biomass, such as starch, cellulose, terpenes, lignins, cashew nut shell liquid (CNSL), and so on,[29–34] as a source for obtaining monomers and polymers. A plethora of difunctional monomers useful for the synthesis of semi-aromatic polymers have been reported.[33,35–37] Cashew nut shell liquid (CNSL), belonging to the class of natural phenols, is an attractive starting material for obtaining aromatic difunctional monomers.

In the present work, a range of monomers (**Tables 3.1 and 3.2**) such as diamines, diacid, dialdehyde, bisphenol, bispropargyl ethers, etc have been designed and synthesised starting from CNSL. Additionally, a diamine incorporating triarylamine

moiety was also developed from CNSL, with a view towards developing partially bio-based polymers for optoelectronic applications.

Table 3.1 Difunctional condensation monomers starting from CNSL

Sr. No.	Monomer Structure	Monomer
1.	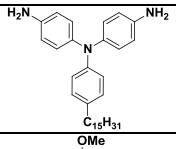	4, 4'-Diamino-4"pentadecyltriphenylamine
2.	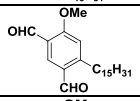	4-Methoxy-6-pentadecylisophthalaldehyde
3.	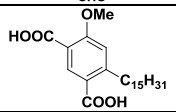	4-Methoxy-6-pentadecylisophthalic acid
4.	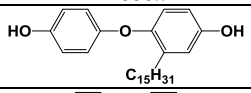	4-(4-Hydroxyphenoxy)-3-pentadecylphenol
5.	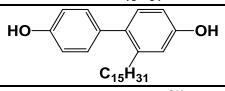	2-Pentadecyl-[1,1'-biphenyl]-4,4'-diol
6.	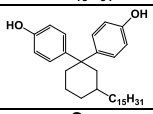	4,4'-(3-Pentadecylcyclohexane-1,1-diyl)diphenol
7.	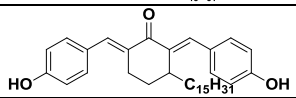	2,6-Bis(4-hydroxybenzylidene)-3-pentadecylcyclohexanone
8.	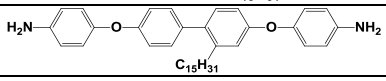	4,4'-((2-Pentadecyl-[1,1'-biphenyl]-4,4'-diyl)bis(oxy))dianiline

Table 3.2 Monomers for thermosetting resins starting from CNSL

Sr. No.	Monomer Structure	Monomer
1.	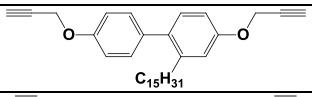	2-Pentadecyl-4,4'-bis(prop-2-yn-1-yloxy)-1,1'-biphenyl
2.	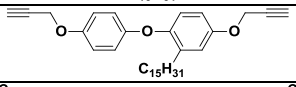	2-Pentadecyl-4-(prop-2-yn-1-yloxy)-1-(4-(prop-2-yn-1-yloxy)phenoxy)benzene
3.	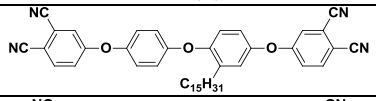	4-(4-(4-(3,4-Dicyanophenoxy)-2-pentadecylphenoxy)phenoxy)phthalonitrile
4.	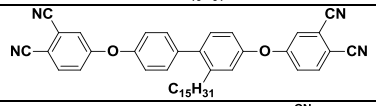	4,4'-((2-Pentadecyl-[1,1'-biphenyl]-4,4'-diyl)bis(oxy))diphthalonitrile
5.	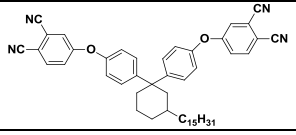	4,4'-(((3-Pentadecylcyclohexane-1,1-diyl)bis(4,1-phenylene))bis(oxy))diphthalonitrile

3.2 Experimental

3.2.1 Materials

Palladium-charcoal (10 wt %, on activated charcoal), 5% Ru/C, 4-fluoro nitro benzene, 4-chloronitrobenzene, 3-pentadecyl phenol, diisobutylaluminiumhydride, *N*-bromosuccinimide, 4-methoxy phenyl boronic acid, tetrakis(triphenyl phosphine)palladium, 3-mercaptopropionic acid, pyridinium chlorochromate, 4-hydroxybenzaldehyde, propargyl bromide (Sigma Aldrich, India), 4-nirophthalonitrile, 4-methoxy phenol (Alfa Aesar, India), ammonium acetate, methanol, potassium hydroxide, hydrazine hydrate (99%), sodium bicarbonate, sodium chlorite, sodium dihydrogen orthophosphate, hydrogen peroxide (30%), potassium carbonate, methanol, hydrochloric acid, glacial acetic acid, hexane, potassium iodide (Thomas Baker, India), fuming nitric acid, methyl iodide (Avra, India),boron tribromide (1M solution in DCM) (Spectrochem, India), absolute ethanol (Himedia, India), sodium hydroxide (SRL, India) and liquid bromine (Loba Chemie), were used as received. Magnesium metal (Loba Chemie, India) was used after activation.[38] Cesium fluoride (Acros, India) was dried at 180 °C under vacuum for 8 h before use.[39] Copper sulphate pentahydrate (Thomas Baker, India) was converted to anhydrous copper sulphate by heating at 250 °C for 12 h in a furnace. Dichloromethane, acetonitrile, dimethyl sulfoxide and *N*, *N* dimethylformamide (Thomas Baker, India) were used after distillation over calcium hydride. Methanesulfonyl chloride (Loba Chemie, India) and triethylamine (Thomas Baker, India) were distilled before use. Zeolite H-β (Si:Al = 28.5 surface area 540 m^2/g, particle size 0.5–1.0 lm, bulk density 0.55 g/cc) was synthesised in CSIR-National Chemical Laboratory.[40] Pentadecyl benzene was synthesised from CNSL according to the reported procedure.[41]

3.2.2 Measurements

Melting points were recorded on Electrothermal MEL-TEMP. Melting points of certain low melting compounds were determined by DSC from the first heating run on TA Q-100 instrument with sample heating rate of 10 °C min^{-1} under nitrogen atmosphere. FT-IR spectra were recorded with ATR mode using Bruker α-T spectrophotometer in the range 4000 to 500 cm^{-1} or on Perkin-Elmer 599B spectrophotometer in chloroform or KBr pellets. ^{1}H-NMR and ^{13}C-NMR spectra were recorded on Bruker-AV 200, 400 or 500 MHz spectrometer using chloroform-*d*, DMSO-d_6 or acetone-d_6 as solvent and TMS

as an internal standard. Elemental analyses were performed on Thermo Finnigan FLASH EA 1112 Series Elemental Analyzer. HRMS were determined on a Thermo Scientific Q-Exacative, with Accela 1250 pump.

3.3 Preparations

3.3.1 Synthesis of 4, 4'-diamino-4''pentadecyltriphenylamine (DPTA)

3.3.1.1 Synthesis of 1-nitro-4-pentadecyl benzene

Into a 250 mL two-necked round bottom flask equipped with a reflux condenser, a guard tube and a magnetic needle were added Zeolite Hβ (1 g) and fuming nitric acid (1.5 mL, 3.45 x 10^{-2} mol) and stirred at 0 °C for 5 minutes. Acetic anhydride (4.5 mL, 4.80 x 10^{-2} mol) was added drop wise into the reaction vessel over a period of 15 minutes to form nitrating mixture, followed by addition of pentadecyl benzene (10 g, 3.45 x 10^{-2} mol) at 0°C, over a period of 30 minutes. The reaction mixture was subsequently stirred at room temperature for 24 h, filtered to remove the zeolite, extracted with ethyl acetate (100 mL), washed successively with saturated sodium bicarbonate (4 x 100 mL), brine (3 x 100 mL) and water (3 x 100 mL) after which the organic layer was separated, dried over anhydrous sodium sulphate and filtered. The crude product was obtained as a mixture of isomers by removing the solvent on a rotary evaporator. Pure 1-nitro-4-pentadecylbenzene was obtained by passing the crude compound through a column of flash silica using petroleum ether (60– 80°C) as an eluent.

Yield = 6.9 g (60 %)

M.P.: 51 °C.

IR (cm^{-1}): 1520 (-NO_2 asymmetric stretch), 1342 (-NO_2 symmetric stretch).

^{1}H-NMR (200 MHz, $CDCl_3$, δ, ppm) 0.87 (s, 3 H, CH_3), 1.13-1.45 (m, 24 H, CH_2), 1.52-1.78 (m., 2 H, CH_2), 2.69 (t, 2H, Ar-CH_2), 7.22 - 7.38 (m, 2 H, Ar-H), 8.12 (d, *J*=8.59 Hz, 2 H, Ar-H)

^{13}C-NMR (50 MHz, $CDCl_3$, δ, ppm) 14.09, 22.67, 28.92 - 29.90, 30.97, 31.90, 35.84, 123.52, 129.11, 146.19, 150.82

3.3.1.2 Synthesis of 4-pentadecylaniline

Into a 250 mL two-necked round bottom flask were charged 1-nitro-4-pentadecylbenzene (15 g, 4.49 x 10^{-2} mol), 10 % Pd/C (0.45 g, 3 wt % of 1-nitro-4-pentadecylbenzene) and absolute ethanol (100 mL). The reaction mixture was heated to

reflux, when hydrazine hydrate (67 mL, 1.347 mol) was added drop wise into the reaction mixture over a period of 15 minutes. The reaction mixture was refluxed for 18 h, filtered to remove Pd/C and extracted with dichloromethane (100 mL). The dichloromethane solution was washed successively with brine (3 x 200 mL) and water (3 x 200 mL). The organic layer was separated, dried over anhydrous sodium sulphate and filtered. The solvent was removed on a rotary evaporator to give the product as a white solid which was dried under reduced pressure at room temperature.

Yield = 10.3 g (76 %)

M.P.: 47 °C.

IR (cm^{-1}): 3400, 3320 and 3220 (-N-H stretch)

^{1}H-NMR (400 MHz, $CDCl_3$, δ, ppm) 0.87 (s, 3H, CH_3), 1.15-1.35 (m., 24 H, CH_2), 1.49-1.63 (m., 2H, CH_2), 2.48 (t, 2 H, Ar-CH_2), 3.52 (br. s., 2 H, O-H), 6.61 (d, *J*=8.28 Hz, 2 H, Ar-H), 6.96 (d, *J*=8.28 Hz, 2 H, Ar-H)

^{13}C-NMR (100 MHz, $CDCl_3$, δ, ppm) 143.96, 133.09, 129.09, 115.17, 35.07, 31.91, 29.67, 29.53, 29.34, 22.67, 14.08

Elemental analysis: (Calcd. for $C_{21}H_{37}N$): C, 83.10; H, 12.29; N, 4.61. Found: C, 82.65; H, 11.98; N, 4.25

3.3.1.3 Synthesis of 4, 4’-dinitro-4''pentadecyltriphenylamine

Into a 100 mL three-necked round bottom flask were taken dry dimethyl sulfoxide (140 mL) and 4-pentadecylaniline (8.3 g, 27.34 x 10^{-3} mol), to which was added caesium fluoride (27.6 g, 18.17 x 10^{-2} mol), under a nitrogen blanket, and the mixture was stirred under continuous nitrogen flow. 4-Fluoro nitro benzene (6.38 mL, 6.01 x10^{-2} mol) was added into the reaction mixture drop wise over a period of 15 minutes. The reaction mixture was then stirred at 120°C under continuous nitrogen flow for 24 h and subsequently poured into ice to precipitate the crude product which was subsequently isolated by filtration. Pure 4, 4’-dinitro-4"pentadecyltriphenylamine was obtained as a bright yellow solid by recrystallisation from glacial acetic acid.

Yield = 9.5 g (64 %)

M. P.: 151 °C

IR (cm^{-1}): 1504 (asymmetric NO_2 stretching), 1328 (symmetric NO_2 stretching).

^{1}H-NMR (400 MHz, $CDCl_3$, δ, ppm) 0.88 (t, 3 H, CH_3), 1.20-1.40 (m, 26 H, CH_2), 1.6-1.7 (m, 2 H, CH_2), 2.64 (t, 2 H, Ar-CH_2), 7.02 - 7.28 (m, 8 H, Ar-H), 8.07 - 8.23 (m, 4 H, Ar-H)

^{13}C-NMR (50 MHz, $CDCl_3$, δ, ppm) 14.10, 22.67, 29.35, 29.47, 29.57, 29.68, 31.33, 31.91, 35.52, 122.06, 125.46, 127.13, 130.42, 142.22, 142.41, 142.55, 151.90

HRMS (m/z) $[M+H]^+$ calculated for $C_{33}H_{44}N_3O_4$, 546.3326; found, 546.3308.

3.3.1.4 Synthesis of 4, 4'-diamino-4''pentadecyltriphenylamine (DPTA)

Into a 100 mL three-necked round bottom flask were added 4, 4'-dinitro-4"pentadecyltriphenylamine (0.5 g, 8.40 x 10^{-4} mol), 10 % Pd/C (0.015 g, 3 wt % of 4, 4'-dinitro-4"pentadecyltriphenylamine) and absolute ethanol (25 mL) and the reaction mixture was heated to reflux. Hydrazine hydrate (2.7 mL, 5.40 x 10^{-2} mol) was added drop wise into the reaction mixture over a period of 15 minutes. Subsequently, the reaction mixture was refluxed for 24 h, filtered to remove Pd/C and extracted with dichloromethane (100 mL). The dichloromethane solution was washed successively with brine (3 x 100 mL) and water (3 x 100 mL). The organic layer was separated, dried over anhydrous sodium sulphate and filtered. The solvent was removed on a rotary evaporator to provide the product as a white solid which was dried under reduced pressure at room temperature.

Yield =0.2 g (76 %)

M. P.: 92 °C

IR (cm^{-1}): 3415, 3320 (N-H stretch), 2917, 2850 (C-H alkyl stretch)

^{1}H-NMR (400 MHz, $CDCl_3$, δ, ppm) 0.89 (s, 3 H, CH_3), 1.17-1.38 (m, 26 H, CH_2), 1.58 (q, 2 H, CH_2), 2.51 (t., 2 H, Ar-CH_2), 3.50 (br. s., 4 H, NH_2), 6.61 (d, *J*=8.24 Hz, 4 H, Ar-H), 6.85 (d, *J*=7.79 Hz, 2 H, Ar-H), 6.89 - 7.01 (m, 6 H, Ar-H)

^{13}C-NMR (100 MHz, $CDCl_3$, δ, ppm) 14.12, 22.67, 29.35, 29.40, 29.54, 29.67, 31.65, 31.90, 35.17, 116.03, 120.46, 126.29, 128.62, 134.57, 139.90, 141.82, 146.68

HRMS (m/z) $[M]^+$ calculated for $C_{33}H_{47}N_3$, 485.3765; found, 485.3755

3.3.2 Synthesis of 4-methoxy-6-pentadecylisophthalaldehyde (MPIAL)

3.3.2.1 Synthesis of 1-methoxy-3-pentadecylbenzene

Into a 1000 mL three- necked round bottom flask equipped with a magnetic stir bar, an addition funnel, a reflux condenser and a guard tube was added 3-

pentadecylphenol (108 g, 3.54 x 10^{-1} mol), to which were added dimethyl sulfoxide (500 mL), potassium hydroxide (79.44 g, 1.4 mol) and methyl iodide (44.17 ml, 7 x 10^{-1} mol) drop wise at 0 °C, over a period of 30 minutes. The reaction mixture was stirred at room temperature for 24 h. After completion of reaction, the reaction mixture was extracted into dichloromethane (500 mL), washed with brine (3 x 500 mL) and water (3 x 500 mL) and dried over sodium sulphate. Evaporation of the solvent afforded crude 1-methoxy-3-pentadecylbenzene. The pure product was obtained by passing the crude product through a silica gel column using pet ether as an eluent.

Yield = 105 g (93 %)

M.P.: 27 °C (Lit. M.P.: 27-28 °C).[42]

IR (cm^{-1}): 1220 (-C-O-C- stretching)

^{1}H-NMR (200 MHz, $CDCl_3$, δ, ppm) 0.88 (t, 3 H,-CH_3), 1.25-1.60 (m, 26 H, -CH_2), 2.57 (t, 2 H, Ar-CH_2), 3.80 (s, 3 H, -OCH_3), 6.69-6.79 (m, 3 H, Ar-H), 7.20 (dd, 1 H, Ar-H)

^{13}C-NMR (50 MHz, $CDCl_3$, δ, ppm)14.11, 22.70, 29.38, 29.71, 31.42, 31.94, 36.04, 54.98, 110.72, 114.15, 12081, 129.09, 144.55, 159.55

Elemental analysis: Calcd. for $C_{22}H_{38}O$: C, 82.95; H, 12.02. Found: C, 82.75; H, 11.86.

3.3.2.2 Synthesis of 1,5-dibromo-2-methoxy-4-pentadecylbenzene

Into a 500 mL three-necked round bottom flask equipped with a magnetic stir bar, an addition funnel, a reflux condenser and a guard tube was added 1-methoxy-3-pentadecylbenzene (29.3 g, 9.1 x 10^{-2} mol) to which was added dichloromethane (150 mL). Liquid bromine (10 mL, 1.9 x 10^{-1} mol) was added drop wise over a period of 1.5 h while maintaining the temperature of the reaction mixture at -5-0 °C and protecting from light. The top of the condenser was equipped with a trap to absorb the hydrogen bromide released during the reaction. After completion of addition, the reaction mixture was stirred at room temperature for 24 h. After completion of reaction, excess bromine was quenched with saturated solution of sodium hydroxide (100 mL) and the dichloromethane solution was washed with brine (3 x 200 mL) and water (3 x 200 mL) and dried over sodium sulphate. The crude product was obtained by evaporation of the solvent and purified by passing through a silica gel column using petroleum ether as an eluent. The pure product was obtained as a white solid.

Yield = 36.36 g (83 %)

M.P.: 38 °C

IR (cm^{-1}): 770 (C-Br stretching).

^{1}H-NMR (200 MHz, $CDCl_3$, δ, ppm) 0.87 (t, 3 H, $-CH_3$), 1.25-1.57 (m, 26 H, $-CH_2$), 2.65 (t, 2 H, Ar-CH_2), 3.86 (s, 3 H, $-OCH_3$), 6.72 (s, 1 H, Ar-H), 7.65 (s, 1 H, Ar-H)

^{13}C-NMR (50 MHz, $CDCl_3$, δ, ppm) 14.10, 22.67, 29.34, 29.66, 31.90, 36.32, 56.28, 109.20, 113.26, 114.81, 135.94, 142.50, 155.10

Elemental analysis: Calcd. for $C_{22}H_{36}Br_2O$: C, 55.47; H, 7.62; Br, 33.55. Found: C, 54.85; H, 7.50; Br, 33.48.

3.3.2.3 Synthesis of 4-methoxy-6-pentadecylisophthalonitrile

Into a 250 mL three-necked round bottom flask equipped with a magnetic stir bar, a reflux condenser and a guard tube was added 1,5-dibromo-2-methoxy-4-pentadecylbenzene (10 g, 2.09 x 10^{-2} mol) to which was added copper cyanide (9.4 g, 10.4 x 10^{-2} mol), anhydrous copper sulphate (0.105 g, 2 x 10^{-5} mol) and *N*,*N*-dimethylformamide (50 mL). The reaction mixture was refluxed overnight. After completion of reaction, *N*,*N*-dimethylformamide was removed from the reaction by distillation. The reaction was quenched by pouring into it concentrated hydrochloric acid (50 mL) and stirred. The reaction mixture was extracted into ethyl acetate (500 mL), washed with sodium bicarbonate till neutral, followed by brine (3 x 500 mL), water (3 x 500 mL) and dried over sodium sulphate. Evaporation of the solvent afforded crude 4-methoxy-6-pentadecylisophthalonitrile. Pure product was obtained by passing the crude product through a column of silica gel, using a mixture of pet ether and ethyl acetate as eluent.

Yield = 5.4 g (70 %)

M.P.: 82 °C.

IR (cm^{-1}): 2225 (-CN)

^{1}H-NMR (400 MHz, $CDCl_3$, δ, ppm) 0.86 (t, 3 H,$-CH_3$), 1.24-1.67 (m, 26 H, $-CH_2$), 2.85 (t, 2 H, Ar-CH_2), 3.99 (s, 3 H, $-OCH_3$), 6.87 (s, 1 H, Ar-H), 7.79 (s, 1 H, Ar-H)

^{13}C-NMR (100 MHz, $CDCl_3$, δ, ppm) 14.01, 22.57, 29.18, 29.24, 29.36, 29.48, 30.56, 29.54, 31.80, 35.43, 56.49, 100.78, 105.00, 112.30, 114.36, 116.27, 137.89, 154.50, 163.43

Elemental analysis: Calcd. for $C_{24}H_{36}N_2O$: C, 78.21; H, 9.85; N, 7.60. Found: C, 78.04; H, 9.65; N, 7.48

3.3.2.4 Synthesis of 4-methoxy-6-pentadecylisophthalaldehyde (MPIAL)

Into a 250 mL three-necked round bottom flask equipped with a magnetic stir bar and a two-way vacuum adaptor was added 4-methoxy-6-pentadecylisophthalonitrile (1.5 g, 4.06 x 10^{-3} mol), to which was added dichloromethane (35 mL) and diisobutylaluminiumhydride (1 M solution in toluene, 9 mL, 9 x 10^{-3} mol) drop wise over a period of 15 minutes while maintaining the reaction mixture at 0 °C, under nitrogen atmosphere. After completion of addition the reaction mixture was stirred under nitrogen atmosphere at room temperature for 4 h. After completion of the reaction, excess diisobutylaluminiumhydride was quenched by adding into the reaction mixture an aqueous solution of potassium sodium tartarate (6.3 g, 2.2 x 10^{-2} mol) and stirring the mixture overnight. The reaction mixture was then washed with water (3 x 50 mL) and dried over sodium sulphate. Evaporation of the solvent afforded crude 4-methoxy-6-pentadecylisophthalaldehyde. The pure product was obtained as a white solid after purification by flash chromatography using a mixture of petroleum ether and ethyl acetate as eluent.

Yield = 1 g (66 %)

M. P.: 88 °C

IR (cm^{-1}): 1732 (C=O stretch, aldehyde functionality), 2928, 2847 (C-H out of plane vibration, aldehyde functionality)

^{1}H-NMR (400 MHz, $CDCl_3$, δ, ppm) 0.88 (t, 3 H, CH_3), 1.18-1.36 (m, 24 H, CH_2), 1.57-1.66 (m, 2 H, CH_2), 3.08 (t, 2 H, Ar-CH_2), 4.03 (s, 3 H, O-CH_3), 6.85 (s, 1 H, Ar-H), 8.30 (s, 1 H, Ar-H), 10.11 (s, 1 H, CHO), 10.41 (s, 1 H, CHO)

^{13}C-NMR (100 MHz, Acetone-d_6, δ, ppm) 14.44, 23.41, 29.35, 29.54, 29.73, 30.11, 30.30, 30.48, 32.72, 33.90, 57.01, 115.43, 124.04, 128.25, 133.69, 155.45, 165.77, 188.42, 191.26

HRMS (m/z) $[M+H]^+$ calculated for $C_{24}H_{39}O_3$, 375.2894; found, 375.2892

3.3.3 Synthesis of diacid with pendent pentadecyl chain

3.3.3.1 Synthesis of 4-methoxy-6-pentadecylisophthalic acid (MPIA)

Into a 250 mL single necked round bottom flask equipped with a magnetic stir bar, an addition funnel and a guard tube were added 4-methoxy-6-pentadecylisophthalaldehyde (0.5 g, 1.3 x 10^{-3} mol), sodium chlorite (0.72 g, 8.0 x 10^{-3} mol), sodium dihydrogen orthophosphate (0.6 g x 10^{-3} mol) and methanol (100 mL). The reaction mixture was stirred at room temperature for 48 h. After completion of reaction, water was added to the reaction mixture to precipitate the product which was isolated by filtration. The pure product was obtained by passing the crude compound through a column of silica gel, using a mixture of pet ether and ethyl acetate as eluent.

Yield = 0.37 g (75 %)

M. P.: 100 °C

IR (KBr, cm^{-1}): 3118 (hydrogen bonded OH), 1673, 1702 (C=O stretch)

^{1}H-NMR (200 MHz, DMSO-d_6, δ, ppm) 0.86 (s, 3 H, CH_3), 1.12-1.38 (m, 24 H, CH_2), 1.53 (br. s., 3 H, CH_2), 2.99 (t, 2 H, Ar-CH_2), 3.88 (s, 3 H, O-CH_3), 7.02 (s, 1 H, Ar-H), 8.21 (s, 1 H, Ar-H), 12.72 (br. s., 2 H, O-H)

^{13}C-NMR (100 MHz, DMSO-d_6, δ, ppm) 14.13, 22.27, 28.88, 29.00, 29.20, 29.31, 31.35, 31.47, 34.28, 39.07, 39.28, 39.49, 39.70, 39.91, 40.11, 40.32, 56.18, 114.80, 118.24, 121.41, 134.66, 151.14, 160.72, 166.48, 167.59

HRMS (m/z) $[M+Na]^+$ calculated for $C_{24}H_{38}O_5Na$, 429.2611; found, 429.2606

3.3.4 Synthesis of 4-(4-hydroxyphenoxy)-3-pentadecylphenol (HPPDP)

3.3.4.1 Synthesis of 1-bromo-4-methoxy-2-pentadecylbenzene

Into a 500 mL round bottom flask equipped with a magnetic strirrer bar were added 1-methoxy-3-pentadecylbenzene (50 g, 1.5 x 10^{-1} mol), *N*-bromosuccinimide (27.94 g, 1.5 x 10^{-1} mol) and dry acetone (300 mL). Subsequently, hydrochloric acid (0.15 mL, 1.5 x 10^{-3} mol) was added to the reaction mixture when the reaction mixture was observed to turn yellow. The reaction mixture was stirred at room temperature until the solution turned colourless, all the while protecting the reaction setup from light. On reaction completion, acetone was removed on a rotary evaporator, hexane (150 mL) was added and the reaction mixture was cooled in an ice bath. The precipitated succinimide was removed by filtration. Evaporation of hexane from the filtrate yielded crude 1-

bromo-4-methoxy-2-pentadecylbenzene, which was purified by column chromatography (eluent: petroleum ether).

Yield = 56 g, (90 %)

M.P.: 41 °C (Lit. M. P.: 40 °C)[43]

IR (cm^{-1}): 801 (C-Br stretching), 1243 (Ar-O-C stretching)

^{1}H-NMR (200 MHz, $CDCl_3$, δ, ppm) 0.89 (t, 3 H), 1.20 - 1.41 (m, 24 H), 1.51 - 1.67 (m, 2 H), 2.67 (t, 2 H), 3.78 (s, 3 H), 6.61 (dd, 1 H), 6.76 (d, 1 H), 7.40 (d, 1 H)

^{13}C-NMR (50 MHz, $CDCl_3$, δ, ppm) 14.11, 22.69, 29.36, 29.68, 29.89, 31.92, 36.40, 55.35, 112.77, 114.93, 115.95, 133.11, 143.15, 158.83

3.3.4.2 Synthesis of 4-methoxy-1-(4-methoxyphenoxy)-2-pentadecylbenzene

Into a 500 mL three-necked round bottom flask equipped with a magnetic stirring bar, a Dean Stark assembly and a reflux condenser were added 4-methoxy phenol (12.9 g, 8.0 x 10^{-2} mol), potassium hydroxide (5.3 g, 8.0 x 10^{-2} mol), *N*,*N* dimethylacetamide (DMAc) (75 mL) and toluene (50 mL). The reaction mixture was refluxed for 7 h. Water formed as a by-product of phenoxide salt formation was removed out of the reaction mixture as an azeotrope with toluene. Subsequently, toluene was distilled out of the reaction mixture and it was cooled to room temperature. Thereafter, 1-bromo-4-methoxy-2-pentadecylbenzene (30 g, 7.5 x 10^{-3} mol), copper powder (0.30 g, 2 wt %) and DMAc (25 mL) were added to the reaction mixture and refluxed for 6 h. After completion of the reaction, the reaction mixture was poured into water (500 mL) and the copper salts were removed by filtration. The filtrate was extracted with ethyl acetate (2 x 250 mL), washed with saturated aqueous sodium chloride solution (2 x 100 mL) followed by water (3 x 250 mL) and dried over sodium sulphate. Solvent evaporation yielded crude 4-methoxy-1-(4-methoxyphenoxy)-2-pentadecylbenzene which was purified by column chromatography (eluent: petroleum ether: ethyl acetate:: 90:10, v/v)

Yield = 20 g (60 %).

IR (cm^{-1}): 1209 (Ar-O-Ar stretching) and 1260 (Ar -O-C stretching)

^{1}H-NMR (200 MHz, $CDCl_3$, δ, ppm) 0.88 (t, 3 H), 1.25 (bs., 24 H), 1.66 - 1.51 (m, 2 H), 2.56 (t, 2 H), 3.78 (s, 3 H), 3.79 (s, 3 H), 6.67 (dd, 1 H), 6.80 - 6.77 (m, 2 H), 6.82 (bs, 4 H)

^{13}C-NMR (50 MHz, $CDCl_3$, δ, ppm), 14.12, 22.68, 29.42, 29.56, 29.68, 29.96, 31.90, 35.87, 55.54, 55.63, 111.73, 114.69, 115.79, 118.01, 120.44, 135.61, 148.62, 152.58, 154.75, 155.63

3.3.4.3 Synthesis of 4-(4-hydroxyphenoxy)-3-pentadecylphenol (HPPDP)

Into a 250 mL round bottom flask equipped with a magnetic stirring bar, an addition funnel and a nitrogen balloon were added 4-methoxy-1-(4-methoxyphenoxy)-2-pentadecylbenzene (6.0 g, 1.4 x 10^{-2} mol) and dichloromethane (100 mL). The mixture was stirred to get a homogeneous solution and cooled in an ice-bath. To this cooled reaction mixture was added boron tribromide (BBr_3, 1 M solution in dichloromethane) (30.53 mL, 3.0 x 10^{-2} mol), drop wise, over a period of 1 h with continuous stirring. Thereafter, the temperature of the reaction mixture was slowly allowed to rise to room temperature and stirred further for a period of 8 h. On completion of the reaction, ice water was added to the reaction mixture and stirred for 1 h. Subsequently, dichloromethane was evaporated from the reaction mixture on a rotary evaporator and the residue was extracted with ethyl acetate. The ethyl acetate solution was washed with brine, dried over sodium sulphate and concentrated in vacuum to obtain crude 4-(4-hydroxyphenoxy)-3-pentadecylphenol (HPPDP) which was purified by column chromatography (eluent: petroleum ether:ethyl acetate :: 70:30 v/v).

Yield = 4.5 g (80 %);

M.P.: 75 ˚C (Lit. M. P.: 76 °C)[43]

IR (cm^{-1}): 3325 (Phenolic O-H); 1204 (Ar-O-Ar stretching)

^{1}H-NMR (400 MHz, $CDCl_3$, δ, ppm) 0.87 (t, 3 H), 1.33 - 1.11 (m, 24 H), 1.65 -1.56 (m, 2 H), 2.51 (t, 2 H), 4.58 (bs, 2 H), 6.61 (dd, 1 H), 6.75 -6.70 (m, 2 H), 6.78 (d, 4 H)

^{13}C-NMR (50 MHz, $CDCl_3$, δ, ppm) 14.12, 22.68, 29.42, 29.56, 29.68, 29.96, 31.91, 113.44, 116.10, 116.89, 118.16, 120.68, 135.92, 148.51, 150.44, 151.43, 152.52

3.3.5 Synthesis of 3-pentadecyl 4,4' biphenol (PDBP)

3.3.5.1 Synthesis of 4, 4'-dimethoxy-2-pentadecyl-1,1'-biphenyl

Into a 250 mL Schlenk tube equipped with a magnetic stirring bar were added 1-bromo-4-methoxy-2-pentadecylbenzene (7.94 g, 2 x 10^{-2} mol), 4-methoxy phenyl boronic acid (4.55 g, 3 x 10^{-2} mol), potassium carbonate (8.29 g, 6 x 10^{-2} mol), tetrakis(triphenyl phosphine)palladium (0.231 g, 2 x 10^{-4} mol) and dry toluene (100 mL). The reaction

mixture was degassed three times by freeze-pump-thaw cycles followed by purging with nitrogen. The nitrogen purging was continued for 1 h. The reaction mixture was heated at 110 °C for 24 h. After completion of the reaction (as monitored by TLC), the reaction mixture was allowed to attain room temperature. Water (50 mL) and ethyl acetate (50 mL) were added. The organic layer was washed with water and brine solution and concentrated to get crude product. The crude product was purified by column chromatography on silica gel using pet ether as an eluent.

Yield = 6.5 g (76 %)

IR (cm^{-1}): 1605 (-C=C- stretching), 1281 (Ar-O-C stretching)

^{1}H-NMR (200 MHz, $CDCl_3$, δ, ppm) 0.88 (t, 3 H), 1.15 - 1.25 (m, 24 H), 1.41 (q, 2 H), 2.30 (d, 2 H), 3.84 (s, 6 H), 6.73 (dd, 2 H), 6.81 (d, 2 H), 6.99 (d, 2 H)

^{13}C-NMR (50 MHz, $CDCl_3$, δ, ppm) 14.10, 22.68, 28.01, 29.36, 29.44, 29.69, 30.67, 31.92, 33.34, 55.11, 110.25, 114.14, 131.19, 133.23, 142.55, 158.53

3.3.5.2 Synthesis of 3-pentadecyl 4, 4' biphenol (PDBP)

Into a 250 mL round bottom flask equipped with a magnetic stirring bar, an addition funnel and a nitrogen balloon were added 4, 4'-dimethoxy-2-pentadecyl-1,1'-biphenyl (10.0 g, 2.35 x 10^{-2} mol) and dichloromethane (100 mL). The mixture was stirred to get a homogeneous solution which was cooled in an ice-bath. To this cooled reaction mixture was added boron tribromide (BBr_3, 1 M solution in dichloromethane) (49.45 mL, 4.945 x 10^{-2} mol), drop wise, over a period of 1 h with continuous stirring. Thereafter, the temperature of the reaction mixture was slowly allowed to rise to room temperature and further stirred for a period of 8 h. On completion of the reaction, ice water was added to the reaction and stirred for 1 h. Subsequently, dichloromethane was evaporated from the reaction mixture on a rotary evaporator and the residue was extracted with ethyl acetate (500 mL). The ethyl acetate solution was washed with brine (3 x 300 mL), water (3 x 300 mL), dried over sodium sulphate and concentrated under vacuum on a rotary evaporator to obtain crude 3-pentadecyl 4, 4' biphenol. The pure product was obtained by recrystallisation from a mixture of dichloromethane:pet ether (50:50, v/v)

Yield = 7.6 g (82 %)

M.P.: 101 °C (Lit. M. P.: 101 °C)[44]

IR (cm^{-1}): 3281 (-O-H stretching), 1604 (-C=C- stretching)

^{1}H-NMR (400 MHz, $CDCl_3$, δ, ppm) 0.88 (t, 3 H), 1.31 - 1.14 (m, 24 H), 1.46 (q, 2 H), 2.52 (t, 2 H), 4.96 (s, 1 H), 5.02 (s, 1H), 6.70 (dd, 1 H), 6.76 (d, 1 H), 6.87 (d, 2 H), 7.03 (d, 1 H), 7.15 (d, 2 H)

^{13}C-NMR (100 MHz, $CDCl_3$, δ, ppm) 14.12, 22.69, 29.37, 29.49, 29.70, 30.57, 31.92, 33.14, 112.07, 115.21, 131.39, 133.22, 142.86, 154.39

3.3.6 Synthesis of 4,4'-(3-pentadecylcyclohexane-1,1-diyl)diphenol (BPC15)

3.3.6.1 Synthesis of 3-pentadecyl cyclohexanol

Into a Parr reactor was added 3-pentadecyl phenol (80 g, 0.26 mol), isopropanol (300 mL) and 5 % Ru/C (2.4 g), as a catalyst. The reaction mixture was hydrogenated at 125 °C and 1000 psi hydrogen pressure. At the end of reduction, the catalyst was filtered off and the filtrate was passed through a short silica column. The product was obtained as a white solid by evaporation of the solvent under reduced pressure.

Yield = 79.9 g (98 %)

M.P.: 47 °C (Lit. M.P.: 46-49 °C)[45]

IR (cm^{-1}): 3334 (-O-H stretching)

3.3.6.2 Synthesis of 3-pentadecyl cyclohexanone

Into a 1000 mL round bottom flask equipped with a mechanical stirrer was added finely ground pyridinium chlorochromate (97 g, 0.45 mol), silica gel (97 g, 100-200 mesh) and dichloromethane (600 mL). The suspension was stirred and 3-pentadecyl cyclohexanol (50 g, 0.22 mol) was added to it in small portions at room temperature. After 30 minutes, the reaction mixture was observed to darken visibly. The suspension was further stirred for 4 h. Subsequently, the reaction mixture was filtered through a short column of silica gel and celite and concentrated to obtain a solid which was dissolved in ethyl acetate (300 mL) and washed with water (3 x 250 mL) and dried over sodium sulphate. Solvent evaporation yielded crude 3-pentadecyl cyclohexanone which was purified by recrystallisation from methanol.

Yield = 46.6 g (94 %)

M.P.: 43 °C (Lit. M.P.: 44 °C)[45]

IR (cm^{-1}): 1705 (C=O stretching)

3.3.6.3 Synthesis of 4,4'-(3-pentadecylcyclohexane-1,1-diyl)diphenol (BPC15)

Into a 250 mL three-necked round bottom flask equipped with a magnetic stirrer, a HCl dip tube and a reflux condenser connected to a scrubber, were added 3-pentadecyl cyclohexanone (20 g, 0.06 mol), phenol (36.62 g, 0.38 mol) and 3-mercaptopropionic acid (0.1 mL). Dry hydrogen chloride gas was bubbled into the reaction mixture at room temperature. The reaction mixture was observed to become solid at the end of 1 h. The solid was dissolved in ethyl acetate (600 mL) and neutralised by washing with aqueous sodium bicarbonate solution (3 x 200 mL), followed by washing with water (3 x 250 mL). The ethyl acetate solution was dried over sodium sulphate. Solvent evaporation yielded crude 4,4'-(3-pentadecylcyclohexane-1,1-diyl)diphenol which was purified by recrystallisation from a mixture of hexane and toluene (9:1, v/v).

Yield = 21.72 g (70 %)

M.P.: 103 °C (Lit. M.P.: 104 °C)[45]

IR (cm^{-1}): 3319 (-O-H stretching)

^{1}H-NMR (400 MHz, $CDCl_3$, δ, ppm) 0.79-0.99 (m, 4 H) 1.13-1.36 (m, 28 H) 1.38-1.57 (m, 3 H) 1.60-1.91 (m, 3 H) 2.48-2.60 (m, 2 H) 6.65 (d, J=7.93 Hz, 2 H) 6.77 (d, J=8.55 Hz, 2 H) 6.99 (d, J=7.93 Hz, 2 H) 7.18 (d, J=7.93 Hz, 2 H)

^{13}C-NMR (100 MHz, $CDCl_3$, δ, ppm) 14.10, 22.68, 26.76, 29.35, 29.69, 30.07, 31.92, 33.28, 33.51, 37.71, 44.38, 45.49, 114.75, 115.19, 127.31, 129.09, 138.05, 144.66, 152.94, 153.00

3.3.7 Synthesis of bisphenol based on 3-pentadecylcyclohexanone

3.3.7.1 Synthesis of 2,6-bis(4-hydroxybenzylidene)-3-pentadecylcyclohexanone (BPC)

Into a 100 mL round bottom flask equipped with a stirring bar, an HCl dip tube and a scrubber were added 3-pentadecylcyclohexanone (5 g, 1.6 x 10^{-2} mol) 4-hydroxybenzaldehyde (4.15 g, 3.4 x 10^{-2}) and glacial acetic acid (50 mL). The reaction mixture was saturated with dry hydrogen chloride at room temperature for 4 h. Thereafter, the reaction mixture was stirred for two days. On completion of reaction, cold water was added to the reaction mixture and was filtered to isolate the precipitate. The solid obtained was washed, dried and purified by column chromatography using a mixture of petroleum ether and ethyl acetate as eluent.

Yield = 6.8 g (82 %)

IR (cm^{-1}): 3298 (-O-H stretching), 1595 (-C=O- stretching), 1634 (-C=C- stretching), 829 (=C-H bending)

M.P.: 138 °C

^{1}H-NMR (200 MHz, $CDCl_3$, δ, ppm) 0.88 (t, 3 H),1.14-1.45 (m, 20 H) 1.49-1.91 (m., 6 H) 1.91-2.11 (m, 2 H) 2.82-2.98 (m, 2 H), 3.30 (br. s., 1 H), 4.75 (br. s., 2 H), 5.59 (br. s., 2 H), 6.88 (d, J=8.65, 2 H), 6.90 (d, 2 H), 7.35 (d, 2 H), 7.45 (d, 2 H), 7.59 (s, 1 H), 7.72 (s, 1 H)

^{13}C-NMR (125 MHz, $CDCl_3$, δ, ppm) 14.10, 22.68, 22.79,26.76, 29.35, 29.69, 29.97, 30.07, 31.92, 33.51, 37.71, 44.38, 45.49, 76.69, 77.32, 114.75, 115.19, 127.31, 127.81, 127.98, 128.37, 128.57, 129.09, 138.05, 144.66, 152.94, 153.00, 194.08

3.3.8 Synthesis of 4,4'-((2-pentadecyl-[1,1'-biphenyl]-4,4'-diyl)bis(oxy))dianiline (PBD)

3.3.8.1 Synthesis of 4,4'-bis(4-nitrophenoxy)-2-pentadecyl-1,1'-biphenyl

Into a 250 mL round bottom flask equipped with a magnetic stirrer bar, a nitrogen inlet and a reflux condenser were added 3-pentadecyl 4, 4' biphenol (10 g, 2.52 x 10^{-2} mol), p-chloronitrobenzene (7.9 g, 5.0 x 10^{-2} mol), potassium carbonate (2.9 g, 5.2 x 10^{-2} mol) and *N*,*N*-dimethylformamide (90 mL) and the reaction mixture was refluxed for 10 h under a continuous flow of nitrogen. Thereafter, the reaction mixture was cooled to room temperature and poured into water (500 mL) and extracted with ethyl acetate (200 mL). The organic layer was subsequently washed with brine (3 x 200 mL) and water (3 x 200 mL). The crude product was obtained by evaporation of the organic layer on a rotary evaporator and purified by column chromatography. (Eluent: pet ether: ethyl acetate; 90:10; v:v)

Yield = 14.4 g (90 %)

M.P.: 57 °C

IR (cm^{-1}): 1519, 1343 (asymmetric and symmetric stretching of $-NO_2$, respectively)

^{1}H-NMR (400 MHz, $CDCl_3$, δ, ppm) 0.88 (t, 3 H), 1.14-1.43 (m, 24 H), 1.48 (q, 2 H), 2.60 (t, 2 H), 6.98 (d, J=8.27 Hz, 2 H), 7.03-7.25 (m, 6 H), 7.28-7.47 (m, 3 H), 8.21-8.40 (m, 4 H)

^{13}C-NMR (100 MHz, $CDCl_3$, δ, ppm) 14.09, 22.66, 29.27, 29.33, 29.66, 31.04, 31.89, 33.10, 117.14, 117.27, 117.57, 120.09, 121.01, 125.98, 131.15, 131.73, 137.89, 138.16, 142.66, 142.80, 143.11, 153.88, 154.09, 163.15, 163.35

3.3.8.2 Synthesis of 4,4'-((2-pentadecyl-[1,1'-biphenyl]-4,4'-diyl)bis(oxy))dianiline (PBD)

Into a 250 mL three-necked round bottom flask were added 4,4'-bis(4-nitrophenoxy)-2-pentadecyl-1,1'-biphenyl (10 g, 1.56 x 10^{-2} mol), 10% Pd/C (0.3 g, 3 wt % of 4,4'-bis(4-nitrophenoxy)-2-pentadecyl-1,1'-biphenyl) and absolute ethanol (100 mL) and the reaction mixture was heated to reflux. Hydrazine hydrate (25 mL, 5.0 x 10^{-1} mol) was added drop wise into the reaction mixture over a period of 20 minutes. Subsequently, the reaction mixture was refluxed for 24 h, filtered to remove Pd/C and extracted with dichloromethane (200 mL). The dichloromethane solution was washed successively with brine (3 x 100 mL) and water (3 x 100 mL). The organic layer was separated, dried over anhydrous sodium sulphate and filtered. The solvent was removed on a rotary evaporator to afford the product as a white solid which was dried under reduced pressure at room temperature.

Yield = 7.88 g (87 %)

IR (cm^{-1}): 3440, 3320 (N-H stretching)

M.P.: 48 °C

^{1}H-NMR (500 MHz, $CDCl_3$, δ, ppm) 0.90 (t, 3 H), 1.18-1.1.36 (m, 24 H), 1.44 (q, 2 H), 2.53 (t, 2 H), 3.47 (br. s., 4 H, NH_2), 6.72 (d, J=8.39, 4 H), 6.76 (dd, J=8.20, 2.48 Hz, 1 H), 6.89 (d, J=2.29 Hz, 1 H), 6.90-7.00 (m, 6 H), 7.10 (d, J=8.39 Hz, 1 H), 7.20 (d, J=8.39 Hz, 2 H)

^{13}C-NMR (125 MHz, $CDCl_3$, δ, ppm) 14.12, 22.67, 29.35, 29.51, 29.68, 31.17, 31.89, 33.11, 114.08, 116.25, 116.56, 117.70, 121.07, 130.48, 131.08, 135.30, 135.36, 142.14, 148.65, 157.67, 157.88

HRMS (m/z) $[M+H]^+$ calculated for $C_{39}H_{51}N_2O_2$, 579.3945; found, 579.3942

3.3.9 Synthesis of bispropargyl ether with biphenylene linkage.

3.3.9.1 Synthesis of 2-pentadecyl-4,4'-bis(prop-2-yn-1-yloxy)-1,1'-biphenyl (PPB)

Into a 100 mL three-necked round bottom flask equipped with a nitrogen inlet, an addition funnel and a reflux condenser were added 3-pentadecyl 4, 4' biphenol (PDBP) (2

g, 5.04 x 10^{-3} mol), potassium carbonate (1.74 g, 1.26 x 10^{-2} mol), potassium iodide (0.083 g, 5.04 x 10^{-4} mol) and *N*,*N*-dimethylformamide (30 mL). The reaction mixture was stirred under continuous nitrogen flow at 60 °C for 1 h. Thereafter, propargyl bromide (0.977 mL, 1.1 x 10^{-2} mol) was added to the reaction mixture drop wise over a period of 10 minutes. After completion of addition, the temperature was raised to 120 °C and stirred at that temperature for 12 h. On completion of the reaction (as monitored by TLC), *N*,*N*-dimethylformamide was distilled out of the reaction mixture under reduced pressure to obtain crude 2-pentadecyl-4,4'-bis(prop-2-yn-1-yloxy)-1,1'-biphenyl (PPB) which was dissolved in ethyl acetate (70 mL) and washed with water (2 x 200 mL). The organic layer was dried over anhydrous sodium sulphate, filtered and ethyl acetate was removed on a rotary evaporator to obtain a residue which was purified by column chromatography using a mixture of petroleum ether and ethyl acetate as eluent to afford pure 2-pentadecyl-4,4'-bis(prop-2-yn-1-yloxy)-1,1'-biphenyl (PPB).

Yield = 1.97 g (83 %)

IR (cm^{-1}): 3280 (≡C-H stretching), 2130 (-C≡C- stretching), 1210 (-C-O-C- stretching)

M.P.: -20 °C [obtained through DSC analysis]

^{1}H-NMR (400 MHz, $CDCl_3$, δ, ppm) 0.90 (t, 3 H), 1.09-1.42 (m, 24 H), 1.48 (q, 2 H), 2.46-2.74 (m, 4 H), 4.73 (br. s., 2 H), 4.75 (br. s., 2 H), 6.85 (dd, J=7.93, 2.44 Hz, 1 H), 6.91 (d, J=2.44 Hz, 1 H), 7.01 (d, J=8.54 Hz, 2 H), 7.13 (d, J=8.54 Hz, 1 H), 7.22 (d, J=8.55 Hz, 2 H)

^{13}C-NMR (100 MHz, $CDCl_3$, δ, ppm) 14.12, 22.69, 29.36, 29.50, 29.69, 31.15, 31.92, 33.21, 55.74, 55.84, 75.42, 75.48, 78.65, 78.75, 111.53, 114.32, 115.60, 130.47, 131.07, 134.82, 134.90, 142.08, 156.36, 156.64

3.3.10 Synthesis of bispropargyl ether with multiple ether linkages

3.3.10.1 Synthesis of 2-pentadecyl-4-(prop-2-yn-1-yloxy)-1-(4-(prop-2-yn-1-yloxy)phenoxy)benzene (PPPB)

Into a 100 mL three-necked round bottom flask equipped with a nitrogen inlet, an addition funnel and a reflux condenser were added 4-(4-hydroxyphenoxy)-3-pentadecylphenol (HPPDP) (2 g, 4.8 x 10^{-3} mol), potassium carbonate (1.67 g, 1.21 x 10^{-2} mol), potassium iodide (0.080 g, 4.84 x 10^{-4} mol) and *N*,*N*-dimethylformamide (30 mL) and stirred at 60 °C for 1 h under continuous flow of nitrogen. Thereafter, propargyl

bromide (0.939 mL, 1.06 x 10^{-2} mol) was added into the reaction mixture drop wise, over a period of 10 minutes. Subsequent to the addition, the reaction mixture was stirred at 120 °C for 12 h. On completion of the reaction, *N*,*N*-dimethylformamide was distilled out from the reaction mixture by distillation under reduced pressure and the crude 2-pentadecyl-4-(prop-2-yn-1-yloxy)-1-(4-(prop-2-yn-1-yloxy)phenoxy)benzene (PPPB) was dissolved in ethyl acetate (70 mL) and washed with water (2 x 200 mL). The organic layer was dried over anhydrous sodium sulphate, filtered and ethyl acetate was removed on a rotary evaporator to obtain a residue which was purified by column chromatography using a mixture of petroleum ether and ethyl acetate as eluent to afford pure 2-pentadecyl-4-(prop-2-yn-1-yloxy)-1-(4-(prop-2-yn-1-yloxy)phenoxy)benzene (PPPB).

Yield = 1.91 g (81 %)

IR (cm^{-1}): 3302 (≡C-H stretching), 2122 (-C≡C- stretching)

M.P.: -22. °C [obtained through DSC analysis]

^{1}H-NMR (400 MHz, $CDCl_3$, δ, ppm) 0.89 (t, J=1.00 Hz, 3 H), 1.16-1.40 (m, 26 H), 1.57 (q, 2 H), 2.46-2.65 (m, 4 H), 4.66 (br. s., 2 H), 4.67 (br. s., 2 H), 6.70 - 6.79 (dd, 2 H), 6.79-6.89 (m, 4 H), 6.92 (d, 2 H)

^{13}C-NMR (100 MHz, $CDCl_3$, δ, ppm) 14.12, 22.69, 29.37, 29.56, 29.69, 29.98, 30.22, 31.92, 56.24, 56.44, 75.39, 78.72, 112.86, 116.01, 116.98, 118.10, 120.36, 135.73, 149.15, 152.74, 153.08, 153.64

3.3.11 Synthesis of phthalonitrile with multiple ether linkages

3.3.11.1 Synthesis of 4-(4-(4-(3,4-dicyanophenoxy)-2-pentadecylphenoxy)phenoxy)phthalonitrile (DCPP)

Into a 100 mL three-necked round bottom flask equipped with a nitrogen inlet and a reflux condenser were added 4-(4-hydroxyphenoxy)-3-pentadecylphenol (HPPDP) (1.42 g, 3.44 x 10^{-3} mol), anhydrous potassium carbonate (1.47 g, 1.06 x 10^{-2} mol) and freshly distilled dimethylsulfoxide (35 mL). The reaction mixture was degassed with nitrogen and stirred at 90 °C for 1h. Subsequently, 4-nitrophthalonitrile (1.25 g, 7.24 x 10^{-3} mol) was added to the reaction mixture and the temperature was raised to 120 °C. The reaction mixture was stirred at that temperature for 24 h. On completion of the reaction (as monitored by TLC), the reaction mixture was poured into ice and stirred with 5 % aqueous HCl (50 mL) for 1 h. Thereafter, ethyl acetate (200 mL) was added to the

mixture and washed with water (2 x 200 mL) until neutral. The organic layer was dried over anhydrous sodium sulphate, filtered and ethyl acetate was removed on a rotary evaporator to obtain a residue which was purified by column chromatography using a mixture of petroleum ether and ethyl acetate as eluent to afford pure 4-(4-(4-(3,4-dicyanophenoxy)-2-pentadecylphenoxy)phenoxy)phthalonitrile (DCPP).

Yield = 1.85 g (81 %)

IR (cm^{-1}): 2236 (-C≡N stretching), 1232 (-C-O-C- stretching)

M.P.: 73 °C

^{1}H-NMR (500 MHz, $CDCl_3$, δ, ppm) 0.87 (t, 3 H), 1.21-1.38 (m, 24 H), 1.62 (q, 2 H), 2.66 (t, 2 H), 6.91 (dd, J=8.77, 3.05 Hz, 1 H), 6.99-7.04 (m, 2 H), 7.04-7.10 (m, 4 H), 7.25-7.31 (m, 4 H), 7.72 - 7.77 (m, 2 H)

^{13}C-NMR (125 MHz, $CDCl_3$, δ, ppm) 14.06, 22.62, 29.29, 29.63, 30.10, 31.85, 108.76, 114.95, 115.31, 117.62, 119.16, 119.48, 121.12, 121.21, 121.28, 122.13, 122.61, 135.38, 137.38, 149.44, 152.06, 155.61, 161.98

3.3.12 Synthesis of phthalonitrile with biphenylene linkage

3.3.12.1 Synthesis of 4,4'-((2-pentadecyl-[1,1'-biphenyl]-4,4'-diyl)bis(oxy))diphthalonitrile (PBP)

Into a 100 mL three-necked round bottom flask equipped with a nitrogen inlet and reflux condenser, were added 3-pentadecyl 4,4' biphenol (PDBP) (1.6 g, 4.03 x 10^{-3} mol), anhydrous potassium carbonate (1.727 g, 1.25 x 10^{-2} mol) and freshly distilled dimethylsulfoxide (35 mL). The resulting mixture was purged with nitrogen and stirred at 90 °C for 1 h. Subsequently, 4-nitrophthalonitrile (1.46 g, 8.47 x 10^{-3} mol) was added to the reaction mixture and the temperature was raised to 120 °C. The reaction mixture was stirred at that temperature for 24 h. On completion of the reaction (as monitored by TLC), the reaction mixture was poured into ice and stirred with 5 % aqueous HCl (50 mL) for 1 h. Thereafter, ethyl acetate (200 mL) was added to the reaction mixture and washed with water (2 x 200 mL) until neutral. The organic layer was dried over anhydrous sodium sulphate, filtered and ethyl acetate was removed on a rotary evaporator to obtain a residue which was purified by column chromatography using a mixture of petroleum ether and ethyl acetate as eluent to afford pure 4,4'-((2-pentadecyl-[1,1'-biphenyl]-4,4'-diyl)bis(oxy))diphthalonitrile (PBP).

Yield = 2.04 g (78 %)

IR (cm^{-1}): 2228 (-C≡N stretching), 1245 (-C-O-C- stretching)

M.P.: 112 °C

^{1}H-NMR (400 MHz, $CDCl_3$, δ, ppm) 0.88 (t, 3 H), 1.15-1.38 (m, 24 H), 1.49 (q, 2 H), 2.60 (t, 2 H), 6.97 (dd, 1 H), 7.04 (d, 1 H), 7.17 (d, J=8.54 Hz, 2 H), 7.28-7.40 (m, 5 H), 7.43 (d, J=8.54 Hz, 2 H), 7.78 (d, J=8.85 Hz, 2 H)

^{13}C-NMR (100 MHz, $CDCl_3$, δ, ppm) 14.08, 22.63, 29.30, 29.63, 30.94, 31.85, 33.06, 109.03, 114.91, 115.29, 115.35, 117.71, 120.29, 121.12, 121.38, 121.60, 131.44, 132.06, 135.44, 138.78, 143.58, 152.78, 153.01, 161.78

3.3.13 Synthesis of phthalonitrile with cyclohexylidene moiety

3.3.13.1 Synthesis of 4,4'-(((3-pentadecylcyclohexane-1,1-diyl)bis(4,1-phenylene))bis(oxy))diphthalonitrile (CPP)

Into a 100 mL three-necked round bottom flask equipped with a nitrogen inlet and a reflux condenser, were added 4,4'-(3-pentadecylcyclohexane-1,1-diyl)diphenol (BPC15) (1.508 g, 3.149 x 10^{-3} mol), anhydrous potassium carbonate (1.349 g, 9.76 x 10^{-3} mol) and freshly distilled dimethylsulfoxide (35 mL). The reaction mixture was degassed with nitrogen and stirred at 90 °C for 1 h. Subsequently, 4-nitrophthalonitrile (1.145 g, 6.61 x 10^{-3} mol) was added to the reaction mixture and the temperature was raised to 120 °C. The reaction mixture was stirred at that temperature for 24 h. On completion of the reaction (as monitored by TLC), the reaction mixture was poured into ice and stirred with 5 % aqueous HCl (50 mL) for one hour. Thereafter, ethyl acetate (200 mL) was added to the mixture and washed with water (2 x 200 mL) until neutral. The organic layer was dried over anhydrous sodium sulphate, filtered and ethyl acetate was removed on a rotary evaporator to obtain a residue which was purified by column chromatography using a mixture of petroleum ether and ethyl acetate as eluent to afford pure 4,4'-(((3-pentadecylcyclohexane-1,1-diyl)bis(4,1-phenylene))bis(oxy))diphthalonitrile (CPP).

Yield = 1.78 g (78 %)

IR (cm^{-1}): 2236 (-C≡N stretching), 1245 (-C-O-C- stretching)

M.P.: 25 °C

^{1}H-NMR (500 MHz, $CDCl_3$, δ, ppm) 0.90 (t, 3 H), 0.99-1.09 (m, 1 H), 1.23-1.41 (m, 28 H), 1.46-1.63 (m, 3 H), 1.78-1.98 (m, 3 H), 2.68-2.77 (m, 2 H), 6.97 (d, J=8.77 Hz, 2 H), 7.09 (d, J=8.39 Hz, 2 H), 7.21-7.35 (m, 6 H), 7.49 (d, J=8.39 Hz, 2 H), 7.77 (d, J=8.39 Hz, 1 H), 7.73 (d, J=8.77 Hz, 1 H)

^{13}C-NMR (125 MHz, $CDCl_3$, δ, ppm) 14.09, 22.66, 26.78, 29.32, 29.66, 30.04, 31.89, 33.02, 33.60, 37.23, 37.57, 44.15, 46.35, 76.74, 77.25, 108.69, 108.89, 114.99, 115.34, 117.53, 117.61, 120.20, 120.43, 121.17, 121.43, 121.54, 121.64, 128.33, 130.14, 135.32, 135.38, 143.49, 149.40, 151.17, 151.36, 161.57, 161.80

3.4 Results and Discussion

3.4.1 Synthesis of 4, 4'-diamino-4''pentadecyltriphenylamine (DPTA)

A new triarylamine containing diamine monomer, namely, 4, 4'-diamino-4''pentadecyltriphenylamine (DPTA), possessing a pendent pentadecyl chain was synthesised following the synthetic route depicted in **Scheme 3.1** starting from 3-pentadecylphenol (A) which in turn is obtained from cashew nut shell liquid (CNSL).

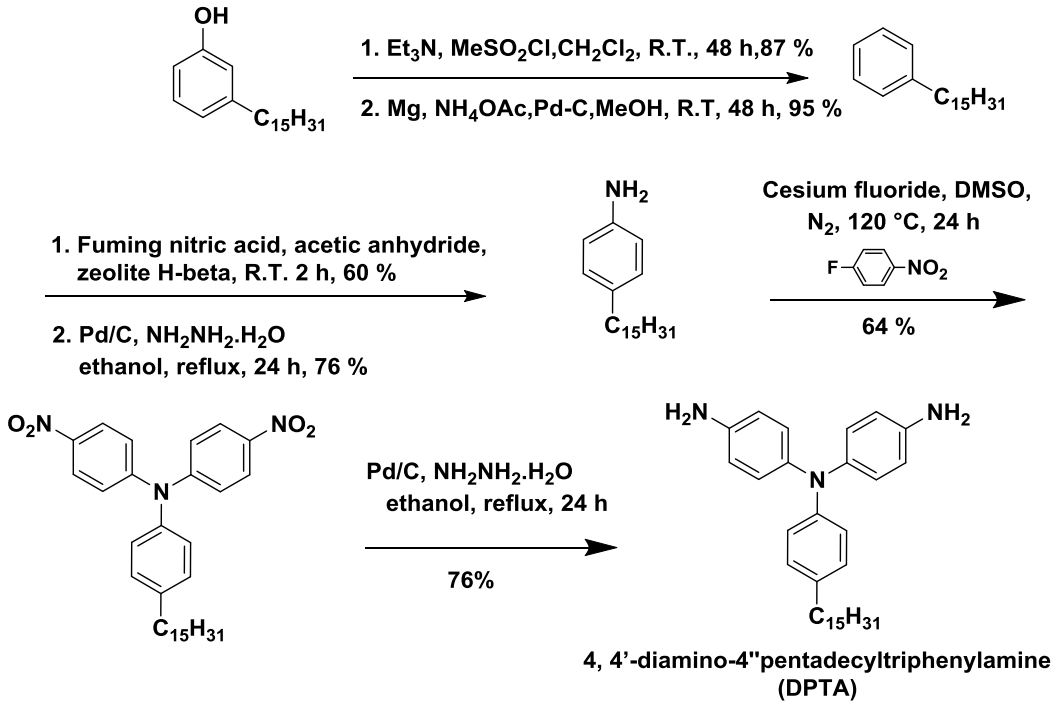

Scheme 3.1 Synthesis of 4, 4'-diamino-4''pentadecyltriphenylamine (DPTA)

Pentadecyl benzene was synthesised from cashew nut shell liquid according to reported procedure[41] and was nitrated using a nitrating system consisting of fuming nitric acid and acetic anhydride in the presence of zeolite H-β[40] to afford 1-nitro-4-

pentadecylbenzene which was reduced to 4-pentadecylaniline in the presence of hydrazine hydrate and Pd/C. 4, 4'-Dinitro-4''pentadecyltriphenylamine was successfully synthesised through double *N*-arylation reaction of 4, 4'-dinitro-4"pentadecyltriphenylamine with 2 equivalents of 4-fluoronitrobenzene in the presence of caesium fluoride and was reduced to yield 4, 4'-diamino-4"pentadecyltriphenylamine (DPTA) in the presence of hydrazine hydrate and Pd/C.[46] 4, 4'-Diamino-4"pentadecyltriphenylamine was characterised through FT-IR, ^{1}H-NMR and ^{13}C-NMR spectroscopy.

FT-IR spectrum of 4, 4'-diamino-4"pentadecyltriphenylamine (DPTA) is depicted in **Fig 3.1.**

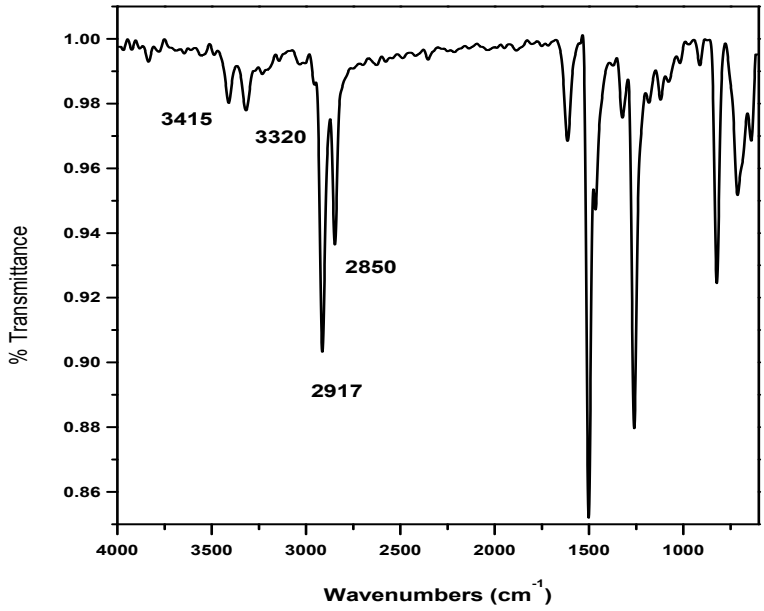

Figure 3.1 FT-IR spectrum of 4, 4'-diamino-4"pentadecyltriphenylamine (DPTA)

Two absorption bands were observed at 3415 cm^{-1} and 3320 cm^{-1} which correspond to N-H stretching of primary amines, while the absorption bands at 2917 cm^{-1} and 2850 cm^{-1} are characteristic of C-H stretching of alkyl groups.

^{1}H-NMR spectrum of 4, 4'-diamino-4"pentadecyltriphenylamine (DPTA) is displayed in **Fig 3.2**

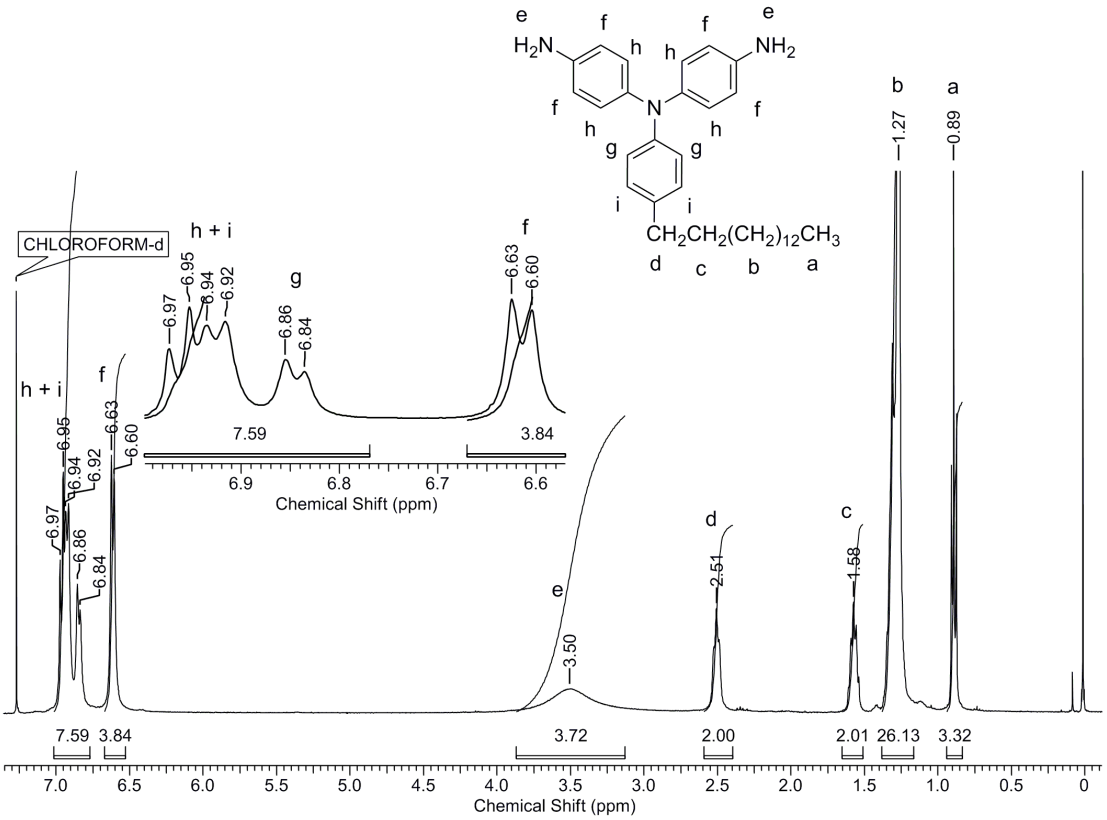

Figure 3.2 ^{1}H-NMR spectrum ($CDCl_3$) of 4, 4'-diamino-4"pentadecyltriphenylamine (DPTA)

The aromatic protons (**f**) *ortho* to the amino group appeared as a doublet at 6.65 δ ppm. The aromatic protons (**g**) resonated at 6.85 δ ppm in the form of a doublet while the remaining aromatic protons (**h** and **i**) appeared in the range of 6.92–6.97 δ ppm. The four protons belonging to the two amine groups resonated as a broad singlet at 3.50 δ ppm. The benzylic protons (**d**) resonated at 2.49 δ ppm as a triplet, while the methylene protons (**c**) appeared at 1.56 δ ppm as a quintet. The protons (**b**) appeared in the range 1.4–1.6 δ ppm and the protons of the methyl group (**a**) resonated at 0.87 δ ppm.

^{13}C-NMR spectrum of 4, 4'-diamino-4"pentadecyltriphenylamine (DPTA) along with assignments is presented in **Fig 3.3**.

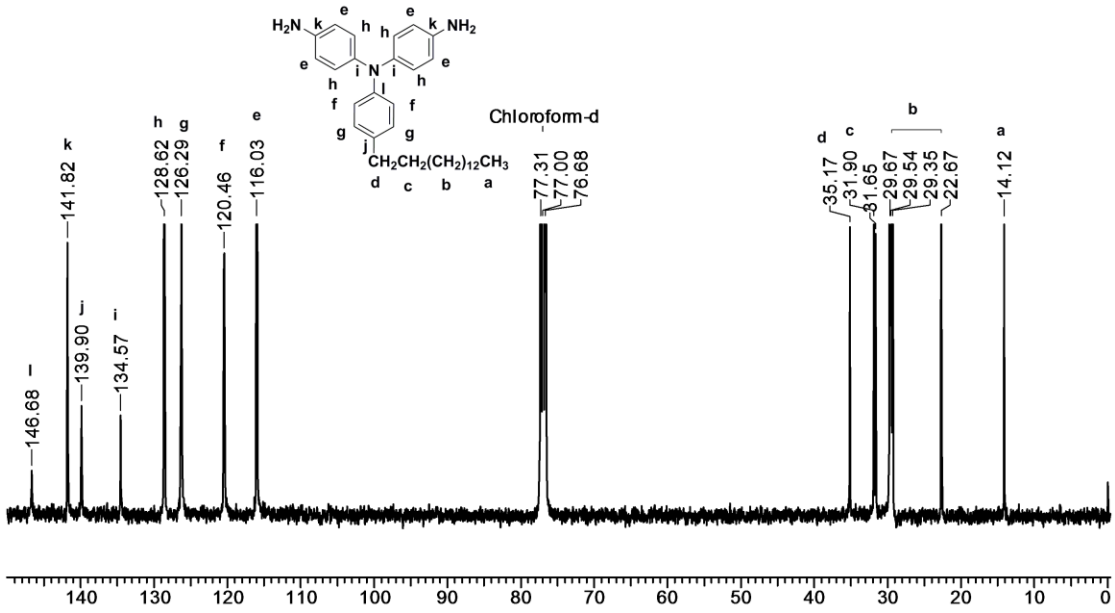

Figure 3.3 ^{13}C-NMR spectrum ($CDCl_3$) of 4, 4'-diamino-4"pentadecyltriphenylamine (DPTA)

Aromatic carbons attached to tertiary nitrogen atom (**i**) of benzene ring containing primary amine group appeared at 134.57 δ ppm, while the quaternary carbon (**l**) attached to tertiary nitrogen atom, belonging to the other benzene ring resonated at 146.68 δ ppm. The carbon atoms (**k**) attached to the primary amine groups appeared at 141.82 δ ppm and the aromatic carbon atom (**j**) attached to the aliphatic chain appeared at 139.90 δ ppm. The aromatic carbons (**e**) *ortho* to the primary amine group appeared shielded at 116.03 δ ppm. Similarly, the carbon atoms (**h**,**f**) *ortho* to the tertiary amine groups appeared at 128.62 δ ppm and 120.46 δ ppm respectively. The aromatic carbon atoms **g** appeared at 126.29 δ ppm. The benzylic carbon atom (**d**) appeared at 35.71 δ ppm, while the methylene carbons (**c**,**b**) appeared at 31.90 δ ppm, 29.67 δ ppm and 22.67 δ ppm. The methyl carbon atom resonated at 14.21 δ ppm.

HRMS results of 4, 4'-diamino-4"pentadecyltriphenylamine (DPTA) showed good agreement with calculated values (**Supporting Information Fig SI 3.1**).

Thus, FT-IR, ^{1}H-NMR, ^{13}C-NMR and HRMS data clearly indicated that the proposed structure of synthesised diamine 4, 4'-diamino-4"pentadecyltriphenylamine (DPTA) was consistent with the observed results.

3.4.2 Synthesis of 4-methoxy-6-pentadecylisophthalaldehyde (MPIAL)

A new dialdehyde containing pentadecyl chain was synthesised from CNSL. The synthesis of the dialdehyde is outlined in **Scheme 3.2**:

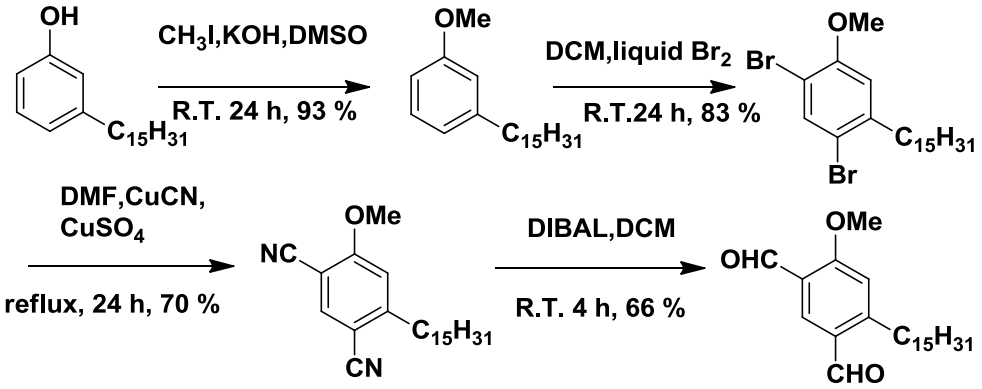

Scheme 3.2 Synthesis of 4-methoxy-6-pentadecylisophthalaldehyde (MPIAL)

4-Methoxy-6-pentadecylisophthalaldehyde was synthesised in four steps. In the first step 3-pentadecyl phenol was converted to its methoxy derivative, 1-methoxy-3-pentadecylbenzene, by the well known Williamson's etherification method according to which the phenol was converted to its phenoxide salt, using potassium hydroxide in dimethyl sulfoxide, followed by methylation using methyl iodide. Dibromination of 1-methoxy-3-pentadecylbenzene was carried out using liquid bromine,[47] which was then converted to the dicyano derivative, 4-methoxy-6-pentadecylisophthalonitrile, by direct cyanation according to Rosenmund-von Braun reaction.[48,49] 4-Methoxy-6-pentadecylisophthalonitrile was later reduced to 4-methoxy-6-pentadecylisophthalaldehyde using diisobutyaluminiumhydride (DIBAL) (1M solution in toluene) as the reducing agent.[50] 4-Methoxy-6-pentadecylisophthalaldehyde was purified by column chromatography and characterised by spectroscopic methods.

FT-IR spectrum of 4-methoxy-6-pentadecylisophthalaldehyde (MPIAL) is presented in **Fig 3.4**

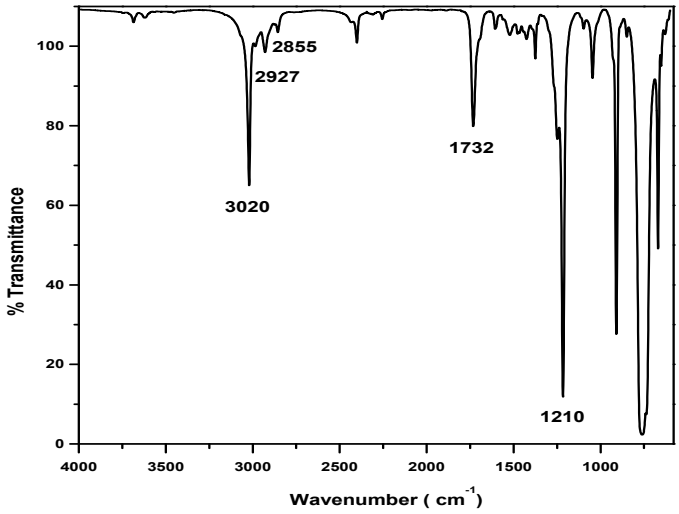

Figure 3.4 FT-IR spectrum of 4-methoxy-6-pentadecylisophthalaldehyde (MPIAL)

The presence of an absorption band at 1732 cm^{-1}, corresponding to C=O stretch, suggested the formation of carbonyl group. Two medium intensity peaks at 2927 cm^{-1} and 2855 cm^{-1}, corresponding to C-H out of plane vibrations, confirmed the formation of aldehyde functionality.

^{1}H-NMR spectrum of 4-methoxy-6-pentadecylisophthalaldehyde (MPIAL) along with assignments is depicted in **Fig 3.5**

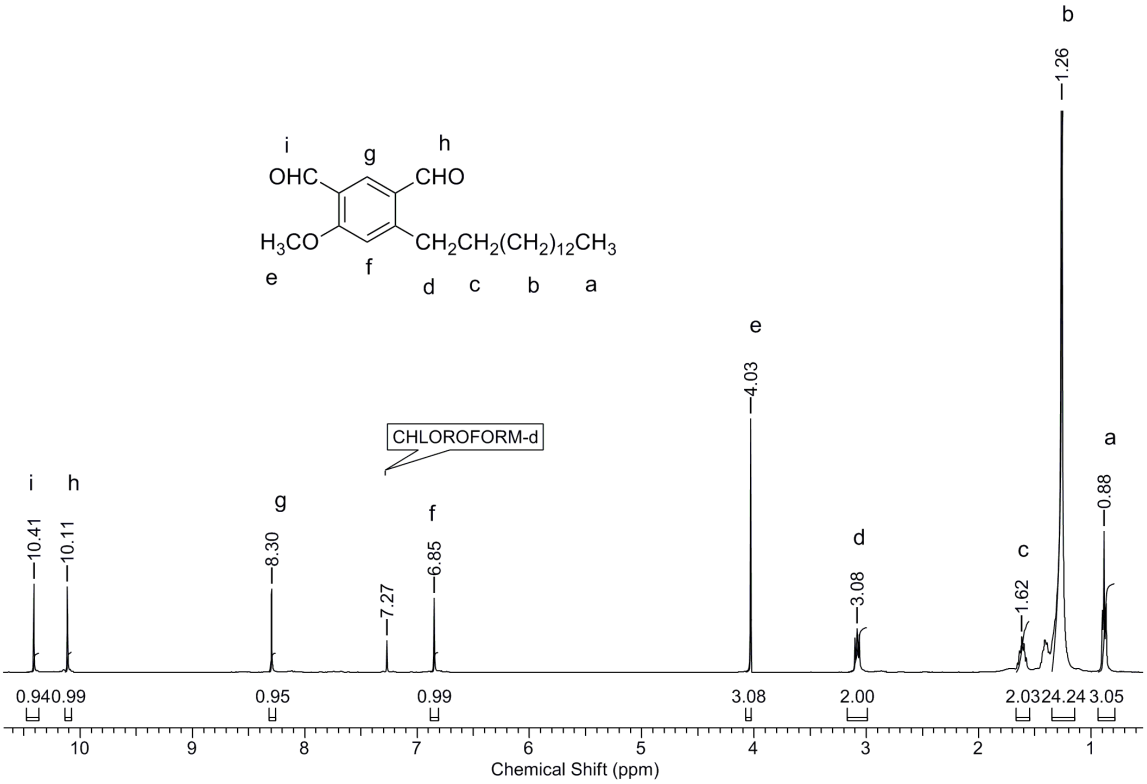

Figure 3.5 ^{1}H-NMR spectrum ($CDCl_3$) of 4-methoxy-6-pentadecylisophthalaldehyde (MPIAL)

The presence of two singlets at 10.11 δ ppm and 10.41 δ ppm, corresponding to aldehyde protons (**h,i**), confirmed the formation of dialdehyde. The aromatic proton *ortho* to the aldehyde groups (**g**) was deshielded, at 8.30 δ ppm compared to the proton *ortho* to the methoxy group (**f**), which appeared at 6.85 δ ppm. The methoxy protons (**e**) appeared at 4.03 δ ppm as a singlet. The benzylic methylene protons (**d**) appeared at 3.08 δ ppm as a triplet, while the methylene protons (**b**) appeared as a multiplet at 1.2 – 1.53 δ ppm. The terminal methyl protons (**a**) appeared as a triplet at 0.88 δ ppm.

^{13}C-NMR spectrum of 4-methoxy-6-pentadecylisophthalaldehyde (MPIAL) along with assignments is presented in **Fig 3.6**

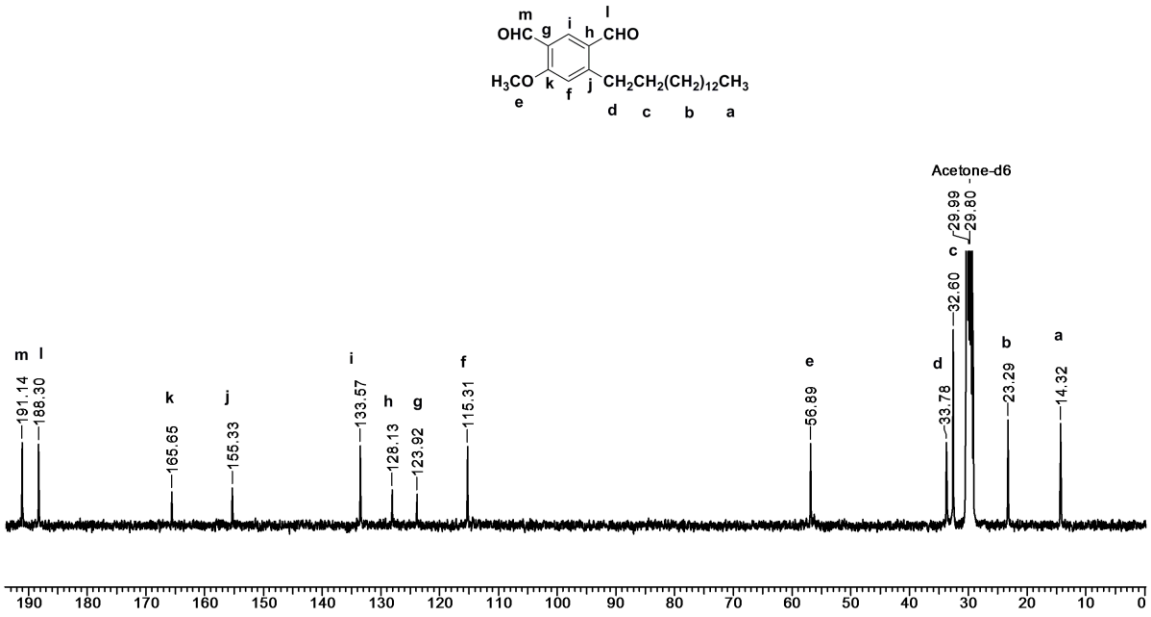

Figure 3.6 ^{13}C-NMR spectrum (Acetone-d_6) of 4-methoxy-6-pentadecylisophthalaldehyde (MPIAL)

The signals at 191.14 δ ppm and 188.30 δ ppm could be readily ascribed to the aldehyde carbons (**l**, **m**). The aromatic carbon flanked by the two aldehyde functionalities (**i**) appeared at 133.57 δ ppm, more downfield than carbon **f** which is positioned *meta* to the aldehyde functionalities and resonated at 115.31 δ ppm. The carbon atoms bearing the aldehyde functionalities appeared at 128.13 δ ppm and 123.42 δ ppm. The remaining aromatic carbon atoms (**k**,**j**) resonated at 165.65 δ ppm and 155.33 δ ppm. The signal appearing at 56.89 δ ppm could be assigned to methoxy carbon (**e**).The benzylic carbon atom (**d**) appeared at 33.78 δ ppm while the terminal methyl carbon (**a**) belonging to the pentadecyl chain resonated at 14.32 δ ppm.

HRMS data of 4-methoxy-6-pentadecylisophthalaldehyde (MPIAL) showed good agreement with calculated values. (**Supporting Information Fig SI 3.2**)

Thus, FT-IR, ^{1}H-NMR, ^{13}C-NMR and HRMS results clearly indicated that the proposed structure of synthesised dialdehyde, 4-methoxy-6-pentadecylisophthalaldehyde (MPIAL), was consistent with the observed results.

3.4.3 Synthesis of 4-methoxy-6-pentadecylisophthalic acid (MPIA)

Scheme 3.3 outlines the synthesis of diacid:

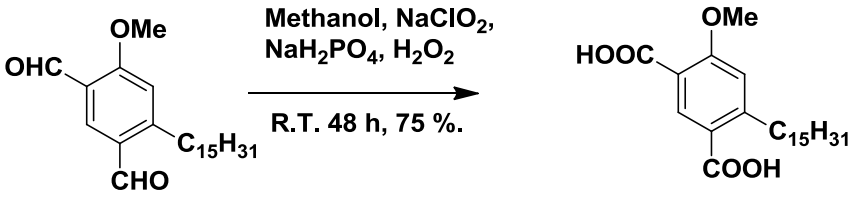

Scheme 3.3 Synthesis of 4-methoxy-6-pentadecylisophthalic acid (MPIA)

4-Methoxy-6-pentadecylisophthalic acid was obtained by oxidation of the dialdehyde, 4-methoxy-6-pentadecylisophthalaldehyde (MPIAL) (**Section 3.4.2**), using sodium chlorite as an oxidant.[51] Hydrogen peroxide was used as a HOCl scavenger while sodium dihydrogen orthophosphate was used to maintain a weakly acidic medium to reduce side reactions. The diacid monomer was purified by column chromatography and characterised by spectroscopic means.

In **Fig 3.7** is depicted FT-IR spectrum of 4-methoxy-6-pentadecylisophthalic acid (MPIA).

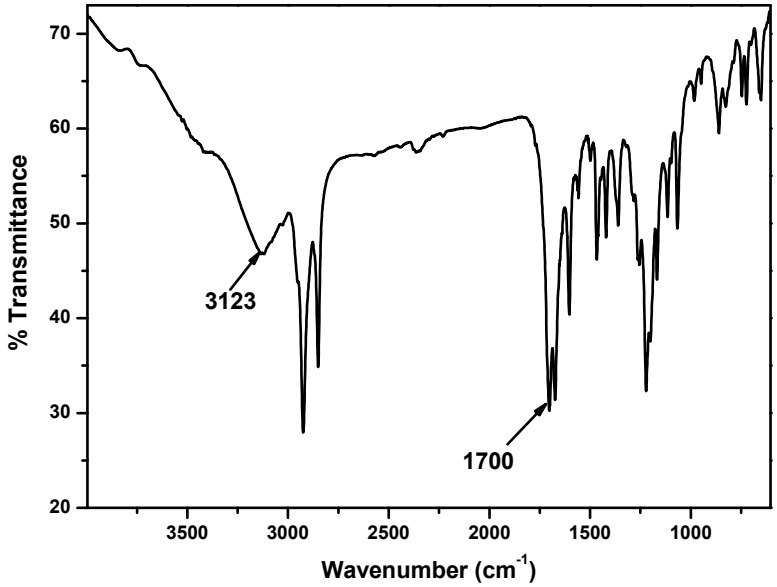

Figure 3.7 FT-IR spectrum of 4-methoxy-6-pentadecylisophthalic acid (MPIA)

IR spectrum showed a broad absorption band at 3123 cm^{-1} corresponding to hydrogen bonded OH. The absorption band at 1700 cm^{-1} is attributed to C=O stretching of carboxyl functionality. The appearance of these absorption bands indicated the formation of diacid.

^{1}H-NMR spectrum of 4-methoxy-6-pentadecylisophthalic acid (MPIA) along with assignments is presented in **Fig 3.8**.

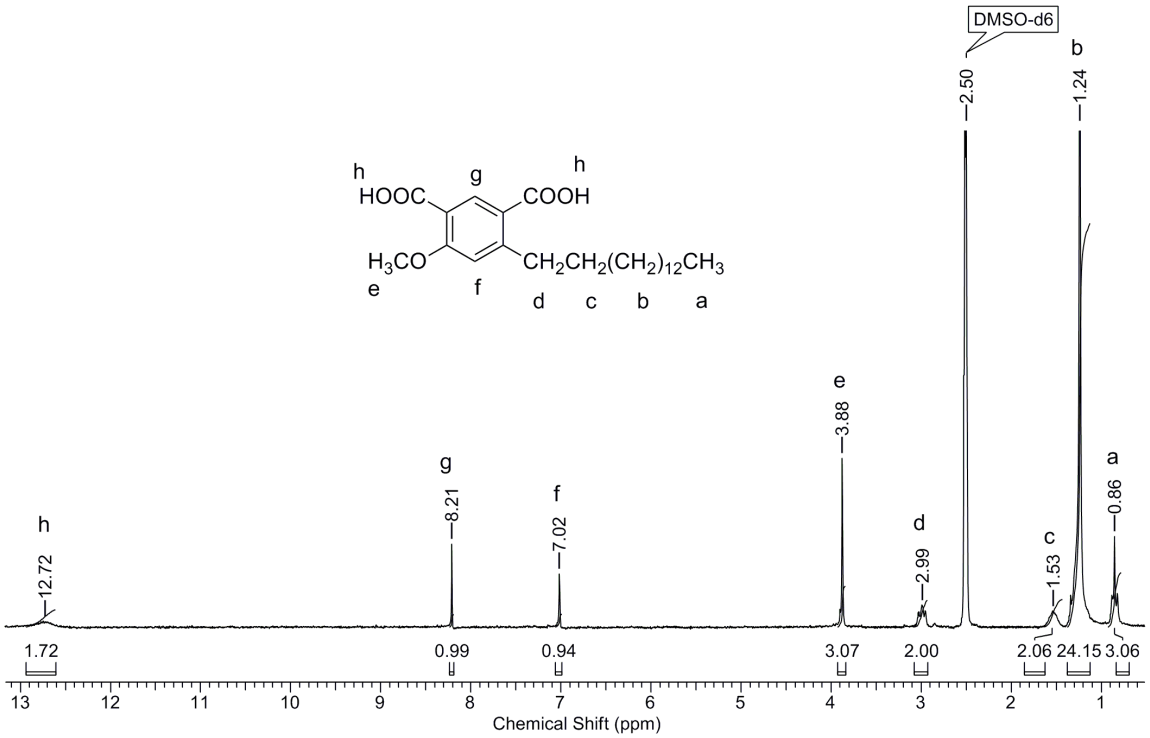

Figure 3.8 ^{1}H-NMR spectrum (DMSO-d_6) of 4-methoxy-6-pentadecylisophthalic acid (MPIA)

A broad singlet at 12.73 δ ppm indicated carboxylic OH protons. The singlets appearing at 8.21 δ ppm and 7.02 δ ppm correspond to aromatic protons (**a**,**b**). Methoxy protons (**e**) appeared as a singlet at 3.88 δ ppm. Benzylic protons (**d**) resonated at 2.99 δ ppm, while the methylene protons (**b**, **c**) appeared as a multiplet in the range 1.00 – 1.56 δ ppm. The terminal methyl protons of the alkyl chain (**a**) appeared at 0.86 δ ppm.

^{13}C-NMR spectrum of 4-methoxy-6-pentadecylisophthalic acid (MPIA) is depicted in **Fig 3.9**.

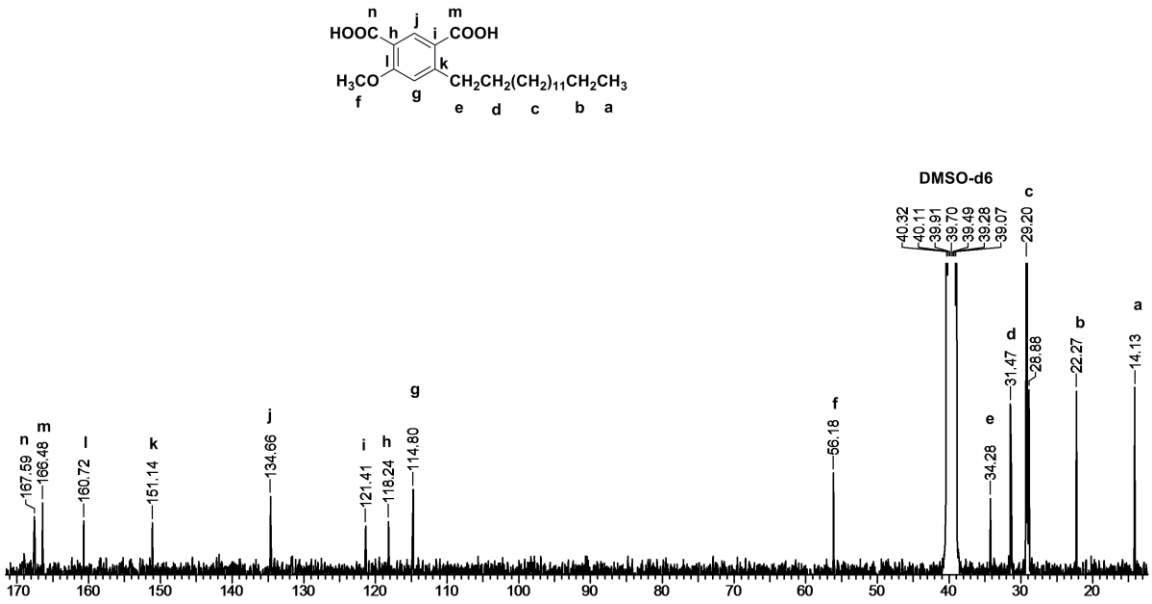

Figure 3.9 ^{13}C-NMR spectrum (DMSO-d_6) of 4-methoxy-6-pentadecylisophthalic acid (MPIA)

The signals at 167.59 δ ppm and 166.48 δ ppm were readily assignable to the carboxyl carbons (**m**,**n**). The aromatic carbon **j**, flanked by the carboxyl groups appeared at 134.66 δ ppm, while the carbon atom **g**, flanked by the methoxy and pentadecyl functionalities resonated upfield at 114.80 δ ppm. The carbon atom **l** linked to the methoxy functionality resonated downfield at 160.72 δ ppm, when compared to the carbon (**k**) linked to the pentadecyl moiety, which appeared at 151.14 δ ppm. The remaining aromatic carbon atoms (**i**, **h**) resonated at 121.41 δ ppm and 118.24 δ ppm. The signal corresponding to the carbon atom of the methoxy functionality (**f**) appeared at 56.18 δ ppm. The benzylic carbon (**e**) resonated at 34.18 δ ppm while the methylene carbons (**b**, **c**, **d**) appeared in the range 22.27 – 31.47 δ ppm. The methyl carbon (**a**) resonated at 14.13 δ ppm.

HRMS data of 4-methoxy-6-pentadecylisophthalic acid (MPIA) showed good agreement with calculated values (**Supporting Information Fig SI 3.3**).

Thus, FT-IR, ^{1}H-NMR, ^{13}C-NMR and HRMS results clearly indicated that the proposed structure of synthesised diacid, 4-methoxy-6-pentadecylisophthalic acid (MPIA), was consistent with the observed results.

3.4.4 Synthesis of 4-(4-hydroxyphenoxy)-3-pentadecylphenol (HPPDP)

This monomer was prepared according to reported procedure.[43]

Scheme 3.4 depicts route for synthesis of 4-(4-hydroxyphenoxy)-3-pentadecylphenol (HPPDP) starting from 3-pentadecyl phenol.

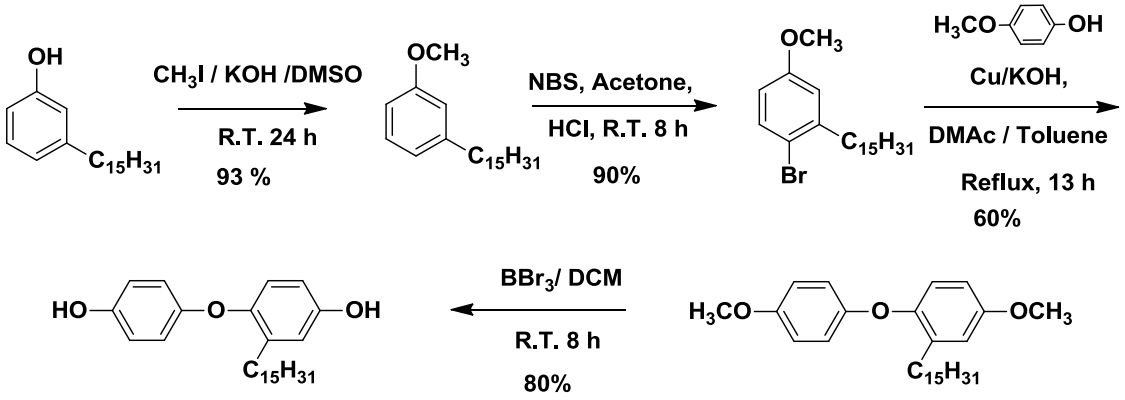

Scheme 3.4 Synthesis of 4-(4-hydroxyphenoxy)-3-pentadecylphenol (HPPDP)

The synthesis of 4-(4-hydroxyphenoxy)-3-pentadecylphenol was accomplished in four steps. In the first step, pentadecyl phenol was methylated to yield 1-methoxy-3-pentadecylbenzene, as discussed in sections **3.3.2** and **3.4.2**. Thereafter, 1-methoxy-3-pentadecylbenzene was brominated using *N*-bromosuccinimide and catalytic quantity of hydrochloric acid. This step yielded the mono bromo product, 1-bromo-4-methoxy-2-pentadecylbenzene.[52,53] Thereafter, 1-bromo-4-methoxy-2-pentadecylbenzene was reacted with 4-methoxy phenol in accordance with classical Ullmann etherification reaction conditions, in the presence of copper powder and potassium hydroxide to provide 4-methoxy-1-(4-methoxyphenoxy)-2-pentadecylbenzene. Subsequently, 4-methoxy-1-(4-methoxyphenoxy)-2-pentadecylbenzene was demethylated following standard demethylation conditions utilising boron tribromide in chloroform to yield the bisphenol, 4-(4-hydroxyphenoxy)-3-pentadecylphenol (HPPDP). 4-(4-hydroxyphenoxy)-3-pentadecylphenol was characterised by standard spectroscopic procedures.

FT-IR spectrum of 4-(4-hydroxyphenoxy)-3-pentadecylphenol (HPPDP) is reproduced in **Fig 3.10**.

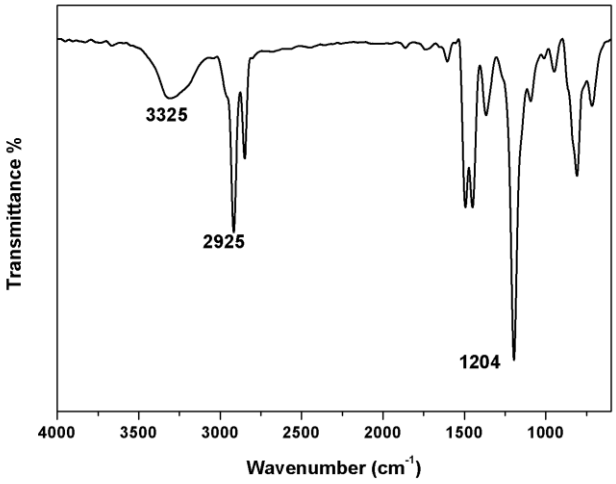

Figure 3.10 FT-IR spectrum 4-(4-hydroxyphenoxy)-3-pentadecylphenol (HPPDP)

A broad absorption band was observed at 3325 cm^{-1}, assignable to the phenolic hydroxyl group. The band at 1204 cm^{-1}appeared due to C–O–C stretching.

^{1}H-NMR spectrum of 4-(4-hydroxyphenoxy)-3-pentadecylphenol (HPPDP) along with assignments is presented in **Fig 3.11**.

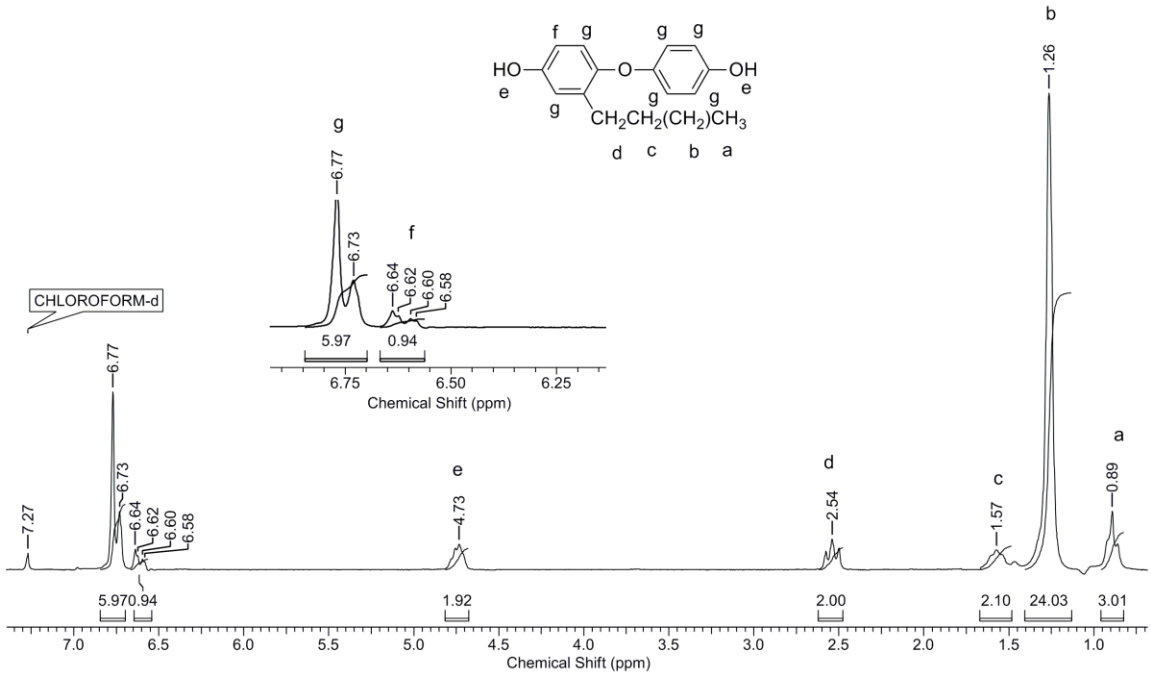

Figure 3.11 ^{1}H-NMR spectrum ($CDCl_3$) of 4-(4-hydroxyphenoxy)-3-pentadecylphenol (HPPDP)

The aromatic proton **e** appeared at 6.61 δ ppm as a doublet of doublet due to *ortho* and *meta* coupling interactions. The remaining aromatic protons (**g**) resonated in the range 6.70 – 6.84 δ ppm in the form of a multiplet. The hydroxyl protons were observed to appear at 4.74 δ ppm as a broad singlet. A triplet at 2.54 δ ppm was assignable to the benzylic methylene protons (**d**) belonging to the pentadecyl chain. The remaining methylene protons (**c**,**b**) appeared in the range 1.13 – 1.67 δ ppm. The methyl protons (**a**) of the pentadecyl chain resonated at 0.89 δ ppm.

^{13}C-NMR spectrum of 4-(4-hydroxyphenoxy)-3-pentadecylphenol (HPPDP) along with assignments is represented in **Figure 3.12.**

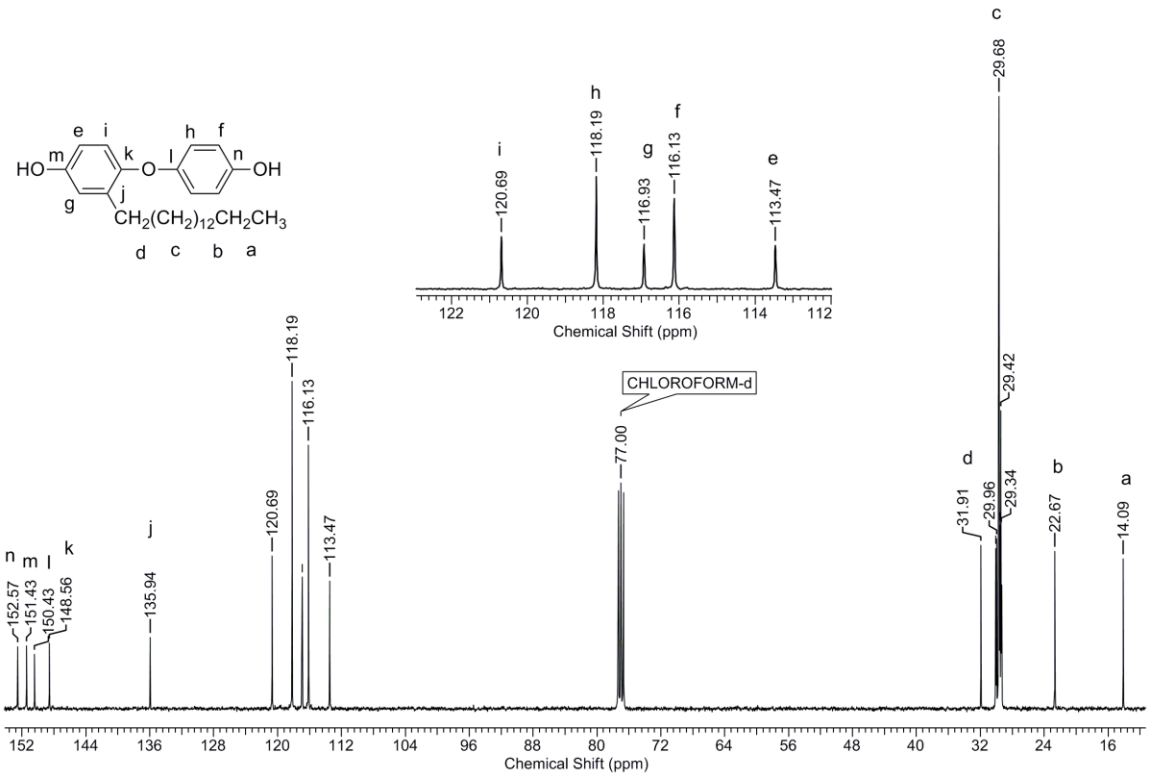

Figure 3.12 ^{13}C-NMR spectrum ($CDCl_3$) of 4-(4-hydroxyphenoxy)-3-pentadecylphenol (HPPDP)

The quaternary carbon atoms attached to the oxygen atoms belonging either to the hydroxyl functionality or ether functionality (**k**-**n**) appeared downfield in the range 148.56 – 152.57 δ ppm. The quaternary carbon linked to pentadecyl chain (**j**) appeared upfield at 135.94 δ ppm. The remaining aromatic carbon atoms (**e**-**i**) resonated in the range 113.47 – 120.69 δ ppm. The signals appearing in the spectrum showed good agreement with the proposed structure. The signal corresponding to the benzylic carbon

(**d**) was observed at 31.91 δ ppm while the signals for the methylene carbons (**b**, **c**) appeared in the range 22.67 – 30.22 δ ppm. The methyl carbon (**a**) appeared at 14.09 δ ppm.

3.4.5 Synthesis of 3-pentadecyl biphenol (PDBP)

This monomer was prepared in accordance to reported procedure.[44]

Scheme 3.5 outlines the route followed for synthesis of 3-pentadecyl biphenol (PDBP).

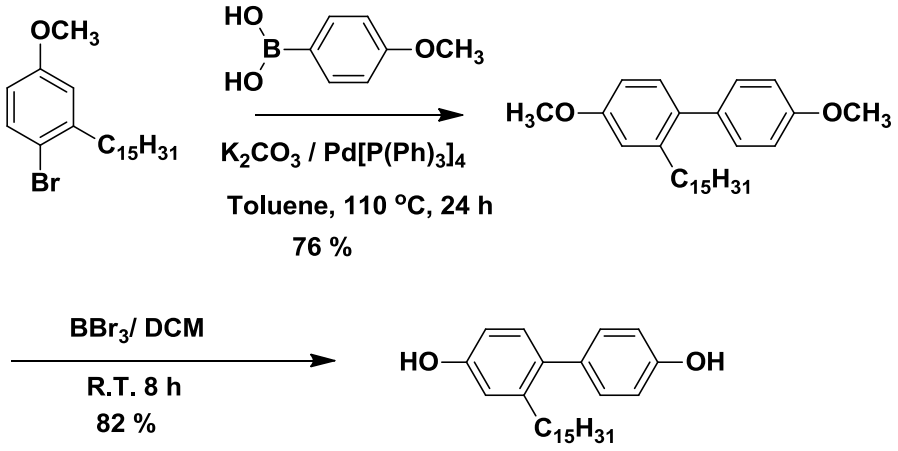

Scheme 3.5 Synthesis of 3-pentadecyl biphenol (PDBP)

3-Pentadecyl biphenol was synthesised from 1-methoxy-3-pentadecylbenzene in two steps, the first step involving Suzuki-Miyaura reaction being the key step. Suzuki-Miyaura is a Palladium catalysed carbon-carbon coupling reaction.[54,55] Although several other carbon-carbon coupling reactions are known, *viz*, Kharash coupling, Negishi coupling, Stille coupling, Himaya coupling, Liebeskind–Srogl coupling and Kumuda coupling, the Suzuki-Miyaura reaction has proven to be the most popular reaction in recent times.[56] 1-Methoxy-3-pentadecylbenzene was treated with 4-methoxy boronic acid and potassium carbonate in the presence of catalytic amount of tetrakis(triphenylphosphine)palladium and toluene as a solvent to yield 4, 4'-dimethoxy-2-pentadecyl-1,1'-biphenyl which was demethylated by boron tribromide in chloroform. The obtained bisphenol, 3-pentadecyl biphenol (PDBP) was purified by recrystallisation from a mixture of petroleum ether and dichloromethane and characterised by spectroscopic methods.

FT-IR spectrum of 3-pentadecyl biphenol (PDBP) is shown in **Fig 3.13**.

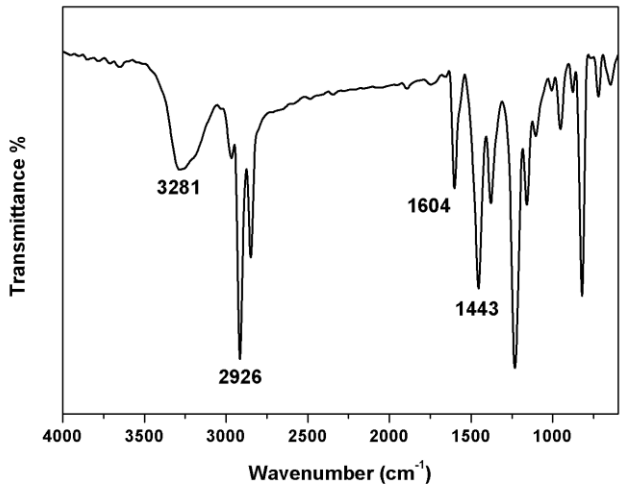

Figure 3.13 FT-IR spectrum of 3-pentadecyl biphenol (PDBP)

The broad absorption band appearing at 3281 cm^{-1} could be assigned to –OH stretching.

^{1}H-NMR spectrum of 3-pentadecyl biphenol (PDBP) is depicted in **Fig 3.14**.

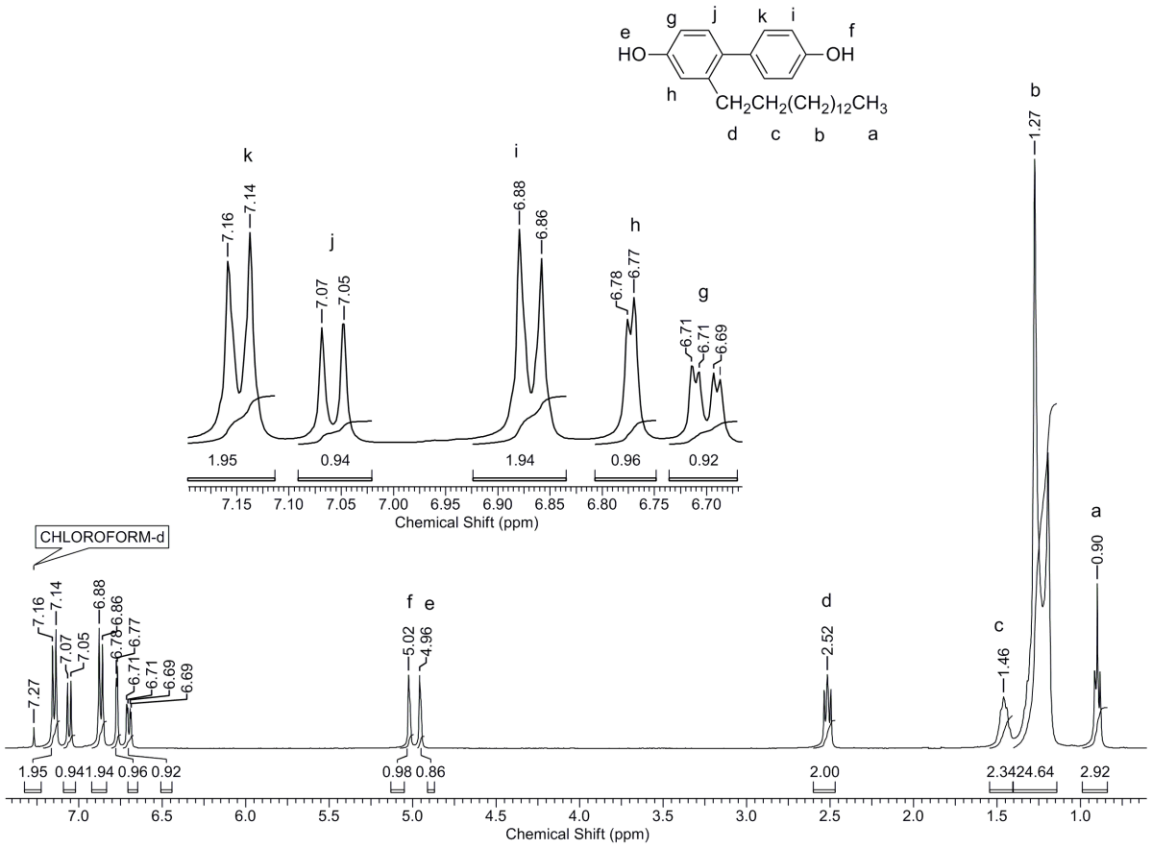

Figure 3.14 ^{1}H-NMR spectrum ($CDCl_3$) of 3-pentadecyl biphenol (PDBP)

Two aromatic protons, **k**, positioned *meta* to –OH functionality appeared as the most deshielded signal at 7.15 δ ppm, as a doublet. The other aromatic proton **j** which is also positioned *meta* to –OH appeared as a doublet at 7.06 δ ppm. The aromatic protons **i** and **h**, both positioned *ortho* to the –OH functionality appeared shielded at 6.87 δ ppm and 6.77 δ ppm, respectively. A doublet of doublet appearing at 6.70 δ ppm could be easily assigned to the aromatic proton **g**, positioned *ortho* to –OH functionality, but *para* to the pentadecyl chain, thus being the most shielded aromatic proton. The protons belonging to the –OH functionality, **f** and **e**, resonated at 5.02 δ ppm and 4.96 δ ppm, respectively. The benzylic protons (**d**) appeared as a triplet at 2.52 δ ppm. The methylene protons (**c**, **b**) resonated in the range 1.25 δ ppm – 1.50 δ ppm, while the methyl protons of the pentadecyl chain (**a**) appeared at 0.90 δ ppm, in the form of a triplet.

^{13}C-NMR spectrum of 3-pentadecyl biphenol (PDBP) along with assignments is presented in **Fig 3.15**.

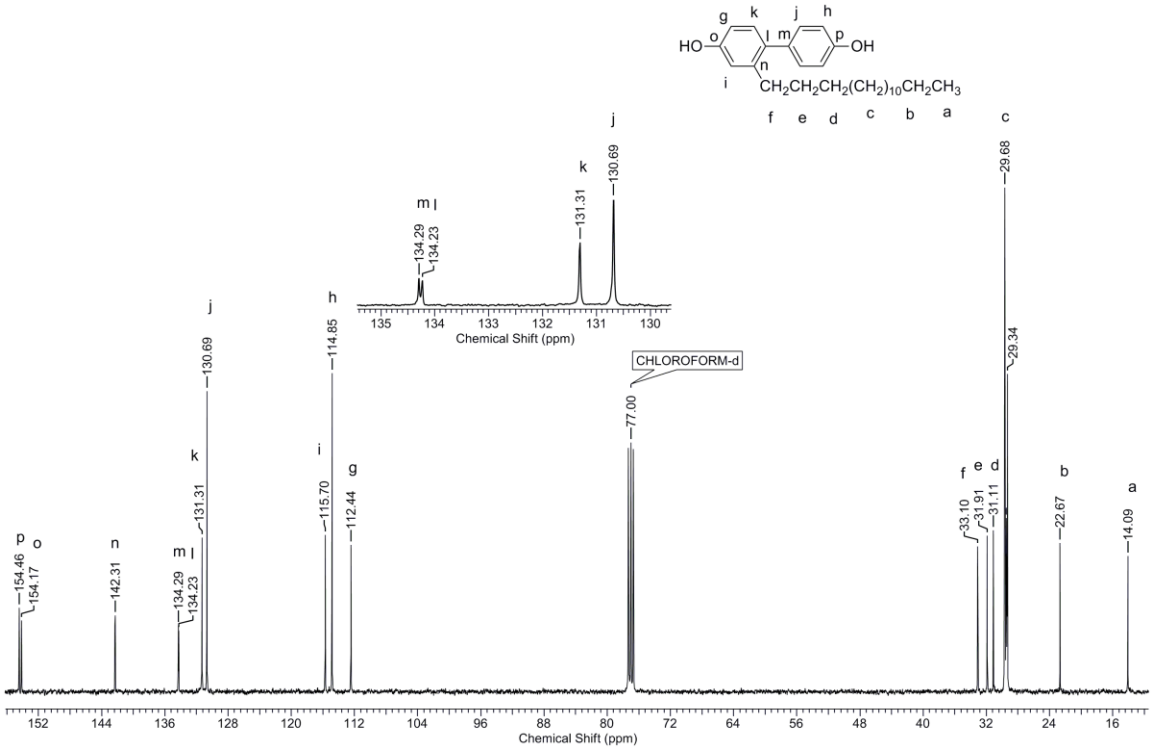

Figure 3.15 ^{13}C-NMR spectrum ($CDCl_3$) of 3-pentadecyl biphenol (PDBP)

The signals appearing at 154.46 δ ppm and 154.17 δ ppm were assignable to the aromatic carbon atoms (**p**, **o**) linked to the –OH functionality. The quaternary carbon linked to the pentadecyl chain (**n**) appeared at 142.31 δ ppm, while the aromatic carbons

linked to each other, **m** and **l**, resonated at 134.29 δ ppm and 134.23 δ ppm, respectively. The aromatic carbon atoms positioned *meta* to the –OH functionality, **k** and **j**, appeared deshielded at 131.31 δ ppm and 130.69 δ ppm, respectively. The remaining aromatic carbons, positioned *ortho* to the –OH group, **i**, **h** and **g**, appeared shielded at 115.70 δ ppm, 114. 85 δ ppm and 112.44 δ ppm, respectively. The signal at 33.10 δ ppm could be ascribed to the benzylic carbon atom (**f**). The methylene carbon atoms (**e-b**) appeared in the range 22.67 δ ppm – 31.91 δ ppm, while the methyl carbon (**a**) resonated at 14.09 δ ppm.

3.4.6 Synthesis of 4,4'-(3-pentadecylcyclohexane-1,1-diyl)diphenol (BPC15)

This monomer was synthesised according to reported procedure.[45]

Scheme 3.6 presents the route for synthesis of 4,4'-(3-pentadecylcyclohexane-1,1-diyl)diphenol (BPC15) starting from 3-pentadecyl phenol.

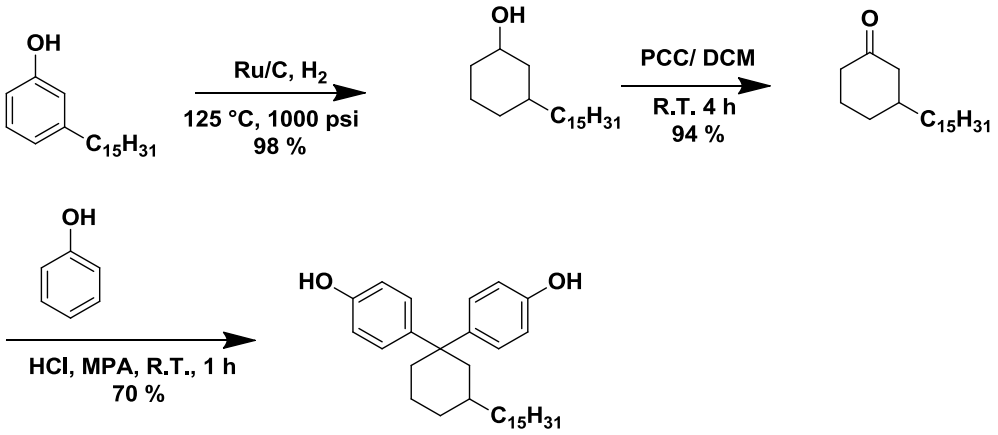

Scheme 3.6 Synthesis of 4,4'-(3-pentadecylcyclohexane-1,1-diyl)diphenol (BPC15)

4,4'-(3-Pentadecylcyclohexane-1,1-diyl)diphenol (BPC15) was synthesised from 3-pentadecyl phenol in three steps. In the first step, 3-pentadecyl phenol was reduced to yield 3-pentadecyl cyclohexanol. Transition metal catalysts, *viz*, Pd, Rh, Co, Ni, Pt, Ru, etc are well known for the hydrogenation of phenols. In this study, 5 % Ru/C was employed for the reduction of 3-pentadecyl phenol to obtain 3-pentadecyl cyclohexanol in a Parr reactor at 125 °C, at hydrogen pressure of 1000 psi. Subsequently, 3-pentadecyl cyclohexanol was oxidised to provide 3-pentadecyl cyclohexanone, using pyridinium chlorochromate (PCC). In the final step, 4,4'-(3-pentadecylcyclohexane-1,1-diyl)diphenol (BPC15) was synthesised by condensation of 3-pentadecyl cyclohexanone with phenol in

the presence of hydrogen chloride and 3-mercaptopropionic acid. In the presence of strong acids, 3-mercaptopropionic acid is known to increase the rate and selectivity for the formation of desired bisphenol (*p,p* isomer). The pure BPC15 was characterised by FTIR, ^{1}H-NMR, HSQC and ^{13}C-NMR spectroscopy.

FT-IR spectrum of 4,4'-(3-pentadecylcyclohexane-1,1-diyl)diphenol (BPC15) is shown in **Fig 3.16**.

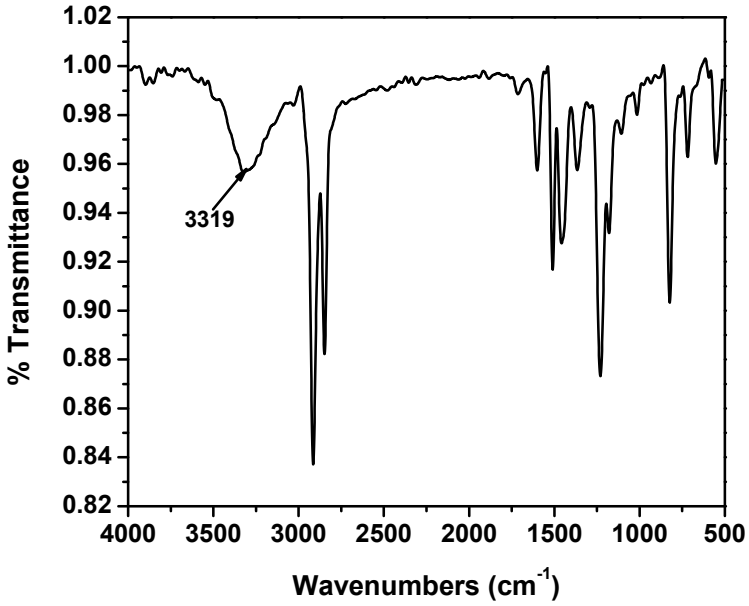

Figure 3.16 FT-IR spectrum of 4,4'-(3-pentadecylcyclohexane-1,1-diyl)diphenol (BPC15)

A broad absorption band at 3319 cm^{-1} (OH stretching) confirmed the presence of hydroxyl functionality.

^{1}H-NMR ($CDCl_3$) spectrum of 4,4'-(3-pentadecylcyclohexane-1,1-diyl)diphenol (BPC15) is shown in **Fig 3.17**.

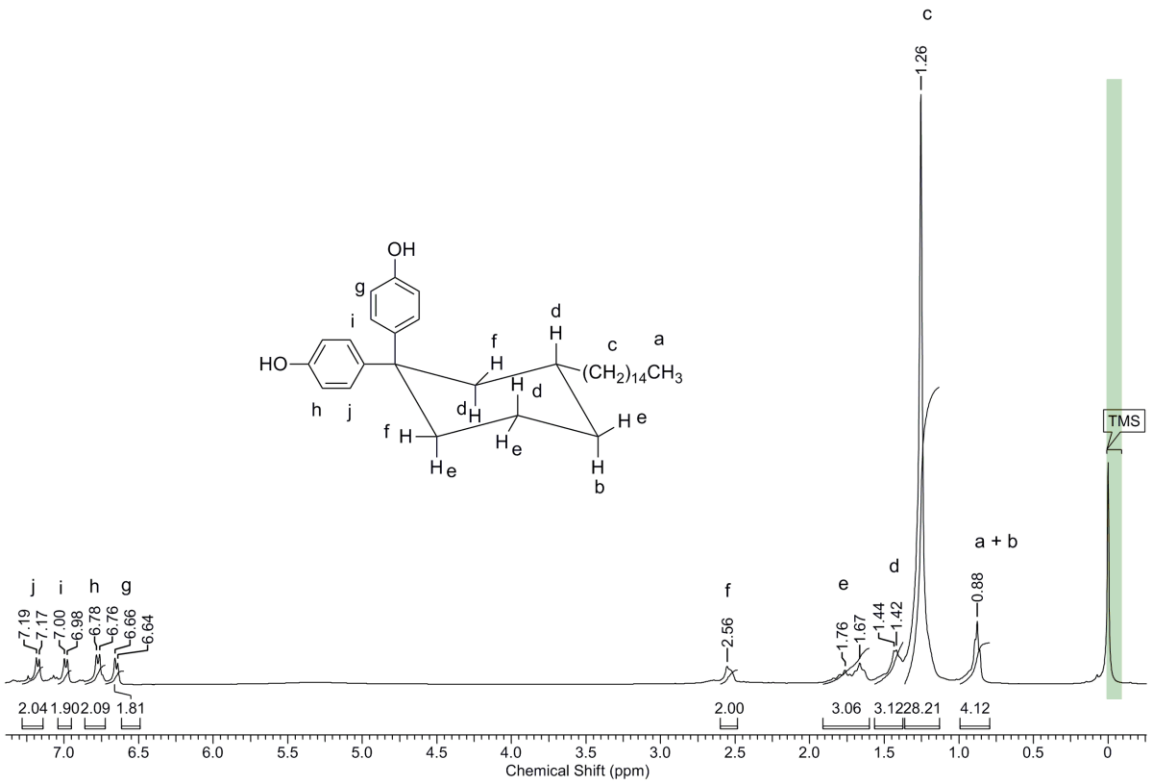

Figure 3.17 ^{1}H-NMR spectrum ($CDCl_3$) of 4,4'-(3-pentadecylcyclohexane-1,1-diyl)diphenol (BPC15)

Detailed study of the ^{1}H-NMR, HSQC and ^{13}C-NMR spectra revealed that the phenyl rings were magnetically non-equivalent. The pentadecyl substituent prevents ring inversion; hence the conformation of the cyclohexyl ring is locked in the chair conformer as depicted in **Fig 3.17**, with the substituent present in the equatorial position. It was found that the equatorial protons appeared up-field compared to corresponding axial protons. The aromatic protons present *ortho* to the hydroxyl functionality on the axial phenyl ring (**g**) appeared at 6.65 δ ppm in the form of a doublet, while those on the equatorial phenyl ring (**h**) resonated downfield at 6.77 δ ppm as a doublet. The aromatic protons *meta* to the hydroxyl functionality, belonging to the axial phenyl ring, (**i**) appeared as a doublet at 6.99 δ ppm. Similarly, the protons **j**, belonging to the equatorial phenyl ring resonated at 7.17 δ ppm as a doublet. Further assignment of the protons was done by a combined study of ^{1}H-NMR, HSQC and ^{13}C-NMR spectra.

HSQC spectrum of 4,4'-(3-pentadecylcyclohexane-1,1-diyl)diphenol (BPC15) is depicted in **Fig 3.18**.

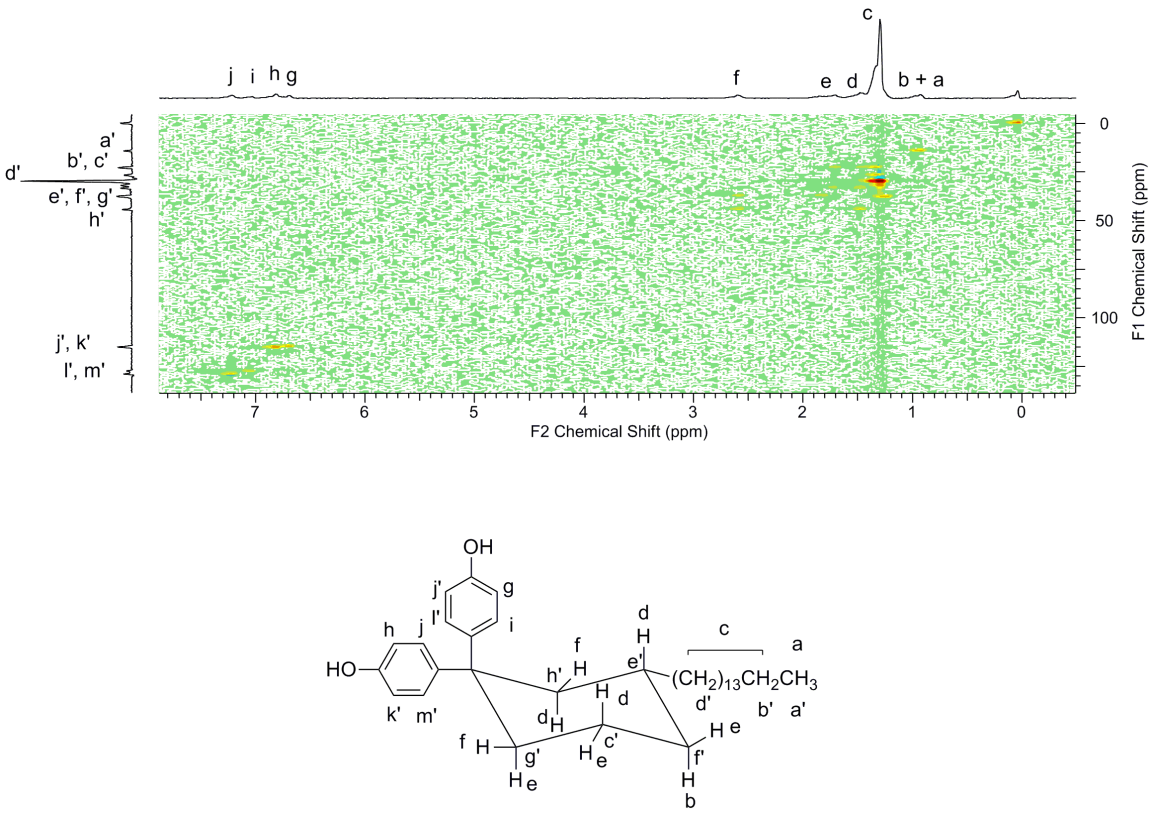

Figure 3.18 HSQC spectrum ($CDCl_3$) of 4,4'-(3-pentadecylcyclohexane-1,1-diyl)diphenol (BPC15).

Protons present on the carbons **e'**, **f'**, **g'**, **h'** and **c'** could be successfully assigned unambiguously on the basis of HSQC spectrum. Equatorial protons (**f**) on carbon **g'** and carbon **h'** appeared at 2.48 – 2.60δ ppm as a multiplet. The axial protons on carbon **g'**, and equatorial protons on carbons **c'** and **f'** (**e**) appeared together as a multiplet at 1.60 – 1.91 δ ppm. The axial protons (**d**) on carbons **e'**, **h'** and **c'** resonated together in the range 1.37 – 1.57 δ ppm as a multiplet. Axial proton (**b**) on carbon **f'** and the methyl protons (**a**) appeared as a multiplet in the range 0.79 – 0.99 δ ppm. The methylene protons (**c**) resonated at 1.13 – 1.36 δ ppm as a multiplet.

^{13}C-NMR spectrum of 4,4'-(3-pentadecylcyclohexane-1,1-diyl)diphenol (BPC15) is shown in **Fig 3.19.**

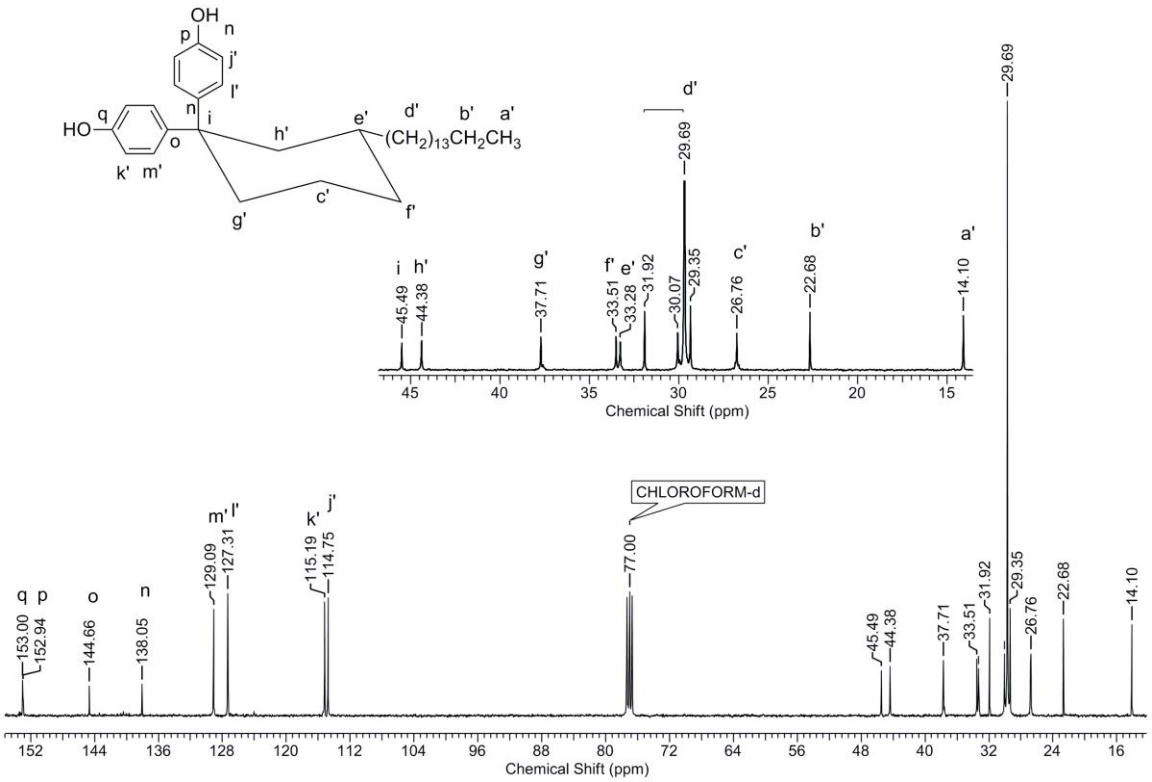

Figure 3.19 ^{13}C-NMR spectrum ($CDCl_3$) of 4,4'-(3-pentadecylcyclohexane-1,1-diyl)diphenol (BPC15)

^{13}C-NMR spectrum of BPC15 was assigned with the help of the corresponding DEPT spectrum and HSQC spectrum. The carbons **c', e'**, **f'**, **g'**, and **h'** appearing at 26.76 δ ppm, 33.28 δ ppm, 33.51 δ ppm, 37.71 δ ppm and 44.38 δ ppm, respectively, could be successfully assigned on the basis of HSQC spectrum. The aromatic carbons positioned *ortho* to the hydroxyl functionality, **j'** and **k'**, on the axial and equatorial phenyl rings, appeared at 114.75 δ ppm and 115.19 δ ppm, respectively. The aromatic carbons *meta* to the hydroxyl functionality, **l'** and **m'**, appeared at 127.31 δ ppm and 129.09 δ ppm, respectively. The aromatic carbons linked to the cyclohexyl ring, **n** and **o**, appeared at 138.05 δ ppm and 144.66 δ ppm, present on the axial and equatorial phenyl rings, respectively. The aromatic carbons linked to the hydroxyl functionality, present on the axial (**p**) and equatorial phenyl rings (**q**), resonated at 152.94 δ ppm and 153.00 δ ppm.

3.4.7 Synthesis of 2,6-bis(4-hydroxybenzylidene)-3-pentadecylcyclohexanone (BPC)

Scheme 3.7 presents the route for synthesis of 2,6-bis(4-hydroxybenzylidene)-3-pentadecylcyclohexanone (BPC) starting from 3-pentadecyl cyclohexanone (**Section 3.4.6**).

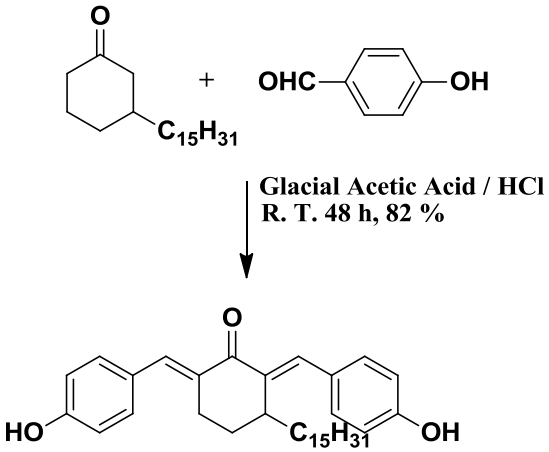

Scheme 3.7 Synthesis of 2,6-bis(4-hydroxybenzylidene)-3-pentadecylcyclohexanone (BPC)

2,6-Bis(4-hydroxybenzylidene)-3-pentadecylcyclohexanone (BPC) was synthesised from 3-pentadecyl cyclohexanone in one step, *via* cross-aldol condensation reaction of one equivalent of ketone with two equivalents of *p*-hydroxybenzaldehyde in glacial acetic acid saturated with anhydrous hydrogen chloride over a period of two days.[57] The crude product obtained was purified by column chromatography and characterised spectroscopically.

FT-IR spectrum of 2,6-bis(4-hydroxybenzylidene)-3-pentadecylcyclohexanone (BPC) is shown in **Fig 3.20**.

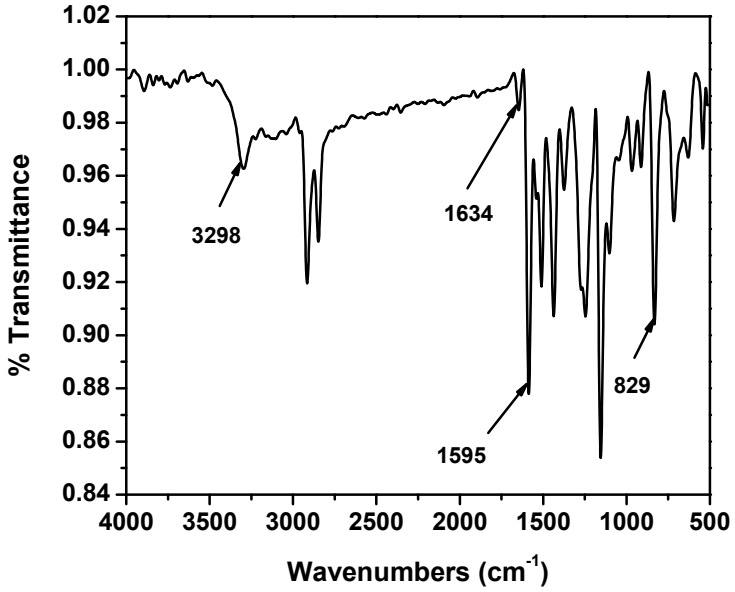

Figure 3.20 FT-IR spectrum of 2,6-bis(4-hydroxybenzylidene)-3-pentadecylcyclohexanone (BPC)

Appearance of a broad absorption band at 3298 cm^{-1} (O-H stretching) confirmed the presence of hydroxyl functionality. The strong absorption band at 1595 cm^{-1}(C=O stretching) indicated the presence of ketone functionality, while the absorption bands at 1634 cm^{-1} (-C=C- stretching) and 829 cm^{-1} (=C-H bending) were suggestive of the presence of alkene functionality.

^{1}H-NMR spectrum of 2,6-bis(4-hydroxybenzylidene)-3-pentadecylcyclohexanone (BPC) is shown in **Fig 3.21**.

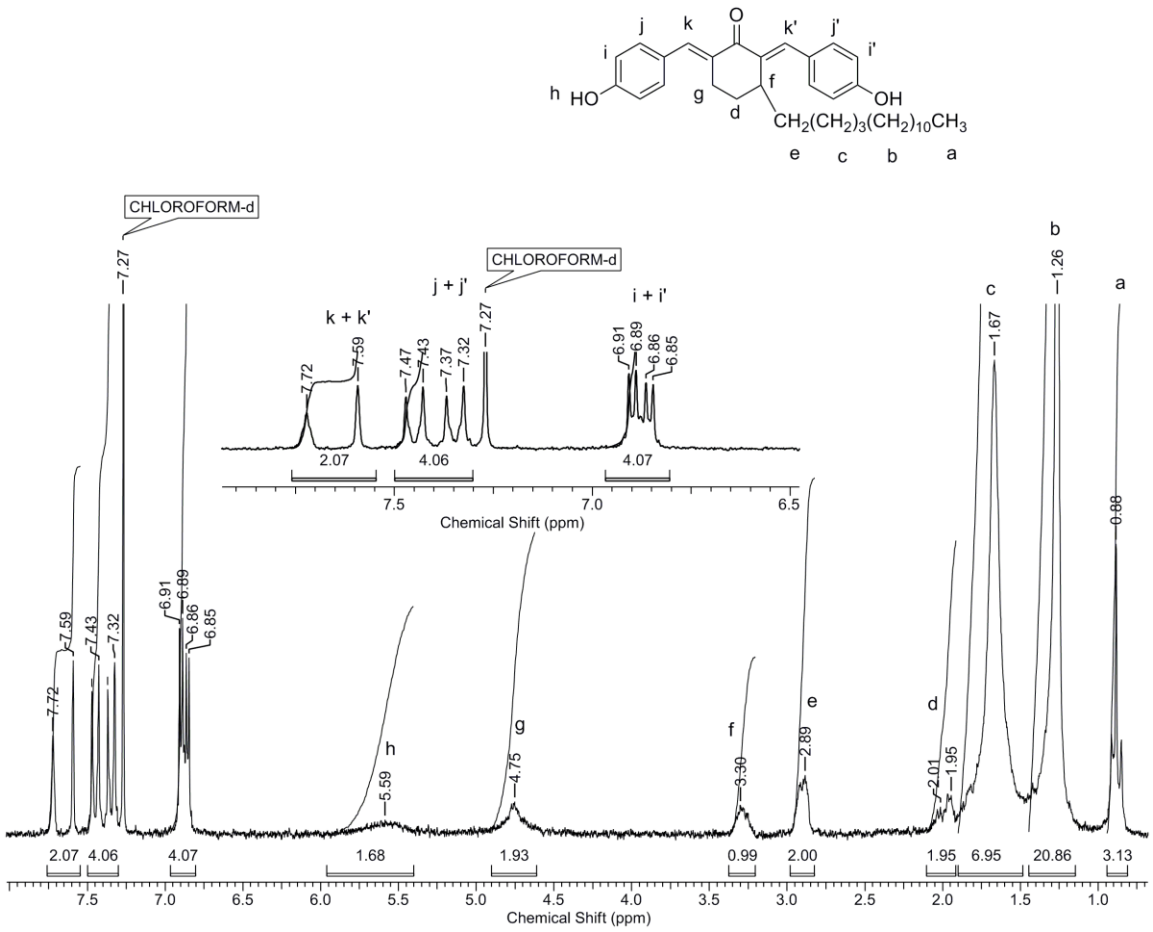

Figure 3.21 ^{1}H-NMR spectrum ($CDCl_3$) of 2,6-bis(4-hydroxybenzylidene)-3-pentadecylcyclohexanone (BPC)

The alkenyl protons (**k** and **k'**) appeared at 7.72 δ ppm and 7.59 δ ppm. The aromatic protons **j** and **j'**, positioned *meta* to the hydroxyl substituent, appeared at 7.45 δ ppm and 7.35 δ ppm, respectively, as doublets, while the aromatic protons present *ortho* to the hydroxyl functionality (**i** and **i'**) resonated as doublets at 6.90 δ ppm and 6.85 δ ppm. A broad singlet (**h**) was observed at 5.59 δ ppm, corresponding to the hydroxyl protons. The proton **f** belonging to the cyclohexanone moiety appeared at 3.30 δ ppm, while the protons **g** and **d** appeared at 4.75 δ ppm and 1.95 δ ppm, respectively. The methylene protons belonging to the pentadecyl chain (**e**, **c** and **b**) appeared in the range 2.82 – 2.98 δ ppm and 1.14 – 1.91 δ ppm. The methyl protons (**a**) appeared at 0.88 δ ppm as a triplet.

^{13}C-NMR spectrum of 2,6-bis(4-hydroxybenzylidene)-3-pentadecylcyclohexanone (BPC) along with assignments is shown in **Fig 3.22**.

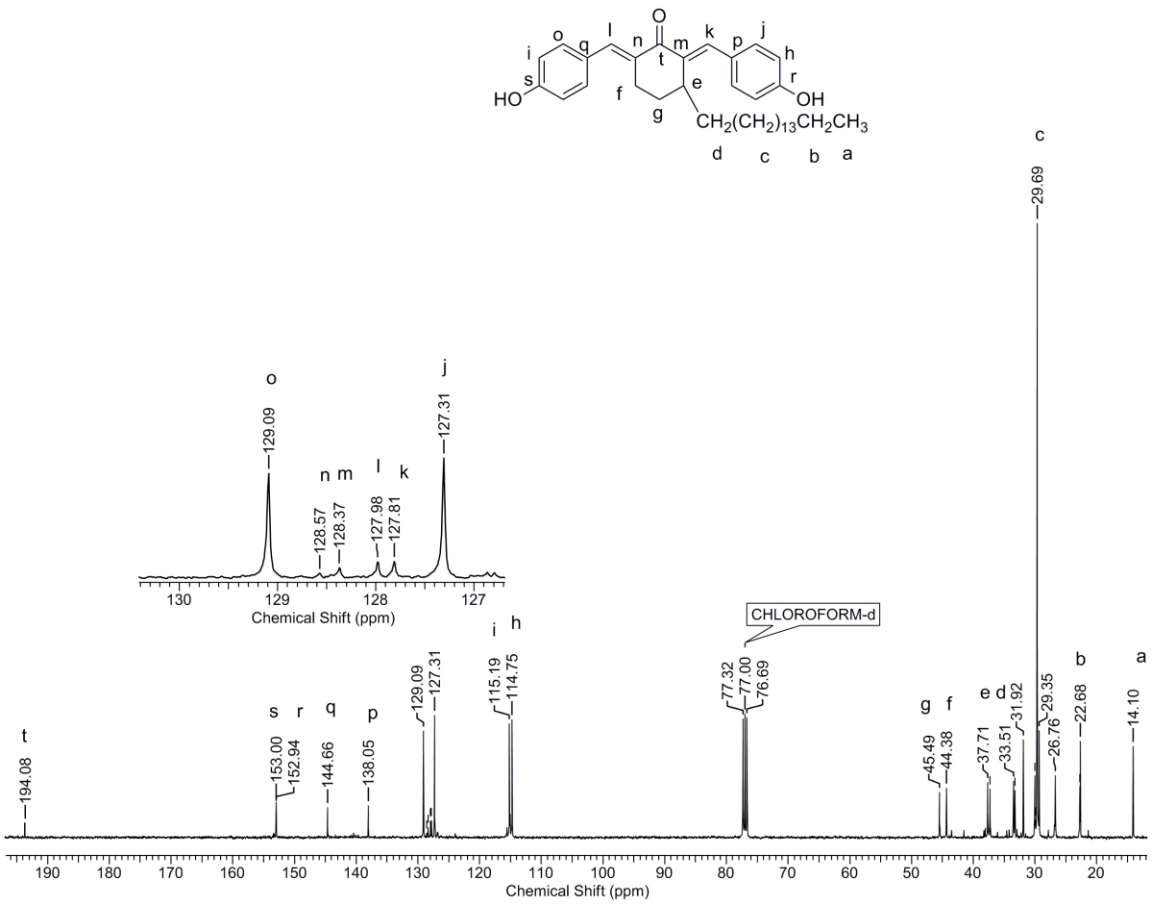

Figure 3.22 ^{13}C-NMR spectrum ($CDCl_3$) 2,6-bis(4-hydroxybenzylidene)-3-pentadecylcyclohexanone (BPC)

The signal at 194 δ ppm was assignable to the ketone carbon (**t**). The aromatic carbons linked to the hydroxyl groups (**s** and **r**) appeared at 153 δ ppm and 152 δ ppm, respectively; the aromatic carbons linked to the alkenyl carbons (**q**, **r**) resonated at 144 δ ppm and 138 δ ppm, respectively. The aromatic carbons present *meta* to the hydroxyl functionality (**o**, **j**) appeared at 129.09 δ ppm and 127.31 δ ppm, while the aromatic carbons positioned *ortho* to the hydroxyl functionality (**i**, **h**) resonated at 115.19 δ ppm and 114.75 δ ppm. The signals corresponding to the alkenyl carbons (**k**-**n**) appeared in the range 127.61 – 128.57 δ ppm. The methylene carbons belonging to the cyclohexyl moiety (**g** and **f**) appeared at 45.49 δ ppm and 44.38 δ ppm, while the methylene carbons of the pentadecyl chain (**b**-**d**) resonated in the range 22.68 – 33.51 δ ppm. The methyl carbon (**a**) appeared at 14.10 δ ppm.

The FT-IR, ^{1}H-NMR and ^{13}C-NMR results clearly indicated that the proposed structure of 2,6-bis(4-hydroxybenzylidene)-3-pentadecylcyclohexanone (BPC) was consistent with the observed results.

3.4.8 Synthesis of 4,4'-((2-pentadecyl-[1,1'-biphenyl]-4,4'-diyl)bis(oxy))dianiline (PBD)

Scheme 3.8 presents the route for synthesis of 4,4'-((2-pentadecyl-[1,1'-biphenyl]-4,4'-diyl)bis(oxy))dianiline (PBD) starting from 3-pentadecyl biphenol (PDBP) (**Section 3.4.5**).

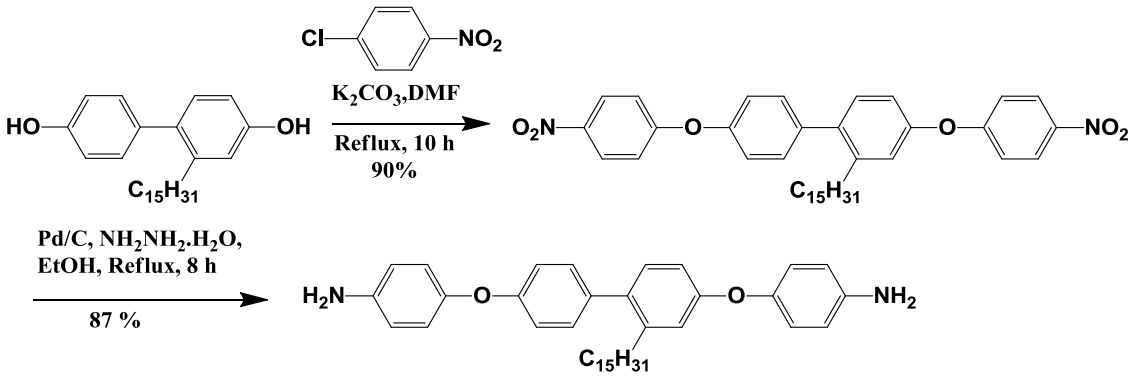

Scheme 3.8 Synthesis of 4,4'-((2-pentadecyl-[1,1'-biphenyl]-4,4'-diyl)bis(oxy))dianiline (PBD)

The diamine, 4,4'-((2-pentadecyl-[1,1'-biphenyl]-4,4'-diyl)bis(oxy))dianiline (PBD) was synthesised from 3-pentadecyl biphenol (PDBP) in two steps. In the first step, 4,4'-bis(4-nitrophenoxy)-2-pentadecyl-1,1'-biphenyl was prepared by nucleophilic substitution reaction of 3-pentadecyl biphenol (PDBP) with *p*-chloronitrobenzene in the presence of potassium carbonate and *N*,*N*-dimethylformamide as the solvent at reflux temperature. The dinitro compound, 4,4'-bis(4-nitrophenoxy)-2-pentadecyl-1,1'-biphenyl, was a yellow solid which was purified by column chromatography. PBD was obtained by reduction of 4,4'-bis(4-nitrophenoxy)-2-pentadecyl-1,1'-biphenyl in refluxing ethanol in the presence of Pd/C.[58] 4,4'-((2-pentadecyl-[1,1'-biphenyl]-4,4'-diyl)bis(oxy))dianiline (PBD) was characterised by spectroscopic methods.

FT-IR spectrum of 4,4'-((2-pentadecyl-[1,1'-biphenyl]-4,4'-diyl)bis(oxy))dianiline (PBD) is shown in **Fig 3.23**.

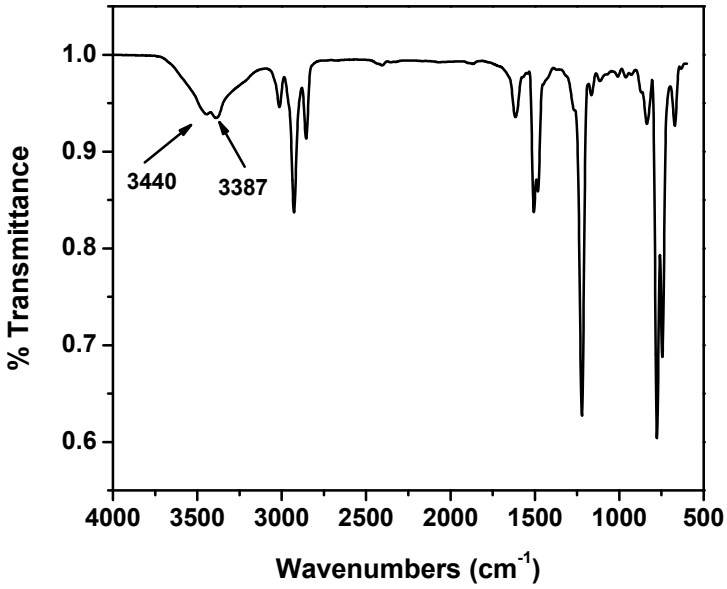

Figure 3.23 FT-IR spectrum of 4,4'-((2-pentadecyl-[1,1'-biphenyl]-4,4'-diyl)bis(oxy))dianiline (PBD)

Absorption bands were observed at 3440 and 3387 cm^{-1} corresponding to -N-H stretching of the amino ($–NH_2$) group.

^{1}H-NMR spectrum of 4,4'-((2-pentadecyl-[1,1'-biphenyl]-4,4'-diyl)bis(oxy))dianiline (PBD)is shown in **Fig 3.24**.

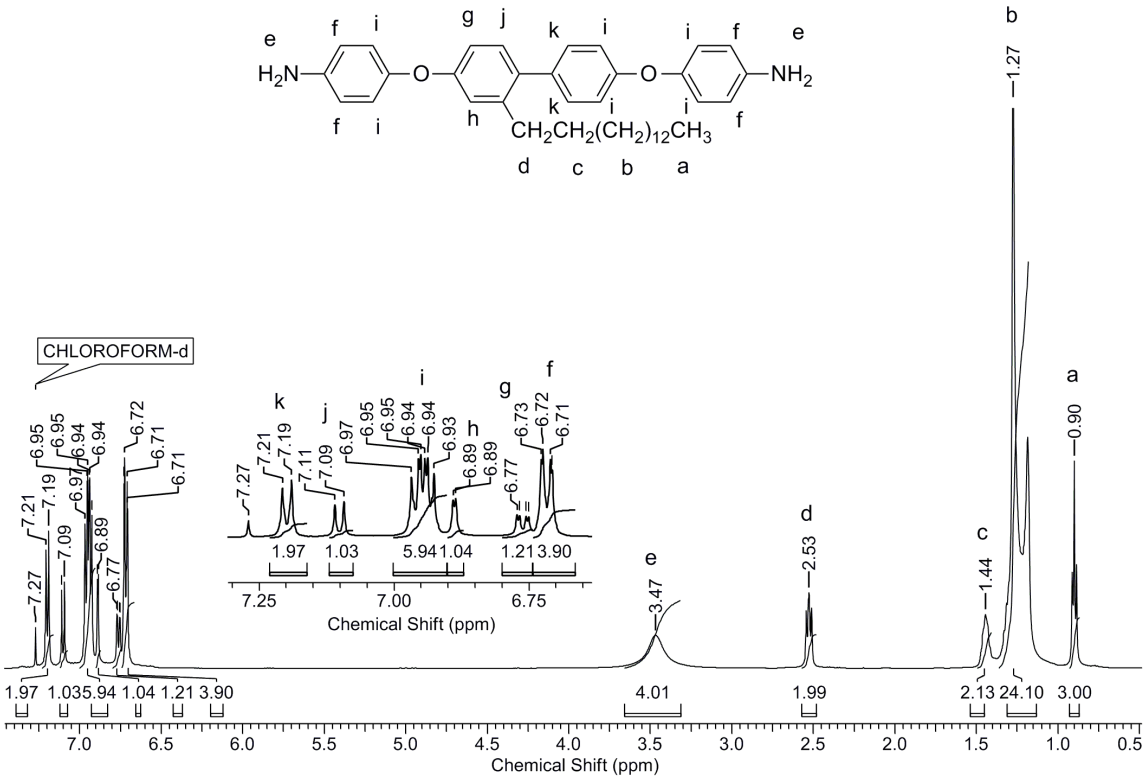

Figure 3.24 ^{1}H-NMR spectrum ($CDCl_3$) of 4,4'-((2-pentadecyl-[1,1'-biphenyl]-4,4'-diyl)bis(oxy))dianiline (PBD)

The two aromatic protons **k**, positioned *meta* to the ethereal oxygen, appeared at 7.20 δ ppm as a doublet. The doublet at 7.10 δ ppm could be assigned to the aromatic proton **j**, oriented *meta* to both ethereal oxygen and the pentadecyl chain, while the multiplet observed in the range 6.90 – 7.00 δ ppm was ascribed to the six aromatic protons, **i**. The aromatic proton, **h**, *ortho* to the ether and the pentadecyl chain appeared as a doublet at 6.89 δ ppm, while the aromatic proton **g** resonated at 6.76 δ ppm in the form of a doublet of doublet. The four aromatic protons, **f**, positioned *ortho* to the amine group appeared shielded at 6.72 δ ppm as a doublet. The amine protons (**e**) resonated as a broad singlet at 3.47 δ ppm. The benzylic protons (**d**) appeared at 2.53 δ ppm as a triplet, while the triplet at 0.90 δ ppm could be assigned to the terminal methyl protons (**a**) belonging to the pentadecyl chain.

^{13}C-NMR spectrum of 4,4'-((2-pentadecyl-[1,1'-biphenyl]-4,4'-diyl)bis(oxy))dianiline (PBD) along with assignments is shown in **Fig 3.25**.

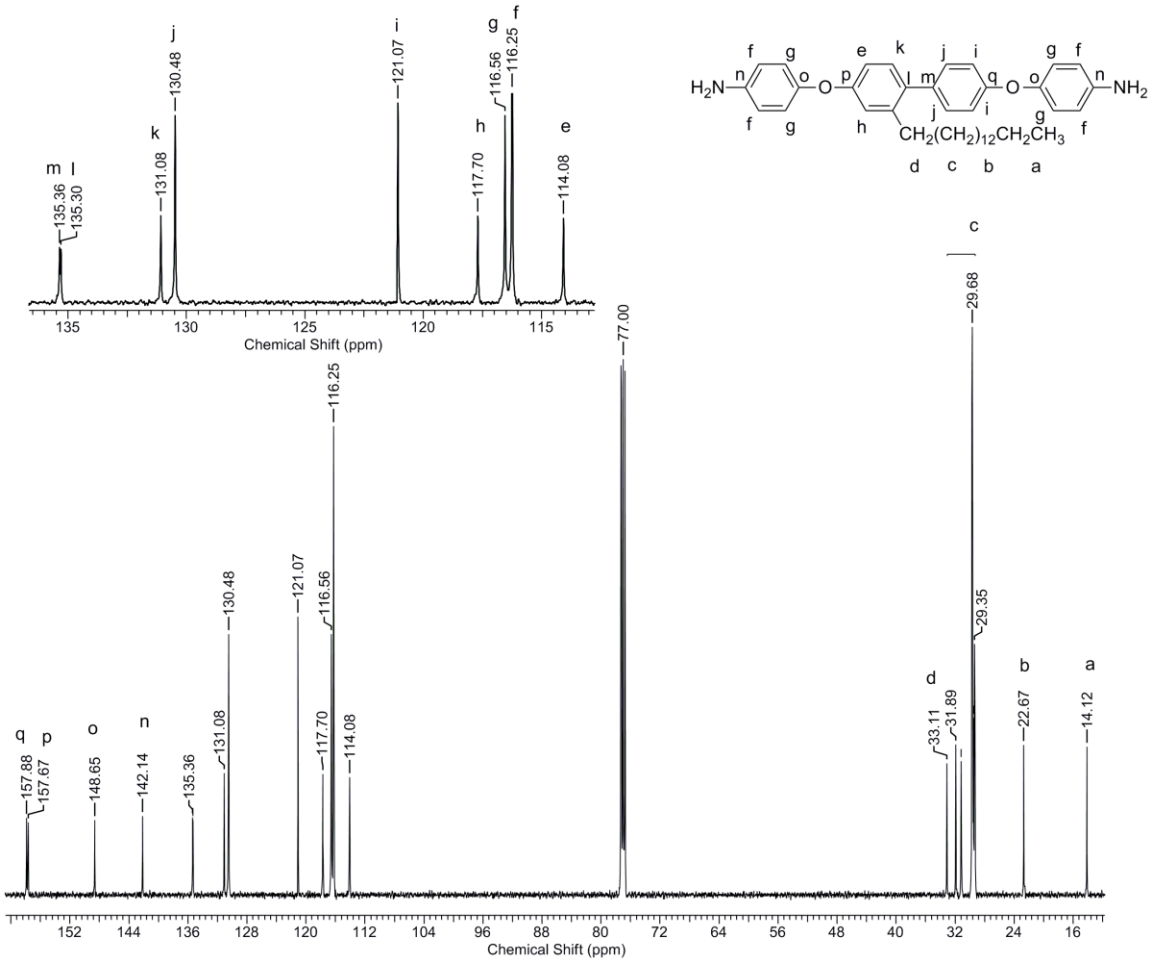

Figure 3.25 ^{13}C-NMR spectrum ($CDCl_3$) 4,4'-((2-pentadecyl-[1,1'-biphenyl]-4,4'-diyl)bis(oxy))dianiline (PBD)

The peaks observed at 157.88 δ ppm, 157.67 δ ppm and 148.65 δ ppm were assigned to the aromatic carbon atoms linked to the ether functionality, **q**, **p** and **o**, respectively. The carbon atoms linked to the amine groups (**n**) appeared at 142.14 δ ppm. The aromatic carbon atoms linked with each other (**m**, **l**) resonated at 135.36 δ ppm and 135.30 δ ppm, respectively. The remaining aromatic carbon atoms (**e**-**k**) appeared in the range 114.08 – 131.08 δ ppm, showing good agreement with the proposed structure. The benzylic carbon atom (**d**) resonated at 33.11 δ ppm, while the methylene carbon atoms (**c**, **b**) appeared in the range 22.67 – 31.89 δ ppm. The methyl carbon (**a**) resonated at 14.12 δ ppm.

HRMS data of 4,4'-((2-pentadecyl-[1,1'-biphenyl]-4,4'-diyl)bis(oxy))dianiline (PBD) showed good agreement with calculated values (**Supporting Information Fig SI 3.4**).

The data obtained from FT-IR, ^{1}H-NMR, ^{13}C-NMR and HRMS clearly indicated that the proposed structure of synthesised diamine, 4,4'-((2-pentadecyl-[1,1'-biphenyl]-4,4'-diyl)bis(oxy))dianiline (PBD), was consistent with the observed results.

3.4.9 Synthesis of 2-pentadecyl-4,4'-bis(prop-2-yn-1-yloxy)-1,1'-biphenyl (PPB)

Bispropargyl ethers are useful monomers for the synthesis of propargyl ether functional phenolic resins (also known as propargyl terminated resins), well known for their good dielectric properties, thermal stability, solvent resistance and attractive physico-mechanical properties. Propargyl terminated resins are a promising hydrophobic alternative for epoxy resins, useful for a number of applications such as adhesives, coatings, advanced composites, electronics, etc.[59,60] The highlighting feature of these monomers is their ability to undergo curing reaction to form resins through addition reaction of the acetylene groups. This involves an initial cyclisation reaction *via* Claisen rearrangement to yield 2-H-1benzopyran (chromene) groups which undergo polymerisation to generate a network with good thermal stability. Bispropargyl ether monomers can be easily and cheaply synthesised from readily available bisphenols in a single step reaction. The generation of bispropargyl ethers from bisphenols has been reported by Hay *et al.*[61,62] Propargylation of bisphenols is generally achieved using propargyl halides in the presence of potassium carbonate or sodium hydroxide.

Scheme 3.9 illustrates the route for the synthesis of 2-pentadecyl-4,4'-bis(prop-2-yn-1-yloxy)-1,1'-biphenyl (PPB) starting from 3-pentadecyl 4,4' biphenol (PDBP) (**Section 3.4.5**)

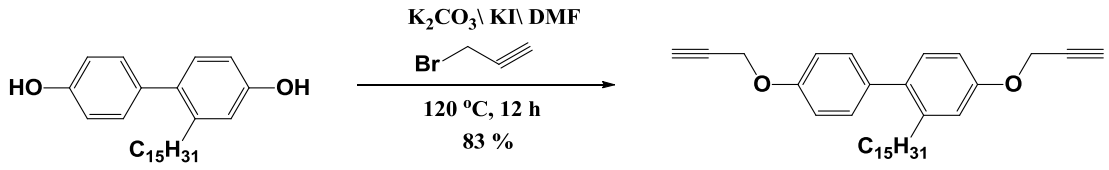

Scheme 3.9 Synthesis of 2-pentadecyl-4,4'-bis(prop-2-yn-1-yloxy)-1,1'-biphenyl (PPB)

In this work, 2-pentadecyl-4,4'-bis(prop-2-yn-1-yloxy)-1,1'-biphenyl (PPB) was synthesised from 3-pentadecyl 4,4' biphenol (PDBP) in one step. Bispropargylation was carried out by the reaction of 3-pentadecyl 4,4' biphenol with a stoichiometric quantity of propargyl bromide at 120 °C for 12 h, using a catalytic amount of potassium iodide. 2-pentadecyl-4,4'-bis(prop-2-yn-1-yloxy)-1,1'-biphenyl (PPB) was obtained after chromatographic purification of the crude product. Pure 2-pentadecyl-4,4'-bis(prop-2-yn-1-yloxy)-1,1'-biphenyl (PPB) was characterised by FT-IR, ^{1}H-NMR and ^{13}C-NMR spectroscopy.

FT-IR spectrum of 2-pentadecyl-4,4'-bis(prop-2-yn-1-yloxy)-1,1'-biphenyl (PPB) is shown in **Fig 3.26**.

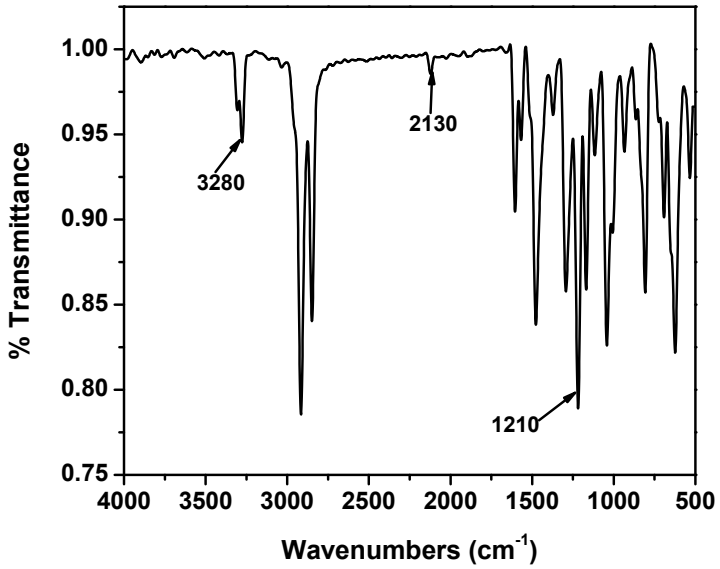

Figure 3.26 FT-IR spectrum of 2-pentadecyl-4,4'-bis(prop-2-yn-1-yloxy)-1,1'-biphenyl (PPB)

A strong absorption band appearing at 3280 cm^{-1} could be assigned to ≡C-H stretching. A weak band at 2130 cm^{-1} appeared as a result of -C≡C- stretching vibrations. The absorption band appearing at 1210 cm^{-1} was assignable to –C-O-C- stretching.

^{1}H-NMR spectrum of 2-pentadecyl-4,4'-bis(prop-2-yn-1-yloxy)-1,1'-biphenyl (PPB) is provided in **Fig 3.27**.

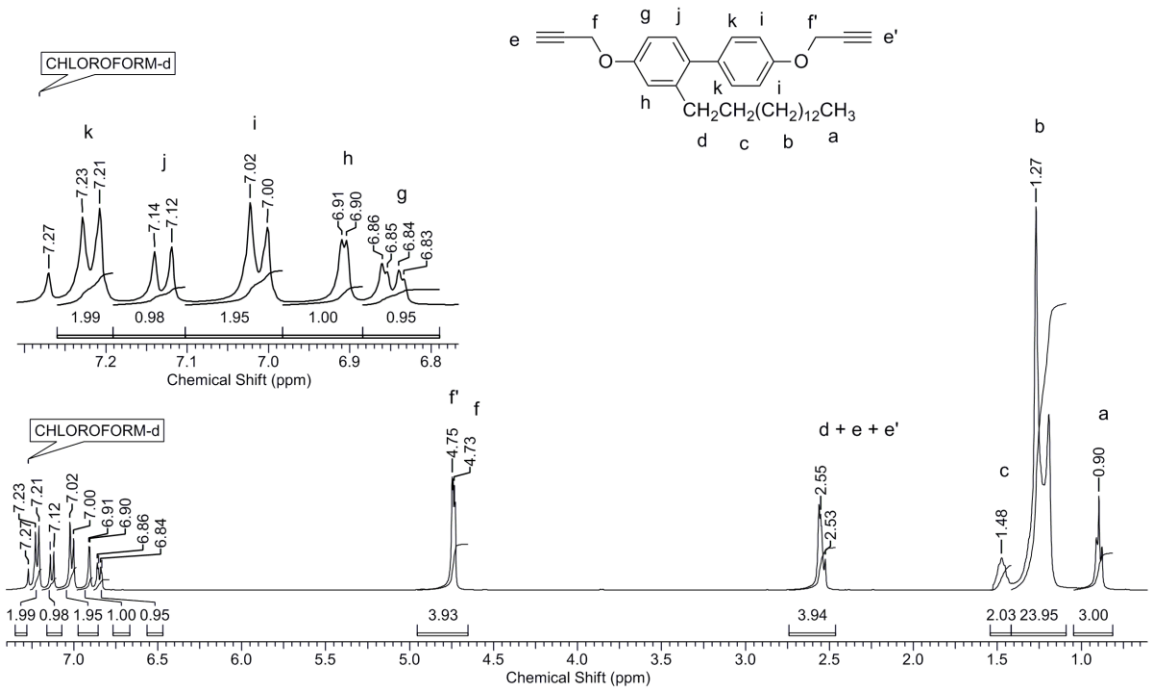

Figure 3.27 ^{1}H-NMR spectrum ($CDCl_3$) of 2-pentadecyl-4,4'-bis(prop-2-yn-1-yloxy)-1,1'-biphenyl (PPB)

Two aromatic protons, **k**, appeared at 7.22 δ ppm in the form of a doublet, while the aromatic proton **j** resonated at 7.13 δ ppm as a doublet. The doublets at 7.01 δ ppm and 6.91 δ ppm could be assigned to the aromatic protons **i** and **h**, respectively. The aromatic proton **g**, positioned *para* to the pentadecyl chain resonated as a doublet of doublet. The methylene protons adjacent to the acetylene linkage (**f'** and **f**) appeared at 4.75 δ ppm and 4.73 δ ppm, respectively, while the acetylene protons (**e'** and **e**) merged with the signal for the benzylic protons of the pentadecyl chain and appeared in the range 2.46 – 2.74 δ ppm. The methylene protons (**c**) appeared at 1.48 δ ppm as a quintet, while the rest of the methylene protons (**b**) resonated in the range 1.09 – 1.42 δ ppm. The methyl protons (**a**) appeared at 0.90 δ ppm in the form of a triplet.

^{13}C-NMR spectrum of 2-pentadecyl-4,4'-bis(prop-2-yn-1-yloxy)-1,1'-biphenyl (PPB) is shown in **Fig 3.28**.

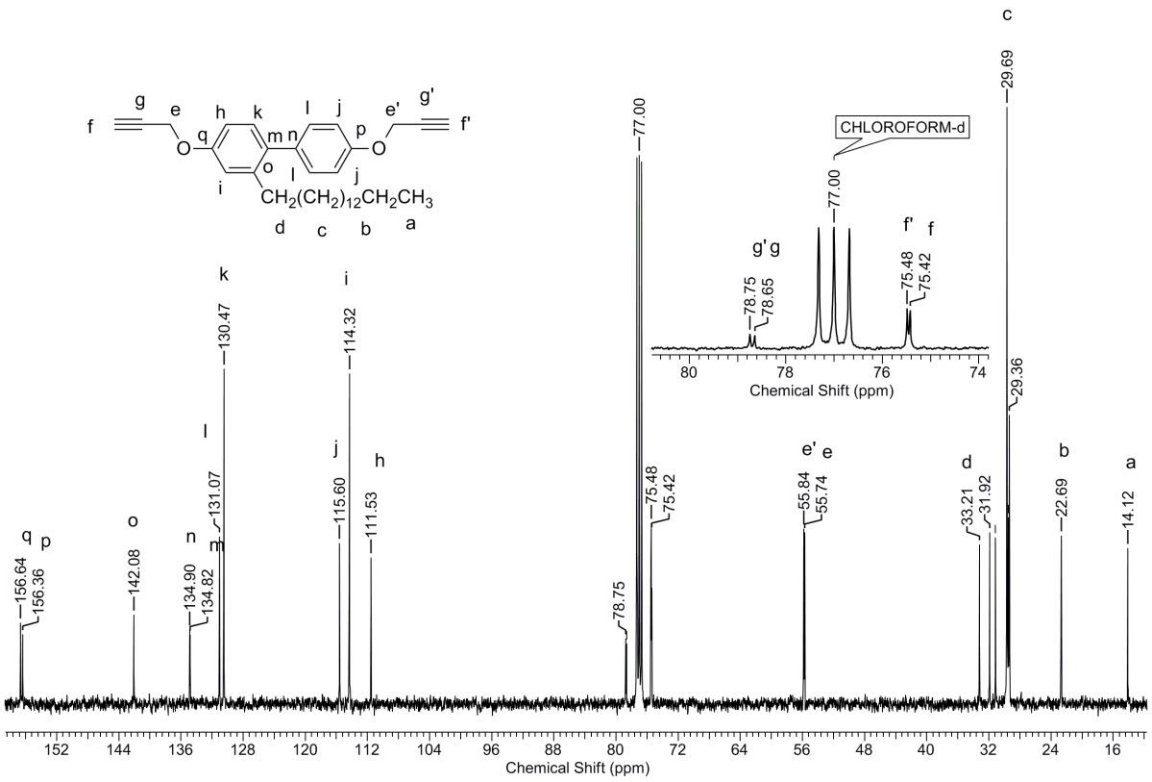

Figure 3.28 ^{13}C-NMR spectrum ($CDCl_3$) of 2-pentadecyl-4,4'-bis(prop-2-yn-1-yloxy)-1,1'-biphenyl (PPB)

The aromatic carbon atoms (**h-q**) resonated in the range 111.56 – 156.67 δ ppm and could be assigned with the assistance of DEPT spectrum. The signals observed showed good agreement with the proposed structure. The acetylenic carbons **g'** and **g** appeared at 78.75 δ ppm and 78.65 δ ppm, respectively. The peaks at 75.48 δ ppm and 75.42 δ ppm could be assigned to the terminal acetylenic carbons **f'** and **f**, respectively, while the peaks observed at 55.84 δ ppm and 55.74 δ ppm could be ascribed to the methylene protons adjacent to the acetylenic moiety, **e'** and **e**, respectively. The benzylic carbon atom (**d**) appeared at 33.21 δ ppm, while the remaining methylene carbons belonging to the pentadecyl chain (**c**, **b**) appeared in the range 22.72 – 31.95 δ ppm. The terminal methyl carbon (**a**) resonated at 14.16 δ ppm.

FT-IR, ^{1}H-NMR and ^{13}C-NMR results clearly indicated that the proposed structure of the synthesised bispropargyl ether PPB was consistent with the observed results.

3.4.10 Synthesis of 2-pentadecyl-4-(prop-2-yn-1-yloxy)-1-(4-(prop-2-yn-1-yloxy)phenoxy)benzene (PPPB)

Scheme 3.10 depicts the route for the synthesis of 2-pentadecyl-4-(prop-2-yn-1-yloxy)-1-(4-(prop-2-yn-1-yloxy)phenoxy)benzene (PPPB) starting from 4-(4-hydroxyphenoxy)-3-pentadecylphenol (HPPDP) (**Section 3.4.4**).

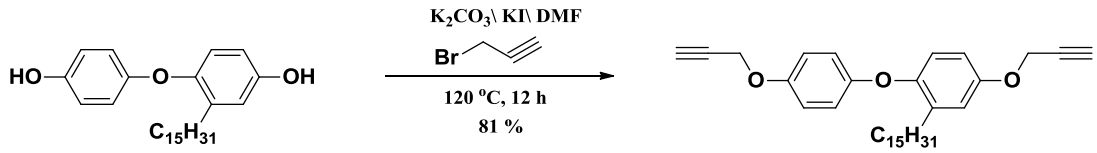

Scheme 3.10 Synthesis of 2-pentadecyl-4-(prop-2-yn-1-yloxy)-1-(4-(prop-2-yn-1-yloxy)phenoxy)benzene (PPPB)

The synthesis of 2-pentadecyl-4-(prop-2-yn-1-yloxy)-1-(4-(prop-2-yn-1-yloxy)phenoxy)benzene (PPPB) from 4-(4-hydroxyphenoxy)-3-pentadecylphenol (HPPDP) was accomplished in one step by the propargylation of phenolic moieties by stoichiometric quantity of propargyl bromide at 120 °C for 12 h in *N*,*N*-dimethylformamide using a catalytic quantity of potassium iodide. Pure 2-pentadecyl-4-(prop-2-yn-1-yloxy)-1-(4-(prop-2-yn-1-yloxy)phenoxy)benzene was obtained after purification of the crude product by column chromatography using petroleum ether as the eluent. The structural characterisation of 2-pentadecyl-4-(prop-2-yn-1-yloxy)-1-(4-(prop-2-yn-1-yloxy)phenoxy)benzene (PPPB) was carried out by spectroscopic analysis.

FT-IR spectrum of 2-pentadecyl-4-(prop-2-yn-1-yloxy)-1-(4-(prop-2-yn-1-yloxy)phenoxy)benzene (PPPB) is shown in **Fig 3.29**.

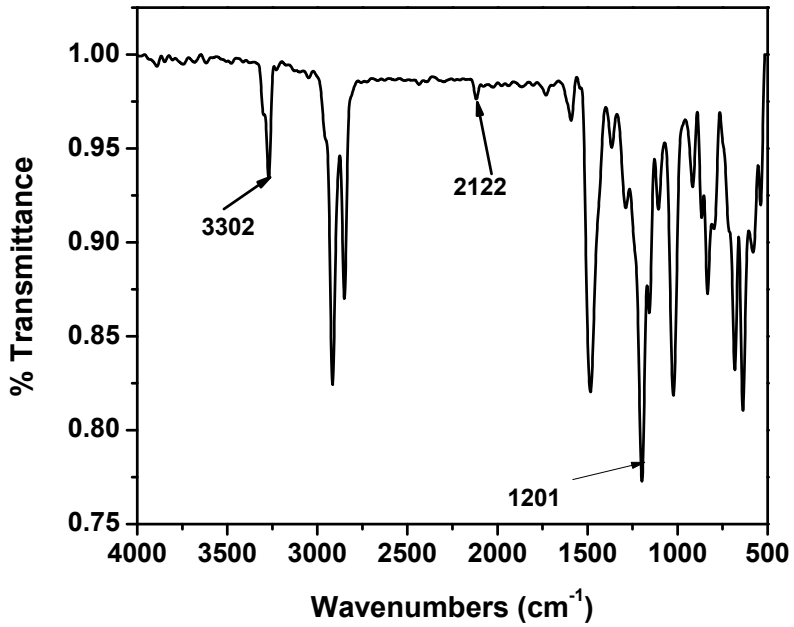

Figure 3.29 FT-IR spectrum of 2-pentadecyl-4-(prop-2-yn-1-yloxy)-1-(4-(prop-2-yn-1-yloxy)phenoxy)benzene (PPPB)

A sharp absorption band was observed at 3302 cm^{-1}, corresponding to ≡C-H stretching. A weak absorption band corresponding to -C≡C- stretching appeared at 2122 cm^{-1}. The strong vibration band at 1201 cm^{-1} was assignable to –C-O-C- stretching.

^{1}H-NMR spectrum of 2-pentadecyl-4-(prop-2-yn-1-yloxy)-1-(4-(prop-2-yn-1-yloxy)phenoxy)benzene (PPPB) is provided in **Fig 3.30.**

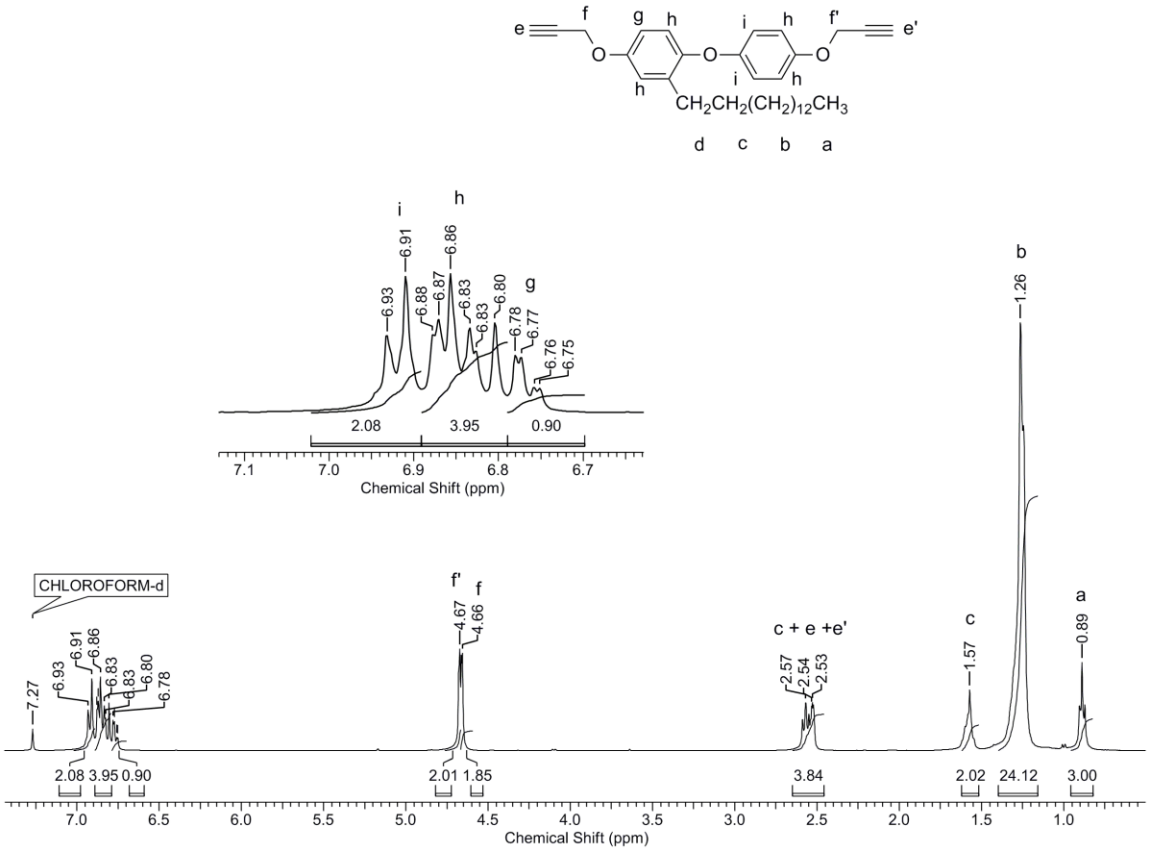

Figure 3.30 ^{1}H-NMR spectrum ($CDCl_3$) of 2-pentadecyl-4-(prop-2-yn-1-yloxy)-1-(4-(prop-2-yn-1-yloxy)phenoxy)benzene (PPPB)

Two aromatic protons (**i**) resonated at 6.92 δ ppm in the form of a doublet. The aromatic proton **g**, positioned *para* to the pentadecyl chain appeared most shielded, at 6.76 δ ppm as a doublet of doublet, due to *ortho* and *meta* coupling. The remaining aromatic protons (**h**) resonated in the range 6.70 δ ppm – 6.89 δ ppm, as a multiplet. The methylene protons adjacent to acetylene groups, **f'**and **f**, appeared at 4.68 δ ppm and 4.66 δ ppm, respectively. The acetylenic protons (**e**, **e'**) and the benzylic protons (**c**) together appeared as a multiplet in the range 2.46 – 2.65 δ ppm. The methylene protons (**c**, **b**) resonated in the range 1.16 – 1.58 δ ppm. The methyl protons belonging to the pentadecyl chain (**a**) appeared at 0.89 δ ppm.

^{13}C-NMR spectrum of 2-pentadecyl-4-(prop-2-yn-1-yloxy)-1-(4-(prop-2-yn-1-yloxy)phenoxy)benzene (PPPB) is shown in **Fig 3.31**.

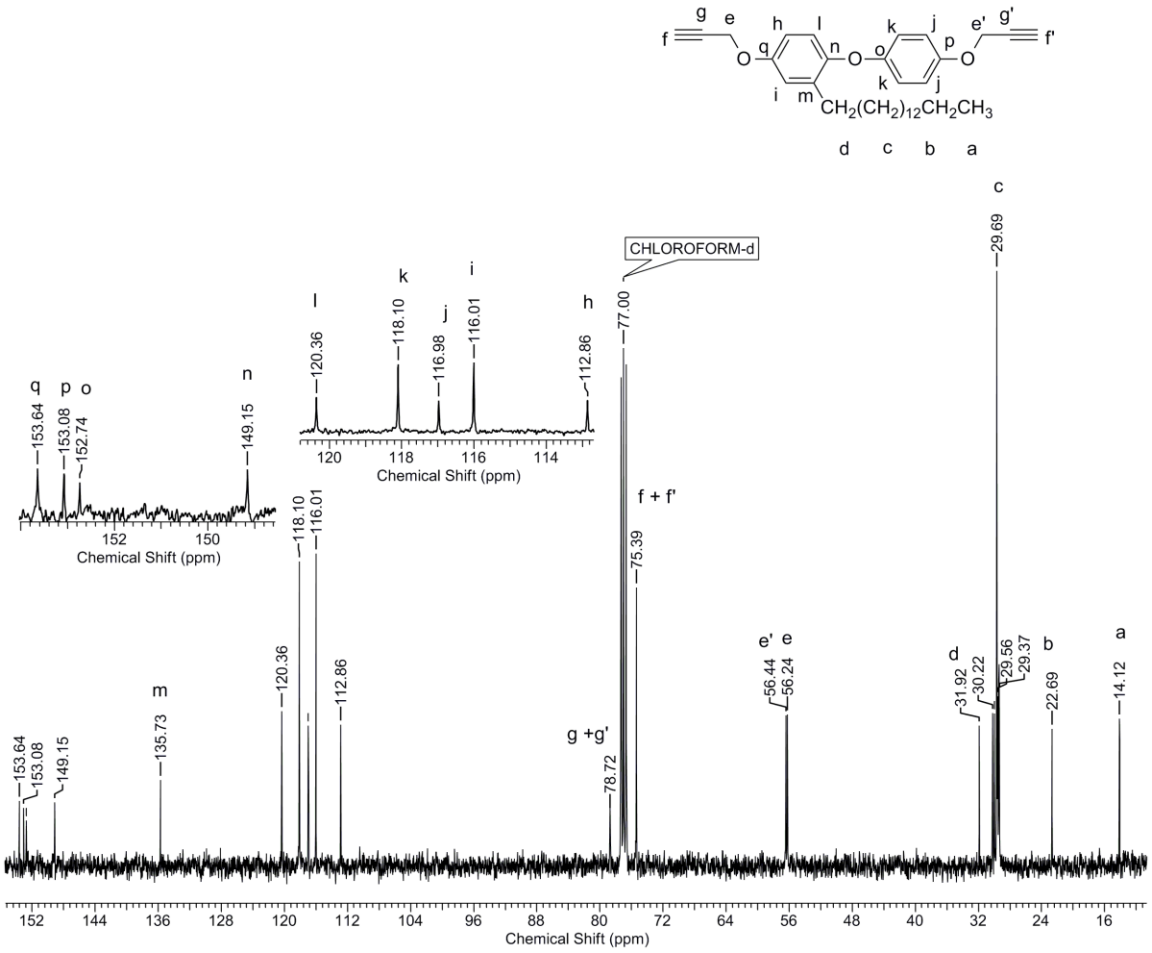

Figure 3.31 ^{13}C-NMR spectrum ($CDCl_3$) of 2-pentadecyl-4-(prop-2-yn-1-yloxy)-1-(4-(prop-2-yn-1-yloxy)phenoxy)benzene (PPPB)

The peaks in the range 112.89 – 153.67 δ ppm were readily assignable to the aromatic carbon atoms, with the assistance of DEPT spectrum. These peaks showed good agreement with the proposed structure. The acetylenic carbons (**g** and **g'**) appeared at 78.76 δ ppm, while the terminal acetylenic carbon atoms (**f** and **f'**) resonated at 75.42 δ ppm. The methylene carbon atoms adjacent to the acetylenic linkage, **e'** and **e**, appeared at 56.47 δ ppm and 56.27 δ ppm, respectively. The benzylic carbon atom (**d**) and methylene carbon atoms (**c**, **b**) belonging to the pentadecyl chain resonated at 31.95 δ ppm and 22.71 – 30.25 δ ppm, respectively.

Thus, FT-IR, ^{1}H-NMR and ^{13}C-NMR results clearly indicated that the proposed structure of synthesised bispropargyl ether 2-pentadecyl-4-(prop-2-yn-1-yloxy)-1-(4-(prop-2-yn-1-yloxy)phenoxy)benzene PPPB was consistent with the observed results.

3.4.11 Synthesis of 4-(4-(4-(3,4-dicyanophenoxy)-2-pentadecylphenoxy)phenoxy)phthalonitrile (DCPP)

Phthalonitrile resins are a class of attractive high temperature resins possessing excellent thermal and thermo-oxidative stabilities, outstanding mechanical properties, high char yields, good moisture resistance in addition to superior flame resistance.[63–69] These resins are most sought after for applications in civilian as well as military fields. Phthalonitrile resins can conveniently be synthesised by thermal polymerisation (in the presence of curing agents) of phthalonitrile monomers. Phthalonitrile monomers with ether linkages can effectively impart good moldability without compromising thermal stability to a great extent.

In **Scheme 3.11** is depicted the route for the synthesis of 4-(4-(4-(3,4-dicyanophenoxy)-2-pentadecylphenoxy)phenoxy)phthalonitrile (DCPP) starting from 4-(4-hydroxyphenoxy)-3-pentadecylphenol (HPPDP) (**section 3.4.4**).

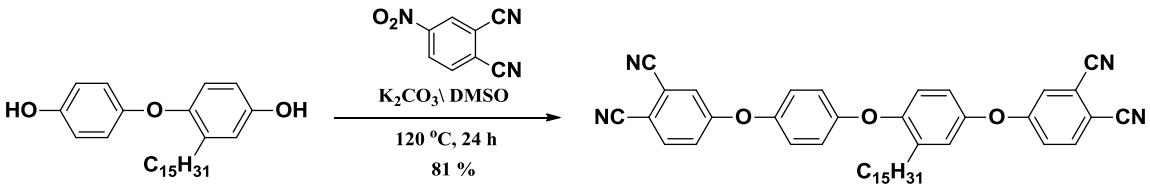

Scheme 3.11 Synthesis of 4-(4-(4-(3,4-dicyanophenoxy)-2-pentadecylphenoxy)phenoxy)phthalonitrile (DCPP)

4-(4-(4-(3,4-Dicyanophenoxy)-2-pentadecylphenoxy)phenoxy)phthalonitrile (DCPP) was synthesised from partially bio-based bisphenol, 4-(4-hydroxyphenoxy)-3-pentadecylphenol (HPPDP), in one step. HPPDP was reacted with 4-nitophthalonitrile in the presence of potassium carbonate in dimethylsulfoxide at 120 °C.[68] Initially, the reaction mixture consisting of HPPDP and potassium carbonate was stirred at 90 °C for one hour leading to the formation of bisphenolate salt. Subsequently, 4-nitrophthalonitrile was added to the reaction mixture which reacted with the bisphenolate salt at 120 °C for 24 h yielding 4-(4-(4-(3,4-dicyanophenoxy)-2-pentadecylphenoxy)phenoxy)phthalonitrile (DCPP). 4-(4-(4-(3,4-dicyanophenoxy)-2-pentadecylphenoxy)phenoxy)phthalonitrile

(DCPP) was characterised by spectroscopic techniques to establish the structure of the synthesised product.

FT-IR spectrum of 4-(4-(4-(3,4-dicyanophenoxy)-2-pentadecylphenoxy)phenoxy)phthalonitrile (DCPP) is shown in **Fig 3.32**.

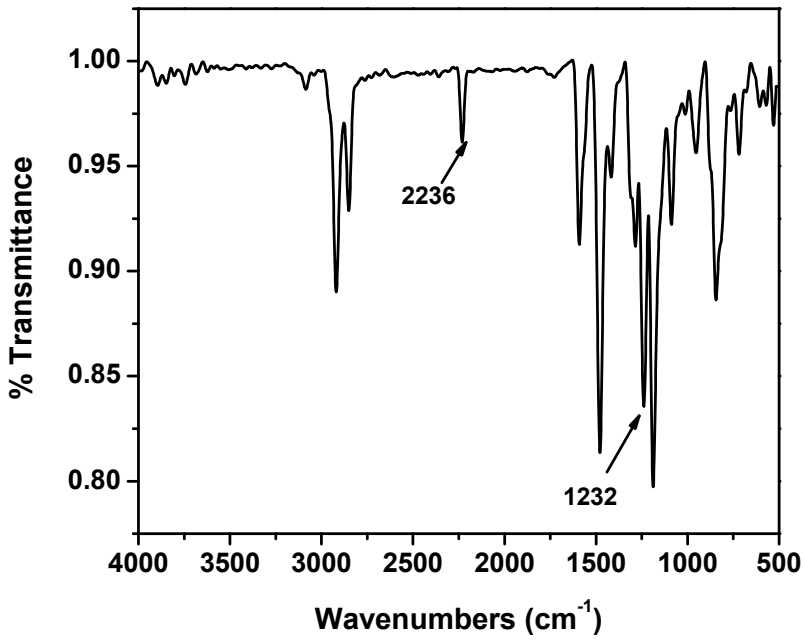

Figure 3.32 FT-IR spectrum of 4-(4-(4-(3,4-dicyanophenoxy)-2-pentadecylphenoxy)phenoxy)phthalonitrile (DCPP)

An absorption band of medium intensity was observed at 2236 cm^{-1}, characteristic of -C≡N stretching. Additionally, a strong absorption band appeared at 1232 cm^{-1}, corresponding to –C-O-C- stretching.

^{1}H-NMR spectrum of 4-(4-(4-(3,4-dicyanophenoxy)-2-pentadecylphenoxy)phenoxy)phthalonitrile (DCPP) is provided in **Fig 3.33.**

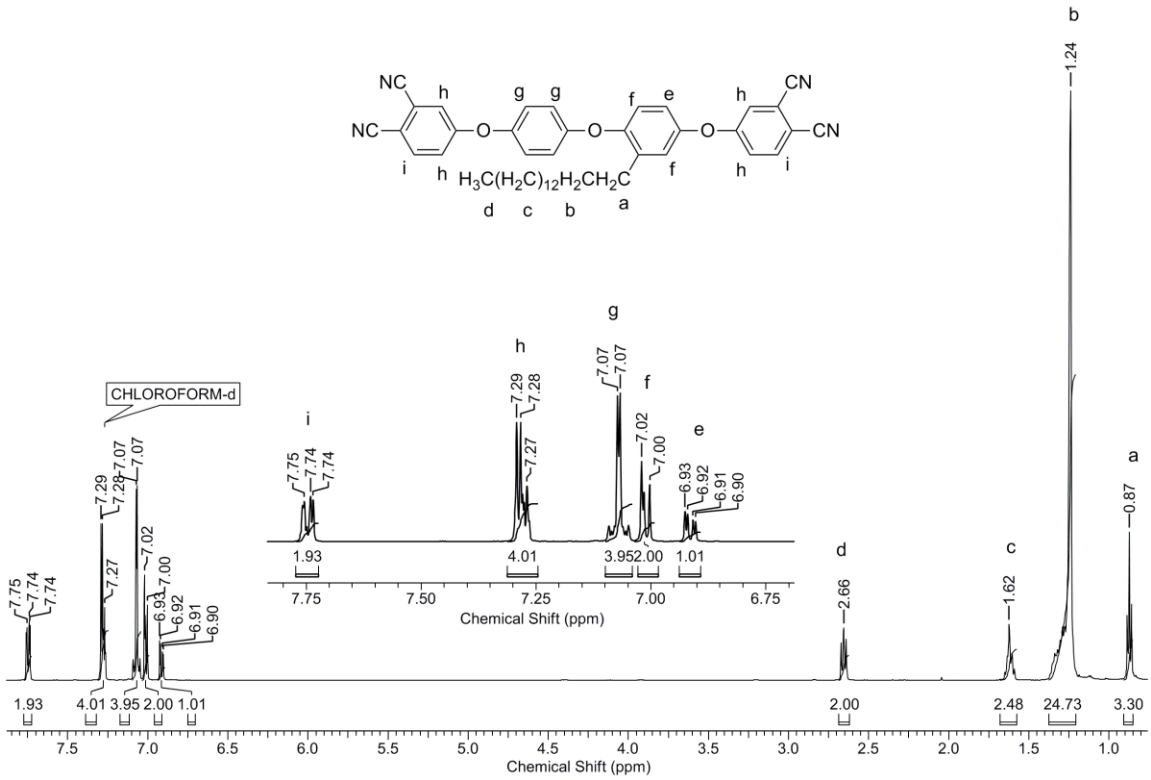

Figure 3.33 ^{1}H-NMR spectrum ($CDCl_3$) of 4-(4-(4-(3,4-dicyanophenoxy)-2-pentadecylphenoxy)phenoxy)phthalonitrile (DCPP)

The two aromatic protons *ortho* to the nitrile group (**i**), appeared most deshielded in the range 7.72 – 7.78 δ ppm, as a multiplet. The aromatic protons **h** appeared as a multiplet in the range 7.25 – 7.31 δ ppm, while the four aromatic protons, **g**, belonging to the aromatic ring linked by ether group, resonated in the range 7.04 – 7.10 δ ppm. The aromatic protons **f** positioned *ortho* and *meta* to the pentadecyl chain appeared in the range 6.99 – 7.04 δ ppm as a multiplet, while the proton **e**, present *para* to the pentadecyl chain appeared most shielded at 6.91 δ ppm in the form of a doublet of doublet. The two benzylic protons (**d**) resonated at 2.66 δ ppm as a triplet, the remaining methylene protons (**b**,**c**) belonging to the pentadecyl chain appearing in the range 1.21 – 1.38 δ ppm. The protons of the methyl group (**a**) resonated at 0.87 δ ppm as a triplet.

^{13}C-NMR spectrum of 4-(4-(4-(3,4-dicyanophenoxy)-2-pentadecylphenoxy)phenoxy)phthalonitrile (DCPP) is shown in **Fig 3.34.**

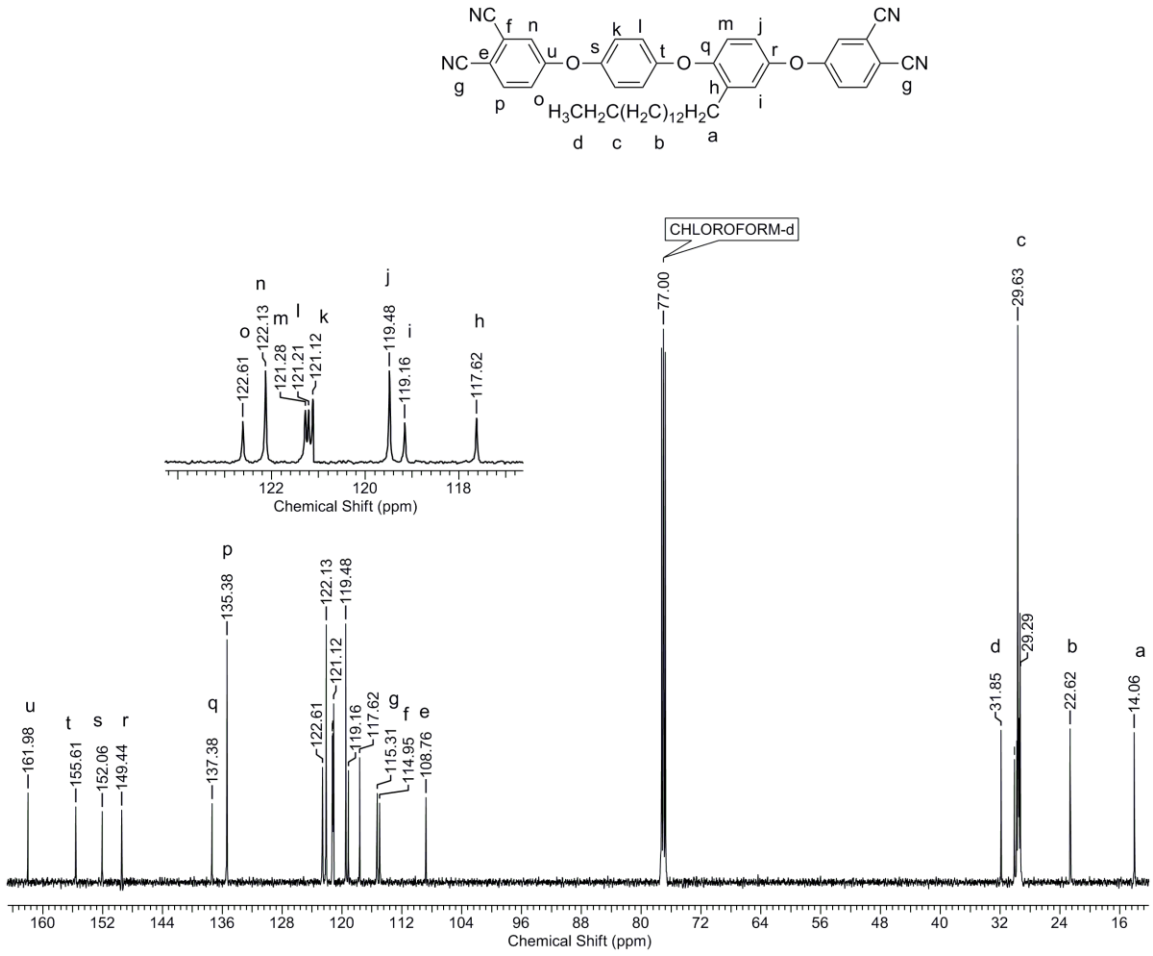

Figure 3.34 ^{13}C-NMR spectrum ($CDCl_3$) of 4-(4-(4-(3,4-dicyanophenoxy)-2-pentadecylphenoxy)phenoxy)phthalonitrile (DCPP)

The aromatic carbon atoms linked to ethereal oxygen (**u**-**q**) resonated at 161.98 δ ppm, 155.61 δ ppm, 152.06 δ ppm, 149.44 δ ppm and 137.38 δ ppm. The aromatic carbon *ortho* to the nitrile functionality (**p**) appeared at 135.38 δ ppm. The remaining aromatic carbon atoms (**j**-**o**) resonated in the range 119.48 – 122.61 δ ppm, while the aromatic carbon linked to the pentadecyl chain (**g**) appeared at 115.31 δ ppm. The nitrile carbon atom (**g**) resonated at 115.31 δ ppm, while the carbon atoms linked to the nitrile group (**f** and **e**) appeared at 114.95 δ ppm and 108.76 δ ppm, respectively. The benzylic carbon (**d**) appeared at 31.85 δ ppm. Additionally, the remaining methylene carbons (**b**,**c**) appeared in the range 22.62 – 30.15 δ ppm, while the methyl carbon (**a**) resonated at 14.06 δ ppm.

Thus, FT-IR, ^{1}H-NMR and ^{13}C-NMR results clearly indicated that the proposed structure of the synthesised phthalonitrile monomer 4-(4-(4-(3,4-dicyanophenoxy)-2-

pentadecylphenoxy)phenoxy)phthalonitrile (DCPP) was consistent with the observed results.

3.4.12 Synthesis of 4,4'-((2-pentadecyl-[1,1'-biphenyl]-4,4'-diyl)bis(oxy))diphthalonitrile (PBP)

In **Scheme 3.12** is depicted the route for the synthesis of 4,4 '-((2-pentadecyl-[1,1'-biphenyl]-4,4'-diyl)bis(oxy))diphthalonitrile (PBP) starting from 3-pentadecyl biphenol (PDBP) (**Section 3.4.5**)

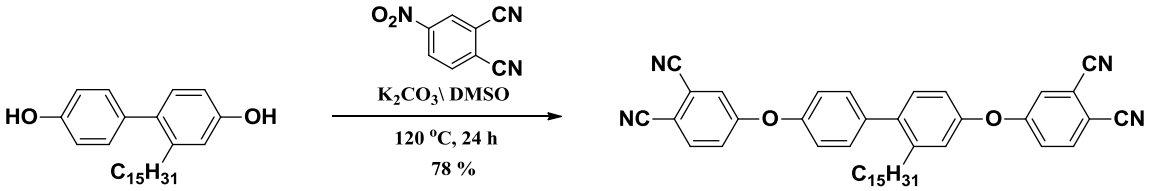

Scheme 3.12 Synthesis of 4,4'-((2-pentadecyl-[1,1'-biphenyl]-4,4'-diyl)bis(oxy))diphthalonitrile (PBP)

4,4 '-((2-Pentadecyl-[1,1'-biphenyl]-4,4'-diyl)bis(oxy))diphthalonitrile (PBP) was synthesised from the partially bio-based bisphenol 3-pentadecyl biphenol (PDBP) in one step, *via* aromatic nucleophilic nitro displacement reaction. Initially, PDBP was stirred with potassium carbonate in dimethyl sulfoxide at 90 °C for 1 h, for the purpose of formation of bisphenolate salt, which was subsequently reacted with 4-nitophthalonitrile for 24 h at 120 °C yielding 4,4 '-((2-pentadecyl-[1,1'-biphenyl]-4,4'-diyl)bis(oxy))diphthalonitrile (PBP). The pure 4,4'-((2-pentadecyl-[1,1'-biphenyl]-4,4'-diyl)bis(oxy))diphthalonitrile was obtained after chromatographic purification of the crude product. The structural analysis of 4,4'-((2-pentadecyl-[1,1'-biphenyl]-4,4'-diyl)bis(oxy))diphthalonitrile (PBP) was carried out spectroscopically.

FT-IR spectrum of 4,4'-((2-pentadecyl-[1,1'-biphenyl]-4,4'-diyl)bis(oxy))diphthalonitrile (PBP) is shown in **Fig 3.35**.

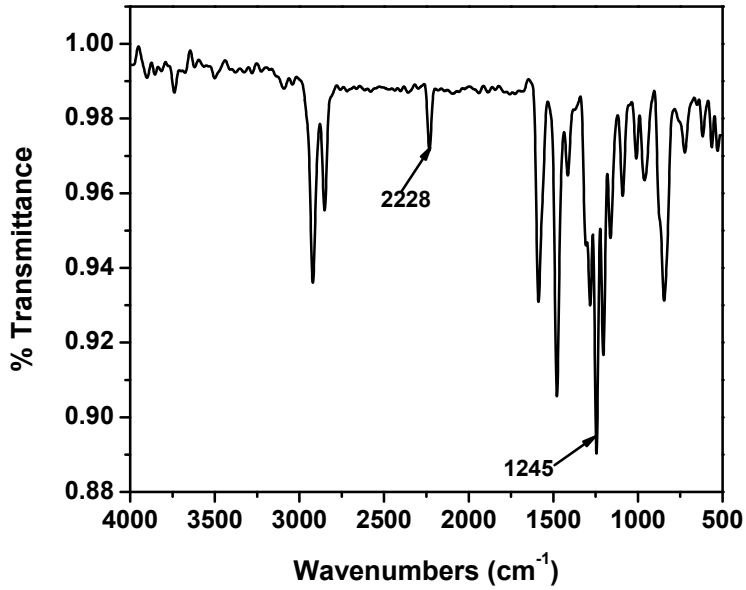

Figure 3.35 FT-IR spectrum of 4,4'-((2-pentadecyl-[1,1'-biphenyl]-4,4'-diyl)bis(oxy))diphthalonitrile (PBP)

A medium intensity absorption band appeared at 2228 cm^{-1}, characteristic of -C≡N stretching, confirming the presence of nitrile functionality. Additionally, a strong absorption band at 1245 cm^{-1} (-C-O-C- stretching) was indicative of the presence of ether functionality.

^{1}H-NMR spectrum of 4,4'-((2-pentadecyl-[1,1'-biphenyl]-4,4'-diyl)bis(oxy))diphthalonitrile (PBP) is provided in **Fig 3.36.**

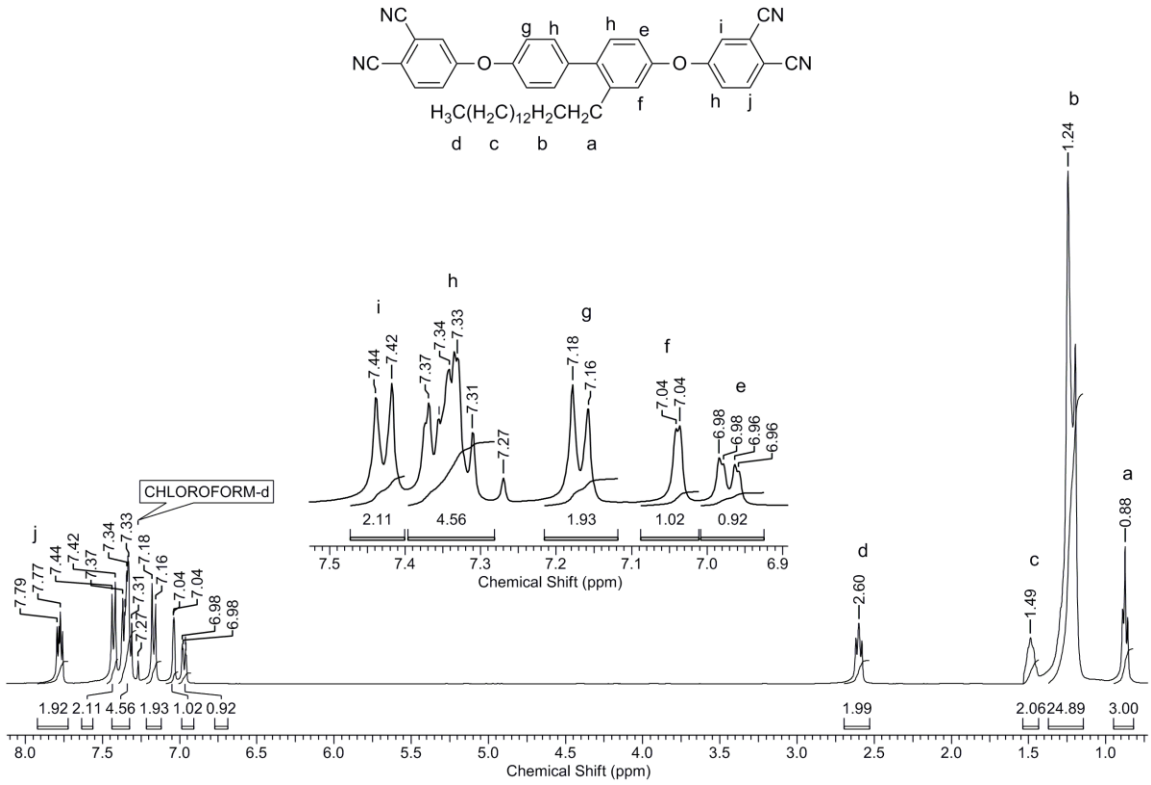

Figure 3.36 ^{1}H-NMR spectrum ($CDCl_3$) of 4,4'-((2-pentadecyl-[1,1'-biphenyl]-4,4'-diyl)bis(oxy))diphthalonitrile (PBP)

The two aromatic protons *ortho* to the nitrile functionality (**j**), appeared in the form of a doublet at 7.78 δ ppm. The two aromatic protons (**i**) appeared at 7.43 δ ppm as a doublet, while the five protons **h** resonated at 7.28 – 7.40 δ ppm as a multiplet. The two aromatic protons **g** appeared as a doublet at 7.17 δ ppm. The aromatic proton **f** resonated as a doublet at 7.04 δ ppm, while the proton **e**, *para* to the pentadecyl chain appeared as a doublet of doublet at 6.97 δ ppm. The benzylic protons (**d**) appeared at 2.60 δ ppm as a triplet, while the methyl protons (**a**) were observed to resonate at 0.88 δ ppm in the form of a triplet.

^{13}C-NMR spectrum of 4,4'-((2-pentadecyl-[1,1'-biphenyl]-4,4'-diyl)bis(oxy))diphthalonitrile (PBP) is shown in **Fig 3.37.**

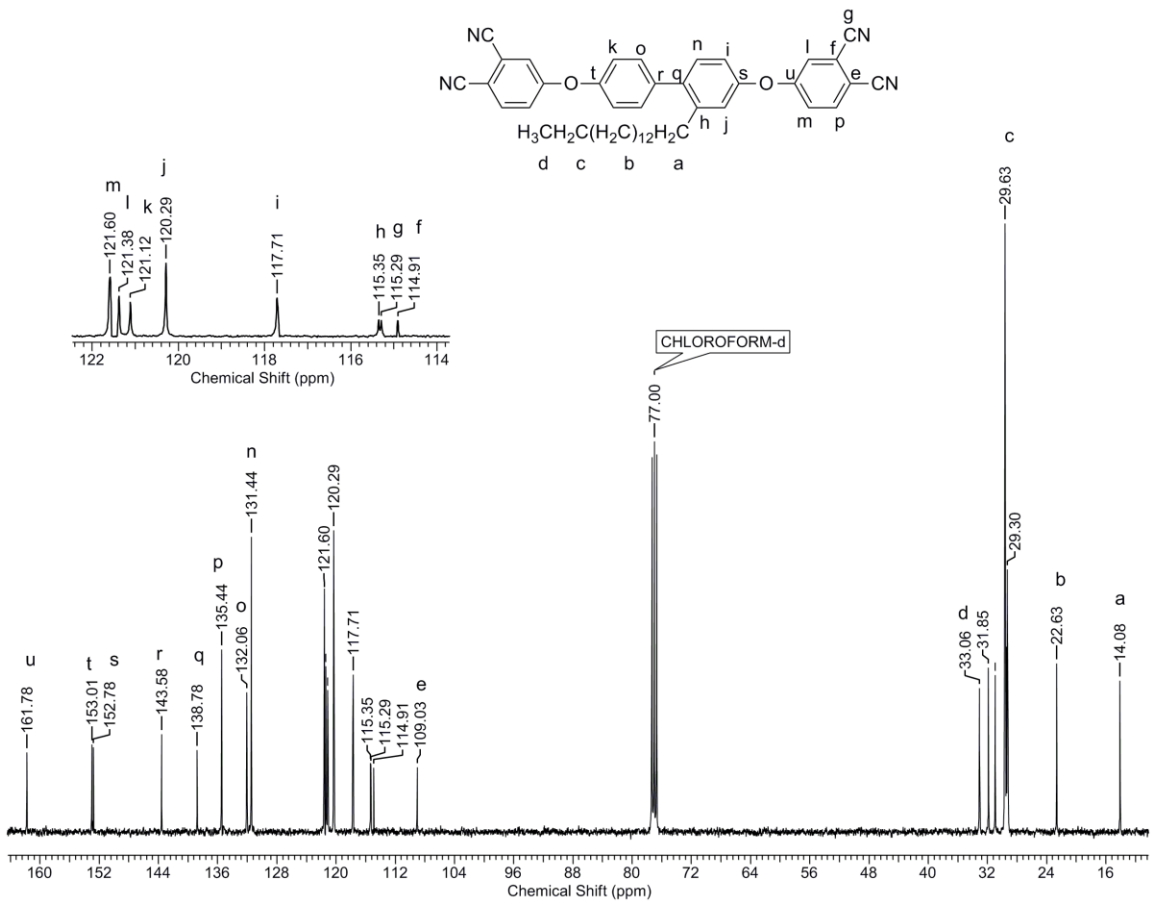

Figure 3.37 ^{13}C-NMR spectrum ($CDCl_3$) of 4,4'-((2-pentadecyl-[1,1'-biphenyl]-4,4'-diyl)bis(oxy))diphthalonitrile (PBP)

The aromatic carbon atoms linked to the oxygen atoms, **s**, **t**, and **u**, appeared at 152.78 δ ppm, 153.01 δ ppm and 161.78 δ ppm, respectively, while aromatic carbon atoms linked to each other (**r** and **q**) resonated at 143.58 δ ppm and 138.78 δ ppm. The other aromatic carbon atoms (**i-p**) appeared at 117.71 – 135.44 δ ppm. The nitrile carbons (**g**) resonated at 115.29 δ ppm, while the signals appearing at 114.91 δ ppm and 109.03 δ ppm were assignable to the aromatic carbon atoms linked to the nitrile groups, **f** and **e**. The benzylic carbon atom (**d**) resonated at 33.06 δ ppm, while the remaining methylene carbons (**b**, **c**) appeared at 22.63 – 31.85 δ ppm. The signal at 14.08 δ ppm could be ascribed to the methyl carbon (**a**).

Thus, FT-IR, ^{1}H-NMR and ^{13}C-NMR results clearly indicated that the proposed structure of synthesised phthalonitrile monomer, 4,4'-((2-pentadecyl-[1,1'-biphenyl]-4,4'-diyl)bis(oxy))diphthalonitrile (PBP), was consistent with the observed results.

3.4.13 Synthesis of 4,4'-(((3-pentadecylcyclohexane-1,1-diyl)bis(4,1-phenylene))bis(oxy))diphthalonitrile (CPP)

In **Scheme 3.13** is depicted the route for the synthesis of 4,4'-(((3-pentadecylcyclohexane-1,1-diyl)bis(4,1-phenylene))bis(oxy))diphthalonitrile (CPP) starting from 4,4'-(3-pentadecylcyclohexane-1,1-diyl)diphenol (BPC15) (**section 3.4.6**).

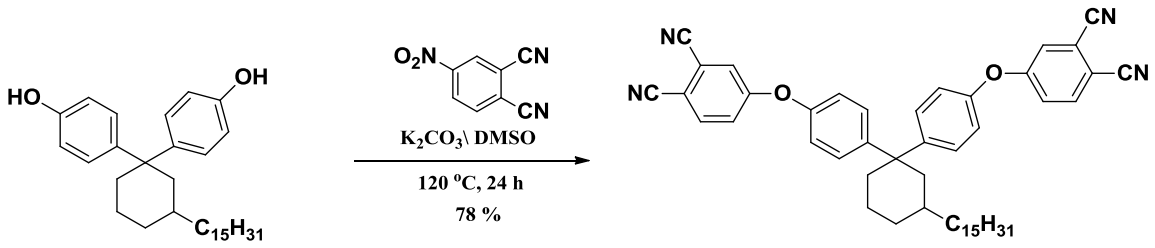

Scheme 3.13 Synthesis of 4,4'-(((3-pentadecylcyclohexane-1,1-diyl)bis(4,1-phenylene))bis(oxy))diphthalonitrile (CPP)

4,4'-(((3-pentadecylcyclohexane-1,1-diyl)bis(4,1-phenylene))bis(oxy))diphthalonitrile (CPP) was synthesised from the partially bio-based bisphenol, 4,4'-(3-pentadecylcyclohexane-1,1-diyl)diphenol (BPC15), containing a cyclohexylidene moiety, in one step. Initially, bisphenolate salt of the bisphenol was generated by stirring the bisphenol with potassium carbonate in dimethyl sulfoxide at 120 °C for one hour. Subsequently, 4-nitrophthalonitrile was added to the reaction mixture and stirred for 24 h at 120 °C, to yield 4,4'-(((3-pentadecylcyclohexane-1,1-diyl)bis(4,1-phenylene))bis(oxy))diphthalonitrile (CPP) by nucleophilic substitution reaction. The structure of pure 4,4'-(((3-pentadecylcyclohexane-1,1-diyl)bis(4,1-phenylene))bis(oxy))diphthalonitrile (CPP) was established spectroscopically.

FT-IR spectrum of 4,4'-(((3-pentadecylcyclohexane-1,1-diyl)bis(4,1-phenylene))bis(oxy))diphthalonitrile (CPP) is shown in **Fig 3.38**.

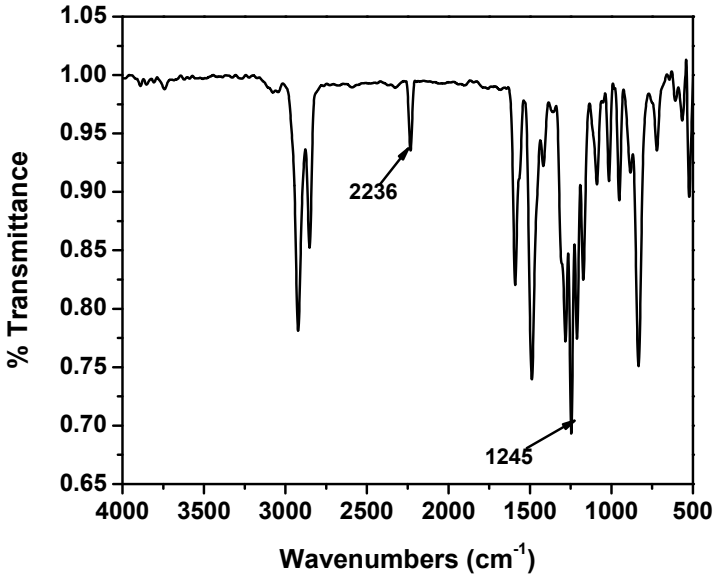

Figure 3.38 FT-IR spectrum of 4,4'-(((3-pentadecylcyclohexane-1,1-diyl)bis(4,1-phenylene))bis(oxy))diphthalonitrile (CPP)

The absorption band at 2236 cm^{-1} (-C≡N stretching) confirmed the presence of nitrile functionality, while the strong absorption band at 1245 cm^{-1} (-C-O-C- stretching) indicated the presence of ether functionality.

^{1}H-NMR spectrum of 4,4'-(((3-pentadecylcyclohexane-1,1-diyl)bis(4,1-phenylene))bis(oxy))diphthalonitrile (CPP) is provided in **Fig 3.39.**

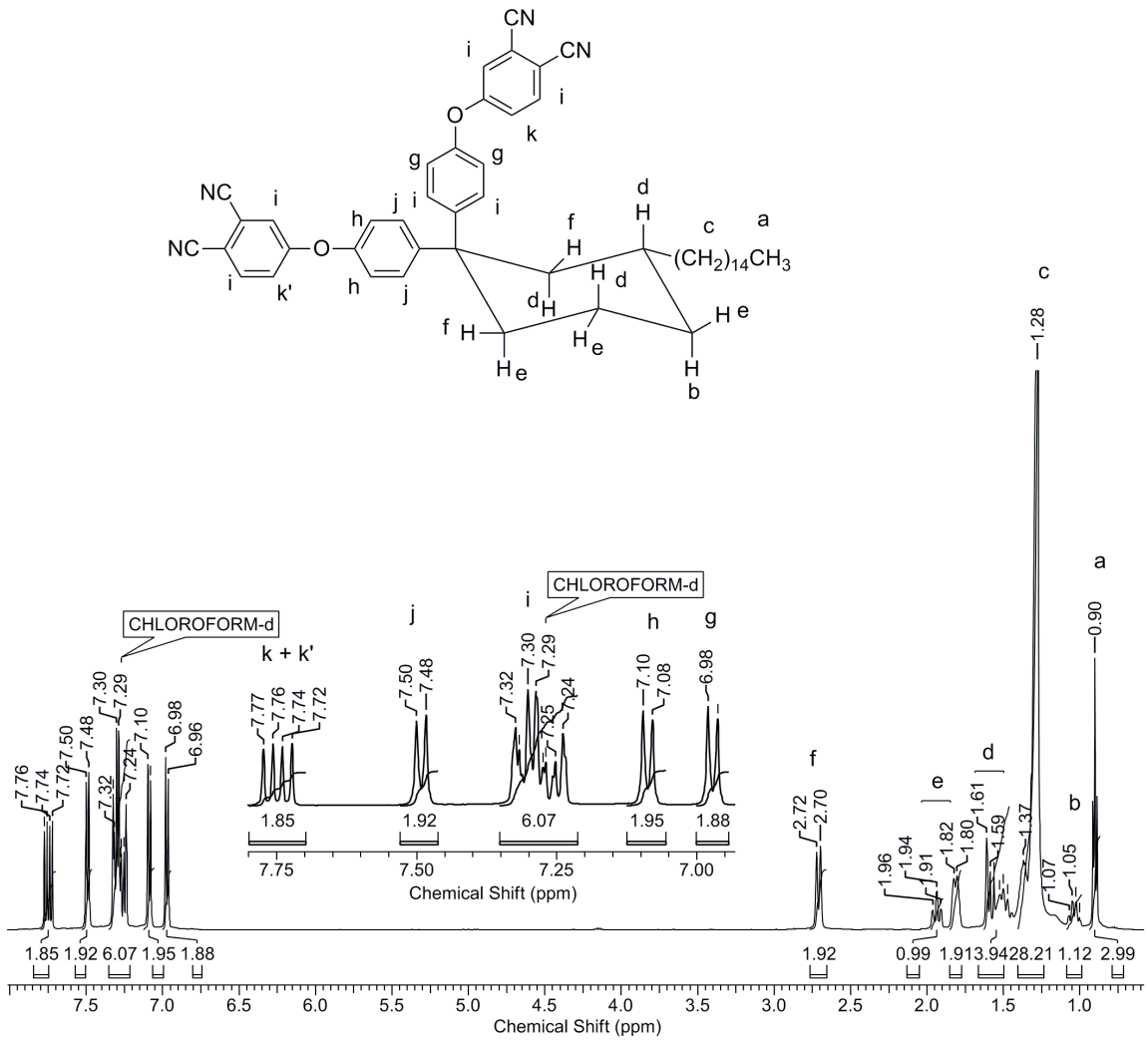

Figure 3.39 ^{1}H-NMR spectrum ($CDCl_3$) of 4,4'-(((3-pentadecylcyclohexane-1,1-diyl)bis(4,1-phenylene))bis(oxy))diphthalonitrile (CPP)

The spectroscopic techniques of ^{1}H-NMR, ^{13}C-NMR, DEPT, COSEY and HSQC were together employed to completely assign the structure of CPP. A detailed study revealed that the phenyl rings attached to the cyclohexyl ring were magnetically non-equivalent. The pentadecyl substituent prevents ring inversion; hence the conformation of the cyclohexyl ring is locked in the chair conformer as depicted in **Fig 3.39**, with the substituent present in the equatorial position. A closer study of the COSEY spectrum along with the HSQC spectrum assisted in the assignment of the ^{1}H-NMR spectrum. It was found that the equatorial protons appeared up-field compared to corresponding axial protons.

In **Fig 3.40** is presented the COSEY spectrum of CPP while the HSQC spectrum of CPP is depicted in **Fig 3.41**.

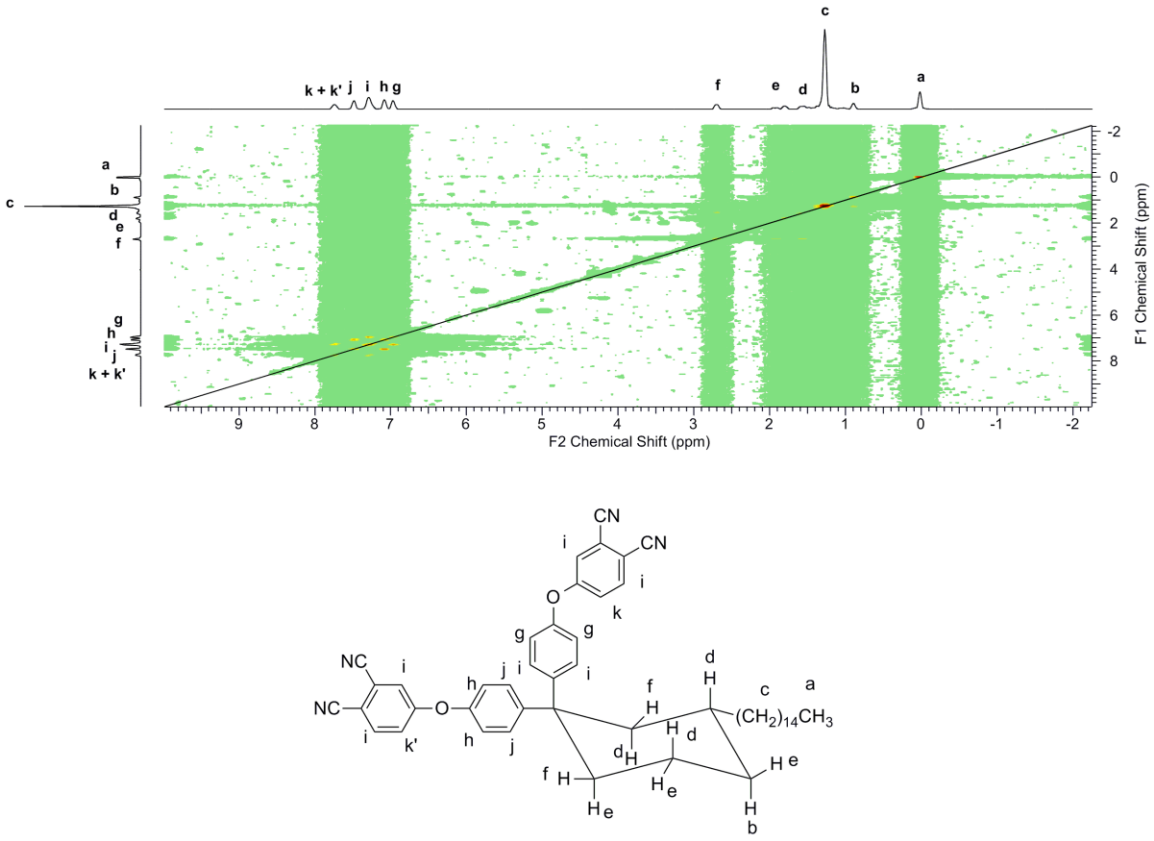

Figure 3.40 COSEY spectrum ($CDCl_3$) of 4,4'-(((3-pentadecylcyclohexane-1,1-diyl)bis(4,1-phenylene))bis(oxy))diphthalonitrile (CPP).

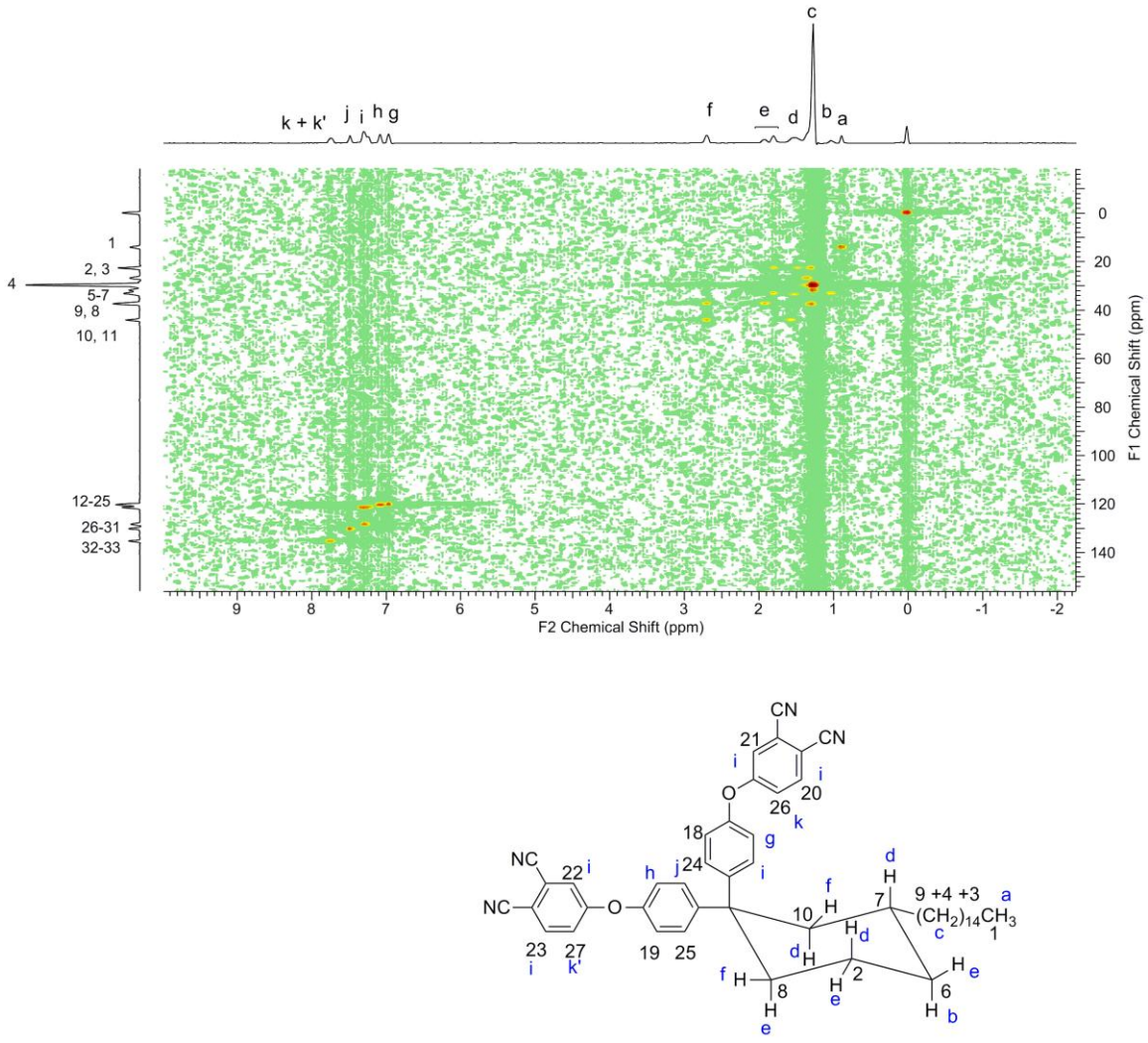

Figure 3.41 HSQC spectrum ($CDCl_3$) of 4,4'-(((3-pentadecylcyclohexane-1,1-diyl)bis(4,1-phenylene))bis(oxy))diphthalonitrile (CPP)

The aromatic protons **k** and **k'** present on carbon **26** and **27** appeared as doublets at 7.73 δ ppm and 7.76 δ ppm, respectively. The aromatic protons **j** present on the equatorial phenyl ring appeared as a doublet at 7.49 δ ppm, while the two aromatic protons **h** present on the same ring also appeared as a doublet, but at 7.09 δ ppm, being *ortho* to the ethereal oxygen. The aromatic protons **g** present on the axial phenyl ring resonated in the form of a doublet at 6.97 δ ppm. The remaining aromatic protons (**i**) appeared in the range 7.21 – 7.35 δ ppm as a multiplet. The two equatorial protons **f** present on the carbons **8** and **10** appeared as a multiplet in the range 2.68 – 2.77 δ ppm. The equatorial protons on carbon **2** and **6**, along with the axial proton on carbon **8** (**e**) appeared at 1.78 – 1.98 δ ppm in the form of a multiplet. The three axial protons on

carbons **2**, **7** and **10** (**d**), appeared as a multiplet in the range 1.46 – 1.63 δ ppm. The multiplet appearing in the range 0.99 – 1.09 δ ppm was assigned to the axial proton (**b**) present on carbon **6**, while the multiplet at 1.23 – 1.41 δ ppm was ascribed to the methylene protons (**c**) belonging to the pentadecyl chain. The methyl protons of the pentadecyl chain (**a**) resonated at 0.90 δ ppm as a triplet.

^{13}C-NMR spectrum of 4,4'-(((3-pentadecylcyclohexane-1,1-diyl)bis(4,1-phenylene))bis(oxy))diphthalonitrile (CPP) is shown in **Fig 3.42.**

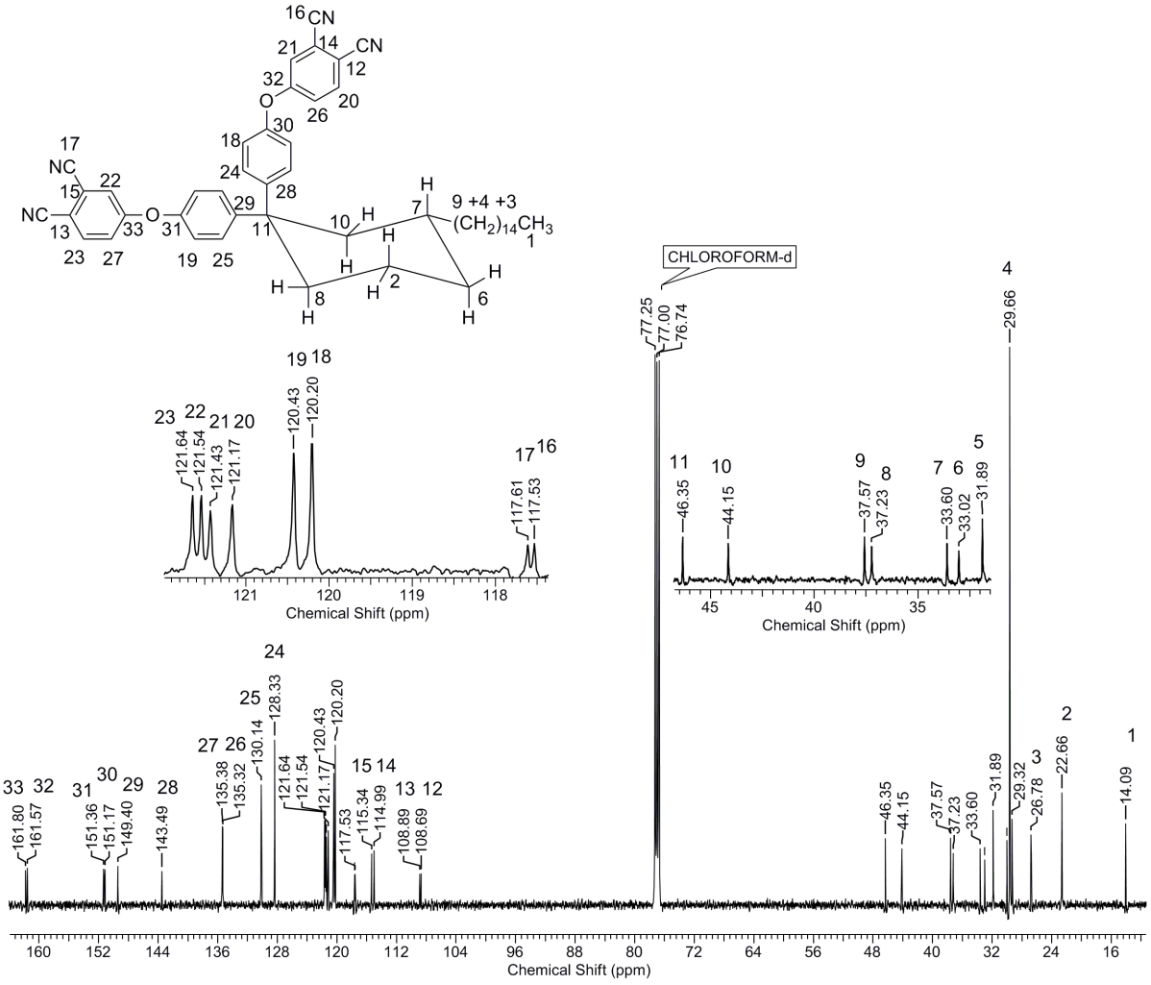

Figure 3.42 ^{13}C NMR spectrum (in $CDCl_3$) of 4,4'-(((3-pentadecylcyclohexane-1,1-diyl)bis(4,1-phenylene))bis(oxy))diphthalonitrile (CPP)

^{13}C-NMR spectrum of 4,4'-(((3-pentadecylcyclohexane-1,1-diyl)bis(4,1-phenylene))bis(oxy))diphthalonitrile (CPP) could be unambiguously assigned with the assistance of DEPT, HSQC and COSEY spectrum. The carbons **8**, **2**, **6**, **10** appeared at 37.23 δ ppm, 22.66 δ ppm, 33.02 δ ppm and 44.15 δ ppm. The carbon **7** linked to the

pentadecyl chain appeared at 33.60 δ ppm, while the quaternary carbon **11** resonated at 46.35 δ ppm. The nitrile carbons **16** and **17** appeared at 117.53 δ ppm and 117.62 δ ppm, respectively, while the carbon atoms linked to the nitrile groups, **12**, **13**, **14** and **15**, resonated at 108.69 δ ppm, 108.89 δ ppm, 114.99 δ ppm and 115.34 δ ppm, respectively. The signals appearing at 143.49 δ ppm and 149.40 δ ppm were assigned to aromatic carbons **28** and **29**, linked to the cyclohexyl moiety, on the axial and equatorial phenyl rings, respectively. The aromatic carbon atoms of the axial phenyl rings linked to ethereal oxygen, **30** and **32**, appeared at 151.17 δ ppm and 161.80 δ ppm, respectively, while those of the equatorial phenyl rings, **31** and **33**, appeared at 151.36 δ ppm and 161.57 δ ppm, respectively. The remaining carbon atoms also showed good agreement with the assigned values.

Thus, FT-IR, ^{1}H-NMR and ^{13}C-NMR results clearly indicated that the proposed structure of the synthesised phthalonitrile monomer 4,4'-(((3-pentadecylcyclohexane-1,1-diyl)bis(4,1-phenylene))bis(oxy))diphthalonitrile (CPP) was consistent with the observed results.

3.5 Conclusions

1. The potential of 3-pentadecyl phenol obtained in turn from cashew nut shell liquid, as a bio-derived starting material for the synthesis of difunctional condensation monomers and monomers for thermosetting resins, was explored in this chapter.

2. A new triarylamine-containing aromatic diamine, *viz*, 4, 4’-diamino-4"pentadecyltriphenylamine (DPTA) was synthesised.

3. A new dialdehyde and a new diacid, namely, 4-methoxy-6-pentadecylisophthalaldehyde (MPIAL) and 4-methoxy-6-pentadecylisophthalic acid (MPIA), respectively, were synthesised.

4. A new diamine containing biphenylene and ether linkages, namely, 4,4'-((2-pentadecyl-[1,1'-biphenyl]-4,4'-diyl)bis(oxy))dianiline (PBD), was synthesised.

5. A new bisphenol containing olefinic unsaturation, *viz.*, 2,6-Bis(4-hydroxybenzylidene)-3-pentadecylcyclohexanone (BPC), was synthesised.

6. Two new CNSL-based bispropargyl ethers were synthesised: one with multiple ether linkages and the other with a biphenylene linkage.

8. Three new phthalonitrile monomers were synthesised from 3-pentadecyl phenol.

9. The synthesised monomers hold great promise for the synthesis of high performance step-growth polymers and thermosetting resins. These monomers are a welcome addition to the family of (partially) bio-based monomers useful as precursors for high performance polymers.

References

1 H. Mark, *J. Macromol. Sci. Part A - Chem.*, 1981, **15**, 1065–1073.

2 M. E. Rogers, T. E. Long and S. R. Turner, in *Synthetic Methods in Step-Growth Polymers*, eds. M. E. Rogers and T. E. Long, John Wiley & Sons, Inc., Hoboken, NJ, USA, 2003, pp. 1–16.

3 D. Feldman, *Des. Monomers Polym.*, 2008, **11**, 1–15.

4 L. Billiet, D. Fournier and F. Du Prez, *Polymer*, 2009, **50**, 3877–3886.

5 C. W. Ulmer II, D. A. Smith, B. G. Sumpter and D. I. Noid, *Comput. Theor. Polym. Sci.*, 1998, **8**, 311–321.

6 P. M. Hergenrother, *High Perform. Polym.*, 2003, **15**, 3–45.

7 K. Lee, J. Y. Kim, S. H. Park, S. H. Kim, S. Cho and A. J. Heeger, *Adv. Mater.*, 2007, **19**, 2445–2449.

8 Y. Shao, G. C. Bazan and A. J. Heeger, *Adv. Mater.*, 2008, **20**, 1191–1193.

9 Y. Shao, X. Gong, A. J. Heeger, M. Liu and A. K. Y. Jen, *Adv. Mater.*, 2009, **21**, 1972–1975.

10 G. Yu, J. Gao, J. C. Hummelen, F. Wudl and A. J. Heeger, *Science*, 1995, **270**, 1789–1791.

11 C. J. Brabec, N. S. Sariciftci and J. C. Hummelen, *Adv. Funct. Mater.*, 2001, **11**, 15–26.

12 G. Li, V. Shrotriya, J. Huang, Y. Yao, T. Moriarty, K. Emery and Y. Yang, *Nat. Mater.*, 2005, **4**, 864–868.

13 M.-H. Chen, J. Hou, Z. Hong, G. Yang, S. Sista, L.-M. Chen and Y. Yang, *Adv. Mater.*, 2009, **21**, 4238–4242.

14 J. Hou, T. L. Chen, S. Zhang, L. Huo, S. Sista and Y. Yang, *Macromolecules*, 2009, **42**, 9217–9219.

15 L. Huo, J. Hou, S. Zhang, H.-Y. Chen and Y. Yang, *Angew. Chemie Int. Ed.*, 2010, **49**, 1500–1503.

16 S. Sista, Z. Hong, M.-H. Park, Z. Xu and Y. Yang, *Adv. Mater.*, 2010, **22**, E77–E80.

17 B. Yao, J. Zhang and X. Wan, in *Electrochromic Materials and Devices*, Wiley-VCH Verlag GmbH & Co. KGaA, Weinheim, Germany, 2015, vol. 44, pp. 211–240.

18 A. Iwan and D. Sek, *Prog. Polym. Sci.*, 2011, **36**, 1277–1325.

19 T. Abidin, Q. Zhang, K.-L. Wang and D.-J. Liaw, *Polymer*, 2014, **55**, 5293–5304.

20 H.-J. Yen and G.-S. Liou, *Polym. Chem.*, 2018, **9**, 3001–3018.

21 T. J. Lee, Y.-G. Ko, H.-J. Yen, K. Kim, D. M. Kim, W. Kwon, S. G. Hahm, G.-S. Liou and M. Ree, *Polym. Chem.*, 2012, **3**, 1276–1283.

22 H.-J. Yen and G.-S. Liou, *Polym. J.*, 2016, **48**, 117–138.

23 W.-P. Lin, S.-J. Liu, T. Gong, Q. Zhao and W. Huang, *Adv. Mater.*, 2014, **26**, 570–606.

24 T. Kurosawa, T. Higashihara and M. Ueda, *Polym. Chem.*, 2013, **4**, 16–30.

25 A. P. Dove and M. A. R. Meier, *Macromol. Chem. Phys.*, 2014, **215**, 2135–2137.

26 G. W. Huber, S. Iborra and A. Corma, *Chem. Rev.*, 2006, **106**, 4044–4098.

27 Y. Zhu, C. Romain and C. K. Williams, *Nature*, 2016, **540**, 354–362.

28 P. F. H. Harmsen, M. M. Hackmann and H. L. Bos, *Biofuels, Bioprod. Biorefining*, 2014, **8**, 306–324.

29 D. Chatterjee, N. V. Sadavarte, R. D. Shingte, A. S. More, B. V. Tawade, A. D. Kulkarni, A. B. Ichake, C. V. Avadhani and P. P. Wadgaonkar, in *Cashew Nut Shell Liquid, A Goldfield for Functional Materials*, ed. P. Anilkumar, Springer International Publishing, Cham, 2017, pp. 163–214.

30 R. Mülhaupt, *Macromol. Chem. Phys.*, 2013, **214**, 159–174.

31 A. Llevot, E. Grau, S. Carlotti, S. Grelier and H. Cramail, *Macromol. Rapid Commun.*, 2016, **37**, 9–28.

32 A. Gandini, T. M. Lacerda, A. J. F. Carvalho and E. Trovatti, *Chem. Rev.*, 2016, **116**, 1637–1669.

33 D. K. Schneiderman and M. A. Hillmyer, *Macromolecules*, 2017, **50**, 3733–3749.

34 H. T. H. Nguyen, P. Qi, M. Rostagno, A. Feteha and S. A. Miller, *J. Mater. Chem. A*, 2018, **6**, 9298–9331.

35 C. Voirin, S. Caillol, N. V. Sadavarte, B. V. Tawade, B. Boutevin and P. P. Wadgaonkar, *Polym. Chem.*, 2014, **5**, 3142–3162.

36 Z. Mi, Z. Liu, C. Tian, X. Zhao, H. Zhou, D. Wang and C. Chen, *J. Polym. Sci. Part A Polym. Chem.*, 2017, **55**, 3253–3265.

37 G. N. Short, H. T. H. Nguyen, P. I. Scheurle and S. A. Miller, *Polym. Chem.*, 2018, **9**, 4113–4119.

38 T. Mukaiyama, F.-C. Pai, M. Onaka and K. Narasaka, *Chem. Lett.*, 1980, **9**, 563–566.

39 A. C. Brown and L. A. Carpino, *J. Org. Chem.*, 1985, **50**, 1749–1750.

40 M. W. Kasture, P. S. Niphadkar, N. Sharanappa, S. P. Mirajkar, V. V. Bokade and P. N. Joshi, *J. Catal.*, 2004, **227**, 375–383.

41 N. V. Sadavarte, M. R. Halhalli, C. V. Avadhani and P. P. Wadgaonkar, *Eur. Polym. J.*, 2009, **45**, 582–589.

42 S. J. Chowdhury, P. P. Wadgaonkar, T. L. Hoeks, S. K. Rajaram, B. D. Sarwade and C. V. Avadhani, US7851524B2, 2010.

43 B. V. Tawade, J. K. Salunke, P. S. Sane and P. P. Wadgaonkar, *J. Polym. Res.*, 2014, **21**, 617.

44 B. V. Tawade, S. V. Shaligram, N. G. Valsange, U. K. Kharul and P. P. Wadgaonkar, *Polym. Int.*, 2016, **65**, 567–576.

45 R. D. Shingte, Ph. D. Thesis, University of Pune, 2006.

46 S.-H. Hsiao, Y.-M. Chang, H.-W. Chen and G.-S. Liou, *J. Polym. Sci. Part A Polym. Chem.*, 2006, **44**, 4579–4592.

47 O. A. Attanasi, S. Buratti and P. Filippone, *Org. Prep. Proced. Int.*, 1995, **27**, 645–650.

48 K. W. Rosenmund and E. Struck, *Berichte der Dtsch. Chem. Gesellschaft (A B Ser.*, 1919, **52**, 1749–1756.

49 J. Lindley, *Tetrahedron*, 1984, **40**, 1433–1456.

50 S. Trofimenko, *J. Org. Chem.*, 1964, **29**, 3046–3049.

51 E. Dalcanale and F. Montanari, *J. Org. Chem.*, 1986, **51**, 567–569.

52 L. Tietze, C. Vock, I. Krimmelbein and L. Nacke, *Synthesis*, 2009, **2009**, 2040–2060.

53 B. Andersh, D. L. Murphy and R. J. Olson, *Synth. Commun.*, 2000, **30**, 2091–2098.

54 A. Suzuki, *J. Organomet. Chem.*, 1999, **576**, 147–168.

55 J. P. Wolfe, R. A. Singer, B. H. Yang and S. L. Buchwald, *J. Am. Chem. Soc.*, 1999, **121**, 9550–9561.

56 J. Hassan, M. Sévignon, C. Gozzi, E. Schulz and M. Lemaire, *Chem. Rev.*, 2002, **102**, 1359–1470.

57 Z. Du, R. Liu, W. Shao, X. Mao, L. Ma, L. Gu, Z. Huang and A. S. C. Chan, *Eur. J. Med. Chem.*, 2006, **41**, 213–218.

58 R. D. Shingte and P. P. Wadgaonkar, US6790993B1, 2004.

59 S. K. Dirlikov, *High Perform. Polym.*, 1990, **2**, 67–77.

60 C. Nair, *Prog. Polym. Sci.*, 2004, **29**, 401–498.

61 A. S. Hay, D. A. Bolon, K. R. Leimer and R. F. Clark, *J. Polym. Sci. Part B Polym. Lett.*, 1970, **8**, 97–99.

62 A. S. Hay, US3594175, 1971.

63 A. Badshah, M. R. Kessler, Z. Heng and A. Hasan, *Polym. Int.*, 2014, **63**, 465–469.

64 Y. Qi, Z. Weng, J. Wang, S. Zhang, L. Zong, C. Liu and X. Jian, *Polym. Int.*, 2018, **67**, 322–329.

65 H. Wang, J. Wang, H. Guo, X. Chen, X. Yu, Y. Ma, P. Ji, K. Naito, Z. Zhang and Q. Zhang, *Polym. Chem.*, 2018, **9**, 976–983.

66 M. Laskoski, A. Neal, T. M. Keller, D. Dominguez, C. A. Klug and A. P. Saab, *J. Polym. Sci. Part A Polym. Chem.*, 2014, **52**, 1662–1668.

67 J. Hu, P. Yuan, K. Zeng and G. Yang, *Thermochim. Acta*, 2014, **590**, 30–39.

68 M. Laskoski, J. S. Clarke, A. Neal, B. G. Harvey, H. L. Ricks-Laskoski, W. J. Hervey, M. N. Daftary, A. R. Shepherd and T. M. Keller, *ChemistrySelect*, 2016, **1**, 3423–3427.

69 N. Sun, Z. Zhou, D. Chao, X. Chu, Y. Du, X. Zhao, D. Wang and C. Chen, *J. Polym. Sci. Part A Polym. Chem.*, 2017, **55**, 213–222.

Supporting Information

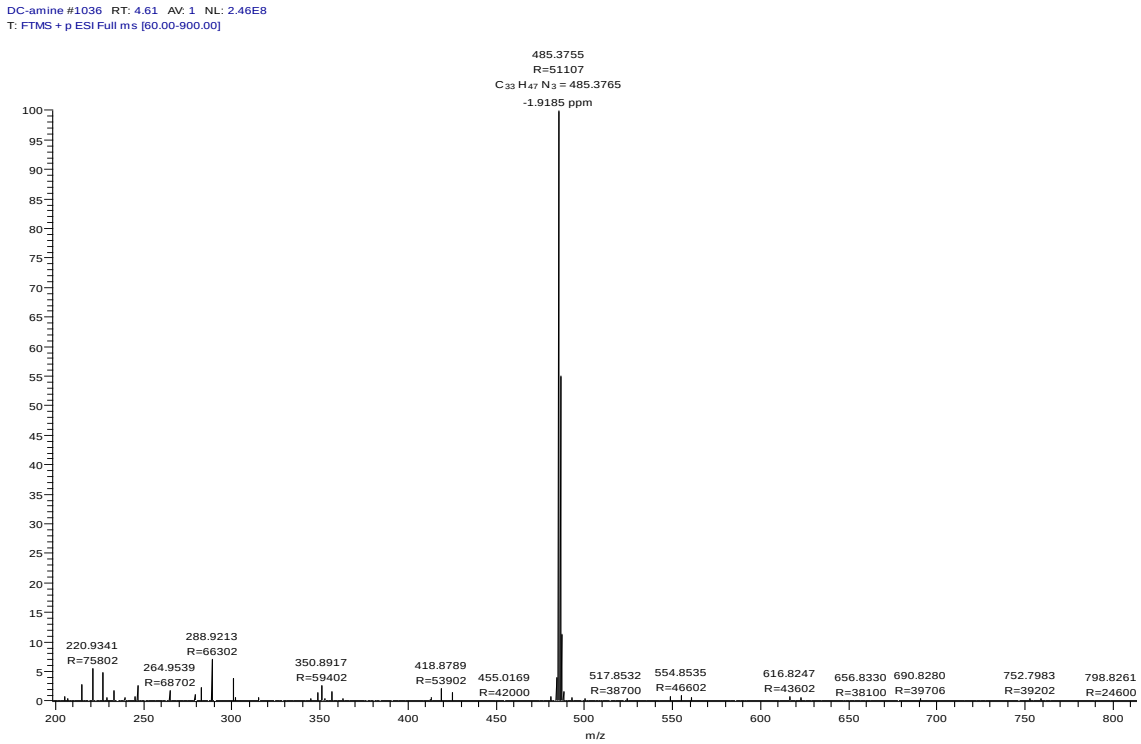

Figure SI 3.1 HRMS of 4, 4’-diamino-4"pentadecyltriphenylamine (DPTA)

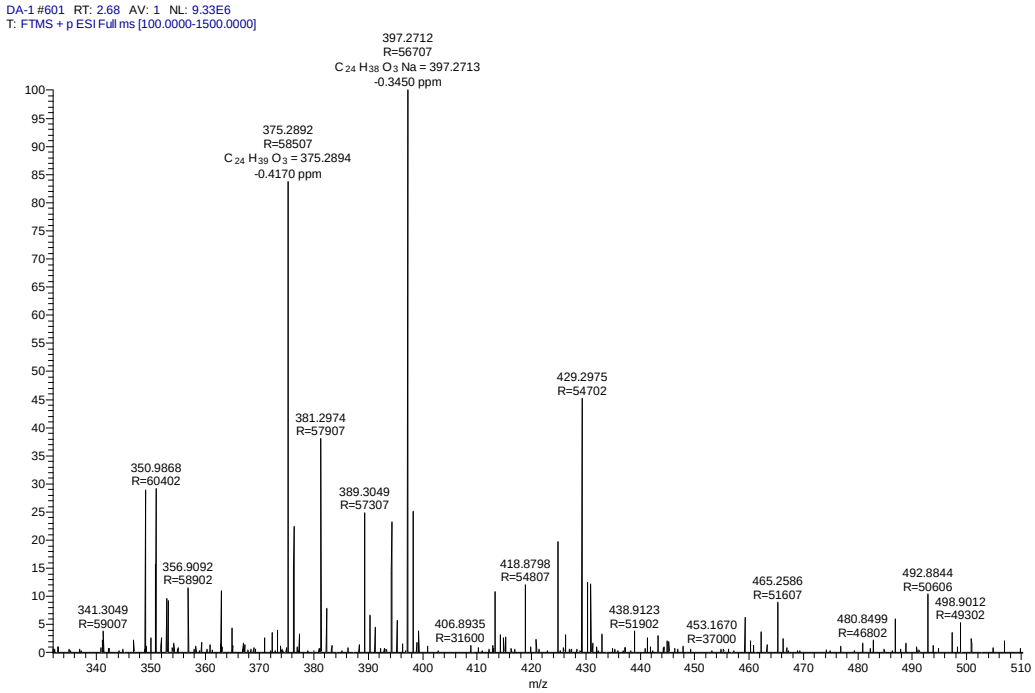

Figure SI 3.2 HRMS of 4-methoxy-6-pentadecylisophthalaldehyde (MPIAL)

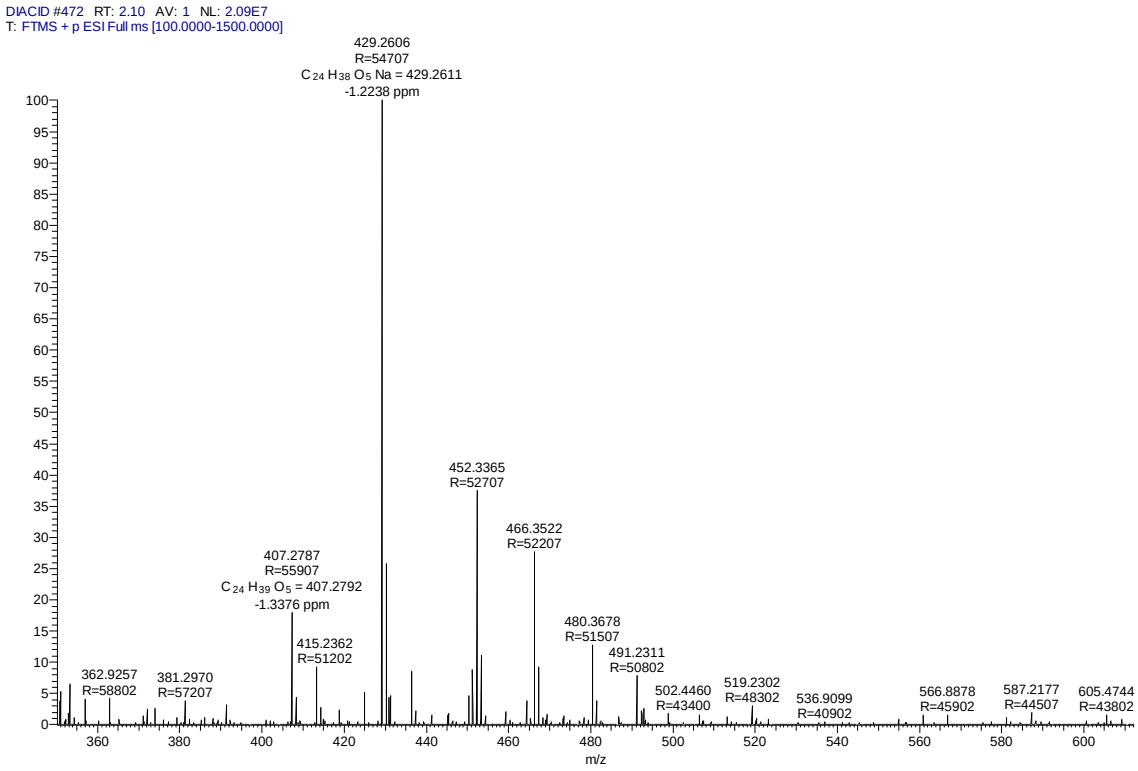

Figure SI 3.3 HRMS of 4-methoxy-6-pentadecylisophthalic acid (MPIA)

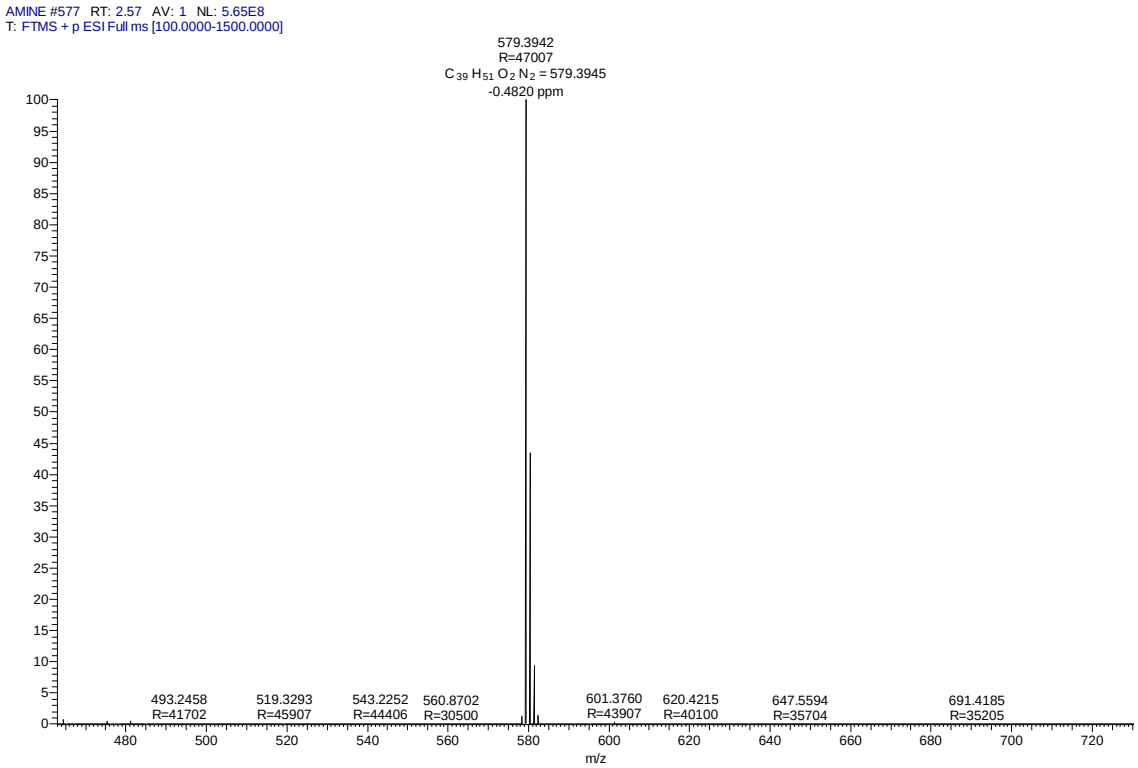

Figure SI 3.4 HRMS of 4,4'-((2-pentadecyl-[1,1'-biphenyl]-4,4'-diyl)bis(oxy))dianiline (PBD)

CHAPTER 4

Partially Bio-Based Triarylamine-Containing High Performance Polymers

CHAPTER 4 (a)

Partially Bio-Based Triarylamine-Containing Polyimides: Synthesis, Characterisation and Evaluation for Memory Devices

4a.1 Introduction

In recent years, considerable research activity has been devoted to the exploration of polymeric materials for optoelectronic applications such as light emitting devices,[1–4] solar cells,[5–11] memory devices[12–14] and electrochromic devices.[15–19] This is in major part a result of the excellent deformation and deterioration resistance, processability, good mechanical strength and opportunity to tune properties of polymeric materials through synthesis. Polymeric materials constitute an interesting emerging alternative for the present-day silicon-based memory devices which suffer from the problems of miniaturisation and requirement to store large volumes of data. In contrast to silicon-based memory cells, polymer RRAM devices (polymer memory) store data in the form of distinct conductivity or resistance states. Additionally, polymer memory devices also have a simple structure, consisting of just a simple metal-insulator-metal setup, eschewing the need of a distinct cell structure as in the case of silicon-based memory. Besides, polymer memory is generally CMOS (complementary metal oxide semiconductor) compatible and so can also be incorporated in existing memory systems.[20]

Aromatic polyimides are a well-known class of materials possessing remarkable electrical and mechanical properties in addition to outstanding chemical properties[21–25] and thus can replace glass and metals in various industrial applications such as aviation, automobiles, electrical packaging, semiconductors and so on.[26–30] Aromatic polyimides containing triarylamine moieties have heretofore been employed for optoelectronic applications such as electrochromic devices, memory devices, electroluminescent devices,[18,31–33] etc. Polyimides have an inherent donor-acceptor nature leading to the formation of charge transfer complex (CTC).[34] Such CTC is crucial for the operation of memory devices, and the incorporation of triarylamine moiety serves to enhance the donor-acceptor nature of polyimides. Due to these reasons, the exploration of aromatic polyimides in the field of memristic devices has become a research topic of great interest. Different types of memory devices fabricated from polyimides have been reported in the literature. Differently substituted triarylamine-based polyimides have exhibited different memory behaviour.[35–40] Similarly, the use of different dianhydrides for the generation of polyimides have yielded polymers with different memory character.[41–43] For example,

Ling[35] et al have reported DRAM type volatile memory behaviour for unsubstituted triphenylamine based polyimides while Lee[36] *et al* were able to obtain polyimides based on triphenylamine substituted with two methyl groups exhibiting WORM type behaviour. Additionally, Liou[43] *et al* have reported polyimides with different electron acceptors exhibiting memory behaviour ranging from DRAM to SRAM to WORM. Hence, it is of interest to investigate the memory properties of new triarylamine-based polyimides with substituted triarylamine and different electron acceptors.

In addition to showing memristive behaviour, triarylamine-based high performance polyimides also show interesting electrochromic properties. Hsiao's and Liou's groups have reported several polyimides with triphenylamine units in the main chain containing pendent methyl,[33,44] t-butyl,[45] methoxy,[46] adamantyl phenoxy,[47] carbazole,[31,48] morpholinyl,[49] cyano[50] and adamantoxy[51] groups. It was demonstrated that the introduction of an electron donating group at the *para* position of the triphenylamine unit stabilised the intermediate radical cation leading to improved electrochromic properties.[46]

To the best of our knowledge, there are no reports of triphenylamine-based aromatic polyimides derived from bio-based sources. In this work is reported the synthesis of triarylamine-based polyimides from 4, 4'-diamino-4"pentadecyltriphenylamine (DPTA) whose synthesis has been described in **Chapter 3**. The synthesised polyimides were characterised by inherent viscosity measurements, GPC studies, FT-IR, ^{1}H-NMR, ^{13}C-NMR spectroscopy, X-ray diffraction, thermogravimetric analysis (TGA) and differential scanning calorimetric studies (DSC). The optical, electrochemical and spectroelectrochemical behaviour of polyimides was also investigated. Memory devices were fabricated from synthesised polyimides and their performance was evaluated.

4a.2 Experimental

4a.2.1 Materials

4, 4'-Diamino-4"pentadecyltriphenylamine (DPTA) was synthesised as described in **Chapter 3**. Tetrabutylammonium perchlorate (TBAP), ferrocene (Sigma Aldrich, India) and isoquinoline (Acros, India), were used as received. 3,3',4,4'-Biphenyltetracarboxylic dianhydride (BPDA), 4,4'-oxydiphthalic anhydride (ODPA) and

4,4'-(hexafluoroisopropylidene) diphthalic anhydride (6-FDA) (Sigma Aldrich, India) were purified by sublimation under reduced pressure. *meta*- Cresol was distilled before use while *N*,*N*-dimethylformamide and acetonitrile (Thomas Baker, India) were distilled over calcium hydride prior to use.

4a.2.2 Measurements

Infrared spectra of polymer films were measured on Perkin-Elmer Spectrum GX spectrometer. ^{1}H and ^{13}C-NMR spectra were recorded on Bruker-AV 400 and 500 MHz spectrometer using chloroform-*d* as solvent and TMS as an internal standard. Molecular weights of polyimides were measured on ThermoFinnigan gel permeation chromatograph (GPC) in chloroform using polystyrene as the calibration standard. Concentration of polymers used was 5 mg dL^{-1}. Inherent viscosity of polymers was measured using 0.5 % (w/v) solution of polymer in chloroform at 25 ± 0.1 °C. Ubbelohde suspended level viscometer was used to determine inherent viscosity according to the following equation:

$$n_{inh} = \frac{2.303}{C} x \log \frac{t}{t_0}$$

where *t* and t_0 are flow times of polymer solution and solvent, respectively and *C* is the concentration of polymer solution. X-Ray diffraction analysis was performed on Rigaku MicroMax-007HF X-ray diffractometer at 40 kV and 30 mA. Thermo gravimetric analysis (TGA) of the polymers was performed on Perkin Elmer: STA 6000 between temperatures of 30 °C to 900 °C with a heating rate of 10 °C min^{-1} under nitrogen. Glass transition temperatures (T_g) were determined from differential scanning calorimetry (DSC) experiments carried out on TA Q-100 instrument with sample heating rate of 10 °C min^{-1} under nitrogen atmosphere. T_g values of polyimides were determined from the second heating cycles. UV–Vis spectra were measured on Specord 210 plus Analytic Jena spectrophotometer. Cyclic voltammetric experiments were carried out on CH Instruments Electrochemical Analyzer.

4a.2.3 Polyimide synthesis: typical procedure

Into a 50 mL three-necked round bottom flask were added 6-FDA (0.274 g, 6.17 x 10^{-2} mol), 4, 4'-diamino-4"pentadecyltriphenylamine (0.3 g, 6.17 x 10^{-2} mol) (TBAP) and freshly distilled *meta*-cresol (5.74 mL) under continuous nitrogen flow and stirred to give a homogeneous solution. The reaction mixture was stirred at room temperature for 1 h after which a few drops of isoquinoline were added. Subsequently, the reaction mixture

was then heated to 150 °C for 8 h and at 220 °C for 6 h, during which period the water produced during imidisation was removed continuously in a stream of nitrogen. The viscous polymer solution was then cooled and poured into methanol with continuous stirring to precipitate the fibrous polymer. The polyimide (PI-6FDA) was further purified by dissolving in chloroform and precipitating in methanol. A similar process was followed for the synthesis of polyimides derived from polycondensation of DPTA with ODPA (PI-ODPA) and BPDA (PI-BPDA)

4a.2.4 Optical, electrochemical and spectroelectrochemical measurements

UV-Vis spectra of chloroform solutions of PI-6FDA, PI-ODPA and PI-BPDA (10^{-5} M) were recorded on Specord 210 plus Analytic Jena spectrophotometer. UV-Vis spectra of free-standing films of the polyimides were also recorded. Cyclic voltammetry was conducted in a three-electrode cell in which platinum foil (0.3 cm x 0.4 cm), on which polyimides were dropcast, was used as a working electrode; a platinum wire was used as counter electrode, while a home-made Ag/AgCl, KCl (sat.) was used as reference electrode in dry acetonitrile (oxidation process/ positive scan) or dry *N*,*N*-dimethylformamide (reduction process/ negative scan) containing 0.1 M TBAP as an electrolyte under nitrogen atmosphere. Ferrocene was employed as an external reference for calibration (4.8 V versus Ag/AgCl). Spectroelectrochemical measurements were carried out by coupling chronoamperometric measurements with UV-Vis spectroscopy. Polyimides drop-casted onto FTO coated glass plates (1 cm x 2 cm) were used as working electrodes for spectroelectrochemical measurements. Other electrodes and electrolyte solutions employed were identical to those employed for cyclic voltammetry experiments.

4a.2.5 Memory device characterisation

Memory devices were fabricated by drop-casting chloroform solutions of PI-6FDA, PI-ODPA and PI-BPDA (1 mg/mL) onto FTO plates (1.5 cm x 1.5 cm) and dried in an oven at 160 °C for 48 h. Uniformity of film thickness was maintained by drop-casting a single layer of polymer onto FTO. The FTO plates used were previously sonicated in dilute soap solution for 10 min, subsequently followed by sequential sonication in deionised water (4 times, 10 min) and isopropyl alcohol (15 min). Finally, the FTO plates were boiled in isopropyl alcohol and dried before memory device

fabrication. **Fig 4a.1** represents the schematic structure of developed memory devices. Programmable memristor characterisation system (Arc ONE) was used to evaluate the resistive switching characteristics of polyimide-based devices. During all electrical measurements, the top aluminium (Al) electrode was biased and bottom FTO electrode was grounded. Following parameters were kept constant during electrical measurements; signal type: staircase, the maximum amplitude of the positive and negative voltage pulse: ±2 V, step width: 100 ms, read voltage: 0.20 V and interpulse time: 10 ms. For the endurance and retention measurements, the pulse width of positive and negative pulses was 100 µs.

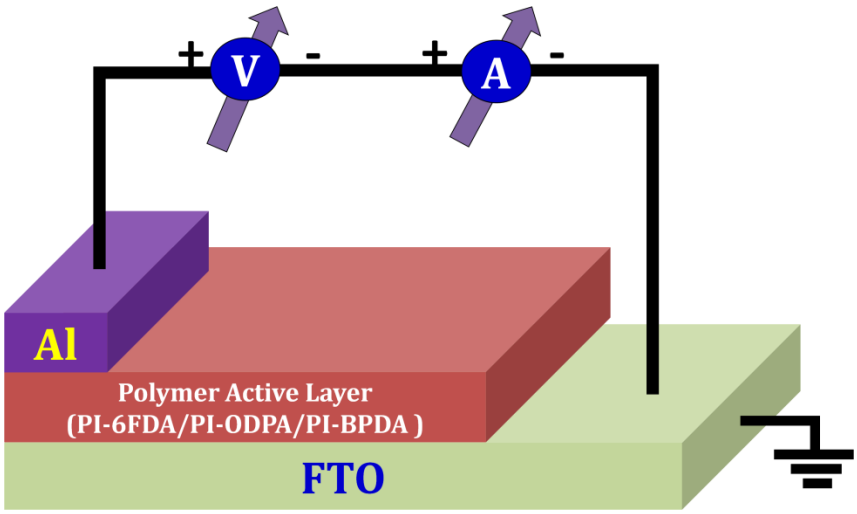

Figure 4a.1 Schematic structure of the triarylamine-containing polyimide based memory devices

4a.3 Results and Discussion

4a.3.1 Polyimide synthesis

DPTA was polycondensed with commercially available aromatic dianhydrides, namely, 6-FDA, ODPA and BPDA in *m*-cresol using one-step high temperature polymerisation method, in the presence of catalytic quantity of isoquinoline, to yield polyimides PI-6FDA, PI-ODPA and PI-BPDA respectively, as depicted in **Scheme 4a.1**

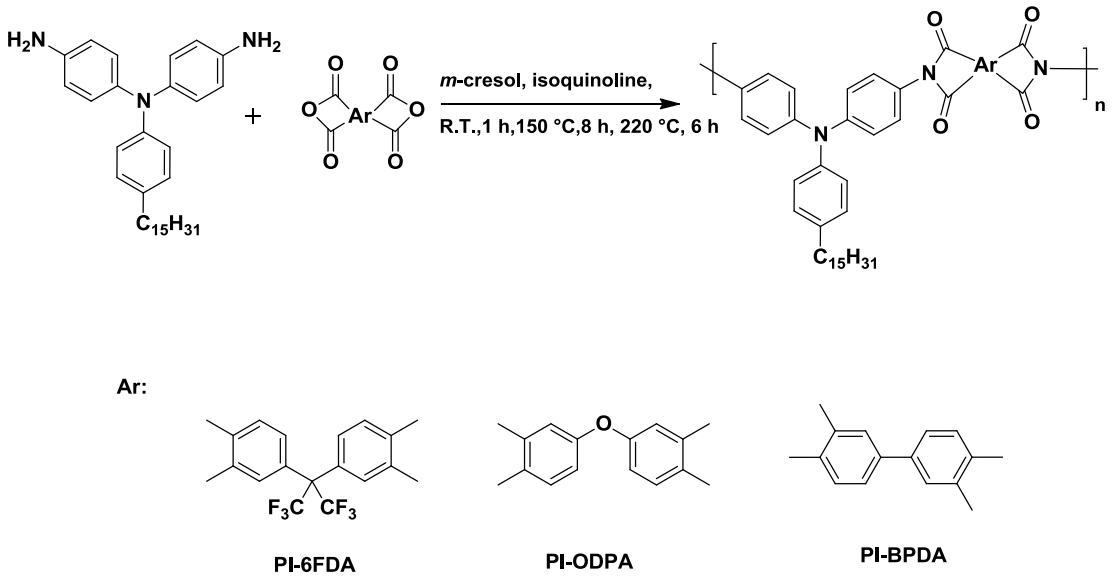

Scheme 4a.1 Synthesis of triarylamine-containing polyimides

The results of polymerisation are tabulated in **Table 4a.1.** The synthesised polyimides were observed to exhibit inherent viscosities in the range 0.57 – 0.60 dL g^{-1} and number average molecular weights (M_n) in the range 26800 – 43500 g mol^{-1}, indicative of the formation of reasonably high molecular weight polyimides. However, it is to be noted that molecular weights determined through GPC utilise polystyrene standards and hence may not be considered absolute molecular weights. The polyimides formed free-standing, flexible transparent films **(Fig 4a.2)**.

Table 4a.1 Results of synthesis of triarylamine-containing polyimides

Polyimide	η_{inh} (dL/g)[a]	Molecular weight[b] (g mol^{-1})		Dispersity (M_w/M_n)
		M_n	M_w	
PI-6FDA	0.57	33200	63600	1.9
PI-ODPA	0.54	26800	74200	2.8
PI-BPDA	0.60	43500	94200	2.2

a: η_{inh} was measured using 0.5% (w/v) solution of polyimides in chloroform at 25 °C ± 1°C
b: Determined through GPC in chloroform, using polystyrenes as calibration standard

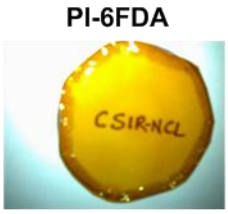

Figure 4a.2 PI-6FDA film cast from chloroform

Structural confirmation of the synthesised polyimides was accomplished through FT-IR, ^{1}H-NMR and ^{13}C-NMR studies. FT-IR spectrum of a representative polyimide, PI-6FDA, is depicted in **Fig 4a.3**. Representative ^{1}H-NMR spectrum of PI-6FDA is presented in **Fig 4a.4**, while ^{13}C-NMR spectrum is presented in **Fig 4a.5**.

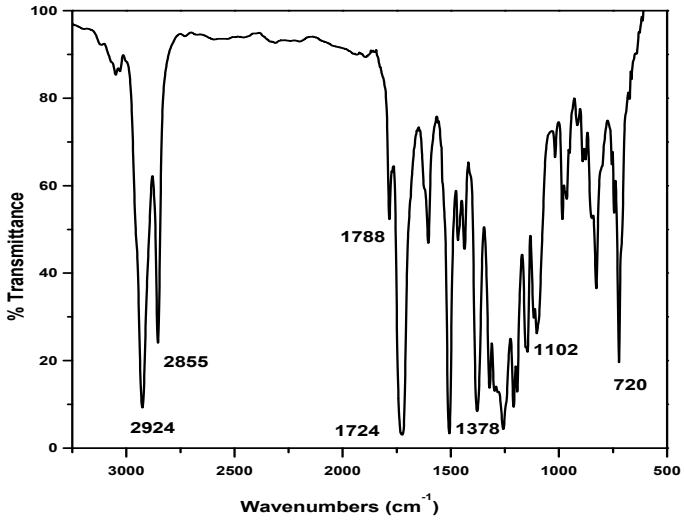

Figure 4a.3 FT-IR spectrum of PI-6FDA film

Absorption bands corresponding to imide functionality appeared at 1788 cm^{-1} (asymmetrical C=O stretch), 1724 cm^{-1} (symmetrical C=O stretch), 1378 cm^{-1} (C-N stretching and bending), 1100 cm^{-1} (C-N stretching) and 720 cm^{-1} (imide ring deformation).[45,46]

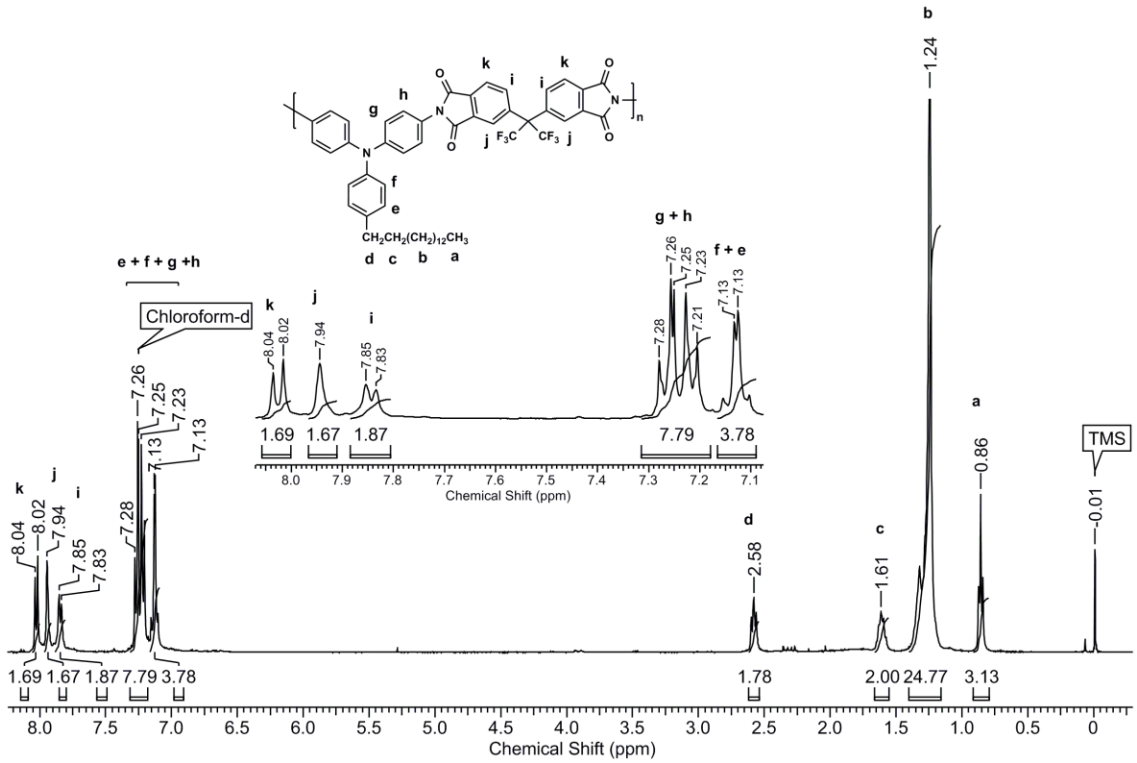

Figure 4a.4 ^{1}H-NMR spectrum ($CDCl_3$) of PI-6FDA.

The aromatic protons corresponding to dianhydride unit appeared in the range 7.8 – 8.04 δ ppm. The aromatic protons belonging to diamine component appeared in the region of 7.13 – 7.28 δ ppm. The benzylic protons appeared as a triplet at 2.58 δ ppm while the methyl protons resonated at 0.86 δ ppm.

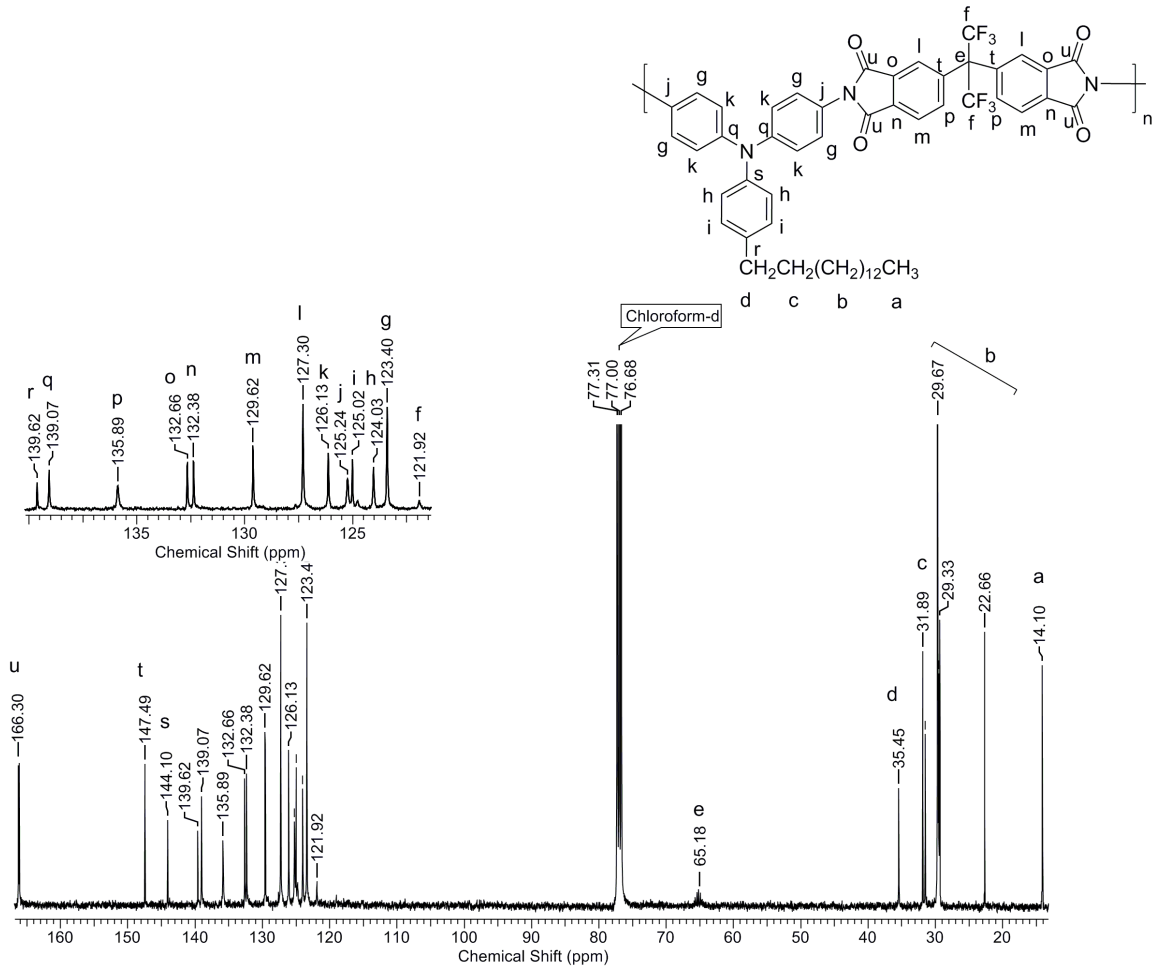

Figure 4a.5 ^{13}C-NMR spectrum ($CDCl_3$) of PI-6FDA.

^{13}C-NMR spectrum of PI-6FDA was assigned with the help of the corresponding DEPT spectrum. The aromatic carbons belonging to the dianhydride unit appeared in the region 127.30 – 135.89 δ ppm and at 147.49 δ ppm while the aromatic carbon atoms of the triarylamine unit resonated in the region 123.40 – 126.13 δ ppm. The aromatic carbons **q** and **s** appeared at 139.07 δ ppm and 144.10 δ ppm, respectively. The signal corresponding to imide carbonyl (**u**) appeared at 166.30 δ ppm.

From the data presented above, it is clear that FT-IR, ^{1}H-NMR and ^{13}C-NMR spectra showed good agreement with proposed structure and thus together confirmed the structure of the synthesised polyimide. ^{1}H-NMR and ^{13}C-NMR spectra of PI-ODPA and PI-BPDA are provided in **Supporting Information** (**Fig SI 4a.1**-**Fig SI 4a.4**)

4a.3.2 Solubility and X-ray diffraction studies

The solubility behaviour of synthesised polyimides at 3 wt % concentration was determined and the results are summarised in **Table 4a.2.**

Table 4a.2 Solubility of triarylamine-containing polyimides

Polyimide	Solvent						
	$CHCl_3$	THF	DMAc	NMP	Pyridine	m-Cresol	Acetone
PI-6FDA	++	++	+	++	+	++	−−
PI-ODPA	++	++	+	++	++	++	−−
PI-BPDA	++	++	++	++	+	++	−−

--, Insoluble; + soluble on heating at 70 °C; ++, soluble at room temperature

Polyimides were soluble in solvents such as chloroform, tetrahydofuran and *m*-cresol at room temperature and they were also soluble in polar solvents such as NMP, DMAc and pyridine either at room temperature or on heating. The C_{15} alkyl chain, together with the bulky triarylamine moiety disrupt interchain packing allowing solvent molecules to penetrate deep within the polymer chains, leading to improved solubility. Such good solubility makes these polymers potentially useful for several practical applications such as spin-coating and inkjet printing techniques.

Wide angle X-ray diffraction (WAXD) patterns for synthesised polyimides are provided in **Fig 4a.6**. A broad hump is observed in the region of around $2\theta \sim 20°$ and a sharp peak at $2\theta \sim 3°$. The broad peak indicates that polyimides were of amorphous nature, while the sharp peak at low angle region is indicative of layered structures. According to literature reports,[52–56] the sharp peak at low angle arises from X-ray reflections from the spacing between the polymer backbones. The long alkyl chains get fully interdigitated and tilted away from the polymer main chain, giving rise to layered structures in the solid state as indicated by XRD patterns.

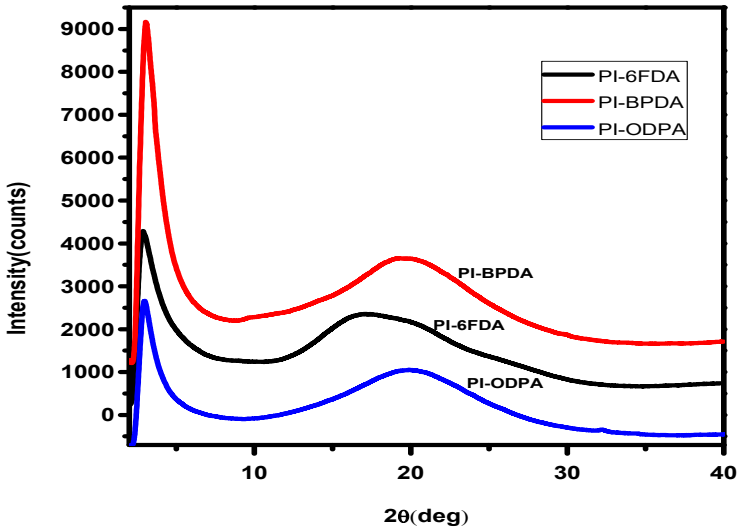

Figure 4a.6 X-Ray diffractograms of triarylamine-containing polyimides

4a.3.3 Thermal properties

The thermal properties of synthesised polyimides were investigated through TGA and DSC measurements and results are collected in **Table 4a.3**. TG curves are presented in **Fig 4a.7**. A representative DTG curve with corresponding TGA curve for PI-ODPA is presented in **Fig 4a.8**. DSC curves are provided in **Fig 4a.9**.

Table 4a.3 Thermal properties of triarylamine-containing polyimides

Polyimide	Polyimide repeat unit	T_g (°C)[a]	T_{10} (°C)[b]	Char yield (%)[c]
PI-6FDA	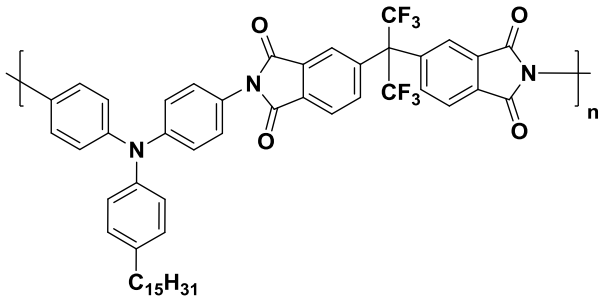	173 (316)	441 (581)	37
PI-ODPA	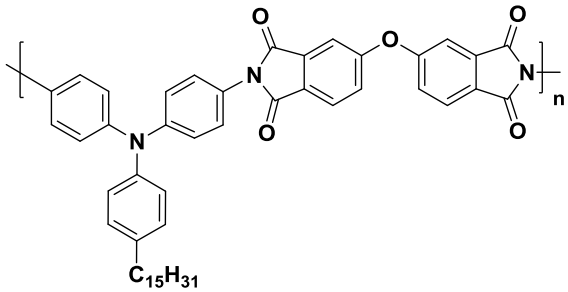	165 (295)	418 (608)	35
PI-BPDA	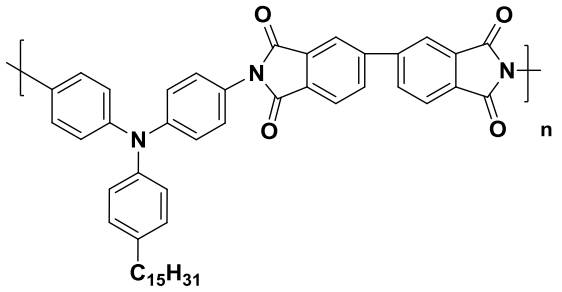	225 (331)	447 (613)	38

a: Measured by DSC from second heating scan with heating rate of 10 °C/min under nitrogen atmosphere.
b: 10 % weight loss on TGA thermograms at a heating rate of 10 °C/min under nitrogen atmosphere.
c: Char yield measured at 900 °C.
values in parenthesis refer to the values of reference polyimides based on 4,4'-diaminotriphenylamine and corresponding dianhydrides and data was taken from available literature.[45]

.

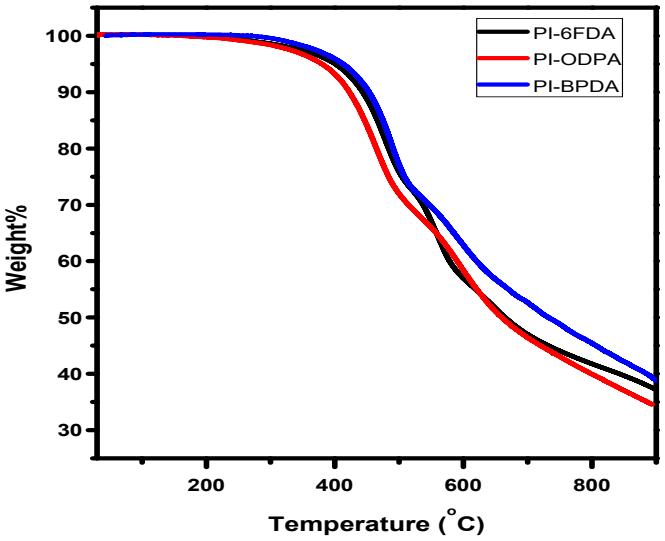

Figure 4a.7 TG curves of triarylamine-containing polyimides

The synthesised polyimides displayed T_{10} values (temperature at 10 % weight loss) in the range 418 – 447 °C with 35 – 38 % char yields at 900 °C. This indicates that polyimides obtained were of reasonably good thermal stability. However, the obtained T_{10} values were lower than the values of corresponding polyimides without C_{15} alkyl chains. This is to be expected due to the lower thermal stability of the alkyl segments.

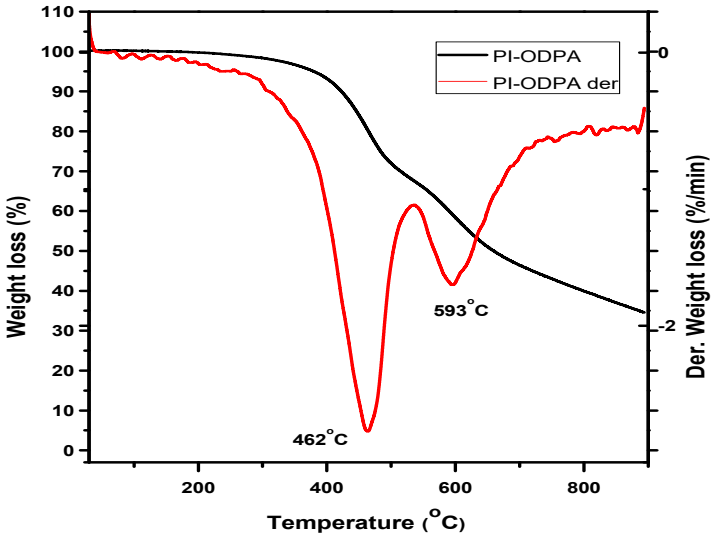

Figure 4a.8 DTG curve of PI-ODPA

Differential thermogravimetric analysis (DTG) of polyimides revealed a two stage weight loss. The first stage of thermal decomposition occurring at 462 °C probably corresponds to decomposition of pendent alkyl chains, while the second stage of thermal decomposition occurring at 593 °C corresponds to decomposition of polyimide backbone.

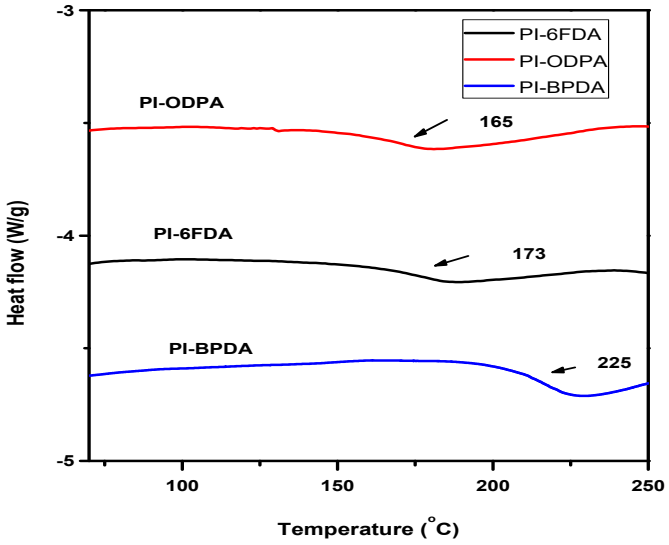

Figure 4a.9 DSC curves of triarylamine-containing polyimides

T_g values of polyimides were obtained in the range 165 – 225 °C. A significant drop in T_g values was observed, compared to reference polyimides (polyimides without

C_{15} alkyl chain). This happened due to the packing disruptive effect of C_{15} alkyl chain, leading to improved segmental mobility and lowering of T_g. Lower T_g values ensure easier polymer processability. The observed T_g values increased with increasing stiffness of the polymer backbone. Higher T_g value (225 °C) was observed in the case of PI-BPDA, possessing the most rigid backbone while PI-ODPA, possessing the most flexible backbone, due to the presence of C-O-C linkage, displayed the lowest T_g value (165 °C). The DSC traces show a total absence of any first order transitions which further support the XRD results suggesting amorphous nature of the polymers.

4a.3.4 Optical and electrochemical properties

The optical and electrochemical characteristics of triarylamine-containing polyimides were investigated by UV-Vis spectroscopy and cyclic voltammetry. UV-Vis spectra of polyimides are depicted in **Supporting Information Fig SI 4a.5**. The λ_{max} values obtained from solution UV spectroscopy and λ_{onset} values (cut-off wavelength) obtained from solid-state UV-Vis spectroscopy are summarised in **Table 4a.4**. The UV absorption bands are generated due to π-π* transitions resulting from conjugation between aromatic rings and the N atoms.[44] It is interesting to note that polyimides with greater CTC (chain transfer complex) interactions were observed to display higher λ_{onset} values. PI-BPDA, with maximum CTC interactions displayed a higher λ_{onset} value. Greater CTC interactions lead to enhanced coloration,[57] broader UV absorption bands and hence higher λ_{onset} values presumably due to formation of a longer effective chromophore. The optical band-gap (E_g^{Opt}) values, the difference between HOMO and LUMO energy levels determined from λ_{onset}, are summarised in **Table 4a.4**, and were found to be in the range 1.95 eV – 1.98 eV. PI-BPDA was found to possess lowest band-gap possibly due to strong CTC interactions between highly electron rich triphenylamine unit and electron deficient dianhydride unit.[45–47]

The redox behaviour of polyimides was studied by cyclic voltammetry

Table 4a.4 Optical and electrochemical properties of triarylamine-containing polyimides

Polyimide	Absorbance		Oxidation[c]			Reduction[f]			E_g^{elec}(eV)[i]
	λ_{max}(nm)[a]	λ_{onset}(nm)[b]	E_g^{Opt}(eV)[d]	$E_{1/2}$ (V)[e]	$E_{oxonset}$	HOMO(eV)[g]	$E_{redonset}$	LUMO(eV)[h]	
PI-6FDA	302,336	630	1.96	0.755	0.67	-5.400	-0.78	-3.903	1.49
PI-ODPA	324	625	1.98	0.715	0.63	-5.360	-0.82	-3.870	1.49
PI-BPDA	329	635	1.95	0.680	0.5	-5.310	-0.77	-3.885	1.42

a: UV-Vis absorption maxima measured in chloroform (10^{-5} M) at room temperature. b: The cut-off wavelength determined from UV-Vis transmission spectra of polymer films. c: From cyclic voltammograms versus Ag/AgCl in CH_3CN. d: Obtained from $E_g^{opt} = 1240/\lambda_{onset}$. e: $E_{1/2}$ is the average potential of redox couple peaks. f: From cyclic voltammograms versus Ag/AgCl in DMF. g: HOMO energy levels calculated from cyclic voltammetry and referenced to ferrocene ($E_{1/2}$ = 0.0785V). h: LUMO energy levels calculated from cyclic voltammetry and referenced to ferrocene ($E_{1/2}$ = 0.232V). i: Obtained from HOMO-LUMO = E_g.

The cyclic voltammograms in the oxidation process are depicted in **Fig 4a.10**. Reductive cyclic voltammograms are provided in the **Supporting Information** (**Fig SI 4a.6**). The obtained half-wave potentials ($E_{1/2}$) and onset potentials (E_{onset}) during oxidation and reduction CV are compiled in **Table 4a.4**.

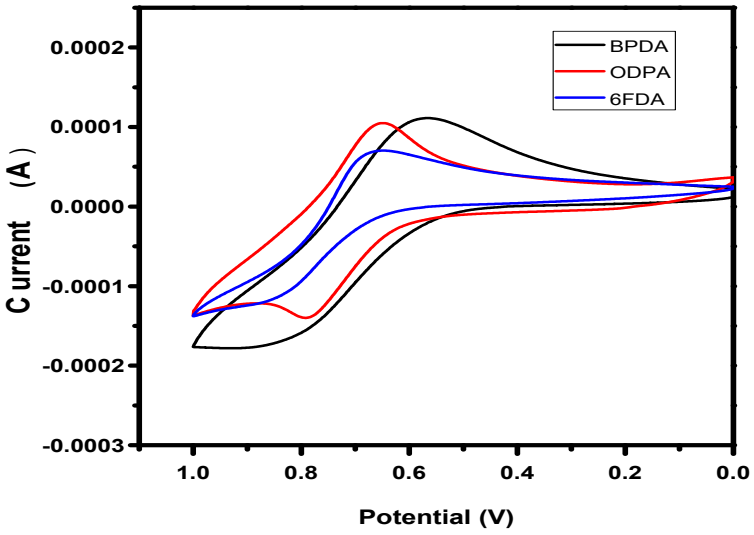

Figure 4a.10 Oxidative cyclic voltammograms of triarylamine-containing polyimides.

Polyimides under study displayed redox peaks under positive CV scan (**Fig 4a.10**). A change in colour from pale yellow/orange to intense green/blue was observed during CV scan from 0 V to 1.2 V against Ag/AgCl. This occurred due to electrochemical oxidation of polyimides. Electron removal from the electron rich

nitrogen atom of the triphenylamine moiety leads to formation of a radical cation. The radical cation belonging to the oxidised polyimides has a very different UV absorption/ transmittance, leading to change in polymer coloration. The HOMO energy levels of respective polyimides were determined from the oxidation onset potentials ($E_{oxonset}$) with respect to Ag/Ag^{+}. The calculations were done considering the HOMO energy level for the ferrocene standard to be 4.80 eV with respect to zero vacuum level. The HOMO energy levels of synthesised polyimides were found to be in the range of -5.31 eV to -5.4 eV, while $E_{1/2}$ values (average potential of the redox peaks or half-wave potential) ranged from 0.68 – 0.755 V. PI-BPDA displayed lowest $E_{oxonset}$ (oxidation onset potential) and $E_{1/2}$ values and was most easily oxidized. Strong CTC interactions lead to lower energy band-gap and hence easier oxidation. Expectedly, PI-6FDA has highest $E_{oxonset}$ amongst the synthesised polyimides. LUMO values were calculated from the onset reduction potentials obtained from reduction CV and were in the range -3.885 eV to -3.903 eV. The electrochemical band-gap (E_g^{elec}) determined from the obtained HOMO and LUMO values was found to be in the range 1.42 – 1.49 eV. The E_g^{elec} values of the synthesised polyimides showed a trend similar to the E_g^{opt} values. The band-gap values of the synthesised polyimides were within the range of semi-conducting materials with hole-transport properties.

4a.3.5 Spectroelectrochemical properties

Spectroelectrochemical investigations of triarylamine-containing polyimides were carried out by chronoamperometric measurements coupled with UV-Vis spectroscopy. The electrochromic transmittance spectra of polyimides are presented in **Fig 4a.11** as a series of UV-Vis transmittance curves in relation to applied electrode potentials.

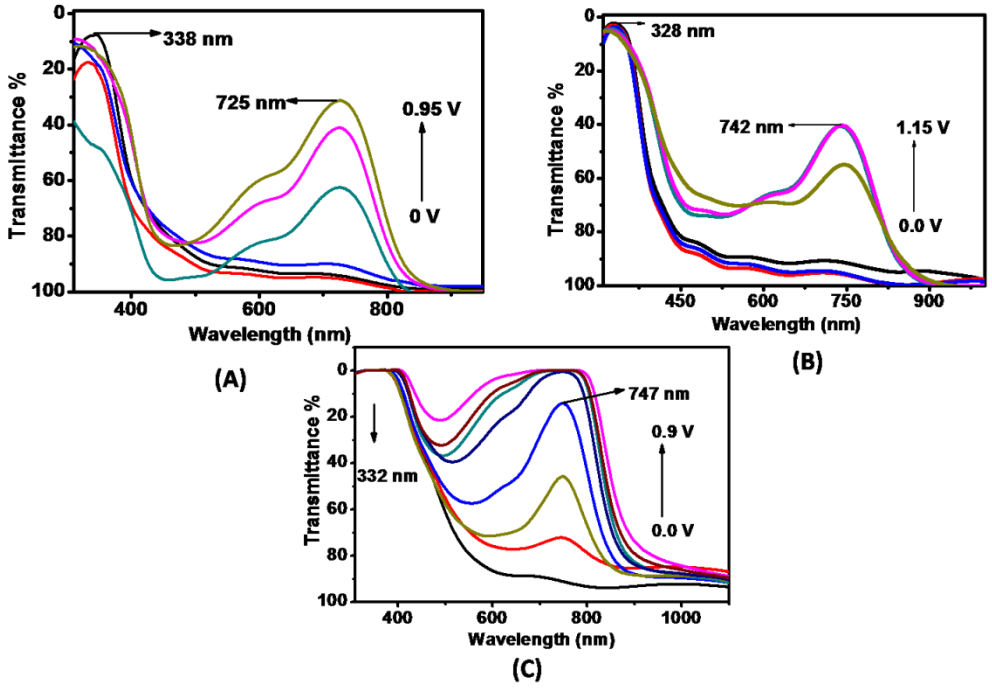

Figure 4a.11 Electrochromic behaviour of **(a)** PI-6FDA thin film, **(b)** PI-ODPA thin film and **(c)** PI-BPDA thin film

When the applied potential was varied positively from 0 V to 0.35 V, the transmittance peak at 338 nm, characteristic for neutral PI-6FDA (**Fig 4a.11(a)**), decreased in intensity and a new peak was observed at 725 nm. Meanwhile, the colour of the film changed from pale yellow to blue-green. The new peak is formed due to the formation of radical cations (oxidized PI-6FDA) which is responsible for the change in colour. In the case of PI-ODPA (**Fig 4a.11 (b)**), the applied potential was varied from 0 V to 1.15 V. The transmittance peak at 328 nm decreased in intensity and a new peak was observed at 742 nm. The film colour changed from pale yellow to green. PI-BPDA polymer film (**Fig 4a.11(c)**) was subjected to potentials ranging from 0 V to 0.9 V and the colour of the film was seen to change from pale orange to intense blue.

The synthesised polyimides showed potential for use in electrochromic devices such as anti-glare car rear-view mirrors, smart windows, protective eye-wear for the military, etc.

4a.3.6 Memory device characterisation

Memory devices based on synthesised polyimides, PI-ODPA, PI-BPDA, and PI-6FDA were studied. The typical I-V graphs of polyimide memory devices in linear and semilog scales are shown in **Fig 4a.12**.

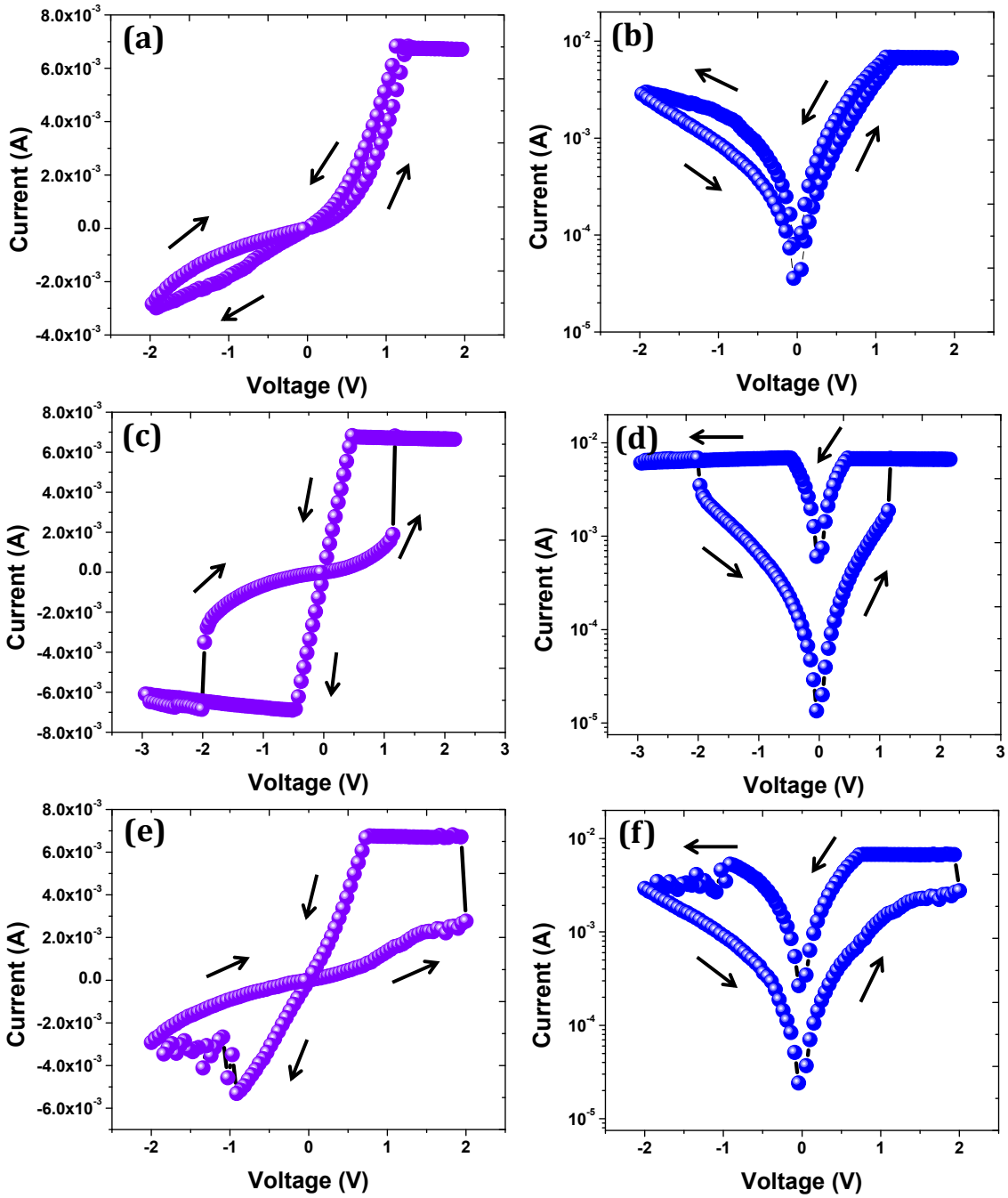

Figure 4a.12 Bipolar resistive switching characteristics of **(a-b)** PI-ODPA, **(c-d)** PI-BPDA, and **(e-f)** PI-6FDA memory devices in linear and semilog scale, respectively. The direction of resistive switching is indicated by arrows.

The typical pinched hysteresis loop in I-V plane is clearly observed for the developed polyimide-based memory devices, indicating that all three polymers legitimately exhibit memristor like behaviour. **Fig 4a.12 (a-b)** represents the bipolar

resistive switching behaviour of PI-ODPA based memory device. Initially, the device is in the HRS and demonstrated low current of about 3.5 x 10^{-5} A. As a positive bias was applied to the device, the current increased smoothly and gradually to 6 x 10^{-3} A, until the voltage reached 1.3 V (V_{SET}) thus transitioning from the "OFF" state to the "ON" state or LRS. Thereafter, up to 2 V, the current remained almost the same and exhibited self compliance effect. The self compliance effect is useful to rectify the irreversible destruction of memory cell during resistive switching process. The memory cell without self compliance property requires external current limiter circuit, which increases the circuit complexity. In view of this, circuit design complexity can be reduced by utilising self-compliance effect based memory cell.[58] As the voltage was varied from 2 V to -2 V, the current gradually decreased to 7.8 x 10^{-5} A and then increased to 3 x 10^{-3} A at -2.00 V when a negative potential sweep was applied from 0 V to -2 V. Subsequently, when the potential was swept from -2.00 V to 0 V, the current decreased gradually from 3 x 10^{-3} A at -2.00 V (V_{RESET}) to 3.5 x 10^{-5} A. This transition from LRS to HRS constitutes an "erasing" or "reset" process. These results indicate that PI-ODPA based memory device is rewritable in nature, showing bipolar resistive switching property.

Fig 4a.12 (c-d) represents the I-V switching curve of memory device based on PI-BPDA. When a positively biased potential sweep was applied from 0 V to 2.2 V, the memory device initially displayed a low current value of 1.2 x 10^{-5} A. The current value gradually increased and reached a value of 2 x 10^{-3} A. At a voltage of 1.15 V the conduction abruptly increased to 7 x 10^{-3} A. This transition from HRS to LRS constitutes a "write" or "set" process where V_{SET} is 1.15 V. Subsequently, as the voltage was varied from 1.15 V to -3 V, the current remained in the range of 7 x 10^{-3}A – 6 x 10^{-4} A. When a negatively biased potential sweep was applied from -3 V to 0 V, the current remained at 7 x 10^{-3} A, until the voltage reached -2 V (V_{RESET}), when the current abruptly decreased to 3.5 x 10^{-3} A. Thereafter, the current decreased gradually to 1.2 x 10^{-5} A. Thus, the device undergoes an "erase" process when V_{RESET} = -2 V. Since both "write" and "erase" processes occur during the entire switching cycle, the memory device fabricated from PI-BPDA is rewritable in nature.

The bipolar resistive switching property of PI-6FDA based memory device is shown in **Fig 4a.12 (e-f)**. Similar to other devices, the PI-6FDA based memory device is

initially in the HRS with current value of 2 x 10^{-5} A. As the device was subjected to a positively biased potential sweep from 0 V to 2 V, the current increased gradually from 2 x 10^{-5} A to 2.8 x 10^{-3} A. At 2 V (V_{SET}), the current increased abruptly to 7 x 10^{-3} A, constituting a "SET" process. During the negative voltage sweep, the PI-6FDA based memory device undergoes the "RESET" process at -2 V. These results indicate that as both "write" and "erase" operations occurred during a switching cycle, the memory device prepared from PI-6FDA is rewritable in nature.

Endurance and retention tests are important to understand the non-volatility nature of the fabricated memory devices. **Fig 4a.13** demonstrates the endurance and retention memory performance of memory devices based on PI-ODPA, PI-BPDA, and PI-6FDA. The endurance and retention properties of the memory devices based on polyimides were studied at room temperature under ambient conditions. In the present study, LRS and HRS were measured by applying the SET and RESET voltage of the particular device with 0.2 V read voltage and 100 µs pulse width was maintained for each measurement. The memory devices were subjected to 10000 repeated "set" and "reset" resistive switching cycles at a read voltage of 0.20 V. The results clearly indicated that two well-defined and distinct resistive states, namely, HRS and LRS were observed in all three memory devices. The respective resistive states were observed to persist with no degradation for the entire range of 10000 resistive switching, indicating that all three devices possessed good endurance and reliability. An excellent memory window in the order of 10^3 was observed for all developed devices. Practically, a memory window greater than 10 is desirable to reliably distinguish the resistance states in circuit design. This indicates that these memory devices can potentially be useful for practical applications. Furthermore, the retention performance of the memory devices was measured at a read voltage of 0.2 V for each second over an extended period of time. The resistive states HRS and LRS were seen to persist without degradation over a period of 1000 s. The endurance and retention studies indicate that the memory devices based on polyimides were non-volatile in nature. However, significant degradation or faulty measurements were observed for each device during endurance or retention measurements and PI-ODPA based memory devices were more susceptible to such faulty measurements during the endurance test. This may be due to significant leakage current

in the devices. In a nutshell, PI-BPDA and PI-6FDA based memory devices show better endurance and retention properties than PI-ODPA based memory device.

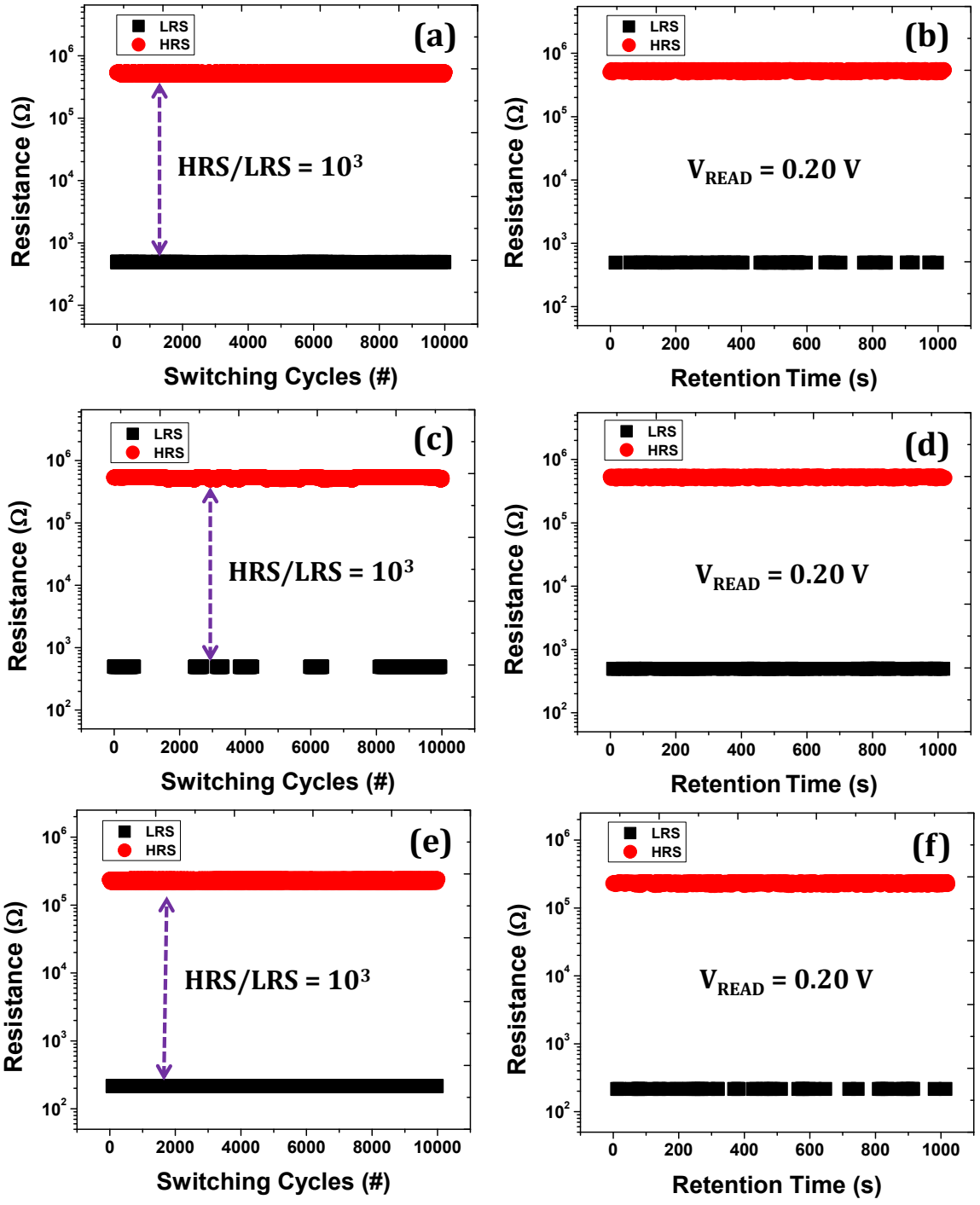

Figure 4a.13 Endurance and retention memory performance of **(a-b)** PI-ODPA, **(c-d)** PI-BPDA, and **(e-f)** PI-6FDA memory devices.

Cumulative probability of the resistive states of fabricated memory devices is shown in **Fig 4a.14**. Furthermore, a performance comparison of the memory devices based on polyimides is summarised in **Table 4a.5**.

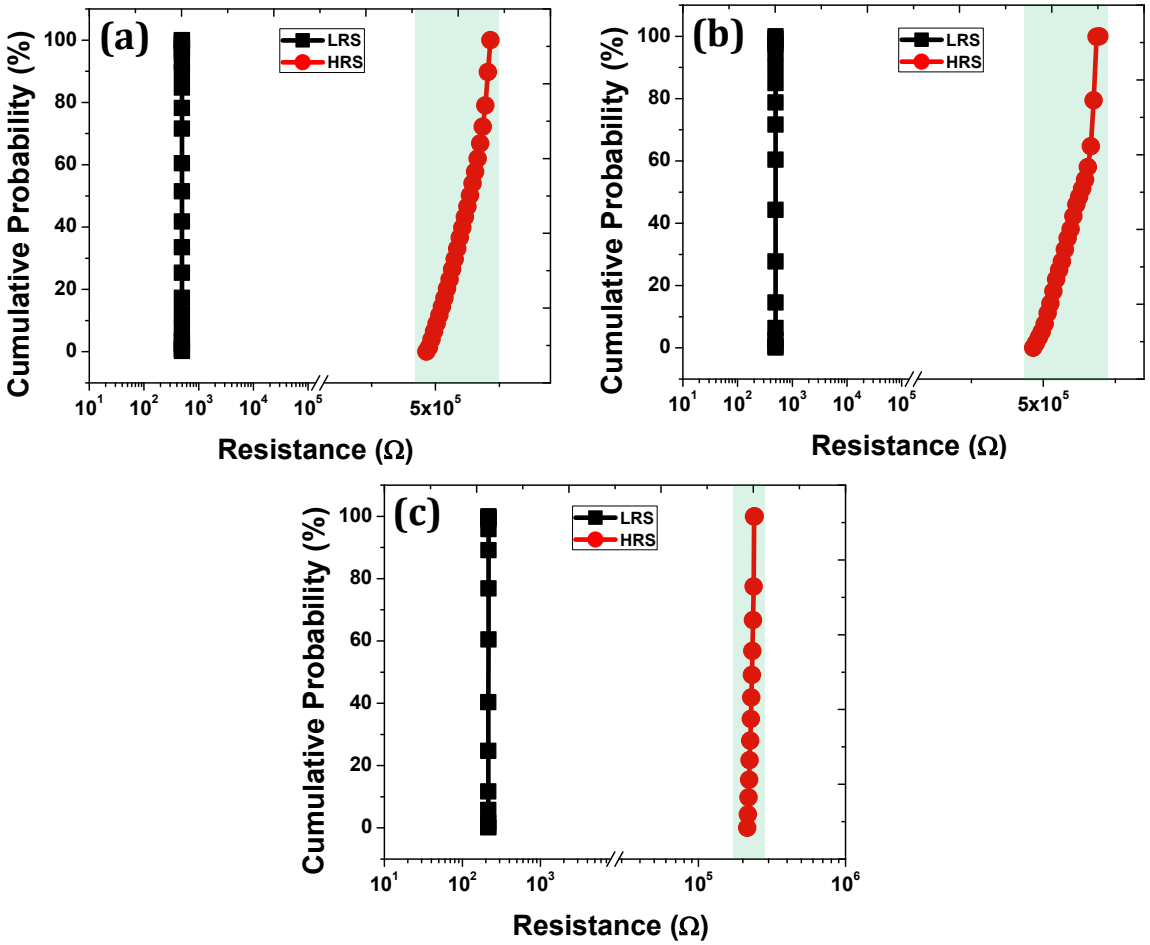

Figure 4a.14 Resistive switching cumulative probability of **(a-b)** PI-ODPA, **(c-d)** PI-BPDA, and **(e-f)** PI-6FDA memory devices.

Table 4a.5 Performance comparison of triarylamine-containing polyimide memory devices

Polyimide	V_{SET}(V)	V_{RESET} (V)	Average, μ (Ω)		Memory window (HRS/LRS)	Standard deviation, σ(Ω)		Coefficient of variation, σ/μ (%)	
			LRS	HRS		LRS	HRS	LRS	HRS
PI-ODPA	1.30	-2.00	493	525083	1065.07	0.1985	14599	0.04	2.78
PI-BPDA	1.15	-2.00	493	523303	1061.46	0.2808	13111	0.05	2.50
PI-6FDA	2.00	-2.00	215	230926	1074.07	0.1028	7107	0.04	3.07

The reliability of the memory devices based on polyimides was investigated statistically. All three memory devices exhibited excellent reliability in terms of memory window, standard deviation, and coefficient of variation. It is interesting to note that LRS of all devices showed very low coefficient of variation (0.04– 0.05 %), suggesting uniformity in the LRS. The uniformity of HRS was slightly low, as was evident from the coefficient of variation values, in the range of 2.50 % to 3.07 %. Memory device based on PI-6FDA gives the best performance as evidenced by the low values of coefficient of variation, standard deviation and highest value of memory window, followed by memory device based on PI-ODPA.

The conduction mechanism of developed memory devices was investigated by analysing the I-V data in further detail. Conduction mechanisms were determined by fitting different regions of the I-V graphs according to conduction mechanisms known in literature.[59–66] **Fig 4a.15** and **Fig 4a.16** represents the double logarithmic I-V characteristics and high slope data fitting to the Schottky conduction mechanism, respectively. In the case of PI-ODPA memory device, the slope is found to be 1.22 for positive biased low voltage region (0 – 0.35 V). On the other hand, the magnitude of the slope increased to 2.27 for high voltage region (0.35 – 1.2 V). A slope of 1.2 indicates that current conduction takes place according to Ohmic conduction model. The region from 0.35 – 1.2 V was fitted in accordance to Schottky conduction model. In negative bias, low voltage region (0 V to 0.40 V) gives 0.94 as slope, indicating conduction occurring in accordance to Ohmic conduction model. Thereafter, from 0.40 – 2.00 V, the linear region had a slope of 1.41. This region was also successfully fitted in accordance to Schottky conduction mechanism. In the case of PI-BPDA, in positive bias, over the range of 0 – 0.3 V, the linear segment of I-V data had a slope of 1.23, suggesting current conduction in this range was occurring in accordance to Ohmic conduction model. The linear segment over the range of 0.3 – 1.2 V had a slope of 1.9. The segment was satisfactorily fitted in accordance to Schottky conduction mechanism. In negative bias, a slope of 1.13 was observed for the linear region from 0 – 0.3 V, while a slope of 1.79 was observed for the region from 0.3 – 2.1 V. This region fitted satisfactorily according to Schottky conduction model indicating that Schottky conduction was dominant over that region. In the case of memory device based on PI-6FDA, in the positive bias, it was

observed that over the voltage range of 0 – 0.4 V, the slope was 1.08, indicating that Ohmic conduction mechanism was prevalent in this region. Over the voltage range of 0.4 – 1.8 V the linear segment of the I-V data had a slope of 1.35. This segment was fitted according to Schottky conduction model. In negative bias, over the voltage range of 0 – 0.3 V, the linear segment had a slope of 1.08; indicating the dominance of Ohmic conduction over this range. From 0.3 – 1.9 V, the observed slope was 1.42. This region was successfully fitted in accordance to Schottky conduction model.

From the above results, it can be concluded that all three memory devices based on polyimides exhibited Ohmic conduction in the low voltage region, in both positive and negative bias. However, as the voltage was increased, there was formation of a Schottky barrier at the electrode – polymer interface. The conduction in this range was limited by charge injection from the aluminium electrode to the polymer film which resulted in the dominance of the Schottky conduction mechanism.

In this study, it has been demonstrated that polyimides containing triarylamine units with pendent pentadecyl chains formed memory devices which were non-volatile and rewritable in nature. It is interesting to note that memory device reported by Ling *et al*, based on polyimide similar to the present work, but without pentadecyl chain, was volatile with DRAM characteristics.[35] Also, memory devices based on triarylamine-containing polyimides possessing three methyl groups, as reported by Lee *et al*, were non-volatile WORM type.[36] It has been postulated that incorporation of electron donating methyl groups probably stabilised the CT complex leading to stable memory characteristics. The results of the present study also support this postulate.

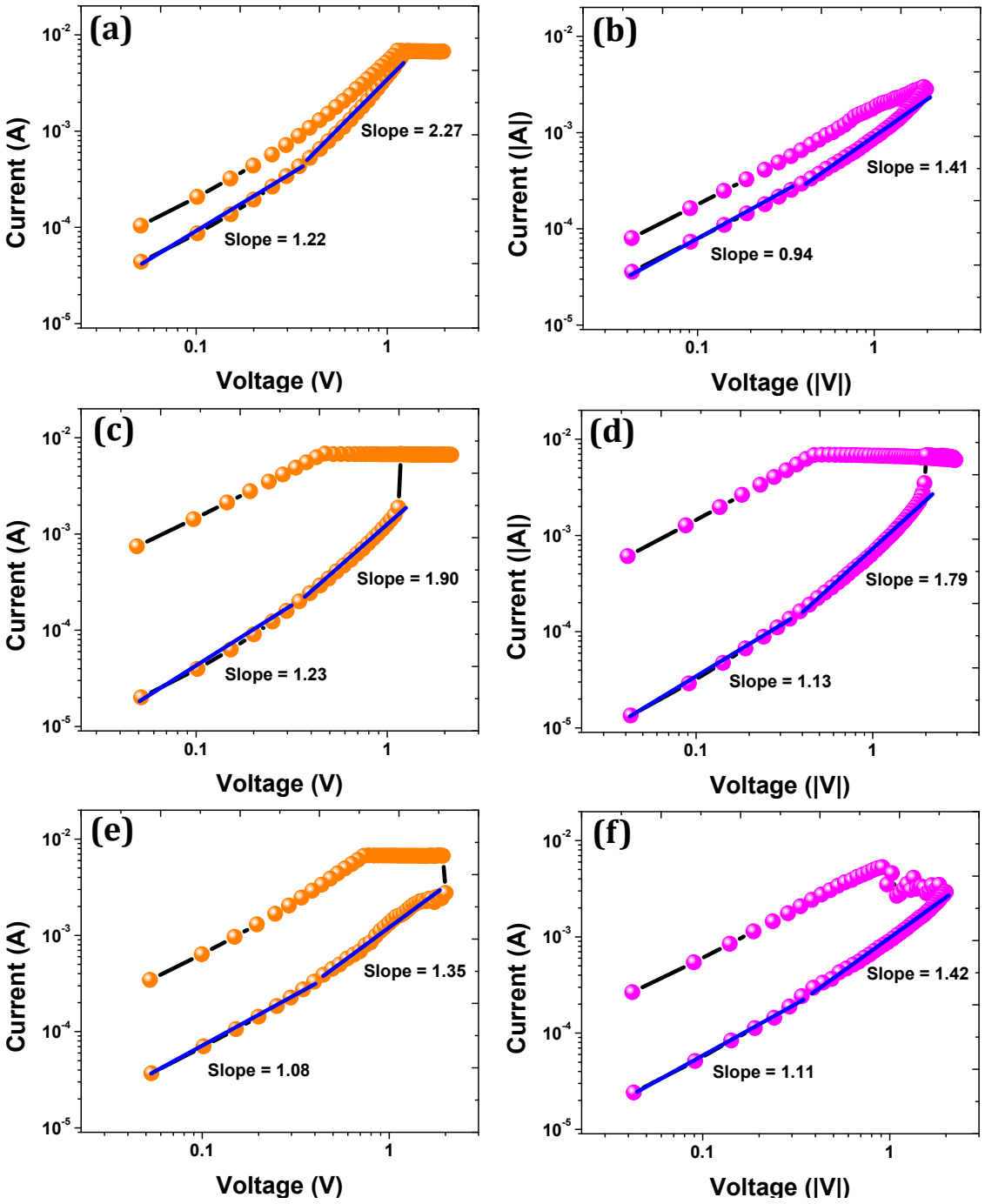

Figure 4a.15 Conduction mechanisms of **(a-b)** PI-ODPA, **(c-d)** PI-BPDA, and **(e-f)** PI-6FDA memory devices in positive and negative bias.

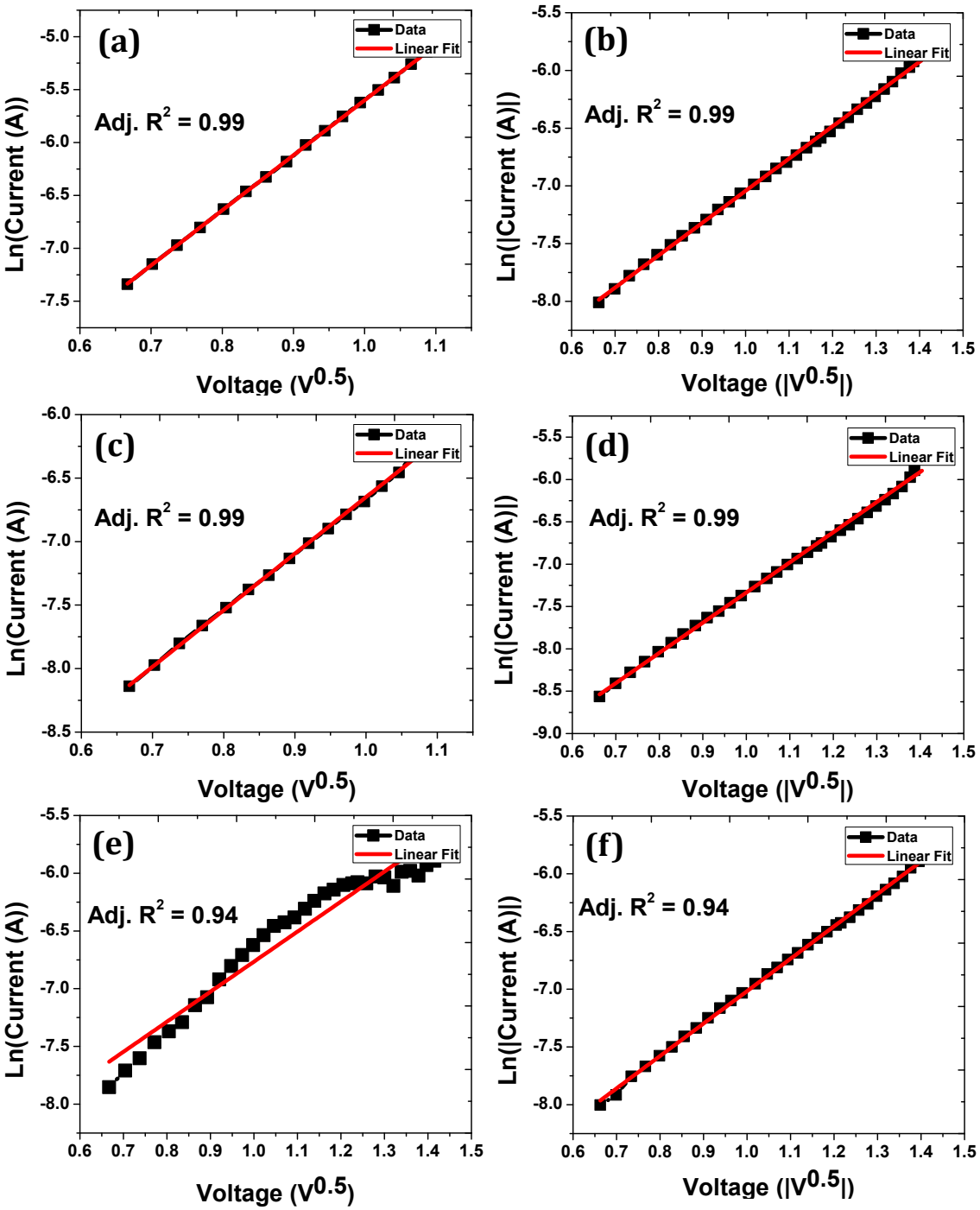

Figure 4a.16 Schottky conduction mechanism fitting to the high slope part data of **(a-b)** PI-ODPA, **(c-d)** PI-BPDA, and **(e-f)** PI-6FDA memory devices.

4a.4 Conclusions

1. Three polyimides, PI-6FDA, PI-ODPA and PI-BPDA were synthesised by polycondensation of a new triphenylamine containing diamine, namely, 4, 4'-diamino-4"pentadecyltriphenylamine (DPTA) with commercially available aromatic dianhydrides, *viz*., 3,3',4,4'-biphenyltetracarboxylic dianhydride (BPDA), 4,4'-oxydiphthalic anhydride (ODPA) and 4,4'-(hexafluoroisopropylidene) diphthalic anhydride (6-FDA).

2. Inherent viscosities and number average molecular weights were in the range 0.54 – 0.60 dL g^{-1} and 26800 – 43500 g mol^{-1}, respectively, indicating the formation of polyimides of reasonably high molecular weights.

3. The synthesised polymers were readily soluble in chloroform, THF, *m*-cresol, and NMP at room temperature. The C_{15} alkyl chain, coupled with the bulky propeller-shaped TPA unit imparted excellent solubility to the synthesised polyimides. Such excellent solubility ensures that the synthesised polyimides are readily solution processable. Flexible, free-standing, yellow coloured films could be cast from chloroform solutions.

4. According to XRD analysis, synthesised polyimides were observed to be amorphous in nature due to combined effect of bulky triarylamine moiety and pendent pentadecyl chains.

5. Observed T_{10} values were in the range 418 – 447 °C while T_g values were in the range 165 – 225 °C. Polyimides exhibited appreciable lowering of T_g values, but possessed good thermal stability. The large difference between T_g values and T_{10} values provide a wide processing window for melt processing.

6. Triarylamine-containing polyimides displayed optical and electrochemical band-gaps in the range 1.95 – 1.98 eV and 1.42 – 1.49 eV respectively, and showed a change in coloration from yellow to intense blue/green on electrochemical oxidation. These partially bio-based polyimides are thus good semiconductor materials with electrochromic properties and may find applications in electrochromic devices as hole-transporting materials.

7. All three polyimides exhibited non-volatile rewritable memory characteristics. Memory device based on PI-ODPA displayed a self compliance effect. Fabricated memory devices displayed well defined high resistive state (HRS) and low resistive state (LRS) with a memory window of 10^3. According to endurance and retention memory

results, the memory devices based on triarylamine-containing polyimides displayed non-volatile memory characteristics. Both LRS and HRS exhibited excellent uniformity, as determined by statistical analysis. Schottky conduction mechanism was observed to dominate in the high voltage region, when the devices were switched from "OFF" state to "ON" state and *vice versa*.

References

1 R. H. Friend, R. W. Gymer, A. B. Holmes, J. H. Burroughes, R. N. Marks, C. Taliani, D. D. C. Bradley, D. A. Dos Santos, J. L. Brédas, M. Lögdlund and W. R. Salaneck, *Nature*, 1999, **397**, 121–128.

2 K. Lee, J. Y. Kim, S. H. Park, S. H. Kim, S. Cho and A. J. Heeger, *Adv. Mater.*, 2007, **19**, 2445–2449.

3 Y. Shao, G. C. Bazan and A. J. Heeger, *Adv. Mater.*, 2008, **20**, 1191–1193.

4 Y. Shao, X. Gong, A. J. Heeger, M. Liu and A. K. Y. Jen, *Adv. Mater.*, 2009, **21**, 1972–1975.

5 C. J. Brabec, N. S. Sariciftci and J. C. Hummelen, *Adv. Funct. Mater.*, 2001, **11**, 15–26.

6 G. Yu, J. Gao, J. C. Hummelen, F. Wudl and A. J. Heeger, *Science*, 1995, **270**, 1789–1791.

7 G. Li, V. Shrotriya, J. Huang, Y. Yao, T. Moriarty, K. Emery and Y. Yang, *Nat. Mater.*, 2005, **4**, 864–868.

8 M.-H. Chen, J. Hou, Z. Hong, G. Yang, S. Sista, L.-M. Chen and Y. Yang, *Adv. Mater.*, 2009, **21**, 4238–4242.

9 J. Hou, T. L. Chen, S. Zhang, L. Huo, S. Sista and Y. Yang, *Macromolecules*, 2009, **42**, 9217–9219.

10 L. Huo, J. Hou, S. Zhang, H.-Y. Chen and Y. Yang, *Angew. Chemie Int. Ed.*, 2010, **49**, 1500–1503.

11 S. Sista, Z. Hong, M.-H. Park, Z. Xu and Y. Yang, *Adv. Mater.*, 2010, **22**, E77–E80.

12 H.-J. Yen and G.-S. Liou, *Polym. J.*, 2016, **48**, 117–138.

13 W.-P. Lin, S.-J. Liu, T. Gong, Q. Zhao and W. Huang, *Adv. Mater.*, 2014, **26**, 570–606.

14 T. Kurosawa, T. Higashihara and M. Ueda, *Polym. Chem.*, 2013, **4**, 16–30.

15 B. Yao, J. Zhang and X. Wan, in *Electrochromic Materials and Devices*, Wiley-VCH Verlag GmbH & Co. KGaA, Weinheim, Germany, 2015, vol. 44, pp. 211–240.

16 A. Iwan and D. Sek, *Prog. Polym. Sci.*, 2011, **36**, 1277–1325.

17 T. Abidin, Q. Zhang, K.-L. Wang and D.-J. Liaw, *Polymer*, 2014, **55**, 5293–5304.

18 H.-J. Yen and G.-S. Liou, *Polym. Chem.*, 2018, **9**, 3001–3018.

19 H.-J. Yen and G.-S. Liou, *Polym. Chem.*, 2012, **3**, 255–264.

20 Q.-D. Ling, D.-J. Liaw, C. Zhu, D. S.-H. Chan, E.-T. Kang and K.-G. Neoh, *Prog. Polym. Sci.*, 2008, **33**, 917–978.

21 M. Ding, *Prog. Polym. Sci.*, 2007, **32**, 623–668.

22 C. E. Sroog, *Prog. Polym. Sci.*, 1991, **16**, 561–694.

23 I. A. Ronova and M. Bruma, *Struct. Chem.*, 2010, **21**, 1013–1020.

24 K. Fukukawa and M. Ueda, *Polym. J.*, 2008, **40**, 281–296.

25 D. M. Stoakley, A. K. St. Clair and C. I. Croall, *J. Appl. Polym. Sci.*, 1994, **51**, 1479–1483.

26 D.-J. Liaw, K.-L. Wang, Y.-C. Huang, K.-R. Lee, J.-Y. Lai and C.-S. Ha, *Prog. Polym. Sci.*, 2012, **37**, 907–974.

27 S. Mallakpour and M. Dinari, *Nano*, 2012, **07**, 1250021.

28 R. Pariser, *Polym. J.*, 1987, **19**, 127–133.

29 C. Marestin, G. Gebel, O. Diat and R. Mercier, in *Fuel Cells II*, Springer Berlin Heidelberg, Berlin, Heidelberg, 2008, vol. 216, pp. 185–258.

30 D. Yin, Y. Li, H. Yang, S. Yang, L. Fan and J. Liu, *Polymer*, 2005, **46**, 3119–3127.

31 Y. Liu, D. Chao and H. Yao, *Org. Electron.*, 2014, **15**, 1422–1431.

32 S. Gong, M. Liu, S. Xia and Y. Wang, *J. Polym. Res.*, 2014, **21**, 542.

33 H. Yen, S. Guo, J. Yeh and G.-S. Liou, *J. Polym. Sci. Part A Polym. Chem.*, 2011, **49**, 3637–3646.

34 M. Hasegawa and K. Horie, *Prog. Polym. Sci.*, 2001, **26**, 259–335.

35 Q.-D. Ling, F.-C. Chang, Y. Song, C.-X. Zhu, D.-J. Liaw, D. S.-H. Chan, E.-T. Kang and K.-G. Neoh, *J. Am. Chem. Soc.*, 2006, **128**, 8732–8733.

36 T. J. Lee, Y.-G. Ko, H.-J. Yen, K. Kim, D. M. Kim, W. Kwon, S. G. Hahm, G.-S. Liou and M. Ree, *Polym. Chem.*, 2012, **3**, 1276–1283.

37 D. M. Kim, S. Park, T. J. Lee, S. G. Hahm, K. Kim, J. C. Kim, W. Kwon and M. Ree, *Langmuir*, 2009, **25**, 11713–11719.

38 D. M. Kim, Y.-G. Ko, J. K. Choi, K. Kim, W. Kwon, J. Jung, T.-H. Yoon and M. Ree, *Polymer*, 2012, **53**, 1703–1710.

39 A.-D. Yu, T. Kurosawa, Y.-C. Lai, T. Higashihara, M. Ueda, C.-L. Liu and W.-C. Chen, *J. Mater. Chem.*, 2012, **22**, 20754–20763.

40 L. Shi, H. Ye, W. Liu, G. Tian, S. Qi and D. Wu, *J. Mater. Chem. C*, 2013, **1**, 7387–7399.

41 C.-J. Chen, H.-J. Yen, W.-C. Chen and G.-S. Liou, *J. Mater. Chem.*, 2012, **22**, 14085–14093.

42 C.-J. Chen, Y.-C. Hu and G.-S. Liou, *Polym. Chem.*, 2013, **4**, 4162–4171.

43 C.-J. Chen, H.-J. Yen, Y.-C. Hu and G.-S. Liou, *J. Mater. Chem. C*, 2013, **1**, 7623–7634.

44 D.-J. Liaw, P.-N. Hsu, W.-H. Chen and S.-L. Lin, *Macromolecules*, 2002, **35**, 4669–4676.

45 S.-H. Hsiao, Y.-M. Chang, H.-W. Chen and G.-S. Liou, *J. Polym. Sci. Part A Polym. Chem.*, 2006, **44**, 4579–4592.

46 C.-W. Chang, H.-J. Yen, K.-Y. Huang, J.-M. Yeh and G.-S. Liou, *J. Polym. Sci. Part A Polym. Chem.*, 2008, **46**, 7937–7949.

47 S.-H. Hsiao, G.-S. Liou, Y.-C. Kung, H.-Y. Pan and C.-H. Kuo, *Eur. Polym. J.*, 2009, **45**, 2234–2248.

48 H.-M. Wang and S.-H. Hsiao, *J. Polym. Sci. Part A Polym. Chem.*, 2014, **52**, 1172–1184.

49 S.-H. Hsiao, Y.-H. Hsiao and Y.-R. Kung, *J. Electroanal. Chem.*, 2016, **764**, 31–37.

50 H.-J. Yen, C.-W. Chang, H. Q. Wong and G.-S. Liou, *Polym. Chem.*, 2018, **9**, 1693–1700.

51 Y.-C. Kung, G.-S. Liou and S.-H. Hsiao, *J. Polym. Sci. Part A Polym. Chem.*, 2009, **47**, 1740–1755.

52 R. Duran, M. Ballauff, M. Wenzel and G. Wegner, *Macromolecules*, 1988, **21**, 2897–2899.

53 H. Kim, S.-B. Park, Jin Chul Jung and W.-C. Zin, *Polymer*, 1996, **37**, 2845–2852.

54 D. H. Wang, Z. Shen, M. Guo, S. Z. D. Cheng and F. W. Harris, *Macromolecules*, 2007, **40**, 889–900.

55 Y. S. Kim and J. C. Jung, *J. Polym. Sci. Part A Polym. Chem.*, 2002, **40**, 1764–1774.

56 Y. Chen, R. Wombacher, J. H. Wendorff and A. Greiner, *Polymer*, 2003, **44**, 5513–5520.

57 V. Ratta, Ph. D. Thesis, Faculty of Virginia Polytechnic Institute and State University, 1999.

58 L. Zou, W. Hu, J. Fu, N. Qin, S. Li and D. Bao, *AIP Adv.*, 2014, **4**, 037106.

59 F. Chiu, *Adv. Mater. Sci. Eng.*, 2014, **2014**, 1–18.

60 A. J. Campbell, D. D. C. Bradley and D. G. Lidzey, *J. Appl. Phys.*, 1997, **82**, 6326–6342.

61 J. Frenkel, *Phys. Rev.*, 1938, **54**, 647–648.

62 K. L. Jensen, *J. Vac. Sci. Technol. B Microelectron. Nanom. Struct.*, 2003, **21**, 1528–1544.

63 C. Laurent, E. Kay and N. Souag, *J. Appl. Phys.*, 1988, **64**, 336–343.

64 P. Mark and W. Helfrich, *J. Appl. Phys.*, 1962, **33**, 205–215.

65 M. A. Lampert, *Phys. Rev.*, 1956, **103**, 1648–1656.

66 S. Ghatak and A. Ghosh, *Appl. Phys. Lett.*, 2013, **103**, 122103.

Supporting Information

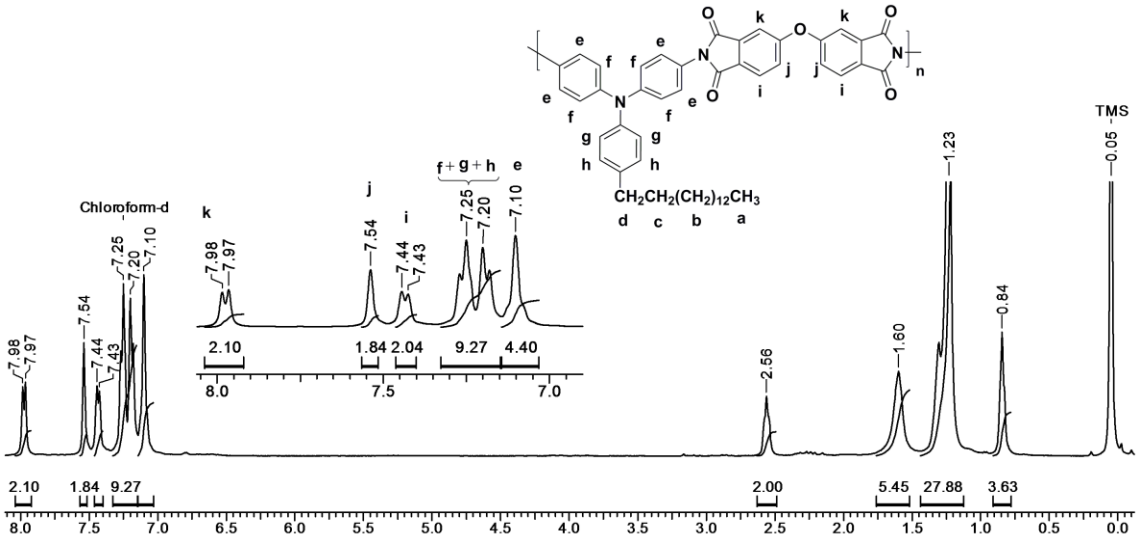

Figure SI 4a.1 ^{1}H-NMR spectrum ($CDCl_3$) of PI-ODPA

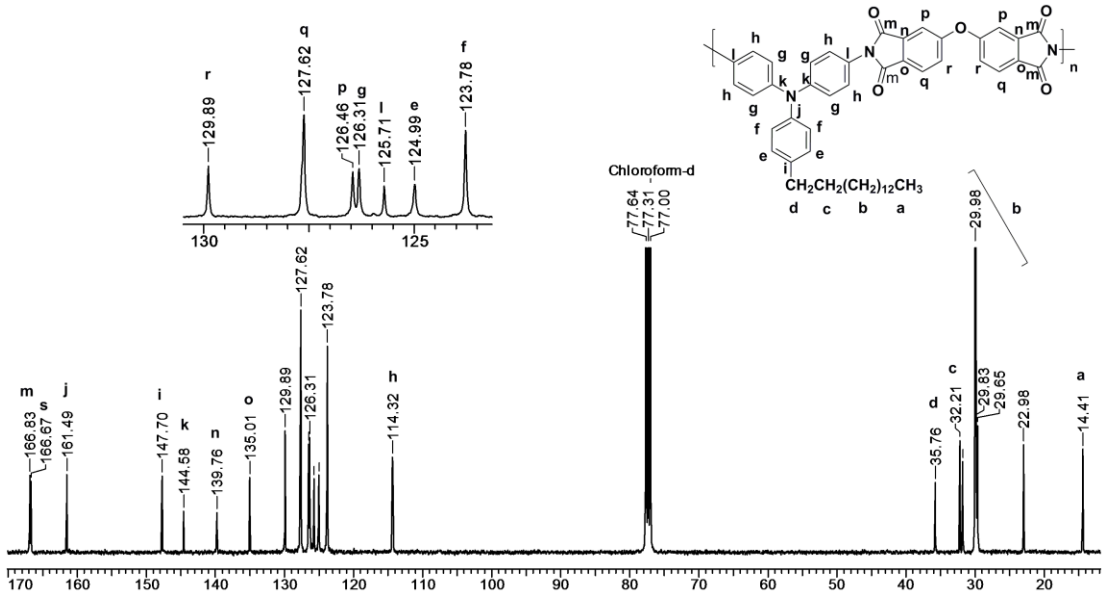

Figure SI 4a.2 ^{13}C-NMR spectrum ($CDCl_3$) of PI-ODPA

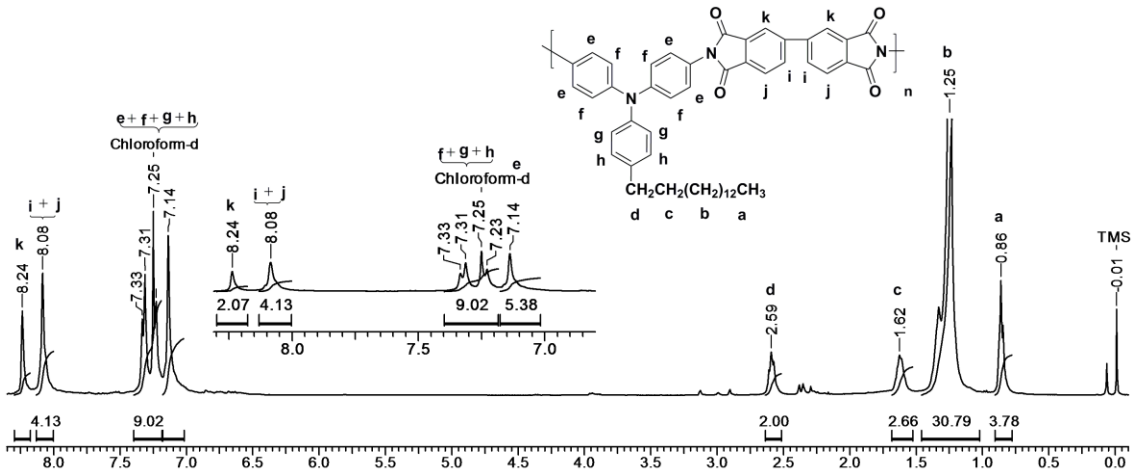

Figure SI 4a.3 ^{1}H-NMR spectrum ($CDCl_3$) of PI-BPDA

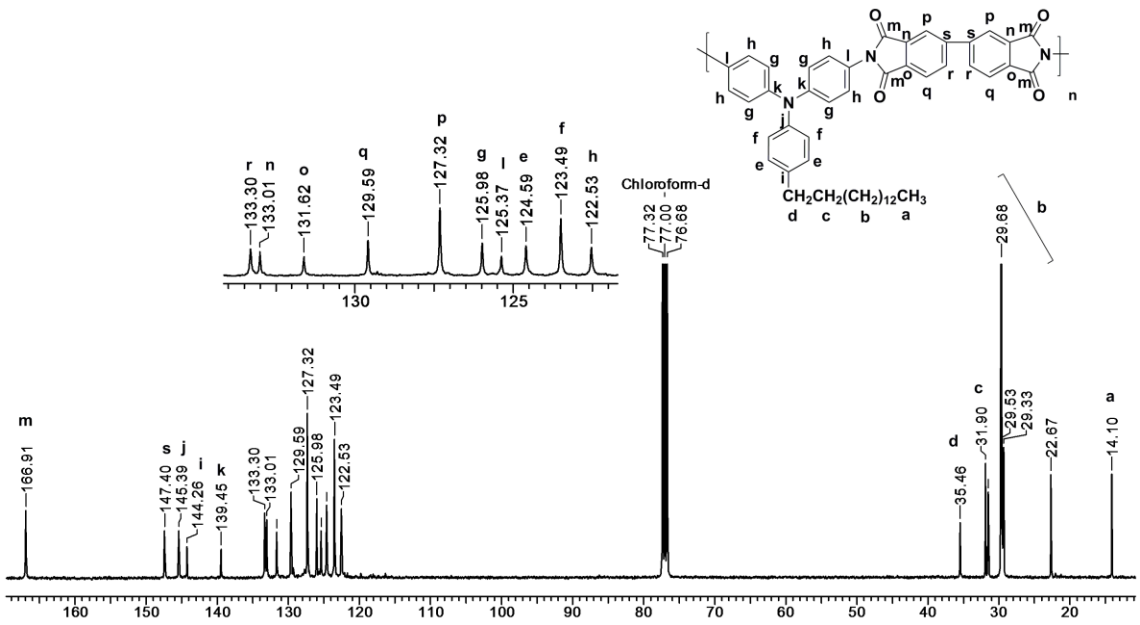

Figure SI 4a.4 ^{13}C-NMR spectrum ($CDCl_3$) of PI-BPDA

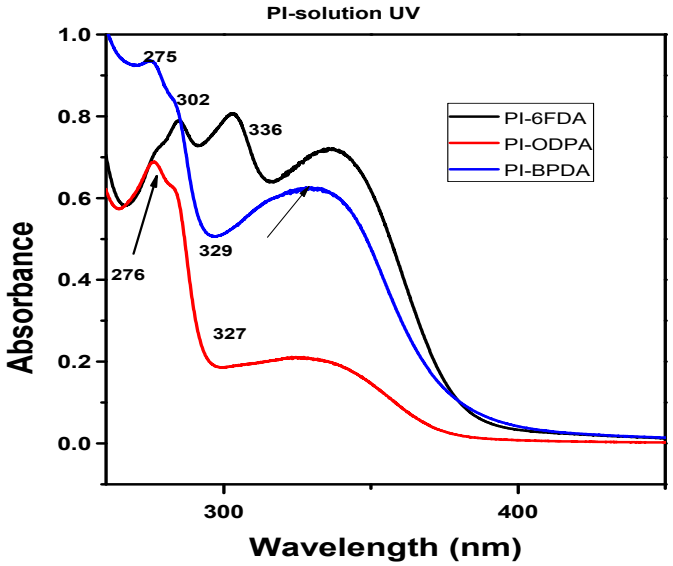

Figure SI 4a.5 UV-Vis absorption spectra of triarylamine-containing polyimides

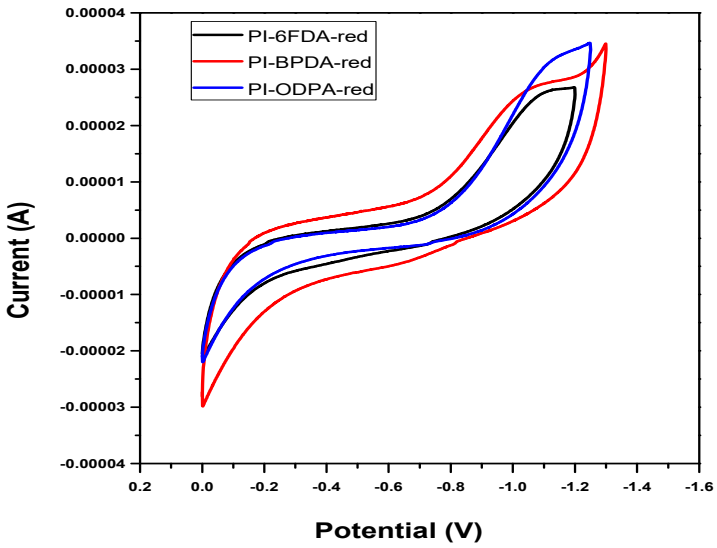

Figure SI 4a.6 Reductive cyclic voltammograms of triarylamine-containing polyimides.

CHAPTER 4 (b)

Partially Bio-Based Triarylamine-Containing Polyamides: Synthesis, Characterisation and Evaluation for Memory Devices

4b.1 Introduction

Aromatic polyamides are well-known for their excellent thermal stability, mechanical strength and oxidative as well as chemical resistance.[1] Triarylamine-based polyamides have been extensively studied for electrochromic,[2–17] electrofluorochromic,[18,19] photoluminescent[18,20] and gas transport properties.[21] Triarylamine-based donor-acceptor polyamides[22–27] are attractive candidates for applications as memristors. However, limited literature is available regarding the behaviour of triarylamine-based polyamides as materials for polymer RRAM devices[28–35]. Liou and co-workers have reported $(OMe)_2$TPPA-6FPA polyamides which revealed volatile SRAM property,[36] and anthraquinone-triphenylamine-based polyamide which was tuned to display SRAM to WORM properties.[37] It would definitely be of interest to explore memristive behaviour of new triarylamine-based polyamides.

In this work, new aromatic polyamides were synthesised from the polycondensation of partially bio-based diamine, *viz.*, 4, 4'-diamino-4"pentadecyltriphenylamine (DPTA), with commercially available diacids, namely, isophthalic acid, 4,4′-(hexafluoroisopropylidene)bis(benzoic acid) and 4,4′-oxybis(benzoic acid) by Yamazaki method at 120 °C. To the best of our knowledge, this is the first report of partially bio-based aromatic triarylamine-containing polyamides evaluated for memory device applications. The synthesised aromatic polyamides were characterised by inherent viscosity measurements, GPC studies, FT-IR, ^{1}H-NMR, ^{13}C-NMR spectroscopy, X-ray diffraction, thermogravimetric analysis (TGA), differential scanning calorimetric studies (DSC), UV analysis and cyclic voltammetry. Memristive behaviour of two polyamides (PA-HBBA and PA-IPA) was investigated.

4b.2 Experimental

4b.2.1 Materials

4, 4'-Diamino-4"pentadecyltriphenylamine (DPTA) was synthesised as described in **Chapter 3**. Tetrabutylammonium perchlorate (TBAP) (Sigma Aldrich, India) was used as received. Isophthalic acid (Sigma Aldrich, India), 4,4′-(hexafluoroisopropylidene)bis(benzoic acid) (Sigma Aldrich, India) and 4,4′-oxybis(benzoic acid) were sublimed before use. Triphenyl phosphite (Sigma Aldrich, India) was used after distillation while N-methyl-2-pyrrolidone (NMP), acetonitrile

(Thomas Baker, India) and pyridine (Thomas Baker, India) were distilled over calcium hydride (Sigma Aldrich, India) prior to use. Calcium chloride (Thomas Baker, India) was activated by heating at 180 °C for 8 h before utilisation for polymerisation.

4b.2.2 Measurements

FT-IR spectra were recorded with ATR mode using Bruker α-T spectrophotometer in the range 4000 to 500 cm^{-1}. ^{1}H and ^{13}C-NMR spectra were recorded on Bruker-AV 400, 500 MHz spectrometer using chloroform-*d* and dimethylsulfoxide-d_6 as solvents, while TMS was used as an internal standard. Inherent viscosities of polyamides was measured using 0.5 % (w/v) solution of polymer in *N*,*N*-dimethyl acetamide at 25 ± 0.1 °C. Ubbelohde suspended level viscometer was used to determine viscosity according to the following equation:

$$n_{inh} = \frac{2.303}{C} x \log \frac{t}{t_0}$$

where *t* and t_0 are flow times of polymer solution and solvent, respectively and *C* is the concentration of polymer solution. X-Ray diffraction analysis was performed on Rigaku MicroMax-007HF X-ray diffractometer at 40 kV and 30 mA. Thermo gravimetric analysis (TGA) of the polymers was performed on Perkin Elmer: STA 6000 between temperatures of 30 °C to 900 °C with a heating rate of 10 °C min^{-1} under nitrogen. Glass transition temperatures (T_g) were determined from differential scanning calorimetry (DSC) experiments carried out on TA Q-100 instrument with sample heating rate of 10 °C min^{-1} under nitrogen atmosphere. T_g values of the polyamides were determined from the second heating cycles. UV–Vis spectra were measured on Specord 210 plus Analytic Jena spectrophotometer.

4b.2.3 Polyamide synthesis: typical procedure

Into a 50 mL three- necked round bottom flask equipped with a magnetic stirring bar, a nitrogen inlet and a reflux condenser were added DPTA (0.3 g, 6.1 x 10^{-4} mol), 4,4′-(hexafluoroisopropylidene)bis(benzoic acid) (0.2422 g, 6.1 x 10^{-4} mol), triphenyl phosphite (0.48 mL, 1.8 x 10^{-3} mol), 1-methyl-2-pyrrolidinone (3 mL), pyridine (0.75 mL) and calcium chloride (0.54 g). The reaction mixture was stirred and heated at 120 °C for 8 h. Subsequently, the viscous reaction mixture was poured into stirred methanol (500 mL) and the fibrous polymer was isolated by filtration. The obtained polymer was further

purified by reprecipitation of the concentrated *N*,*N*-dimethylacetamide solution of the polymer into stirred methanol (500 mL), filtration and drying under reduced pressure. This polymer was designated as PA-HBBA.

A similar procedure was followed for the synthesis of polyamides by polycondensation of DPTA with isophthalic acid (PA-IPA) and 4,4′-oxybis(benzoic acid) (PA-OBBA).

4b.2.4 Optical and electrochemical characterisation

UV-Vis spectra of dimethylacetamide (DMAc) solutions of PA-HBBA and PA-IPA (10^{-5} M) were recorded on Specord 210 plus Analytic Jena spectrophotometer. UV-Vis spectra of polyamide thin films were also recorded. Cyclic voltammetry was conducted in a three-electrode cell with platinum foil (0.3 cm x 0.4 cm) as a working electrode. Polyamide film was formed on the platinum electrode by drop casting from *N*,*N*-dimethylacetamide solutions. A platinum wire was used as counter electrode, while a home-made Ag/AgCl, KCl (sat.) was used as reference electrode in dry acetonitrile (oxidation process/ positive scan). 0.1 M TBAP was used as an electrolyte under nitrogen atmosphere. Ferrocene was employed as an external reference for calibration (4.8 V versus Ag/AgCl).

4b.2.5 Memory device characterisation

Memory devices were fabricated by drop-casting *N*,*N*-dimethylacetamide solutions of PA-HBBA and PA-IPA onto ITO plates (1.5 cm x 1.5 cm) and dried in an oven at 160 °C for 48 h. Uniform thickness of polyamide film was maintained by drop-casting a single layer onto ITO plates.The ITO plates used were previously sonicated in dilute soap solution for 10 min, followed by sequential sonication in deionised water (4 times, 10 min) and isopropyl alcohol (15 min). Finally, the ITO plates were boiled in isopropyl alcohol and dried before memory device fabrication. **Fig 4b.1** represents schematic structure of the developed memory devices. Programmable memristor characterisation system (Arc ONE) was used to evaluate the resistive switching characteristics of polyamide-based devices. During all electrical measurements, the top Aluminium (Al) electrode was biased and bottom ITO electrode was grounded. Following parameters were kept constant during electrical measurements; signal type: staircase, the maximum amplitude of the positive and negative voltage pulse: ±2 V, step

width: 100 ms, read voltage: 0.20 V and interpulse time: 10 ms. For endurance and retention measurements, the pulse width of positive and negative pulses was 100 µs.

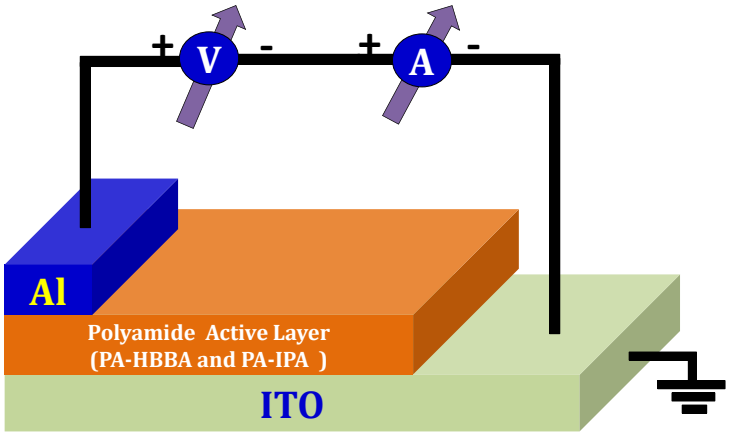

Figure 4b.1 Schematic structure of triarylamine-containing polyamide based memory devices

4b.3 Results and Discussion

4b.3.1 Polyamide synthesis

Aromatic polyamides are conventionally synthesised through polycondensation of aromatic diamines and diacyl chlorides. However, the synthesis, isolation, purification, storage and handling of moisture sensitive acid chlorides presents challenges which may be avoided by utilising the synthetic procedure reported for the first time in 1974 by Yamazaki.[38] This synthetic approach employs aromatic diacids in the place of aromatic diacyl chlorides for the synthesis of polyamides.[39–41]

In the present work, Yamazaki phosphorylation polycondensation method was employed to synthesise aromatic polyamides, as depicted in **Scheme 4b.1**.

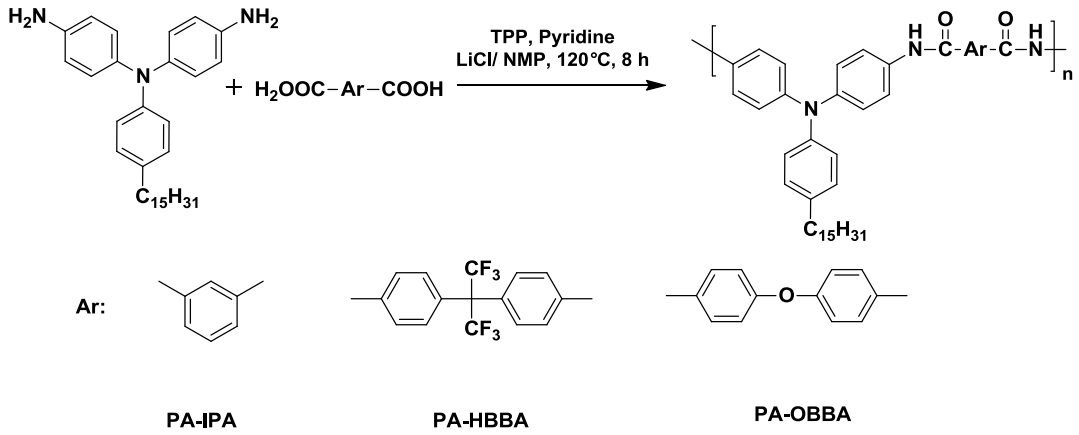

Scheme 4b.1 Synthesis of triarylamine-containing polyamides

DPTA, an aromatic diacid, a mixture of NMP and pyridine, triphenyl phosphite and calcium chloride were stirred and heated at 120 °C for 8 h. It has been proposed that the reaction progresses *via* an acyloxy N-phosphonium salt of pyridine formed by dephenoxylation of triphenyl phosphite.[38,41] Calcium chloride added to the reaction mixture assists by solubilisation of the growing polymer chains that allows the realisation of high molecular weights. The polymers were isolated by precipitation into methanol followed by reprecipitation from *N*,*N*-dimethylacetamide solutions.

The results of polymerisation reactions are collected in **Table 4b.1**. Polyamides PA-HBBA and PA-IPA displayed inherent viscosities of 0.71 dL g^{-1} and 0.6 dL g^{-1}, respectively, as determined from *N*,*N*-dimethylacetamide solutions. This indicates that the polyamides synthesised were of reasonably high molecular weights. Flexible, free-standing films could be cast from *N*,*N*-dimethylacetamide solutions (**Fig 4b.2**).

Table 4b.1 Results of synthesis of triarylamine-containing polyamides

Polyamide	Polyamide repeat unit	η_{inh} (dL/g)[a]
PA-HBBA	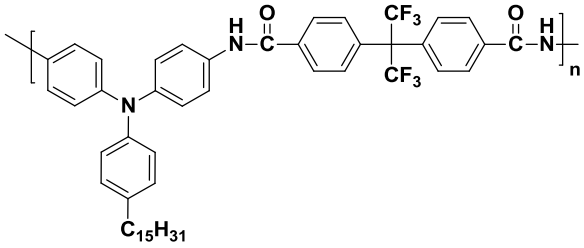	0.71
PA-IPA	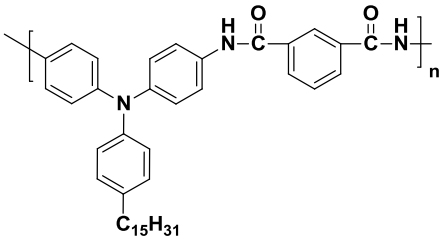	0.6
PI-OBBA	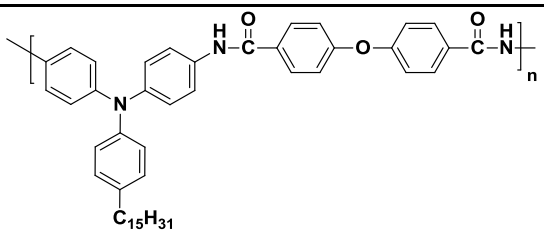	N. D.[b]

a: η_{inh} was measured using 0.5% (w/v) solution of polyamides in DMAc at 25 °C ± 1°C
b: N.D. Not determined due to lack of solubility in DMAc

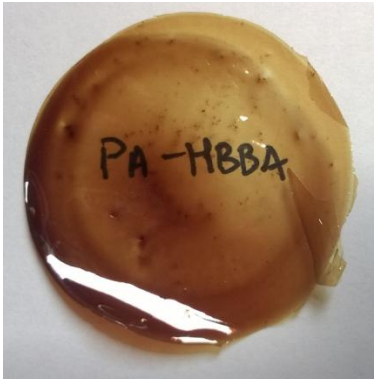

Figure 4b.2 PA-HBBA film cast from DMAc

The structural analysis of polyamides synthesised from DPTA was performed through FT-IT, ^{1}H-NMR and ^{13}C-NMR spectroscopic studies. Representative FT-IR spectrum of PA-HBBA is provided in **Fig 4b.3**. In **Fig 4b.4** is depicted ^{1}HNMR spectrum of PA-HBBA, while in **Fig 4b.5** is presented ^{13}C-NMR spectrum of PA-HBBA.

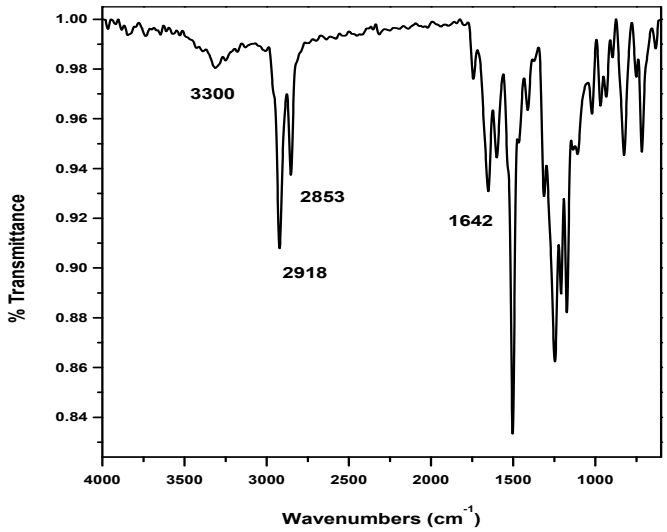

Figure 4b.3 FT-IR spectrum of PA-HBBA film

A broad absorption band appearing at 3300 cm^{-1} was attributable to N-H stretching vibration. The absorption band at 1642 cm^{-1} could be ascribed to stretching vibrations of carbonyl (C=O) belonging to the amide linkage. Both observations confirm the successful formation of polyamides.

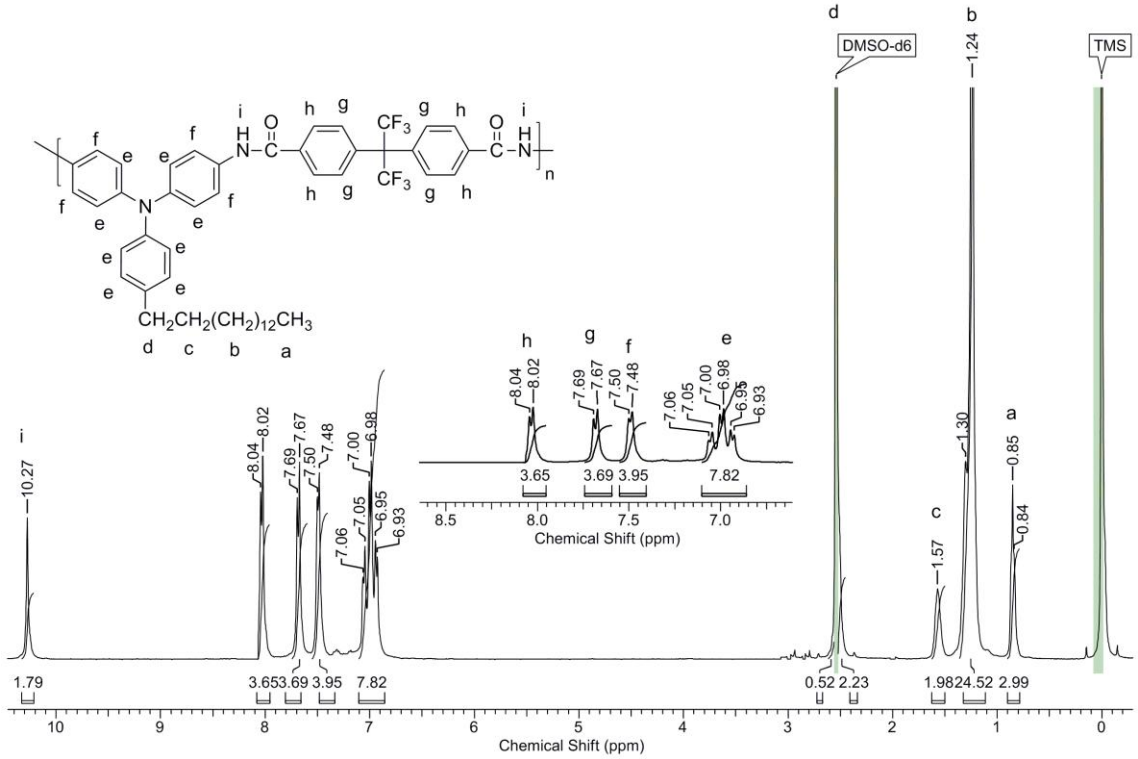

Figure 4b.4 ^{1}H-NMR spectrum (DMSO-d_6 + $CDCl_3$) of PA-HBBA.

The singlet at 10.27 δ ppm for two protons was attributable to N-H protons (**i**). Aromatic protons (**e**) belonging to the triarylamine moiety resonated in the range 6.86 – 7.09 δ ppm. The remaining protons (**f**) appeared at 7.49 δ ppm as a doublet. The signals corresponding to the acid component appeared at 7.68 δ ppm (**g**) and 8.03 δ ppm (**h**) as doublets. The benzylic protons (**d**) overlapped with the signal for DMSO-d_6 at 2.52 δ ppm, while the methylene protons (**c**) resonated in the range 1.47 – 1.65 δ ppm. The remaining methylene protons (**b**) belonging to the pentadecyl chain appeared in the range 1.08 – 1.45 δ ppm as a multiplet. The signal for the terminal methyl group of the pentadecyl chain (**a**) appeared at 0.85 δ ppm as a triplet.

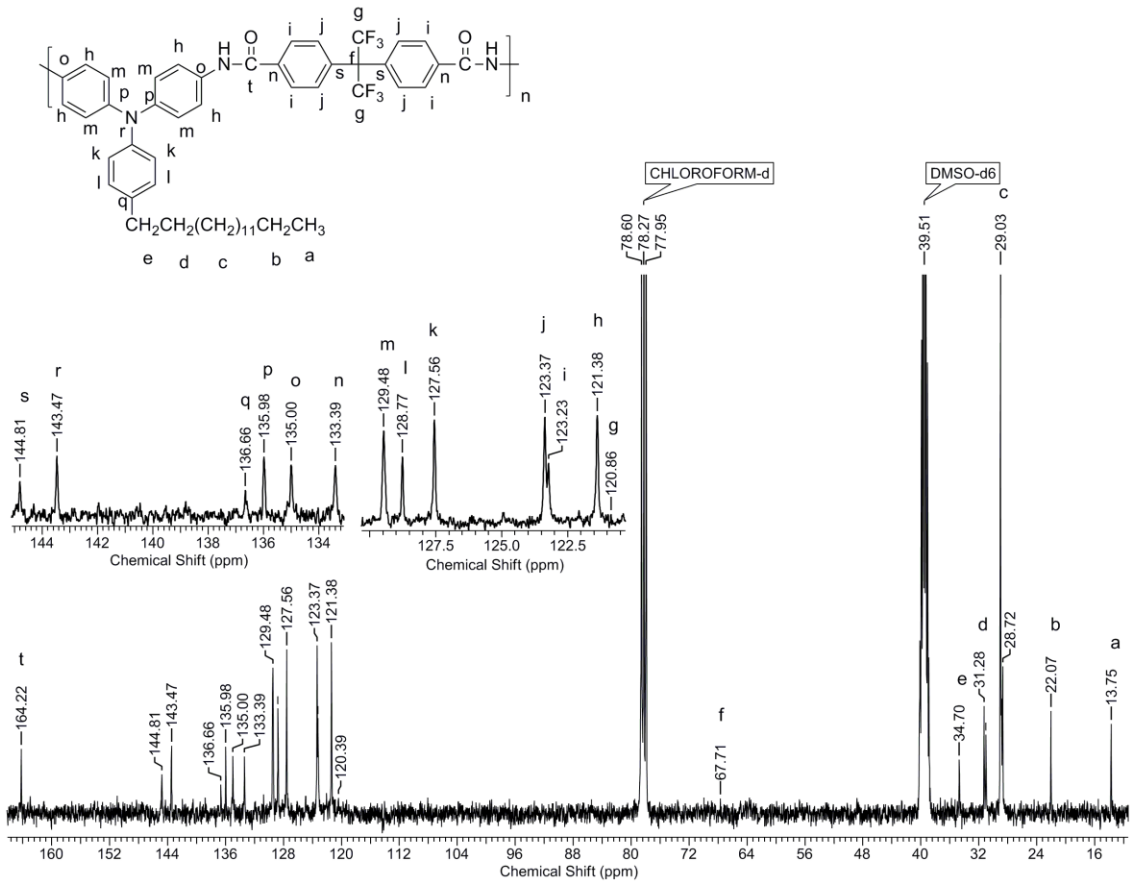

Figure 4b.5 ^{13}C-NMR spectrum (DMSO-d_6 + $CDCl_3$) of PA-HBBA.

^{13}C-NMR spectrum of PA-HBBA was successfully assigned with the assistance of DEPT spectrum. The amide carbonyl carbon (**t**) resonated at 164.22 δ ppm. Aromatic carbons (**h-s**) appeared in the range 121.38 δ – 144.81 δ ppm. The signal appearing at 34.70 δ ppm was assignable to benzylic carbon (**e**) while the signal at 31.28 δ ppm could be ascribed to the methylene carbon **d.** The signal corresponding to the remaining methylene carbons (**c**) appeared in the range 28.164 δ – 29.26 δ ppm. Signals corresponding to the methyl carbon (**a**) and the methylene carbon **b** resonated at 13.75 δ ppm and 22.07 δ ppm, respectively.

Results obtained from FT-IR, ^{1}H-NMR and ^{13}C-NMR analysis indicated that the synthesised polyamide shows good agreement with the proposed structure and thus together confirm the structure of the synthesised polyamide. ^{1}H-NMR and ^{13}C-NMR spectra of PA-IPA are depicted in **Supporting Information** (**Fig SI 4b.1**, **Fig SI 4b.2**).

4b.3.2 Solubility and X-ray diffraction studies

The solubility data of the synthesised polyamides at 3 wt % concentration is summarised in **Table 4b.2**.

Table 4b.2 Solubility of triarylamine-containing polyamides

Polyamide	Solvent								
	DMAc	NMP	DMF	DMSO	*m*-cresol	Pyridine	$CHCl_3$	THF	Nitro benzene
PA-HBBA	++	++	+	+-	++	++	+-	+	+-
PA-OBBA	+-	+-	+-	--	+-	+-	--	--	--
PA-IPA	++	++	+	+-	++	++	+-	+	+

--, Insoluble; + soluble on heating at 70°C; ++, soluble at room temperature; +-, partially soluble or swollen

From the data in **Table 4b.2** it was observed that PA-HBBA and PA-IPA were both soluble in *N*,*N*-dimethylacetamide, 1-methyl-2-pyrrolidinone, *m*-cresol and pyridine at room temperature while PA-OBBA was found to be insoluble or partially soluble in the mentioned solvents. The better solubility of PA-HBBA is attributable to the presence of bulky hexafluoroisopropylidene linkages, while that of PA-IPA is ascribed to the unsymmetrical *m*-orientation. When the solubility of PA-HBBA and PA-IPA was compared to the solubility of polyamides based on 4,4'-diaminotriphenylamine, it was found that the presence of pentadecyl chains hampered solubility to a certain extent, since the reference poyamides are reported to be readily soluble in DMF and dimethyl sulfoxide.[42] This may be attributed to the presence of non-polar alkyl chains, for which polar solvents such as DMF and dimethyl sulfoxide are bad solvents.

Wide angle XRD (WAXD) patterns for the synthesised polyamides are provided in **Fig 4b.6**. A broad hump observed around 2θ ~ 20° for all three polyamides suggested that the polyamides were amorphous in nature. Additionally, sharp peaks were observed in the low angle region 2θ ~ 2.5° as well. It has been reported in literature[43–47] that such peaks in the low angle region are generated from reflections from spacings between the polymer chains, suggesting the formation of layered or stacked structures in the solid

state. Such layered structures are formed due to the presence of pendent alkyl chains which interdigitate and orient away from the backbone of the polymer giving rise to layered structures. It is to be noted that unlike in the case of the other polyamides, a shoulder peak was observed at 2θ ~ 4.6° in the X-ray diffraction curve of PA-OBBA. The origin of shoulder peak cannot be explained at this stage.

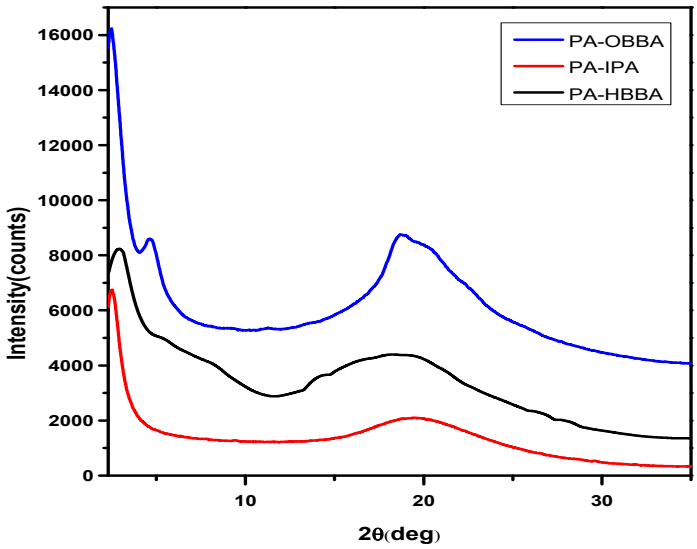

Figure 4b.6 X-Ray diffractograms of triarylamine-containing polyamides

4b.3.3 Thermal Properties

The thermal properties of synthesised polyamides were investigated *via* thermogravimetric analysis (TGA) and differential scanning calorimetry (DSC). The results are collected in **Table 4b.3**. TG curves are depicted in **Fig 4b.7**. A representative DTG curve with corresponding TGA curve for PA-IPA is presented in **Fig 4b.8**. In **Fig 4b.9** is provided DSC curves of synthesised polyamides.

Table 4b.3 Thermal properties of triarylamine-containing polyamides

Polyamide	Polyamide repeat unit	T_g (°C)[a]	T_{10} (°C)[b]	Char yield (%)[c]
PA-HBBA	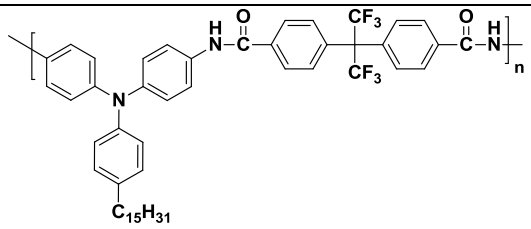	206 (290)	448 (490)	43
PA-IPA	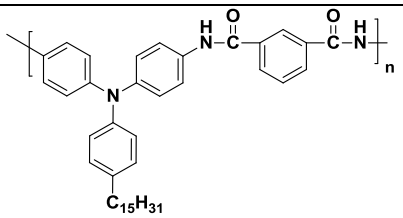	193 (281)	434 (515)	45
PI-OBBA	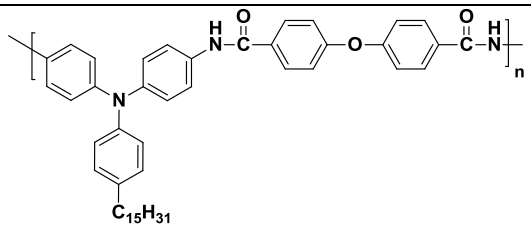	189 (273)	420 (571)	39

a: Measured by DSC from second heating scan with heating rate of 10 °C/min under nitrogen atmosphere.
b: 10 % weight loss on TGA thermograms at a heating rate of 10 °C/min under nitrogen atmosphere.
c: Char yield measured at 900 °C.
values in parenthesis refer to the values of reference polyamides based on 4,4'-diaminotriphenylamine and corresponding diacids and data was taken from available literature.[5,42]

.

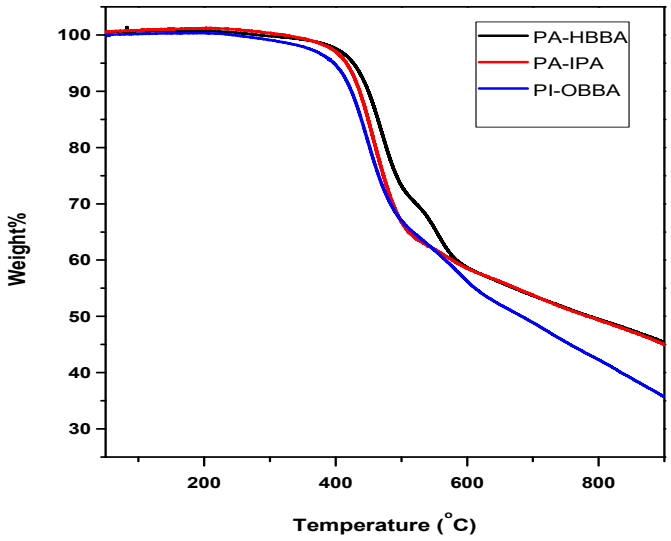

Figure 4b.7 TG curves of triarylamine-containing polyamides

From data in **Table 4b.3** it was observed that the synthesised polyamides displayed T_{10} values in the range 420 – 448 °C suggesting their good thermal stability. However, these polymers exhibited lower T_{10} values, and thus lower thermal stability, when compared with reference polyamides based on 4,4'-diaminotriphenylamine. This is reasonable due to the presence of thermally labile pendent alkyl chains. Observed char yields were in the range of 39 – 45 %.

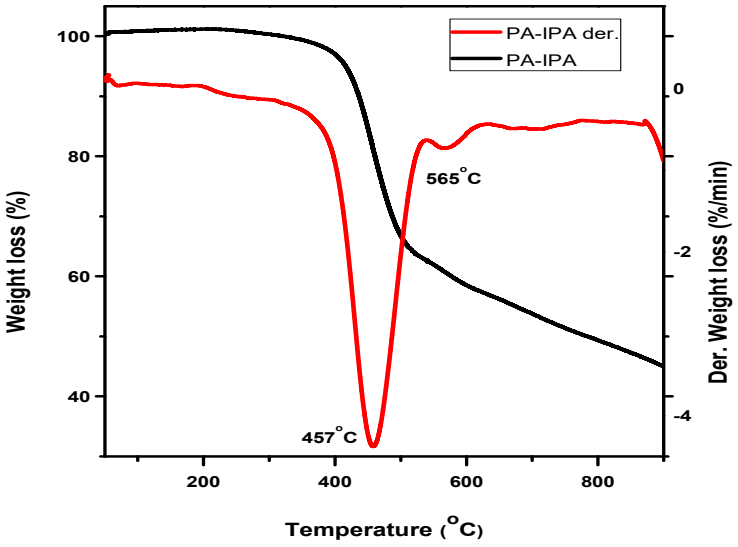

Figure 4b.8 DTG curve of PA-IPA

From the DTG curve it was observed that maximum polymer degradation occurred at 457 °C. Minor degradation occurred at 565 °C, presumably due to degradation of products formed by thermally induced cyclisation.

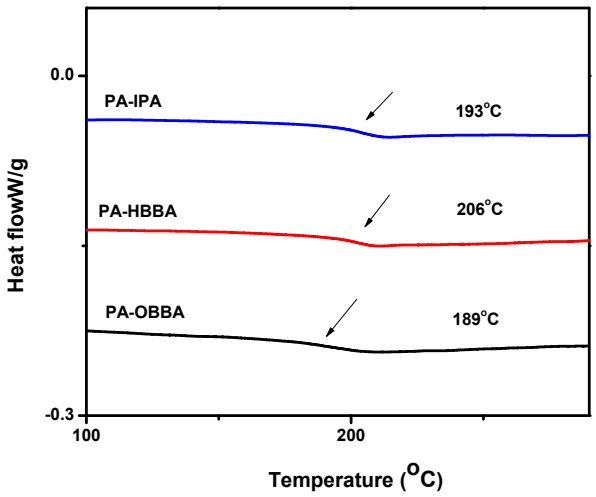

Figure 4b.9 DSC curves of triarylamine-containing polyamides

Glass transition temperatures (T_g) were observed to be in the range 189 – 206 °C. PA-OBBA, containing a flexibilising ether linkage in the polymer backbone, displayed the lowest T_g value, followed by PA-IPA whose *meta*-orienting moiety causes a "kink" in

the polymer chain. Additionally, it is to be noted that all the synthesised polyamides displayed T_g values much lower than those of reference polyamides based on 4,4'-diaminotriphenylamine. This clearly suggests that the pentadecyl chains exert a packing disruptive effect and improve segmental mobility, leading to a lowering of T_g. Further, first order transitions were not observed in the DSC scans, which additionally supports the results from XRD, suggesting the amorphous nature of polyamides.

4b.3.4 Optical and electrochemical properties

The optical and electrochemical characteristics of polyamides were investigated by UV-Vis spectroscopy and cyclic voltammetry. UV-Vis spectra of polyamides are depicted in **Fig 4b.10**. The λ_{max} values obtained from solution UV spectroscopy and λ_{onset} values (cut-off wavelength) obtained from solid-state UV-Vis spectroscopy are summarised in **Table 4b.4**. The cyclic voltammograms in oxidation process are depicted in **Fig 4b.11**. The obtained half-wave potentials ($E_{1/2}$) and onset potentials (E_{onset}) during oxidation CV are summarised in **Table 4b.4**.

Table 4b.4 Optical and electrochemical properties of triarylamine-containing polyamides

Polyamide	Absorbance		Oxidation[c]			Energy Levels	
	λ_{max}(nm)[a]	λ_{onset}(nm)[b]	E_g^{Opt}(eV)[d]	$E_{1/2}$(V)[e]	$E_{oxonset}$	HOMO(eV)[f]	LUMO(eV)
PA-HBBA	344	761	1.6	0.763	0.432	-5.16	-3.56
PA-IPA	342	780	1.58	0.756	0.267	-4.997	-3.47

a: UV-vis absorption maxima measured in *N*,*N*-dimethylacetamide (10^{-5} M) at room temperature. b: The cut-off wavelength determined from UV-vis transmission spectra of polymer films. c: From cyclic voltammograms versus Ag/AgCl in CH_3CN. d: Obtained from $E_g^{opt} = 1240/\lambda_{onset}$. e: $E_{1/2}$ is the average potential of redox couple peaks. f: HOMO energy levels calculated from cyclic voltammetry and referenced to ferrocene ($E_{1/2}$ = 0.0785V).

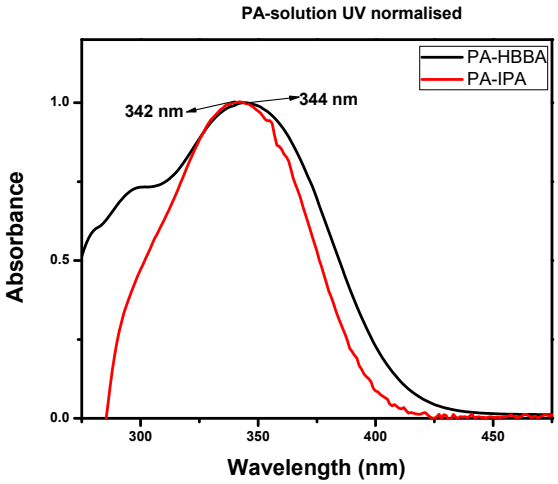

Figure 4b.10 UV-Vis spectra of triarylamine-containing polyamides.

The UV absorption bands at 342 nm and 344 nm are observed due to π-π* transitions resulting from conjugation between aromatic rings and the N atoms. Both PA-HBBA and PA-IPA exhibit very close λ_{max} values. The optical band-gap (E_g^{Opt}) values, the difference between HOMO and LUMO energy levels determined from λ_{onset}, are summarised in **Table 4b.4**, and were found to be in the range 1.58 eV – 1.6 eV.

The redox behaviour of the polyamides was studied by cyclic voltammetry

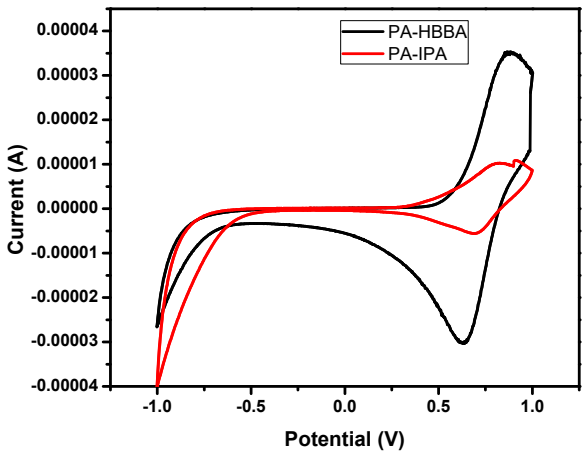

Figure 4b.11 Oxidative cyclic voltammograms of triarylamine-containing polyamides

Redox peaks were observed under positive CV scan (**Fig 4b.11**) from -1 V to 1.0 V against Ag/AgCl. The HOMO energy levels of respective polyamides were determined from oxidation onset potentials ($E_{oxonset}$) with respect to Ag/Ag^{+}. The calculations were done taking the value of HOMO energy level for the ferrocene standard to be 4.80 eV with respect to zero vacuum level. The HOMO energy levels of the synthesised polyamides were found to be in the range of -4.99 eV to -5.16 eV, while the $E_{1/2}$ values (average potential of the redox peaks or half-wave potential) ranged from 0.756 – 0.755 V. PA-IPA displayed lowest $E_{oxonset}$ (oxidation onset potential) and $E_{1/2}$ values and was most easily oxidized. PA-IPA allows better extended conjugation contrasted with PA-HBBA and hence was more easily oxidised. LUMO values were calculated from the E_g^{Opt} values, obtained from UV spectroscopy, and were observed to be from -3.47 eV to -3.56 eV. The HOMO values were determined from CV measurements and were from -4.99 eV to -5.16 eV. The band-gap values of the synthesised polyamides were observed to be in the range 1.58 – 1.6 eV, within the range of semi-conducting materials with hole-transport properties,.

4b.3.5 Memory device characterisation

Memory devices fabricated from polyamides PA-HBBA and PA-IPA, were evaluated for resistive memory applications. **Fig 4b.12** represents current-voltage (I-V) characteristics obtained from memory devices based on PA-HBBA and PA-IPA in linear and semilog scale. The resistive switching direction is indicated by the arrows.

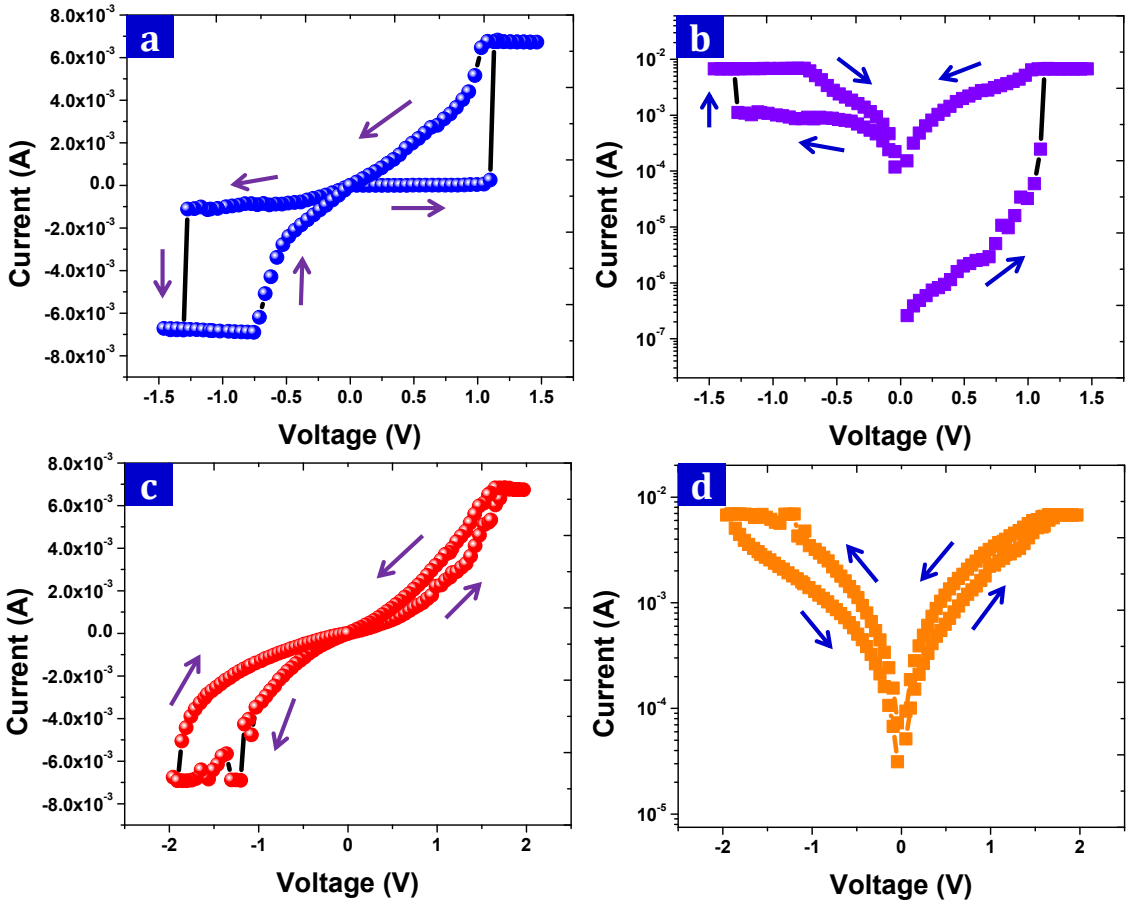

Figure 4b.12 Bipolar resistive switching characteristics of **(a-b)** PA-HBBA and **(c-d)** PA-IPA memory devices in linear and semilog scale, respectively.

Generally, the I-V hysteresis loop in first and third quadrant is a fingerprint characteristic of memristor, which is a fourth fundamental circuit element. Similar kind of I-V hysteresis loop is observed for the devices based on PA-HBBA and PA-IPA, as shown in **Fig 4b.12**. In addition to this, bistable I-V curves were observed for PA-HBBA and PA-IPA based memory devices. In the case of PA-HBBA memory device (**Fig. 4b.12(a-b)**), initially, current through the device was found to be very low (2.2 x 10^{-7} A). This condition is considered as a high resistive state (HRS). When the voltage was positively swept from 0 V to 1.5 V, the current increased gradually. At 1.1 V, the current was observed to increase abruptly from 2.49 x 10^{-4} A to 7.1 x 10^{-3} A. This voltage is referred to as V_{SET} voltage which transitions the memory device from HRS to low resistance state (LRS). This transition constitutes a "SET" or "write" process. The current conduction was observed to remain in the same range as the voltage was increased further

to 1.5 V. Thereafter, when the voltage was changed continuously from 1.5 V to 0 V, the observed current decreased gradually to 1.43 x 10^{-4} A. Subsequently, the device was subjected to a negative sweep voltage from 0 V to -1.5 V. The observed current increased gradually to 1.1 x 10^{-3} A. When the voltage reached -1.3 V, the current increased to 7.0 x 10^{-3} A. The current remained in this range as the voltage was changed continuously to -1.5 V. As the voltage changed from -1.5 V to 0 V, the current observed started decreasing gradually when the voltage reached -0.7 V to a value of 1.6 x 10^{-4} A. Thus during the entire negative sweep voltage, the device remained in LRS. Since during entire resistive cycle only "SET"/ "write" process occurred and during subsequent voltage sweeps the device remained in LRS, the memory device based on PA-HBBA is "write once read many times" (WORM) type in nature.

Fig 4b.12 (c-d) represents the I-V curves of memory device based on PA-IPA. It was observed that the memory device was initially in an "OFF" state / HRS. The observed current was 1.92 x 10^{-5} A. The current increased gradually to 6.8 x 10^{-3} A as the voltage was positively swept from 0 V to 2 V. The V_{SET} was observed to be 1.75 V, at which the device was "switched" into "ON" state. As the voltage changed continuously from 2 V to 0 V, the current was observed to decrease gradually to 7.6 x 10^{-5} A. Subsequently, the device was subjected to a negative voltage sweep from 0 V to -2 V during which the current continuously increased and reached 6.8 x 10^{-3} A at -1.19 V and remained in this range up to -2 V. The device was further subjected to another voltage sweep from -2 V to 0 V. At -1.9 V (V_{RESET}), the current measured was observed to decrease gradually as the voltage changed from -1.9 V to 0 V, thus putting the device into "OFF" state. Unlike the memory device based on PA-HBBA, the memory device based on PA-IPA showed the occurrence of both "SET" as well as a "RESET" process during the complete resistive cycle, thus pointing towards its rewritable nature. Additionally, the memory device based on PA-HBBA showed an abrupt transition from "ON" state to "OFF" state, while the device based on PA-IPA displayed a gradual increase or decrease in current conduction during device switching.

In addition to the analysis of I-V curves of memory devices, it is also important to evaluate the performance of memory devices in terms of endurance and retention. **Fig 4b.13** represents endurance and retention memory performance of the memory devices

based on PA-HBBA and PA-IPA. The endurance of the memory devices was determined by subjecting the memory devices to 10000 repetitive resistive switching cycles at a read voltage of 0.25 V. ±2 V positive and negative voltage pulses with a pulse width of 100 µs was applied to obtain the results of endurance tests. It was observed that two well-defined memory states, the high resistive state (HRS) and low resistive state (LRS), were observed in both memory devices. The HRS and LRS were observed to persist without significant degradation even after 10000 resistive switching cycles, indicating that both memory devices showed good endurance. PA-HBBA exhibited an excellent "memory window" (HRS/LRS) of 10^3, while PA-IPA displayed a memory window of 10. For practical applications, a memory window of 10 and above is necessary to minimise reading errors. PA-HBBA, with a memory window of 10^3, shows good potential for applications in memory devices. Furthermore, the memory retention performance of the memory devices was conducted at a read voltage of 0.25 V for each second over an extended period of time (1000 s). Both the resistive states, HRS and LRS, were observed to maintain their integrity with no degradation over the entire time period. The results of endurance and retention studies indicated that memory devices based on PA-HBBA and PA-IPA are non-volatile in nature.

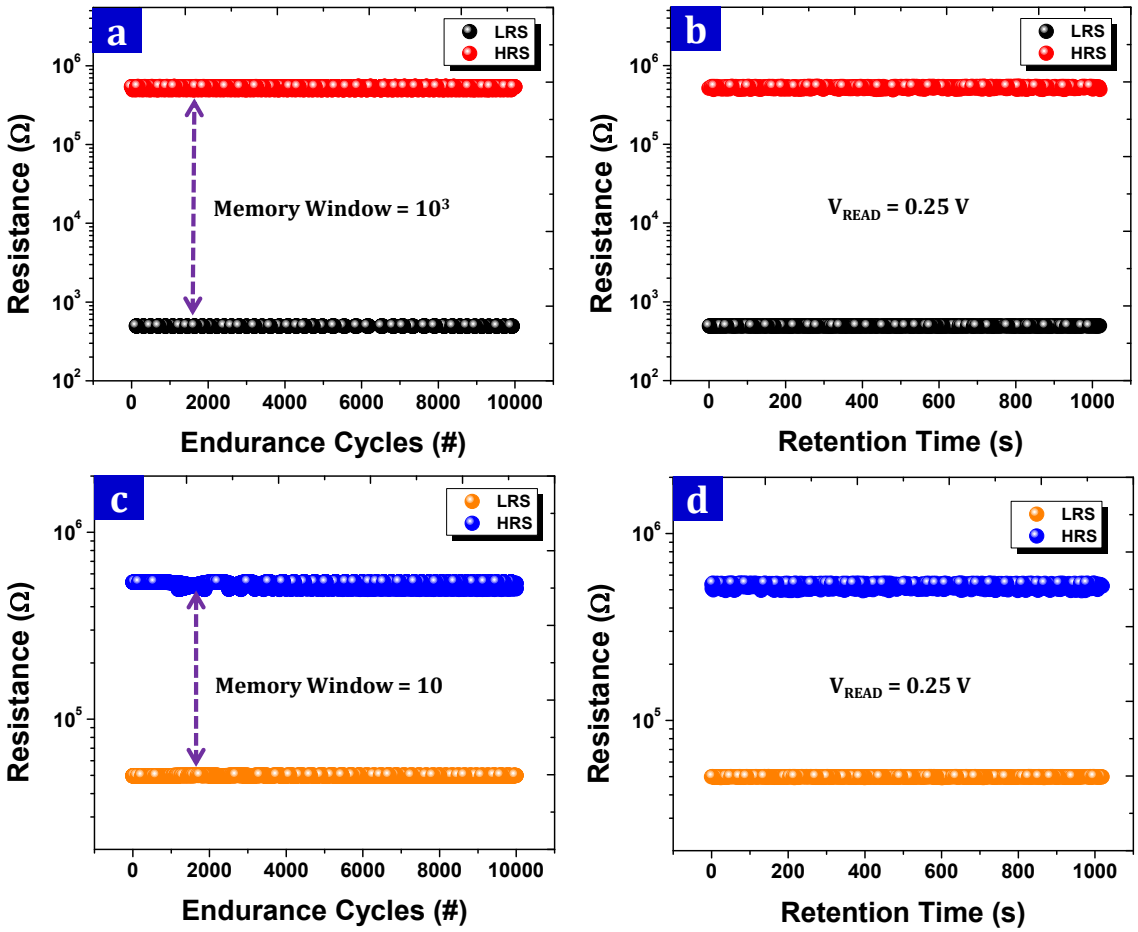

Figure 4b.13 Endurance and retention memory performance of **(a-b)** PA-HBBA and **(c-d)** PA-IPA memory devices.

The stability of the resistive states developed was studied through statistical analysis. The statistical distribution of cumulative probability of the resistive switching states of PA-HBBA and PA-IPA is provided in **Fig 4b.14**. In addition, the performance comparison of the memory devices, in terms of statistical parameters is summarised in **Table 4b.5**.

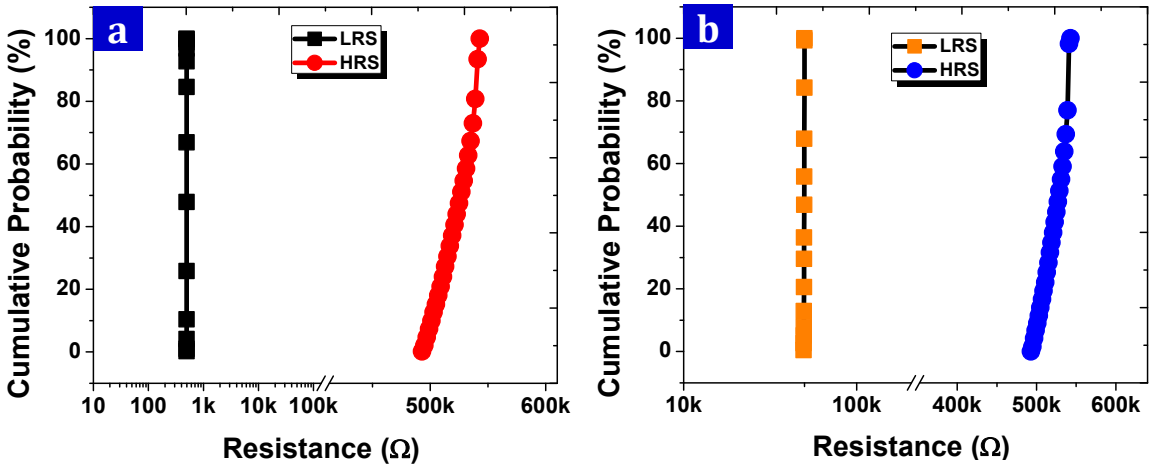

Figure 4b.14 LRS and HRS cumulative probability of **(a)** PA-HBBA and **(b)** PA-IPA memory devices.

Table 4b.5 Performance comparison of triarylamine-containing polyamide memory devices

Polyamide	V_{SET}(V)	V_{RESET} (V)	Average, μ (Ω)		Memory window (HRS/LRS)	Standard deviation, σ(Ω)		Coefficient of variation, σ/μ (%)	
			LRS	HRS		LRS	HRS	LRS	HRS
PA-HBBA	1.10	-	493	524660	~1000	0.1891	14690	0.03	2.79
PA-IPA	1.75	-1.90	49789	525599	~10	152	14548	0.30	2.76

The statistical parameters provide a good idea of the stability and reliability of the resistive states observed in the devices. Both developed memory devices showed excellent stability of LRS, with a low coefficient of variation of 0.03 % while coefficient of variation of HRS was slightly higher, in the range of 2.76 % - 2.79 %, indicating slightly lower uniformity of the HRS. The LRS of PA-HBBA also exhibited a very low standard deviation of 0.1891, in contrast to the value of 152, in the case of PA-IPA. Overall, memory device based on PA-HBBA showed much better performance in terms of standard deviation, coefficient of variation and memory window.

The current conduction mechanisms prevalent in the developed memory devices were ascertained by taking a closer look at the I-V data of the memory devices. Towards this end, different regions of the I-V data curves were fitted in accordance to current

conduction models known in literature (**Fig 4b.15**).[48–55] In **Fig 4b.15 (a)**, it is observed that the low voltage region (0 – 0.425 V) of the memory device based on PA-HBBA in positive bias has a slope of 0.67. This suggests that current conduction over this voltage range occurs in accordance to Ohmic conduction model. In the higher voltage region (0.423 – 1.13 V), a slope of 5.18 was observed. This region was successfully fitted in accordance to Schottky conduction model, indicating that Schottky conduction mechanism dominates over this voltage range (**Fig 4b.16 (a)**). In negative bias (**Fig 4b.15 (b)**), it was observed that in the low voltage region, from 0 – 0.30 V, a slope of 0.84 was observed. Furthermore, in the high voltage region, from 0.30 – 1.35 V, a slope of 1.00 was observed. This suggests that Ohmic conduction mechanism dominates in negative bias. In the case of PA-IPA, in positive bias (**Fig 4b.15 (c)**), a slope of 1.10 was observed in the low voltage region (0 – 0.32 V), while a slope of 1.84 was observed in the high voltage region, from 0.32 – 1.85 V. This indicates that Ohmic conduction mechanism was dominant in the low voltage region. The higher voltage region was fitted according to Schottky conduction model (**Fig 4b.16 (b)**), suggesting that Schottky conduction prevailed in the high voltage region. In negative bias (**Fig 4b.15 (d)**) a slope of 1.14 was observed in low voltage region (0 – 0.30 V), followed by a slope of 1.57 in the high voltage region (0.30 – 1.90 V). The higher voltage region was fitted according to Schottky conduction model (**Fig 4b.16 (c)**). Hence in negative bias Ohmic conduction dominated at lower voltage and Schottky conduction prevailed in high voltage region. Equations (1) and (2) represent the equations of Ohmic and Schottky conduction models which have been used for the fitting of experimental data.[48,49,51]

$$J \propto V \qquad (1)$$

$$J \propto T^2 exp\left[\frac{-q\left(\Phi - \sqrt{\frac{qV}{4\pi\varepsilon d}}\right)}{k_B T}\right] \qquad (2)$$

where, J is the current density, T is the temperature, Φ is the barrier height, ε is the dynamic dielectric permittivity, q is the electronic charge, V is the applied electric field,

kB is the Boltzmann's constant, and d is the thickness. Hence, it is clear that in both the devices, in the low voltage region, current conduction takes place in accordance to Ohmic conduction model, in both positive and negative bias. As the voltage was increased, a Schottky conduction barrier develops at the aluminium-polymer interface and current is limited by charge injection from the electrode to the polymer film, leading to dominance of Schottky conduction mechanism. Thereafter, as the barrier is overcome, the device transitions into "ON" state. As an exception, Ohmic conduction was observed to dominate over the entire voltage range in the case of PA-HBBA in negative bias. This happened because in this case there was no transition occurring from "ON" state to "OFF" state.

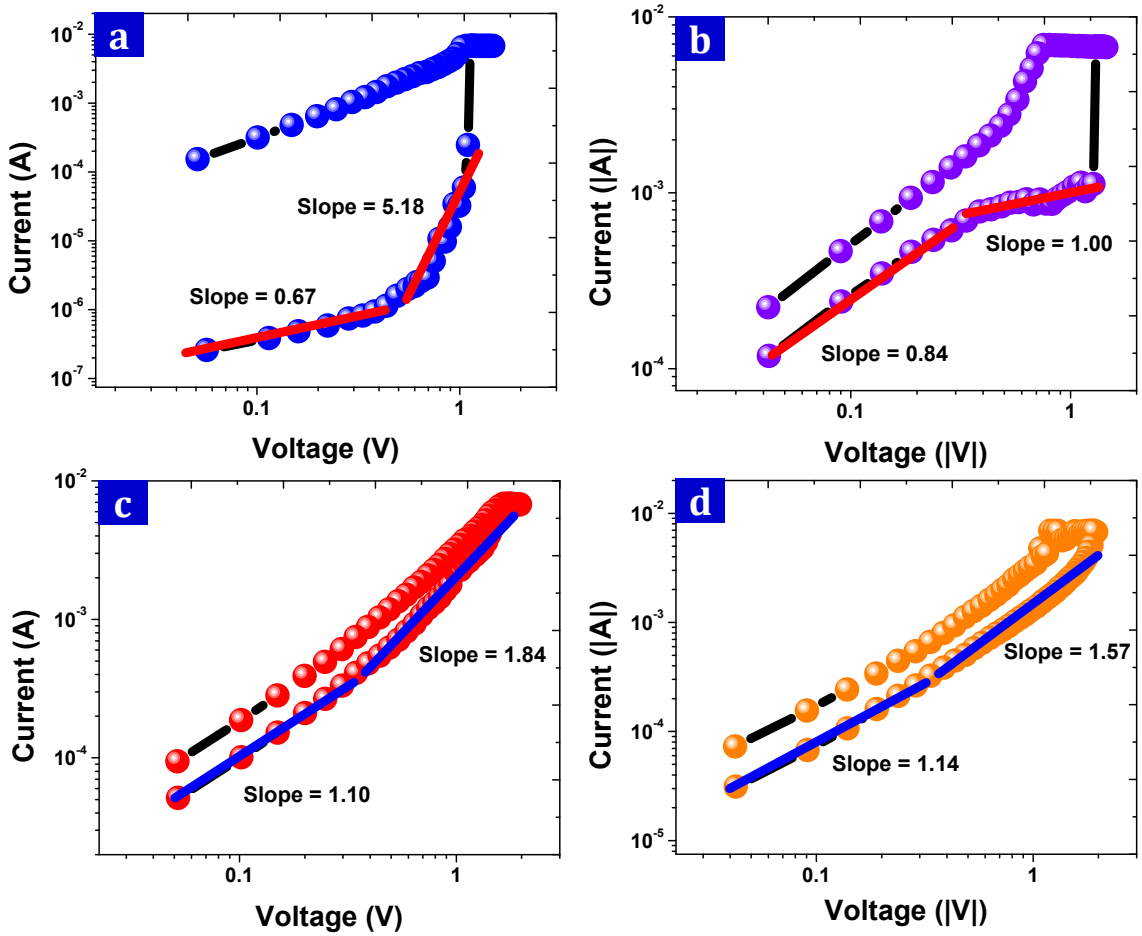

Figure 4b.15 Conduction mechanisms of **(a-b)** PA-HBBA and **(c-d)** PA-IPA memory devices in positive and negative bias, respectively.

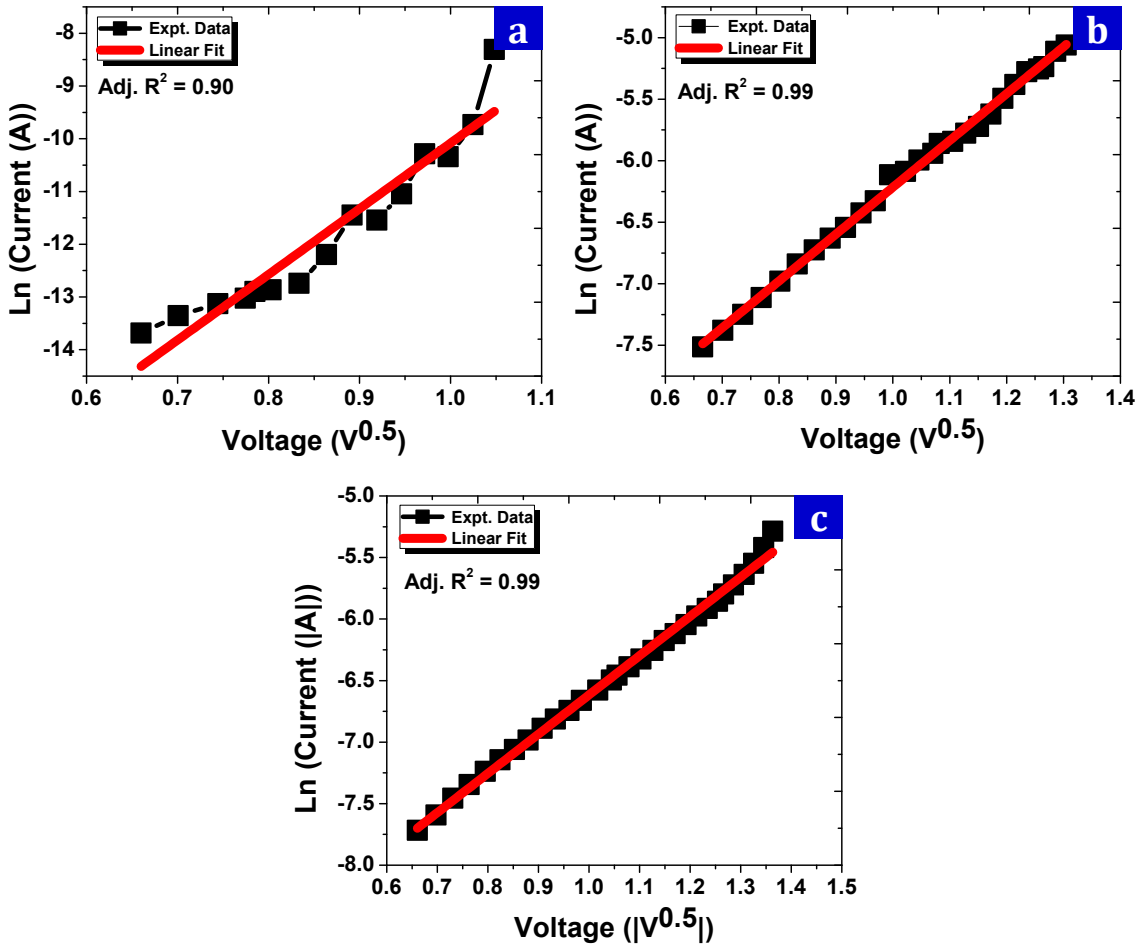

Figure 4b.16 Schottky conduction mechanism fitting to the high slope part data of **(a)** PA-HBBA (positive bias) memory device and **(b)** PA-IPA memory device in positive bias and **(c)** negative bias.

4b.4 Conclusions

1. Three new triarylamine-containing aromatic polyamides bearing pentadecyl chains, PA-HBBA, PA-IPA and PA-OBBA, were synthesised from the polycondensation of 4, 4’-diamino-4"pentadecyltriphenylamine (DPTA) with 4,4′-(hexafluoroisopropylidene)bis(benzoic acid), isophthalic acid (and 4,4′-oxybis(benzoic acid) by Yamazaki polymerisation at 120 °C.

2. The formation of polyamides of reasonably high molecular weights was inferred from the inherent viscosity values.

3. The synthesised polyamides were amorphous in nature, as ascertained from XRD analysis. This was due to the packing disruptive effect exerted by the bulky triarylamine moiety and the pentadecyl chain.

4. T_{10} values were observed in the range 420 – 448 °C while T_g values obtained were in the range 189 – 206 °C. T_{10} values indicate that the polyamides synthesised were of good thermal stability.

5. Optical band-gap values were found to be in the range 1.58 eV – 1.6 eV. These values indicate that the synthesised polyamides showed good potential for semiconductor applications.

6. Memory device fabricated from PA-IPA was observed to exhibit rewritable memory characteristics, while the memory device base on PA-HBBA displayed WORM memory behaviour. Two well defined memory states, high resistive state (HRS) and low resistive state (LRS), were observed. A memory window of 10 was observed in the case of PA-IPA and 10^3 in the case of PA-HBBA. The results of endurance and retention studies indicated that memory devices based on the two polyamides were non-volatile in nature. Statistical analysis of resistive states revealed that developed resistive states possessed good stability. Schottky conduction mechanism dominated for "OFF" to "ON" and "ON" to "OFF" transitions.

References

1 P. E. Cassidy, *Thermally stable polymers*, Marcel Dekker, New York, 1980.

2 S.-H. Hsiao, Y.-M. Chang, H.-W. Chen and G.-S. Liou, *J. Polym. Sci. Part A Polym. Chem.*, 2006, **44**, 4579–4592.

3 S.-H. Hsiao and Y.-T. Chiu, *RSC Adv.*, 2015, **5**, 90941–90951.

4 H.-J. Yen and G.-S. Liou, *J. Mater. Chem.*, 2010, **20**, 9886.

5 Y.-C. Kung and S.-H. Hsiao, *J. Mater. Chem.*, 2010, **20**, 5481.

6 S. Hsiao, G. Liou, Y. Kung and H. Yen, *Macromolecules*, 2008, **41**, 2800–2808.

7 S.-H. Hsiao, Y.-H. Hsiao and Y.-R. Kung, *J. Polym. Sci. Part A Polym. Chem.*, 2016, **54**, 1289–1298.

8 G. Liou and C. Chang, *Macromolecules*, 2008, **41**, 1667–1674.

9 M. J. Lee, Y. J. Kwak, W. C. Seok and S. W. Lee, *Polym. Bull.*, 2016, **73**, 2427–2438.

10 H.-J. Yen, S.-M. Guo and G.-S. Liou, *J. Polym. Sci. Part A Polym. Chem.*, 2010, **48**, 5271–5281.

11 H.-M. Wang and S.-H. Hsiao, *Polym. Chem.*, 2010, **1**, 1013–1023.

12 G.-S. Liou, N.-K. Huang and Y.-L. Yang, *Polymer*, 2006, **47**, 7013–7020.

13 N. Sun, Z. Zhou, D. Chao, X. Chu, Y. Du, X. Zhao, D. Wang and C. Chen, *J. Polym. Sci. Part A Polym. Chem.*, 2017, **55**, 213–222.

14 S.-H. Hsiao, H.-M. Wang and S.-H. Liao, *Polym. Chem.*, 2014, **5**, 2473–2483.

15 S.-H. Hsiao and C.-N. Wu, *Polym. Int.*, 2017, **66**, 916–924.

16 S.-H. Hsiao and J.-S. Han, *J. Polym. Sci. Part A Polym. Chem.*, 2017, **55**, 1409–1421.

17 Y.-C. Kung, G.-S. Liou and S.-H. Hsiao, *J. Polym. Sci. Part A Polym. Chem.*, 2009, **47**, 1740–1755.

18 H.-J. Yen and G.-S. Liou, *Chem. Commun.*, 2013, **49**, 9797–9799.

19 S.-W. Cheng, T. Han, T.-Y. Huang, B.-Z. Tang and G.-S. Liou, *Polym. Chem.*, 2018, **9**, 4364–4373.

20 Y.-C. Kung and S.-H. Hsiao, *J. Polym. Sci. Part A Polym. Chem.*, 2011, **49**, 3475–3490.

21 D. Bera, V. Padmanabhan and S. Banerjee, *Macromolecules*, 2015, **48**, 4541–4554.

22 H.-J. Yen, C.-L. Tsai, S.-H. Chen and G.-S. Liou, *Macromol. Rapid Commun.*, 2017, **38**, 1600715.

23 L.-C. Lin, H.-J. Yen, C.-J. Chen, C.-L. Tsai and G.-S. Liou, *Chem. Commun.*, 2014, **50**, 13917–13920.

24 W. Zhang, C. Wang, G. Liu, J. Wang, Y. Chen and R.-W. Li, *Chem. Commun.*, 2014, **50**, 11496–11499.

25 C.-J. Chen, H.-J. Yen, Y.-C. Hu and G.-S. Liou, *J. Mater. Chem. C*, 2013, **1**, 7623–7634.

26 L. Shi, H. Ye, W. Liu, G. Tian, S. Qi and D. Wu, *J. Mater. Chem. C*, 2013, **1**, 7387–7399.

27 C.-J. Chen, Y.-C. Hu and G.-S. Liou, *Polym. Chem.*, 2013, **4**, 4162–4171.

28 J. S. Meena, S. M. Sze, U. Chand and T.-Y. Tseng, *Nanoscale Res. Lett.*, 2014, **9**,

1–33.

29 Q.-D. Ling, D.-J. Liaw, C. Zhu, D. S.-H. Chan, E.-T. Kang and K.-G. Neoh, *Prog. Polym. Sci.*, 2008, **33**, 917–978.

30 Y. Yang, J. Ouyang, L. Ma, R. J.-H. Tseng and C.-W. Chu, *Adv. Funct. Mater.*, 2006, **16**, 1001–1014.

31 L. Fu, L. Cao, Y. Liu and D. Zhu, *Adv. Colloid Interface Sci.*, 2004, **111**, 133–157.

32 C. Li, W. Fan, B. Lei, D. Zhang, S. Han, T. Tang, X. Liu, Z. Liu, S. Asano, M. Meyyappan, J. Han and C. Zhou, *Appl. Phys. Lett.*, 2004, **84**, 1949–1951.

33 Y. Yang, L. Ma and J. Wu, *MRS Bull.*, 2004, **29**, 833–837.

34 R. F. Service, *Science*, 2001, **293**, 1746.

35 J. C. Scott, *Science*, 2004, **304**, 62–63.

36 C.-J. Chen, H.-J. Yen, W.-C. Chen and G.-S. Liou, *J. Polym. Sci. Part A Polym. Chem.*, 2011, **49**, 3709–3718.

37 H.-J. Yen, J.-H. Chang, J.-H. Wu and G.-S. Liou, *Polym. Chem.*, 2015, **6**, 7758–7763.

38 N. Yamazaki, F. Higashi and J. Kawabata, *J. Polym. Sci. Polym. Chem. Ed.*, 1974, **12**, 2149–2154.

39 F. Higashi, S.-I. Ogata and Y. Aoki, *J. Polym. Sci. Polym. Chem. Ed.*, 1982, **20**, 2081–2087.

40 N. Yamazaki and F. Higashi, in *Polymerization Processes. Advances in Polymer Science*, Springer Berlin Heidelberg, Berlin, Heidelberg, 1981, vol. 38, pp. 1–25.

41 N. Yamazaki, M. Matsumoto and F. Higashi, *J. Polym. Sci. Polym. Chem. Ed.*, 1975, **13**, 1373–1380.

42 Y. Oishi, H. Takado, M. Yoneyama, M.-A. Kakimoto and Y. Imai, *J. Polym. Sci. Part A Polym. Chem.*, 1990, **28**, 1763–1769.

43 R. Duran, M. Ballauff, M. Wenzel and G. Wegner, *Macromolecules*, 1988, **21**, 2897–2899.

44 H. Kim, S.-B. Park, Jin Chul Jung and W.-C. Zin, *Polymer*, 1996, **37**, 2845–2852.

45 D. H. Wang, Z. Shen, M. Guo, S. Z. D. Cheng and F. W. Harris, *Macromolecules*, 2007, **40**, 889–900.

46 Y. S. Kim and J. C. Jung, *J. Polym. Sci. Part A Polym. Chem.*, 2002, **40**, 1764–

1774.

47 Y. Chen, R. Wombacher, J. H. Wendorff and A. Greiner, *Polymer*, 2003, **44**, 5513–5520.

48 F. Chiu, *Adv. Mater. Sci. Eng.*, 2014, **2014**, 1–18.

49 A. J. Campbell, D. D. C. Bradley and D. G. Lidzey, *J. Appl. Phys.*, 1997, **82**, 6326–6342.

50 J. Frenkel, *Phys. Rev.*, 1938, **54**, 647–648.

51 K. L. Jensen, *J. Vac. Sci. Technol. B Microelectron. Nanom. Struct.*, 2003, **21**, 1528–1544.

52 C. Laurent, E. Kay and N. Souag, *J. Appl. Phys.*, 1988, **64**, 336–343.

53 P. Mark and W. Helfrich, *J. Appl. Phys.*, 1962, **33**, 205–215.

54 M. A. Lampert, *Phys. Rev.*, 1956, **103**, 1648–1656.

55 S. Ghatak and A. Ghosh, *Appl. Phys. Lett.*, 2013, **103**, 122103.

Supporting Information

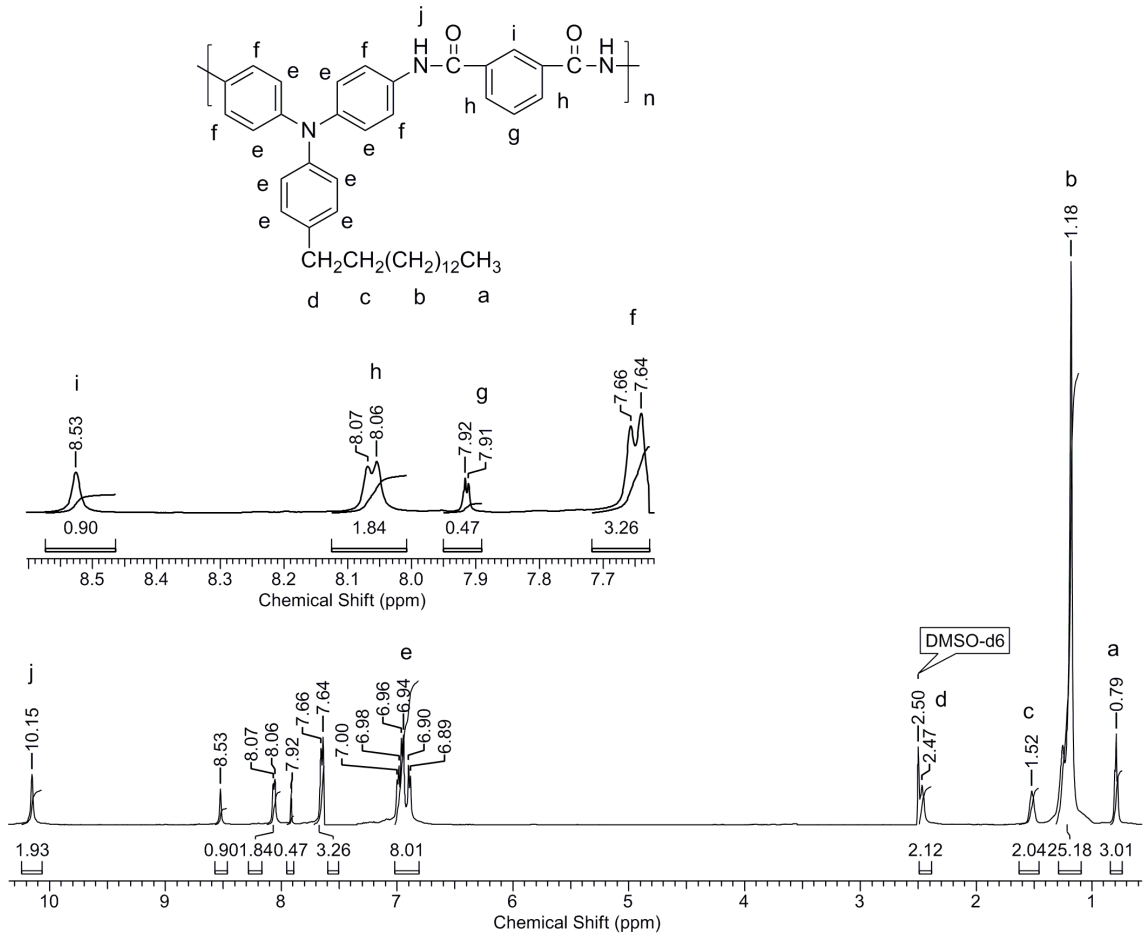

Figure SI 4b.1 ^{1}H-NMR spectrum ($CDCl_3$ + DMSO-d_6) of PA-IPA

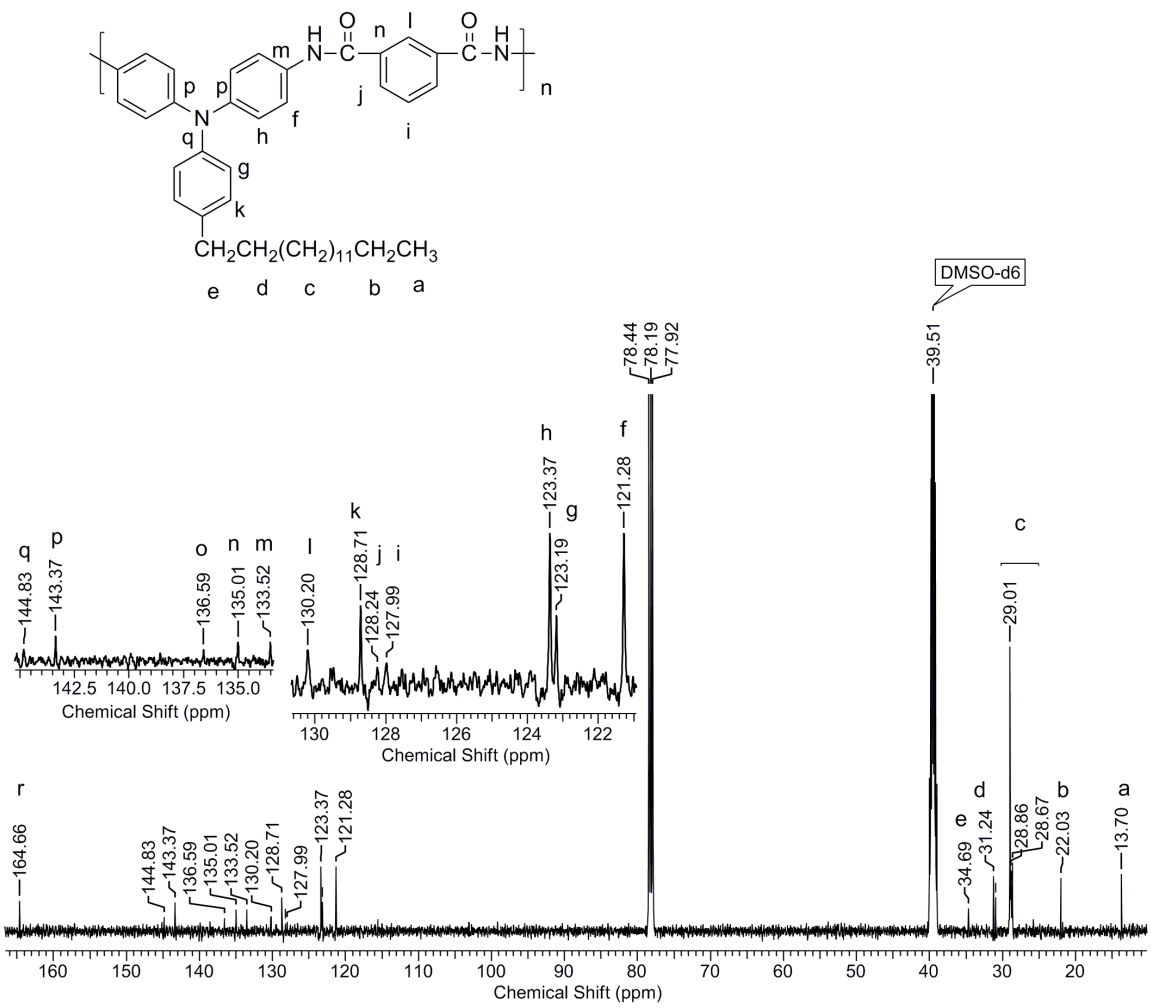

Figure SI 4b.2 ^{13}C-NMR spectrum ($CDCl_3$ + DMSO-d_6) of PA-IPA

CHAPTER 4 (c)

Partially Bio-Based Triarylamine-Containing Polyazomethines: Synthesis, Characterisation and Evaluation for Memory Devices

4c.1 Introduction

Aromatic polyazomethines (PAMs) are high performance polymers with excellent thermal, mechanical, optical and electronic properties. PAMs are conjugated polymers which are isoelectronic with polyphenylenevinylenes.[1] They are formed from the polycondensation of aromatic diamines and dialdehydes. Their applications in various fields currently under research include biological fields, liquid crystal materials, photoluminescence, photovoltaic devices (eg. solar cells), etc.[2] Introduction of the interesting triphenylamine moiety into the polyazomethine structure leads to the formation of polymers with interesting properties.[3–6] Such polymers have mostly been investigated for optoelectronic applications. Donor-acceptor[7–15] type polyazomethines based on triarylamines are interesting applicants for polymer-based RRAM devices.[16–28] Scanty literature is available regarding the evaluation of triarylamine-containing polyazomethines in polymer resistive random access materials (RRAM), which include the protonic-acid doped polyazomethine with excellent operative uniformity and multilevel storage reported by Hu[29] *et al*. Zhang[10] *et al* have reported linear and hyperbranched triarylamine-based polyazomethines with uniform distribution of HRS and LRS.

In the present work, aromatic triarylamine-containing polyazomethines were synthesised from a partially bio-based triarylamine-containing diamine derived from cashew nut shell liquid, namely, 4, 4’-diamino-4"pentadecyltriphenylamine (DPTA). DPTA was polycondensed with terephthalaldehyde and isophthalaldehyde and a 50:50 mol % mixture of isophthalaldehyde and terephthalaldehyde in NMP and HMPA (1:1 v/v) at room temperature. The synthesised aromatic polyazomethines were characterised by inherent viscosity measurements, GPC studies, FT-IR, ^{1}H-NMR, ^{13}C-NMR spectroscopy, X-ray diffraction, thermogravimetric analysis (TGA), differential scanning calorimetric studies (DSC) and UV analysis. Thereafter, PAZ-based memory devices were fabricated and their performance was evaluated. To the best of our knowledge, this is the first report of partially bio-based polyazomethines evaluated for memory devices.

4c.2 Experimental

4c.2.1 Materials

4, 4'-Diamino-4"pentadecyltriphenylamine (DPTA) was synthesised as described in **Chapter 3**. Terephthalaldehyde (Sigma Aldrich, India) and isophthalaldehyde (Sigma Aldrich, India) were sublimed before use. Hexamethylphosphoramide (HMPA) (Sigma Aldrich, India) was used after distillation while N-methyl-2-pyrrolidone (NMP) was distilled over calcium hydride (Sigma Aldrich, India) prior to use. Lithium chloride (LiCl) (Sigma Aldrich, India) was activated by heating at 180 °C for 8 h before utilisation for polymerisation.

4c.2.2 Measurements

FT-IR spectra were recorded with ATR mode using Bruker α-T spectrophotometer in the range of 4000 to 500 cm^{-1}. ^{1}H and ^{13}C-NMR spectra were recorded on Bruker-AV 400 and 500 MHz spectrometer using chloroform-*d* as solvent and TMS as an internal standard. Molecular weights of the polyazomethines were measured on ThermoFinnigan gel permeation chromatograph (GPC) in chloroform using polystyrene as the calibration standard. Concentration of polymers used was 5 mg dL^{-1}. Inherent viscosity of the polymers was measured using 0.5 % (w/v) solution of polymer in chloroform at 25 ± 0.1 °C. Ubbelohde suspended level viscometer was used to determine inherent viscosity according to the following equation:

$$n_{inh} = \frac{2.303}{C} x \log \frac{t}{t_0}$$

where t and t_0 are flow times of polymer solution and solvent, respectively and C is the concentration of polymer solution. X-Ray diffraction analysis was performed on Rigaku MicroMax-007HF X-ray diffractometer at 40 kV and 30 mA. Thermo gravimetric analysis (TGA) of the polymers was performed on Perkin Elmer: STA 6000 between temperatures of 30 °C to 900 °C with a heating rate of 10 °C min^{-1}, under nitrogen. Glass transition temperatures (T_g) were determined from differential scanning calorimetry (DSC) experiments carried out on TA Q-100 instrument with sample heating rate of 5 °C min^{-1} under nitrogen atmosphere. T_g values of the polyazomethines were determined from the second heating cycles. UV–Vis spectra were measured on Specord 210 plus Analytic Jena spectrophotometer. Cyclic voltammetric experiments were carried out on CH Instruments Electrochemical Analyzer.

4c.2.3 Polyazomethine synthesis: typical procedure

Into a 50 mL three- necked round bottom flask equipped with a magnetic stirring bar, a nitrogen inlet and a guard tube were added DPTA (0.3 g, 6.6 x 10^{-4} mol), terephthalaldehyde (0.0809 g, 6.6 x 10^{-4} mol), 1-methyl-2-pyrrolidinone (1.9 mL), hexamethylphosphoramide (1.9 mL) and lithium chloride (0.103 g). The reaction mixture was stirred at room temperature for 48 h under a steady stream of nitrogen. Thereafter, the viscous reaction mixture was poured into methanol (500 mL) to yield the fibrous polymer which was isolated by filtration. The polymer was further purified by reprecipitation of concentrated chloroform solution of the polymer into methanol (500 mL). This polymer was designated as PAZ-TPA.

A similar synthetic protocol was applied for the synthesis of polyazomethines from the polycondensation of DPTA with isophthalaldehyde (PAZ-IPA) and a 50:50 mole % of terephthalaldehyde and isophthalaldehyde (PAZ-IPA+TPA).

4c.2.4 Optical measurements

UV-Vis spectra of chloroform solutions of polyazomethines (10^{-5} M) were recorded on Specord 210 plus Analytic Jena spectrophotometer. UV-Vis spectra of free-standing films of polyazomethines were also recorded.

4c.2.5 Memory device characterisation

Memory devices were fabricated by drop-casting chloroform solutions of PAZ-TPA, PAZ-IPA and PAZ-IPA+TPA (1 mg/mL) onto FTO plates (1.5 cm x 1.5 cm) and dried in an oven at 160 °C for 48 h. Uniformity of polyazomethine thin films was ensured by drop-casting a single layer onto the FTO glass plates. The FTO plates used were previously sonicated in dilute soap solution for 10 min, followed by sequential sonication in deionised water (4 times, 10 min) and isopropyl alcohol (15 min). Finally, the FTO plates were boiled in isopropyl alcohol and dried before memory device fabrication. **Fig 4c.1** represents schematic structure of developed memory devices. Programmable memristor characterisation system (Arc ONE) was used to evaluate the resistive switching characteristics of polyazomethine-based devices. During all electrical measurements, the top Aluminium (Al) electrode was biased and bottom FTO electrode was grounded. Following parameters were kept constant during electrical measurements; signal type: staircase, maximum amplitude of the positive and negative voltage pulse: ±2

V, step width: 100 ms, read voltage: 0.20 V and interpulse time: 10 ms. For endurance and retention measurements, the pulse width of positive and negative pulses was 100 µs.

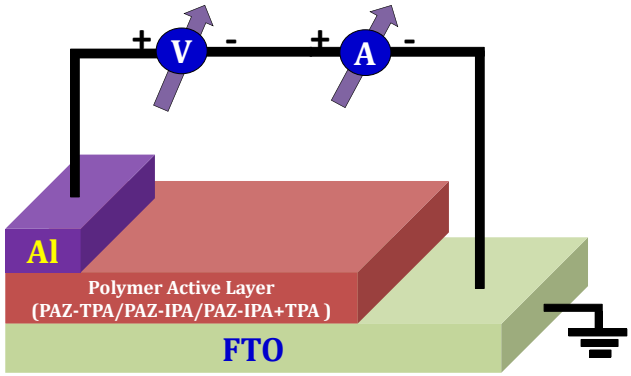

Figure 4c.1 Schematic structure of triarylamine-containing polyazomethine based memory devices.

4c.3 Results and Discussion

4c.3.1 Polyazomethine synthesis

Aromatic polyazomethines are generally synthesised by the polycondensation of aromatic diamines and dialdehydes in polar aprotic solvents such as *N*,*N*-dimethylacetamide, 1-methyl-2-pyrrolidinone, *N*,*N*-dimethylformamide, dimethyl sulfoxide, hexamethylphosphoramide or polar protic solvents, such as *m*-cresol.In this study, a mixture of DPTA, a commercially available dialdehyde (terephthalaldehyde, isophthalaldehyde or a mixture of both) and LiCl was stirred in a 1:1 mixture of 1-methyl-2-pyrrolidinone and hexamethylphosphoramide for a period of 48 h (**Scheme 4c.1**).

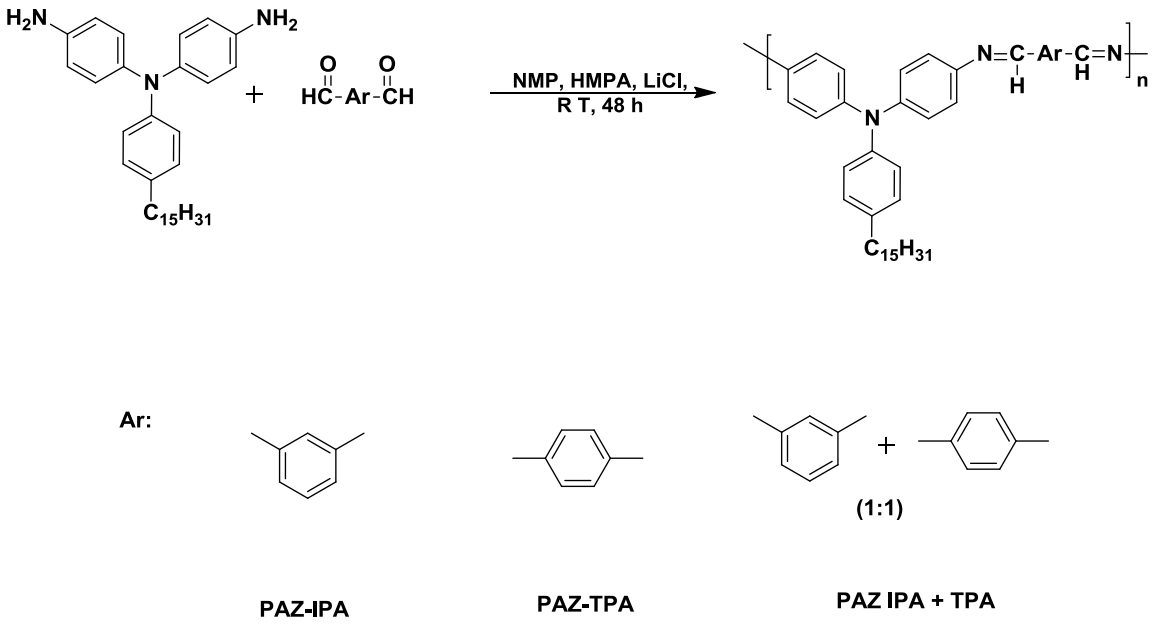

Scheme 4c.1 Synthesis of triarylamine-containing polyazomethines

The results of synthesis of polyazomethines are collected in **Table 4c.1**. Inherent viscosities of the synthesised polyazomethines were observed to be in the range 0.51 – 0.65 dL g^{-1}, indicating the formation of reasonably high molecular weights. This is further supported by the values of number average molecular weights (M_n), which were obtained in the range 12700 – 22000 g mol^{-1}. Molecular weights (M_n) determined by GPC measurements are not absolute due to the employment of polystyrene as standard. Orange free-standing, flexible films were cast from chloroform solutions of the polymers (**Fig 4c.2**).

Table 4c.1 Results of synthesis of triarylamine-containing polyazomethines

Polyazomethine	η_{inh} (dL/g)[a]	Molecular weight[b] (g mol^{-1})		Dispersity (M_w/M_n)
		M_n	M_w	
PAZ-TPA	0.65	22000	40000	1.8
PAZ-IPA	0.51	12700	21800	1.7
PAZ-IPA +TPA	0.56	18300	35400	1.9

a: η_{inh} was measured using 0.5% (w/v) solution of polyazomethines in chloroform at 25 °C ± 1°C
b: Determined through GPC in chloroform, using polystyrenes as calibration standard

Figure 4c.2 PAZ-TPA film cast from chloroform

The molecular structures of polyazomethines were investigated by FT-IR, ^{1}H-NMR and ^{13}C-NMR spectroscopic analysis. In **Fig 4c.3** is presented the representative FT-IR spectrum of PAZ-TPA. ^{1}H-NMR spectrum of PAZ-TPA is depicted in **Fig 4c.4** while the ^{13}C-NMR spectrum is presented in **Fig 4c.5**.

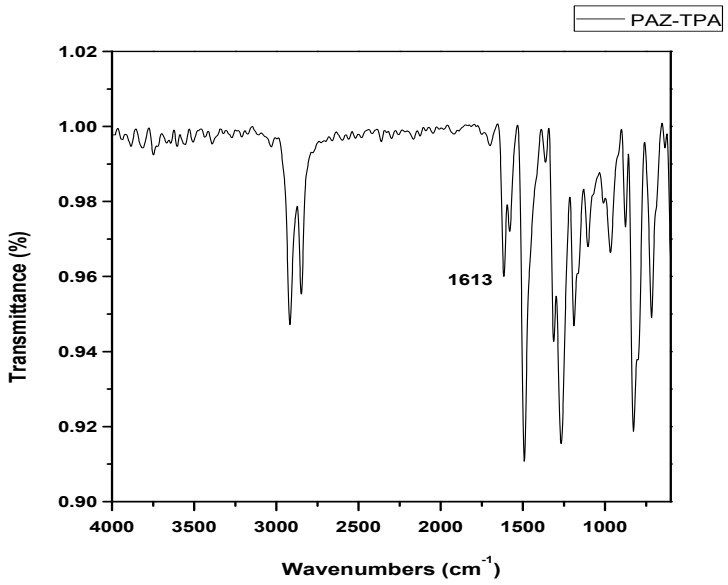

Figure 4c.3 FT-IR spectrum of PAZ-TPA film

An absorption band was observed at 1613 cm^{-1}, characteristic of imine linkage (HC=N-), thus confirming the formation of polyazomethine.

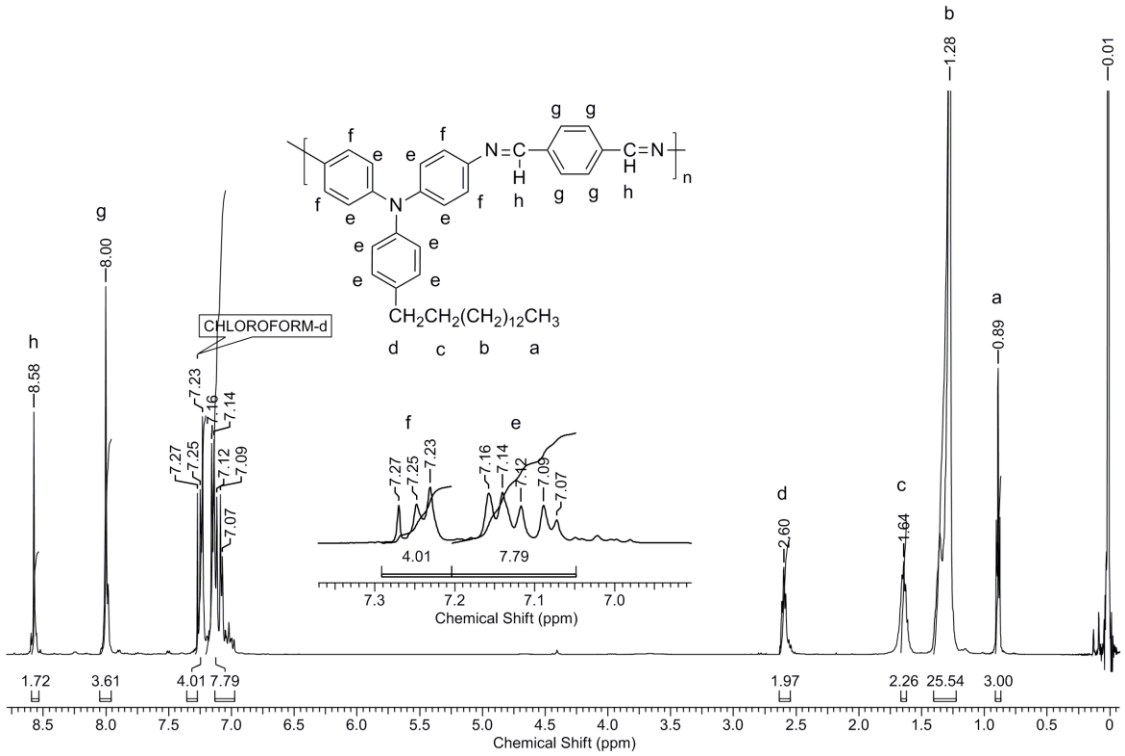

Figure 4c.4 ^{1}H-NMR spectrum ($CDCl_3$) of PAZ-TPA.

A singlet observed at 8.58 δ ppm was assignable to proton attached to the azomethine linkage (**h**). The protons belonging to the phenylene moiety derived from terephthalaldehyde (**g**) resonated at 8.00 δ ppm in the form of a singlet. A doublet which appeared at 7.24 δ ppm could be ascribed to four protons (**f**) belonging to the triarylamine moiety. The remaining protons of the triarylamine moiety (**e**) resonated as a multiplet in the range 7.06 – 7.17 δ ppm. The benzylic protons (**d**) of the pentadecyl chain appeared as a triplet at 2.60 δ ppm. The methylene protons adjacent to the benzylic protons (**c**) appeared at 1.64 δ ppm as a quintet while the remaining methylene protons resonated in the range 1.23 – 1.40 δ ppm as a multiplet. The terminal methyl protons belonging to the pentadecyl chain appeared at 0.89 δ ppm as a triplet.

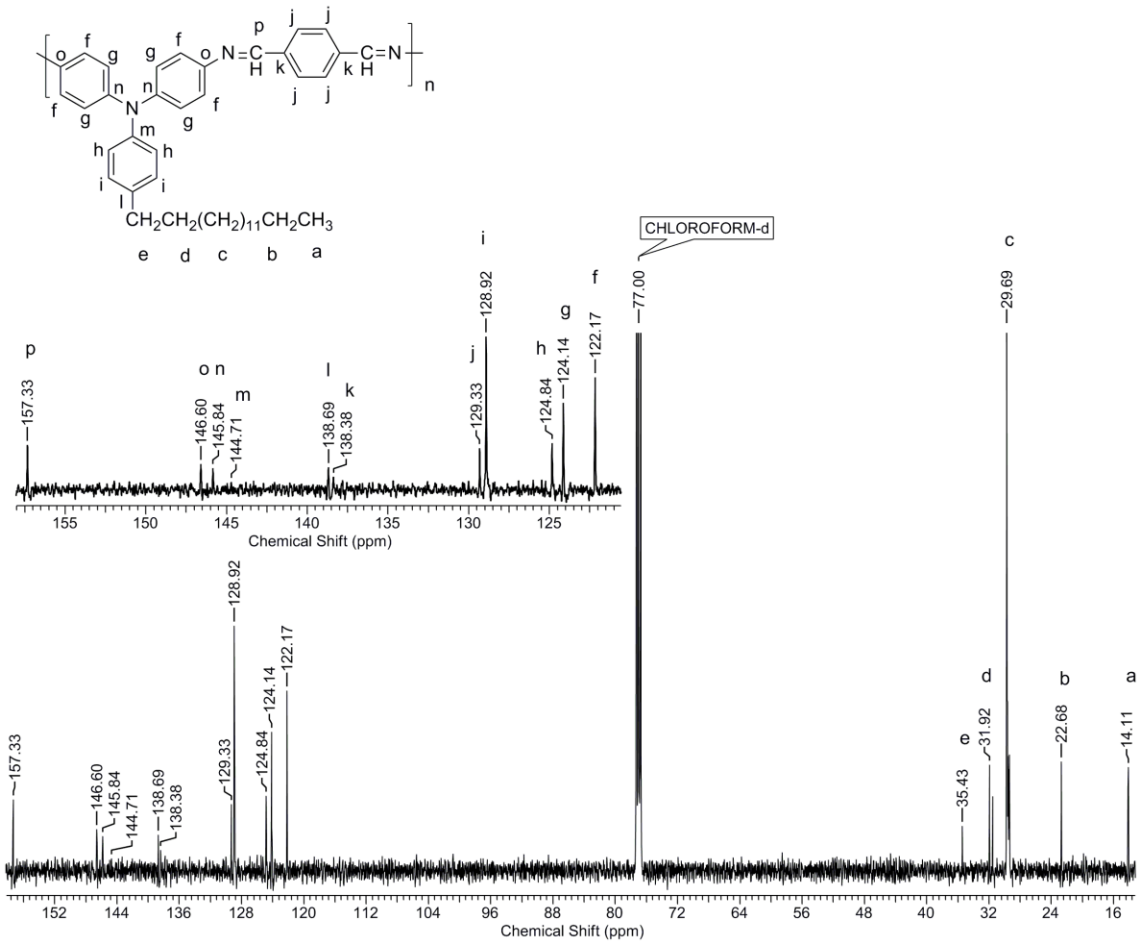

Figure 4c.5 ^{13}C-NMR spectrum ($CDCl_3$) of PAZ-TPA.

^{13}C-NMR spectrum of PAZ-TPA was assigned with the help of the corresponding DEPT spectrum. The signal corresponding to imine carbon (**p**) resonated at 157.33 δ ppm. The aromatic carbons belonging to triarylamine moiety (**f-i**, **l-o**) appeared in the range 127.17 – 124.84 δ ppm and 138.69 – 157.33 δ ppm while the carbon atom belonging to phenylene moiety derived from terephthalaldehyde (**j**, **k**) resonated at 129.33 δ ppm and 138.38 δ ppm. The signal appearing at 35.43 δ ppm could be ascribed to the benzylic carbon of the pentadecyl chain (**e**). The methylene carbon atoms (**d**, **c**, **b**) appeared in the range 22.68 – 31.92 δ ppm. The terminal methyl carbon of the pentadecyl chain resonated at 14.11 δ ppm.

FT-IR, ^{1}H-NMR and ^{13}C-NMR spectroscopy together contributed towards confirmation of the structure of the synthesised polyazomethine.

4c.3.2 Solubility and X-ray diffraction studies

The solubility of the synthesised polyazomethines at 3 wt % was studied and the results are compiled in **Table 4c.2**.

Table 4c.2 Solubility of triarylamine-containing polyazomethines

Polyazomethine	Solvent								
	$CHCL_3$	THF	NMP	DMAc	DMF	DMSO	*m*-cresol	Pyridine	Nitro benzene
PAZ-IPA	++	++	+	+-	+-	--	++	++	++
PAZ-TPA	++	++	+	+-	+-	--	++	++	++
PAZ-IPA+TPA	++	++	+	+-	+-	--	++	++	++

--, Insoluble; + soluble on heating at 70 °C; ++, soluble at room temperature; +-, partially soluble or swollen

The synthesised polyazomethines were soluble in chloroform, tetrahydrofuran, *m*-cresol, pyridine and nitro benzene at room temperature and in NMP on heating. This excellent solubility of the polyazomethines results due to the presence of the pendent pentadecyl chain which disrupts interchain packing thus acting as a handle for interaction with solvent molecules, in addition to the presence of bulky triarylamine moiety which also has a packing disruptive effect. Consequently, the synthesised polyazomethines are easily solution processable.

Wide angle X-ray diffraction (WAXD) patterns of the synthesised polyazomethines are collected in **Fig 4c.6**. The broad hump observed around the region $2\theta \sim 20°$ suggests that the polyazomethines are amorphous in nature. The amorphous nature of the polyazomethines arises due to the introduction of the packing disruptive pentadecyl chains and the bulky triphenylamine moiety. In addition, a sharp peak was observed in the low angle region, $2\theta \sim 2.9°$. As reported in literature[30–34] such a peak results from X-ray diffractions occurring from the spacing between the polymer chains, implying the existence of layered or stacked structures. Such layered/ stacked structures result due to the presence of pendent alkyl chains which are oriented away from the main chain and interdigitated.

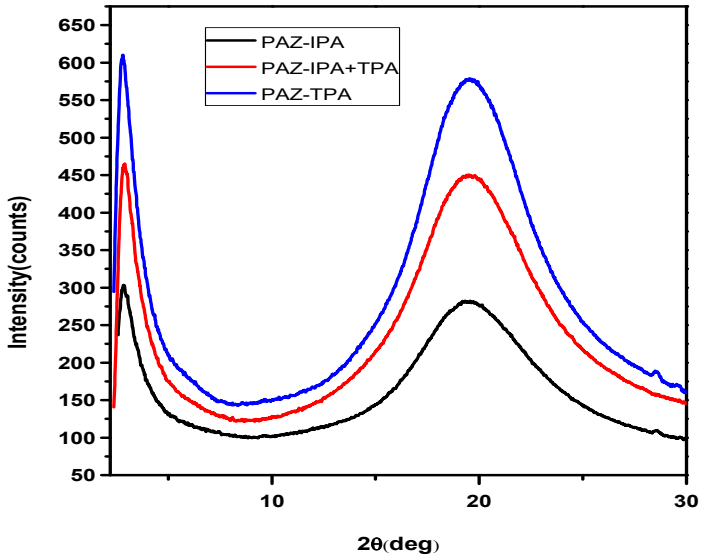

Figure 4c.6 X-Ray diffractograms of triarylamine-containing polyazomethines

4c.3.3 Thermal Properties

The thermal properties of synthesised polyazomethines were studied through thermogravimetric analysis (TGA) and differential scanning calorimetry (DSC) studies. The results of these studies are summarised in **Table 4c.3**. In **Fig 4c.7** is depicted the TG curves of synthesised polyazomethines while in **Fig 4c.8** is presented DTG curve of PAZ-TPA, along with the TG curve. The DSC curves are provided in **Fig 4c.9**.

Table 4c.3 Thermal properties of triarylamine-containing polyazomethines

Polyazomethine	Polyazomethine structure	T_g (°C)[a]	T_{10} (°C)[b]	T_5 (°C)[c]	Char yield (%)[d]
PAZ-IPA	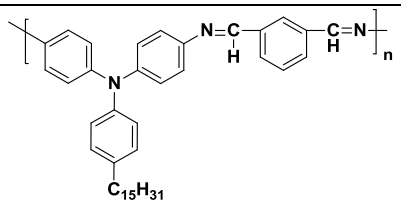	56 (251)	436	421 (T_5=452)	24
PAZ-TPA	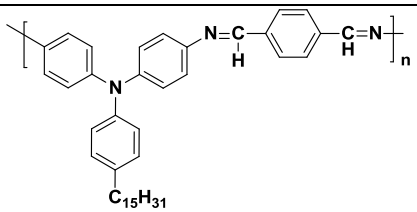	78 (310)	431	423 (T_5=450)	25
PAZ-IPA+TPA	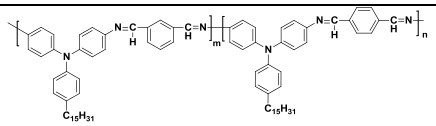	69	435	420	25

a: Measured by DSC from second heating scan with heating rate of 10 °C/min under nitrogen atmosphere.
b: 10 % weight loss on TGA thermograms at a heating rate of 10 °C/min under nitrogen atmosphere.
c: 5 % weight loss on TGA thermograms at a heating rate of 10 °C/min under nitrogen atmosphere.
d: Char yield measured at 900 °C.
values in parenthesis refer to the values of reference polyazomethines based on 4,4'-diaminotriphenylamine and corresponding dialdehydes and the data was collected from relevant reference.[3]

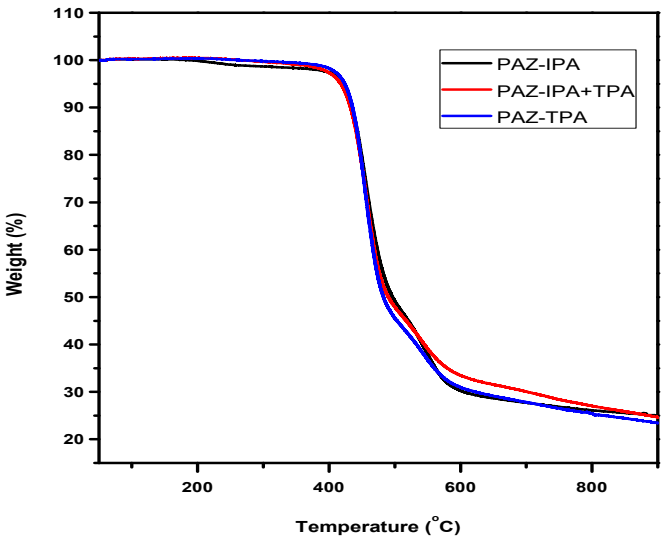

Figure 4c.7 TG curves of triarylamine-containing polyazomethines

The synthesised polyazomethines were observed to display T_{10} and T_5 values in the range 431 – 436 °C, and 420 – 423 °C, respectively, indicating good thermal stability. When the T_5 values are compared with corresponding reference polyazomethines devoid of pentadecyl chains, it is observed that the T_5 values of synthesised polyazomethines are slightly lower. The pentadecyl chains present in the synthesised polymers thus lower the thermal stability to a certain extent due to their thermally labile nature.

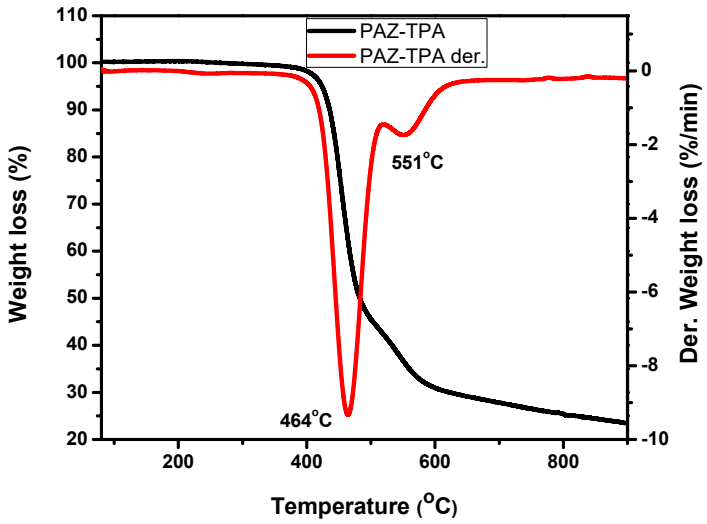

Figure 4c.8 DTG curve of PAZ-TPA

DTG curve of PAZ-IPA revealed that maximum degradation occurred at 464 °C accompanied by minor degradation at 551 °C.

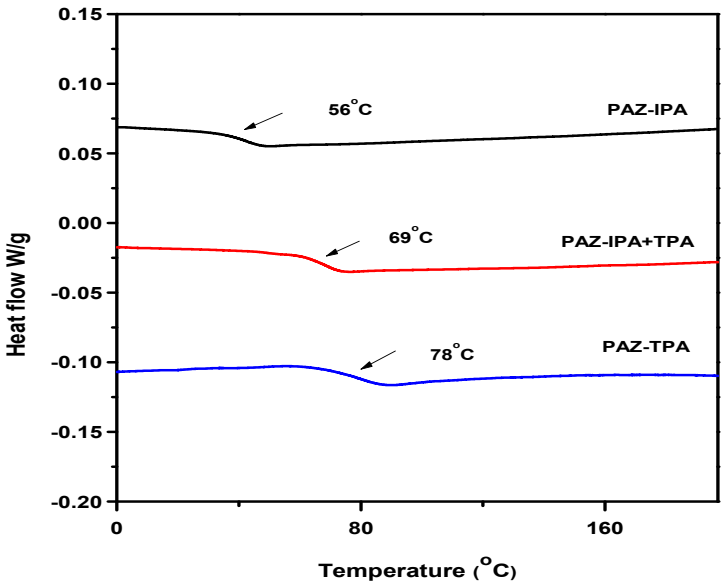

Figure 4c.9 DSC curves of triarylamine-containing polyazomethines

From the DSC curves of the synthesised polyazomethines it was observed that T_g values were obtained in the range 56 – 78 °C. PAZ-TPA, being most rigid in nature, displayed highest T_g value, while PAZ-IPA, possessing least rigidity due to "kinked" backbone structure, displayed lowest T_g value. PAZ-IPA+TPA, displayed T_g value in between that of PAZ-TPA and PAZ-IPA. When these T_g values are compared with those of reference polyazomethines, it was observed that a drastic decrease in T_g values occurred with the introduction of pentadecyl chains in the polymer backbone. The pentadecyl chain disrupts chain packing, thus exerting a flexibilising effect leading to improved segmental mobility and lowering of T_g. The huge difference in T_{10} and T_g values indicate that a large processing window is available for processing these polymers through melt processing. Additionally, it is to be noted that these polymers also display excellent solubility. Thus these polyazomethines show excellent potential for solution as well as melt processability.

4c.3.4 Optical properties

The optical properties of the synthesised polyazomethines were investigated through UV-Vis spectroscopic studies. UV-Vis spectra of polyazomethines in chloroform solutions are depicted in **Fig 4c.10** and the λ_{max} values and λ_{onset} (cut-off wavelength) values along with band-gap energies is compiled in **Table 4c.4**.

Table 4c.4 Optical properties of triarylamine-containing polyazomethines

Polyazomethine	Absorbance		Optical band gap energy
	λ_{max} (nm)[a]	λ_{onset} (nm)[b]	E_g^{Opt}(eV)[c]
PAZ-IPA	410	926	1.33
PAZ-IPA+TPA	435	955	1.29
PAZ-TPA	453	981	1.26

a: UV-Vis absorption maxima measured in chloroform (10^{-5} M) at room temperature.
b: The cut-off wavelength determined from UV-vis transmission spectra of polymer films
c: Obtained from $E_g^{opt} = 1240/\lambda_{onset}$.

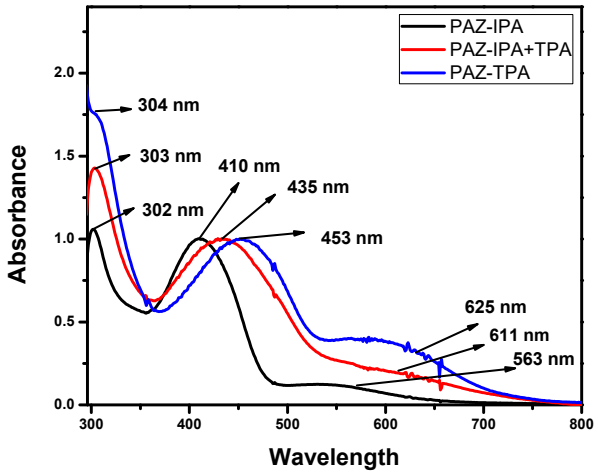

Figure 4c.10 UV-Vis spectra of triarylamine-containing polyazomethines.

The absorption bands at 302 – 304 nm were generated from the π-π* transitions occurring in the aromatic rings; while the absorption bands at 410 – 453 nm was observed due to π-π* transitions along the conjugated backbone as well as due to the conjugation between aromatic rings and the nitrogen atom. The bands at 563 – 525 nm were observed due to occurrence of *n*-π* transitions. PAZ-TPA, with maximum conjugation, exhibited maximum red-shifted UV absorption values. A similar trend was observed in the case of λ_{onset} values. Optical band-gap energy values were observed to be in the range 1.26 – 1.33 eV. Lowest band-gap energy value was observed in the case of PAZ-TPA with maximum conjugation. Additionally, the values of band-gap energy

indicate that synthesised polyazomethines exhibit semiconductor-like behaviour and may appropriately be investigated for semiconductor applications.

4c.3.5 Memory device characterisation

The memory devices based on synthesised polyazomethines, PAZ-TPA, PAZ-IPA and PAZ-IPA+TPA, were evaluated for resistive memory application. **Fig 4c.11** represents the current-voltage (I-V) characteristics of PAZ-TPA, PAZ-IPA, and PAZ-TPA+IPA memory devices in linear and semilog scale, respectively. The resistive switching direction is indicated by the continuous arrows.

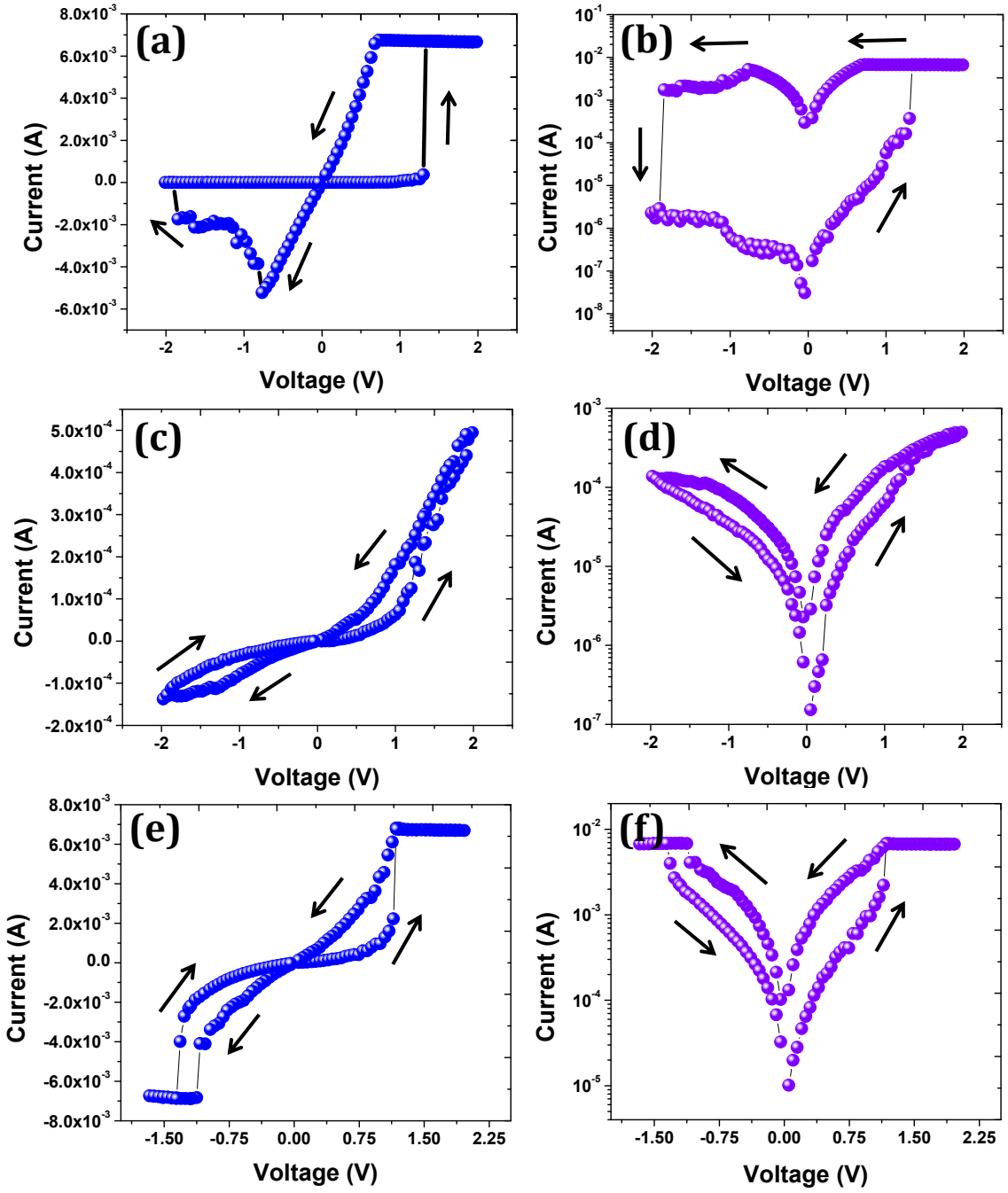

Figure 4c.11 Current-voltage (I-V) characteristics of **(a-b)** PAZ-TPA, **(c-d)** PAZ-IPA, and **(e-f)** PAZ-TPA+IPA memory devices in linear and semilog scale, respectively. The arrows indicate the direction of resistive switching.

All three fabricated devices exhibited typical pinched hysteresis loop confined to the first and third quadrant, qualifying these devices as memristors (**Fig 4c.11 (a)**, **Fig 4c.11 (c)** and **Fig 4c.11 (e)**). The memristor is a fourth fundamental circuit element with

memory, passivity and nonlinearity properties. These properties are very important for the development of next-generation memory devices and to rectify the scaling, power consumption and speed issues of the conventional complementary metal-oxide-semiconductor based memory devices.[35] **Fig 4c.11 (a-b)** shows the bistable I-V characteristics of memory device fabricated from PAZ-TPA. Initially, the device exhibited low conduction (current: 2.6 x 10^{-8} A) or "OFF" state or high resistive state (HRS). As the voltage was increased from 0 V to 1.29 V, the current gradually increased to 3.7 x 10^{-4} A. Thereafter, the current increased abruptly to 6.6 x 10^{-3} A. The device thus transitioned from a HRS ("OFF" state) to a low resistance state (LRS) ("ON" state) at a particular voltage, 1.29 V, called V_{SET} (SET voltage). This electrical transition in a memory device functions as a "SET" process. In the next voltage sweeping, i.e. 2 V to -2V, the current varied between 6.6 x 10^{-3} A to 2.84 x 10^{-4} A. At voltage of -1.90 V, there was an abrupt change in current from 1.7 x 10^{-3} A to 2.8 x 10^{-6} A which further decreased gradually to 2.9 x 10^{-8} A. This particular voltage (-1.90 V) serves as the V_{RESET} voltage, at which the device transitions from LRS to HRS. This electrical transition is referred to as the "RESET" process. These results indicated that the memory device fabricated from PAZ-TPA showed excellent bipolar ON and OFF switching behaviour, in addition to being rewritable in nature.

Fig 4c.11 (c-d) shows the I-V characteristics of memory device fabricated from PAZ-IPA. A positively biased potential sweep was applied from 0 V to 2 V. Contrary to the memory device prepared from PAZ-TPA, the device fabricated from PAZ-IPA showed a smooth and gradual increase in current from 1.5 x 10^{-7} A to 5 x 10^{-4} A. Thus the device transitioned from HRS to LRS culminating at 2 V (V_{SET} voltage). Subsequently, as the voltage was varied from 2 V to 0 V, the current decreased smoothly from 5 x 10^{-4} A to 2 x 10^{-6} A. When a negatively biased potential sweep was applied from 0 V to -2 V, the current was again observed to increase gradually to 1.42 x 10^{-4} A at -2.0 V. Subsequently, on change of voltage from -2 V to 0 V, the current of the device was observed to decrease smoothly from 1.4 x 10^{-4} A to 1.3 x 10^{-7} A. This transition constitutes an HRS process, occurring on changing voltage from -2.0 V (V_{RESET}) to 0 V. The observed results indicated that memory device based on PAZ-IPA was rewritable in nature, showing a smooth transition between "ON" state and "OFF" state.

Fig 4c.11 (e-f) demonstrates I-V curves generated from memory device based on PAZ-IPA+TPA. The device was initially in a low conduction state, with current in the order of 1.5 x 10^{-7} A. As a positively biased potential sweep from 0 V to 2 V was applied, the current was observed to increase gradually to 2.2 x 10^{-3} A, which further increased abruptly to 7.6 x 10^{-3} A at 1.15 V (V_{SET}). Subsequently, as the voltage was varied from 2 V to -2 V, the current remained in the range of 1 x 10^{-4} A to 7 x 10^{-3} A. The transition into LRS constitutes a "set" process. At the voltage of -1.3 V (V_{RESET}), current decreased abruptly from 6 x 10^{-3} A to 4 x 10^{-3} A, undergoing the "RESET" process. Thereafter, as the voltage was swept from -1.3 V to 0 V, the current decreased gradually to 1 x 10^{-5} A. Since both LRS and HRS processes were observed to occur during one switching cycle, the memory device fabricated from PAZ-IPA+TPA was also rewritable in nature. It is interesting to note that the I-V characteristics of the memory device fabricated from PAZ-IPA+TPA showed both smooth increase/decrease of conduction (as in the case of PAZ-IPA) and an abrupt change in conduction (as seen in the case of PAZ-TPA).The co-existence of both abrupt and smooth resistive switching properties is useful for the development of the high-performance resistive switching memory devices and to mimic the biological synaptic properties

In addition to observing the electrical switching effect of fabricated memory devices, it is important to evaluate the performance of the memory devices in terms of endurance and retention. **Fig 4c.12 (a)** and **Fig 4c.12 (b**) represent the endurance and retention memory performance of PAZ-TPA, PAZ-IPA, and PAZ-IPA+TPA memory devices, respectively. The endurance cycling (**Fig 4c.12 (a)**) data was obtained from repetitive "set" and "reset" processes for 10000 cycles at a read voltage of 0.2 V. The multilevel data storage capability was investigated by applying ± 2 V positive and negative voltage pulse with a pulse width in the order of 100 µs. Formation of three resistive states, namely, high resistive state (HRS), intermediate resistive state (IRS) and low resistive state (LRS) was observed in all three memory devices, indicating that the developed devices are potential candidates for multilevel data storage application. All three resistive states were observed to persist even after 10000 switching cycles for PAZ-TPA and PAZ-IPA based devices. However, degradation in endurance was observed for PAZ-TPA+IPA based memory device. It is interesting to note that excellent memory

window (HRS to IRS and IRS to LRS ratio) was achieved for all three devices. The memory window for HRS to IRS is 10; while for IRS to LRS the memory window is about 100. These memory devices thus can potentially provide multi-level memory. Since the memory window is 10 and above, the memory devices can be used for practical purposes.[36] The retention memory performance (**Fig 4c.12 (b)**) test was done at a read voltage of 0.2 V. The three resistive states (HRS, IRS, and LRS) were seen to persist without degradation for over a test period of 1000 s. The endurance and retention studies indicated that the memory devices under study were non-volatile in nature.The results obtained for the developed devices are promising for the development of polymer-based multilevel data storage devices.

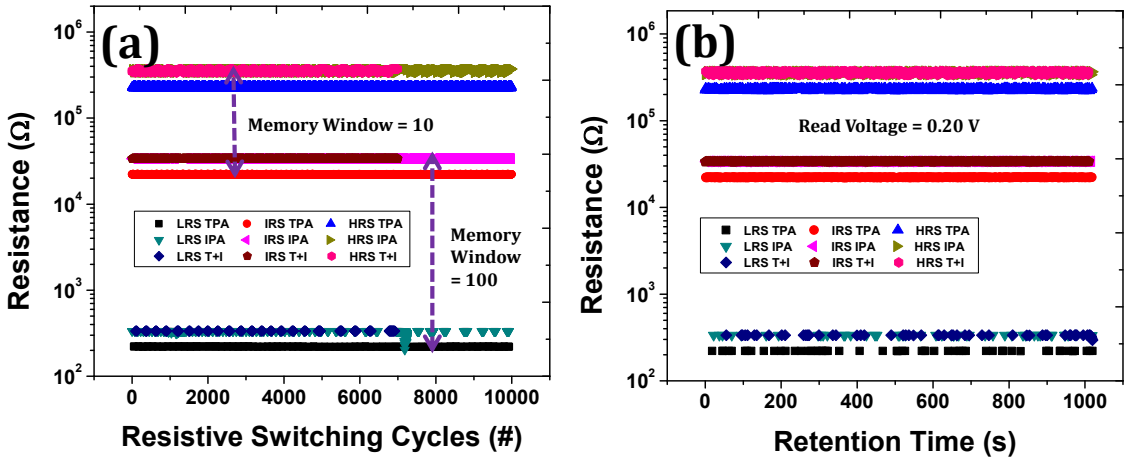

Figure 4c.12 (a) Endurance and **(b)** retention memory performance of PAZ-TPA, PAZ-IPA, and PAZ-TPA+IPA memory devices. Three resistance states *viz.* LRS, IRS, and HRS are observed in the developed devices.

The statistical distribution or cumulative probability of resistive switching states of PAZ-TPA, PAZ-IPA, and PAZ-TPA+IPA memory devices are shown in **Fig. 4c.13**. Furthermore, the performance comparison of polyazomethine memory devices based on statistical analysis is summarised in **Table 4c.5**.

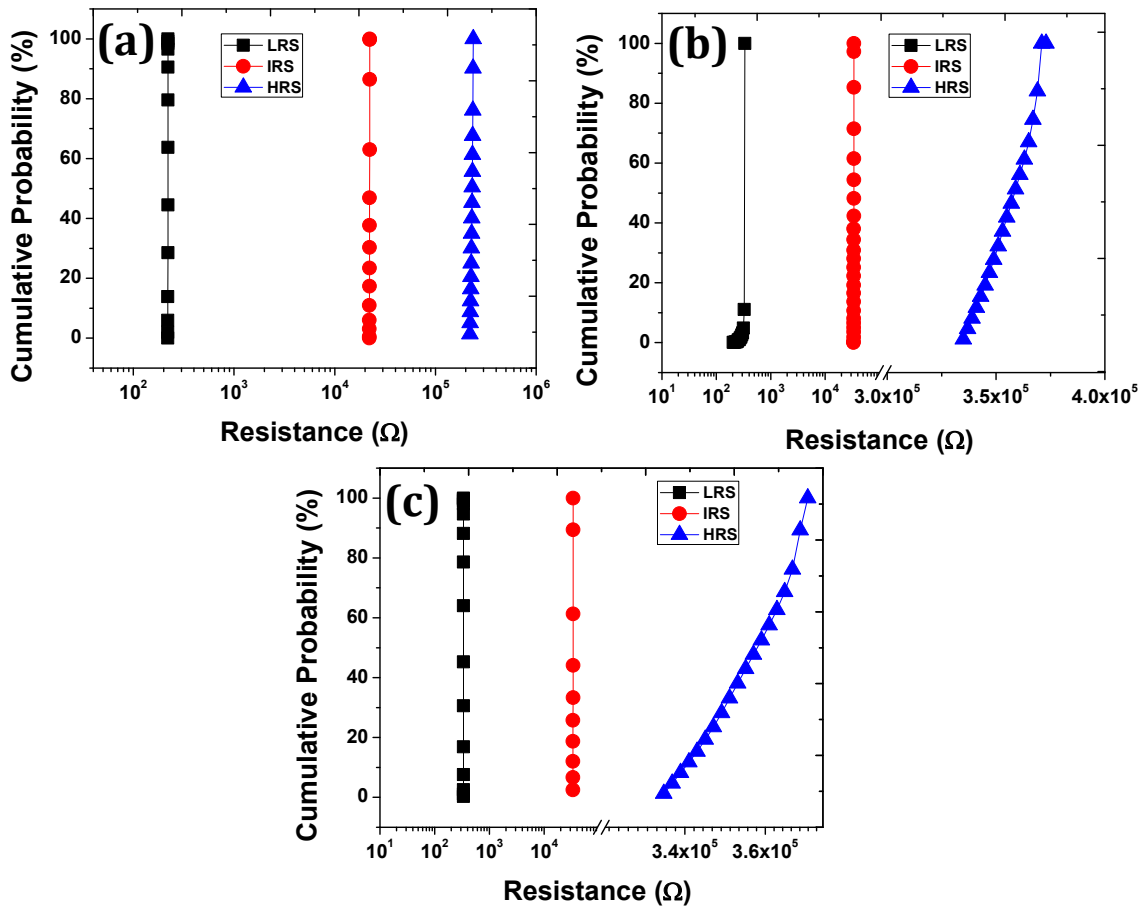

Figure 4c.13 Cumulative probability of resistive switching states of **(a-b)** PAZ-TPA, **(c-d)** PAZ-IPA, and **(e-f)** PAZ-TPA+IPA memory devices.

Table 4c.5 Performance comparison of triarylamine-containing polyazomethine memory devices

Polyazomethine	Average, μ (Ω)			Standard deviation, σ(Ω)			The coefficient of variation, σ/μ (%)		
	LRS	IRS	HRS	LRS	IRS	HRS	LRS	IRS	HRS
PAZ-TPA	220.46	22184.89	231076.64	0.1039	56.45	5057.04	0.04	0.25	2.18
PAZ-IPA	331.69	33785.02	357759.61	11.26	120.80	11004.63	3.39	0.35	3.07
PAZ-IPA+TPA	334.81	33778.15	357366.35	0.1160	120.73	10765.53	0.03	0.35	3.01

The statistical calculations give a good idea of the stability of resistive states of developed memory devices. The memory devices showed excellent stability for IRS and LRS with a low coefficient of variation in the range of 0.25 – 0.35 and 0.03 – 0.04, respectively, except for LRS of PAZ-IPA, which showed a coefficient of variation of 3.39. The stability of HRS was slightly low, with coefficient of variation in the range

2.18 – 3.07. The stability of the resistive states is graphically demonstrated in **Fig 4c.13**. PAZ-TPA, followed by PAZ-IPA+TPA showed excellent device stability as evidenced by very low values of standard deviation and coefficient of variation. The better stability of PAZ-TPA can be explained due to better extended π-π conjugation taking place in PAZ-TPA. The extended conjugation stabilises the CT (charge transfer complex) which, in turn, leads to the generation of stable resistive states. Memory device based on PAZ-IPA+TPA is stable due to more conjugated character by virtue of the presence of para-phenylene moieties which originate from the use of TPA as comonomer. In addition to this, the standard deviation of LRS and IRS are excellent for all three devices, whereas, HRS shows higher values of standard deviation for all three devices. This may be due to stochastic switching of HRS and leakage current. Considering the data obtained from the statistical analysis, PAZ-TPA and PAZ-TPA+IPA are good candidates for memory application, whereas gradual resistive switching observed in PAZ-IPA based memory devices makes it a good candidate for neuromorphic computing applications. Literature suggests that abrupt resistive switching devices are superior to gradual resistive switching counterparts for memory applications.[37,38] On the other hand, synaptic plasticity can be efficiently mimicked by gradual resistive switching based devices.[39–41]

The electrical switching characteristics and current conduction mechanisms prevalent in the memory devices were investigated by taking a closer look at I-V data. For this purpose, different regions of I-V curves were fitted in accordance with current conduction mechanisms known in literature.[42–49] The conduction mechanism of the developed devices is shown in **Fig 4c.14**. The double logarithmic I-V plot of the PAZ-TPA memory devices is shown in **Fig 4c.14 (a)**. The slope of the lower voltage range was found to be 1.28. This indicates that Ohmic conduction mechanism was dominant over this voltage range. The higher voltage region, with a slope of 5.24, was fitted according to Schottky conduction model, suggesting that Schottky conduction mechanism dominated over this voltage range (**Fig. 4c.14 (b)**). In the case of PAZ-IPA (**Fig. 4c.14 (c)**), the lower voltage region is well fitted with Ohmic conduction mechanism with a slope of 1.06. On the other hand, Schottky conduction mechanism is well fitted to the higher voltage region experimental data. Similarly, conduction mechanisms of the PAZ-IPA+TPA based memory device were governed by Ohmic and Schottky models in low

and high voltage regions, respectively. Thus, all three polyazomethine-based memory devices exhibited electrical conduction in accordance with Ohmic conduction model in the low voltage region. As the voltage was increased, a Schottky barrier was formed at Al and polymer interface due to the difference in work function between Al and HOMO of the polymers. The current is limited by charge injection. Subsequently, at the threshold voltage (V_{SET}), the electric-field induced charge transfer occurs, resulting in the generation of holes in HOMO of polymer, which delocates over conjugated triarylamine moieties and C=N linkages. The hole migration leads to a surge in current and the devices transition from OFF state to the ON state.

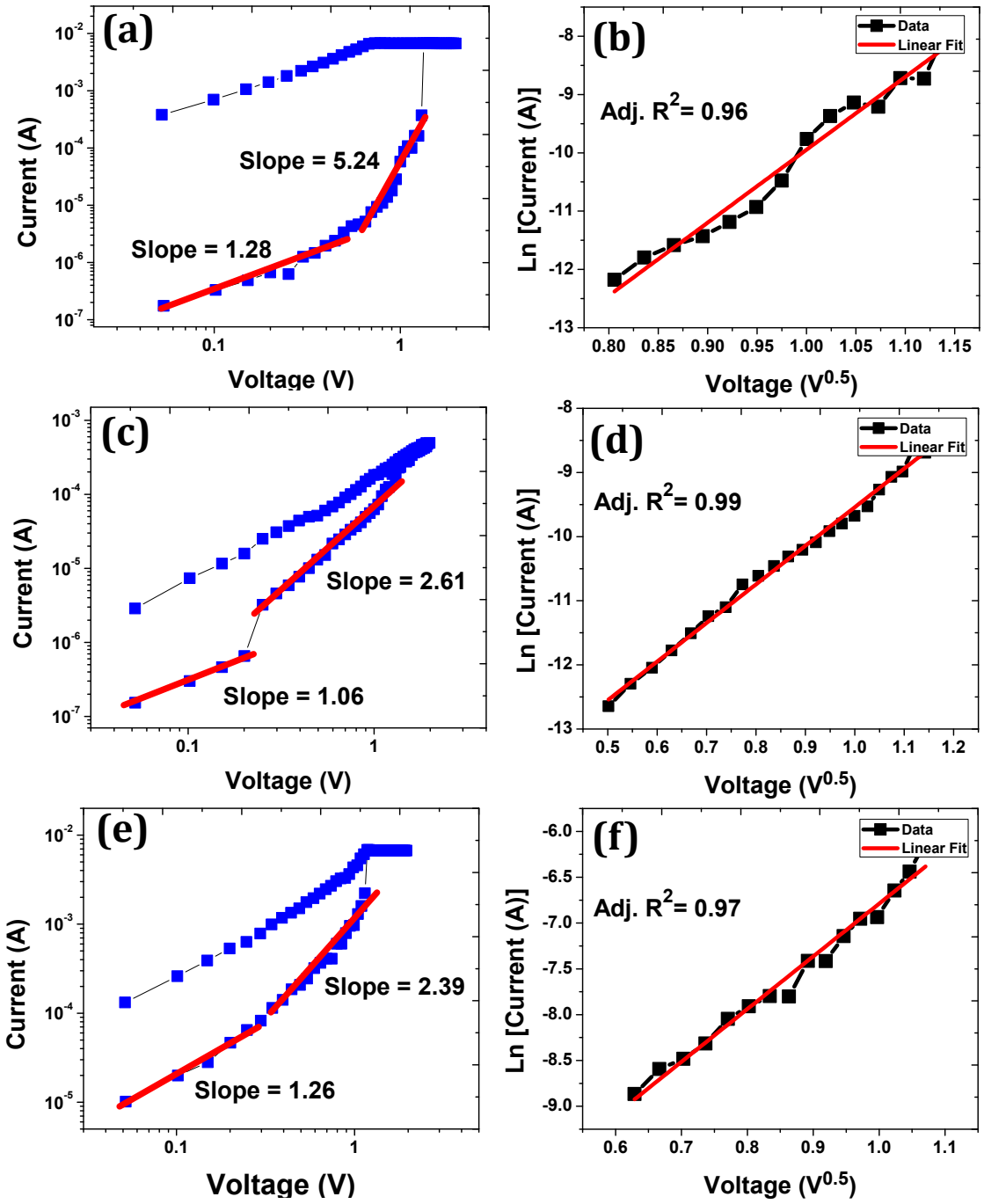

Figure 4c.14 Conduction mechanisms and high slope part data fitting of **(a-b)** PAZ-TPA, **(c-d)** PAZ-IPA, and **(e-f)** PAZ-TPA+IPA memory devices.

4c.4 Conclusions

1. Aromatic polyazomethines containing triarylamine moieties and pendent pentadecyl chains were synthesised by polycondensation of 4, 4'-diamino-4"pentadecyltriphenylamine (DPTA) with commercially available dialdehydes, namely,

terephthaldehyde, isophthaldehyde and a 50:50 % mixture of terephthaldehyde and isophthaldehyde.

2. Inherent viscosities and number average molecular weights were in the range 0.51 – 0.65 dL g^{-1} and 12700 – 22000 g mol^{-1}, respectively, suggestive of the formation of polyazomethines of reasonably high molecular weights.

3. The synthesised polymers were readily soluble in chloroform, tetrahydrofuran, *m*-cresol, pyridine and nitro benzene at room temperature. Flexible, free-standing, orange coloured films could be cast from chloroform solutions.

4. According to XRD analysis, synthesised polyazomethines were observed to be amorphous in nature due to the packing disruptive action of bulky triarylamine moiety and pendent pentadecyl chains.

5. T_{10} values obtained were in the range 431 – 463 °C, while T_g values were in the range 53 – 78 °C. The wide difference in T_g values and T_{10} values suggest that these polymers may be thermoplastically processed in melt state before thermal decomposition.

6. Optical band-gap values were found to be in the range 1.26 – 1.3 eV. These values indicated that synthesised polyazomethines show good potential for semiconductor applications.

7. The memory devices fabricated displayed three well defined memory states: HRS, IRS and LRS, with memory window of 10 and 100. Thus, these memory devices can provide multi-level data storage. The endurance and retention performance indicated that the fabricated memory devices were non-volatile in nature. It was determined from statistical analysis of the developed resistive states in the memory devices that HRS, IRS and LRS exhibited good uniformity. Schottky conduction mechanism was observed to dominate in the high voltage region.

References

1 J. Cai, H. Niu, C. Wang, L. Ma, X. Bai and W. Wang, *Electrochim. Acta*, 2012, **76**, 229–241.

2 A. Iwan, B. Boharewicz, K. Parafiniuk, I. Tazbir, L. Gorecki, A. Sikora, M. Filapek and E. Schab-Balcerzak, *Synth. Met.*, 2014, **195**, 341–349.

3 J. C. Hindson, B. Ulgut, R. H. Friend, N. C. Greenham, B. Norder, A. Kotlewski and T. J. Dingemans, *J. Mater. Chem.*, 2010, **20**, 937–944.

4 D. Sek, A. Iwan, B. Jarzabek, B. Kaczmarczyk, J. Kasperczyk, Z. Mazurak, M. Domanski, K. Karon and M. Lapkowski, *Macromolecules*, 2008, **41**, 6653–6663.

5 H.-J. Niu, Y.-D. Huang, X.-D. Bai and X. Li, *Mater. Lett.*, 2004, **58**, 2979–2983.

6 A. Iwan, M. Palewicz, A. Chuchmała, L. Gorecki, A. Sikora, B. Mazurek and G. Pasciak, *Synth. Met.*, 2012, **162**, 143–153.

7 C.-J. Chen, Y.-C. Hu and G.-S. Liou, *Polym. Chem.*, 2013, **4**, 4162–4171.

8 Q.-D. Ling, F.-C. Chang, Y. Song, C.-X. Zhu, D.-J. Liaw, D. S.-H. Chan, E.-T. Kang and K.-G. Neoh, *J. Am. Chem. Soc.*, 2006, **128**, 8732–8733.

9 C.-J. Chen, H.-J. Yen, W.-C. Chen and G.-S. Liou, *J. Polym. Sci. Part A Polym. Chem.*, 2011, **49**, 3709–3718.

10 W. Zhang, C. Wang, G. Liu, J. Wang, Y. Chen and R.-W. Li, *Chem. Commun.*, 2014, **50**, 11496–11499.

11 G. Liu, B. Zhang, Y. Chen, C.-X. Zhu, L. Zeng, D. Siu-Hung Chan, K.-G. Neoh, J. Chen and E.-T. Kang, *J. Mater. Chem.*, 2011, **21**, 6027–6033.

12 K.-L. Wang, Y.-L. Liu, J.-W. Lee, K.-G. Neoh and E.-T. Kang, *Macromolecules*, 2010, **43**, 7159–7164.

13 H.-C. Wu, A.-D. Yu, W.-Y. Lee, C.-L. Liu and W.-C. Chen, *Chem. Commun.*, 2012, **48**, 9135–9137.

14 D.-J. Liaw, K.-L. Wang, Y.-C. Huang, K.-R. Lee, J.-Y. Lai and C.-S. Ha, *Prog. Polym. Sci.*, 2012, **37**, 907–974.

15 J.-H. Wu, H.-J. Yen, Y.-C. Hu and G.-S. Liou, *Chem. Commun.*, 2014, **50**, 4915–4917.

16 Q.-D. Ling, D.-J. Liaw, C. Zhu, D. S.-H. Chan, E.-T. Kang and K.-G. Neoh, *Prog. Polym. Sci.*, 2008, **33**, 917–978.

17 C.-U. Pinnow and T. Mikolajick, *J. Electrochem. Soc.*, 2004, **151**, K13–K19.

18 G. Marsh, *Mater. Today*, 2003, **6**, 38–43.

19 J. S. Meena, S. M. Sze, U. Chand and T.-Y. Tseng, *Nanoscale Res. Lett.*, 2014, **9**, 1–33.

20 S. Seo, M. J. Lee, D. H. Seo, E. J. Jeoung, D.-S. Suh, Y. S. Joung, I. K. Yoo, I. R. Hwang, S. H. Kim, I. S. Byun, J.-S. Kim, J. S. Choi and B. H. Park, *Appl. Phys. Lett.*, 2004, **85**, 5655–5657.

21 M.-C. Wu, Y.-W. Lin, W.-Y. Jang, C.-H. Lin and T.-Y. Tseng, *IEEE Electron Device Lett.*, 2011, **32**, 1026–1028.

22 C.-Y. Huang, C.-Y. Huang, T.-L. Tsai, C.-A. Lin and T.-Y. Tseng, *Appl. Phys. Lett.*, 2014, **104**, 062901.

23 M.-H. Lin, M.-C. Wu, C.-H. Lin and T.-Y. Tseng, *IEEE Trans. Electron Devices*, 2010, **57**, 1801–1808.

24 J. J. Yang, M. D. Pickett, X. Li, D. A. A. Ohlberg, D. R. Stewart and R. S. Williams, *Nat. Nanotechnol.*, 2008, **3**, 429–433.

25 Y. Yang, J. Ouyang, L. Ma, R. J.-H. Tseng and C.-W. Chu, *Adv. Funct. Mater.*, 2006, **16**, 1001–1014.

26 L. Fu, L. Cao, Y. Liu and D. Zhu, *Adv. Colloid Interface Sci.*, 2004, **111**, 133–157.

27 C. Li, W. Fan, B. Lei, D. Zhang, S. Han, T. Tang, X. Liu, Z. Liu, S. Asano, M. Meyyappan, J. Han and C. Zhou, *Appl. Phys. Lett.*, 2004, **84**, 1949–1951.

28 Y. Yang, L. Ma and J. Wu, *MRS Bull.*, 2004, **29**, 833–837.

29 B. Hu, X. Zhu, X. Chen, L. Pan, S. Peng, Y. Wu, J. Shang, G. Liu, Q. Yan and R.-W. Li, *J. Am. Chem. Soc.*, 2012, **134**, 17408–17411.

30 R. Duran, M. Ballauff, M. Wenzel and G. Wegner, *Macromolecules*, 1988, **21**, 2897–2899.

31 H. Kim, S.-B. Park, Jin Chul Jung and W.-C. Zin, *Polymer*, 1996, **37**, 2845–2852.

32 D. H. Wang, Z. Shen, M. Guo, S. Z. D. Cheng and F. W. Harris, *Macromolecules*, 2007, **40**, 889–900.

33 Y. S. Kim and J. C. Jung, *J. Polym. Sci. Part A Polym. Chem.*, 2002, **40**, 1764–1774.

34 Y. Chen, R. Wombacher, J. H. Wendorff and A. Greiner, *Polymer*, 2003, **44**, 5513–5520.

35 A. C. Khot, N. D. Desai, K. V. Khot, M. M. Salunkhe, M. A. Chougule, T. M. Bhave, R. K. Kamat, K. P. Musselman and T. D. Dongale, *Mater. Des.*, 2018, **151**, 37–47.

36 T. D. Dongale, K. V. Khot, S. V. Mohite, N. D. Desai, S. S. Shinde, V. L. Patil, S. A. Vanalkar, A. V. Moholkar, K. Y. Rajpure, P. N. Bhosale, P. S. Patil, P. K. Gaikwad and R. K. Kamat, *Int. Nano Lett.*, 2017, **7**, 209–216.

37 C. Tan, Z. Liu, W. Huang and H. Zhang, *Chem. Soc. Rev.*, 2015, **44**, 2615–2628.

38 Y. Chen, G. Liu, C. Wang, W. Zhang, R.-W. Li and L. Wang, *Mater. Horizons*, 2014, **1**, 489–506.

39 P. Heremans, G. H. Gelinck, R. Müller, K.-J. Baeg, D.-Y. Kim and Y.-Y. Noh, *Chem. Mater.*, 2011, **23**, 341–358.

40 W.-P. Lin, S.-J. Liu, T. Gong, Q. Zhao and W. Huang, *Adv. Mater.*, 2014, **26**, 570–606.

41 J. Sun, Y. Fu and Q. Wan, *J. Phys. D. Appl. Phys.*, 2018, **51**, 314004.

42 F. Chiu, *Adv. Mater. Sci. Eng.*, 2014, **2014**, 1–18.

43 A. J. Campbell, D. D. C. Bradley and D. G. Lidzey, *J. Appl. Phys.*, 1997, **82**, 6326–6342.

44 J. Frenkel, *Phys. Rev.*, 1938, **54**, 647–648.

45 K. L. Jensen, *J. Vac. Sci. Technol. B Microelectron. Nanom. Struct.*, 2003, **21**, 1528–1544.

46 C. Laurent, E. Kay and N. Souag, *J. Appl. Phys.*, 1988, **64**, 336–343.

47 P. Mark and W. Helfrich, *J. Appl. Phys.*, 1962, **33**, 205–215.

48 M. A. Lampert, *Phys. Rev.*, 1956, **103**, 1648–1656.

49 S. Ghatak and A. Ghosh, *Appl. Phys. Lett.*, 2013, **103**, 122103.

CHAPTER 5

Partially Bio-Based Poly(arylene ether)s Containing Pendent Pentadecyl Chains

CHAPTER 5 (a)

Synthesis and Characterisation of Partially Bio-Based Poly(ether ether ether ketone)s Containing Pendent Pentadecyl Chains

5a.1 Introduction

Poly(ether ether ketone)s (PEEK) are a type of poly(arylene ether)s, belonging to the class of engineering thermoplastics endowed with excellent chemical resistance, thermo-oxidative stability, mechanical strength, excellent ultraviolet resistance and improved dielectric stability over a broad range.[1–9] PEEK are being actively pursued for several applications[10,11] such as fibres,[12,13] coatings,[14] nanocomposites[15–17] and membrane technology, especially membranes for fuel cells,[10,18–21] sorptive extraction[22] and gas separation.[23] However, commercially available PEEK (Victrex, which is based on 4,4'-difluorobenzophenone and hydroquinone) is generally difficult to process due to lack of solubility. It would be of interest to further expand the commercial applications of PEEK by developing new processable PEEK through structural modifications. Over the past few decades, active research efforts have been expended towards the development of processable PEEKs. Introduction of bulky groups such as phthalazinone,[24] phenyl,[25] biphenyl,[26] *t*-butyl,[27] naphthyl,[26] 9,9-diarylfluorene[28] and 3-(trifluoromethyl)phenyl[29] groups and flexible alkyl chains, eg., pentadecyl chains[30,31] and ethyl[32] groups, constitute two major strategies. It is interesting to note that in many such instances, introduction of such groups have also imparted interesting properties and opened up opportunities for exploration of applications in new fields. Kawasaki[28] *et al* developed PEEK based on 9,9-diarylfluorene which besides being processable, exhibited high refractive index and low birefringence. Wang *et al*[29] have reported PEEK bearing pendent 3-(trifluoromethyl)phenyl groups which displayed liquid crystalline properties. Ueda *et al*[32] developed photoreactive PEEK containing pendent ethyl groups which showed potential for use as negative photoresist materials. Additionally, most PEEK under study are derived from petrochemical sources. In the face of depleting oil-resources, it would also be advisable to develop PEEK based on monomers from renewable resources. A few reports concerning bio-derived poly(ether ketone)s based on 2,5-furandicarboxylic acid, isosorbide, isomannide and CNSL are known.[30,31,33–35]

In the present work is reported the synthesis and characterisation of a series of (co)poly(ether ether ether ketone)s possessing pendent pentadecyl chains as part of our continuing efforts in the quest to obtain processable high performance polymers. Additionally, the alkyl groups also hold potential for being UV-reactive and may be

explored for photoresist applications. (Co)poly(ether ether ether ketone)s were synthesised from partially bio-based bisphenol 4-(4-hydroxyphenoxy)-3-pentadecylphenol (HPPDP) obtained from renewable natural phenol CNSL. (Co)poly(ether ether ether ketone)s were synthesised by polycondensation of mixtures of HPPDP and bisphenol A (BPA) with 4,4'-difluorobenzophenone in *N*,*N*-dimethylacetamide at 180 °C. (Co)poly(ether ether ether ketone)s were characterised by inherent viscosity measurements, GPC studies, FT-IR, ^{1}H-NMR, ^{13}C-NMR spectroscopy, X-ray diffraction, thermogravimetric analysis (TGA) and differential scanning calorimetric studies (DSC). The influence of the pentadecyl chain on polymer properties was studied.

5a.2 Experimental

5a.2.1 Materials

4-(4-Hydroxyphenoxy)-3-pentadecylphenol (HPPDP) was synthesised as described in **Chapter 3**. Bisphenol A (BPA) (Sigma Aldrich, India) was sublimed before use. 4,4'-Difluorobenzophenone (Sigma Aldrich, India) was recrystallised from dry toluene and vacuum dried before use. *N*,*N*-Dimethylacetamide (Merck, India) was used after distillation over calcium hydride (Sigma Aldrich, India), while toluene (Merck, India) was distilled twice over calcium hydride before use. Anhydrous potassium carbonate (Thomas Baker, India) was utilised after drying under vacuum at 180 °C for 8 h.

5a.2.2 Measurements

FT-IR spectra of synthesised polymers were recorded with ATR mode using Bruker α-T spectrophotometer in the range of 4000 to 500 cm^{-1}. ^{1}H and ^{13}C-NMR spectra were recorded on Bruker-AV 400 and 500 MHz spectrometer using chloroform-*d* as solvent and TMS as an internal standard. Molecular weights of (co)poly(ether ether ether ketone)s were measured on ThermoFinnigan gel permeation chromatograph (GPC) in chloroform using polystyrene as the calibration standard. Concentration of polymers used was 3 mg dL^{-1}. Inherent viscosity of the polymers was measured using 0.5 % (w/v) solution of polymer in chloroform at 25 ± 0.1 °C. Ubbelohde suspended level viscometer was used to determine inherent viscosity according to the following equation:

$$n_{inh} = \frac{2.303}{C} x \log \frac{t}{t_0}$$

where t and t_0 are flow times of polymer solution and solvent, respectively and C is the concentration of polymer solution. X-Ray diffraction analysis was performed on Rigaku MicroMax-007HF X-ray diffractometer at 40 kV and 30 mA. Thermogravimetric analysis (TGA) of the polymers was performed on Perkin Elmer: STA 6000 between temperatures of 30 °C to 900 °C with a heating rate of 10 °C min^{-1}, under nitrogen. Glass transition temperatures (T_g) were determined from differential scanning calorimetry (DSC) experiments carried out on TA Q-100 instrument with sample heating rate of 10 °C min^{-1} under nitrogen atmosphere. T_g values of (co)poly(ether ether ether ketone)s were determined from the second heating cycles.

5a.2.3 Synthesis of (co)poly(ether ether ether ketone)s: typical procedure

Into a 50 mL three-necked round bottom flask equipped with a magnetic stirring bar, a nitrogen inlet, a reflux condenser and a Dean-Stark trap were added 4-(4-hydroxyphenoxy)-3-pentadecylphenol (HPPDP) (0.4 g, 9.69 x 10^{-4} mol), freshly distilled *N*, *N*-dimethylacetamide (6.75 mL, 14 wt % of total solute), anhydrous potassium carbonate (0.334 g, 2.42 x 10^{-3} mol), and dry toluene (50 mL). The reaction mixture was heated to reflux with stirring under a steady stream of nitrogen for 3 h and water was removed by azeotropic distillation with toluene. At the end of 3 h, toluene was removed from the reaction mixture and the reaction mixture was cooled to room temperature. 4,4'-Difluorobenzophenone (0.211 g, 9.69 x 10^{-4} mol) was added in one lot under a steady stream of nitrogen, and the reaction mixture was heated at 180 °C for 8 h. Subsequently, the viscous polymer solution was cooled to room temperature and poured into methanol (500 mL) with continuous stirring to precipitate the fibrous polymer. The polymer was isolated by filtration and further purified by reprecipitation from methanol. It was designated as PEK-100.

A similar procedure was followed for the synthesis of (co)poly(ether ether ether ketone)s with HPPDP feed mol % of 75 %, 50 %, 25 %, 10 % and 5 % designated as PEK-75, PEK-50, PEK-25, PEK-10 and PEK-05, respectively.

5a.3 Results and Discussion

5a.3.1 Synthesis of (co)poly(ether ether ether ketone)s

Aromatic polyetherketones have mainly been synthesised by nucleophilic substitution reaction[6,36–44] and electrophilic substitution reaction.[45–48] Aromatic

polyethers were reported for the first time by Bonner, who in 1962, obtained low molecular weight polyethers by Friedel-Crafts reaction of diphenyl ether and isophthaloyl chloride.[49] The electrophilic substitution route mainly suffers from difficulty in choosing suitable solvents and disposal of reaction by-products.[44] Synthesis of polyetherketones by nucleophilic aromatic substitution was reported for the first time by Johnson and Farnham in 1967.[50]

In this work, (co)poly(ether ether ether ketone)s were synthesised by nucleophilic aromatic substitution polycondensation of HPPDP or varying compositions of HPPDP and BPA with 4,4'-difluorobenzophenone in DMAc (**Scheme 5a.1**).

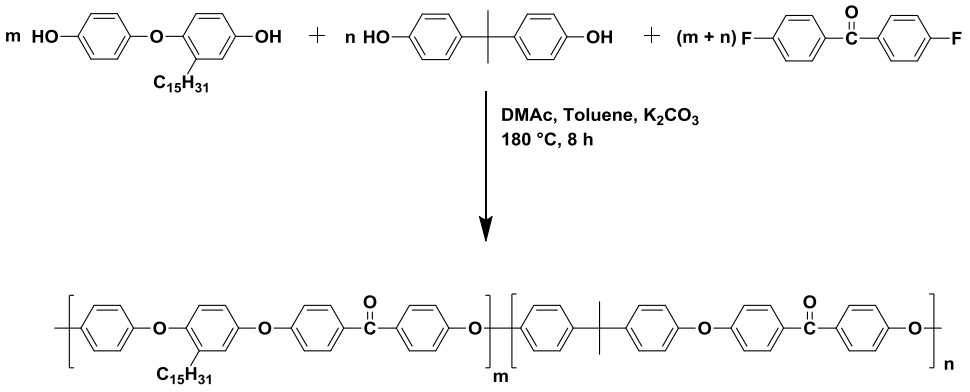

Scheme 5a.1 Synthesis of (co)poly(ether ether ether ketone)s

Anhydrous potassium carbonate was added to a stirred homogeneous solution of HPPDP or a mixture of HPPDP and BPA in DMAc and toluene. Water was formed as a result of generation of potassium bisphenolate salt, which was continuously removed from the reaction mixture as an azeotrope with toluene. Subsequent to expulsion of water and toluene, 4,4'-difluorobenzophenone was added to the reaction mixture. The formation of (co)poly(ether ether ether ketone)s resulted at 180 °C from aromatic nucleophilic substitution reaction (S_NAr) as the polymer forming reaction *via* the formation of an intermediate Meisenheimer complex.[51] The polymers were isolated by precipitation from viscous reaction mixture into methanol.

Polycondensation of HPPDP and that of BPA with 4.4'-difluorobenzophenone is expected to lead to formation of polymer containing ether-ether-ether-ketone units and ether-ether-ketone units, respectively. Thus, the copolymers formed by polycondensation

of a mixture of HPPDP and BPA with 4.4'-difluorobenzophenone would contain both types of sequences arranged in a random fashion.

The results of polymerisation are tabulated in **Table 5a.1.** The synthesised (co)poly(ether ether ether ketone)s were observed to have inherent viscosities in the range 0.61 – 0.73 dL g^{-1}, measured from respective chloroform solutions, indicating the formation of polymers possessing reasonably high molecular weights. This was further supported by the number average molecular weights (M_n), which were obtained from GPC analysis, in the range 26900 – 93400 g mol^{-1}. It is to be noted that the values obtained from GPC analysis are determined against polystyrene standards and hence cannot be considered as absolute values of molecular weights. Dispersities were in the range of 1.6 – 2.6. The (co)poly(ether ether ether ketone)s formed flexible, free-standing films by solution casting from corresponding chloroform solutions (**Fig 5a.1**).

Table 5a.1 Results of synthesis of (co)poly(ether ether ether ketone)s

(Co)poly(ether ether ether ketone)	Composition of diols (mol%)		η_{inh}(dL/g)[a]	Molecular weight[b] (g/mol)		Dispersity (M_w/M_n)
	HPPDP	BPA		M_n	M_w	
PEK-100	100	0	0.69	45900	76500	1.7
PEK-75	75	25	0.61	26900	43100	1.6
PEK-50	50	50	0.64	27000	53200	2.0
PEK-25	25	75	0.70	42800	70000	1.6
PEK-10	10	90	0.72	60400	160000	2.6
PEK-05	05	95	0.73	93400	180000	1.9

a: $\eta_{inh}$was measured using 0.5% (w/v) solution of (co)poly(ether ether ether ketone)s in chloroform at 25 °C ± 1°C
b: Determined through GPC in chloroform, using polystyrenes as calibration standard

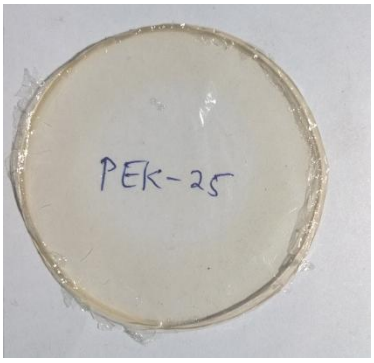

Figure 5a.1 PEK-25 film cast from chloroform

The synthesised (co)poly(ether ether ether ketone)s were analysed by FT-IR, ^{1}H-NMR and ^{13}C-NMR spectroscopic studies. FT-IR spectrum of a representative poly(ether ether ether ketone), PEK-100, is depicted in **Fig 5a.2**.

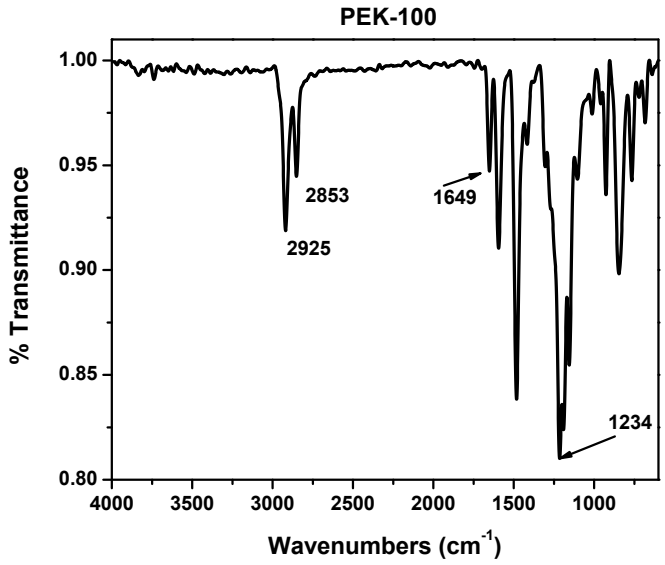

Figure 5a.2 FT-IR spectrum of PEK-100 film

Absorption band corresponding to ketone functionality appeared at 1649 cm^{-1} (C=O stretching) and a strong absorption band characteristic of ether functionality was observed at 1234 cm^{-1} (C-O-C stretch).

Representative ^{1}H-NMR spectrum of PEK-100 is presented in **Fig 5a.3**, while ^{13}C-NMR spectrum is presented in **Fig 5a.4**.

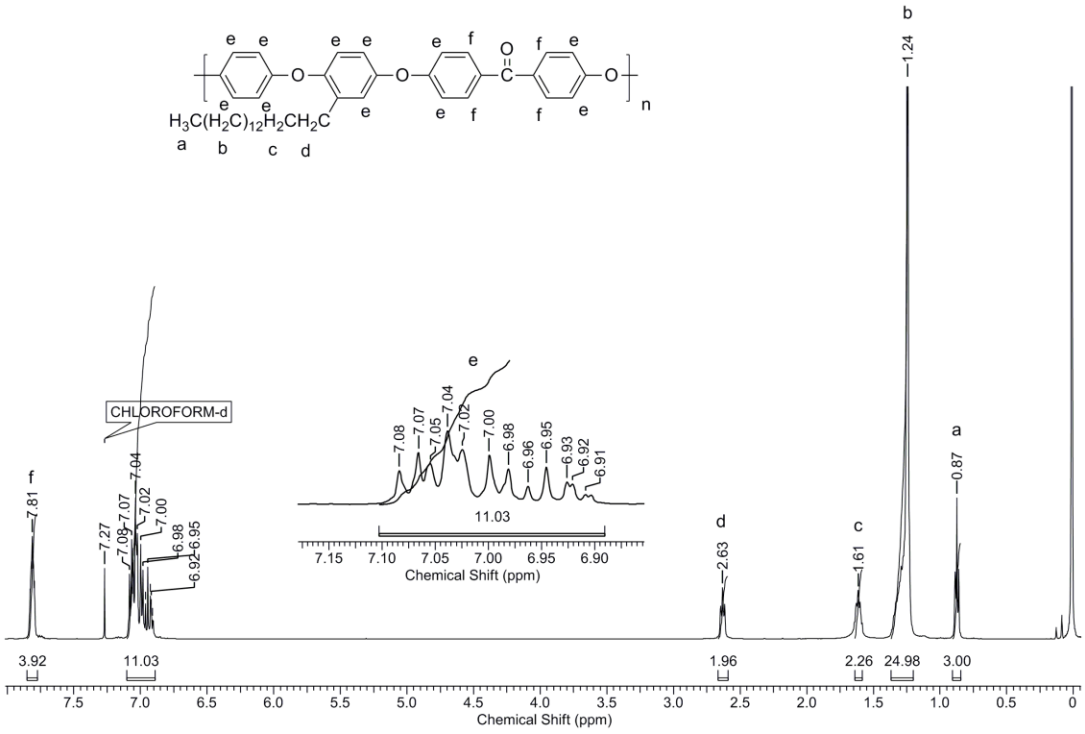

Figure 5a.3 ^{1}H-NMR spectrum ($CDCl_3$) of PEK-100.

The four aromatic protons *ortho* to the carbonyl group (**f**), appeared as a broad singlet in the region 7.88 – 7.85 δ ppm. The remaining aromatic protons (**e**) appeared as a complex multiplet in the range 6.89 – 7.10 δ ppm. The benzylic methylene protons (**d**) were observed as a triplet at 2.63 δ ppm while the methylene protons (**c**) appeared as a quintet centred at 1.61 δ ppm. Twenty four methylene protons (**b)** appeared as a multiplet in the range 1.19 – 1.37 δ ppm. The methyl protons (**a**) belonging to the pentadecyl chain resonated at 0.87 δ ppm as a triplet.

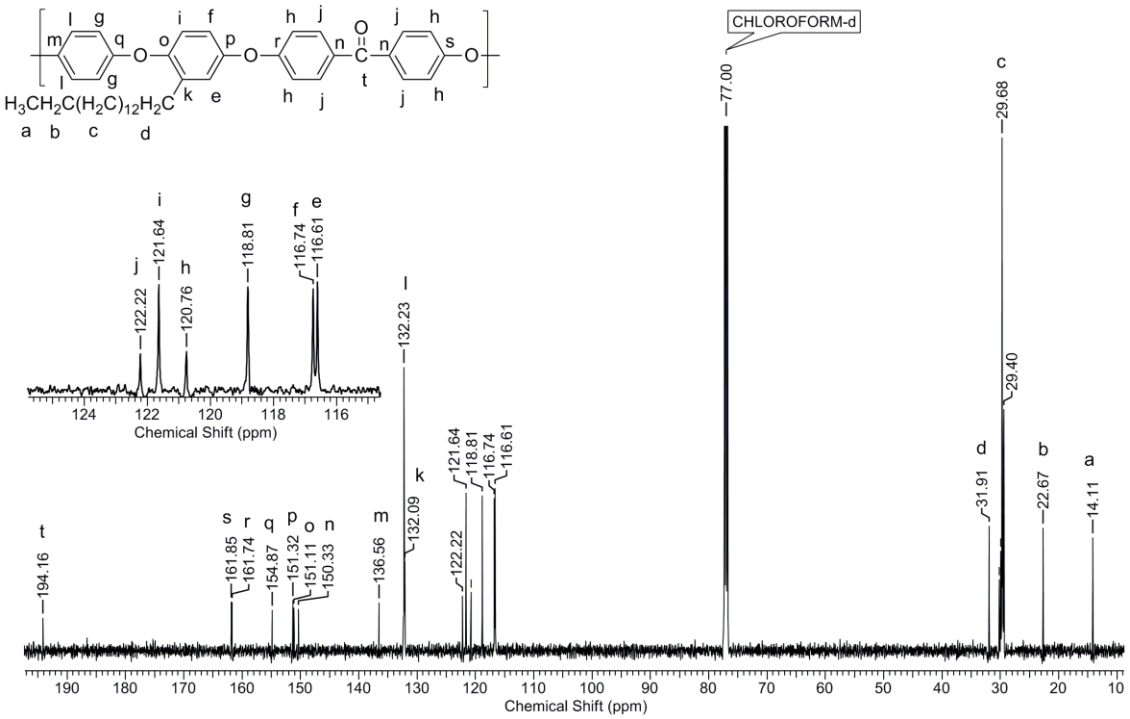

Figure 5a.4 ^{13}C-NMR spectrum ($CDCl_3$) of PEK-100.

^{13}C-NMR spectrum of PEK-100 was assigned with the help of the corresponding DEPT spectrum. The signal corresponding to carbonyl carbon (**t**) appeared at 194.16 δ ppm. The signals corresponding to aromatic carbon atoms (**e**-**s**) appeared in the region 161.85 – 116.61 δ ppm. The benzylic carbon atom (**d**) belonging to the pentadecyl chain resonated at 31.91 δ ppm while the methylene carbons (**c**) adjacent to it appeared in the range 29.24 – 30.31 δ ppm. Methylene carbon (**b**) adjacent to the terminal methyl group of the pentadecyl chain resonated at 22.67 δ ppm, while the signal corresponding to the methyl carbon (**a**) was observed at 14.11 δ ppm.

FT-IR, ^{1}H-NMR and ^{13}C-NMR spectral analysis indicated that the proposed structure of homopolymer PEK-100 showed good agreement with the proposed structure and thus together confirmed the structure of the synthesised polymer.

The composition of the synthesised copoly(ether ether ether ketone)s was investigated by ^{1}H-NMR spectroscopy (**Fig 5a.5**).

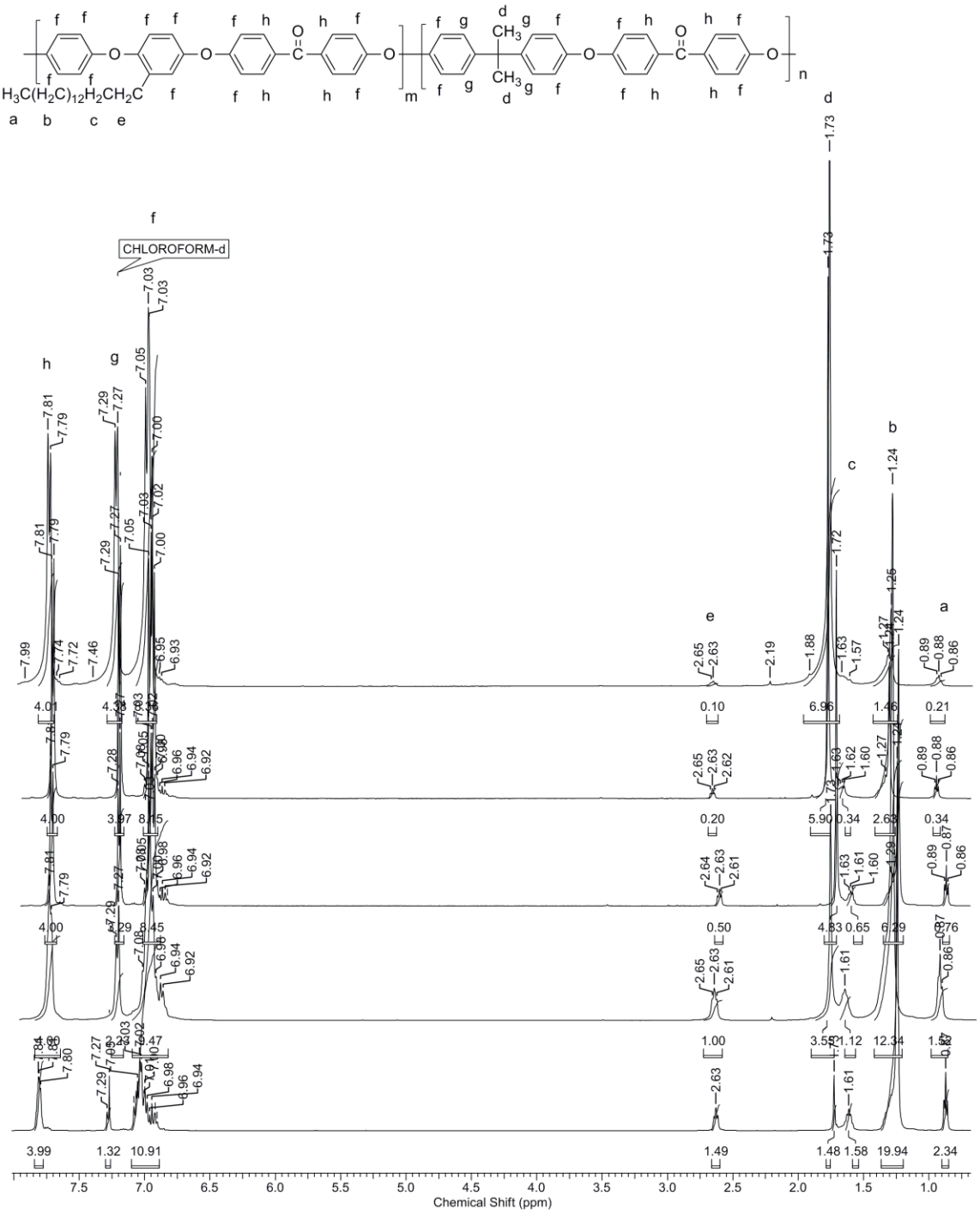

Figure 5a.5 ^{1}H-NMR spectra ($CDCl_3$) of copoly(ether ether ether ketone)s derived from HPPDP, BPA and 4,4'-difluorobenzophenone

^{1}H-NMR spectra of copoly(ether ether ether ketone)s were compared to determine the actual mol % incorporation of HPPDP monomer. For this purpose, the integrated intensity of the peak **h**, belonging to 4,4'-difluorobenzophenone component and **e**,

belonging to the HPPDP component were correlated to determine the actual mol % incorporation of HPPDP into the synthesised copoly(ether ether ether ketone)s, as summarised in **Table 5a.2**.

Table 5a.2 Composition of copoly(ether ether ether ketone)s determined from ^{1}H-NMR spectra

Copoly(ether ether ether ketone)	Feed HPPDP, mol %	Observed HPPDP, mol %
PEK-75	**75**	**75**
PEK-50	**50**	**50**
PEK-25	**25**	**25**
PEK-10	**10**	**10**
PEK-05	**5**	**5**

Results obtained from **Table 5a.2** indicated that an excellent agreement existed between the feed mol % HPPDP taken for polymerisation and the actual mol % incorporation of HPPDP in the obtained polymers. This suggests that copolymers of desired compositions were successfully obtained.

5a.3.2 Solubility and X-ray diffraction studies

The solubility behaviour of synthesised (co)poly(ether ether ether ketone)s at 3 wt % concentration was determined and the results are summarised in **Table 5a.3.**

Table 5a.3 Solubility of (co)poly(ether ether ether ketone)s

(Co)poly(ether ether ether ketone)	Solvent							
	$CHCl_3$	DCM	THF	DMF	DMAc	NMP	Pyridine	DMSO
PEK-100	++	++	++	+-	+-	++	++	+-
PEK-75	++	++	++	+-	+-	++	++	+-
PEK-50	++	++	++	+-	+	++	++	+-
PEK-25	++	++	++	+-	+	++	++	+-
PEK-10	++	++	++	+-	+-	++	++	+-
PEK-05	++	++	++	+-	+-	++	++	+-

--, Insoluble; + soluble on heating at 70 °C; ++, soluble at room temperature; +-, partially soluble or swollen

From the data presented in **Table 5a.3** it is clear that all the synthesised (co)poly(ether ether ether ketone)s were easily soluble at room temperature in chloroform, dichloromethane, tetrahydrofuran, 1-methyl-2-pyrrolidinone and pyridine. They were also partially soluble in *N*,*N*-dimethylformamide, *N*,*N*-dimethylacetamide and dimethyl sulfoxide. It is well known that both hydroquinone and BPA-based PEEKS are not easily soluble in common organic solvents. It can be deduced that this excellent solubility of synthesised (co)poly(ether ether ether ketone)s arises from incorporation of the pentadecyl chain containing HPPDP monomer into the polymers. Even 5 mol % incorporation of the HPPDP monomer greatly improved polymer solubility. The presence of the pentadecyl chains disturbs chain packing of polyetherketones into crystal lattice structures,[44] thus allowing solvent molecules to penetrate within the polymer and solvating the polymer chains easily. Such solubility characteristics suggest that (co)poly(ether ether ether ketone)s containing pendent pentadecyl chains can be readily

solution processed into membranes and films suitable for applications in gas separation and microelectronic devices.

Wide angle X-ray diffraction (WAXD) patterns obtained for the synthesised (co)poly(ether ether ether ketone)s are depicted in **Fig 5a.6**. The broad halo observed in the region of 2θ ~ 20° indicated that (co)poly(ether ether ether ketone)s were amorphous in nature. It is to be noted that both hydroquinone and BPA-based poly(ether ether ketone) are semicrystalline in nature.[4] Strikingly, even 5 mol % incorporation of HPPDP in copolymers was sufficient to disrupt the crystalline nature and make it essentially amorphous. It is surmised that the pentadecyl chains disrupt polymer chain packing, as stated earlier, which leads to the formation of amorphous polymers. Additionally, the peak observed at 2θ ~ 3° is indicative of the formation of layered structures.[52–56] With gradual increase in incorporation of the pentadecyl chain containing HPPDP monomer, the peak at 2θ ~ 3° was well developed with a concomitant increase in relative peak intensity.

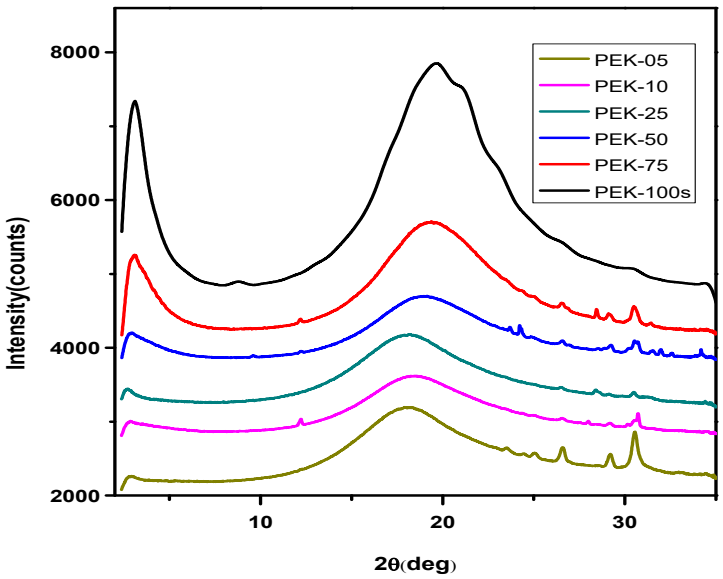

Figure 5a.6 X-Ray diffractograms of (co)poly(ether ether ether ketone)s

The solubility behaviour of the synthesised polymers as well as the results obtained from XRD analysis both indicate that incorporation of pentadecyl chains

containing HPPDP monomer led to the formation of amorphous (co)poly(ether ether ether ketone)s readily soluble in common organic solvents.

5a.3.3 Thermal properties

The thermal properties of synthesised (co)poly(ether ether ether ketone)s were explored through thermogravimetric analysis (TGA) and differential scanning calorimetry (DSC). The data obtained from TGA and DSC studies is summarised in **Table 5a.4**. TG curves are presented in **Fig 5a.7**, while DSC curves are depicted in **Fig 5.9**. In **Fig 5a.8** is presented a representative DTG curve along with corresponding TG curve of PEK-100.

Table 5a.4 Thermal properties of (co)poly(ether ether ether ketone)s

(Co)poly(ether ether ether ketone)	Composition of diols (mol %)		T_g (°C)[a]	T_{10} (°C)[b]	Char yield (%)[c]
	HPPDP	BPA			
PEK-100	100	0	25	431	22
PEK-75	75	25	32	434	26
PEK-50	50	50	55	439	32
PEK-25	25	75	72	446	34
PEK-10	10	90	111	460	38
PEK-05	05	95	125	463	40

a: 10 % weight loss on TGA thermograms at a heating rate of 10 °C/min under nitrogen atmosphere.
b: Measured by DSC from second heating scan with heating rate of 10 °C/min under nitrogen atmosphere.
c: Char yield measured at 900 °C.

.

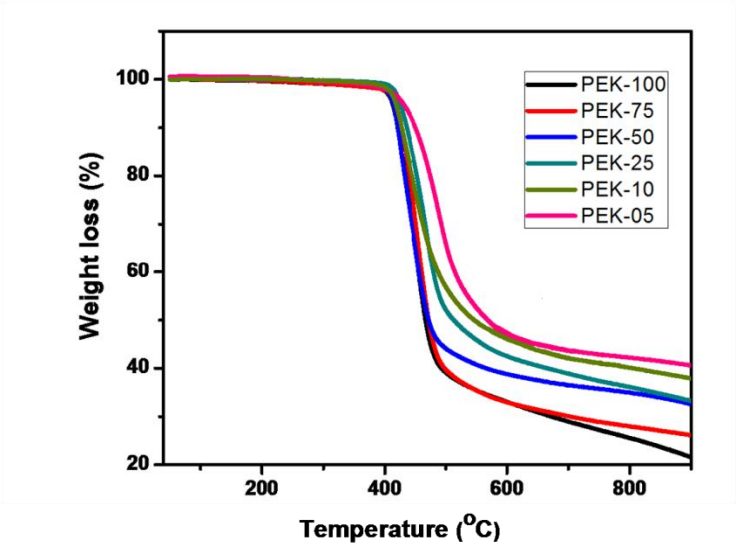

Figure 5a.7 TG curves of (co)poly(ether ether ether ketone)s

The synthesised (co)poly(ether ether ether ketone)s displayed T_{10} values in the range 431 – 463 °C. A decrease in T_{10} values was observed with increase in mol % incorporation of pentadecyl chain containing HPPDP monomer. This is reasonable on account of the increase in content of thermally labile pentadecyl chains in the polymers. Char yields at 900 °C were obtained in the range 22 – 40 %. As the mol % of HPPDP increased, the char yields decreased, due to the increase in aliphatic content in the copolymers.

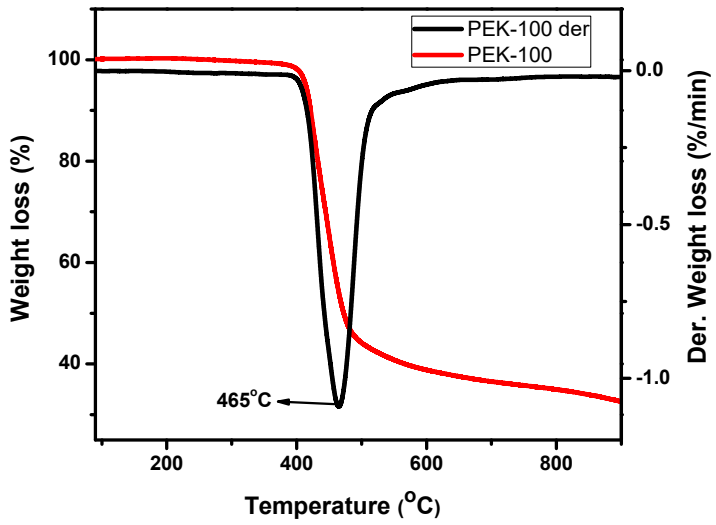

Figure 5a.8 DTG curve of PEK-100

Differential thermogravimetric analysis (DTG) of the (co)poly(ether ether ether ketone)s revealed a single step weight loss. Maximum degradation was observed to occur at 465 °C.

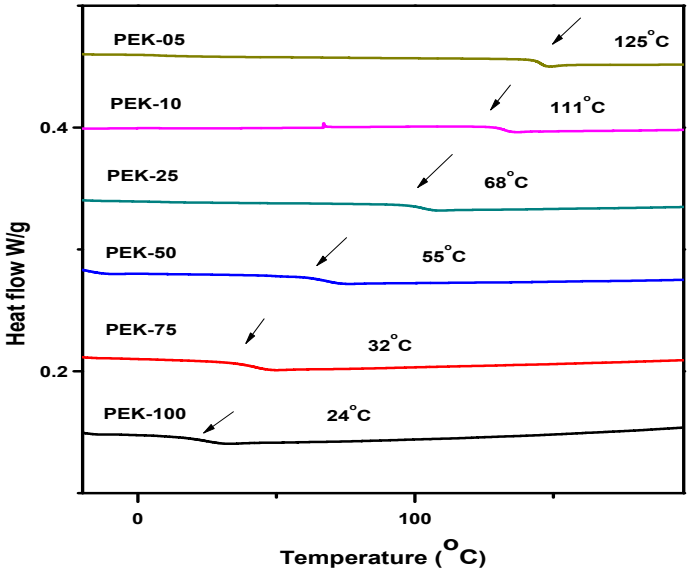

Figure 5a.9 DSC curves of (co)poly(ether ether ether ketone)s

Glass transition temperatures (T_g) observed for the synthesised (co)poly(ether ether ether ketone)s ranged from 25 – 125 °C. T_g values for all copolymers were less than the T_g value reported for BPA-based polyetherketone (T_g=157 °C).[57] The T_g values were observed to decrease progressively as the mol % incorporation of pentadecyl chain containing monomer (HPPDP) was increased. Thus, the presence of pentadecyl chain had a T_g lowering effect. This happens because the pentadecyl chains exert a packing disruptive effect leading to greater segmental mobility and lower T_g values. The obtained DSC traces were devoid of any melting transitions thus signifying that all the copolymers were amorphous in nature. This observation further supports the results obtained from XRD analysis.

The experimentally obtained T_g values were compared with the T_g values calculated using the Fox Equation:

$$\frac{1}{T_{gc}} = \frac{W_1}{T_{g1}} + \frac{W_2}{T_{g2}}$$

Where;

T_{gc} refers to the calculated T_g of copoly(ether ether ether ketone)s, T_{g1} and T_{g2} refer to T_g values obtained from homopolymer derived from HPPDP and BPA, respectively. (T_{g1} = 24 °C and T_{g2} = 157 °C[57]). W_1 and W_2 represent weight fractions of HPPDP and BPA, respectively, in the copoly(ether ether ether ketone)s. The $1/T_{gc}$ values calculated were plotted against W_1. At the same time, experimentally determined $1/T_g$ values were also plotted (**Fig 5a.10**).

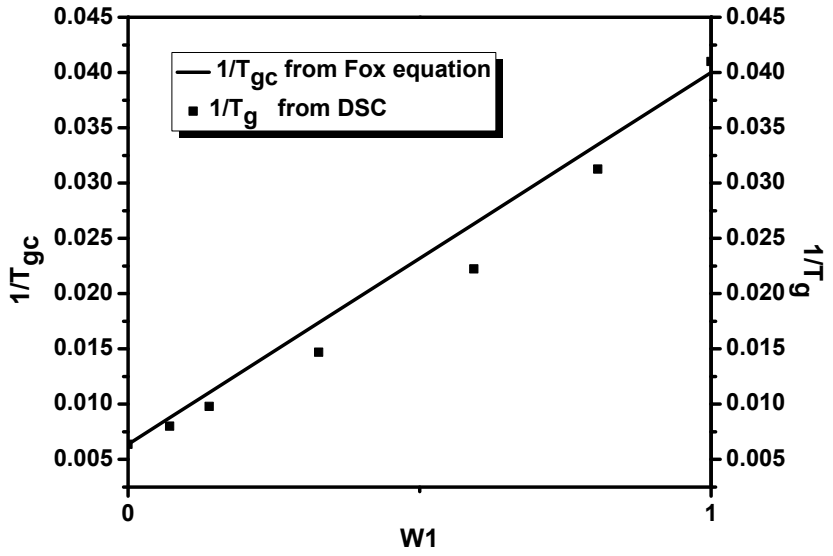

Figure 5a.10 T_g as a function of composition of HPPDP in copoly(ether ether ether ketone)s derived from polycondensation of a mixture of HPPDP and BPA with 4,4'-difluorobenzophenone

The observed T_g values showed acceptable agreement with theoretical T_{gc} values determined from Fox Equation, within range of experimental error.

5a.4 Conclusions

1. A series of new (co)poly(ether ether ether ketone)s containing pendent pentadecyl chains were synthesised by nucleophilic aromatic substitution polycondensation in *N*,*N*-dimethylacetamide of HPPDP and varying mixtures of HPPDP and BPA with 4,4'-difluorobenzophenone.

2. Inherent viscosities and number average molecular weights ranged from 0.61 – 0.73 dL g^{-1} and 26900 – 93400 g mol^{-1}, respectively, indicating the formation of (co)poly(ether ether ether ketone)s of reasonably high molecular weights.

3. The synthesised polymers were readily soluble in chloroform, dichloromethane, tetrahydrofuran, 1-methyl-2-pyrrolidinone and pyridine at room temperature. All (co)poly(ether ether ether ketone)s are readily solution processable, unlike commercial PEEK. (Co)poly(ether ether ether ketone)s could be cast into flexible, free-standing films from chloroform solutions.

4. (Co)poly(ether ether ether ketone)s under study were found to be amorphous in nature, as deduced from XRD analysis due to incorporation of packing disruptive pentadecyl chains into the polymers.

5. Observed T_{10} values ranged from 431 – 463 °C while T_g values were in the range 25 – 125 °C. The T_g and T_{10} values progressively decreased with increase in % incorporation of pentadecyl chain containing HPPDP.

References

1 T. E. Attwood, P. C. Dawson, J. L. Freeman, L. R. J. Hoy, J. B. Rose and P. A. Staniland, *Polymer*, 1981, **22**, 1096–1103.

2 J. Pan, K. Li, S. Chuayprakong, T. Hsu and Q. Wang, *ACS Appl. Mater. Interfaces*, 2010, **2**, 1286–1289.

3 H. Wang, G. Wang, W. Li, Q. Wang, W. Wei, Z. Jiang and S. Zhang, *J. Mater. Chem.*, 2012, **22**, 21232–21237.

4 J. M. Chalmers, W. F. Gaskin and M. W. Mackenzie, *Polym. Bull.*, 1984, **11**, 433–435.

5 V. Carlier, J. Devaux, R. Legras and P. T. McGrail, *Macromolecules*, 1992, **25**, 6646–6650.

6 P. M. Hergenrother, B. J. Jensen and S. J. Havens, *Polymer*, 1988, **29**, 358–369.

7 N. Yonezawa, S. Mori, S. Miyata, Y. Ueha-Anyashiki and K. Maeyama, *React. Funct. Polym.*, 2002, **53**, 11–17.

8 K. H. Gardner, B. S. Hsiao, R. R. Matheson and B. A. Wood, *Polymer*, 1992, **33**, 2483–2495.

9 D. Shukla, Y. S. Negi, J. Sen Uppadhyaya and V. Kumar, *Polym. Rev.*, 2012, **52**, 189–228.

10 F. Trotta, S. C. Mio, K. Martina, E. Drioli and P. Finocchiaro, *Asia-Pacific J. Chem. Eng.*, 2010, **5**, 249–255.

11 T. Hoffmann, D. Pospiech, L. Häußler, H. Komber, D. Voigt, C. Harnisch, C. Kollann, M. Ciesielski, M. Döring, R. Perez-Graterol, J. Sandler and V. Altstädt, *Macromol. Chem. Phys.*, 2005, **206**, 423–431.

12 Y. Ding and B. Bikson, *J. Memb. Sci.*, 2010, **357**, 192–198.

13 X. Zhao, C. Wang, K. Zhang, Z. Zhou and M. Zhu, *Colloid Polym. Sci.*, 2010, **288**, 907–914.

14 W. Guan, F. Xu, W. Liu, J. Zhao and Y. Guan, *J. Chromatogr. A*, 2007, **1147**, 59–65.

15 R. K. Goyal, A. N. Tiwari and Y. S. Negi, *J. Appl. Polym. Sci.*, 2011, **124**, 4612–4619.

16 M. J. Kayser, M. X. Reinholdt and S. Kaliaguine, *J. Phys. Chem. B*, 2010, **114**, 8387–8395.

17 R. K. Nagarale, W. Shin and P. K. Singh, *Polym. Chem.*, 2010, **1**, 388–408.

18 X. C. Ge, Y. Xu, M. Xiao, Y. Z. Meng and A. S. Hay, *Eur. Polym. J.*, 2006, **42**, 1206–1214.

19 E. Chauveau, C. Marestin, R. Mercier, E. Espuche and A. Morin, *J. Polym. Sci. Part B Polym. Phys.*, 2017, **55**, 771–777.

20 H. Li, G. Zhang, J. Wu, C. Zhao, Y. Zhang, K. Shao, M. Han, H. Lin, J. Zhu and H. Na, *J. Power Sources*, 2010, **195**, 6443–6449.

21 T. Mikami, K. Miyatake and M. Watanabe, *ACS Appl. Mater. Interfaces*, 2010, **2**, 1714–1721.

22 W. Guan, Y. Wang, F. Xu and Y. Guan, *J. Chromatogr. A*, 2008, **1177**, 28–35.

23 J. C. Jansen and E. Drioli, *Polym. Sci. Ser. A*, 2009, **51**, 1355–1366.

24 Y. Meng, A. R. Hlil and A. S. Hay, *J. Polym. Sci. Part A Polym. Chem.*, 1999, **37**, 1781–1788.

25 T. Wu, P. Liu, M. Shi, J. Lu, G. Ye and J. Xu, *Polym. Int.*, 2011, **60**, 1318–1323.

26 P. N. Honkhambe, N. A. Dhamdhere, B. V. Tawade, M. M. Salunkhe and P. P. Wadgaonkar, *High Perform. Polym.*, 2013, **25**, 260–267.

27 W. Risse and D. Y. Sogah, *Macromolecules*, 1990, **23**, 4029–4033.

28 S. Kawasaki, M. Yamada, K. Kobori, F. Jin, Y. Kondo, H. Hayashi, Y. Suzuki and T. Takata, *Macromolecules*, 2007, **40**, 5284–5289.

29 G. Wang, Z. Jiang, S. Zhang, C. Chen and Z. Wu, *Polym. Int.*, 2006, **55**, 657–661.

30 A. S. More, S. K. Pasale, P. N. Honkhambe and P. P. Wadgaonkar, *J. Appl. Polym. Sci.*, 2011, **121**, 3689–3695.

31 B. V. Tawade, S. V. Shaligram, N. G. Valsange, U. K. Kharul and P. P. Wadgaonkar, *Polym. Int.*, 2016, **65**, 567–576.

32 M. Ueda, H. Toyoda, T. Nakayama and T. Abe, *J. Polym. Sci. Part A Polym. Chem.*, 1996, **34**, 109–115.

33 Y. Kanetaka, S. Yamazaki and K. Kimura, *Macromolecules*, 2016, **49**, 1252–1258.

34 H. Ben Abderrazak, A. Fildier, H. Ben Romdhane, S. Chatti and H. R. Kricheldorf, *Macromol. Chem. Phys.*, 2013, **214**, 1423–1433.

35 S. R. Sriram, C. R. Hoppin, N. Taylor and S. Srinivasan, US20140186624A1, 2014.

36 H. R. Kricheldorf and G. Bier, *Polymer*, 1984, **25**, 1151–1156.

37 V. Percec, R. S. Clough, M. Grigoras, P. L. Rinaldi and V. E. Litman, *Macromolecules*, 1993, **26**, 3650–3662.

38 K. Maeyama and S. Ito, *Polym. Bull.*,2018 , DOI:10.1007/s00289-018-2347-5.

39 V. Percec, M. Grigoras, R. S. Clough and J. Fanjul, *J. Polym. Sci. Part A Polym. Chem.*, 1995, **33**, 331–344.

40 S. K. Park and S. Y. Kim, *Macromolecules*, 1998, **31**, 3385–3387.

41 V. Percec, R. S. Clough, P. L. Rinaldi and V. E. Litman, *Macromolecules*, 1991, **24**, 5889–5892.

42 J. W. Labadie, J. L. Hedrick and M. Ueda, in *Step-Growth Polymers for High-Performance Materials*, eds. J. L. Hedrick and J. W. Labadie, American Chemical Society, Washington, DC, 1996, pp. 210–225.

43 B. E. Jennings, M. E. B. Jones and J. B. Rose, *J. Polym. Sci. Part C Polym. Symp.*, 1967, **16**, 715–724.

44 P. T. McGrail, *Polym. Int.*, 1996, **41**, 103–121.

45 V. Jansons and K. Dahl, *Makromol. Chemie. Macromol. Symp.*, 1991, **51**, 87–101.

46 Y. Iwakura, K. Uno and T. Takiguchi, *J. Polym. Sci. Part A-1 Polym. Chem.*, 1968, **6**, 3345–3355.

47 M. Ueda and M. Sato, *Macromolecules*, 1987, **20**, 2675–2678.

48 B. M. Marks, US3441538, 1969.

49 W. H. Bonner, US3065205, 1962.

50 R. N. Johnson, A. G. Farnham, R. A. Clendinning, W. F. Hale and C. N. Merriam, *J. Polym. Sci. Part A-1 Polym. Chem.*, 1967, **5**, 2375–2398.

51 M. Jayakannan and S. Ramakrishnan, *Macromol. Rapid Commun.*, 2001, **22**, 1463–1473.

52 R. Duran, M. Ballauff, M. Wenzel and G. Wegner, *Macromolecules*, 1988, **21**, 2897–2899.

53 H. Kim, S.-B. Park, Jin Chul Jung and W.-C. Zin, *Polymer*, 1996, **37**, 2845–2852.

54 D. H. Wang, Z. Shen, M. Guo, S. Z. D. Cheng and F. W. Harris, *Macromolecules*, 2007, **40**, 889–900.

55 Y. S. Kim and J. C. Jung, *J. Polym. Sci. Part A Polym. Chem.*, 2002, **40**, 1764–1774.

56 Y. Chen, R. Wombacher, J. H. Wendorff and A. Greiner, *Polymer*, 2003, **44**, 5513–5520.

57 S. S. Nagane, Ph. D. Thesis, Academy of Scientific and Innovative Research, 2018.

CHAPTER 5 (b)

Synthesis and Characterisation of Partially Bio-Based Poly(ether sulfone)s Containing Pendent Pentadecyl Chains

5b.1 Introduction

Poly(ether sulfone)s are a well-known class of engineering thermoplastics possessing excellent chemical, hydrolytic, thermal and radiation resistance.[1–4] Besides their general applications as an engineering thermoplastic,[2] researchers over the past few decades have been attempting to widen the applications of poly(ether sulfone)s into newer fields by tuning of properties. For example, sulfonated poly(ether sulfone)s and their nanocomposites have been successfully explored for proton exchange membrane fuel cells,[5–9] while cyclohexylidene-based poly(ether sulfone)s have been explored for anion exchange membrane fuel cells.[10] Antifouling hybrid poly(ether sulfone) membranes have been developed for ultrafiltration.[11–14] Jurs *et al*[15] have developed flame retardant poly(ether sulfone)s by incorporating bisphenol C, while Mir *et al*[16] have synthesised deoxybenzoin-based poly(ether sulfone)s to improve flame-resistance. Poly(ether sulfone) membranes are also attractive candidates for gas transport applications.[17–19] Liu *et al*[20] developed methylated and trifluoromethylated poly(ether sulfone)s with low dielectric constants for microelectronics. However, this burgeoning research involving poly(ether sulfone)s depends on their synthesis from petrochemical feedstocks. In light of expected future oil crisis, it is advisable to replace oil-based feedstocks with chemicals derived from plentiful renewable resources. The myriad of applications which have been explored till date for poly(ether sulfone)s should be attempted for polymers derived from renewable feedstocks. Poly(ether sulfone)s derived from isosorbide, isomannide and isoidide[21–24] are reported. Aromatic poly(ether sulfone)s derived from renewable resources are mostly limited to a few reports.[25,26]

In this work, a series of (co)poly(ether sulfone)s containing pendent pentadecyl chains were synthesised from the bisphenol 4-(4-hydroxyphenoxy)-3-pentadecylphenol (HPPDP), which was in turn synthesised from CNSL. Poly(ether sulfone)s based on CNSL may be interesting materials for gas permeation evaluation. Only a few reports are known concerning the gas permeation properties of alkyl chain containing poly(ether sulfone)s.[25,27–30] (Co)poly(ether sulfone)s were synthesised by polycondensation of mixtures of HPPDP and BPA with bis(4-fluorophenyl)sulfone in *N*,*N*-dimethylacetamide at 180 °C. (Co)poly(ether sulfone)s were characterised by inherent viscosity measurements, GPC studies, FT-IR, ^{1}H-NMR, ^{13}C-NMR spectroscopy, X-ray diffraction,

thermogravimetric analysis (TGA) and differential scanning calorimetric studies (DSC). The influence of the pentadecyl chain on polymer properties was studied.

5b.2 Experimental

5b.2.1 Materials

4-(4-Hydroxyphenoxy)-3-pentadecylphenol (HPPDP) was synthesised as described in **Chapter 3**. Bisphenol A (BPA) (Sigma Aldrich, India) was used after sublimation, while bis(4-fluorophenyl)sulfone was recrystallised from toluene (Merck, India) before use. *N*,*N*-Dimethylacetamide (DMAc) (Merck, India) and toluene were utilised after distillation over calcium hydride (Sigma Aldrich, India). Anhydrous potassium carbonate (Thomas Baker, India) was heated at 180 °C for 8 h before use.

5b.2.2 Measurements

FT-IR spectra of synthesised polymers were recorded with ATR mode using Bruker α-T spectrophotometer in the range of 4000 to 500 cm^{-1}.^{1}H-NMR and ^{13}C-NMR spectra were recorded on Bruker-AV 400 and 500 MHz spectrometer using chloroform-*d* as solvent and TMS as an internal standard. Molecular weights of (co)poly(ether sulfone)s were measured on Waters 2707 chromatograph (GPC) equipped with Viscotek 270 dual detector in tetrahydrofuran using polystyrene as the calibration standard. Concentration of polymers used was 3 mg dL^{-1}. Inherent viscosity of the polymers was measured using 0.5 % (w/v) solution of polymer in chloroform at 25 ± 0.1 °C. Ubbelohde suspended level viscometer was used to determine inherent viscosity according to the following equation:

$$n_{inh} = \frac{2.303}{C} x \log \frac{t}{t_0}$$

where *t* and t_0 are flow times of polymer solution and solvent, respectively and *C* is the concentration of polymer solution. X-Ray diffraction analysis was performed on Rigaku MicroMax-007HF X-ray diffractometer at 40 kV and 30 mA. Thermogravimetric analysis (TGA) of the polymers was performed on Perkin Elmer: STA 6000 between temperatures of 30 °C to 900 °C with a heating rate of 10 °C min^{-1} under nitrogen. Glass transition temperatures (T_g) were determined from differential scanning calorimetry experiments (DSC) carried out on TA Q-100 instrument with sample heating rate of 10 °C min^{-1} under nitrogen atmosphere. T_g values of (co)poly(ether sulfone)s were determined from the second heating cycles.

5b.2.3 Synthesis of (co)poly(ether sulfones)s: typical procedure

Into a 50 mL three-necked round bottom flask equipped with a magnetic stirring bar, a nitrogen inlet, a Dean-Stark trap and a reflux condenser, were added HPPDP (0.4 g, 9.69 x 10^{-4} mol), freshly distilled *N*,*N*-dimethylacetamide (7 mL), anhydrous potassium carbonate (0.334 g, 2.42 x 10^{-3} mol) and freshly distilled toluene (30 mL). The reaction mixture was stirred at reflux under a steady stream of nitrogen. Water formed during the reaction was continuously distilled out as an azeotrope with toluene for 3 h, after which the toluene was removed out of the reaction mixture by raising the temperature to 150 °C. Thereafter, the reaction mixture was cooled to room temperature and bis(4-fluorophenyl)sulfone (0.246 g, 9.69 x 10^{-4} mol) was added in one lot in a steady stream of nitrogen. Subsequently, the reaction mixture was heated to 180 °C after removal of the Dean-Stark trap and stirred at that temperature for 8 h. The viscous polymer solution was poured into methanol (500 mL) to precipitate the poly(ether sulfone) designated as PES-100. PES-100 was further purified by reprecipitating from concentrated chloroform solution (15 mL) into methanol (500 mL) and drying under reduced pressure at room temperature for 8 h.

Copoly(ether sulfone)s derived from HPPDP feed mol % of 75 %, 50 %, 25 % and 10 % are designated as PES-75, PES-50, PES-25 and PES-10, respectively, and were synthesised by following the above procedure.

5b.3 Results and Discussion

5b.3.1 Synthesis of (co)poly(ether sulfone)s

Aromatic polyethersulfones, similar to polyetherketones, are mainly synthesised through electrophilic substitution reactions[31] and nucleophilic substitution reactions.[32–36] Polyethersulfones were reported for the first time by Johnson and Farnham in 1967 by nucleophilic substitution polymerisation.[34]

In the present study, a series of (co)poly(ether sulfone)s were synthesised by aromatic nucleophilic substitution polymerisation of HPPDP or varying compositions of HPPDP and bisphenol A with bis(4-fluorophenyl)sulfone (**Scheme 5b.1**).

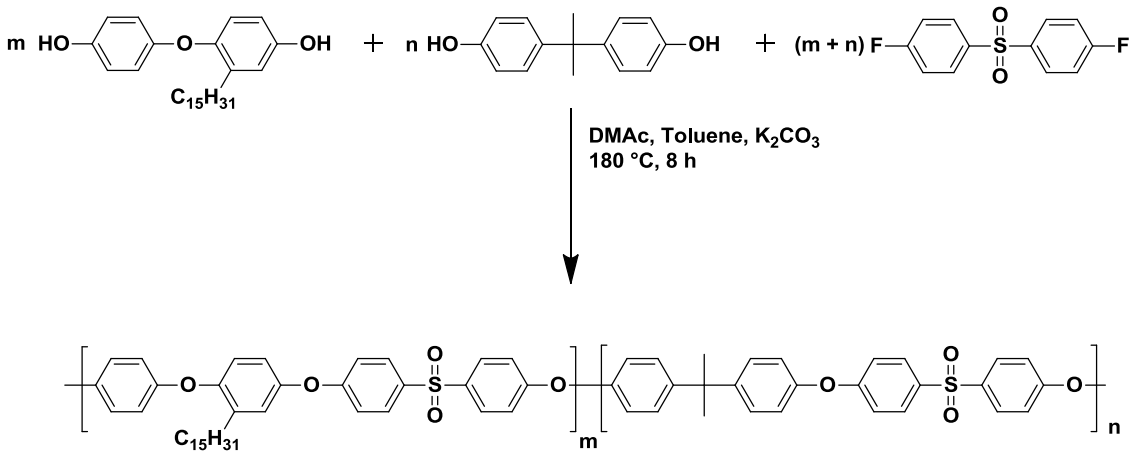

Scheme 5b.1 Synthesis of (co)poly(ether sulfone)s

HPPDP or a mixture of HPPDP and BPA along with anhydrous potassium carbonate was refluxed in a mixture of *N*,*N*-dimethylacetamide and toluene. The water formed as a result of formation of bisphenolate salt was removed from the reaction mixture continuously through azeotropic distillation with toluene. Thereafter, toluene was removed from the reaction mixture by raising the temperature to 150 °C. Subsequently, the reaction mixture was cooled to room temperature and bis(4-fluorophenyl)sulfone was added under a steady stream of nitrogen. The bisphenolate salt(s) and the activated bisfluoride reacted in accordance to aromatic nucleophilic substitution reaction mechanism (S_NAr) *via* the formation of an intermediate Meisenheimer complex.[37] The polymer forming reaction leads to the generation of ether linkages in the backbone.

The results of polymerisation are tabulated in **Table 5b.1.** Inherent viscosities, of the (co)poly(ether sulfone)s measured from the chloroform solutions, were found to be in the range 0.56 – 0.69 g dL^{-1}. Number average molecular weights (M_n) determined through GPC analysis were found to be in the range 50200 – 87000 g mol^{-1}. Both these observations point towards the formation of (co)poly(ether sulfone)s of reasonably high molecular weights. Dispersities obtained from GPC measurements were found to lie in the range 1.7 – 2.1. However, molecular weights obtained through GPC measurements are not absolute since these measurements were carried out using polystyrenes as standard. PES-100 formed flexible, free-standing film (**Fig 5b.1**).

Table 5b.1 Results of synthesis of (co)poly(ether sulfone)s

(Co)poly(ether sulfone)	Composition of diols (mol %)		η_{inh} (dL/g)[a]	Molecular weight (g/mol)[b]		Dispersity (M_w/M_n)
	HPPDP	BPA		M_n	M_w	
PES-100	100	0	0.67	81700	177700	2.1
PES-75	75	25	0.56	50200	90500	1.7
PES-50	50	50	0.61	46000	91000	1.9
PES-25	25	75	0.69	87000	151900	1.7
PES-10	10	90	0.58	56400	108900	1.9

a: η_{inh} was measured using 0.5% (w/v) solution of (co)poly(ether sulfone)s in chloroform at 25 °C ± 1°C
b: Determined through GPC in tetrahydrofuran, using polystyrenes as calibration standard

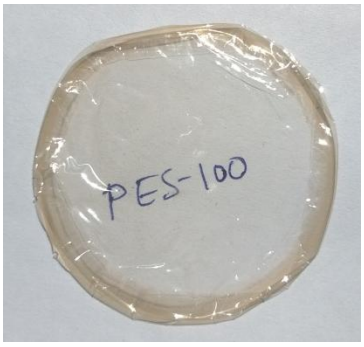

Figure 5b.1 PES-100 film cast from chloroform

The molecular structure of synthesised (co)poly(ether sulfone)s were analysed in detail and confirmed by FT-IR, ^{1}H-NMR and ^{13}C-NMR spectroscopic studies. FT-IR spectrum of a representative poly(ether sulfone), PES-100, is presented in **Fig 5b.2**.

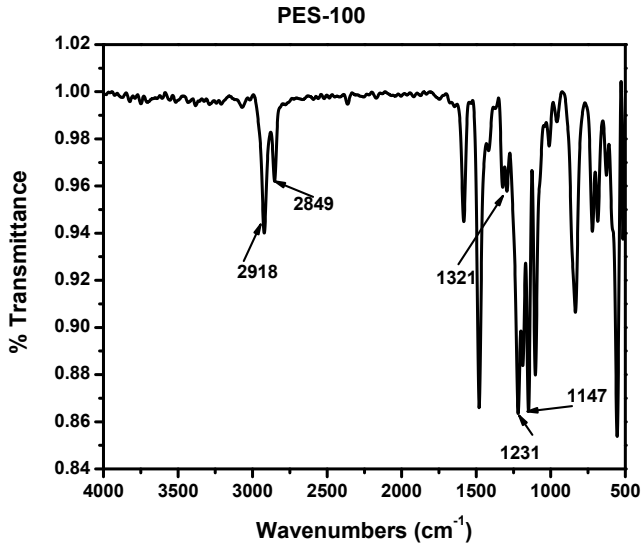

Figure 5b.2 FT-IR spectrum of PES-100 film

Absorption bands characteristic of sulfone functionality appeared at 1321 cm^{-1} (asymmetrical S=O stretch) and 1147 cm^{-1} (symmetrical S=O stretch). Additionally, a strong band indicative of ether functionality was observed at 1231 cm^{-1} (C-O-C stretching).

Representative ^{1}H-NMR spectrum of PES-100 is presented in **Fig 5b.3**, while ^{13}C-NMR spectrum is presented in **Fig 5b.4**.

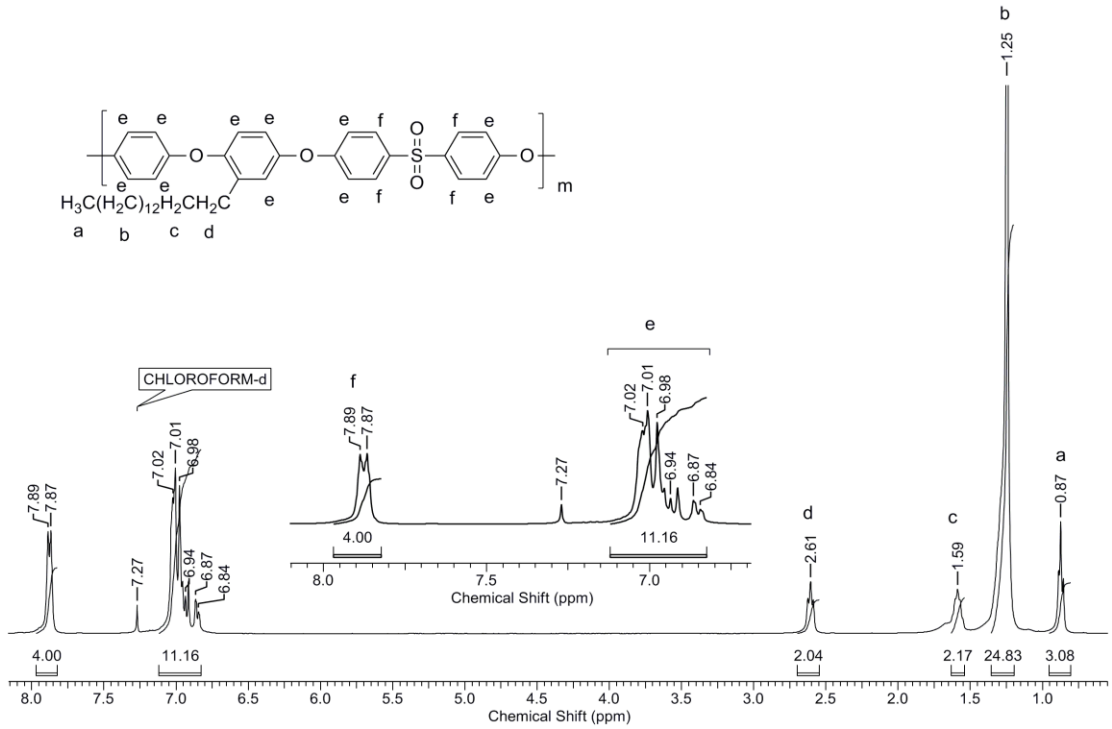

Figure 5b.3 ^{1}H-NMR spectrum ($CDCl_3$) of PES-100.

The four aromatic protons present *ortho* to the sulfonyl moiety (**f**) appeared as a doublet at 7.88 δ ppm. The remaining aromatic protons belonging to the polymer repeat unit (**e**) resonated at 6.83 – 7.12 δ ppm in the form of a multiplet. Benzylic protons (**d**) appeared as a triplet at 2.61 δ ppm, while the methylene protons (**c**) resonated at 1.59 δ ppm as a quintet. The remaining methylene protons (**b**) belonging to the pentadecyl chain appeared as a multiplet in the range 1.20 – 1.35 δ ppm. Methyl protons (**a**) appeared as a triplet at 0.87 δ ppm.

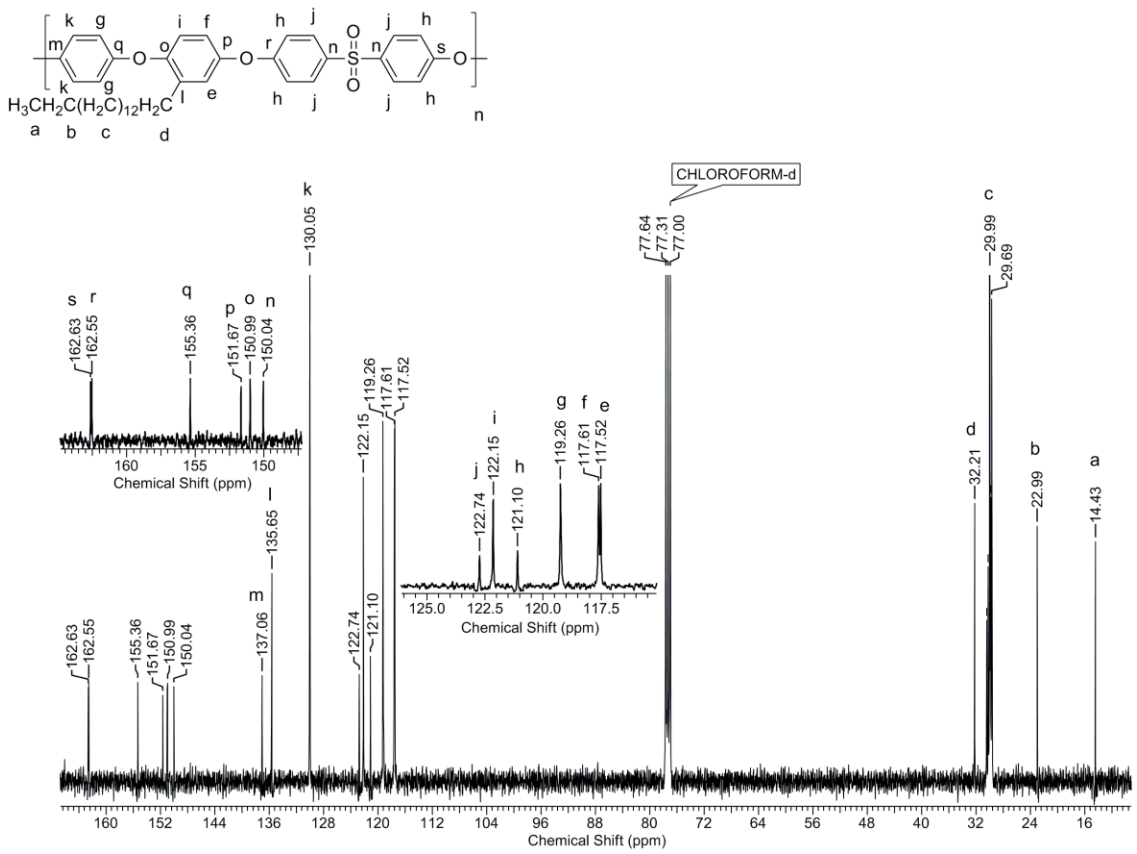

Figure 5b.4 ^{13}C-NMR spectrum ($CDCl_3$) of PES-100.

^{13}C-NMR spectrum of PES-100 was assigned with the additional assistance of DEPT spectrum. The signals corresponding to the aromatic carbons belonging to the PES-100 repeat unit (**e-s**) appeared in the range 117.62 – 162.63 δ ppm. The chemical shift values observed for these carbon atoms showed good agreement with the proposed structure as shown in **Fig 5b.4**. The benzylic carbon (**d**) resonated at 132.21 δ ppm while the twelve methylene carbons (**c**) appeared in the range 29.53 – 30.54 δ ppm. The benzylic carbon (**b**) appeared at 22.99 δ ppm while the methyl carbon (**a**) resonated at 14.43 δ ppm.

The composition of synthesised copoly(ether sulfone)s was determined by ^{1}H-NMR spectroscopy (**Fig 5b.5**).

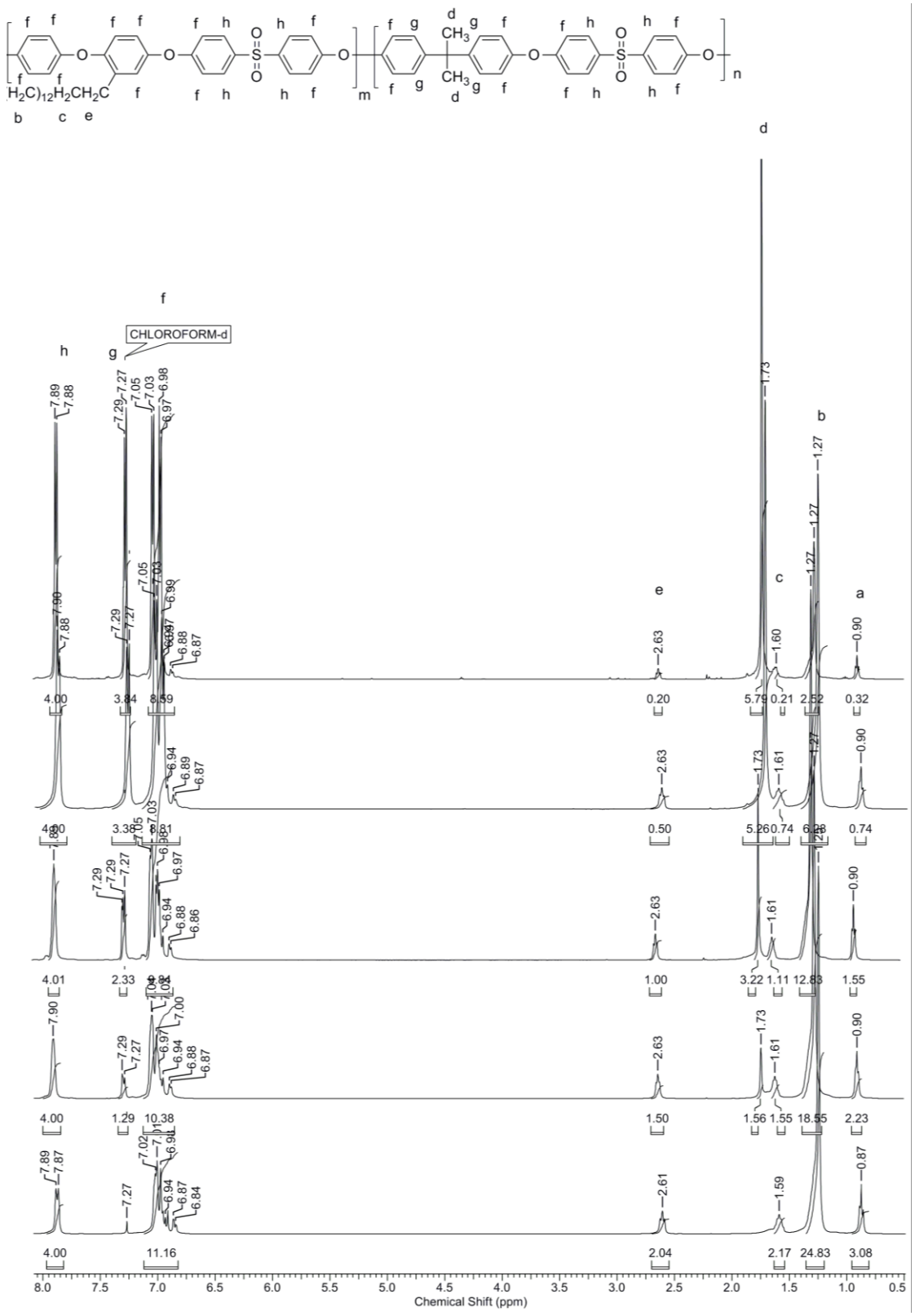

Figure 5b.5 ^{1}H-NMR ($CDCl_3$) spectra of (co)poly(ether sulfone)s derived from HPPDP, BPA and bis(4-fluorophenyl)sulfone

^{1}H-NMR spectra of synthesised (co)poly(ether sulfone)s were compared to determine the actual % incorporation of the HPPDP monomer in the resultant polymer structures. Towards this end, the integrated intensity ratio of **h**, corresponding to the four protons *ortho* to the sulfone moiety, and **e**, assigned to the benzylic methylene protons, was determined to elucidate the composition of the synthesised copoly(ether sulfone)s as summarised in **Table 5b.2**.

Table 5b.2 Composition of copoly(ether sulfone)s determined from ^{1}H-NMR spectra

Copoly(ether sulfone)	Feed HPPDP, mol %	Observed HPPDP, mol %
PEK-75	**75**	**75**
PEK-50	**50**	**50**
PEK-25	**25**	**25**
PEK-10	**10**	**10**

From the data in **Table 5b.2** it is clear that an excellent agreement exists between the mol % of HPPDP taken for polymerisation and the actual incorporation of HPPDP, as determined from ^{1}H-NMR spectra.

5b.3.2 Solubility and X-ray diffraction studies

The solubility behaviour of synthesised (co)poly(ether sulfone)s at 3 wt % concentration was determined and the results are summarised in **Table 5b.3.**

Table 5b.3 Solubility of poly(ether sulfone)s

(Co)poly(ether sulfone)	Solvent							
	$CHCl_3$	DCM	THF	DMF	DMAc	NMP	Pyridine	DMSO
PES-100	++	++	++	+-	++	++	+	+-
PES-75	++	++	++	+-	++	++	+	+-
PES-50	++	++	++	+-	++	++	+-	+-
PES-25	++	++	++	++	++	++	+-	+-
PES-10	++	++	++	++	++	++	+-	+-

--, Insoluble; + soluble on heating at 70 °C; ++, soluble at room temperature; +-, partially soluble or swollen

All the synthesised (co)poly(ether sulfone)s were observed to be soluble in chloroform, dichloromethane, tetrahydrofuran, *N*,*N*-dimethylacetamide and 1-methyl-2-pyrrolidinone at room temperature.

Wide angle X-ray diffractograms (WAXD) of the synthesised polymers are presented in **Fig 5b.6**. A broad hump in the region around $2\theta \sim 20°$ indicated that all the polymers synthesised were amorphous in nature due to the packing disruptive effect of the C_{15} alkyl chain in addition to inability of polysulfones to not pack into definite crystal structures.[4] A sharp peak was observed at $2\theta \sim 3°$, indicative of the formation of layered or stacked structures in the solid state[38–42] due to the incorporation of pendent C_{15} alkyl chains. It was observed that as the incorporation of the pentadecyl chain containing HPPDP was gradually increased, there was an increase in the relative intensity of the peak at $2\theta \sim 3°$.

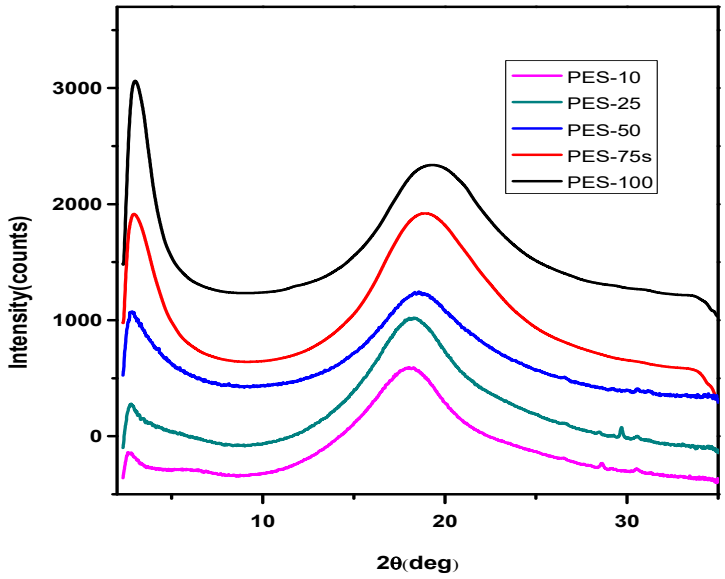

Figure 5b.6 X-Ray diffractograms of (co)poly(ether sulfone)s

5b.3.3 Thermal properties

The thermal properties of synthesised (co)poly(ether sulfone)s were evaluated through thermogravimetric analysis (TGA) and differential scanning calorimetry (DSC) studies. In **Table 5b.4** are compiled the results of TG and DSC analyses. TG curves are presented in **Fig 5b.7** and DSC curves are depicted in **Fig 5b.9**. A representative differential thermogravimetric analysis (DTG) curve along with corresponding TG curve for PES-100 is depicted in **Fig 5b.8**.

Table 5b.4 Thermal properties of (co)poly(ether sulfone)s

(Co)poly(ether sulfone)	Composition of diols (mol %)		T_g (°C)[a]	T_{10} (°C)[b]	Char yield (%)[c]
	HPPDP	BPA			
PES-100	100	0	47	414	23
PES-75	75	25	61	415	25
PES-50	50	50	82	420	30
PES-25	25	75	115	432	32
PES-10	10	90	149	444	34

a: 10% weight loss on TGA thermograms at a heating rate of 10 °C/min under nitrogen atmosphere.
b: Measured by DSC from second heating scan with heating rate of 10 °C/min under nitrogen atmosphere.
c: Char yield measured at 900 °C.

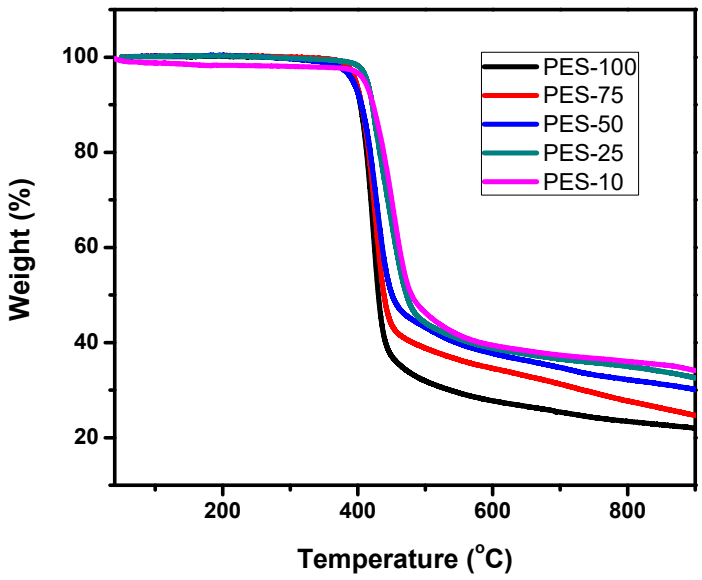

Figure 5b.7 TG curves of (co)poly(ether sulfone)s

The T_{10} values observed for synthesised (co)poly(ether sulfone)s were in the range 414 – 444 °C, indicating that synthesised polymers were of good thermal stability. Additionally, it was observed that as the mol % incorporation of HPPDP was increased, the T_{10} values decreased. This happened because incorporation of the thermally labile aliphatic pentadecyl chain decreased the thermal stability of the polymers. As the mol %

incorporation of HPPDP was increased, the thermally labile pentadecyl content increased, leading to decrease in the thermal stability. Char yields recorded ranged from 23 – 44%. As the aliphatic content increased with increasing mol % incorporation of HPPDP, decrease in char yields was observed.

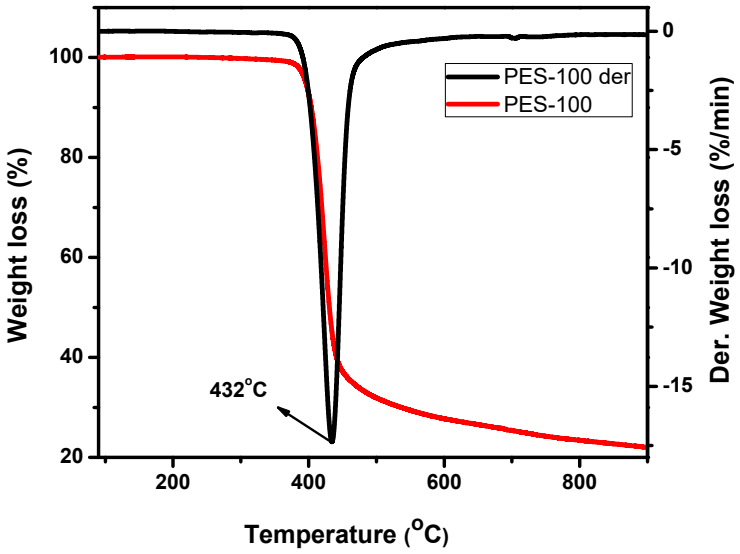

Figure 5b.8 DTG curve of PES-100

From the differential thermogravimetric (DTG) analysis curve it was observed that PES-100 underwent single step degradation. Maximum degradation occurred at 432 °C.

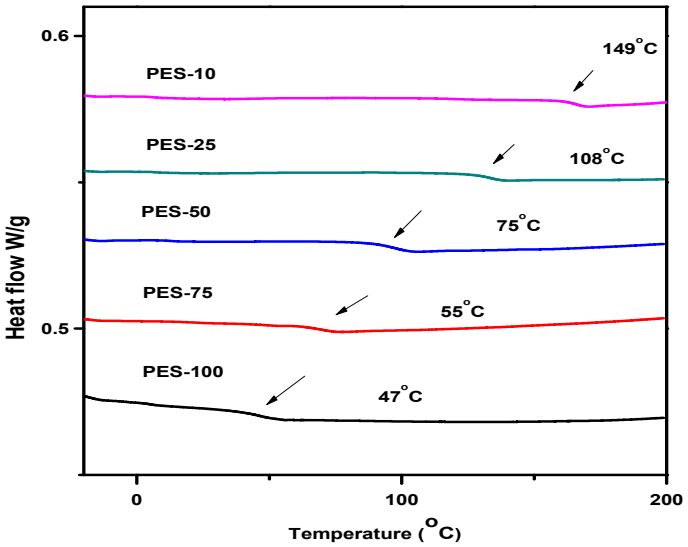

Figure 5b.9 DSC curves of (co)poly(ether sulfone)s

DSC analysis revealed that synthesised (co)poly(ether sulfone)s exhibited glass transition temperatures (T_g) in the range 47 °C – 149 °C. All the observed T_g values were also lower than the reported T_g value of BPA-based polyethersulfone (190 °C).[43] Similar to the case of (co)poly(ether ether ether ketone)s, a progressive decrease in T_g values was observed with increase in incorporation of pentadecyl chain containing HPPDP. The pentadecyl chain exerts a packing disruptive effect which enhances chain mobility leading to decrease in T_g values.

The T_g values of the (co)poly(ether sulfone)s were correlated with theoretical T_g values calculated from the Fox Equation:

$$\frac{1}{T_{gc}} = \frac{W_1}{T_{g1}} + \frac{W_2}{T_{g2}}$$

Where;

T_{gc} refers to the calculated T_g of copoly(ether sulfone)s, T_{g1} and T_{g2} refer to T_g values obtained from homopolymer derived from HPPDP and BPA, respectively. (T_{g1} = 47 °C and T_{g2} = 190 °C[43]). W_1 and W_2 represent weight fractions of HPPDP and BPA, respectively, in copoly(ether sulfone)s. The $1/T_{gc}$ values calculated were plotted against W_1. At the same time, experimentally determined $1/T_g$ values were also plotted (**Fig 5b.10**).

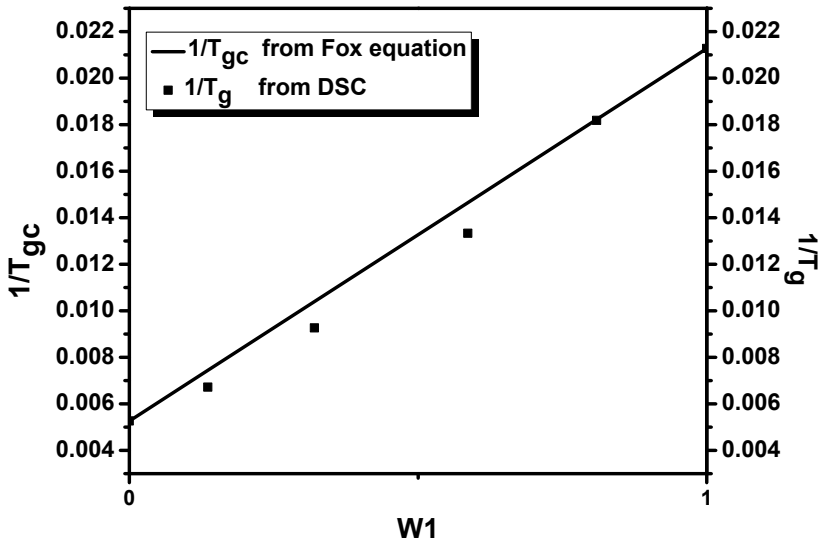

Figure 5b.10 T_g as a function of composition of HPPDP in copoly(ether sulfone)s derived from polycondensation of a mixture of HPPDP and BPA with bis(4-fluorophenyl)sulfone

The obtained T_g values showed a good correlation with theoretical T_g values within range of experimental error.

5b.4 Conclusions

1. A series of (co)poly(ether sulfone)s were synthesised from polycondensation of pentadecyl chain containing 4-(4-hydroxyphenoxy)-3-pentadecylphenol (HPPDP) and varying mixtures of HPPDP and BPA with bis(4-fluorophenyl)sulfone *via* aromatic nucleophilic substitution polymerisation in *N*,*N*-dimethylacetamide at 180 °C.

2. Observed inherent viscosities were in the range 0.56 – 0.69 dL g^{-1}, while number average molecular weights were in the range 50200 – 87000 g mol^{-1}, indicating that the synthesised (co)poly(ether sulfone)s were of reasonably high molecular weights.

3. (Co)poly(ether sulfone)s were easily soluble in chloroform, dichloromethane, tetrahydrofuran, *N*,*N*-dimethylacetamide and 1-methyl-2-pyrrolidinone at room temperature. Films cast from chloroform solutions were flexible, transparent and free-standing in nature.

4. Observed T_{10} values were in the range 414 – 444 °C while the T_g values were in the range 47 – 149 °C. T_{10} values indicate that the (co)poly(ether sulfone)s possessed good

thermal stability. Both T_{10} and T_g values showed a progressive decrease with increase in % incorporation of pentadecyl chain containing HPPDP.

References

1 S. Maiti and B. K. Mandal, *Prog. Polym. Sci.*, 1986, **12**, 111–153.

2 P. M. Hergenrother, B. J. Jensen and S. J. Havens, *Polymer*, 1988, **29**, 358–369.

3 V. L. Rao, *J. Macromol. Sci. Part C Polym. Rev.*, 1999, **39**, 655–711.

4 P. T. McGrail, *Polym. Int.*, 1996, **41**, 103–121.

5 E. Yılmaz and E. Can, *J. Polym. Sci. Part B Polym. Phys.*, 2018, **56**, 558–575.

6 K. Kim, J. Bae, M.-Y. Lim, P. Heo, S.-W. Choi, H.-H. Kwon and J.-C. Lee, *J. Memb. Sci.*, 2017, **525**, 125–134.

7 Z. Hu, Y. Lu, X. Zhang, X. Yan, N. Li and S. Chen, *Front. Mater. Sci.*, 2018, **12**, 156–167.

8 H. Lade, V. Kumar, G. Arthanareeswaran and A. F. Ismail, *Int. J. Hydrogen Energy*, 2017, **42**, 1063–1074.

9 S.-W. Lee, J.-C. Chen, J.-A. Wu and K.-H. Chen, *ACS Appl. Mater. Interfaces*, 2017, **9**, 9805–9814.

10 D. Lu, D. Li, L. Wen and L. Xue, *J. Memb. Sci.*, 2017, **533**, 210–219.

11 J. Zhang, Y. Xu, S. Chen, J. Li, W. Han, X. Sun, D. Wu, Z. Hu and L. Wang, *Appl. Surf. Sci.*, 2018, **434**, 806–815.

12 Z. Geng, X. Yang, C. Boo, S. Zhu, Y. Lu, W. Fan, M. Huo, M. Elimelech and X. Yang, *J. Memb. Sci.*, 2017, **529**, 1–10.

13 A. Rahimpour, S. S. Madaeni, A. H. Taheri and Y. Mansourpanah, *J. Memb. Sci.*, 2008, **313**, 158–169.

14 C. Zhao, J. Xue, F. Ran and S. Sun, *Prog. Mater. Sci.*, 2013, **58**, 76–150.

15 J. L. Jurs and J. M. Tour, *Polymer*, 2003, **44**, 3709–3714.

16 A. A. Mir, S. Wagner, R. H. Krämer, P. Deglmann and T. Emrick, *Polymer*, 2016, **84**, 59–64.

17 A. Naderi, W. F. Yong, Y. Xiao, T.-S. Chung, M. Weber and C. Maletzko, *Polymer*, 2018, **135**, 76–84.

18 J. S. Chiou, Y. Maeda and D. R. Paul, *J. Appl. Polym. Sci.*, 1987, **33**, 1823–1828.

19 M. R. Pixton and D. R. Paul, *Polymer*, 1995, **36**, 3165–3172.

20 B. Liu, W. Hu, X. Rao, G. Wang, Z. Jiang, Z. Wu and T. Matsumoto, *Polym. Bull.*, 2004, **52**, 235–242.

21 S. Chatti, M. A. Hani, K. Bornhorst and H. R. Kricheldorf, *High Perform. Polym.*, 2009, **21**, 105–118.

22 H. R. Kricheldorf and M. Al Masri, *J. Polym. Sci. Part A Polym. Chem.*, 1995, **33**, 2667–2671.

23 C. Belgacem, R. Medimagh, A. Fildier, A. Bulete, H. Kricheldorf, H. Ben Romdhane and S. Chatti, *Des. Monomers Polym.*, 2015, **18**, 64–72.

24 W. U. Yuhong, N. Taylor, V. Leo and C. Ward, EP3088442A1, 2016.

25 B. V. Tawade, S. V. Shaligram, N. G. Valsange, U. K. Kharul and P. P. Wadgaonkar, *Polym. Int.*, 2016, **65**, 567–576.

26 A. S. More, S. K. Pasale, P. N. Honkhambe and P. P. Wadgaonkar, *J. Appl. Polym. Sci.*, 2011, **121**, 3689–3695.

27 C.-L. Lee, H. L. Chapman, M. E. Cifuentes, K. M. Lee, L. D. Merrill, K. L. Ulman and K. Venkataraman, *J. Memb. Sci.*, 1988, **38**, 55–70.

28 J. S. McHattie, W. J. Koros and D. R. Paul, *Polymer*, 1991, **32**, 840–850.

29 T. Sakaguchi, K. Yumoto, Y. Shida, M. Shiotsuki, F. Sanda and T. Masuda, *J. Polym. Sci. Part A Polym. Chem.*, 2006, **44**, 5028–5038.

30 J. W. Simmons, US5393323, 1995.

31 B. E. Jennings, M. E. B. Jones and J. B. Rose, *J. Polym. Sci. Part C Polym. Symp.*, 1967, **16**, 715–724.

32 J. Ding, X. Du, M. Day, J. Jiang, C. L. Callender and J. Stupak, *Macromolecules*, 2007, **40**, 3145–3153.

33 H. R. Kricheldorf and G. Bier, *J. Polym. Sci. Polym. Chem. Ed.*, 1983, **21**, 2283–2289.

34 R. N. Johnson, A. G. Farnham, R. A. Clendinning, W. F. Hale and C. N. Merriam, *J. Polym. Sci. Part A-1 Polym. Chem.*, 1967, **5**, 2375–2398.

35 F. Liu, J. Ding, M. Li, M. Day, G. Robertson and M. Zhou, *Macromol. Rapid Commun.*, 2002, **23**, 844–848.

36 V. Percec, R. S. Clough, M. Grigoras, P. L. Rinaldi and V. E. Litman, *Macromolecules*, 1993, **26**, 3650–3662.

37 M. Jayakannan and S. Ramakrishnan, *Macromol. Rapid Commun.*, 2001, **22**, 1463–1473.

38 R. Duran, M. Ballauff, M. Wenzel and G. Wegner, *Macromolecules*, 1988, **21**, 2897–2899.

39 H. Kim, S.-B. Park, Jin Chul Jung and W.-C. Zin, *Polymer*, 1996, **37**, 2845–2852.

40 D. H. Wang, Z. Shen, M. Guo, S. Z. D. Cheng and F. W. Harris, *Macromolecules*, 2007, **40**, 889–900.

41 Y. S. Kim and J. C. Jung, *J. Polym. Sci. Part A Polym. Chem.*, 2002, **40**, 1764–1774.

42 Y. Chen, R. Wombacher, J. H. Wendorff and A. Greiner, *Polymer*, 2003, **44**, 5513–5520.

43 S. S. Nagane, Ph. D. Thesis, Academy of Scientific and Innovative Research, 2018.

CHAPTER 6

Synthesis and Characterisation of Partially Bio-Based Polycarbonates Containing Pendent Pentadecyl Chains

6.1 Introduction

Polycarbonates represent a prominent member of the group of engineering thermoplastics.[1] Polycarbonates were synthesised for the first time in 1881 by Birnbaum and Lurie *via* polycondensation of resorcinol and phosgene in the presence of pyridine.[2] The early polycarbonates possessed undesirable properties: they were brittle, crystalline, insoluble in most solvents and were of low molecular weights. It was only after Herman Schnell of Bayer AG (Germany) developed BPA-based polycarbonate, under the commercial name of Makrolon in 1959,[3,4] that the commercial utilisation of polycarbonates started. Daniel Fox of GE (USA) independently developed bisphenol-based polycarbonates in 1960 with the trade name Lexan.[5] Polycarbonate obtained from bisphenol A possesses good thermal stability, excellent impact resistance, high flame retardancy, easy moldability, excellent transparency, high refractive index and UV absorption. Such attractive properties make polycarbonates compelling alternatives and substitutes for metals, glass and wood. Polycarbonates find applications as shatter-proof window glass replacements, storage of digital data on CDs and DVDs, safety eyewear, sunglasses, corrective lenses, medical appliances (blood filters, dialysers and pacemaker components) and in packaging.[6,7]

Commercially, polycarbonates are mostly derived from bisphenol A (BPA). The annual production of BPA in 2016 was 5 million tonnes in USA alone; with a 13 % annual growth reported from Asia and 19 % growth in demand for polycarbonates in India. The major use of BPA was in the manufacture of polycarbonates, followed by epoxy resins, caprolactum, alkyl phenols, aniline and adipic acid.[8] Unfortunately, BPA is toxic in nature, being a known endocrine disruptor.[9–11] In addition, BPA is derived from non-renewable petrochemical resources. Due to finite nature of petrochemical resources, interest in chemicals derived from biomass has been progressively growing.[12,13]

In the past few decades a lot of research activities in both academia and industries have focused on developing bisphenols and polycarbonates from sustainable sources. Meylemann *et al* have reported renewable bisphenols from creosol[14,15] obtained from lignin. Several aliphatic polycarbonates have been developed from renewable feedstocks, notably: high T_g polycarbonates obtained from limonene oxide,[16] carbohydrate-based polycarbonates,[17] plant oil based polycarbonates,[18] and isosorbide-based

polycarbonates.[12] Aromatic polycarbonates generated from sustainable resources include polycarbonates derived from vanillin,[19] softwood lignin feedstock[20] and carvacol obtained from turpentine,[21] di(hydroxyphenyl) alkane monomers obtained by metathesis from eugenol and CNSL.[22] Additionally, several functional polycarbonates have been reported from renewable resources.[23]

The synthesis of bisphenol containing pendent pentadecyl chains, namely, 1,1-bis(4-hydroxyphenyl)-3-pentadecylcyclohexane (BPC15), starting from CNSL has been reported in the patent literature and polycarbonates based on BPC15 have been claimed.[24] The utility of BPC15 for synthesis of (co)polyesters and poly(arylene ether)s[25,26] has also been demonstrated.

In the present work, a series of partially bio-based (co)polycarbonates with cyclohexylidene units and pentadecyl chains were synthesised by polycondensation of varying compositions of BPC15 and BPA with triphosgene in dichloromethane at room temperature. (Co)polycarbonates were characterised by inherent viscosity measurements, GPC studies, FT-IR, ^{1}H-NMR, ^{13}C-NMR spectroscopy, X-ray diffraction, thermogravimetric analysis (TGA) and differential scanning calorimetric studies (DSC). The influence of the pentadecyl chains on polymer properties was studied.

6.2 Experimental

6.2.1 Materials

1,1-Bis(4-hydroxyphenyl)-3-pentadecylcyclohexane (BPC15) was synthesised as described in **Chapter 3**. Triphosgene (Sigma Aldrich, India) and hydrochloric acid (Thomas Baker, India) were used as received. Bisphenol A (Sigma Aldrich, India) was utilised after sublimation. Dichloromethane and triethylamine (Thomas Baker, India) were used after distillation over calcium hydride (Sigma Aldrich, India) and potassium hydroxide (Thomas Baker, India), respectively.

6.2.2 Measurements

FT-IR spectra of synthesised (co)polycarbonates were recorded with ATR mode using Bruker α-T spectrophotometer in the range 4000 to 500 cm^{-1}. ^{1}H-NMR and ^{13}C-NMR spectra were recorded on Bruker-AV 400 and 500 MHz spectrometer using chloroform-*d* as solvent and TMS as an internal standard. Molecular weights of polycarbonates were measured on Waters 2707 chromatograph (GPC) equipped with

Viscotek 270 dual detector in tetrahydrofuran using polystyrene as the calibration standard. Concentration of polymers used was 3 mg dL^{-1}. Inherent viscosity of (co)polycarbonates was measured using 0.5 % (w/v) solution of (co)polycarbonates in chloroform at 25 ± 0.1 °C using Ubbelohde suspended level viscometer. Inherent viscosity was determined according to the following equation:

$$n_{inh} = \frac{2.303}{C} x \log \frac{t}{t_0}$$

where *t* and t_0 are flow times of polymer solution and solvent, respectively and *C* is the concentration of polymer solution. X-Ray diffraction analysis was performed on Rigaku MicroMax-007HF X-ray diffractometer at 40 kV and 30 mA. Thermo gravimetric analysis (TGA) of the polymers was performed on Perkin Elmer: STA 6000 between temperatures of 30 °C to 900 °C with a heating rate of 10 °C min^{-1}, under nitrogen. Glass transition temperatures (T_g) were determined from differential scanning calorimetry experiments (DSC) carried out on TA Q-100 instrument with sample heating rate of 10 °C min^{-1} under nitrogen atmosphere. T_g values of the polycarbonates were determined from the second heating cycles.

6.2.3 Synthesis of (co)polycarbonates: typical procedure

Into a 50 mL three-necked round bottom flask equipped with a nitrogen balloon, an addition funnel and a magnetic stirrer bar were added BPC15 (1.9159 g, 4 x 10^{-3} mol) and dry dichloromethane (15 mL). The reaction mixture was cooled to 0 °C, to which a solution of triethylamine (1.67 mL, 1.2 x 10^{-2} mol) in dry dichloromethane (3 mL) was added drop wise over a period of 10 minutes. Subsequently, a solution of triphosgene (0.499 g, 1.68 x 10^{-3} mol) in dry dichloromethane (3 mL) was added drop wise into the reaction mixture, which was then allowed to warm to 25 °C and stirred continuously for a period of 4 h. Thereafter, the reaction was quenched by the addition of 2 N hydrochloric acid (5 mL), extracted with dichloromethane (2 x 100 mL), washed with water (2 x 100 mL), dried over anhydrous sodium sulphate and concentrated under reduced pressure. Due precautions were taken to carry out the work-up in a fume hood. All the glassware used were immersed in sodium hydroxide solution prior to washing to neutralise phosgene. The concentrated polycarbonate solution was poured into methanol (1000 mL) and the precipitated polycarbonate was filtered and washed with methanol. The obtained polycarbonate was subsequently dissolved in dichloromethane, reprecipitated in methanol

(1000 mL), filtered and dried under reduced pressure. This polycarbonate was designated as PC-100.

A similar procedure was employed for the synthesis of copolycarbonates with BPC15 feed mol % of 70 %, 50 % and 30 % designated as PC-70, PC-50 and PC-30, respectively.

6.3 Results and Discussion

6.3.1 Synthesis of (co)polycarbonates

Presently, several methods for the synthesis of polycarbonates are known. These include (1) interfacial or solution polymerisation (Schotten Baumann reaction) of phosgene with diols[27] (2) interfacial or solution polymerisation of phosgene substitutes, such as *N*, *N'*-carbonyl diimidazole, trichloromethyl chloroformate, triphosgene, and bis (2,4,6-trichlorophenyl)carbonate with diols[28,29] (3) melt polymerisation of diaryl carbonate and diols[30,31] (4) ring opening polymerisation of cyclic oligomeric carbonates[32] (5) catalytic oxidative carbonylation reaction of BPA with carbon monoxide in the presence of oxygen.[33–37] Phosgene is an extremely toxic chemical, which being gaseous, renders it highly dangerous and inconvenient for use at the laboratory scale. It has been reported that high molecular weight polycarbonates may be obtained by using triphosgene, a solid which acts as a source for phosgene, on laboratory scale.[38–42]

In the present work, aromatic (co)polycarbonates were synthesised by polycondensation of BPC15 or a mixture of BPC15 and BPA with triphosgene (**Scheme 6.1**)

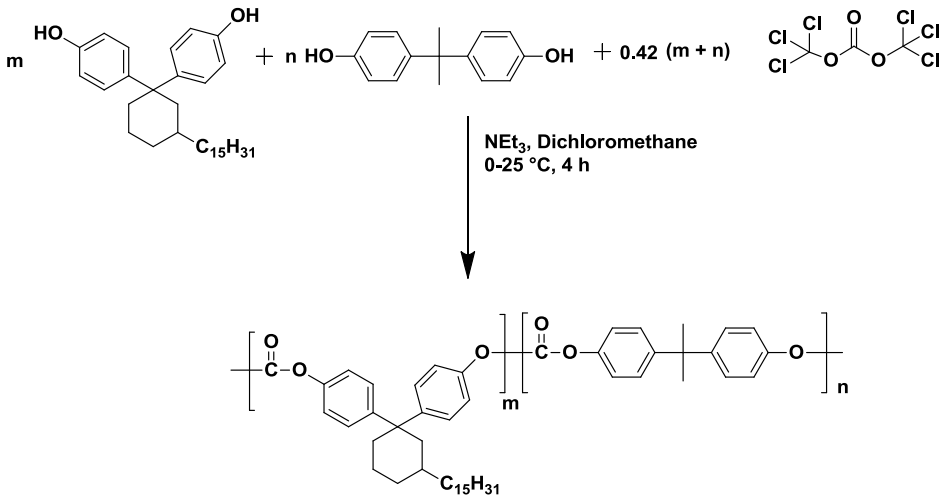

Scheme 6.1 Synthesis of (co)polycarbonates

To a solution of BPC15 or a mixture of BPC15 and BPA in dry dichloromethane (9-10 wt % solid) was successively added triethylamine and triphosgene in dichloromethane drop wise at 0 °C. A mole ratio of bisphenol:triphosgene of 1:0.42 was maintained in accordance with the work reported by Boyles *et al*,[43] who obtained high molecular weight polycarbonates under similar molar stoichiometric conditions. The polycondensation reaction was allowed to proceed at 25 °C for a period of 4 h. During the reaction work up, involving extraction of dichloromethane solution with water, the by-product of triethylamine hydrochloride dissolved in water along with the decomposition of the chloroformate-triethylamine complex at both ends of the polymer chain.[43] Subsequently, the dichloromethane solution was concentrated and the solid polycarbonates were obtained by precipitation in methanol.

The results of synthesis of (co)polycarbonates are tabulated in **Table 6.1.** The synthesized polycarbonates were observed to have inherent viscosities in the range 0.71 – 0.86 dL g^{-1} and number average molecular weights (M_n) in the range 40200 – 69800 g mol^{-1}, indicative of the formation of reasonably high molecular weight polycarbonates. However, it is to be noted that molecular weights determined through GPC utilise polystyrene standards and hence may not be considered absolute molecular weights. Dispersities of (co)polycarbonates were in the range 1.6-1.9. The polycarbonates formed free-standing, flexible transparent films (**Fig 6.1**) when drop-casted from respective chloroform solutions.

Table 6.1 Results of synthesis of (co)polycarbonates

(Co)polycarbonate	Composition of diols (mol %)		η_{inh} (dL/g)[a]	Molecular weight[b] (g mol^{-1})		Dispersity (M_w/M_n)
	BPC15	BPA		M_n	M_w	
PC-100	100	0	0.71	40200	67300	1.6
PC-70	75	25	0.78	52900	96700	1.8
PC-50	50	50	0.79	66400	127400	1.9
PC-30	25	75	0.86	69800	125800	1.8

a: η_{inh} was measured using 0.5% (w/v) solution of polycarbonates in chloroform at 25 °C ± 1°C
b: Determined through GPC in tetrahydrofuran, using polystyrenes as calibration standard

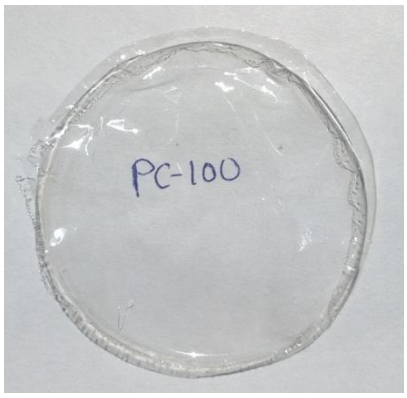

Figure 6.1 PC-100 film cast from chloroform

The structure of the synthesised polycarbonates was studied through FT-IR, ^{1}H-NMR and ^{13}C-NMR spectroscopic studies. FT-IR spectrum of homo polycarbonate, PC-100, is depicted in **Fig 6.2**.

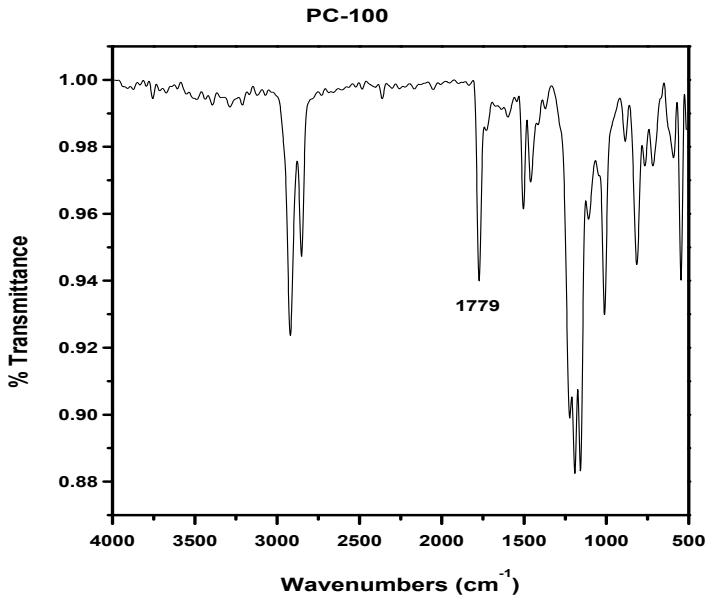

Figure 6.2 FT-IR spectrum of PC-100 film

A strong absorption band was observed at 1779 cm^{-1}, which is characteristic of carbonyl group (C=O) of carbonate functionality confirming the formation of polycarbonate.

Representative ^{1}H-NMR, HSQC and ^{13}C-NMR spectra of PC-100 are presented in **Fig 6.3**, **Fig 6.4** and **Fig 6.5**, respectively.

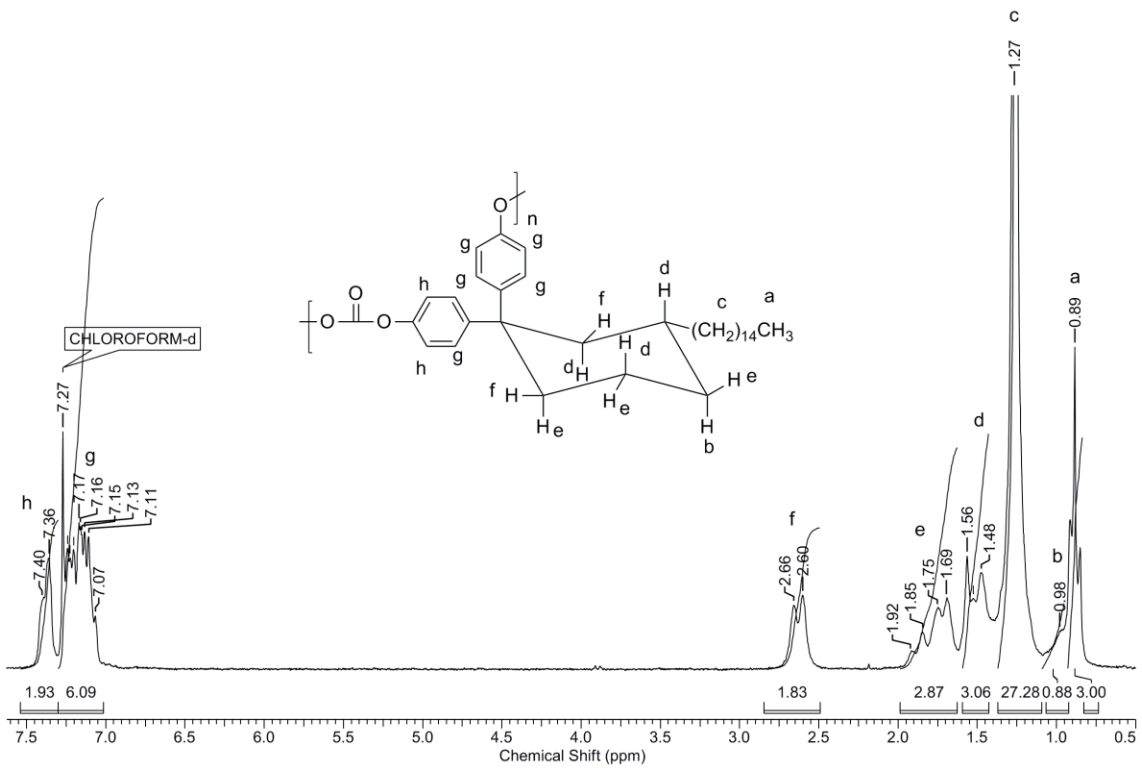

Figure 6.3 ^{1}H-NMR spectrum ($CDCl_3$) of PC-100

Detailed study of the ^{1}H-NMR, HSQC and ^{13}C-NMR spectra revealed that the phenyl rings were magnetically non-equivalent. The pentadecyl substituent prevents ring inversion; hence the conformation of the cyclohexyl ring is locked in the chair conformer as depicted in **Fig 6.3**, with the substituent present in the equatorial position. Aromatic protons (**g)** present on the axial phenyl ring and the protons *meta* to oxygen of carbonate linkage, present on the equatorial phenyl ring appeared as a multiplet in the range 7.03 – 7.31 δ ppm. The aromatic protons present on the equatorial phenyl ring adjacent to the carbonate linkage resonated as a multiplet in the range 7.32 – 7.44 δ ppm. Further assignment of the protons was done by a combined study of ^{1}H-NMR, HSQC and ^{13}C-NMR spectra. It was found that the equatorial protons appeared up-field compared to corresponding axial protons.

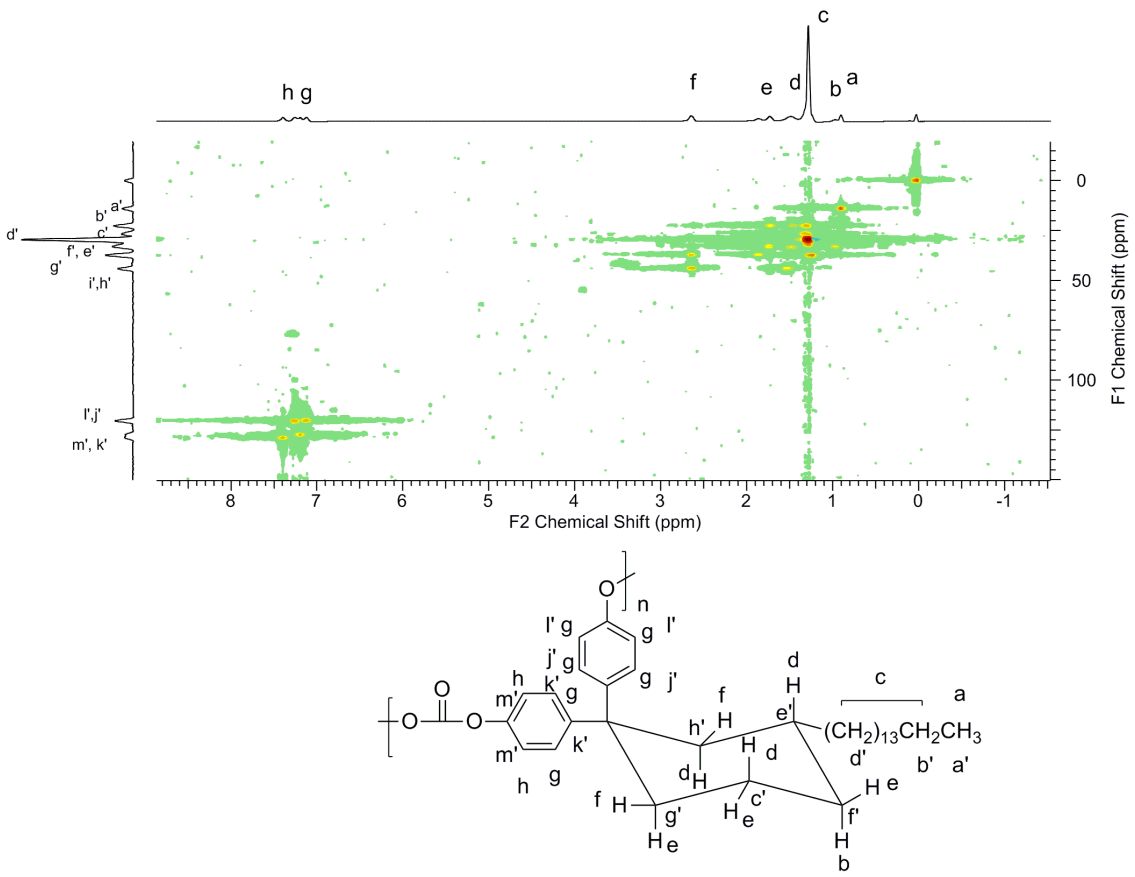

Figure 6.4 HSQC spectrum ($CDCl_3$) of PC-100

Protons present on the carbons **e'**, **f'**, **g'**, **h'** and **c'** could be successfully assigned unambiguously on the basis of HSQC spectrum. Equatorial protons (**f**) on carbon **g'** and carbon **h'** appeared at 2.54 – 2.72 δ ppm as a multiplet. The axial protons on carbon **g'**, and equatorial protons on carbons **c'** and **f'** (e) appeared together as a multiplet at 1.63 – 1.96 δ ppm. The axial protons (**d**) on carbons **e'**, **h'** and **c'** resonated together in the range 1.39 – 1.63 δ ppm as a multiplet. Axial proton (**b**) on carbon **f'** appeared as a multiplet in the range 0.94 – 1.08 δ ppm. Methyl protons (**a**) belonging to the pentadecyl chain appeared as a triplet at 0.89 δ ppm, while the methylene protons (**c**) resonated in the range 1.09 – 1.38 δ ppm as a multiplet.

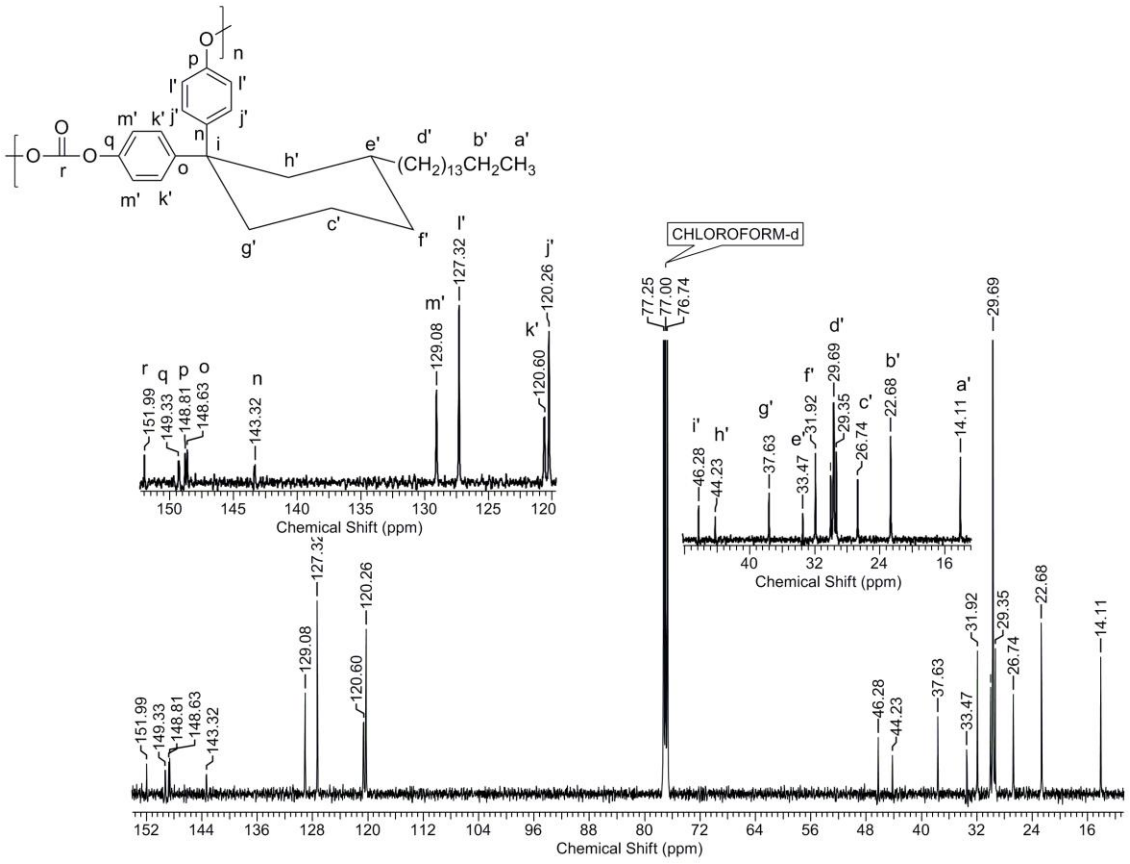

Figure 6.5 ^{13}C-NMR spectrum ($CDCl_3$) of PC-100

^{13}C-NMR spectrum of PC-100 was assigned with the help of the corresponding DEPT and HSQC spectra. The carbons **c', e'**, **f'**, **g'**, and **h'** appearing at 26.74 δ ppm, 33.47 δ ppm, 31.92 δ ppm, 37.63 δ ppm and 44.23 δ ppm, respectively, could be successfully assigned on the basis of HSQC spectrum. The aromatic carbons **j'** and **l'**, belonging to the axial phenyl ring, resonated at 120.26 δ ppm and 127.32 δ ppm, respectively, while the carbons **k'** and **m'** appeared at 120.60 δ ppm and 129.08 δ ppm, respectively. Carbonyl carbon (**r**) belonging to the carbonate linkage resonated at 151.99 δ ppm.

The composition of the synthesised copolycarbonates was determined by ^{1}H-NMR spectroscopy (**Fig 6.6**).

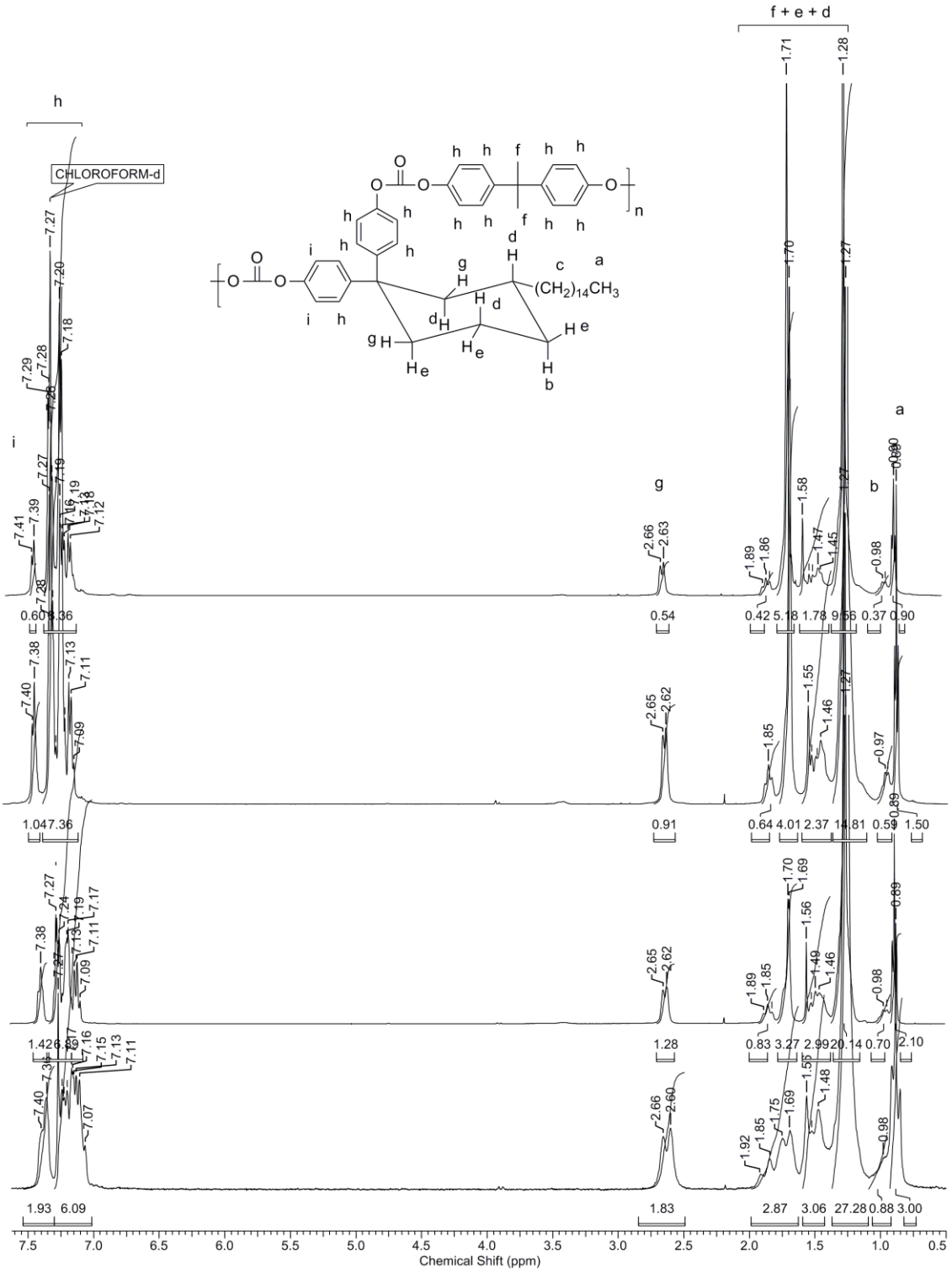

Figure 6.6 ^{1}H-NMR spectra ($CDCl_3$) of (co)polycarbonates derived from BPC15, BPA and triphosgene

^{1}H-NMR spectra of (co)polycarbonates were compared to determine the mol % incorporation of BPC15 in the synthesised (co)polycarbonates. The integrated intensity

ratio of peaks **g** and **a** belonging to the (co)polycarbonates was determined to find out composition of the (co)polycarbonates and is summarised in **Table 6.2**.

Table 6.2 Composition of copolycarbonates determined from ^{1}H-NMR spectra

Copolycarbonate	Feed BPC15, mol %	Observed BPC15, mol %
PC-70	**70**	**70**
PC-50	**50**	**50**
PC-30	**30**	**30**

The data obtained from **Table 6.2** demonstrates that there is an excellent agreement between the observed % incorporation of bisphenol BPC15 in copolycarbonates and the amount taken for polymerisation.

6.3.2 Solubility and X-ray diffraction studies

The solubility behaviour of synthesised (co)polycarbonates at 3 wt % concentration was determined. All synthesised (co)polycarbonates were soluble in chloroform, dichloromethane and tetrahydrofuran.

Wide angle X-ray diffraction (WAXD) patterns for the synthesized polymers are provided in **Fig 6.7**. A broad hump is observed around 2θ ~ 20° while a sharp peak was observed at 2θ ~ 3°. The broad hump indicates that the (co)polycarbonates were amorphous in nature. However, the sharp peak at low angle region is indicative of the formation of layered structures. According to literature reports,[44–47] the sharp peak at low angle arises from the reflection from the spacing between the polymer backbones with pendent alkyl chains. The long alkyl chains get fully interdigitated and tilted away from the polymer main chain, giving rise to the layered structure in the solid state as indicated by the XRD pattern. Notably, relative intensity of the peak at low angle increased with increase in % incorporation of pentadecyl chain containing BPC15 in the (co)polycarbonates.

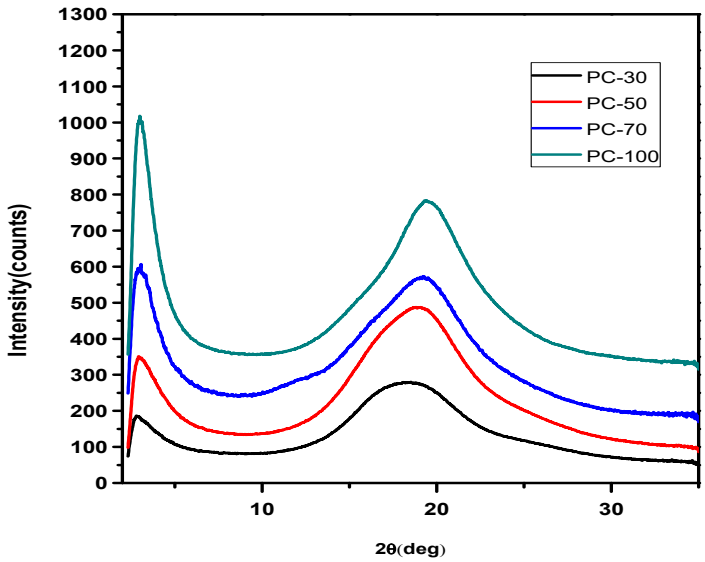

Figure 6.7 X-Ray diffractograms of (co)polycarbonates

6.3.3 Thermal properties

The thermal properties of (co)polycarbonates were studied through TG and DSC analyses. The results obtained are summarised in **Table 6.3** and the TG and DSC curves are displayed in **Fig 6.8** and **Fig 6.10**. A representative differential thermogravimetric analysis (DTG) curve along with corresponding TG curve for PC-100 is reproduced in **Fig 6.9**.

Table 6.3 Thermal properties of (co)polycarbonates

(Co)polycarbonate	Composition of diols (mol %)		T_g (°C)[a]	T_{10} (°C)[b]	Char yield (%)[c]
	BPC15	BPA			
PC-100	100	0	47	438	1.6
PC-70	70	30	56	446	2.2
PC-50	50	50	67	449	5.9
PC-30	30	70	79	450	6.4

a: 10 % weight loss on TGA thermograms at a heating rate of 10 °C/min under nitrogen atmosphere.
b: Measured by DSC from second heating scan with heating rate of 10 °C/min under nitrogen atmosphere.
c: Char yield measured at 900 °C.

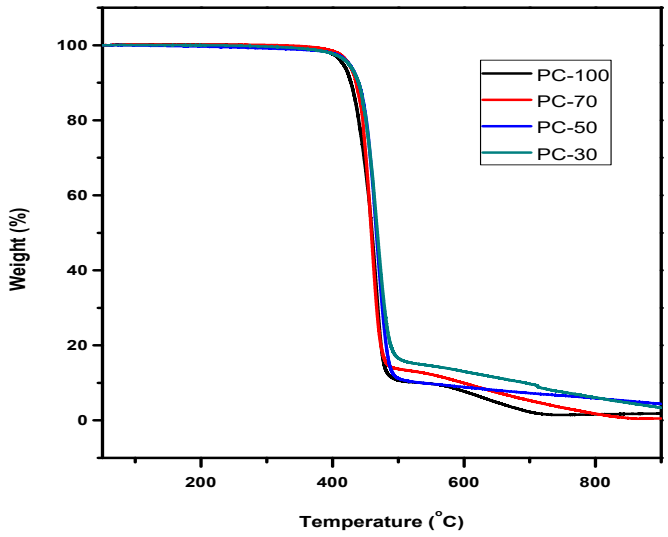

Figure 6.8 TG curves of (co)polycarbonates

TG analysis of (co)polycarbonates was carried out at temperatures ranging from 30 – 900 °C at a heating rate of 10 °C/min. The T_{10} values (temperature at which 10 % weight loss of polymers occurred) obtained were in the range of 438 – 450 °C. It was observed that the T_{10} values of the (co)polycarbonates decreased in the order PC-30, PC-50, PC-70 and PC-100. This trend is observed because from PC-30 to PC-100, there is an increase in % incorporation of pentadecyl chain containing monomer, BPC15. The pentadecyl chain being a thermally labile group, leads to decrease in thermal stability. Char yields obtained at 900 °C were in the range of 1.6 – 6.4 %. A decrease in char yields was observed with increase in incorporation of BPC15 monomer. This is due to decreasing aromatic content in (co)polycarbonates with increase in mole % incorporation of pentadecyl chain and cyclohexylidene containing BPC15.

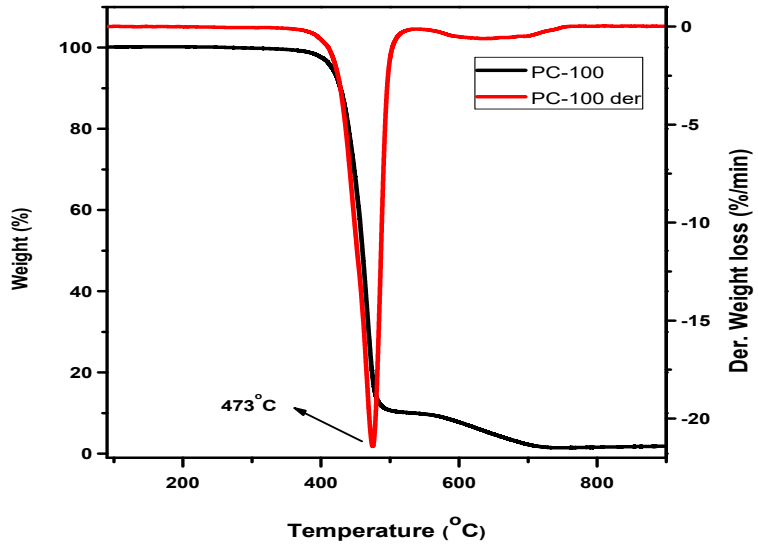

Figure 6.9 DTG curve of PC-100

From the differential thermogravimetric (DTG) analysis curve it was determined that PC-100 underwent single-step degradation. Maximum degradation occurred at 473 °C.

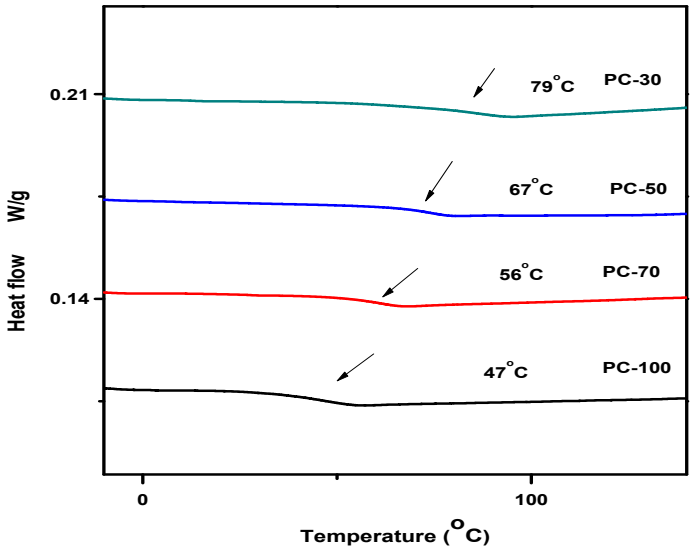

Figure 6.10 DSC curves of (co)polycarbonates

(Co)polycarbonates displayed T_g values in the range 47 °C – 79 °C. There was a distinct decrease in T_g values with increase in % incorporation of pentadecyl chain

containing BPC15 in the (co)polycarbonates. This observation can be explained by the packing disruptive effect the pentadecyl chain exerts on the polymers in the solid state, leading to enhanced segmental mobility and lowered T_g values. A wide gap is observed between the T_g values (47 – 79 °C) and the T_{10} values (438 – 450 °C). This indicates that these (co)polycarbonates afford a large processing window for melt processing.

The experimentally obtained T_g values were compared with the theoretical T_{gc} values, calculated from the Fox equation:

$$\frac{1}{T_{gc}} = \frac{W_1}{T_{g1}} + \frac{W_2}{T_{g2}}$$

Where;

T_{gc} refers to the calculated T_g of copolycarbonates, T_{g1} and T_{g2} refer to T_g values obtained from homopolycarbonates derived from BPC15 and BPA, respectively. (T_{g1} = 47 °C and T_{g2} = 147 °C). W_1 and W_2 represent weight fractions of BPC15 and BPA, respectively, in the copolycarbonates. The $1/T_{gc}$ values calculated were plotted against W_1. At the same time, experimentally determined $1/T_g$ values were also plotted (**Fig 6.11**).

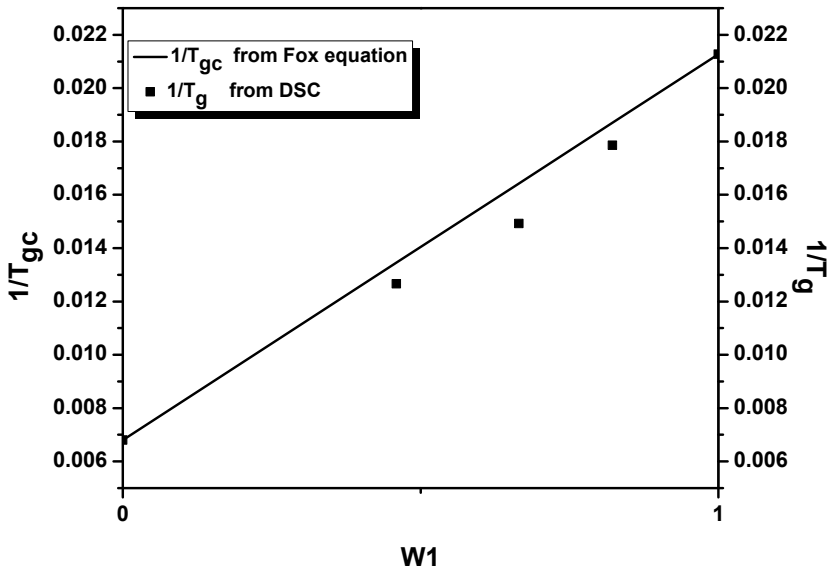

Figure 6.11 T_g as a function of composition of BPC15 in copolycarbonates derived from polycondensation of a mixture of BPC15 and BPA with triphosgene

The calculated T_{gc} values express the net effect of the interaction between the monomeric components of a copolymer on the T_g values. The experimentally determined

T_g values were observed to follow the Fox-Flory rule within experimental error. This also indicated that the (co)polycarbonates synthesised are random in nature.

6.4 Conclusions

1. A series of (co)polycarbonates containing cyclohexylidene and pendent pentadecyl chains were synthesised from polycondensation of 1,1-bis(4-hydroxyphenyl)-3-pentadecylcyclohexane (BPC15) and varying mixtures of BPC15 and BPA with triphosgene as phosgene substitute *via* low temperature solution polycondensation.

2. Inherent viscosities and number average weights of the (co)polycarbonates were in the range 0.71 – 0.86 dL g^{-1} and 40200 – 69800 g mol^{-1}, respectively, indicating the formation of (co)polycarbonates of reasonably high molecular weights.

3. (Co)polycarbonates were soluble in chloroform, dichloromethane and tetrahydofuran. Flexible, transparent and free-standing films of synthesised (co)polycarbonates were obtained by drop-casting from chloroform solutions.

4. The T_g values (47 – 79 °C) of (co)polycarbonates showed a significant decrease with increase in % incorporation of BPC15. T_{10} values (438 – 450 °C) of (co)polycarbonates indicated that they possessed good thermal stability.

References

1 D. Freitag, G. Fengler and L. Morbitzer, *Angew. Chemie Int. Ed. English*, 1991, **30**, 1598–1610.

2 K. Birnbaum and G. Lurie, *Berichte der Dtsch. Chem. Gesellschaft*, 1881, **14**, 1753–1755.

3 H. Schnell, *Angew. Chemie*, 1956, **68**, 633–640.

4 H. Schnell, *Ind. Eng. Chem.*, 1959, **51**, 157–160.

5 D. W. Fox, US3153008, 1964.

6 D. J. Brunelle, in *Advances in Polycarbonates*, eds. D. J. Brunelle and M. R. Korn, American Chemical Society, 2005, pp. 1–5.

7 K. Takeuchi, in *Polymer Science: A Comprehensive Reference*, eds. K. Matyjaszewski and M. Möller, Elsevier, 2012, vol. 5, pp. 363–376.

8 N. Jalal, A. R. Surendranath, J. L. Pathak, S. Yu and C. Y. Chung, *Toxicol. Reports*, 2018, **5**, 76–84.

9 C. V. Sartain and P. A. Hunt, *Fertil. Steril.*, 2016, **106**, 820–826.

10 M. K. Björnsdotter, J. de Boer and A. Ballesteros-Gómez, *Chemosphere*, 2017, **182**, 691–706.

11 J. S. Siracusa, L. Yin, E. Measel, S. Liang and X. Yu, *Reprod. Toxicol.*, 2018, **79**, 96–123.

12 F. Fenouillot, A. Rousseau, G. Colomines, R. Saint-Loup and J.-P. Pascault, *Prog. Polym. Sci.*, 2010, **35**, 578–622.

13 L. Shen, E. Worrell and M. Patel, *Biofuels, Bioprod. Biorefining*, 2010, **4**, 25–40.

14 H. A. Meylemans, B. G. Harvey, J. T. Reams, A. J. Guenthner, L. R. Cambrea, T. J. Groshens, L. C. Baldwin, M. D. Garrison and J. M. Mabry, *Biomacromolecules*, 2013, **14**, 771–780.

15 H. A. Meylemans, T. J. Groshens and B. G. Harvey, *ChemSusChem*, 2012, **5**, 206–210.

16 N. Kindermann, À. Cristòfol and A. W. Kleij, *ACS Catal.*, 2017, **7**, 3860–3863.

17 M. G. García-Martín, R. R. Pérez, E. B. Hernández, J. L. Espartero, S. Muñoz-Guerra and J. A. Galbis, *Macromolecules*, 2005, **38**, 8664–8670.

18 M. Winkler, C. Romain, M. A. R. Meier and C. K. Williams, *Green Chem.*, 2015, **17**, 300–306.

19 B. G. Harvey, A. J. Guenthner, H. A. Meylemans, S. R. L. Haines, K. R. Lamison, T. J. Groshens, L. R. Cambrea, M. C. Davis and W. W. Lai, *Green Chem.*, 2015, **17**, 1249–1258.

20 S.-F. Koelewijn, S. Van den Bosch, T. Renders, W. Schutyser, B. Lagrain, M. Smet, J. Thomas, W. Dehaen, P. Van Puyvelde, H. Witters and B. F. Sels, *Green Chem.*, 2017, **19**, 2561–2570.

21 B. G. Harvey, A. J. Guenthner, T. A. Koontz, P. J. Storch, J. T. Reams and T. J. Groshens, *Green Chem.*, 2016, **18**, 2416–2423.

22 A. S. Trita, L. C. Over, J. Pollini, S. Baader, S. Riegsinger, M. A. R. Meier and L. J. Gooßen, *Green Chem.*, 2017, **19**, 3051–3060.

23 K. S. Bisht and T. F. Al-Azemi, in *Green Polymer Chemistry: Biocatalysis and Biomaterials*, eds. H. N. Cheng and R. A. Gross, American Chemical Society, 2010, pp. 175–199.

24 C. V. Avadhani, P. P. Wadgaonkar and S. Sivaram, US6255439B1, 2001.

25 R. D. Shingte, Ph. D. Thesis, University of Pune, 2006.

26 A. S. More, S. K. Pasale, P. N. Honkhambe and P. P. Wadgaonkar, *J. Appl. Polym. Sci.*, 2011, **121**, 3689–3695.

27 H. Schnell, *Polymer Review. Volume 9: Chemistry and Physics*, New York, 1964.

28 T. Kanno and M. Ueda, *Die Makromol. Chemie, Rapid Commun.*, 1990, **11**, 181–183.

29 Y. Saegusa, M. Kuriki, A. Kawai and S. Nakamura, *J. Polym. Sci. Part A Polym. Chem.*, 1990, **28**, 3327–3335.

30 S. Sun and T.-C. Chang, *J. Polym. Sci. Part A Polym. Chem.*, 1993, **31**, 2237–2243.

31 S. Sun and T.-C. Chang, *J. Polym. Sci. Part A Polym. Chem.*, 1993, **31**, 2711–2719.

32 D. J. Brunelle and T. G. Shannon, *Macromolecules*, 1991, **24**, 3035–3044.

33 J. E. Hallgren and R. O. Matthews, *J. Organomet. Chem.*, 1979, **175**, 135–142.

34 J. E. Hallgren, G. M. Lucas and R. O. Matthews, *J. Organomet. Chem.*, 1981, **204**, 135–138.

35 H. Ishii, M. Goyal, M. Ueda, K. Takeuchi and M. Asai, *Catal. Letters*, 2000, **65**, 57–60.

36 K. Okuyama, J. Sugiyama, R. Nagahata, M. Asai, M. Ueda and K. Takeuchi, *Green Chem.*, 2003, **5**, 563–566.

37 K. Okuyama, J. Sugiyama, R. Nagahata, M. Asai, M. Ueda and K. Takeuchi, *Macromolecules*, 2003, **36**, 6953–6955.

38 S.-J. Sun, K.-Y. Hsu and T.-C. Chang, *Polym. J.*, 1997, **29**, 25–32.

39 S. Sun, Y. Liao and T. Chang, *J. Polym. Sci. Part A Polym. Chem.*, 2000, **38**, 1852–1860.

40 M. J. Marks, S. Munjal, S. Namhata, D. C. Scott, F. Bosscher, J. A. De Letter and B. Klumperman, *J. Polym. Sci. Part A Polym. Chem.*, 2000, **38**, 560–570.

41 J. Eiffler and G. A. Jueptner, US6225436 B1, 2001.

42 T. F. McCarthy, D. B. Schwind and G. C. Smith, US6153721, 2000.

43 D. A. Boyles, T. S. Filipova, J. T. Bendler, G. Longbrake and J. Reams, *Macromolecules*, 2005, **38**, 3622–3629.

44 R. Duran, M. Ballauff, M. Wenzel and G. Wegner, *Macromolecules*, 1988, **21**, 2897–2899.

45 H. Kim, S.-B. Park, Jin Chul Jung and W.-C. Zin, *Polymer*, 1996, **37**, 2845–2852.

46 Y. S. Kim and J. C. Jung, *J. Polym. Sci. Part A Polym. Chem.*, 2002, **40**, 1764–1774.

47 Y. Chen, R. Wombacher, J. H. Wendorff and A. Greiner, *Polymer*, 2003, **44**, 5513–5520.

CHAPTER 7

Synthesis and Characterisation of Partially Bio-Based Polyimides Containing Pendent Pentadecyl Chains

7.1 Introduction

Aromatic polyimides belong to the class of high performance/ high temperature polymers which exhibit outstanding heat resistance, excellent mechanical properties, oxidative stability, solvent resistance and low dielectric constants allowing their use in niche applications, especially in the fields of aerospace, microelectronics, optoelectronics and microelectronics.[1–10] However, conventional aromatic polyimides generally possess high glass transition and melting temperatures in addition to limited solubility in common solvents, making the processing of polyimides difficult and expensive. This is attributable to the rigid rod-like structure of the aromatic polyimide which fosters strong inter-chain interactions. Over many years research efforts have been expended towards the development of processable polyimides to widen the scope of applications of polyimides. Such efforts generally include the incorporation of bulky substituents, flexible linkages, structurally unsymmetrical units and flexible pendent groups in the polyimides.[11–18] Such groups reduce close-chain packing of macromolecular chains leading to decreased inter-chain interactions and increased flexibility. This leads to decrease in T_g values, reduction in crystallinity and improvement in solubility, together leading to easier processability.

Polyimides are generally intensely coloured as a result of the generation of charge transfer complex (CTC) interactions resulting from inter-molecular and intra-molecular interactions.[19–22] Fabrication of transparent polyimides are useful in advanced optoelectronic applications, especially flexible printing circuit boards, flexible displays and optical waveguides.[23–28] The design of transparent polyimides include attempts to decrease CTC interactions. CTC interactions may be reduced by the incorporation of bent or bulky units, flexible linkages or pendents and fluorinated substituents in the polyimide structure, which effectively reduce molecular aggregation leading to weakened CTC interactions.[24]

Incorporation of pendent alkyl chains and flexible ether linkages in the polyimide structure would lead to improved processability as well as weakened CTC interactions yielding transparent polyimides. Aromatic ether linkages also significantly improve polyimide toughness besides improving processability, without compromising thermal stability.[25,28–32] Development of transparent shape memory polyimides would be

especially useful in deployable space structures, high temperature sensors, jet propulsion systems, etc.[33–36]

Taking into consideration the advantages of incorporation of alkyl chains and ether linkages, both of which are known to lead to processable polymers with improved transparency, the monomer 4,4'-((2-pentadecyl-[1,1'-biphenyl]-4,4'-diyl)bis(oxy))dianiline(PBD) (**Chapter 3**) was employed for the synthesis of a series of polyimides possessing pendent pentadecyl chains and ether linkages. The pendent alkyl groups and ether linkages are both expected to improve polyimide processability and generate colourless polyimides. Polyimides were synthesised by polycondensation of PBD with commercially available aromatic dianhydrides, namely, 3,3',4,4'-biphenyltetracarboxylic dianhydride (BPDA), 4,4'-oxydiphthalic anhydride (ODPA), 4,4'-(hexafluoroisopropylidene) diphthalic anhydride (6-FDA) and 4,4′-(4,4′-isopropylidenediphenoxy)bis(phthalic anhydride) (IDBP) in *m*-cresol by single step high temperature solution polymerisation strategy. Polyimides were characterised by inherent viscosity measurements, GPC studies, FT-IR, ^{1}H-NMR, ^{13}C-NMR spectroscopy, X-ray diffraction, thermogravimetric analysis (TGA) and differential scanning calorimetric studies (DSC). The influence of pentadecyl chains on polymer properties was studied.

7.2 Experimental

7.2.1 Materials

4,4'-((2-Pentadecyl-[1,1'-biphenyl]-4,4'-diyl)bis(oxy))dianiline (PBD) was synthesised as described in **Chapter 3**. Isoquinoline (Acros, India), was used as received. 3,3',4,4'-Biphenyltetracarboxylic dianhydride (BPDA), 4,4'-oxydiphthalic anhydride (ODPA), 4,4'-(hexafluoroisopropylidene) diphthalic anhydride (6-FDA) and 4,4′-(4,4′-isopropylidenediphenoxy)bis(phthalic anhydride) (IDBP) (Sigma Aldrich, India) were purified by sublimation under reduced pressure. *meta*- Cresol (Thomas Baker, India) was distilled before use.

7.2.2 Measurements

Infrared spectra of the polymer films were measured on Perkin-Elmer Spectrum GX spectrometer. ^{1}H-NMR and ^{13}C-NMR spectra were recorded on Bruker-AV 400 and 500 MHz spectrometer using chloroform-*d* as solvent and TMS as an internal standard. Molecular weights of the polyimides were measured on Waters 2707 chromatograph

(GPC) equipped with Viscotek 270 dual detector in tetrahydrofuran using polystyrene as the calibration standard. Concentration of polymers used was 3 mg dL^{-1}. Inherent viscosity of the polymers was measured using 0.5 % (w/v) solution of polymer in chloroform at 25 ± 0.1 °C. Ubbelohde suspended level viscometer was used to determine viscosity according to the following equation:

$$n_{inh} = \frac{2.303}{C} x \log \frac{t}{t_0}$$

where *t* and t_0 are flow times of polymer solution and solvent, respectively and *C* is the concentration of polymer solution. X-Ray diffraction analysis was performed on Rigaku MicroMax-007HF X-ray diffractometer at 40 kV and 30 mA. Thermo gravimetric analysis (TGA) of the polymers was performed on TA Instrument SDT-Q600 Simultaneous TGA/DSC between temperatures of 30 °C to 800 °C with a heating rate of 10 °C min^{-1}, under nitrogen. Glass transition temperatures (T_g) were determined from differential scanning calorimetry experiments (DSC) carried out on TA Q-10 instrument with sample heating rate of 10 °C min^{-1} under nitrogen atmosphere. T_g values of the polyimides were determined from the second heating cycles.

7.2.3 Polyimide synthesis: typical procedure

Into a 50 mL three-necked round bottom flask equipped with a magnetic stirring bar and a calcium chloride guard tube were added 4,4'-((2-pentadecyl-[1,1'-biphenyl]-4,4'-diyl)bis(oxy))dianiline (PBD) (0.6 g, 1.04 x 10^{-3} mol), 6-FDA (0.426 g, 1.04 x 10^{-3} mol) and *m*-cresol (5.31 mL) and stirred under a steady stream of nitrogen for 1 h. The viscosity of the reaction mixture was observed to visibly increase, when a few drops of isoquinoline was added. Thereafter, the temperature of the reaction mixture was raised to 150 °C and stirred at that temperature for 8 h. Subsequently, the reaction mixture was stirred at 220 °C for six hours, during which the water formed as a result of imidisation was continuously removed out of the reaction mixture in a steady stream of nitrogen. The viscous polymer solution was poured into methanol (1000 mL) with continuous stirring to precipitate the fibrous polymer (PEI-6FDA). PEI-6FDA was further purified by repeated reprecipitation of its viscous chloroform solution into methanol (1000 mL).

A similar procedure was employed for the synthesis of other polyimides by polycondensation of PBD with ODPA (PEI-ODPA), BPDA (PEI-BPDA) and IDBP (PEI-IDBP).

7.3 Results and Discussion

7.3.1 Synthesis of polyimides

In this work, a series of polyimides was synthesised by single step high temperature solution polycondensation of PBD with commercially available aromatic dianhydrides, namely, 6FDA, BPDA, ODPA and IDBP (**Scheme 7.1**).

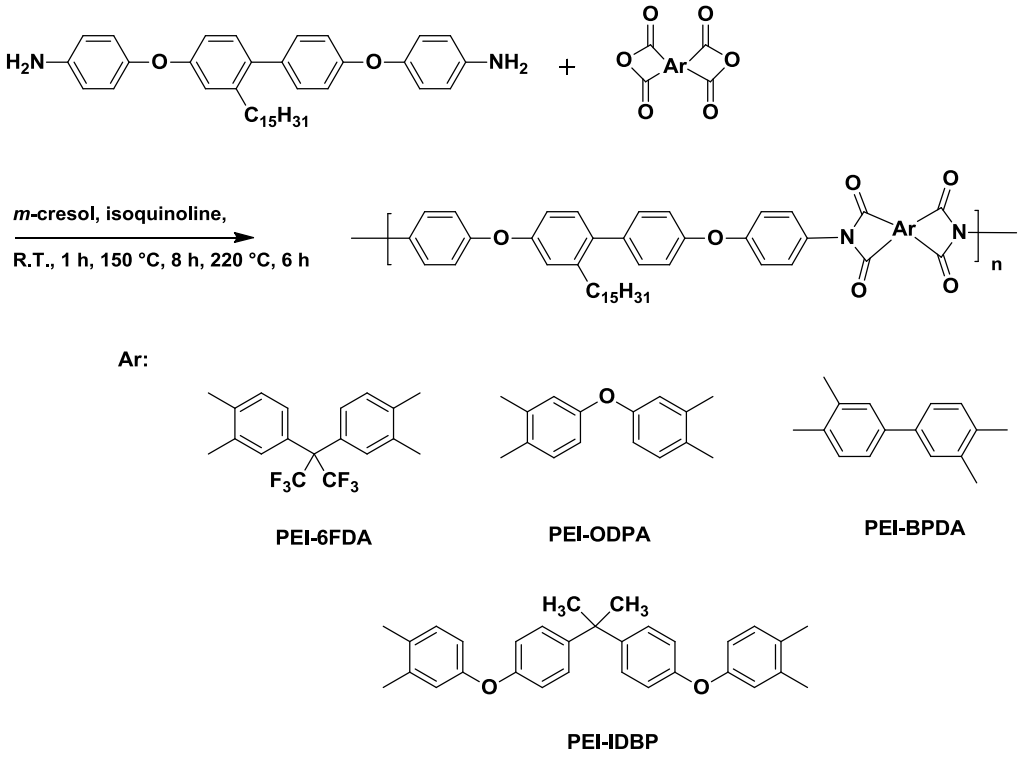

Scheme 7.1 Synthesis of polyimides

PBD and commercially available aromatic dianhydrides (6-FDA, ODPA, BPDA or IDBP) were stirred in *m*-cresol at room temperature for 1 h, during which the viscosity of the reaction mixture increased visibly. A few drops of isoquinoline were added to the reaction mixture, which acts as a catalyst for the imidisation process,[2] and heated at 150 °C for 8 h. Thereafter, the temperature was raised to 220 °C and stirred at that temperature to complete the imidisation process during which the water of imidisation was removed out of the reaction continuously in a steady stream of nitrogen.

The results of polymerisation are summarised in **Table 7.1.** Inherent viscosities of the synthesised polyimides were observed to be in the range 0.5 – 1.53 dL g^{-1}, which is suggestive of the formation of polyimides of reasonably high molecular weights. Number average molecular weights (M_n) of polyimides in tetrahydrofuran determined by GPC

were found to be in the range 19600 – 46500 g mol^{-1}. This observation also indicated that the polyimides synthesised were of reasonably high molecular weights. However, PEI-BPDA was insoluble in tetrahydrofuran, so its M_n could not be determined. The dispersities obtained were in the range 1.6 – 2.0. Flexible, free-standing, transparent films of polyimides were obtained from the corresponding chloroform solutions (**Fig 7.1**).

Table 7.1 Results of synthesis of polyimides

Polyimide	η_{inh} (dL/g)[a]	Molecular weight (g mol^{-1})[b]		Dispersity (M_w/M_n)
		M_n	M_w	
PEI-6FDA	0.56	46500	106900	1.6
PEI-ODPA	0.50	19600	40000	2.0
PEI-BPDA	1.53	-[c]	-[c]	-
PEI-IDBP	0.73	45100	84000	1.8

a: η_{inh} was measured using 0.5% (w/v) solution of polyimides in chloroform at 25 °C ± 1°C
b: determined through GPC in THF, using polystyrenes as calibration standard
c: not determined due to lack of solubility in THF

Figure 7.1 PEI-IDBP film cast from chloroform

The structure of synthesised polyimides was confirmed by FT-IR, ^{1}H-NMR and ^{13}C-NMR spectroscopic analysis. In **Fig 7.2** is presented FT-IR spectrum of representative polyimide, PEI-6FDA. In **Fig 7.3** is depicted the ^{1}H-NMR spectrum of PEI-6FDA while ^{13}C-NMR spectrum of PEI-6FDA is provided in **Fig 7.4**.

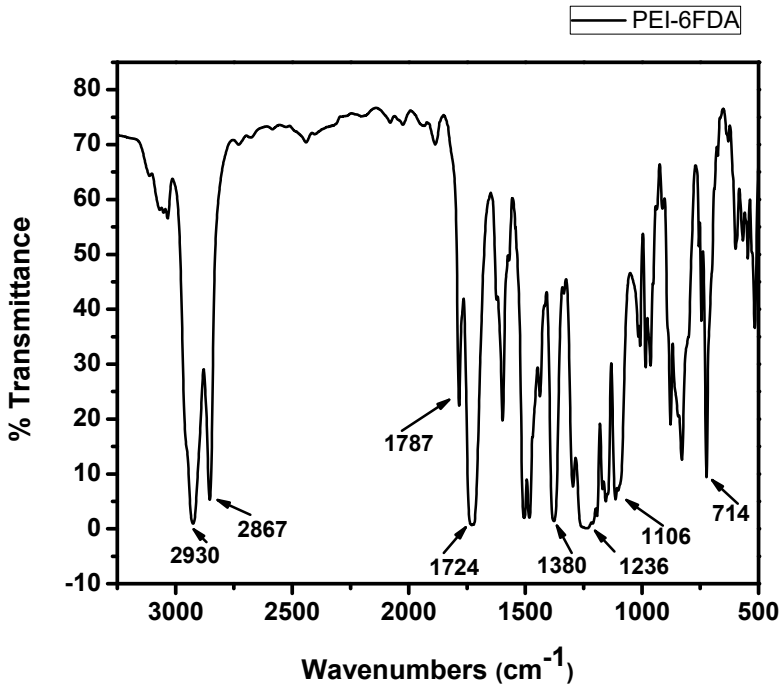

Figure 7.2 FT-IR spectrum of PEI-6FDA film

The absorption band at 1787 cm^{-1} was attributable to asymmetrical C=O stretch of imide functionality. A strong absorption band was observed at 1724 cm^{-1} corresponding to symmetrical C=O stretching. The band at 1380 cm^{-1} could be assigned to C-N stretching and bending vibrations while the absorption band at 1106 cm^{-1} could be ascribed to C-N stretching. The absorption band corresponding to imide ring deformation appeared at 714 cm^{-1}. The strong absorption band at 1236 cm^{-1} was ascribable to C-O-C stretching vibrations.

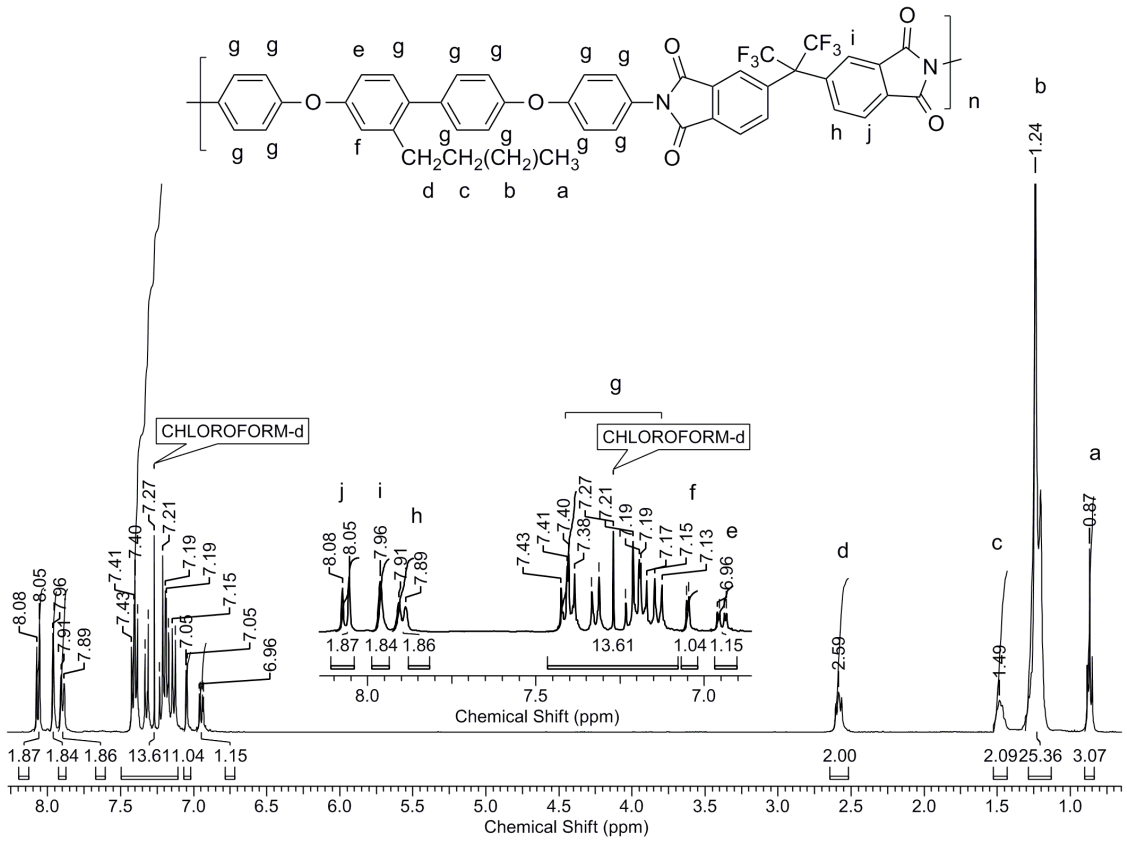

Figure 7.3 ^{1}H-NMR spectrum ($CDCl_3$) of PEI-6FDA

The aromatic proton **j**, *ortho* to the imide carbonyl resonated at 8.06 δ ppm as a doublet. The proton **i** flanked by imide carbonyl and quaternary carbon bearing trifluoromethyl groups appeared at 7.96 δ ppm in the form of a singlet. The aromatic protons **h** could be readily ascribed to the doublet at 7.90 δ ppm. The aromatic proton *ortho* to the pentadecyl chain (**f**) appeared at 7.05 δ ppm as a doublet. The aromatic proton *para* to pentadecyl chain (**e**), resonated at 6.95 δ ppm in the form of a doublet. The remaining aromatic protons (**g**) appeared in the range 7.44 – 7.11 δ ppm. The benzylic protons (**d**) of the pentadecyl chain appeared as a triplet at 2.59 δ ppm, while the methylene protons adjacent to it resonated at 1.49 δ ppm as a quintet. The remaining methylene protons (**b**) appeared in the range 1.33 – 1.15 δ ppm as a multiplet. The protons of the terminal methyl group (**a**) belonging to the pentadecyl chain appeared as a triplet at 0.87 δ ppm.

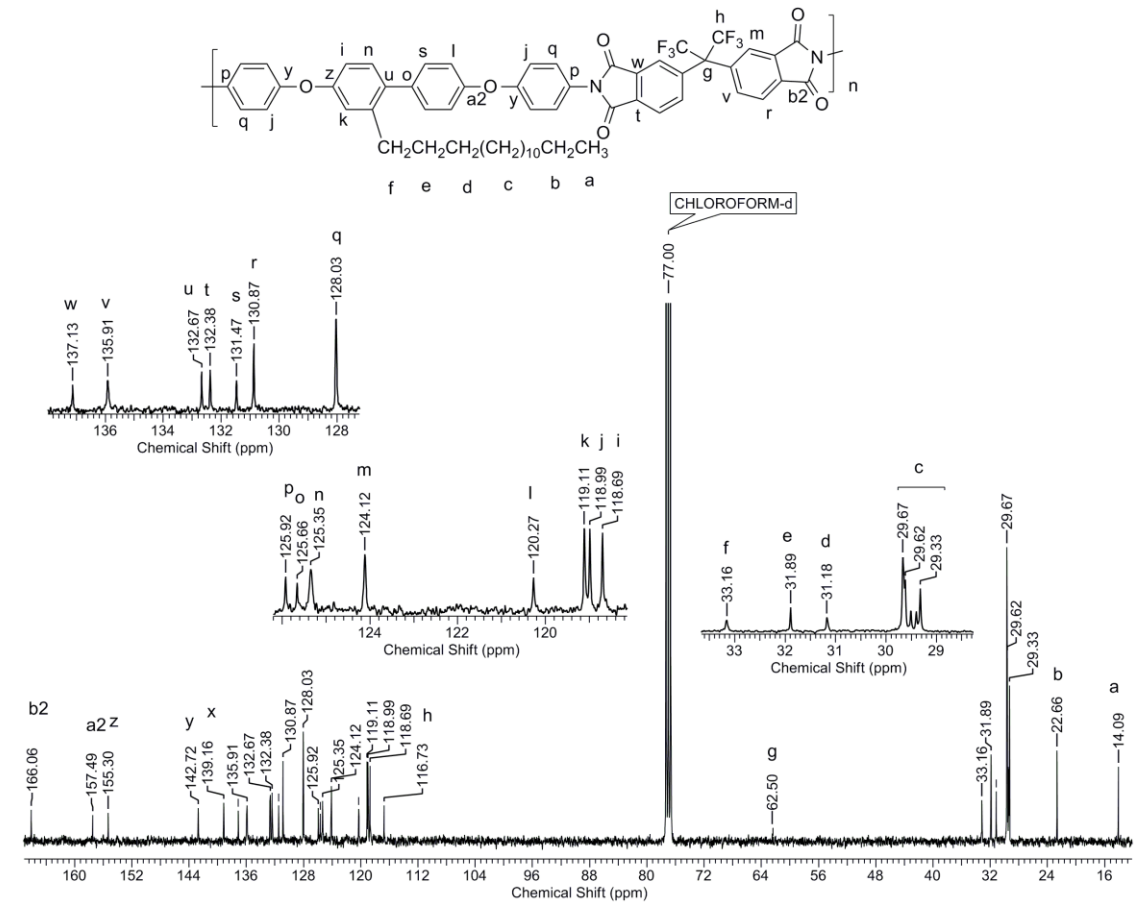

Figure 7.4 ^{13}C-NMR spectrum ($CDCl_3$) of PEI-6FDA

The peak appearing at 166.06 δ ppm was readily assignable to the carbonyl carbons (**b2**) of the imide moiety. The aromatic carbons of the diamine and dianhydride moiety (**i-a2**) appeared in the range 118.69 – 151.49 δ ppm. The carbon bearing fluorine atoms (**h**) resonated at 116.73 δ ppm, while the weak signal appearing at 62.50 δ ppm could be ascribed to the quaternary carbon bearing trifluoromethyl groups (**g**). The benzylic carbon (**f**) resonated at 33.16 δ ppm, while the methylene carbons belonging to the pentadecyl chain (**c**-**e**) appeared in the range 29.33 – 31.89 δ ppm. The methyl carbon (**a**) appeared at 14.09 δ ppm.

FT-IR, ^{1}H-NMR and ^{13}C-NMR spectral analysis indicated that structure of the representative polyimide PEI-6FDA showed good agreement with the proposed structure.

7.3.2 Solubility and X-ray diffraction studies

The solubility behaviour of synthesised polyimides at 3 wt % concentration was determined and the results are summarised in **Table 7.2.**

Table 7.2 Solubility of polyimides

Polyimide	Solvent								
	$CHCl_3$	THF	DMAc	NMP	Pyridine	DMSO	Nitro benzene	*m*-cresol	Acetone
PEI-6FDA	++	++	++	++	++	+-	++	++	--
PEI-ODPA	++	++	++	++	++	--	++	++	--
PEI-BPDA	++	+-	+-	++	+	--	+	++	--
PEI-IDBP	++	++	++	++	++	+-	++	++	--

--, Insoluble; + soluble on heating at 70°C; ++, soluble at room temperature; +-, partially soluble or swollen

The synthesised polyimides were found to be soluble in chloroform, 1-methyl-2-pyrrolidinone, pyridine, *m*-cresol and nitro benzene either at room temperature or on heating at 70 °C. This excellent solubility of polyimides can be readily attributed to the presence of pendent pentadecyl chains which exert a packing disruptive effect, decreasing the inter-chain interactions leading to improved polymer solubility.

X-Ray diffractograms of the synthesised polyimides are depicted in **Fig 7.5**. A broad hump was observed at around $2\theta \sim 20°$, which indicated that all the synthesised polyimides were amorphous in nature. It is postulated that the amorphous nature of the polyimides arises due to the presence of the pentadecyl chains, which disturb polymer close chain packing. Interestingly, a sharp peak is also observed in the region of $2\theta \sim 3°$. According to literature reports,[37–41] a sharp peak in this region is indicative of layered or stacked structures arising due to the presence of pendent long alkyl chains.

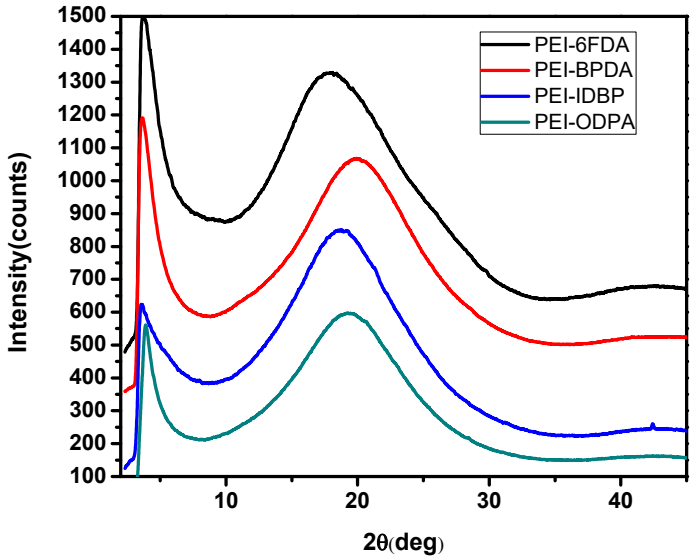

Figure 7.5 X-Ray diffractograms of polyimides

The solubility results and XRD analysis together support that the incorporation of pendent chains leads to disturbed chain packing leading to improved polymer solubility.

7.3.3 Thermal properties

The thermal behaviour of synthesised polyimides was investigated by thermogravimetric analysis (TGA) and differential scanning calorimetry (DSC) analysis. The results of TG and DSC analyses are tabulated in **Table 7.3**. In **Fig 7.6** is provided the TG curves of the synthesised polyimides, while DSC curves of polyimides are depicted in **Fig 7.8**. In **Fig 7.7** is presented a representative DTG curve along with corresponding TG curve of PEI-BPDA.

Table 7.3 Thermal properties of polyimides

Polyimide	Polyimide repeat unit	T_g (°C)[a]	T_d^{10} (°C)[b]	Char yield (%)[c]
PEI-6FDA	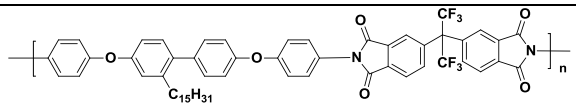	127	462	33
PEI-ODPA	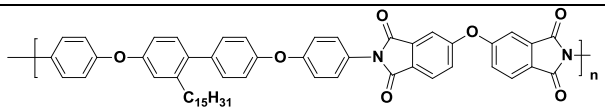	100	476	44
PEI-BPDA	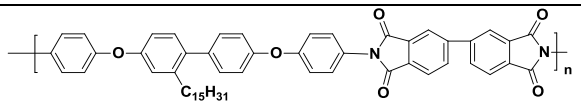	134	460	46
PEI-IDBP	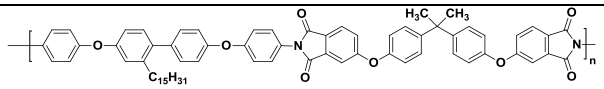	110	470	35

a: Measured by DSC from second heating scan with heating rate of 10 °C/min under nitrogen atmosphere.
b: 10% weight loss on TGA thermograms at a heating rate of 10 °C/min under nitrogen atmosphere.
c: Char yield measured at 800 °C.

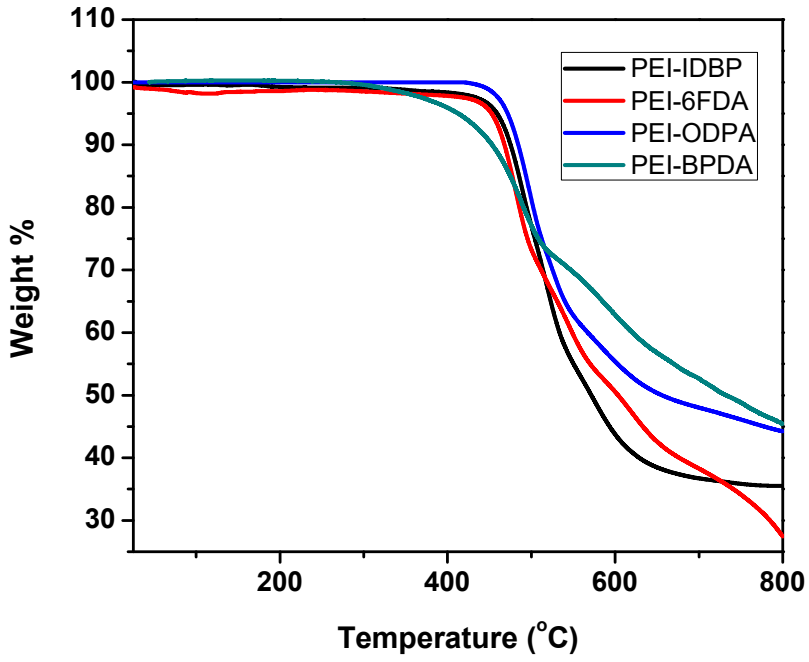

Figure 7.6 TG curves of polyimides

The T_{10} values of synthesised polyimides were observed in the range 460 °C – 476 °C. This indicates that the polyimides possessed good thermal stability. The char yields obtained were in the range 30 % – 46 %.

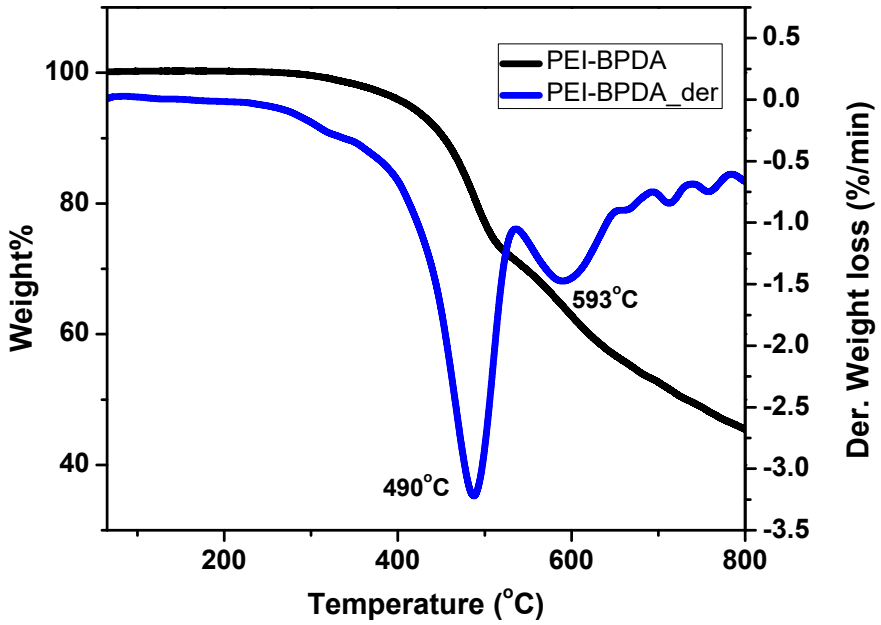

Figure 7.7 DTG curve of PEI-BPDA

Differential thermogravimetric analysis (DTG) of the polyimides revealed a two stage weight loss. The first stage of thermal decomposition occurring at 490 °C probably corresponded to decomposition of pendent alkyl chains, while the second stage of thermal decomposition occurring at 593°C corresponded to decomposition of polyimide backbone.

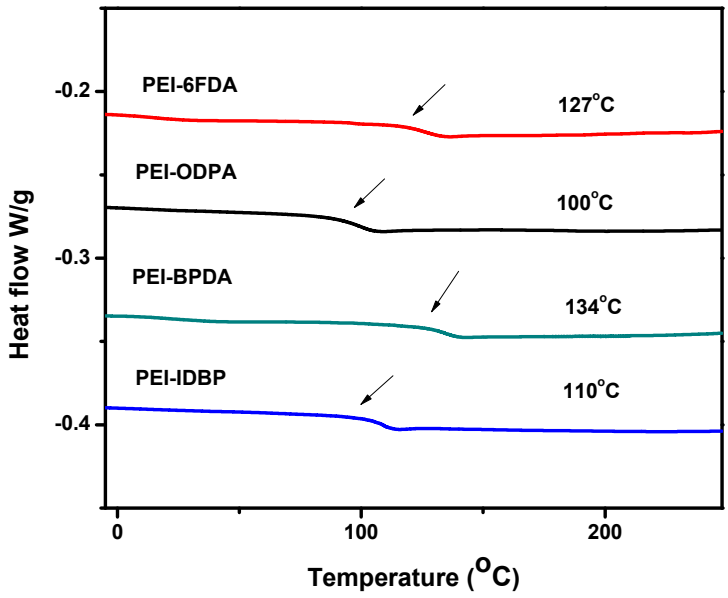

Figure 7.8 DSC curves of polyimides

Glass transition temperatures of the synthesised polyimides were observed in the range 110 – 134 °C. The observed T_g values increased with increase in polymer chain rigidity, depending on the structure of dianhydride used for synthesis. PEI-BPDA, possessing the most rigid backbone, displayed highest T_g value (134 °C). PEI-ODPA displayed the lowest T_g value of 100 °C, due to its backbone being the most flexible due to presence of additional ether linkages coming from ODPA. The T_g value of PEI-ODPA is much lower than the T_g value of polymer derived from 4,4'-oxydianiline and ODPA (242 °C). This implies that the T_g lowering effect observed was due to the cumulative effect of the flexibilising ether linkages and pendent pentadecyl chains. Both these groups exert a packing disruptive effect leading to decreased inter-chain interactions and improved segmental mobility leading to lowered T_g values. Additionally, no melting transitions were observed, further supporting the XRD results signifying that polyimides synthesised were amorphous in nature.

7.4 Conclusions

1. A new series of ether containing polyimides with pendent pentadecyl chains was synthesised by single step high temperature polycondensation of 4,4'-((2-pentadecyl-[1,1'-biphenyl]-4,4'-diyl)bis(oxy))dianiline (PBD) with commercially available dianhydrides, namely, 3,3',4,4'-biphenyltetracarboxylic dianhydride (BPDA), 4,4'-

oxydiphthalic anhydride (ODPA), 4,4'-(hexafluoroisopropylidene) diphthalic anhydride (6-FDA) and 4,4′-(4,4′-isopropylidenediphenoxy)bis(phthalic anhydride) (IDBP) in *meta*-cresol.

2. Inherent viscosities and number average molecular weights were in the range 0.5 – 1.53 dL g^{-1} and 19600 – 46500 g mol^{-1}, respectively, indicating the formation of polyimides of reasonably high molecular weights.

3. The synthesised polyimides were soluble in chloroform, 1-methyl-2-pyrrolidinone and *m*-cresol. As a result of excellent solubility in common organic solvents, synthesised polyimides are readily solution processable. Flexible, free-standing, transparent films could be cast from chloroform solutions.

4. The polyimides under study were found to be amorphous in nature, as deduced from XRD analysis due to incorporation of packing disruptive pentadecyl chains into the polymers.

5. Observed T_{10} values were in the range 460 – 476 °C while T_g values were in the range 100 – 134 °C. T_g values were governed by structure of the dianhydride monomer used for polyimide synthesis. A wide gap between T_g and T_{10} values provides a large processing window for melt processability.

References

1 M. Ding, *Prog. Polym. Sci.*, 2007, **32**, 623–668.

2 C. E. Sroog, *Prog. Polym. Sci.*, 1991, **16**, 561–694.

3 I. A. Ronova and M. Bruma, *Struct. Chem.*, 2010, **21**, 1013–1020.

4 K. Fukukawa and M. Ueda, *Polym. J.*, 2008, **40**, 281–296.

5 D. M. Stoakley, A. K. St. Clair and C. I. Croall, *J. Appl. Polym. Sci.*, 1994, **51**, 1479–1483.

6 D.-J. Liaw, K.-L. Wang, Y.-C. Huang, K.-R. Lee, J.-Y. Lai and C.-S. Ha, *Prog. Polym. Sci.*, 2012, **37**, 907–974.

7 S. Mallakpour and M. Dinari, *Nano*, 2012, **07**, 1250021.

8 R. Pariser, *Polym. J.*, 1987, **19**, 127–133.

9 C. Marestin, G. Gebel, O. Diat and R. Mercier, in *Fuel Cells II*, Springer Berlin Heidelberg, Berlin, Heidelberg, 2008, vol. 216, pp. 185–258.

10 D. Yin, Y. Li, H. Yang, S. Yang, L. Fan and J. Liu, *Polymer*, 2005, **46**, 3119–

3127.

11 C.-H. Chang, K.-L. Wang, J.-C. Jiang, D.-J. Liaw, K.-R. Lee, J.-Y. Lai and K.-H. Lai, *Polymer*, 2010, **51**, 4493–4502.

12 M. Dinari and H. Ahmadizadegan, *RSC Adv.*, 2015, **5**, 26040–26050.

13 G.-S. Liou, S.-H. Hsiao and Y.-K. Fang, *Eur. Polym. J.*, 2006, **42**, 1533–1540.

14 G.-S. Liou and S.-H. Hsiao, *Polym. J.*, 2003, **35**, 402–406.

15 T. M. Long and T. M. Swager, *J. Am. Chem. Soc.*, 2003, **125**, 14113–14119.

16 L. Yi, W. Huang and D. Yan, *J. Polym. Sci. Part A Polym. Chem.*, 2017, **55**, 533–559.

17 J. de Abajo and J. G. de la Campa, in *Progress in Polyimide Chemistry I Advances in Polymer Science*, ed. H. R. Kricheldorf, Springer, Berlin, Heidelberg, 1999, vol. 140, pp. 23–59.

18 A. Ghosh, S. K. Sen, S. Banerjee and B. Voit, *RSC Adv.*, 2012, **2**, 5900–5926.

19 A. Arbelaiz, B. Fernández, J. A. Ramos and I. Mondragon, *Thermochim. Acta*, 2006, **440**, 111–121.

20 S. Ando, T. Matsuura and S. Sasaki, *Polym. J.*, 1997, **29**, 69–76.

21 M. Hasegawa and K. Horie, *Prog. Polym. Sci.*, 2001, **26**, 259–335.

22 V. Ratta, Ph. D. Thesis, Faculty of Virginia Polytechnic Institute and State University, 1999.

23 J.-C. Kim and J.-H. Chang, *Macromol. Res.*, 2014, **22**, 1178–1182.

24 K. Takizawa, J. Wakita, S. Azami and S. Ando, *Macromolecules*, 2011, **44**, 349–359.

25 C.-P. Yang, Y.-Y. Su and S.-H. Hsiao, *J. Polym. Sci. Part A Polym. Chem.*, 2006, **44**, 5909–5922.

26 C.-P. Yang and Y.-Y. Su, *Polymer*, 2005, **46**, 5797–5807.

27 M. Dinari, H. Ahmadizadegan and P. Asadi, *New J. Chem.*, 2015, **39**, 4478–4487.

28 Y.-Y. Chen, C.-P. Yang and S.-H. Hsiao, *Eur. Polym. J.*, 2006, **42**, 1705–1715.

29 M. Chao, K. C. Kou, Z. C. Wang, G. L. Wu, D. N. Zhang and J. Q. Zhang, *Adv. Mater. Res.*, 2011, **199**–**200**, 13–18.

30 H. Li, S. Zhang, C. Gong, Y. Liang, Z. Qi and Y. Li, *Polym. Int.*, 2015, **64**, 352–360.

31 D. H. Wang, Z. Shen, S. Z. D. Cheng and F. W. Harris, *Polymer*, 2007, **48**, 2572–2584.

32 T. F. da Conceição and M. I. Felisberti, *J. Appl. Polym. Sci.*, 2014, **131**, 40351–40360.

33 H. Koerner, R. J. Strong, M. L. Smith, D. H. Wang, L.-S. Tan, K. M. Lee, T. J. White and R. A. Vaia, *Polymer*, 2013, **54**, 391–402.

34 J. A. Shumaker, A. J. W. McClung and J. W. Baur, *Polymer*, 2012, **53**, 4637–4642.

35 M. Yoonessi, Y. Shi, D. A. Scheiman, M. Lebron-Colon, D. M. Tigelaar, R. A. Weiss and M. A. Meador, *ACS Nano*, 2012, **6**, 7644–7655.

36 X. Xiao, X. Qiu, D. Kong, W. Zhang, Y. Liu and J. Leng, *Soft Matter*, 2016, **12**, 2894–2900.

37 R. Duran, M. Ballauff, M. Wenzel and G. Wegner, *Macromolecules*, 1988, **21**, 2897–2899.

38 H. Kim, S.-B. Park, Jin Chul Jung and W.-C. Zin, *Polymer*, 1996, **37**, 2845–2852.

39 D. H. Wang, Z. Shen, M. Guo, S. Z. D. Cheng and F. W. Harris, *Macromolecules*, 2007, **40**, 889–900.

40 Y. S. Kim and J. C. Jung, *J. Polym. Sci. Part A Polym. Chem.*, 2002, **40**, 1764–1774.

41 Y. Chen, R. Wombacher, J. H. Wendorff and A. Greiner, *Polymer*, 2003, **44**, 5513–5520.

CHAPTER 8

Summary and Conclusions

8.1 Summary

Being remarkably useful, polymers form the cornerstone of our modern lives. Yet, they are "challenged" from the point of view of sustainability: modern polymers are born out of petrochemical sources, which constitute a finite carbon source, under extreme stress from escalating energy demands as a result of burgeoning human population and improving standards of living. It is indeed the need of our times to explore the development of low-cost polymers from cheap and readily available renewable resources. Scientific efforts towards the conception, synthesis and fabrication of sustainable polymers have escalated in the past few decades. CNSL constitutes an attractive low-cost renewable starting material for the design and synthesis of monomers and polymers.

The overall goal of this thesis was the conception and design of difunctional monomers from CNSL and their utilisation for the synthesis of high performance polymers. It was envisioned that the nature-gifted alkyl chain present in cardanol, when incorporated into the synthesised polymers would greatly improve their processability and endow interesting properties. Another goal of this project was to design and synthesise high performance polymers containing a triarylamine moiety from CNSL to yield smart optoelectronic materials. Towards this end, following monomers were synthesised, as depicted in **Tables 8.1 and 8.2**, starting from 3-pentadecyl phenol, which in turn is derived from CNSL:

Table 8.1 Difunctional condensation monomers starting from CNSL

Sr. No.	Monomer Structure	Monomer
1.	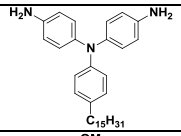	4, 4'-Diamino-4"pentadecyltriphenylamine
2.	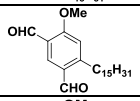	4-Methoxy-6-pentadecylisophthalaldehyde
3.	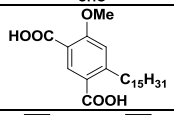	4-Methoxy-6-pentadecylisophthalic acid
4.	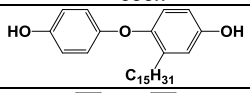	4-(4-Hydroxyphenoxy)-3-pentadecylphenol
5.	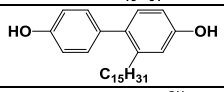	2-Pentadecyl-[1,1'-biphenyl]-4,4'-diol
6.	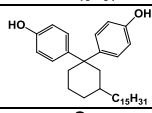	4,4'-(3-Pentadecylcyclohexane-1,1-diyl)diphenol
7.	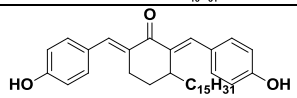	2,6-Bis(4-hydroxybenzylidene)-3-pentadecylcyclohexanone
8.	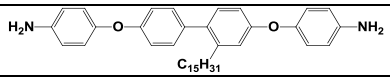	4,4'-((2-Pentadecyl-[1,1'-biphenyl]-4,4'-diyl)bis(oxy))dianiline

Table 8.2 Monomers for thermosetting resins starting from CNSL

Sr. No.	Monomer Structure	Monomer
1.	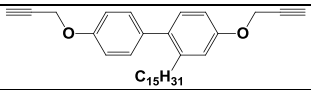	2-Pentadecyl-4,4'-bis(prop-2-yn-1-yloxy)-1,1'-biphenyl
2.	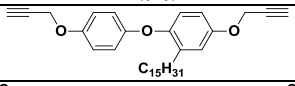	2-Pentadecyl-4-(prop-2-yn-1-yloxy)-1-(4-(prop-2-yn-1-yloxy)phenoxy)benzene
3.	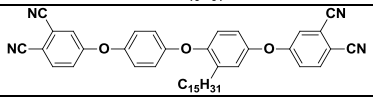	4-(4-(4-(3,4-Dicyanophenoxy)-2-pentadecylphenoxy)phenoxy)phthalonitrile
4.	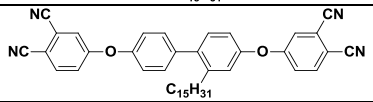	4,4'-((2-Pentadecyl-[1,1'-biphenyl]-4,4'-diyl)bis(oxy))diphthalonitrile
5.	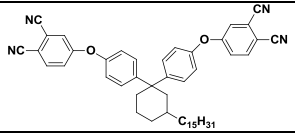	4,4'-(((3-Pentadecylcyclohexane-1,1-diyl)bis(4,1-phenylene))bis(oxy))diphthalonitrile

The synthesised monomers were characterised by FT-IR, ^{1}H-NMR and ^{13}C-NMR spectroscopy and in certain cases by HRMS analysis. The difunctional monomers were employed for the synthesis of step-growth polymers. Although not investigated in the present work, the monomers for thermosetting resins **(Table 8.2)** are potentially useful for the synthesis of partially bio-based thermosets.

Three polyimides were synthesised by the polycondensation of 4, 4'-diamino-4"pentadecyltriphenylamine with commercially available aromatic dianhydrides, namely, 3,3',4,4'-biphenyltetracarboxylic dianhydride (BPDA), 4,4'-oxydiphthalic anhydride (ODPA) and 4,4'-(hexafluoroisopropylidene) diphthalic anhydride (6-FDA). The polyimides were designated as PI-BPDA, PI-ODPA and PI-6FDA. Inherent viscosities and number average molecular weights were in the range 0.54 – 0.60 dL g^{-1} and 26800 – 43500 g mol^{-1}, respectively, indicating the formation of polyimides of reasonably high molecular weights. The synthesised polymers were readily soluble in chloroform, tetrahydrofuran, *m*-cresol and 1-methyl-2-pyrrolidinone at room temperature. The C_{15} alkyl chain, coupled with the bulky propeller-shaped triphenylamine unit imparted excellent solubility to the synthesised polyimides. Due to such excellent solubility the synthesised polyimides are readily solution processable. Flexible, free-standing, yellow coloured films could be cast from chloroform solutions. According to XRD analysis, the synthesised polyimides were observed to be amorphous in nature due to the combined effect of bulky triarylamine moiety and pendent pentadecyl chains. Additionally, a sharp peak was observed in the low angle region (~3 °) which was ascribable to the formation of stacked or layered structures in the solid state, typically observed in the case of high performance polymers bearing pendent long alkyl chains. T_{10} values (418 – 447 °C) indicated that synthesised polyimides possessed good thermal stability. Polyimides demonstrated appreciable lowering of T_g (165 – 225 °C) values when compared with reference polyimides based on 4,4'-diaminotriphenylamine (295 °C – 316 °C). It was also observed that the polymers exhibited two-stage degradation, with degradation occurring at ~ 462 °C and ~ 593 °C presumably corresponding to decomposition of alkyl chains and polyimide backbone, respectively. The polyimides displayed optical and electrochemical band-gap values in the range 1.95 – 1.98 eV and 1.42 – 1.49 eV, respectively, and showed a change in colour from yellow to intense blue/green on

electrochemical oxidation. These partially bio-based polyimides thus are good semiconductor materials with electrochromic properties and may find applications in electrochromic devices as hole-transporting materials. All three polyimides exhibited non-volatile rewritable memory characteristics, as determined from I-V, endurance and retention studies. Fabricated memory devices displayed memory window of 1000 along with excellent uniformity of memory states as evidenced from statistical analysis. Schottky conduction mechanism was observed to dominate in the high voltage region.

Three new triarylamine and pentadecyl chain containing aromatic polyamides, PA-HBBA, PA-IPA and PA-OBBA, were synthesised from the polycondensation of 4, 4'-diamino-4"pentadecyltriphenylamine with commercially available aromatic diacids *viz*. 4,4′-(hexafluoroisopropylidene)bis(benzoic acid) (HBBA), isophthalic acid (IPA) and 4,4′-oxybis(benzoic acid) (OBBA) by Yamazaki polymerisation at 120 °C. Inherent viscosities were in the range 0.6 – 0.7 dL g^{-1}, indicating the formation polyamides of reasonably high molecular weights. The synthesised polyamides were amorphous in nature, as ascertained from XRD analysis. This was due to the packing disruptive effect exerted by bulky triarylamine moiety and pentadecyl chains. It was evidenced from T_{10} values (420 – 448 °C) that polyamides synthesised were of good thermal stability. T_g values ranged from 189 – 206 °C. Optical band-gap values were found to be in the range 1.58 – 1.6 eV. These values indicated that the synthesised polyamides showed good potential for semiconductor applications. Memory device fabricated PA-HBBA displayed WORM memory behaviour, while memory device based on PA-IPA exhibited bipolar rewritable memory characteristics. Two well defined memory states, HRS and LRS were developed in the devices, with a memory window of 1000 in the case of PA-HBBA and 10 in the case of PA-IPA, suggesting that the memory devices would be useful for practical purposes. Endurance and retention studies indicated that the memory devices are non-volatile in nature. Additionally, statistical analysis of the developed memory states indicated good stability. Schottky conduction mechanism dominated for "OFF" to "ON" and "ON" to "OFF" transitions.

Three new aromatic polyazomethines containing triarylamine moiety and pendent pentadecyl chains were synthesised by solution polycondensation of 4, 4'-diamino-4"pentadecyltriphenylamine with commercially available aromatic dialdehydes such as

terephthaldehyde, isophthaldehyde and a mixture of terephthaldehyde and isophthaldehyde. The polyazomethines were designated as PAZ-TPA, PAZ-IPA and PAZ-IPA+TPA. Inherent viscosities and number average molecular weights were in the range 0.5 – 0.65 dL g^{-1} and 12700 – 22000 g mol^{-1}, respectively, indicating the formation of polyazomethines of reasonably high molecular weights. The synthesised polymers were readily soluble in chloroform, tetrahydrofuran, *m*-cresol, pyridine and nitro benzene at room temperature. Such excellent solubility allows the synthesised polyazomethines to be readily solution processable. Flexible, free-standing, orange coloured films could be cast from chloroform solutions. According to XRD analysis, the synthesised polyazomethines were observed to be amorphous in nature due to the combined effect of bulky triarylamine moiety and pendent pentadecyl chains. Polyazomethines exhibited 10 % weight loss temperature (T_{10}) in the range 431 – 463 °C pointing towards good thermal stability. A sharp decline in T_g values (53 – 78 °C), when compared with T_g values of polyazomethines based on 4,4'-diaminotriphenylamine (251 °C – 310 °C), resulting from the introduction of packing disruptive and flexibilising pentadecyl chains, afforded a wide processing window for melt processing. Optical band-gap values were found to be in the range 1.26 – 1.3 eV. These values indicated that the synthesised polyazomethines may appropriately be employed for semiconductor applications. All three polyazomethines were evaluated for applications in memory devices. The memory devices were found to be rewritable in nature from I-V studies. Three well developed resistive states were observed: HRS, IRS and LRS, with memory window of 10 and 100. Thus multi-level memory behaviour was observed, which indicates that the fabricated memory devices can potentially afford high density data storage. It was evidenced from endurance and retention studies that the memory devices had good endurance and exhibited non-volatile memory characteristics. Statistical analysis of the resistive states revealed excellent uniformity of memory states. Schottky conduction mechanism was observed to dominate in the high voltage region.

A new series of (co)poly(ether ether ether ketone)s containing pendent pentadecyl chains was synthesised by nucleophilic aromatic substitution polycondensation in *N*,*N*-dimethylacetamide of 4-(4-hydroxyphenoxy)-3-pentadecylphenol with 4,4'-difluorobenzophenone or a mixture of 4-(4-hydroxyphenoxy)-3-pentadecylphenol and

bisphenol A with 4,4'-difluorobenzophenone. Inherent viscosities and number average molecular weights were in the range 0.61 – 0.73 dL g^{-1} and 26900 – 93400 g mol^{-1}, respectively, indicating the formation of (co)poly(ether ether ether ketone)s of reasonably high molecular weights. The synthesised polymers were readily soluble in chloroform, dichloromethane, tetrahydrofuran, 1-methyl-2-pyrrolidinone and pyridine at room temperature. As a result of such excellent solubility, the (co)poly(ether ether ether ketone)s are readily solution processable. Flexible, free-standing, transparent films could be cast from chloroform solutions. (Co)poly(ether ether ether ketone)s under study were found to be amorphous in nature, as deduced from XRD analysis, due to incorporation of packing disruptive pentadecyl chains into the polymers. 10 % thermal degradation (T_{10} values) observed in the case of (co)poly(ether ether ether ketone)s ranged from 431 – 463 °C indicating good thermal stability. T_g values ranged from 25 – 125 °C. The T_g and T_{10} values progressively decreased with increase in % incorporation of 4-(4-hydroxyphenoxy)-3-pentadecylphenol. T_g values obtained from DSC analysis showed good agreement with theoretical T_g values obtained from Fox equation within range of experimental error.

A series of (co)poly(ether sulfone)s were synthesised from polycondensation of pentadecyl chain containing 4-(4-hydroxyphenoxy)-3-pentadecylphenol with bis(4-fluorophenyl)sulfone or a mixture of 4-(4-hydroxyphenoxy)-3-pentadecylphenol and bisphenol A with bis(4-fluorophenyl)sulfone in *N*,*N*-dimethylacetamide at 180 °C. Inherent viscosities were observed to be in the range 0.56 – 0.69 dL g^{-1}, while number average molecular weights obtained were in the range 46000 – 87000 g mol^{-1}, indicating that the synthesised (co)poly(ether sulfone)s possessed reasonably high molecular weights. (Co)poly(ether sulfone)s were easily soluble in chloroform, dichloromethane, tetrahydrofuran, *N*,*N*-dimethylacetamide and 1-methyl-2-pyrrolidinone at room temperature. Films cast from chloroform solutions were flexible, transparent and free-standing in nature. T_{10} values were observed in the range 414 – 444 °C, suggesting good thermal stability. T_g values obtained from DSC analysis were in the range 47 – 149 °C. Both T_{10} and T_g values showed a progressive decrease with increasing % incorporation of pentadecyl chain containing 4-(4-hydroxyphenoxy)-3-pentadecylphenol into copoly(ether sulfone)s.

A series of polycarbonates containing cyclohexylidene and pendent pentadecyl chains were synthesised from polycondensation of 1,1-bis(4-hydroxyphenyl)-3-pentadecylcyclohexane with triphosgene or a mixture of 1,1-bis(4-hydroxyphenyl)-3-pentadecylcyclohexane and bisphenol A with triphosgene *via* low temperature solution polymerisation. Inherent viscosities obtained were in the range 0.7 – 0.86 dL g^{-1}, while number average molecular weights were determined to be in the range 40200 – 69800 g mol^{-1}, suggesting the formation of (co)polycarbonates of reasonably high molecular weights. (Co)polycarbonates were soluble in chloroform, dichloromethane and tetrahydrofuran. Flexible, transparent and free-standing films of synthesised (co)polycarbonates were obtained by drop-casting from chloroform solutions. The T_g values (47 – 79 °C) and the T_{10} values (438 – 450 °C) of the (co)polycarbonates showed a distinct decrease with increase in incorporation of 1,1-bis(4-hydroxyphenyl)-3-pentadecylcyclohexane. Additionally, the T_{10} values indicated that the (co)polycarbonates possessed good thermal stability.

A new series of ether containing polyimides with pendent pentadecyl chains was synthesised by single step high temperature solution polycondensation of 4,4'-((2-pentadecyl-[1,1'-biphenyl]-4,4'-diyl)bis(oxy))dianiline with commercially available aromatic dianhydrides, namely, 3,3',4,4'-biphenyltetracarboxylic dianhydride (BPDA), 4,4'-oxydiphthalic anhydride (ODPA), 4,4'-(hexafluoroisopropylidene) diphthalic anhydride (6-FDA) and 4,4′-(4,4′-isopropylidenediphenoxy)bis(phthalic anhydride) (IDBP) in *m*-cresol. Inherent viscosities and number average molecular weights were in the range 0.5 – 1.53 dL g^{-1} and 19600 – 46500 g mol^{-1}, respectively, indicating the formation of polyimides of reasonably high molecular weights. The synthesised polyimides were soluble in chloroform, 1-methyl-2-pyrrolidinone and *m*-cresol. Such excellent solubility ensures that all the polyimides are readily solution processable. Flexible, free-standing, transparent films could be cast from chloroform solutions. The polyimides under study were found to be amorphous in nature, as deduced from XRD analysis due to incorporation of packing disruptive pentadecyl chains into the polymers. T_{10} values in the range 460 °C – 476 °C indicated good thermal stability. T_g values ranged from 100 – 134 °C. The polyimides displayed two-step thermal degradation, with degradation occurring at 490 °C and 593 °C, presumably due to degradation of alkyl

chains and polyimides backbone, respectively. T_g values varied with change in the polymer backbone flexibility, as influenced by the structure of the aromatic dianhydride used.

In summary, it was observed that the incorporation of pentadecyl chains in the synthesised polymers resulted in improved solubility and the formation of amorphous polymers. This can be attributed to the packing disruptive effect of pentadecyl chains, which reduce the inter-chain interactions due to effective chain separation effect, allowing solvent molecules to penetrate within the polymer chain and thus improving solubility. The packing disruptive effect does not allow the polymer chain to pack into specific crystal lattices, thus leading to the formation of amorphous polymers in the solid state. A decrease in T_g and T_{10} values are observed due to the introduction of the pentadecyl chains. A large difference in T_g and T_{10} values observed in the case of synthesised polymers leads to the generation of a wider processing window and better polymer processing possibilities. Additionally, the high performance polymers containing triarylamine moieties derived from CNSL showed impressive memory characteristics, making them good smart materials for memristive applications.

8.2 Future Perspectives

The work presented in this thesis on the design and synthesis of difunctional monomers starting from CNSL and the synthesis of high performance polymers has opened up several avenues for future work.

1. The difunctional monomers reported in this thesis, including diacid, dialdehyde, diamines and bisphenol, have broadened the library of bio-based monomers available to chemists for the purpose of synthesis of new high performance polymers.
2. 4-Methoxy-6-pentadecylisophthalaldehyde may potentially be used for the synthesis of new partially bio-based polyazomethines. Similarly, 4-methoxy-6-pentadecylisophthalic acid may be employed for the synthesis of a host of polymers, such as polyesters, polyamides and poly(1,3,4-oxadiazole)s.
3. 2,6-Bis(4-hydroxybenzylidene)-3-pentadecylcyclohexanone may be utilised for the synthesis of polyesters, polycarbonates, poly(arylene ether)s, etc containing

olefinic unsaturation in the backbone. These unsaturated sites could be used for cross-linking *via* UV irradiation.

4. Although polyimides were targeted in the present work, 4,4'-((2-pentadecyl-[1,1'-biphenyl]-4,4'-diyl)bis(oxy))dianiline may be exploited for the synthesis of polyamides, polyazomethines and poly(amideimide)s.
5. The thermosetting monomers reported in the present work, namely, 2-pentadecyl-4,4'-bis(prop-2-yn-1-yloxy)-1,1'-biphenyl, 2-pentadecyl-4-(prop-2-yn-1-yloxy)-1-(4-(prop-2-yn-1-yloxy)phenoxy)benzene, 4-(4-(4-(3,4-dicyanophenoxy)-2-pentadecylphenoxy)phenoxy)phthalonitrile, 4,4'-((2-pentadecyl-[1,1'-biphenyl]-4,4'-diyl)bis(oxy))diphthalonitrile and 4,4'-(((3-pentadecylcyclohexane-1,1-diyl)bis(4,1-phenylene))bis(oxy))diphthalonitrile could be employed to generate partially bio-based bispropargyl ether resins and phthalonitrile resins. Bispropargyl ether resins are a useful alternative for epoxy resins, while phthalonitrile resins have attractive civilian as well as military applications.
6. Although the triarylamine-containing polyimides, polyamides and polyazomethines under study exhibited excellent memristive behaviour, smooth resistive switching properties observed in the case of PAZ-IPA, PI-ODPA and PA-IPA suggest that these polymers may be useful to mimic biological synaptic properties. Memristors exhibiting analog-type switching may be useful in neuromorphic computing. Such memristor-based neuromorphic systems may revolutionalise conventional computing systems to perform judging, learning and decision-making actions that are characteristic of higher life forms.
7. Electrochemical analysis of the synthesised polyazomethines would yield a better understanding of their memristic characteristics.
8. Additionally, the polyazomethines under study may also be investigated for applications in bulk heterojunction solar cells.
9. Morphological analysis of the triarylamine-based memory devices would provide a deeper understanding of memory characteristics.
10. Dielectric properties of polymers are known to be dependent on their hydrophobicity. Therefore the synthesised polymers in this study, especially poly(arylene ether)s, polyimides, etc containing pendent pentadecyl chains would

be expected to have low dielectric constants, making them useful as interlayer dielectrics.

11. Polymers containing alkyl groups in the main chain are also known to be useful as high-sensitive negative resist materials. It would be interesting to explore the synthesised poly(arylene ether)s containing pendent pentadecyl chains for applications in lithography.
12. The ether containing polyimides reported in this study may be useful as transparent materials in optoelectronic applications such as transparent flexible displays, flexible printing circuit boards, etc. Additionally, PEI-IDBP, containing a flexible bisphenol-A type dianhydride may be useful as a transparent shape memory material.

Synopsis of the Thesis Entitled "Utilisation of Cashew Nut Shell Liquid as a Starting Material for the Synthesis of Difunctional Monomers Useful in the Preparation of High Performance Polymers"

Introduction:

Polymers are the most important class of materials useful both in day-to-day life and in advanced applications such as aircrafts, automobiles, electronics, etc. Most of the monomers for industrially relevant synthetic polymers are generally derived from petrochemical sources.[1] However, complete dependence on fossil-based resources is risky. The fossil-based resources are formed through biological and chemical processes which take place over millions of years, while their rate of consumption is several times greater than the rate of formation.[2–5] This implies that fossil-based resources such as petro-chemicals are in imminent danger of depletion. Consequently, over the years, and in particular in the recent past, academic and industrial researchers have been intensely exploring renewable resources as starting materials for chemicals. Biomass, which refers to any organic matter of recent biological origin, is a promising renewable resource for value-added chemicals.[6] The products obtained from biomass may be intermediates, final products or other materials useful in chemical processes.[7–10] Biochemicals derived from biomass may either be edible or non-edible. Utilisation of non-edible bio-derived chemicals is desirable to avoid stressing the food industry. Non-edible bio-derived chemicals include lignins, tannins, natural phenols, etc. Several reports are available in the literature which enumerate monomers and polymers synthesised from a variety of biomass sources.[11–19]

Cashew nut shell liquid (CNSL) belongs to the class of naturally occurring phenols, and is abundantly available (4,898,360 tonnes worldwide and 671,000 tonnes in India in 2016) at low cost (around 0.27 $/Kg in 2017). It is an industrial waste of the cashew processing industry. Utilisation of CNSL for production of useful chemicals is highly desirable as it would involve the exploitation of a waste product for the generation of value-added chemicals. CNSL is mainly composed of anacardic acid, cardanol and 2-methyl cardol.[20–22] Cardanol, which is the major product of high temperature distillation process of CNSL, possesses interesting reactive sites:

phenolic –OH, aromatic ring and double bonds in the C_{15} chain, making it an attractive starting material for the synthesis of difunctional condensation monomers.[23] There are several reports in the literature dealing with cardanol-based monomers, high performance polymers[24], resins, additives and other value-added chemicals.[9,25–31]

High performance polymers such as aromatic polyimides, polyamides, polyazomethines, etc possess excellent mechanical strength, thermo-oxidative stability, good electrical properties and solvent resistance.[32] These polymers find applications in fields such as electronics, aerospace, automobiles, coatings, adhesives, membranes for separation of gases or liquids, etc.[33–37] However, these polymers generally possess high glass transition temperatures, sometimes above decomposition temperatures and exhibit poor solubility in common organic solvents, leading to difficulties in processing. Approaches employed to overcome these difficulties include (1) insertion of flexible spacers between rigid units, (2) insertion of bent or "crankshaft" units or kinks along the polymer backbone, and (3) introduction of bulky side groups or flexible side chains to the aromatic backbone.[38]

In consideration of the aforementioned issues, our research efforts were directed towards exploiting the intriguing structural features presented by cardanol, for the synthesis of difunctional monomers and processable high performance polymers therefrom. Difunctional monomers were designed starting from 3-pentadecyl phenol, which in turn is obtained from side-chain hydrogenation of cardanol, (1) to incorporate the flexible hydrocarbon chain pendent to the polymer backbone, and (2) to introduce asymmetry into the monomer structure. Furthermore, an aromatic diamine was designed starting from 3-pentadecyl phenol such that the hole-transporting triarylamine unit could be incorporated into aromatic polyimides, polyamides and polyazomethines. This strategy can potentially lead to the formation of partially bio-based high performance polymers possessing attractive electron-donating and hole-transporting/ injection properties. Additionally, thermosetting monomers such as bispropargyl ethers and bisphthalonitriles were synthesised based on bisphenols obtained from 3-pentadecyl phenol.

Objectives:

- The design and synthesis of aromatic difunctional monomers, *viz*., aromatic diamines, diacid, dialdehyde and bisphenol starting from 3-pentadecyl phenol.

- ❖ The design and synthesis of triarylamine-containing diamine starting from 3-pentadecyl phenol.
- ❖ The design and synthesis of bispropargyl ethers and bisphthalonitriles starting from 3-pentadecyl phenol.
- ❖ Synthesis of triarylamine-containing partially bio-based high performance polymers such as polyimides, polyamides and polyazomethines and their evaluation for applications in memory devices.
- ❖ Synthesis of aromatic polyimides, poly(arylene ether)s and polycarbonates containing pendent pentadecyl chains and study of the effects of incorporation of pentadecyl chains on polymer properties.

This thesis is divided into eight chapters

Chapter 1: Introduction and Literature Survey

This chapter provides a brief overview of cashew nut shell liquid (CNSL) — an important bio-derived chemical obtained as a by-product of the cashew processing industry. A particular emphasis has been laid on the work carried out pertaining to the synthesis of aromatic difunctional monomers based on cardanol and their utilisation for the preparation of high performance polymers. The properties of high performance polymers are also mentioned in brief.

Chapter 2: Scope and Objectives

This chapter presents the scope and objectives of the work.

Chapter 3: Synthesis and Characterisation of Monomers Starting from CNSL

This chapter describes the synthesis of monomers depicted in **Tables 1 and 2**:

Table 1 Difunctional condensation monomers starting from CNSL

Sr. No.	Monomer Structure	Monomer
1.	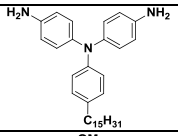	4, 4'-Diamino-4"pentadecyltriphenylamine
2.	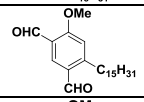	4-Methoxy-6-pentadecylisophthalaldehyde
3.	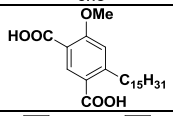	4-Methoxy-6-pentadecylisophthalic acid
4.	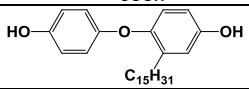	4-(4-Hydroxyphenoxy)-3-pentadecylphenol
5.	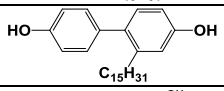	2-Pentadecyl-[1,1'-biphenyl]-4,4'-diol
6.	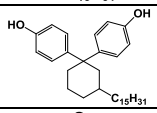	4,4'-(3-Pentadecylcyclohexane-1,1-diyl)diphenol
7.	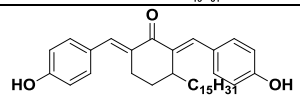	2,6-Bis(4-hydroxybenzylidene)-3-pentadecylcyclohexanone
8.	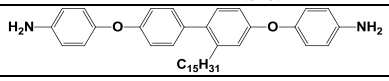	4,4'-((2-Pentadecyl-[1,1'-biphenyl]-4,4'-diyl)bis(oxy))dianiline

Table 2 Monomers for thermosetting resins starting from CNSL

Sr. No.	Monomer Structure	Monomer
1.	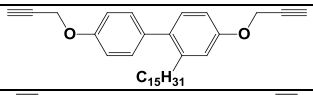	2-Pentadecyl-4,4'-bis(prop-2-yn-1-yloxy)-1,1'-biphenyl
2.	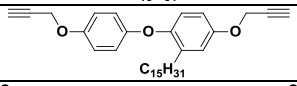	2-Pentadecyl-4-(prop-2-yn-1-yloxy)-1-(4-(prop-2-yn-1-yloxy)phenoxy)benzene
3.	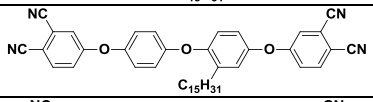	4-(4-(4-(3,4-Dicyanophenoxy)-2-pentadecylphenoxy)phenoxy)phthalonitrile
4.	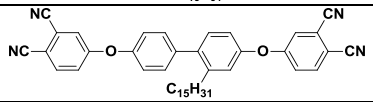	4,4'-((2-Pentadecyl-[1,1'-biphenyl]-4,4'-diyl)bis(oxy))diphthalonitrile
5.	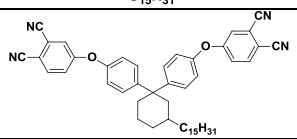	4,4'-(((3-Pentadecylcyclohexane-1,1-diyl)bis(4,1-phenylene))bis(oxy))diphthalonitrile

The synthesised monomers and the intermediates involved were characterised by FT-IR, ^{1}H-NMR spectroscopy, ^{13}C-NMR spectroscopy and HRMS.

Chapter 4: Partially Bio-based Triarylamine-Containing High Performance Polymers

This chapter has been sub-divided into three sections

Chapter 4(a): Partially Bio-based Triarylamine-Containing Polyimides: Synthesis, Characterisation and Evaluation for Memory Devices

This section describes:

- Synthesis of triarylamine-containing polyimides bearing pendent pentadecyl chains by polycondensation of 4, 4'-diamino-4"pentadecyltriphenylamine with commercially available aromatic dianhydrides *viz.* 3,3',4,4'-biphenyltetracarboxylic dianhydride (BPDA), 4,4'-oxydiphthalic anhydride (ODPA) and 4,4'-(hexafluoroisopropylidene) diphthalic anhydride (6-FDA).
- Polyimides were characterised by FT-IR, NMR, GPC, TGA, DSC and XRD studies. The optical, electrochemical and spectroelectrochemical behavior of polyimides and structure property relationship was also investigated.
- Memory devices were prepared from the synthesised triarylamine-containing polyimides. The I-V characteristics of the devices were studied. Performance parameters with respect to endurance and retention were investigated. The stability of resistive states and conduction mechanisms were also studied.

Chapter 4(b): Partially Bio-based Triarylamine-Containing Polyamides: Synthesis, Characterisation and Evaluation for Memory Devices

This section describes:

- Synthesis of triarylamine-containing polyamides possessing pendent pentadecyl chains by polycondensation of 4, 4'-diamino-4"pentadecyltriphenylamine with commercially available aromatic diacids *viz.* 4,4′-(hexafluoroisopropylidene)bis(benzoic acid) (HBBA), isophthalic acid (IPA) and 4,4′-oxybis(benzoic acid) (OBBA).
- Polyamides were characterised by FT-IR, NMR, GPC, TGA, DSC and XRD studies. The optical and electrochemical behaviour of polyamides along with structure property relationship was also investigated.
- Memory devices were prepared from the synthesised triarylamine-containing polyamides. The I-V characteristics of the devices were studied. Performance parameters with respect to endurance and retention were investigated. The stability of resistive states and conduction mechanisms were also studied.

Chapter 4(c): Partially Bio-based Triarylamine-Containing Polyazomethines: Synthesis, Characterisation and Evaluation for Memory Devices

This section describes:

- Synthesis of triarylamine-containing (co)polyazomethines containing pendent pentadecyl chains by polycondensation of 4, 4'-diamino-4"pentadecyltriphenylamine with aromatic dialdehydes such as terephthaldehyde, isophthaldehyde and a mixture of terephthaldehyde and isophthaldehyde.
- (Co)polyazomethines were characterised by FT-IR, NMR, GPC, TGA, DSC and XRD studies. The optical behavior of (co)polyazomethines and structure property relationships were also investigated.
- Memory devices were prepared from the synthesised triarylamine-containing (co)polyazomethines. The I-V characteristics of the devices were studied. Performance parameters with respect to endurance and retention were investigated. The stability of resistive states and conduction mechanisms were also studied.

Chapter 5: Partially Bio-based Poly(arylene ether)s Containing Pendent Pentadecyl Chains

This chapter has been sub-divided into two sections

Chapter 5(a): Synthesis and Characterisation of Partially Bio-based Poly(ether ether ether ketone)s Containing Pendent Pentadecyl Chains

This section describes:

- Synthesis of aromatic poly(ether ether ether ketone) from polycondensation of 4-(4-hydroxyphenoxy)-3-pentadecylphenol with 4,4'-difluorobenzophenone. Copoly(ether ether ether ketone)s were obtained by polycondensation of mixtures of 4-(4-hydroxyphenoxy)-3-pentadecylphenol and bisphenol-A with 4,4'-difluorobenzophenone.
- (Co)poly(ether ether ether ketone)s were characterised by FT-IR, NMR, GPC, TGA, DSC and XRD studies and influence of incorporation of pentadecyl chains on polymer properties was elucidated.

Chapter 5(b): Synthesis and Characterisation of Partially Bio-based Poly(ether sulfone)s Containing Pendent Pentadecyl Chains

This section describes:

- Synthesis of aromatic poly(ether sulfone) from polycondensation of 4-(4-hydroxyphenoxy)-3-pentadecylphenol with bis(4-fluorophenyl)sulfone. Copoly(ether sulfone)s were obtained by polycondensation of mixtures of 4-(4-hydroxyphenoxy)-3-pentadecylphenol and bisphenol-A with bis(4-fluorophenyl)sulfone.
- (Co)poly(ether sulfone)s were characterised by FT-IR, NMR, GPC, TGA, DSC and XRD studies and influence of incorporation of pentadecyl chains on polymer properties was elucidated.

Chapter 6: Synthesis and Characterisation of Partially Bio-based Polycarbonates Containing Pendent Pentadecyl Chains

This chapter describes:

- Synthesis of aromatic polycarbonates from polycondensation of 1,1-bis(4-hydroxyphenyl)-3-pentadecylcyclohexane with triphosgene. Copolycarbonates were obtained by polycondensation of mixtures of 1,1-bis(4-hydroxyphenyl)-3-pentadecylcyclohexane and bisphenol-A with triphosgene.
- (Co)polycarbonates were characterised by FT-IR, NMR, GPC, TGA, DSC and XRD studies and structure property relationship was developed.

Chapter 7: Synthesis and Characterisation of Partially Bio-based Polyimides Containing Pendent Pentadecyl Chains

This chapter describes:

- Synthesis of polyimides containing ether linkages in the backbone and pendent pentadecyl chains by polycondensation of 4,4'-((2-pentadecyl-[1,1'-biphenyl]-4,4'-diyl)bis(oxy))dianiline with commercially available aromatic dianhydrides, namely, 3,3',4,4'-biphenyltetracarboxylic dianhydride (BPDA), 4,4'-oxydiphthalic anhydride (ODPA), 4,4'-(hexafluoroisopropylidene) diphthalic anhydride (6-FDA) and 4,4′-(4,4′-isopropylidenediphenoxy)bis(phthalic anhydride) (IDBP).
- Polyimides were characterised by FT-IR, NMR, GPC, TGA, DSC and XRD studies and structure property relationship was studied. Incorporation of pentadecyl chains on polymer properties was elucidated.

Chapter 8: Summary and Conclusions

This chapter summarises the results and describes the salient conclusions and future prospects of the investigations reported in this thesis.

References:

1 Y. Xu, M. A. Hanna and L. Isom, *Open Agric. J.*, 2008, **2**, 54–61.

2 R. A. Berner, *Nature*, 2003, **426**, 323–326.

3 J. D. Brooks and J. W. Smith, *Geochim. Cosmochim. Acta*, 1969, **33**, 1183–1194.

4 F. D. Mango, *Org. Geochem.*, 1997, **26**, 417–440.

5 B. P. Tissot and D. H. Welte, *Petroleum Formation and Occurrence*, Springer Berlin Heidelberg, Berlin, Heidelberg, Heidelberg, 1984.

6 M. Crocker and C. Crofcheck, *Energeia*, 2006, **17**, 1–6.

7 M. FitzPatrick, P. Champagne, M. F. Cunningham and R. A. Whitney, *Bioresour. Technol.*, 2010, **101**, 8915–8922.

8 S. N. Naik, V. V. Goud, P. K. Rout and A. K. Dalai, *Renew. Sustain. Energy Rev.*, 2010, **14**, 578–597.

9 M. Stöcker, *Angew. Chemie Int. Ed.*, 2008, **47**, 9200–9211.

10 C. Williams and M. Hillmyer, *Polym. Rev.*, 2008, **48**, 1–10.

11 A. Gandini and T. M. Lacerda, *Prog. Polym. Sci.*, 2015, **48**, 1–39.

12 C. Vilela, A. F. Sousa, A. C. Fonseca, A. C. Serra, J. F. J. Coelho, C. S. R. Freire and A. J. D. Silvestre, *Polym. Chem.*, 2014, **5**, 3119–3141.

13 A. Gandini, T. M. Lacerda, A. J. F. Carvalho and E. Trovatti, *Chem. Rev.*, 2016, **116**, 1637–1669.

14 A. F. Sousa, C. Vilela, A. C. Fonseca, M. Matos, C. S. R. Freire, G.-J. M. Gruter, J. F. J. Coelho and A. J. D. Silvestre, *Polym. Chem.*, 2015, **6**, 5961–5983.

15 M. A. Hillmyer, *Science*, 2017, **358**, 868–870.

16 S. A. Miller, *ACS Macro Lett.*, 2013, **2**, 550–554.

17 D. K. Schneiderman and M. A. Hillmyer, *Macromolecules*, 2017, **50**, 3733–3749.

18 B. Gyarmati and B. Pukánszky, *Eur. Polym. J.*, 2017, **93**, 612–617.

19 R. Mülhaupt, *Macromol. Chem. Phys.*, 2013, **214**, 159–174.

20 M. T. Harvey and S. Caplan, *Ind. Eng. Chem.*, 1940, **32**, 1306–1310.

21 R. Paramashivappa, P. P. Kumar, P. J. Vithayathil and A. S. Rao, *J. Agric. Food Chem.*, 2001, **49**, 2548–2551.

22 J. H. P. Tyman, *Synthetic and Natural Phenols*, Elsevier, Amsterdam, 1st edn.,

1996.

23 C. Voirin, S. Caillol, N. V. Sadavarte, B. V. Tawade, B. Boutevin and P. P. Wadgaonkar, *Polym. Chem.*, 2014, **5**, 3142–3162.

24 D. Chatterjee, N. V. Sadavarte, R. D. Shingte, A. S. More, B. V. Tawade, A. D. Kulkarni, A. B. Ichake, C. V. Avadhani and P. P. Wadgaonkar, in *Cashew Nut Shell Liquid, A Goldfield for Functional Materials*, ed. P. Anilkumar, Springer International Publishing, Cham, 2017, pp. 163–214.

25 B. Lochab, S. Shukla and I. K. Varma, *RSC Adv.*, 2014, **4**, 21712–21752.

26 M. C. Lubi and E. T. Thachil, *Des. Monomers Polym.*, 2000, **3**, 123–153.

27 P. H. Gedam and P. S. Sampathkumaran, *Prog. Org. Coatings*, 1986, **14**, 115–157.

28 P. Blazdell, *Interdiscip. Sci. Rev.*, 2000, **25**, 220–226.

29 G. Mele and G. Vasapollo, *Mini. Rev. Org. Chem.*, 2008, **5**, 243–253.

30 V. S. Balachandran, S. R. Jadhav, P. K. Vemula and G. John, *Chem. Soc. Rev.*, 2013, **42**, 427–438.

31 S. Caillol, *Curr. Opin. Green Sustain. Chem.*, 2018, **14**, 26–32.

32 P. M. Hergenrother, *High Perform. Polym.*, 2003, **15**, 3–45.

33 O. J. Dautel, G. Wantz, D. Flot, J.-P. Lere-Porte, J. J. E. Moreau, J.-P. Parneix, F. Serein-Spirau and L. Vignau, *J. Mater. Chem.*, 2005, **15**, 4446–4452.

34 M.-S. Jung, T.-W. Lee, J. Hyeon-Lee, B. Hee Sohn and I.-S. Jung, *Polymer*, 2006, **47**, 2670–2676.

35 A. Kausar, S. Zulfiqar, Z. Ahmad and M. I. Sarwar, *Polym. Degrad. Stab.*, 2010, **95**, 1826–1833.

36 M. Rubal, C. W. Wilkins, P. E. Cassidy, C. Lansford and Y. Yamada, *Polym. Adv. Technol.*, 2008, **19**, 1033–1039.

37 B. Zhang, W. Li, J. Yang, Y. Fu, Z. Xie, S. Zhang and L. Wang, *J. Phys. Chem. C*, 2009, **113**, 7898–7903.

38 A. P. Dove and M. A. R. Meier, *Macromol. Chem. Phys.*, 2014, **215**, 2135–2137.

(Deepshikha Chatterjee)
Student

(Prakash P. Wadgaonkar)
Research Guide

List of Publications

1. **Deepshikha Chatterjee** et al. (2017) Step-Growth Polymers from Cashew Nut Shell Liquid (CNSL)-Based Aromatic Difunctional Monomers. In: Anilkumar P. (eds) Cashew Nut Shell Liquid. A Goldfield for Functional Materials. Springer

2. Kavita Garg, **Deepshikha Chatterjee** and Prakash P. Wadgaonkar

Clickable Polyurethanes Based on *s*-Triazine Ring Containing Aromatic Diisocyanate Bearing Pendent Alkyne Group: Synthesis and Postmodification.

J. Polym. Sci. Part A: Polym. Chem. 2017, 55, 1008–1020.

3. Kavita Garg, **Deepshikha Chatterjee** and Prakash P. Wadgaonkar

New Difunctional Monomers Containing Furyl as a Clickable Pendant Group and Polymers Therefrom.

WO 2016/098129 A1

4., Rahul Shingte, **Deepshikha Chatterjee**, Bhausaheb Tawade, Bharat Shrimant and Prakash P. Wadgaonkar

Aromatic Polyesters Containing Cardo Perhydrocumyl Cyclohexylidene Groups: Synthesis, Characterization and Gas Permeation Study

Journal of Macromolecular Science, Part A: Pure and Applied Chemistry (*Manuscript Accepted*)

4. **Deepshikha Chatterjee**, Tukaram Dongale, Uday Jadhav and Prakash P. Wadgaonkar

Non-volatile memory behavior of partially bio-based electrochromic polyimides with different electron withdrawing groups. (*Manuscript under preparation*)

5. **Deepshikha Chatterjee**, Tukaram Dongale, Uday Jadhav and Prakash P. Wadgaonkar

Partially bio-based aromatic polyamides with non-volatile memory behavior. (*Manuscript under preparation*)

6. **Deepshikha Chatterjee**, Tukaram Dongale, Uday Jadhav and Prakash P. Wadgaonkar

Multi-level non-volatile memory devices based on partially bio-derived aromatic polyazomethines. (*Manuscript under preparation*)

7. **Deepshikha Chatterjee**, and Prakash P. Wadgaonkar

Partially bio-based poly(arylene ether)s bearing pendent pentadecyl chains: synthesis and properties.(*Manuscript under preparation*)

8. **Deepshikha Chatterjee**, and Prakash P. Wadgaonkar

Synthesis and characterisation of partially bio-based polyimides containing ether linkages and pendent pentadecyl chains. (*Manuscript under preparation*)